

VOLTAGE STABILITY LIMITS FOR WEAK POWER SYSTEMS WITH HIGH
WIND PENETRATION

by

ALA TAMIMI

B.S., Jordan University of Science and Technology, 1990
M.S., Wichita State University, Wichita, Kansas, 1993

AN ABSTRACT OF A DISSERTATION

submitted in partial fulfillment of the requirements for the degree

DOCTOR OF PHILOSOPHY

Department of Electrical and Computer Engineering
College of Engineering

KANSAS STATE UNIVERSITY
Manhattan, Kansas

2011

Abstract

Analysis of power system voltage stability has practical value in increasing wind penetration levels. As wind penetration levels increase in power systems, voltage stability challenges arise due to locating wind resources far away from load centers. This dissertation presents several different voltage stability methods for sizing new wind farms. Power system wind penetration levels depend on the available voltage stability margins (*VSMs*) of the existing power system and system load characteristics. Three new iterative methods have been developed to maximize wind penetration level in weak power systems based on systems' *VSMs*. The first two methods use an iterative approach for increasing the size of each wind farm until reaching the collapse point. Wind farms with less negative impact on system *VSMs* are sized larger than others. A third wind farm sizing method has been developed using modal analysis in conjunction with the traditional voltage stability method (Q-V method). Wind farms are placed at buses in the power system which have the lowest negative impact on voltage instability modes (strong wind injection buses). By placing the wind farms at the strongest wind injection buses, higher amounts of wind power can be injected into the power system. To further increase wind penetration in weak power systems, two additional techniques are introduced and applied to the western Kansas power system. The first technique uses modes of voltage instability to place voltage support equipment like static var compensators at locations in the power system where they provide the needed reactive power support for increasing levels of wind penetration. The second technique uses the fact that wind patterns at a wind farm site may rarely allow the wind farm to produce its maximum capacity during the peak loading hours. Wind farm maximum sizes can be increased above their maximum voltage stable size limit without driving the power system into becoming voltage unstable. Preventing voltage collapse for the additional increases in wind farm sizes is accomplished by disconnecting some wind turbines inside the wind farm during critical times to reduce its power output to a voltage stable level.

VOLTAGE STABILITY LIMITS FOR WEAK POWER SYSTEMS WITH HIGH
WIND PENETRATION

by

ALA TAMIMI

B.S., Jordan University of Science and Technology, 1990
M.S., Wichita State University, Wichita, Kansas, 1993

A DISSERTATION

submitted in partial fulfillment of the requirements for the degree

DOCTOR OF PHILOSOPHY

Department of Electrical and Computer Engineering
College of Engineering

KANSAS STATE UNIVERSITY
Manhattan, Kansas

2011

Approved by:

Co-Major Professor
Anil Pahwa

Approved by:

Co-Major Professor
Shelli Starrett

Copyright

ALA TAMIMI

2011

Abstract

Analysis of power system voltage stability has practical value in increasing wind penetration levels. As wind penetration levels increase in power systems, voltage stability challenges arise due to locating wind resources far away from load centers. This dissertation presents several different voltage stability methods for sizing new wind farms. Power system wind penetration levels depend on the available voltage stability margins (*VSMs*) of the existing power system and system load characteristics. Three new iterative methods have been developed to maximize wind penetration level in weak power systems based on systems' *VSMs*. The first two methods use an iterative approach for increasing the size of each wind farm until reaching the collapse point. Wind farms with less negative impact on system *VSMs* are sized larger than others. A third wind farm sizing method has been developed using modal analysis in conjunction with the traditional voltage stability method (Q-V method). Wind farms are placed at buses in the power system which have the lowest negative impact on voltage instability modes (strong wind injection buses). By placing the wind farms at the strongest wind injection buses, higher amounts of wind power can be injected into the power system. To further increase wind penetration in weak power systems, two additional techniques are introduced and applied to the western Kansas power system. The first technique uses modes of voltage instability to place voltage support equipment like static var compensators at locations in the power system where they provide the needed reactive power support for increasing levels of wind penetration. The second technique uses the fact that wind patterns at a wind farm site may rarely allow the wind farm to produce its maximum capacity during the peak loading hours. Wind farm maximum sizes can be increased above their maximum voltage stable size limit without driving the power system into becoming voltage unstable. Preventing voltage collapse for the additional increases in wind farm sizes is accomplished by disconnecting some wind turbines inside the wind farm during critical times to reduce its power output to a voltage stable level.

Table of Contents

Table of Contents	vi
List of Figures	xii
List of Tables	xvii
Dedication.....	xxi
Chapter 1 - Introduction	1
1.1 Motivation.....	1
1.2 Objectives	2
1.3 Contributions.....	3
1.4 Publications of this Dissertation.....	4
1.5 Organization of Dissertation	5
1.6 Overview of Renewable Energy Resources and Wind Integration in Power Systems	7
1.6.1 Wind Resources Potential in Kansas	11
1.6.2 Challenges to Wind Power Integration in Power Systems.....	15
1.7 Wind Power and Wind Generation Types	18
1.7.1 Wind Power and Wind Generation Types	19
1.7.2 Wind Turbine Components	21
1.7.3 Wind Turbine Characteristics.....	22
1.7.4 Pitching	23
1.7.5 Generator.....	25
1.7.5.1 Squirrel-Cage Induction Generator (SCIG)	26
1.7.5.2 Doubly-Fed Induction Generator (DFIG)	28
1.7.5.3 Direct-Drive Synchronous Generator (DDSG)	30
1.7.6 Converter.....	32
1.8 Literature Survey.....	34
1.8.1 Wind Turbines	34
1.8.2 Wind Farm Aggregate Models	35
1.8.3 Voltage Stability	35
Chapter 2 - Steady-State Voltage Stability Methods and Load Modeling	41

2.1 Voltage Collapse and Power System Black-Out.....	41
2.1.1 Reactive Power System Limitation Cases.....	41
2.1.2 Control and Protection Scheme Limitation Cases	43
2.2 Definition of Voltage Stability and Voltage Collapse.....	44
2.3 Steady-State Voltage Stability Methods.....	46
2.3.1 The P-V Curve Method.....	46
2.3.2 The Q-V Curve Method.....	48
2.3.3 The P-Q Curve Method.....	50
2.4 Load Models for Voltage Stability Analysis in Power Systems with High Wind Penetration	53
2.4.1 Load Modeling Impact on Power System Voltage Stability.....	58
2.4.2 Case Studies for Load Modeling Impact on Power System Voltage Stability.....	58
2.4.2.1 Stability Limit Calculations for Constant Power (P), Constant Current (I), and Constant Impedance (Z) Load Types Using Different Stability Analysis Methods	60
2.4.3 Stability Boundaries Load-Type Buffer Analysis Using P-Q Curve Method.....	71
2.4.3.1 Case Study for the Application of Load Type Stability Buffer Calculations Applied to the Western Kansas Power System.....	75
2.5 Conclusions.....	82
Chapter 3 - Application of Steady-State Voltage Stability Methods for Wind Integration in Western Kansas.....	85
3.1 Wind Farm Aggregate Models for Steady-State Voltage Stability Analysis	85
3.2 Bus Type Models for Aggregated Wind Farms for Steady-State Stability Analysis.....	87
3.3 Maximum Wind Penetration for Different Turbine Type Wind Farms in the Western Kansas Power System	89
3.5 Conclusions.....	100
Chapter 4 - Voltage Stability Based Calculations of the Maximum Wind Penetration Using Voltage Stability Iterative Methods	102
4.1 Impact of Load Modeling on Voltage Stability Assessment for Power Systems with High Wind Penetration.....	103
4.2 Voltage Stability Based Methods for Determining Maximum Wind Farm Sizes	104
4.2.1 Method I: Simultaneous Wind Farm Power Output Incremental Increase	105

4.2.2 Method II: Independent Wind Farm Power Output Incremental Increase.....	107
4.3 Simulation Model Formulation & Results.....	110
4.3.1 Simulation Model Formulation	110
4.3.2 Simulation Results	112
4.4 Conclusions.....	119
Chapter 5 - Methods for Assessing System Impact of Increasing Wind Farm Sizes Above Their Maximum Limits.....	121
5.1 Voltage Stability Assessment Criteria.....	122
5.2 New Expected Voltage Stability Method for Assessing the Voltage Stability Impact of Wind Farm Sizes on Weak Power Systems.....	123
5.2.1 Details of the New Expected Voltage Stability Method.....	124
5.3 Simulation Model Formulation and Results	128
5.3.1 Simulation Model Formulation	128
5.3.2 Simulation Results	128
5.4 Conclusions.....	138
Chapter 6 - Effective Wind Farm Sizing Using Modes of Voltage Instability	140
6.1 Q-V Modal Analysis Method.....	140
6.2 Developing a Q-V Modal Method for Increasing Wind Penetration in Weak Power Systems.....	143
6.2.1 Development of a Systematic Voltage Stability Procedure for Increasing Wind Penetration in Weak Power Systems.....	143
6.2.2 Voltage Stability Method for Increasing Wind Penetration Using Modes of Instability	146
6.3 Simulation and Performance Using Simultaneous Increase of Wind Farms' Power Outputs	151
6.3.1 Case I: Base Case - No Wind Injection	152
6.3.2 Maximum Wind Penetration Using SCIG Wind Turbine Type.....	154
6.3.2.1 Case II: Maximum Wind Penetration from Individual Bus Wind Injection Using SCIG Wind Type Turbines	154
6.3.2.2 Case III: Maximum Wind Penetration from 3-Combined Bus for Wind Injections Using SCIG Wind Turbine Type.....	158

6.3.3 Maximum Wind Penetration Using DFIG Wind Turbine Type.....	159
6.3.3.1 Case II: Maximum Wind Penetration from Individual Bus Wind Injection Using DFIG Wind Turbine Type	160
6.3.3.2 Case III: Maximum Wind Penetration from 3-Combined Bus for Wind Injections Using DFIG Wind Turbine Type	164
6.3.4 Maximum Wind Penetration Using DDSG Wind Turbine Type	167
6.3.4.1 Case II: Maximum Wind Penetration from Individual Bus Wind Injection Using DDSG Wind Turbine Type.....	167
6.3.4.2 Case III: Maximum Wind Penetration from 3-Bus Combination for Wind Injections Using DDSG Wind Turbine Type.....	170
6.3.5 Comparison of the Impact of Using Three Different Types of Wind Generators on Maximum Wind Penetrations and on System Critical Eigenvalues	172
6.4 Increasing Wind Penetration by Placing SVCs Using the Different Types of Wind Turbines for the 3-Strong Bus Combination	175
6.4.1 Increasing Wind Penetration Using SVC Placement for the Combined 3-Strong Bus Combination Using SCIG Wind Type Turbines.....	176
6.4.2 Increasing Wind Penetration Using SVC Placement for the 3-Strong Bus Combination Using DFIG Wind Type Turbines.....	179
6.4.3 Increasing Wind Penetration Using SVC Placement for the 3-Strong Bus Combination Using DDSG Wind Type Turbines	184
6.5 Comparison of the Amount of SVCs Required for Reaching 410 MW of Wind Power Injection Using Different Wind Turbine Types for the 3-Strong Bus Combination Using Option II	187
6.6 Load Model Sensitivity Impact on Maximum Wind Penetration for the 3-Weak & the 3-Strong Bus Wind Combinations	188
6.7 Conclusions.....	192
Chapter 7 - Increasing Wind Farm Sizes Using Iterative Modal Voltage Stability Method.....	195
7.1 Increasing Wind Penetration Using the Iterative Voltage Stability Margins (VSM) Method (Method II) for the Combined Bus Wind Injection Cases	195
7.2 Iterative Method (Method III) for Increasing Wind Penetration Using Modal Analysis of Voltage Instability for the Combined Bus Wind Injection Cases.....	201

7.3 Conclusions.....	207
Chapter 8 - Conclusions and Future Work.....	212
References	216
Appendix A – Month of July Maximum Power Output Based on the Maximum Hourly Wind Speed Data Occurred from 2005 – 2007 for the Selected Six Wind Farms in Western Kansas Using SCIG Wind Turbine Type Manufactured by Suzlone “S64-1,250 kW”.....	228
Appendix B – The PSS/E Load Flow Data Format and Sample Power System Load Flow Data for the Western Kansas Power System	247
Appendix C - Additional Results of Simulations “Load Modeling Impact on Voltage Stability”	260
C.2 Constant Impedance (Z) Load Modeling Impact on Voltage Stability Using the P-V Curve Method (Area I to Area II Transfer)	262
C.3 Constant Current (I) Load Modeling Impact on Voltage Stability Using the Q-V Curve Method.....	263
C.4 Constant Impedance (Z) Load Modeling Impact on Voltage Stability Using the Q-V Curve Method	264
Appendix D – Additional Modal Analysis Results of Simulation for Wind Integration in the Western Kansas Power System.....	266
D.1 Additional Results of Simulation for Western Kansas Power System Critical Eigenvalues and the “Normalized” Participation Factors for Individual Buses for Wind Injections Using DFIG Wind Turbine Type	267
D.2 Additional Results of Simulation of System Critical Eigenvalue and “Normalized” Participation Factors for the 3-Weak Bus Combination Wind Injections Using DFIG Wind Turbine Type.....	292
D.3 Additional Results of Simulation of System Critical Eigenvalue and “Normalized” Participation Factors for the 3-Strong Bus Combination Wind Injections Using DFIG Wind Turbine Type.....	296
D.4 Additional Results of Simulation of System Critical Eigenvalue and “Normalized” Participation Factors for the 3-Strong Bus Combination Wind Injections Using DFIG Wind Turbine Type and Using SVCs to Increase Wind Penetration	301

D.5 Sample of Additional Results of Simulation of System Critical Eigenvalue and “Normalized” Participation Factors for Individual Bus Wind Injections Using SCIG Wind Turbine Type.....	304
D.6 Additional Results of Simulation of System Critical Eigenvalue and “Normalized” Participation Factors for the 3-Weak Bus Combination Wind Injections Using SCIG Wind Turbine Type.....	314
D.7 Additional Results of Simulation of System Critical Eigenvalue and “Normalized” Participation Factors for the 3-Strong Bus Combination Wind Injections Using SCIG Wind Turbine Type.....	316
D.8 Additional Results of Simulation of System Critical Eigenvalue and “Normalized” Participation Factors for Individual Bus Wind Injections Using DDSG Wind Turbine Type	319
D.9 Additional Results of Simulation of System Critical Eigenvalue and “Normalized” Participation Factors for the 3-Weak Bus Combination Wind Injections Using DDSG Wind Turbine Type.....	333
D.10 Additional Results of Simulation of System Critical Eigenvalue and “Normalized” Participation Factors for the 3-Strong Bus Combination Wind Injections Using DDSG Wind Turbine Type.....	336

List of Figures

Figure 1.1 The 2008 Available Renewable Energy Resources World Wide [4].....	8
Figure 1.2 July 2008 USA Electrical Energy 2030 Generation Mix Output without any Additional Wind and with Additional 20% Wind Resources [21].....	10
Figure 1.3 Kansas Renewable Energy Potential [23]	11
Figure 1.4 The United State Available Wind Resources [23]	12
Figure 1.5 Kansas Wind Resource Map [23]	12
Figure 1.6 Annual Wind Energy Potential on Steady-State Basis for the USA in TWh (A) and as a Ratio with Respect to Retail Sales in Each State (B) [25]	13
Figure 1.7 Southwest Power Pool (SPP) Service Area Map [26].....	14
Figure 1.8 Wind Turbine Power Versus Wind Speed Curve [28]	16
Figure 1.9 Average Daily Available Wind Profile by Season for 3 years (2005 -2007)	17
Figure 1.10 Maximum 3 years' (2005 -2007) Available Wind Power Output as a % of Maximum Wind Farm Rated Power (Maximum Size) at a Wind Injection Bus (Bus 95) for the Month of July	18
Figure 1.11 2010 Kansas Proposed and Existing Large Wind Generation Projects [31]	19
Figure 1.12 Coefficient of Parameter C_p as a Function of λ and for Various Values of Parameter θ [35].....	21
Figure 1.13 Wind Turbine Components [35]	21
Figure 1.14 The Turbine Power and Turbine Speed Versus Wind Speed [36].....	23
Figure 1.15 Pitch Controller Open Loop Controller [32].....	24
Figure 1.16 Wind Turbine Output Fluctuations Caused by Blade Pitching [32]	24
Figure 1.17 “3-Plades” Effect of Blade Tower Shadow [32].....	25
Figure 1.18 Squirrel-Cage Induction Generator (SCIG) Type Grid Connectivity [32].....	26
Figure 1.19 Per-Phase Equivalent Circuit for SCIG [39].....	27
Figure 1.20 Doubly-Fed Induction Generator (DFIG) Type Grid Connectivity [40].....	28
Figure 1.21 Per-Phase Equivalent Circuit for DFIG [40]	29
Figure 1.22 Direct-Drive Synchronous Generator (DDSG) Type Grid Connectivity [39].....	31
Figure 1.23 Per-Phase Equivalent Circuit for DDSG [39].....	31
Figure 1.24 Self Commutated Voltage Source Inverter [39]	33

Figure 1.25 Self-Commutated Current Source Inverter [39].....	33
Figure 2.1 Typical Scenario of Voltage Collapse.....	45
Figure 2.2 Voltage Stability Time Response [84]	46
Figure 2.3 P-V Curve Method	47
Figure 2.4 Single Phase Equivalent of Three Phase Power System	48
Figure 2.5 Q-V Curve Method.....	49
Figure 2.6 P-Q Curve Method	51
Figure 2.7 Component Approach Load Model.....	56
Figure 2.8 Western Kansas Power System (Areas I & II).....	59
Figure 2.9 P-V Curves for Constant Power (P) Load Type in the Western Kansas Power System (Area I to Area II Transfer).....	62
Figure 2.10 Maximum Power Transfer from Area I to Area II in the Western Kansas Power System Using Constant Current (I) & Constant Impedance (Z) Load Types as a Percent of the Constant Power (P) Load Type	64
Figure 2.11 Curves for Voltage Stability Margins Using Q-V Curve Method for Constant Power (P) Load Type Applied to the Western Kansas Power System (Area I)	65
Figure 2.12 <i>VSMs</i> Obtained Using Constant Current (I) & Constant Impedance (Z) Load Types as a Percent of <i>VSMs</i> Obtained Using Constant Power (P) Load Type in Area I of the Western Kansas Power System.....	66
Figure 2.13 Stability Boundary Calculated in P-Q Curve Method for Constant Power (P) Load Type Applied to the Western Kansas Power System (Area I).....	69
Figure 2.14 Illustration of the Use of the P-Q Stability Curve Method in Calculating Load Mix Sensitivity Index “ S_i ”	72
Figure 2.15 Equivalent (ZIP) Load Bus Model.....	74
Figure 2.16 Maximum Voltage Stability Buffer Calculation Process for Uncertainties in Load Type Models	76
Figure 2.17 Stability Margins for the Three Different Load Models	80
Figure 3.1 Wind Farm Collector System Network.....	86
Figure 3.2 Flow Chart for Active (P) and Reactive (Q) Power Model for a Wind Farm	87
Figure 3.3 Stability Boundaries for Increasing Wind Injection at Bus 105 Using SCIG Wind Turbine Type for the Western Kansas Power System (Area I) - P-Q Curve Method.....	97

Figure 3.4 Stability Boundary Limits in MVA for Increasing Wind Injection at Bus 105 Using SCIG Wind Turbine Type for the Western Kansas Power System (Area I) - P-Q Curve Method Results.....	97
Figure 3.5 Wind Injection Impact on Stability Boundaries Using DFIG Wind Turbine Type for the Western Kansas Power System (Area I) – P-Q Curve Method Results	98
Figure 3.6 Stability Boundary Limits for Increasing Wind Injection at Bus 105 Using DFIG Wind Turbine Type for the Western Kansas Power System (Area I) - P-Q Curve Method Results.....	98
Figure 3.7 Wind Injection Impact on Stability Boundaries Using DDSG Wind Turbine Type for the Western Kansas Power System (Area I) – P-Q Curve Method Results	99
Figure 3.8 Stability Boundary Limits for Increasing Wind Injection at Bus 105 Using DDSG Wind Turbine Type for the Western Kansas Power System (Area I) - P-Q Curve Method Results.....	99
Figure 4.1 Sizing Wind Farms Using Method I – Simultaneous Increase of Wind Farms’ Power Outputs.....	107
Figure 4.2 Sizing Wind Farms Using Method II - Wind Farm Power Output Increases Based on their <i>VSM</i> Impacts	110
Figure 4.3 “2010” July Peak MW Load for the Western Kansas Power System (Area I).....	113
Figure 4.4 Lowest Hourly <i>VSMs</i> in Mvar for July 2010 (Month of July).....	114
Figure 5.1 Q-V Curve Stability Regions per Criteria	122
Figure 5.2 Flow Chart for Calculating <i>EVSMs</i> and the Number of Expected Curtailment Hours	127
Figure 5.3 Western Kansas Maximum Hourly Peak Load for the Month of July 2010	129
Figure 5.4 Impact of Increasing Wind Farm Sizes on Western Kansas System <i>EVSMs</i> for Each of the Heavy Loading Hours for the Month of July 2010.....	134
Figure 5.5 Number of Wind Farm Operating Hours as a Percent of the Total “744” July Hours for the Selected Heavy Loading Hours at Bus 105 in Western Kansas	137
Figure 5.6 Number of Expected Curtailment Hours for Each Maximum Wind Farm Size Case for the Heavy Loading Hours in the Month of July.....	137
Figure 6.1 Systematic Voltage Stability Procedure for Assessing Weak Power Systems with High Wind Penetration Using Modal Analysis and the Q-V Voltage Stability Method.....	145

Figure 6.2 Process for Calculating Maximum Wind Injection Using Modal Analysis	149
Figure 6.3 Locating New SVCs for Increasing Wind Penetration	150
Figure 6.4 Participation Factors for Mode of Instability without Any Wind Injection	153
Figure 6.5 Impact on System Eigenvalues for Increasing Wind Injections From Each of the Weak Buses Individually Using SCIG Wind Turbine Type.....	156
Figure 6.6 Impact on System Eigenvalues for Increasing Wind Injections From Each of the Strong Buses Individually Using SCIG Wind Turbine Type	156
Figure 6.7 Normalized Bus Participation Factor to the Most Critical Mode of Voltage Instability for the Combined Weak Bus Wind Injection of 90 MW Using SCIG Wind Turbine Type	159
Figure 6.8 Normalized Bus Participation Factor to the Most Critical Mode of Voltage Instability for the Combined Strong Bus Wind Injection of 180 MW Using SCIG Wind Turbine Type	159
Figure 6.9 The Impact on Eigenvalues of Increasing Wind Injection from Each of the Weak Buses Using DFIG Wind Turbine Type	161
Figure 6.10 The Impact on Eigenvalues of Increasing Wind Injection from Each of the Strong Buses Using DFIG Wind Turbine Type	162
Figure 6.11 The Impact on the “Q-V” Voltage Stability Margins (<i>VSMs</i>) of Increasing Wind Injections Using DFIG Wind Turbine Type	164
Figure 6.12 Impact on System Eigenvalues of Increasing Wind Injections from the Combined Strong and the Weak Buses Using Modal Analysis for DFIG	166
Figure 6.13 The Impact of Increasing Wind Injection from the Combined Weak and Strong Buses on Voltage Stability Margins (<i>VSMs</i>) Using the Q-V Curve Method for DFIG	167
Figure 6.14 Impact on System Eigenvalues for Increasing Wind Injections from.....	169
Figure 6.15 Impact on System Eigenvalues for Increasing Wind Injections from Each	169
Figure 6.16 Combined Weak Buses Wind Injection of 150 MW on System Bus Normalized Participation Factors Using DDSG Wind Turbine Type.....	171
Figure 6.17 Combined Strong Buses Wind Injection of 350 MW on System Bus Normalized Participation Factors Using DDSG Wind Turbine Type.....	172
Figure 6.18 SVCs Connected to an Equivalent Wind Farm for Voltage Support [115].....	175
Figure 6.19 Using Option II for SVC Placement s for Reaching 410 MW of Total Wind Injection Using SCIG Wind Type Turbines.....	179

Figure 6.20 Normalized Participation Factors for Combined Strong Bus Wind Injection of 330 MW	182
Figure 6.21 Normalized Participation Factors for Combined Strong Bus Wind Injection of 360 MW	182
Figure 6.22 Normalized Participation Factors for Combined Strong Bus Wind Injection of 390 MW	183
Figure 6.23 Comparison of the Amount of the Reactive Power Installed (SVCs) Using the Two SVC Placement Options for Reaching 410 MW of Total Wind Injection Using DFIG Wind Type Turbines	184
Figure 6.24 Comparison of the Amount of the Reactive Power Installed (SVCs) Using the Two SVC Placement Options for Reaching 410 MW of Total Wind Injection Using DDSG Wind Type Turbines	186
Figure 6.25 Comparison of the Required Number and Size of SVCs for Each Type of Wind Turbine Using Option II for Reaching a Total Combined Bus Wind Injection of 410 MW	188
Figure 7.1 Combined Wind Power Output for the 3-Weak Bus Combined Using Different Methods	210
Figure 7.2 Combined Wind Power Output for the 3-Strong Bus Combined Using Different Methods	210

List of Tables

Table 1.1 Comparison of the Maximum Wind Generation Levels Installed for the Top 10 Countries in Wind Generation [21]	9
Table 2.1 Load Types α and β Constants [47] and [55]	54
Table 2.2 Typical Load Composition for the Component Load Model [52] and [58]	56
Table 2.3 Load Mixes Multiplying Factors	57
Table 2.4 Classifications of Power System Loads [52, 53]	57
Table 2.5 Maximum Power Transfer Calculated Using the P-V Curve Method for Constant Power (P) Load Type Applied to the Western Kansas Power System (Area I to Area II Transfer)	61
Table 2.6 Comparison of P-V Curves Based on Maximum Power Transfer for Voltage Sensitive Loads (ZIP) in the Western Kansas Power System (Area I)	63
Table 2.7 Voltage Stability Margins (VSMs) Obtained Using Q-V Curve Method for Constant Power (P) Load Type Applied to the Western Kansas Power System (Area I)	64
Table 2.8 Comparison of Q-V Curves Based on Maximum Power Transfer for Voltage Sensitive Loads (ZIP) in the Western Kansas Power System (Area I)	66
Table 2.9 P-Q Curve Method Applied to the Western Kansas Power System (Area I) Assuming Constant Power (P) Load (Opening the Branch between Bus 83 and Bus 128)	68
Table 2.10 P-Q Curve Method for Constant Current (I) & Constant Impedance (Z) Load Types Applied to the Western Kansas Power System	70
Table 2.11 Stability Margins for the Three Constant Load Models in Western Kansas	70
Table 2.12 Load Class k -Factors Multiplier for Converting Load Classes to a ZIP Load Model	75
Table 2.13 Load Types for the Summer Peak in Western Kansas Power System	77
Table 2.14 Constant ZIP Model as a % of the Western Kansas Total Summer 2010 System Peak Load ($S_{Total} = 557.59$ MVA)	78
Table 2.15 Stability Limits for Constant Power (P), Constant Impedance (Z) and The ZIP Mixed Load Model Applied to the Western Kansas Power System Using The P-Q Curve Method	79
Table 2.16 Variances of Stability Boundary Limits between Constant Power (P) and ZIP Load Models for Determining Appropriate VSM Buffer	80

Table 2.17 Load Type Impact on Sensitivity Index " S_i " for the Range of Load Power Factors Considered	81
Table 2.18 Stability Boundary Buffer Calculations for Western Kansas (Area I) Power System	82
Table 3.1 Summary of Steady-State Models of SCIG, DFIG and DDSS Wind Turbine Generators	89
Table 3.2 Stability Limits on Maximum Wind Injection from Bus 105	90
Table 3.3 Wind Injection Impact on Stability Boundaries Using SCIG Wind Turbine Type for the Western Kansas Power System (Area I) – P-Q Curve Method Results	91
Table 3.4 Wind Injection Impact on Stability Boundaries Using DFIG Wind Turbine Type for the Western Kansas Power System (Area I) – P-Q Curve Method Results	92
Table 3.5 Wind Injection Impact on Stability Boundaries Using DDSG Wind Turbine Type for the Western Kansas Power System (Area I) – P-Q Curve Method Results	94
Table 4.1 Load Types and Load Characteristics for the July 2010 (Daily Hours 1 through 15 and Daily Hours 21 Through 24).....	111
Table 4.2 Load Types and Load Characteristics for July 2010 (Daily Hours 16 Through 20)...	112
Table 4.3 July 2010 Peak Load in MW and the Hourly <i>VSMs</i> in Mvars before Wind Injections	113
Table 4.4 Maximum Wind Penetration in MW for Each Daily Hour During the Summer 2010 for Three Wind Turbine Types Using Method I (Simultaneously Increasing All Wind Injection Sites Until Reaching the Collapse Point).....	115
Table 4.5 Maximum Hourly Wind Penetration Using Method II.....	116
Table 4.6 Iterative Steps for Calculating Maximum Wind Farm Sizes for the SCIG, DFIG and DDSG Wind Turbine Types Using Method II for Daily Hour “4 pm – 5 pm” for the Contingency of Losing the 115 kV Transmission Line from Bus 83 to Bus 128.....	117
Table 5.1 Maximum Wind Injections in MW from the Wind Farm Site Using DFIG Wind Turbine Type before Reaching the Collapse Point Using the Q-V Curve Method	130
Table 5.2 <i>EVSM</i> Calculations for 150 MW Wind Farm in Western Kansas for Daily Hour 17 in the Month of July 2010.....	132
Table 5.3 Expected Wind Farm Power Outputs and their Probabilities as a % of the Maximum DFIG’s Size at the Wind Farm Site for Daily Hour 17 (4 pm – 5 pm) for the Month of July 2010	133

Table 5.4 Wind Farm Power Output Curtailment Limits for Voltage Stability	135
Table 5.5 Summary of the Impact of Increasing Wind Farm Size on System <i>EVSMs</i> and Expected Curtailment Hours for the Heavy Loading Hours in the Month of July 2010.....	136
Table 5.6 Expected Voltage Stability Index L_i for Changes in the Wind Farm Maximum Size During the Heavy Loading Hours	138
Table 6.1 Ranking & Classification of the Proposed Wind Injection Buses before Wind Injection Using Modal Analysis	153
Table 6.2 Maximum Wind Injected Separately From Each Individual Bus before Reaching the Collapse Point Using SCIG Wind Turbine Type.....	155
Table 6.3 Impact of Gradual Increases of Wind Penetration from Each Individual Bus on System Eigenvalues and Bus Normalized Participation Factors Using SCIG Wind Turbine Type	157
Table 6.4 Maximum Wind Injection from Each Individual Bus in MW Using DFIG Wind Turbine Type Before Reaching the Voltage Collapse Point.....	161
Table 6.5 Bus Participation Factors for all Six Buses as Wind Injection Gradually Increased from Each Bus Individually Using DFIG Wind Turbine Type.....	163
Table 6.6 Maximum Wind Injections in MW for Case III with DFIG.....	165
Table 6.7 Maximum Wind Injected Separately from Each Individual Bus Before.....	168
Table 6.8 Impact of Gradual Increases of Wind Penetration from Each Individual Bus on System Eigenvalues and Bus Normalized Participation Factors Using DDSG Wind Turbine Type	170
Table 6.9 Comparison of Maximum Wind Penetration Using the Weak Buses for Each Wind Turbine Type.....	174
Table 6.10 Comparison of Maximum Wind Penetration Using the Strong Buses for Each Wind Turbine Type.....	174
Table 6.11 Placement of SVCs to Increase Wind Penetration from Strong Buses Using SCIG Wind Turbine Type Using Option I	177
Table 6.12 Placement of SVCs to Increase Wind Penetration from Strong Buses Using SCIG Wind Turbine Type Using Option II.....	178
Table 6.13 Locating SVCs to Increase Wind Penetration for DFIG Wind Turbine Type Using Option I.....	180

Table 6.14 Locating new SVCs to Increase Wind Penetration for DFIG Wind Turbine Type Using Option II	181
Table 6.15 Placement of SVCs to Increase Wind Penetration from Strong Buses Using DDSG Wind Turbine Type Using Option I	185
Table 6.16 Placement of SVCs to Increase Wind Penetration from Strong Buses Using DDSG Wind Turbine Type Using Option II.....	186
Table 6.17 Maximum Size for the 3-Strong Bus Based on Load-Type for DFIG - Constant Power (P) Versus Exact (ZIP) Load Mix	189
Table 6.18 Sensitivity Index “ S_i ” for Different Load Power Factors for the 3-Strong Bus Combination with DFIG at the Maximum Wind Sizes of the Constant P Model.....	190
Table 6.19 Load-Type Voltage Stability Buffer for the 3-Strong Bus Combination with DFIG	191
Table 6.20 Load-Type Voltage Stability Buffer for the 3-Weak Bus Combination for Different Type of Turbines	192
Table 6.21 Load-Type Voltage Stability Buffer for the 3-Strong Bus Combination for Different Type of Turbines	192
Table 7.1 Iterative Steps for Calculating Maximum Wind Injections for the 3-Weak Bus Combination Using the “Q-V” Method (Method II).....	196
Table 7.2 Iterative Steps for Calculating Maximum Wind Injections for the 3-Strong Bus Combination Using the “Q-V” Method (Method II).....	198
Table 7.3 Iterative Steps for Calculating Maximum Wind Injections for the 3-Weak Bus Combination Using the “Bus Participation Factor” Method (Method III).....	202
Table 7.4 Iterative Steps for Calculating Maximum Wind Injections for the 3-Strong Bus Combination Using the “Bus Participation Factor” Method (Method III).....	205
Table 7.5 Summary of the Maximum Amount of Wind Injection from the 3-Weak and the 3- Strong Buses Obtained from Each Sizing Method.....	209
Table 7.6 Summary of the Maximum Amount of Wind Injection from each of the 3-Weak and the 3-Strong Buses Obtained from Each Sizing Method.....	211

Dedication

I dedicate this dissertation to my family, mom and dad.

Chapter 1 - Introduction

Large amounts of wind power can stress power systems that are under heavily loaded conditions. This is due to the fact that wind power integration usually takes place in high wind speed areas of power systems, which are usually located in areas with weak transmission lines and are located far from load centers. As more wind penetrates such power systems, one of the major problems associated with such high wind penetration will be voltage collapse or instability. The motivations, objectives, and contribution of this dissertation are focused on developing new voltage stability methods that can be applied to maximize wind penetration levels in weak power systems so that high wind penetration can be integrated into the system with an adequate voltage stability margin that will prevent voltage collapse.

1.1 Motivation

Maximum wind integration in power systems largely depends on the number and size of wind injection sites, type of wind turbine used, and the reactive power strength of the system. Voltage stability and its dependency on the systems available reactive power can be an effective mean for increasing wind penetration in power systems. The current procedures used in the utility industry do not incorporate the available reactive power when sizing new wind farms. This has a negative impact when trying to achieve the maximum wind penetration levels. In weak power systems, where wind generation is placed in locations far from the load centers, excessive amounts of voltage support equipment are needed to achieve high levels of wind penetration.

The research presented herein has been conducted in pursuit of the objective that has direct impact on maximizing the amount of wind penetration in weak power systems. For this purpose, systematic procedures using voltage stability methods for sizing new wind farms to maximize wind penetration in weak power systems are developed and applied to a weak power system in the state of Kansas (the western Kansas power system). These procedures and methods can be used to maximize wind penetration in any weak power system where wind generation is located far from load centers. Since the maximum size of a wind farm directly impacts the amount of wind penetration level in power systems, the procedures and methods developed can be used for maximizing wind penetration levels by increasing the size of wind farms based on

their impact on system voltage stability achieved by optimizing the use of system available reactive power resources. The new methods for sizing new wind farms increases the size of the wind farms which have low impact on system voltage stability for their size increases. Wind farms with size increases that require large amounts of the available system reactive power are sized smaller than other wind farms that require less reactive power for a size increase. Applying the developed procedures and methods can result in an effective combination of wind farms maximum power outputs using the least amount of the available reactive power resources.

1.2 Objectives

The objectives of this dissertation are summarized below.

The first objective is to develop a voltage stability method to use in calculating the maximum wind farm penetration before reaching the voltage collapse. The P-Q method is developed for this purpose.

The second objective is to develop a new method for calculating a voltage stability buffer to reduce uncertainties when calculating the voltage collapse point. Composite load mix is developed and used for calculating the voltage stability buffer at any wind penetration level.

The third objective of this research is to determine the optimal wind farm sizes in weak power systems using the available system's reactive power. Four methods are developed to determine the maximum wind farm sizes needed to optimize the use of available reactive power for increasing wind farm sizes. Three of these methods determine maximum wind farm sizes without requiring any wind curtailments related to voltage instability. One method uses the expected voltage stability margin concept and special protection schemes for wind curtailments to prevent voltage instability.

The fourth objective is to develop methods for sizing and locating voltage support equipment to further increase wind farm sizes above the maximum sizes found using the previous four methods. For each increase of wind farm sizes, Static Var Compensators (SVCs) are placed in the power system at locations where the reactive power output of the placed SVCs have the most positive impact on voltage stability. SVCs are placed at buses with high contribution to modes of instability using participation factors calculated using modal voltage analysis.

The fifth objective is to investigate how the new procedures and methods developed for maximizing wind farm sizes can be applied to a weak power system. The western Kansas power system is used to study and test the new procedures and methods mentioned above.

1.3 Contributions

Advances made on the above five objectives represent the eight contributions of this dissertation to the overall body of knowledge.

- 1. Derived the P-Q voltage stability method for voltage stability analysis of power systems with high wind penetration.** The P-Q voltage stability method given in [1] was expanded to include calculation of voltage stability boundaries for power systems with large changes of real and reactive power caused by the wind power output fluctuations.
- 2. Applied the P-Q voltage stability method to a power system with load-type model sensitivities (constant power, constant current and constant impedance).** The P-Q voltage stability method derived in [1] was expanded to incorporate composite load-type models in calculating voltage stability boundaries and in determining suitable voltage stability boundary load buffers. A voltage stability sensitivity index (S_i) was introduced to provide a measure to system voltage stability sensitivity to load-type changes.
- 3. Developed and applied iterative methods for maximizing wind penetration levels based on voltage stability margins.** These iterative methods can effectively increase wind farm sizes to maximize wind penetration using existing system reactive power margins.
- 4. Developed the expected voltage stability margin index (L_i) which incorporates both the probability of wind farms power output and their corresponding voltage stability margins.** The new index provides a voltage stability stiffness measure which can be used to determine the best areas in the power system for wind power injections.
- 5. Developed and applied a systematic procedure to assess the impact of increasing wind farm sizes above their maximum limits found in contributions (3) and (4).** This method uses system expected voltage stability margins and special protection schemes for wind curtailments to prevent voltage instability for the increase of wind farm sizes above their maximum limits. The new method quantifies voltage stability risk of increasing wind farm sizes above the voltage stable limits by calculating the number of

wind curtailment hours. The new method eliminates the need for calculating *VSMs* for all of the operating hours of a wind farm. Only the hours with potential voltage collapse are analyzed for possible voltage stability problems

- 6. Developed the essential components of a systematic modal voltage stability method for increasing wind penetration in power systems.** The developed modal method can be used to increase wind farm sizes based on the wind injection site contribution to modes of voltage instability. Wind farms with high contribution to modes of instability are sized smaller than the ones with low contribution to instability modes.
- 7. Developed and applied a procedure using the voltage instability modes and voltage support equipment like SVCs for maximizing wind penetration.** Maximum wind farm sizes obtained in contributions (3) and (4) can be increased by placing dynamic voltage support equipment like static var compensators (SVCs) at locations within the power system where high participation in modes of instability is observed.
- 8. Developed and applied iterative wind farm sizing method based on system eigenvalues and bus participation factors to voltage instability modes.** This iterative method can effectively increase wind farm sizes to maximize wind penetration using existing reactive power margins.

1.4 Publications of this Dissertation

All publications associated with this research were submitted to the Institute of Electrical & Electronics Engineers (IEEE). The first IEEE published paper with a title of “Maximizing Wind Penetration Using Voltage Stability Based Methods for Sizing and Locating New Wind Farms in Power System” introduced two voltage stability based iterative methods for maximizing wind farm sizes in weak power systems[2]. A second accepted IEEE publication with a title of “Method for Assessing System Impact of Increasing Wind Farm Sizes Above Their Maximum Limits” introduced a new method which calculates the risk of increasing wind farm sizes above the secured voltage stable limits using the probabilistic nature of wind in addition to voltage stability margins for planning studies [3]. A third pending IEEE publication with a title of “Effective Wind Farm Sizing Method in Weak Power Systems Using Critical Modes of Voltage Instability” illustrates that voltage stability modal analysis can be used to pre-determine buses that have the most contribution to voltage instability for any wind penetration

level. All of the methods developed in these publications were applied to the western Kansas power system and are included in this dissertation.

1.5 Organization of Dissertation

This dissertation consists of eight chapters. Chapter 1 is an introduction which explains the motivation, the objectives, and the contributions of theory development for voltage stability based methods used in sizing wind farms to maximize wind penetration levels in weak power systems. The chapter gives an overview of wind power integration in power systems starting with an overview of renewable energy resources and wind power potential in the state of Kansas. Challenges to high wind generation integration into power systems are discussed. A brief introduction to wind generator types and their characteristics are included in this chapter. Introduction to the Squirrel-Cage Induction Generator (SCIG), Doubly-Fed Induction Generator (DFIG) and the Direct-Drive Synchronous Generator (DDSG) are presented and their one-line (single-phase equivalent) circuit representation in steady-state are shown. Topics in this dissertation are based on several high quality references that are summarized in this chapter under literature survey.

The second chapter introduces steady-state voltage stability methods and power system load models. Definition of voltage instability and voltage collapse is provided followed by derivations of three steady-state voltage stability methods used to calculate voltage stability limits in power systems. The P-V, Q-V and P-Q curve methods are derived and applied to western Kansas power system. Load models are incorporated in the P-Q curve method calculations and used to calculate suitable voltage stability boundary buffers based on load composite variations.

Wind generators modeling for power system steady-state stability are detailed in Chapter 3. Detail analysis of SCIG, DFIG and DDSG are presented and their representation in the steady-state voltage stability power flow analysis is investigated. Maximum wind penetration in the western Kansas power system using the three wind generation types was calculated and compared.

Chapter 4 includes the development and application of two voltage stability based iterative methods for maximizing wind penetration levels in power systems. The first method is based on uniform increase in wind farm sizes until reaching the collapse point. The second

method is based on increasing wind farm sizes in steps. For each step a wind farm size is increased, voltage stability margins are monitored. Wind farms, which have a low impact on system *VSM*, are sized larger than the others. Both methods are applied to western Kansas power system and results of maximum wind penetration using both methods are compared.

A new method for assessing the impact of increasing wind farm sizes above their maximum limit is developed and applied to a wind farm in western Kansas in Chapter 5. The expected voltage stability margin method is expanded to include both wind nature and their probabilities in calculating the probability of reaching voltage collapse for additional increases in wind generation above the maximum limits obtained using the methods in Chapter 4. The new method shows that the risk of increasing wind farm sizes above the voltage stable limits can be assessed and an expected number of wind curtailment hours are calculated for each wind level increase.

Chapter 6 includes the development of essential components of the modal voltage stability procedure for assessing systems with high wind penetration. The developed modal voltage stability method for wind farm size increases is based on each wind injection site contribution to modes of instability. The new method provides for the identification of system weaknesses for each wind penetration level which is used to increase wind farm sizes. The new methods incorporate modal analysis as well as the traditional voltage stability methods (Q-V curve) in sizing and placing new wind farms. To further increase wind farm sizes, modal analysis is used to determine the location and amount of Static Var Compensators (SVCs) need to be added to the power system to reach a desired wind penetration level.

Chapter 7 includes the development of iterative wind sizing method using modes of voltage instability to further increase wind penetration. A new modal sizing methods is developed and implemented using the western Kansas power system. The method is based on a step increase of wind injections while monitoring system eigenvalues and bus participation factors in modes of voltage instability. Results of applying all of the wind farm-sizing methods are presented and compared. A wind farm sizing method is recommended for use in weak power systems for maximizing wind penetration levels.

Chapter 8 incorporates both conclusions and future work. Voltage stability based methods have proved to be very effective in increasing wind penetration level in weak power systems. Increasing wind penetration in weak power system requires optimization of the existing

power system voltage stability margins. Results of the iterative voltage stability methods developed in this dissertation indicated that incorporating voltage stability margins in sizing new wind farms increases wind penetration in the weak power systems. A further increase in wind penetration levels using voltage stability modal analysis was also analyzed. The ability to identify best locations for wind injections and voltage support equipment using modal analysis resulted in higher wind penetration level when compared to any other voltage stability sizing methods. For future work, the use of the methods developed in this dissertation can be expanded on in future research for maximizing wind penetration in areas with low wind resources. With wind power mainly available in areas far from the load centers, wind penetration can be maximized using similar voltage stability based methods which maximizes the power transfer from areas with high wind resources to areas with low wind resources. The voltage stability methods developed in this dissertation can be modified to incorporate additional steps which makes them useful for calculating maximum wind farm sizes in strong power systems where the lowest voltage stability margins may not happen when maximum wind power output occurs simultaneously with maximum peak loading conditions.

1.6 Overview of Renewable Energy Resources and Wind Integration in Power Systems

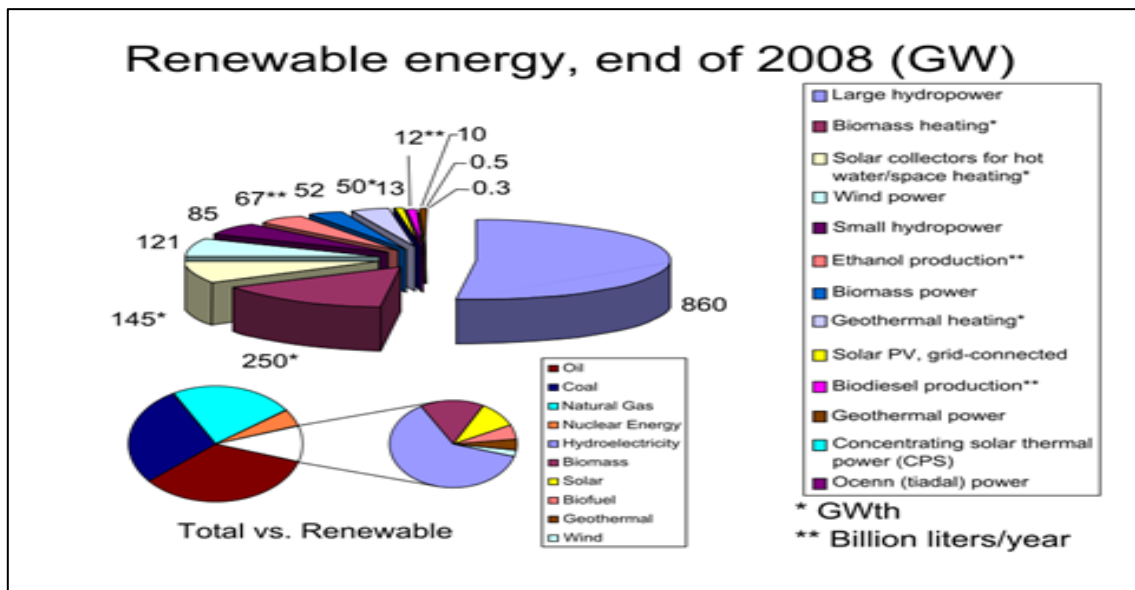
Renewable energy is energy which is generated from natural resources such as sunlight, wind, rain, tides, and geothermal heat, that are renewable [4]. In 2008, about 19% of global energy consumption was generated from renewables, with 13% generated from traditional biomass, which is mainly used for heating, and 3.2% from hydroelectricity as shown in Figure 1.1 [4]. New renewables (small hydro, modern biomass, wind, solar, geothermal, and biofuels) accounted for another 2.7% and are growing very rapidly [4]. The share of renewables in electricity generation is around 18%, with 15% of global electricity coming from hydroelectricity and 3% from new renewables [4, 5].

Renewable power generated from wind resources is growing at the rate of 30% annually, with a worldwide installed capacity of 158 gigawatts (GW) in 2009, and is widely used in Europe, Asia, and the United States (USA) [6, 7]. At the end of 2009, cumulative global photovoltaic (PV) installations surpassed 21 GW with most of the PV power stations located in Germany and Spain [8 – 11]. Solar thermal power stations operate in the USA and Spain, and the

largest of these is the 354 megawatt (MW) SEGS power plant in the Mojave Desert in the USA [12]. The world's largest geothermal power installation is The Geysers in California, with a rated capacity of 750 MW. Brazil has one of the largest renewable energy programs in the world, involving production of ethanol fuel from sugar cane, and ethanol now provides 18% of the country's automotive fuel [13]. Ethanol fuel is also widely available in the USA.

Climate change concerns, coupled with high oil prices, peak oil, and increasing government support, are driving more renewable energy legislation, incentives and commercialization [14]. New government spending, regulation and policies helped the industry weather the global financial crisis better than many other sectors [15, 16, 17].

Figure 1.1 The 2008 Available Renewable Energy Resources World Wide [4]



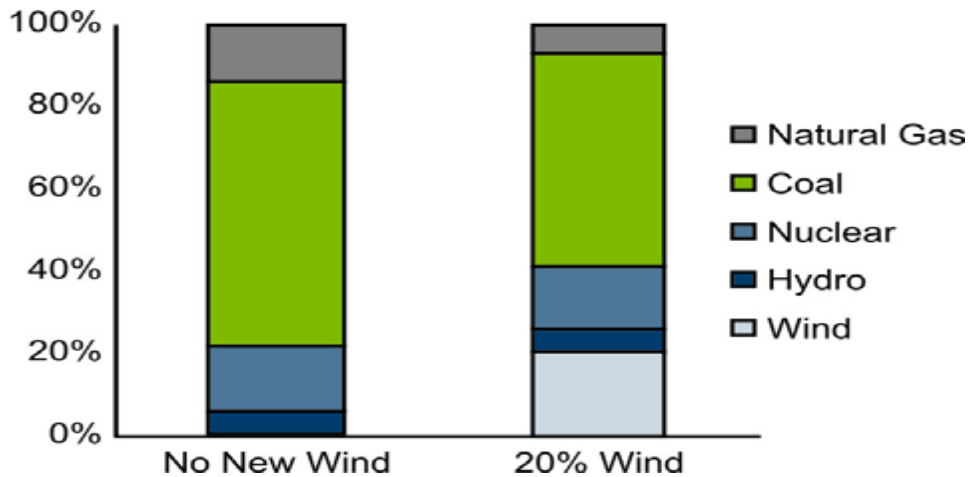
Global wind power installations increased by 35,800 MW in 2010, bringing the total installed capacity up to 194,400 MW, a 22.5% increase over the 158,700 MW installed at the end of 2009. For the first time, more than half of all new wind power was added outside of the traditional markets of Europe and North America. This was mainly driven by the continuing boom in China which accounted for nearly half of all of the installations at 16,500 MW. China now has 42,300 MW of wind power installed [18 – 20]. Wind power accounts for approximately 19% of electricity generated in Denmark, 9% in Spain and Portugal, and 6% in Germany and the Republic of Ireland [21].

Table 1.1 Comparison of the Maximum Wind Generation Levels Installed for the Top 10 Countries in Wind Generation [21]

Country	Total Capacity in MW	
	2009	2010
United States	35,159	36,300
China	26,010	33,800
Germany	25,777	26,400
Spain	19,149	19,500
India	10,925	12,100
Italy	4,850	5,300
France	4,521	5,000
United Kingdom	4,092	4,600
Portugal	3,535	3,800
Denmark	3,497	3,700
Rest of world	21,698	24,500
Total	159,213	175,000

In response to the climate change crises, the USA government is committed to support renewable development for the next ten years [21]. A goal of 20% of total generation mix made up of renewables by 2020 has been set as a target for many states in the USA. The U.S. Energy Information Administration (EIA) estimates that electricity demand in the USA will grow by 39% from 2005 to 2030, reaching 5.8 billion MWh by 2030. The USA electrical energy mix output for 2008 and the forecasted 2030-generation mix as of July 2008 is shown in Figure 1.2. The figure shows that in 2030 without new wind resources, coal will have approximately 60% of the total energy mix. However, it is expected that by 2030, 20% of the USA electrical energy mix will be composed of wind energy while the coal energy mix is expected to decrease by 15% of the total generation mix.

Figure 1.2 July 2008 USA Electrical Energy 2030 Generation Mix Output without any Additional Wind and with Additional 20% Wind Resources [21]



The electricity network (electric grid) plays a significant role in facilitating integration of large amounts of renewables in the USA. Companies in the USA have already identified approximately 37 billion U.S. Dollars in transmission investment needed by 2020 to facilitate integration of renewables [21]. The ability to accommodate the near-maximum simultaneous renewable power outputs of all generators has driven most of the projected investment in the transmission system. High levels of renewable generation may result in stressing power system equipment since the transmission system capacity has to be shared by conventional and renewable generation. Therefore, major transmission system reinforcement may be required to integrate large amounts of renewable energy in the USA [21].

The large increase in renewable energy resources may cause some adverse impact on the existing power systems due to the nature of renewable resources. Power quality may suffer from large amounts of renewable resources penetration [22]. Renewable power output fluctuations may cause voltage rise and fluctuations that have a direct impact on power system voltage profiles. These fluctuations can lead to frequent operation of power system transformer's load tap changers (LTCs) and voltage controlled capacitor banks. More frequent operation of LTCs and voltage control equipment may shorten the expected life cycle of these devices and increase maintenance requirements. If the penetration level of the renewables is large, voltage fluctuations may affect sub-transmission (below 69 kV) and transmission system (above 100 kV) voltages and may impact power quality for customers far from the renewable resource sites.

1.6.1 Wind Resources Potential in Kansas

Renewable energy resources in the state of Kansas consist of mainly wind and geothermal resources. Development of wind energy resources in the state of Kansas has accelerated due to the abundance of wind resources, which bring excellent return on the investments when compared to other renewable resources in the state. A Kansas renewable energy potential map is shown in Figures 1.3 [23]. The state of Kansas' available wind resources, where the yearly average wind speed is classified as excellent "class 4", are shown in Figures 1.4 [23] and Figure 1.5 [24]. The wind resources are located in the southwest and northwest portions of the state as shown in Figure 1.5. The state of Kansas is ranked third in the USA in available wind resources as shown in Figure 1.6. The potential wind generation resources for Kansas exceeds its current total electricity retail load by a factor of 110 [25].

Figure 1.3 Kansas Renewable Energy Potential [23]

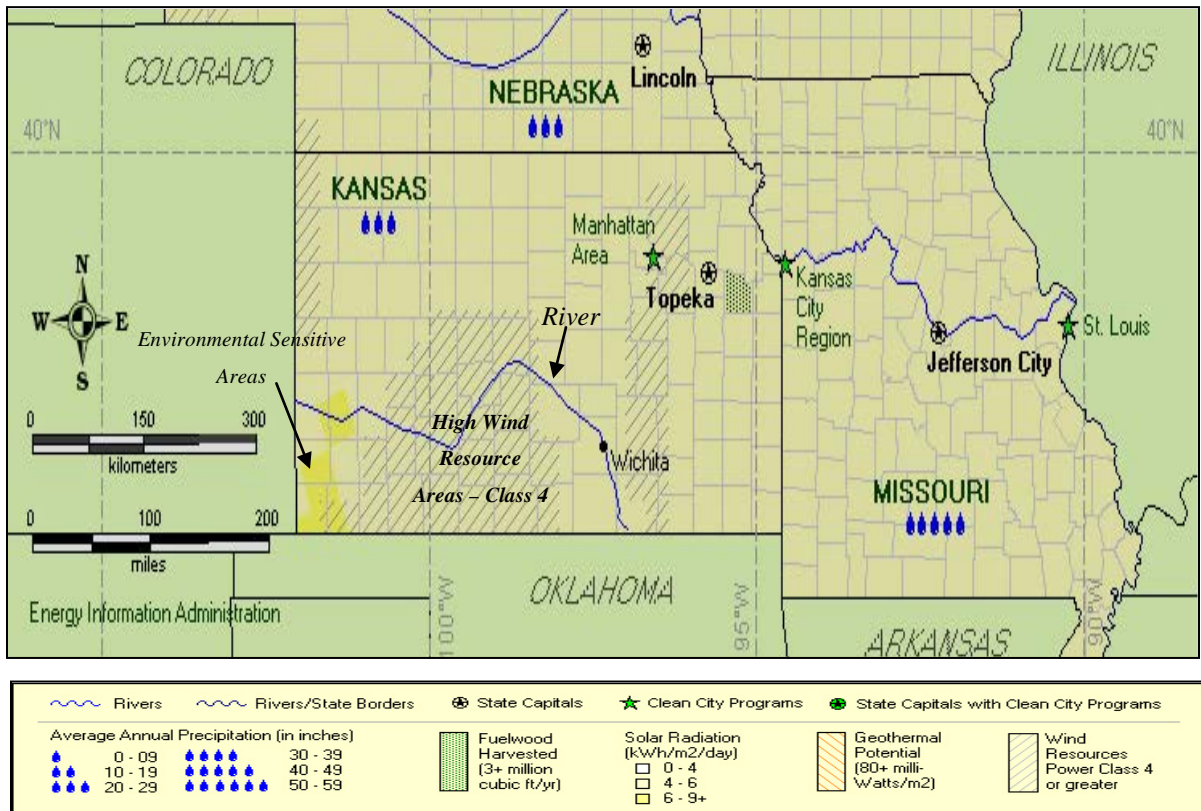


Figure 1.4 The United State Available Wind Resources [23]

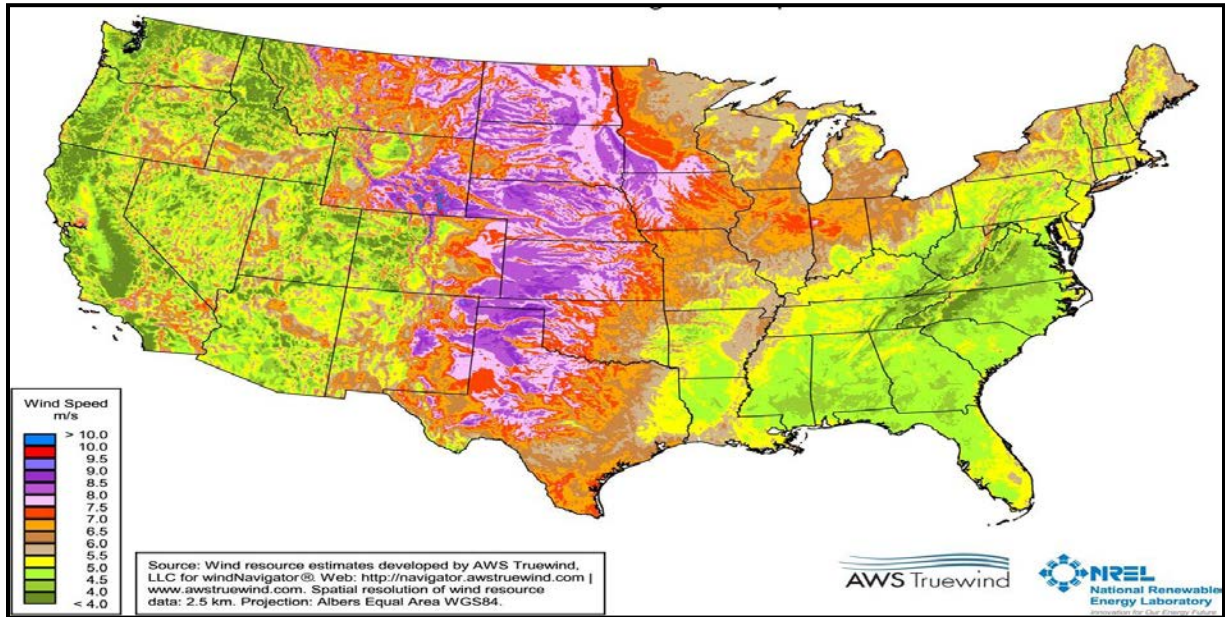
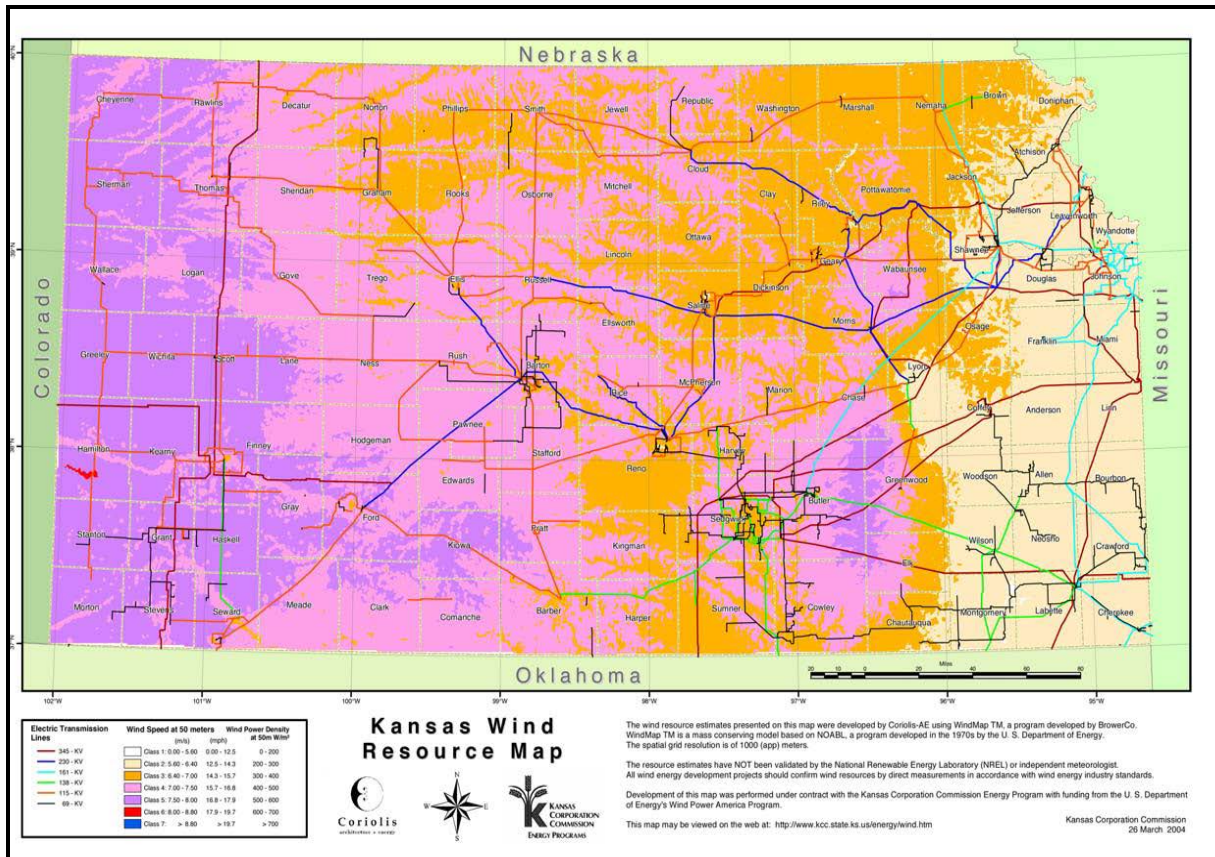
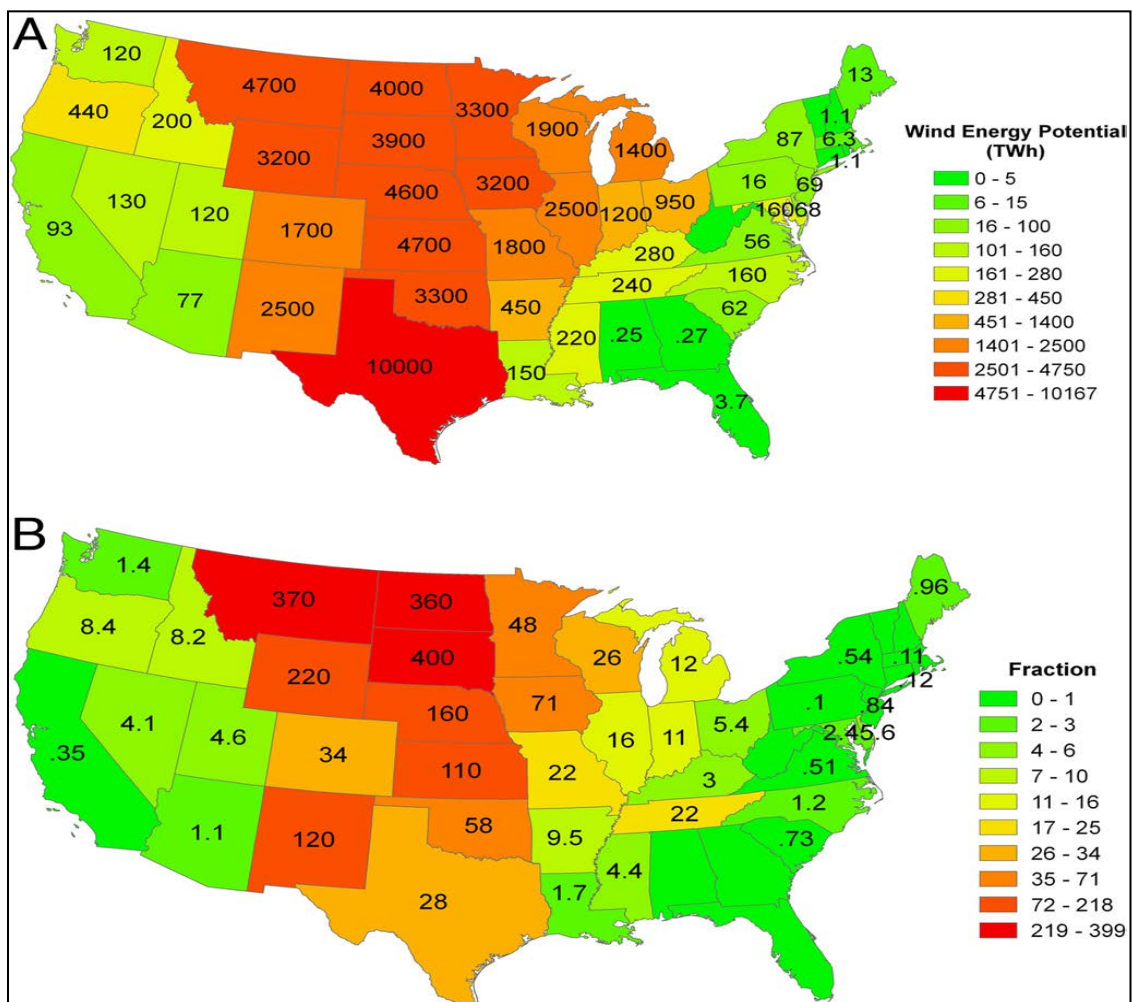


Figure 1.5 Kansas Wind Resource Map [23]



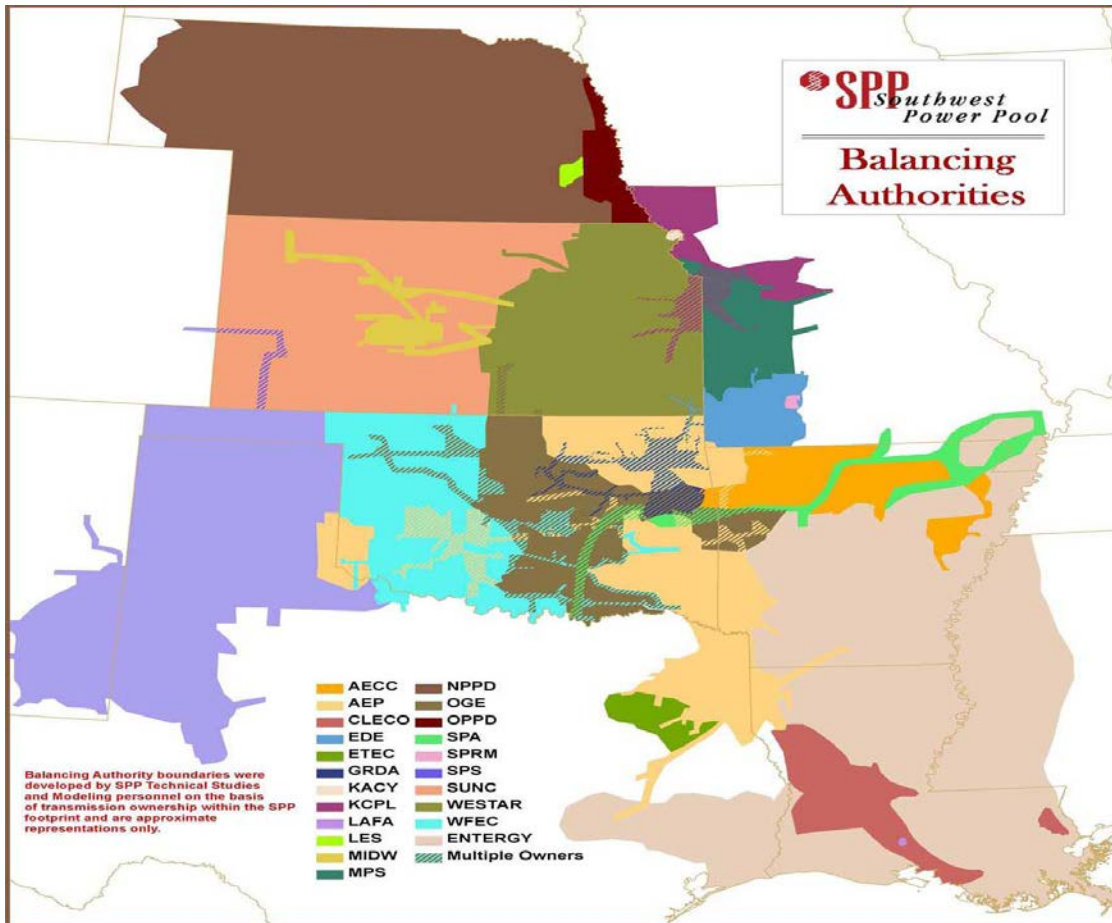
Large wind integration in the state Kansas is governed by the Southwest Power Pool (SPP). SPP is a Regional Transmission Organization (RTO) designed to ensure reliable supplies of power in nine states in the USA. A map of the SPP service area (footprint) is shown in Figure 1.7 [26]. SPP coordinates the generation interconnection process and oversees the planning study requirements on behalf of the transmission providers in Kansas and all other states under their jurisdiction within the SPP footprint. SPP is the authority which perform wind integration studies for all new wind generation interconnections within the SPP footprint [27]. SPP provides recommendations for the maximum size of new wind generation for each new site and any additional voltage support equipment needed to maintain system reliability.

Figure 1.6 Annual Wind Energy Potential on Steady-State Basis for the USA in TWh (A) and as a Ratio with Respect to Retail Sales in Each State (B) [25]



Current SPP wind integration planning studies use maximum thermal limits of the existing power system at the point of interconnection to determine maximum size for each new wind injection site. A power factor range of +/- 0.95 is specified for each new wind generator site. This is the range that a wind farm must maintain for the specific maximum size [27]. The SPP clustering study does not attempt to maximize wind penetration; it is simply performed to ensure that the power system reliability is not negatively impacted by incorporating the additional wind resources. It is also used to determine additional system upgrades needed for system reliability.

Figure 1.7 Southwest Power Pool (SPP) Service Area Map [26]



1.6.2 Challenges to Wind Power Integration in Power Systems

Integrating wind power into power systems does not pose significant operational challenges when the wind penetration level is low, especially in portfolios with abundant resources having high response rates like Hydro or combustion turbines [28]. As the wind penetration level increases, challenges arise due to the unique nature of the wind resource. Proper integration of the wind power into the grid becomes important as the extent of penetration of wind power increases [28].

The nature of wind plays a big part in complicating wind integration studies due to the variation of real and reactive power output as functions of time. The balance between power system loads and generation resources has become a big challenge due to uncertainties in wind generation resources. The variability leads to a greater need for reserves; disturbances of the generation-to-load balance due to high ramp events require supplementation by traditional generators. Additional reserves have additional costs and increase operational challenges, especially in a market like that of the Kansas region, in which the generation is primarily thermal with few hydro resources. Furthermore, the peak hours for wind generation usually occur in the early morning (off-peak) just before sunrise and do not coincide with the peak hours (on-peak) for the load, which occur mid-afternoon. As a result, net load (load minus wind generation) exhibits more significant fluctuations between off-peak and on-peak periods.

This fluctuation leads to more operational challenges in controlling non-wind generators serving the net load. For a primarily thermal generation portfolio like that of the Kansas region, this means that additional challenges arise during the off-peak hours because of minimum generation requirements. The variation of wind output and forecast errors have a significant impact on non-wind unit commitment. Under-forecasting wind generation leads to over-commitment of non-wind generation, and over-forecasting wind generation leads to under-commitment. Over commitment can result in a suboptimal economic dispatch and high uplift costs as well as wind generator curtailment. Under-commitment can result in shortage of supply which may lead to voltage collapse and other reliability issues. In order to avoid these commitment problems, the uncertainty introduced by wind power in the unit commitment timeframe must be minimized, especially with high wind power penetration levels [28].

Another factor complicating wind integration is the output characteristic of a wind farm power curve. Figure 1.8 shows a representative wind turbine power versus wind speed curve

[28]. As seen in Figure 1.8, the forecast error in wind speed can vary greatly the output of the wind generator. If the wind speed is in the range between the cut-in wind speed and the rated power wind speed, a small forecast error in wind speed leads to a large error in wind generation output. If wind speed is close to the cut-out wind speed, there is a risk of a cutoff event, which shuts down the wind turbine to avoid mechanical failure. These potential forecasting errors will lead to different reserve requirement needs, further complicating the challenge of wind integration.

Figure 1.8 Wind Turbine Power Versus Wind Speed Curve [28]

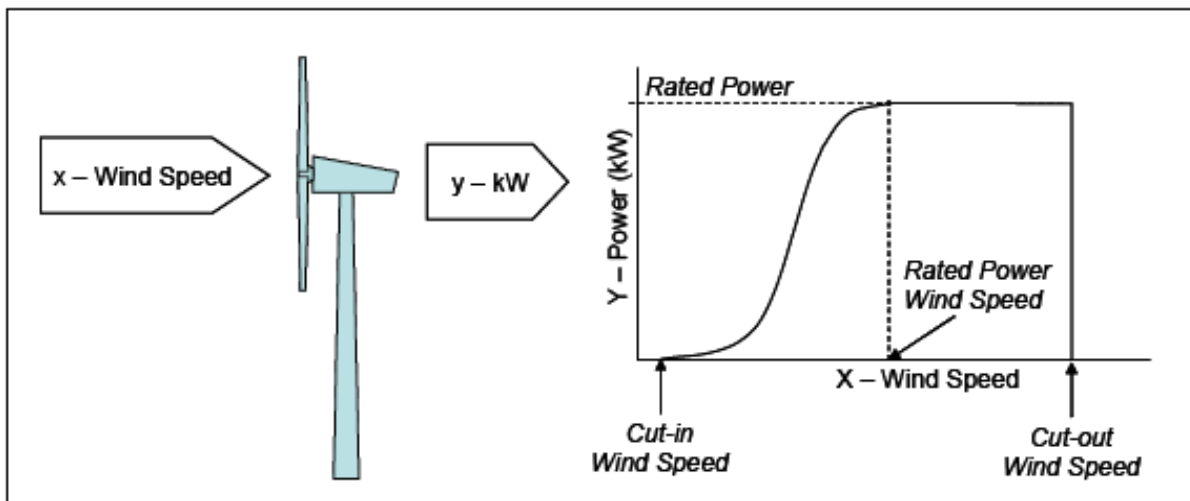


Figure 1.9 shows the average daily available wind profile by season for a wind injection point in western Kansas. The average profiles are different for different seasons, although the fall and winter profiles are quite similar. All seasons have the highest average available wind in the morning, with the spring, summer, and fall average peaks occurring around 6 am, while the winter peak occurs around 10 am. The season with the steepest average hourly ramps is summer, followed by spring, fall, and winter. Average yearly wind power output in western Kansas can be as high as 50% to 60% of the maximum installed rated power. A sample of the hourly wind power outputs for six different wind farm sites in western Kansas are shown in Appendix A. The wind profiles used to calculate the maximum hourly power output for each site are based on the wind profiles developed by “AWS Truewind” [29] for the National Renewable Energy Laboratory (NREL) Eastern Wind Integration and Transmission Study (EWITS) [28]. The EWITS wind profile dataset contains simulated 10-minute wind power output for 2005 – 2007

for a large number of sites in Kansas. Each EWITS site is composed of several cells. The EWITS dataset provides the 10-minute wind power profile for each cell, as well as the cell location. The calculated power output provided in Table A.1 in Appendix A are based on using the squirrel-cage induction generator (SCIG) wind turbine type manufactured by Suzlon with product number S64 which has a rated power of 1,250 kW [30].

Wind speed can peak in any day at any hour for any season. As an example, a single wind farm in western Kansas produced close to its maximum rated power for several random times in the month of July as shown in Figure 1.10. The figure shows that the power output profile of a wind farm is time-independent. In other words, for a given month and a day, the maximum observed wind power output can occur in any hour.

Figure 1.9 Average Daily Available Wind Profile by Season for 3 years (2005 -2007)

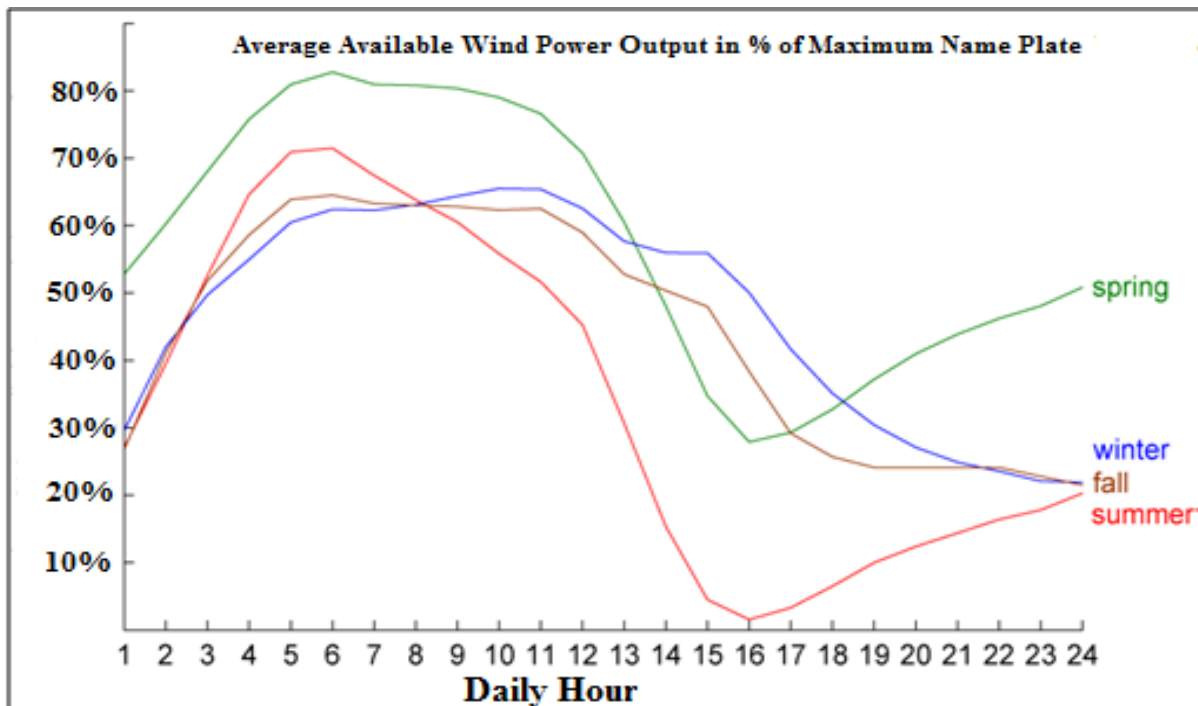
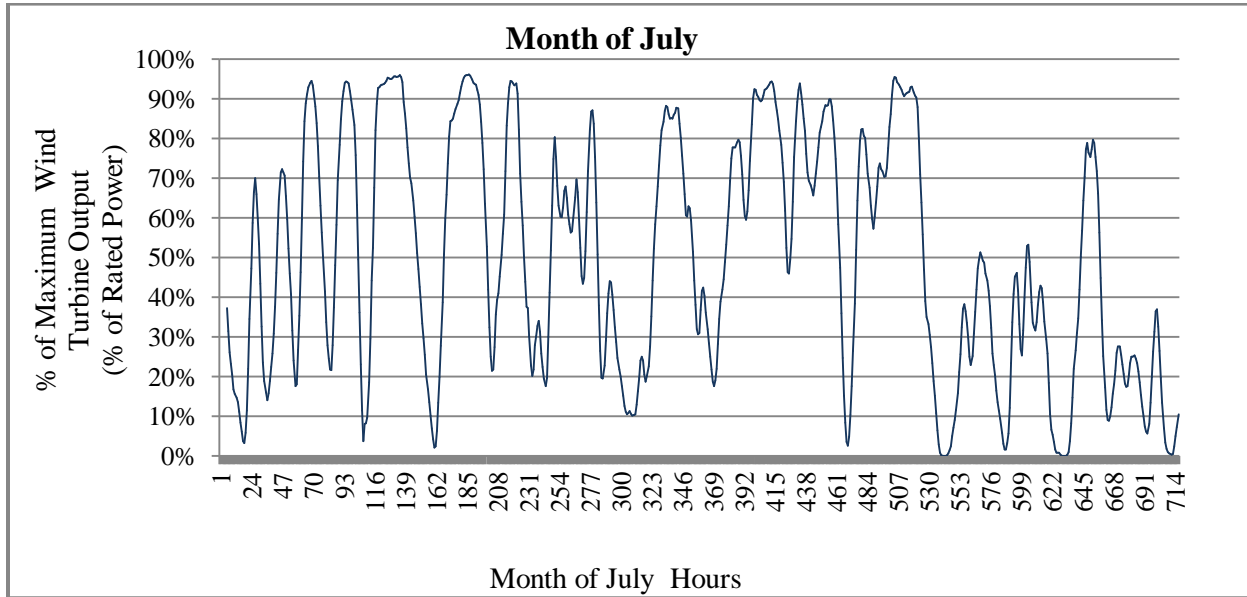


Figure 1.10 Maximum 3 years' (2005 -2007) Available Wind Power Output as a % of Maximum Wind Farm Rated Power (Maximum Size) at a Wind Injection Bus (Bus 95) for the Month of July



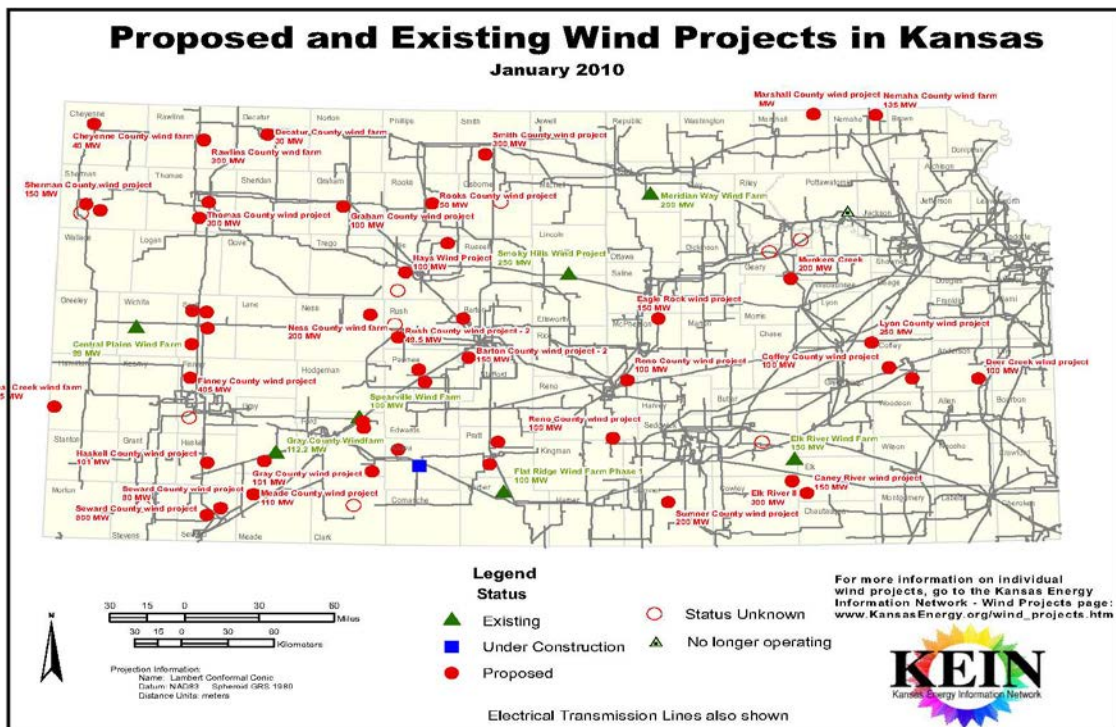
An additional challenge to wind integration is the lack of understanding of wind generation models which can be used by power system planners for wind integration planning studies [22]. Models for conventional power system elements, such as generators and their various controls, power system loads, transmission network elements and static compensation devices are well understood by power system analysts. Large wind power plants (wind farms) and wind power integration in power systems pose several new challenges. The technology employed in commercial wind turbines deviates from the much better understood conventional generation equipment. Induction generators, rather than conventional synchronous generators, are used in nearly all USA commercial wind turbines. The new trend in wind turbines is the use of power electronic controllers to isolate the wind farm from the grid. These controllers alter the fundamental behavior of the induction machines in both steady-state and transient operation.

1.7 Wind Power and Wind Generation Types

In recent years, there have been rapid increases in new wind-power generation connecting to the electric grid in the USA [31]. Wind power is the most rapidly growing renewable resource in the last decade as a result of the increased environmental concern over the

use of fossil fuels for producing electric energy. Wind turbines convert wind airflow power into electricity. A recently updated map of proposed wind projects in the state of Kansas (shown in Figure 1.11) indicated that over 2 GW of total wind capacity is being developed in the state of Kansas [23, 27, 31]. In addition, the capacity of the new wind resources has grown in the last decade from just a fraction of MW per turbine to 4 MW per turbine [32, 33].

Figure 1.11 2010 Kansas Proposed and Existing Large Wind Generation Projects [31]



For modern large wind turbines, the tendency is to group tens or even hundreds of these turbines within a limited geographical area referred to it as a wind farm. The grouping helps to reduce the cost of running underground or overhead cables to connect wind turbines to the transmission grid and to limit visual impact of wind turbines to a certain area.

1.7.1 Wind Power and Wind Generation Types

The simplest turbine model assumes a constant input wind speed, constant rotor speed and constant pitch angle. This model can be used in small distribution systems where small wind turbines are installed and the variation of rotor speed and pitch angle can be neglected.

In large wind integration applications, wind speed is no longer assumed constant. With changing wind speed, wind power variations impact wind turbine rotor speed and the pitch angle. The wind power that is extracted by the wind turbine is characterized by the performance coefficient (C_P). The total wind power (P_w) multiplied by C_P is the total power that the wind turbine can generate [32]. The kinetic energy of a mass of air “ m ” moving at an average speed V_w is given by

$$\text{Kinetic Energy} = \frac{1}{2} m V_w^2 \quad (1.1)$$

to convert the kinetic energy of the wind (E) to power (P_w), take the derivative of the kinetic energy with respect of time

$$P_w = \frac{dE}{dt} = \frac{1}{2} \frac{dm}{dt} V_w^2 \quad (1.2)$$

Where dm/dt is the mass of air transferred per unit time. If the mass of air is crossing an area “ A ”, then $dm/dt = \rho A V_w$ where “ ρ ” is the air density. The power of the air passing through an area (power in the wind) can be expressed as

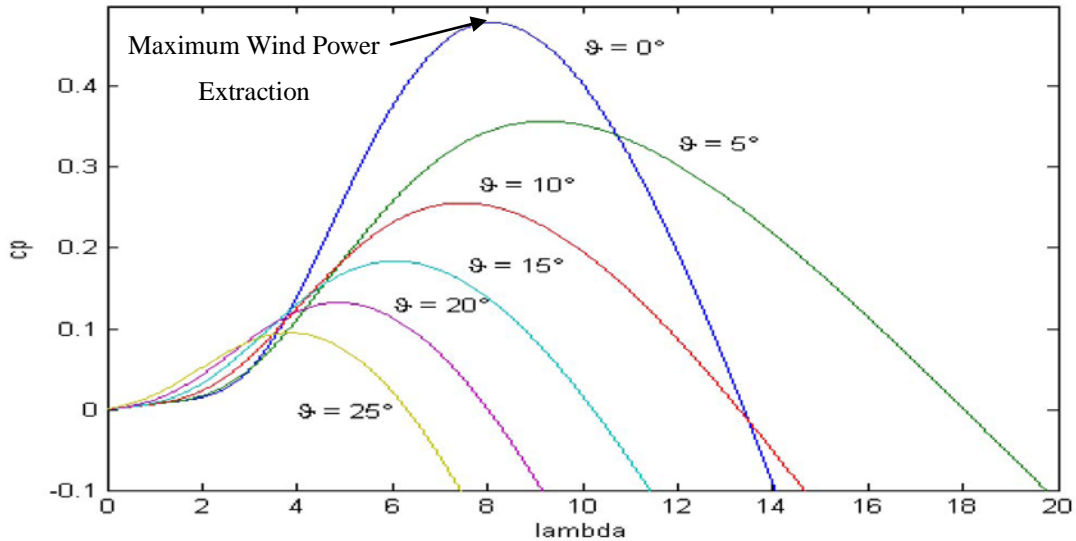
$$P_w = \frac{1}{2} \rho A V_w^3 \quad (1.3)$$

The power extracted by the wind turbine can written as

$$P_t = \frac{1}{2} \rho \pi R^2 C_p V_w^3 \quad (3.5)$$

Where R is the radius of the area wind flow crosses, and the performance coefficient C_p is a manufacturer specific coefficient which is approximated by field test measurements of the tip-speed ratio (λ) of the wind turbine blades and the pitch angle (Θ) [35]. The tip-speed ratio is the ratio between the speed at the tip of the blade and the average wind speed. An example of coefficient C_p from manufacturing data is shown in Figure 1.12.

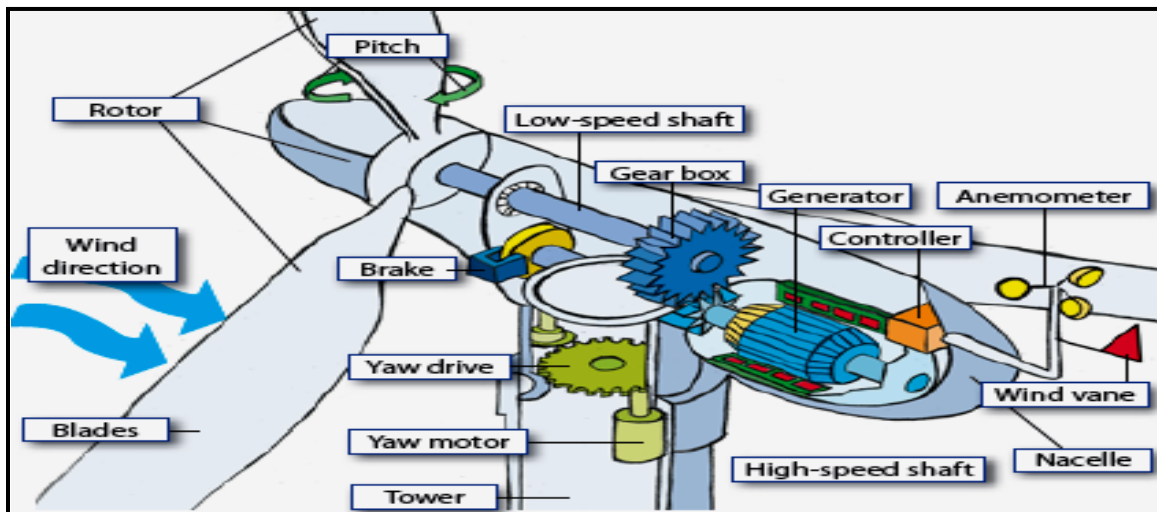
Figure 1.12 Coefficient of Parameter C_p as a Function of λ and for Various Values of Parameter θ [35]



1.7.2 Wind Turbine Components

The main components of a wind turbine generator are shown in Figure 3.13. The turbine is formed by the blades, the hub and the connecting components (bearing and pitching actuators). It transforms wind energy to a kinetic energy which generates torque to rotate the wind turbine shaft. For multi-megawatt wind turbines, dimensions are large with blade span ranging from 30 to 70 meters [35].

Figure 1.13 Wind Turbine Components [35]



The drive train is formed by the turbine rotating shaft, low-speed shaft, gearbox, high-speed shaft and generator rotating mass. The gearbox's function is to adjust the rotating speed of the turbine shaft which is much slower than that of the generator. For multi-megawatt wind turbines, the gearbox ratio is about 50-100 as the typical speed range of the turbine is 10-20 rpm while the generator rotates at about 1,000-2,000 rpm [36]. The low speed shaft contains pipes for the hydraulic system that operates the aerodynamic breaks [36]. The high speed shaft contains emergency breaks to back-up the aerodynamic breaks in case of failure [36]. The generator converts mechanical power into electrical power. For SCIG type, no AC-DC-AC convertor is required since this type of generator operates at a constant speed. For DFIG and DDSG types, an AC-DC-AC convertor is required to allow for variable speed operation.

Generators usually produce power at 690 volts and a step-up transformer steps it up to 34.5 kV [37]. The transformer may be placed at the bottom of the tower or inside the nacelle (where turbine is located) to reduce distribution circuit losses [38]. The power loss reduction is due to transmitting the wind power generated at a higher voltage level (34.5 kV) right at the Nacelle location (Higher voltage means less current for the same amount of power). The power is then transmitted to the wind farm collector substation (point of interconnection with the transmission grid) where an additional voltage step-up transformer steps it up to 115 kV or above.

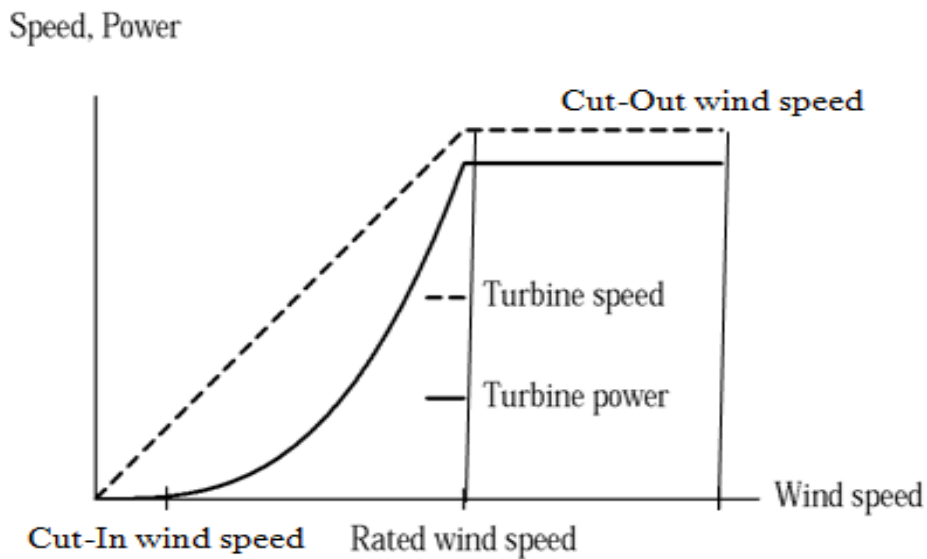
Other components include the vane and anemometer which measure the wind speed and direction separately. Measured wind speed is used to determine when to start or stop the turbine. Wind speed direction is used as an input signal to the yaw-control system for aerodynamic torque controls.

1.7.3 Wind Turbine Characteristics

The operating regimes of wind turbines can be illustrated using the power versus wind speed curve shown in Figure 1.14 [36]. The power curve cut-in wind speed is the wind speed at which usable electric power generation starts. The rated wind speed is the wind speed at which the turbine generates its designated rated power output. The cut-out wind speed is the wind speed at which the turbine is shut down to protect the turbine from mechanical damage [32]. To keep the turbine efficiency at its maximum, the speed of the turbine should be changed linearly with

the wind speed until reaching the rated wind speed. However, since the wind power is proportional to the cube of the wind speed, the shaft speed power function is limited by the turbine dependency on the ratio between the blade tip speed and the wind speed (tip speed ratio). The maximum aerodynamic efficiency is obtained at a fixed tip speed ratio. In this Dissertation, the turbine speed is assumed to be controllable above the rated wind speed by blade pitch control [36]. The generator speed can then be considered constant at wind speeds above the rated wind speed. An ordinary wind turbine has a rated wind speed of about 13 to 14 m/s but the median wind speed is much lower, about 5 to 7 m/s. Therefore, the power of the turbine most of the times considerably less than the rated power.

Figure 1.14 The Turbine Power and Turbine Speed Versus Wind Speed [36]



1.7.4 Pitching

Wind turbine speed control in the DFIG and DDSG types uses blade speed pitch controls to reduce stress on the induction machine shaft [32]. The control of the pitch angle is obtained by means of a Proportional-Integral (PI) controller that compares the electrical generated power with the mechanical power provided by the turbine as shown in the block diagram of Figure 1.15 where ω^* is the desired rotor speed at which the generator power output is reduced. The PI

controller controls the position of the blades for maximum wind energy capturing under a variety of wind speeds and operating conditions. So when the turbine is operating in wind speeds below rated ω^* , the PI controller will position the blades with a pitch to maximize energy capture. As the wind speed increases above rated, the blades are feathered to reduce the power output of the generator and maintain constant rotor speed to prevent overpowering the turbine. The impact of wind speed control by blade pitching is shown in Figure 1.16 [32].

Figure 1.15 Pitch Controller Open Loop Controller [32]

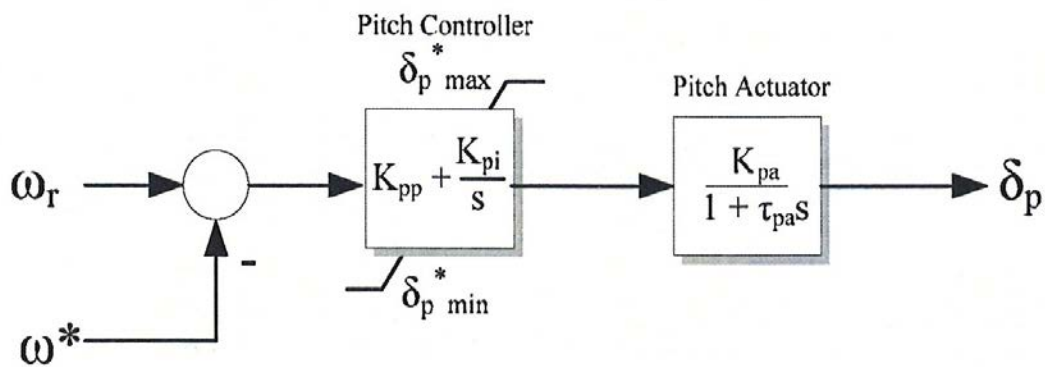
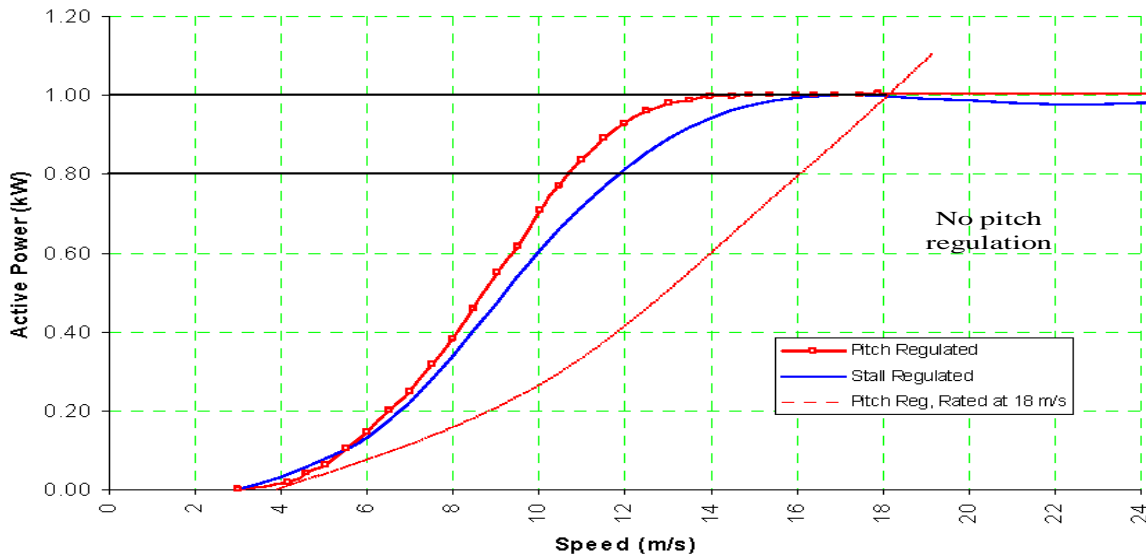
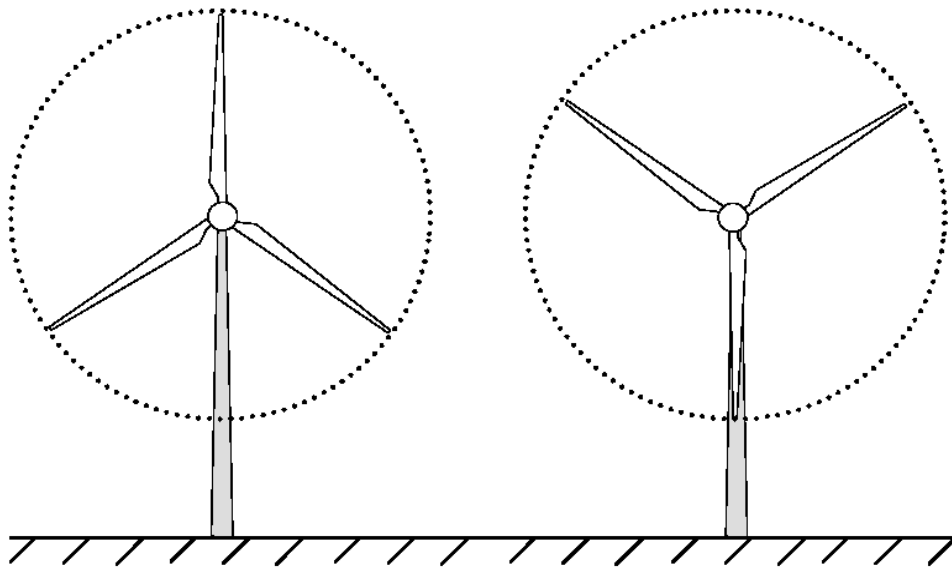


Figure 1.16 Wind Turbine Output Fluctuations Caused by Blade Pitching [32]



Blade pitching is another pitching that may influence the wind speed versus power output characteristic for wind turbines. As the blades rotate and pass the turbine tower post structure, slight variations of mechanical torque are produced due to the tower affecting the flow of wind across the sweep area of the blades. The turbine tower introduces a resistance to the wind flow past it, and it will disturb the flow both upstream and downstream of the tower when the blade is in the tower “shadow” [32]. For modern wind turbines with 3-blades as shown in Figure 1.17, this phenomena is often referred to as the 3-blade effect because the blades will pass the front of the tower three times per revolution of the rotor. Tower shadowing can result in wind power output power fluctuations of 0.5 to 1.5 Hz in range for modern large wind turbines depending on the number of generator poles and gearbox ratio.

Figure 1.17 “3-Plades” Effect of Blade Tower Shadow [32]



1.7.5 Generator

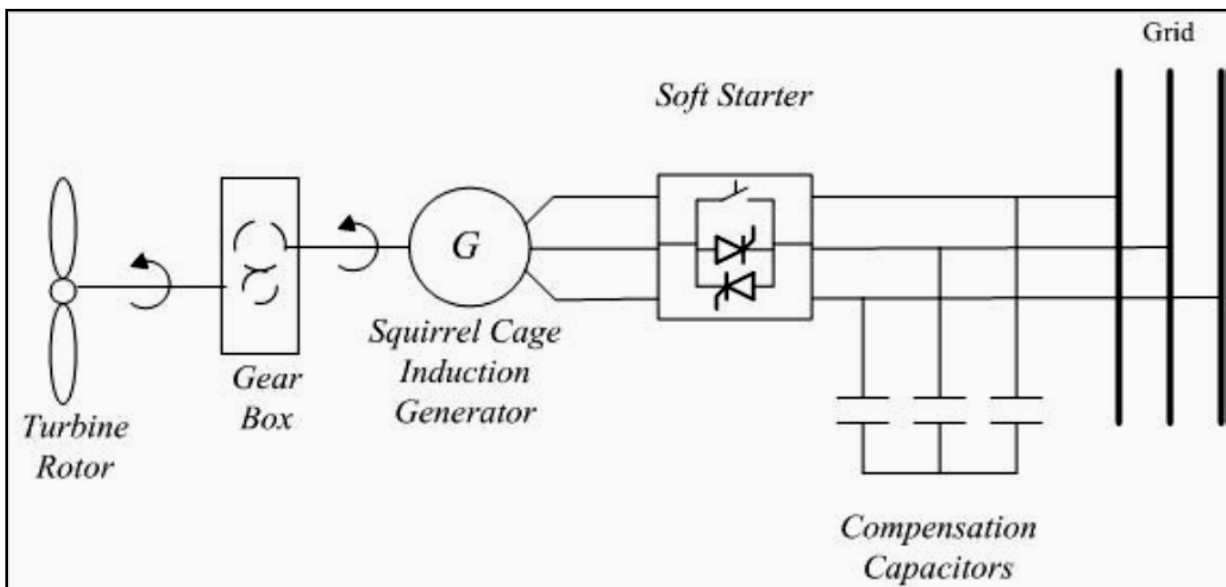
Regardless of the type of wind turbine used, the working principle of a wind turbine is based on two energy conversion processes. The rotor of the turbine extracts kinematic energy from the wind airflow and converts it to a generator torque. The available torque is converted to electricity by the induction or synchronous generator. Wind generation systems for large wind integration projects generally use either Squirrel-Cage Induction Generator (SCIG), a Doubly-

Fed (wound rotor) Induction Generator (DFIG) or a Direct-Drive Synchronous Generator (DDSG) type.

1.7.5.1 Squirrel-Cage Induction Generator (SCIG)

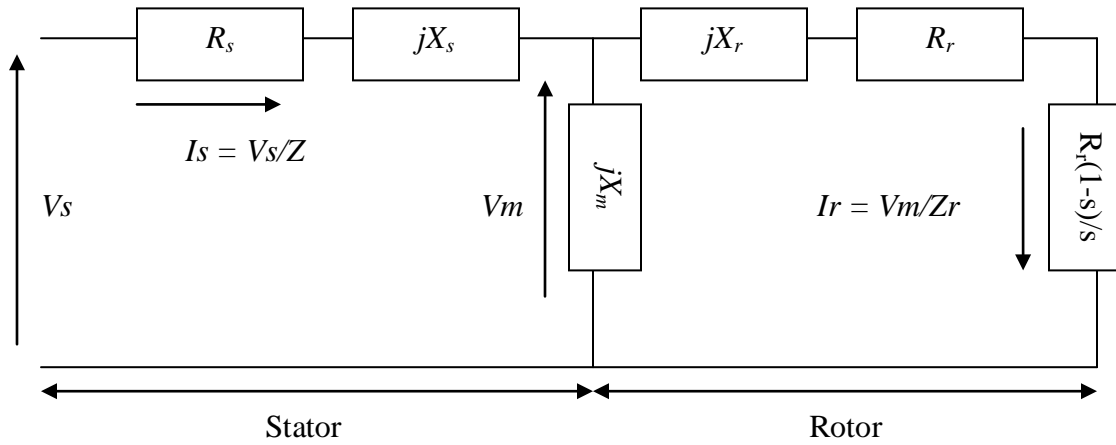
The SCIG type consists of fixed-speed induction machine that is directly connected to the transmission grid as shown in Figure 1.18 [32]. This type is the oldest wind turbine machine and it is the cheapest. The SCIG wind turbine type uses a gearbox to couple the wind turbine shaft to the generator shaft. SCIGs have no pitch angle control since they are fixed speed machines and their rotor's efficiency decreases at high wind speeds which results in reducing the amount of torque that can be extracted from the airflow. Even though these machines are referred to as fixed speed, they can operate at two different fixed speeds by changing the number of poles of the stator winding [32]. The rotor of this type of wind turbines is short circuited. The advantage of this type of machine is its robustness [32]. SCIG consumes reactive power from compensation capacitors connected to the transmission grid. For large wind farms in weak grid systems like the power system in Kansas, it is undesirable to use the SCIG type in new installations due to the lack of active and reactive power control in this type of wind farm.

Figure 1.18 Squirrel-Cage Induction Generator (SCIG) Type Grid Connectivity [32]



The equivalent circuit model for the SCIG wind turbine type is shown in Figure 1.19 [39]. For power flow studies, the SCIG wind turbine type is modeled as a PQ bus with the real power specified and the reactive power demand calculated. To calculate the reactive power “ Q ” absorption for specified real power generated values, the per-phase equivalent circuit is used and the following equations determine the relationship between P and Q for the SCIG wind turbine type.

Figure 1.19 Per-Phase Equivalent Circuit for SCIG [39]



$$Z = R_s + jX_s + [jX_m \text{ parallel with } \left(\frac{R_r}{s} + jX_r \right)] \quad (1.4)$$

$$V_m = V_s + I_s (R_s + jX_s) \quad (1.5)$$

$$P = 3 |V_s| |I_s| \cos \theta \quad (1.6)$$

$$Q = 3 |V_s| |I_s| \sin \theta \quad (1.7)$$

Where, Z is the equivalent impedance of the circuit, R_r and R_s are rotor and stator resistances, X_r and X_s are rotor and stator reactances, S is the machine slip and I_r and I_s are the rotor and the stator currents respectively. If the magnetization reactance is neglected; $X_m = 0$, a simplified effective P and Q relationship of the SCIG can be written as follows [40].

$$Q = \frac{X_s + X_r}{v_s^2} P^2 \quad (1.8)$$

1.7.5.2 Doubly-Fed Induction Generator (DFIG)

The Doubly-Fed Induction Generator (DFIG) is a variable speed induction generator with its rotor consisting of conductors with slip-rings fed by an ac-dc-ac convertor connected to the transmission grid as shown in Figure 1.20. To enable variable-speed operation, the mechanical rotor speed and the electrical grid frequency are decoupled in the DFIG turbine types. The rotors in these machines are capable of operating at variable speeds since the rotor has a non-zero voltage with a typical slip range of $\pm 30\%$ determined by the size of the converter [40]. The advantages of the DFIG are the speed variability which reduces mechanical stress [40] and the ability of controlling reactive power independently from the controlling the electrical torque of the machine [40]. The equivalent circuit model for the DFIG wind turbine type is shown in Figure 1.21.

Figure 1.20 Doubly-Fed Induction Generator (DFIG) Type Grid Connectivity [40]

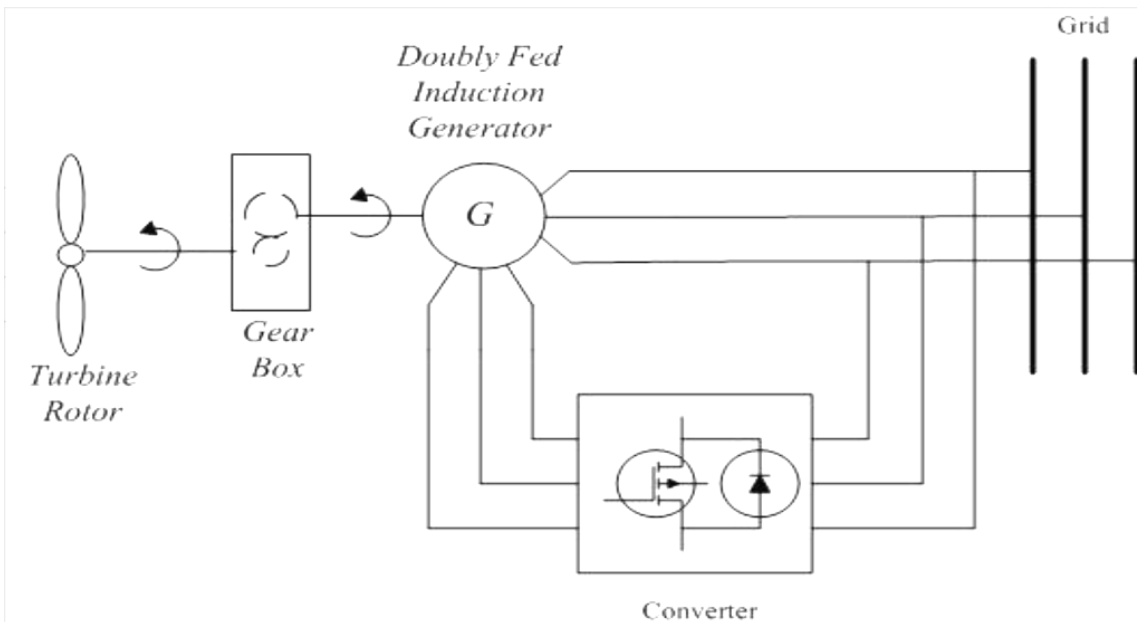
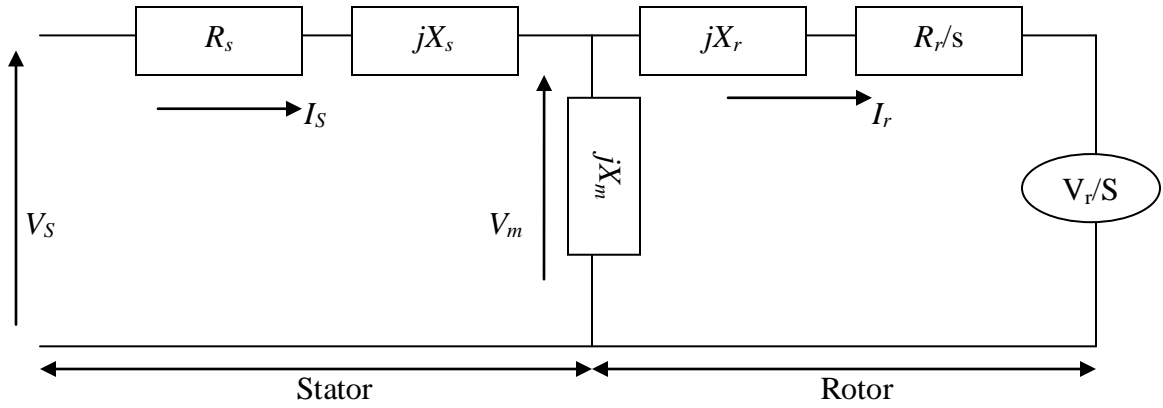


Figure 1.21 Per-Phase Equivalent Circuit for DFIG [40]



For power flow studies, the DFIG wind turbine type is also modeled as a PQ bus with the real power specified and the reactive power demand calculated. To calculate the reactive power “ Q ” absorption for specified real power values, the per-phase equivalent circuit is used and the following equations give the relationship between P and Q for the DFIG wind turbine type.

$$V_S = R_S I_S + jX_S I_S + jX_m (I_S + I_r) \quad (1.9)$$

$$\frac{V_r}{S} = \frac{R_r}{S} I_r + jX_r I_r + jX_m (I_S + I_r) \quad (1.10)$$

Again, R_r and R_S are rotor and stator resistances, X_r and X_S are rotor and stator reactances, S is the machine slip and I_r and I_S are the rotor and the stator currents respectively. The magnetization reactance is X_m . The power generated from the DFIG turbine can be written as the sum of the power values of the stator and rotor as follows.

$$P_S + jQ_S = 3 V_S I_S^* \quad (1.11)$$

$$P_r + jQ_r = 3 V_{Sr} I_{Sr}^* \quad (1.12)$$

$$P_{equivalent} = P_S + P_r \quad (1.13)$$

$$Q_{equivalent} = Q_s + Q_r \quad (1.14)$$

DFIG wind turbine type uses the AC-DC-AC conversion process to allow the generator to operate with variable speed, which improves energy capturing and allows better management of loads during wind turbulence. The characteristic of the inverter dominates the behavior of the wind turbine with respect to the grid [39]. DFIG are equipped with high-frequency, pulse-width-modulated, current-regulated, voltage-fed invertors. This implies that they are supplied with a DC voltage source, and operate to regulate their prospective AC power output currents in response to an external current control signal through high carrier frequency of approximately 3 kHz pulse width modulation of the DC voltage source. This provides a high quality sinusoidal current output that is both synchronized to the grid voltage frequency as well as phase locked to the grid voltage displacement power factor.

The reactive power control (power factor controller) uses a separate power factor control system that consists of thyristor-switched capacitors and/or thyristor-controlled reactors to control reactive power at the point of common coupling with the transmission system. The DFIG power factor controller senses real power (P) and reactive power (Q) flow and voltage level at the point of common coupling. The power factor controller uses a closed loop control of voltage and reactive power (Q) within a range of power factors from 0.95 leading to 0.95 lagging.

1.7.5.3 Direct-Drive Synchronous Generator (DDSG)

The DDSG is a variable speed synchronous generator which is completely decoupled from the electric grid by a voltage convertor connected to the stator winding of the generator [39]. These turbine types are equipped with direct drive synchronous generators as shown in Figure 1.22 [39]. Such types are equipped with back-to-back voltage source converters or diode rectifiers and voltage source converters to couple the generators with the grids.

The DDSG is excited using an excitation winding or permanent magnet. The permanent magnet generators offer advantages over induction generators in terms of increased power density, increased efficiencies at lower wind speeds, improved low-voltage ride-through capability when combined with full power conversion and simplicity of design [41]. For low-speed gearless wind turbine generators, the permanent magnet generator is more competitive

than the conventional synchronous generator because it has higher pole numbers which reduce the impact of speed changes on the machine.

Figure 1.22 Direct-Drive Synchronous Generator (DDSG) Type Grid Connectivity [39]

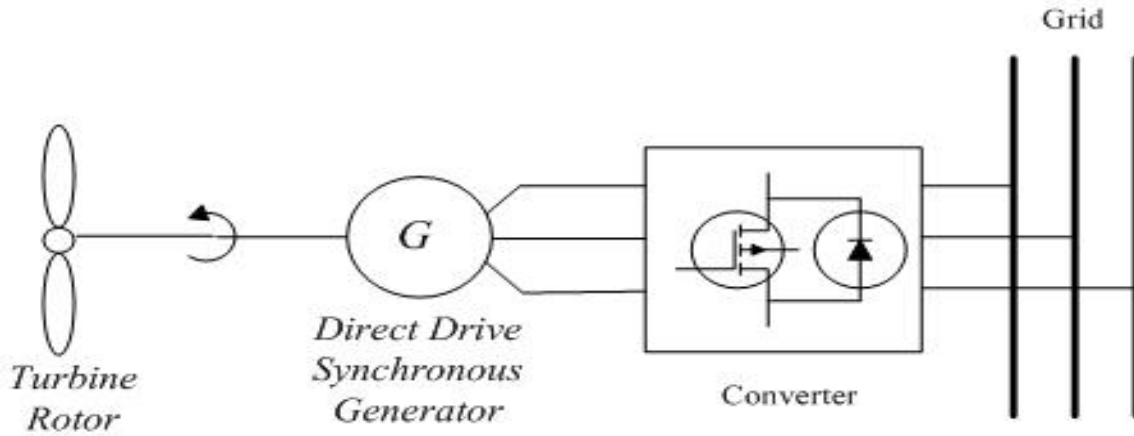
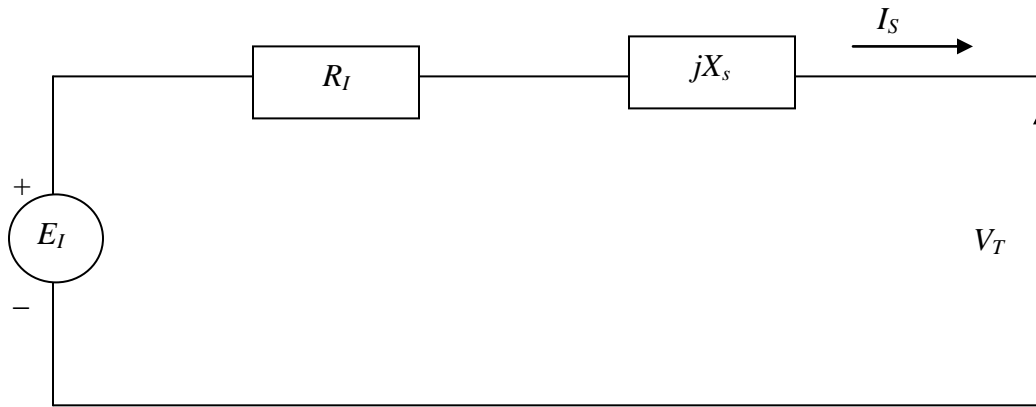


Figure 1.23 Per-Phase Equivalent Circuit for DDSG [39]



The per-phase equivalent circuit of DDSG wind turbine types is shown in Figure 1.23. The following equations describe the DDSG type wind turbine.

$$V_T = E_l - jX_s I_s - R_l I_s \quad (1.15)$$

V_T is the per-phase terminal voltage, E_f is the internal generator voltage, X_S is the internal generator synchronous reactance, I_S is the current and R_f is the stator resistance. The power generated by the DDSG wind turbines can be written as

$$P = 3 |V_T| |I_S| \cos \theta \quad (1.16)$$

$$Q = 3 |V_T| |I_S| \sin \theta \quad (1.17)$$

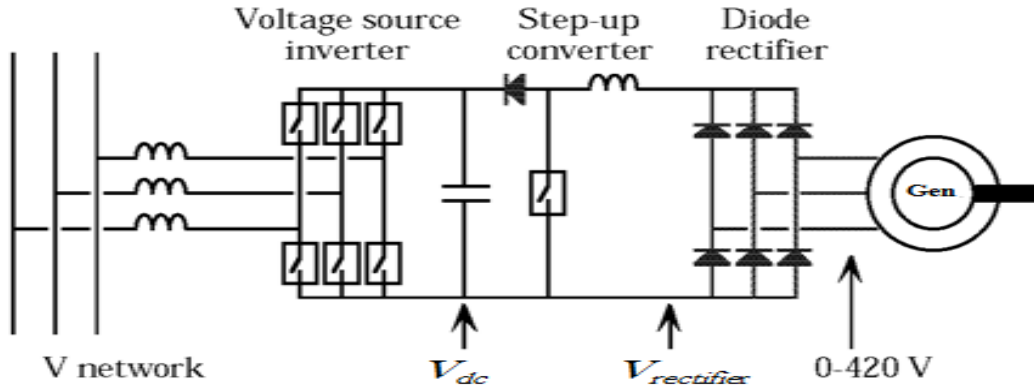
1.7.6 Converter

Many types of converters can be used in variable-speed wind turbine generator systems today [39]. They can be characterized as either network-commutated or self-commutated. Self-commutated converters are either current source or voltage source inverters. Self-commutated converters use high switching frequencies, up to several kHz. Control of the reactive power flow is possible for this type of converter making it easier to connect them to weak networks. Self-commutated converters use a pulse width modulation (PWM) technique to reduce the harmonics. To make the harmonics low, the switching frequency is often 3 kHz or higher. Self-commutated converters are usually made either with Gate Turn Off thyristors, GTOs, or transistors. The GTO converters are not capable of switching frequencies higher than “1” kHz. That is not enough for reducing the harmonics substantially below those of a thyristor converter with a filter. Therefore, the GTO converter is not considered as a choice for wind turbines in weak power systems [38]. Today the most common transistor for this type of application is the insulated gate bipolar transistor, IGBT. It is capable of handling large phase currents, about 400 A, and it is today used in converters with rated AC voltage up to 690 V.

A self-commutated converter with a voltage source inverter is shown in Figure 1.24. Today the voltage source inverter is the most common type used in the wind industry [38, 39]. When this type of converter is used to feed power to the network, it must have a constant voltage on the DC shunt capacitor (V_{dc}) which is higher than the peak voltage of the network ($V_{network}$). Due to wind speed fluctuation, the generator can't produce constant high voltage especially during low wind speed periods. A self-commutated rectifier provides constant high voltage

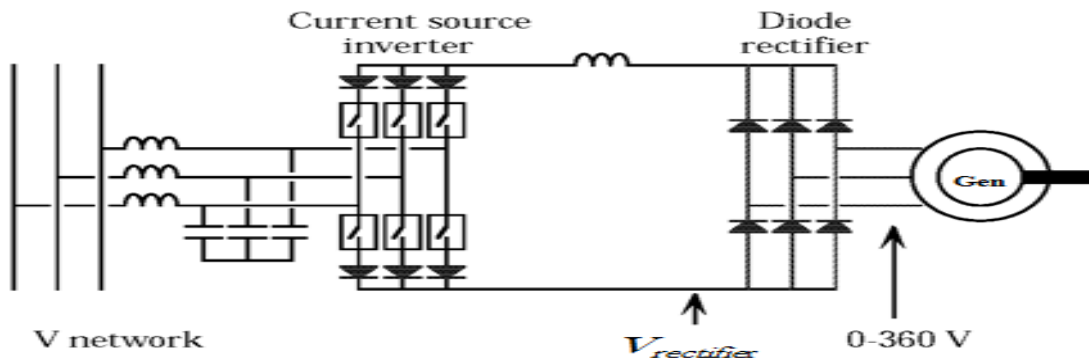
($V_{rectifier}$) even during low wind speed periods which makes it attractive for use in wind generator design.

Figure 1.24 Self Commutated Voltage Source Inverter [39]



A self-commutated current source inverter diagram is shown in Figure 1.25. For a generator connected to a diode rectifier, the self-commutated current source inverter is capable of feeding power to the network from very low voltages. For networks with voltage-stiff characteristics, this type of converter is very reliable since DC voltage across the inverter is constant regardless of the available wind speed. Current source inverters are not suitable for a weak power systems since the network does not always provide constant voltage across the inverter [39].

Figure 1.25 Self-Commutated Current Source Inverter [39]



1.8 Literature Survey

This literature survey is divided into three sections: wind turbines, wind farm aggregate models and voltage stability. In the survey of wind turbine components, their types, operation and representation in power flow models are introduced. Aggregation methods for wind farms are described in the wind farm aggregation survey. In the voltage stability survey, steady-state voltage stability techniques and the modal voltage stability method are described. Voltage stability boundary limit calculation methods are also introduced. Power system load characteristics and their impact on voltage stability limit are described in the voltage stability section. Although a large amount of literature is available on wind power and voltage stability, none was found which addresses maximization of wind farms using voltage stability methods. This dissertation content is the first that the author is aware of that optimizes using the existing power system reactive power margins in maximizing wind penetration in power systems.

1.8.1 Wind Turbines

The working principle of a wind turbine encompasses two conversion processes: the rotor that extracts kinetic energy from the wind and the generator that converts that energy into electricity [31, 36]. Currently, there are three wind turbine types widely available. The three wind turbine types are: Squirrel-Cage Induction Generator (SCIG), a Doubly-Fed (wound rotor) Induction Generator (DFIG) or a Direct-Drive Synchronous Generator (DDSG) type. The textbook by S. Heier [31] explains the detailed components of each generator type and lists the advantages and disadvantages of each wind turbine type. The main difference between these types is the way the wind generator is configured (wind turbine component differences) and the way the aerodynamic efficiency of the rotor is limited during high wind speeds (pitching) to prevent rotor damages [37].

As for the wind turbine generation system, the first generation type is the squirrel-cage induction generator which consists of a conventional, directly-coupled squirrel-cage induction generator connected to the grid [38]. This type of generator is a fixed speed generator and does not produce or have the ability to control reactive power [38, 39, 66]. The advantages of the squirrel-cage induction generator are its simplicity and robustness [90, 91]. The other two generating turbines are variable-speed generators in which the mechanical rotor speed is decoupled from the electrical frequency. The Doubly-fed induction generator uses a convertor

between the rotor and the stator of the machine. The rotor circuit which consists of conductors with slip-rings fed by an ac-dc-ac convertor connected to the grid. Typically, the slip-ring range is +/- 30% of the maximum rated power which is limited by the size of the convertor [92]. Reactive power and voltage control can be obtained by varying the firing angle of the connected convertor [30, 93, 94].

Direct drive permanent magnet synchronous generator offer several advantages over induction generators in terms of increased power density, increased efficiencies at lower wind speeds, and improved low-voltage ride-through capability when combined with full power convertor [78]. This type of generator provides full power factor control (reactive power control) and full isolation from the grid [40, 79, 95]. The permanent magnet synchronous generators are more compact than the electrically excited synchronous generators but they are more expensive and require more advance rectifiers [37, 50, 114, 115].

1.8.2 Wind Farm Aggregate Models

A wind farm consisting of tens or hundreds of wind turbines can be aggregated into a minimal set of equivalent wind generator models combining all turbines into a single equivalent turbine since all wind turbines inside a wind farm are connected to a common point (point of interconnection) that connects them to the grid [62, 87, 98]. To study the impact of a wind farm on the grid, it is acceptable to aggregate all wind turbines inside the wind farm to a single large wind turbine at the point of common coupling with the grid [54, 63, 99, 100, 101, 102]. The geographical spread of individual wind turbines inside a wind farm is necessary only for evaluating the wind farm internal dynamics [61, 65, 103, 104].

1.8.3 Voltage Stability

Power system voltage stability is mainly classified into short-term referred to as transient voltage stability, and long-term, referred to as steady-state voltage stability [76]. Several references defined each category differently; however, all of them are based on the time it takes to develop a stability problem as it appears in [46, 47, 60, 76, 84, 88, 105, 106, 107]. Authors of these references agree on using the time response chart which has been reported in [46, 47] in which power system equipment models for voltage stability analysis are classified as transient models if the time span for voltage instability and collapse is less than five seconds. For longer-

term voltage stability which exceeds five seconds to develop, voltage stability is considered a steady-state phenomenon.

Voltage collapse is defined in [46, 47] as a power system behavior at a given operating point that is subjected to certain disturbances and, as a result, undergoes voltage collapse. Voltage collapse can occur as a result of a sequence of system disturbance events which lead to low-voltage profile in a major part of the power system. After clearing the disturbance in an unstable power system, system voltages stay below acceptable limits and existing system reactive power sources are unable to raise voltages to an acceptable level. Several references cited some major collapse incidents which have occurred in the last 40 years. In [42], the North East black-out is analyzed. A computer bug prevented system operators from shedding loads or starting emergency generation units to prevent a voltage collapse. System operators were unable to react to tripping of a major generation unit in Ohio due to losing two major tie lines from Ohio to Canada. This resulted in deficiency in generation in the North East which led to a major black-out. Some voltage collapse scenarios were avoided using system operator intervention. The 1987 Tokyo black-out is discussed in [43]. Tokyo suffered from a major black-out due to lack of reactive power resources during a very hot summer day in July, and voltages on a major 500 kV transmission line decayed significantly. After 15 to 20 minutes, the voltage started decaying to low values throughout the Tokyo power system and protection relays disconnected about 8,000 MW of load to maintain voltage stability. Lack of generation may also lead to voltage collapse as was the case in Texas where several wind generation sites experienced power interruption. This was due to sudden unexpected loss of wind generation caused by wind disturbances which was reported in [120].

For steady-state voltage stability calculations, many references presented the P-V and the Q-V curve methods for assessing power system voltage stability [45, 48, 108]. The P-V curve method is one of the simplest methods where the P-V curves are computed for load increases. The power transfer is increased in steps, and the distance in MW from the nose of the curve provides the voltage stability margin. The Q-V curve method assumes a fictitious synchronous condenser is applied at a test bus [49]. The test bus becomes a PV bus where bus voltage is specified and the corresponding reactive power generated from the condenser is monitored. A series of voltages and their corresponding reactive power are computed and a Q-V curve can be

plotted for the bus. The distance from the bottom of the Q-V curve to the zero reactive power axes is the voltage stability margin.

Both the P-V and the Q-V methods only incorporate the changes in either real power for voltage changes as in the P-V method or the change in reactive power for voltage changes as in the Q-V method. The authors of [50, 67] applied a new P-Q method which incorporate changes in both real and reactive power for voltage changes. In [68, 109], voltage stability boundaries were defined as the minimum values of system load (active and reactive power demand) which result in voltage collapse. The equation required to generate the voltage stability boundary is derived in [51].

In [110], *EVSM* is defined as the mean value of the voltage stability margins determined for each probable contingency and load level in the power system. The author of this dissertation expanded on the concept of using the *EVSM* which is developed in [110]. The importance of this concept is its ability to calculate a voltage stability margin which incorporates wind speed probability in the calculations of the voltage stability margins. In [5], the authors used the expected voltage stability concept for selecting the most important contingencies, which reduced the expected voltage stability margin (*EVSM*) computational efforts by narrowing the number of deterministic voltage stability evaluations. The *EVSM* can be used as a voltage stability “fitness” measure for the power systems.

Power system voltage stability limit estimation methods have been developed [75, 111, 112]. Most of these methods use system sensitivity for voltage stability calculations. In [75], to detect the occurrence of voltage instability in the network, the sensitivity of voltage to reactive power input is observed. The sign of the sensitivity is used to decide if a calculated network condition is above or below the voltage instability point. In [111, 112], the risk based calculation provided accounts for both the future uncertainties on the system and the consequences associated with voltage collapse and violation of limits. Several uncertainties associated with the voltage collapse are analyzed including deviations of load sharing and generation dispatch.

Power system equipment models appropriate for voltage stability studies depend on the time it takes to reach voltage instability and collapse. Time dependant models for voltage stability studies have been introduced in [46, 47, 70, 118]. Some power system equipment models need to include their dynamic behavior for voltage stability studies; others do not. The authors of [46, 47] indicated that voltage stability is a dynamic phenomenon when analyzing

equipment like induction motors, air conditioners and High Voltage DC (HVDC) links. However, when analyzing equipment like mechanical tap changers on transformers, generation change (AGC) units, and load diversity voltage stability is a slow phenomenon and can be studied using steady-state equipment models. In [118], the impact of equipment modeling accuracy on the results of voltage stability analysis is evaluated based on the type, kind, and class of stability problems in power systems. In [69] and [70], types of power system loads and their representation in voltage stability studies are defined. Dynamic and static load models required for voltage stability studies are also analyzed in [72, 113]. The effects of load modeling on the analysis of power system voltage stability has been evaluated in [74].

Power system load characteristics vitally affect voltage stability and unfavorable load characteristics may lead to complete voltage collapse [53, 54, 56, 57, 70, 73, 74, 120]. In [46, 76], impacts of two cases of load sensitivity on voltage stability have been studied. Using slightly voltage sensitive load, like electric heating load versus a highly voltage sensitive load, like motor loads, resulted in a great impact on voltage stability results. The authors of [60] considered practical issues in load modeling for voltage stability like the impact of tap changers on load characteristics. Load tap changers have a detrimental effect on voltage stability when power system loads consist of mainly residential and commercial loads since these loads have high sensitivity to system voltages. This is the opposite of induction motors with virtually constant real power that is not voltage sensitive. Location of tap changers and their impact on voltage stability is reported in [118]. The worst location for tap changing is close to voltage sensitive loads having little or no shunt compensation. In [53, 54], the Q-V curve method was used to evaluate the impact of load characteristics on voltage stability considering voltage and load control methods. The result of the analysis indicates that static var compensators are superior to mechanically switched capacitors and are one of the best solutions to prevent severe voltage instability.

Integrating large amounts of wind generation has great impact on system voltage stability. The authors of [49, 50, 67, 68] indicated that large amounts of wind penetration in power systems may lower voltage stability margins. Excessive wind integration may also lead to voltage collapse. Changes in wind speed often result in wind turbine active and reactive power fluctuations. [49] focuses on the relationship between the ratio of power system short circuit capacity and its impact on voltage drop across the power system. Power systems are classified

strong voltage stability systems when the short circuit ratio is high (high fault currents). The short circuit capacity plays a big part in determining the amount of wind power which can be injected from each wind injection site. Short circuit capacity ratio at the point of interconnection of the wind farm limits the maximum size of the wind farm. In [50, 67, 68] a large transmission network upgrades were found necessary to integrate large amounts of wind in the Southwest Power Pool (SPP) region. SPP plan of integrating 2.1 GW of wind in western Kansas required the construction of several 345 kV transmission line with estimated cost of \$600,000,000 Dollars to transfer half of the wind energy produced to low wind resources states line Missouri and Arkansas.

Voltage instability can be avoided or prevented using several techniques as introduced in [71, 110, 111, 112]. Following are a list of these techniques.

- 1) In [71], the authors investigated voltage stability impact of changes in generators' voltage set points to prevent generators from reaching their maximum reactive power limits and hence prevent voltage collapse.
- 2) The author of [110] used automatic shunt switching devices like static var compensators to increase reactive power support automatically to prevent voltage collapse during system disturbances or during heavy loading hours.
- 3) To reduce the potential for voltage collapse, installing and adjusting controls of series compensation equipment like series capacitor banks, used to reduce line reactive power losses, when generators reach their reactive capability limits is discussed in [111].
- 4) Blocking of transformers tap changers to keep distribution loads at their lowest voltage levels can prevent voltage collapse as described by the authors of [112]. Authors of [112] also investigated the impact of reducing amount of loads to reduce system demand which can relieve generators operating at their reactive power limits.

In [115], the basic structure and model of an SVC operating under typical bus voltage control are described. The model is based on representing the controller as variable impedance that changes with the firing angle of the Thyristor Controlled Reactor (TCR), which is used to control voltage in the system. Simulations carried out confirmed that the static var compensator could provide the fast acting voltage support necessary to prevent the possibility of voltage reduction and voltage collapse at the bus to which it is connected.

Due to complexity of today's transmission networks, computer software is necessary to perform steady-state voltage stability studies since all current voltage stability methods rely on solving the power flow model. Power flow models contain thousands of transmission lines, generators, and other equipment, and simulations are usually calculated based on several tries to solve the differential-algebraic equations describing the power system. This is time consuming to do manually. There are many software packages available which can be used for long-term simulation of power systems. A comparison between several different softwares and their applications in power system studies can be found in [119]. In this dissertation, two power flow software tools were used. The first one is called Power System Simulation for Engineers (PSS/E) from PTI Inc. [82]. This software is well recognized at power companies worldwide and is beginning to be used among higher education institutions in the USA. PSS/E has the capability of solving the power flow for networks with over 150,000 buses. PSS/E has integrated voltage stability functions like P-V and Q-V curves making it easy to use for generating voltage stability boundaries. The other software, which has been used for modal voltage stability analysis is Matlab with a third party power stability tool box [83]. Power flow solutions and modal voltage stability analysis can easily be completed for a power system network. Matlab software was used in this dissertation for calculating eigenvalues and participation factors for modal voltage stability calculations.

Chapter 2 - Steady-State Voltage Stability Methods and Load Modeling

Voltage stability issues are of major concern in weak power systems. Weak power systems are characterized by long transmission lines and lack of reactive resources to compensate for high reactive power losses. Voltage instability can cause disruption to power supplies in major parts of the power system. Several black-outs worldwide have been attributed to voltage instability. Major black-outs caused by voltage instability include the Tokyo black-out in 1987, the Israeli black-out in 1996, the French black-out in 1978, and the 2003 northeast black-out in the USA. Detailed discussion of these black-outs can be found in [42 - 45]. Many disturbances that can cause black-outs have common properties. Power system limitations which can cause system black-outs are summarized in the next section.

2.1 Voltage Collapse and Power System Black-Out

A voltage collapse which may lead to black-outs is usually caused by voltage instability. Voltage instability occurs when the power system can't provide enough reactive power to system loads in an area causing voltages to decay slowly until reaching zero. In most known voltage collapse black-outs, the cause is usually one contingency or a series of related contingencies that trigger a sequence of switching events which result in voltage black-outs. A voltage black-out takes time to develop. Every part of the power system, from generation to transmission to distribution, can trigger a black-out. Losing a generator situated in an area that needs voltage support could cause large increases in reactive power demand that other generators or voltage support equipment cannot provide. This may result in initiating a voltage stability problem due to high voltage drops in the transmission network. Some common factors that may lead to voltage black-outs, system reactive power limitations and control and protection scheme limitations are discussed in the following sections.

2.1.1 Reactive Power System Limitation Cases

In August 4, 1982, lack of reactive power resources caused the power system of Belgium to collapse (voltage black-out). The collapse was initiated due to having most of the online generation units operating at their maximum reactive power limits. Very few generators were

online at the time due to low load periods which made it economical to only a few generators to serve the load. With fewer generators online, the generators serving the load were operating close to their maximum reactive power limits. When a disturbance occurred which caused one of the available generators to go off line, the surrounding area load was exposed to a lack of reactive power because the other generators were operating at their maximum field current limits. Due to reactive power demand not being met by the generators, the voltages across the Belgium power system started declining, and several generators started tripping creating an island that separated the Belgium system from the European transmission network.

Lack of reactive power resources was also the cause of other voltage collapses worldwide. The 1979 disturbance in New Zealand, loss of the generation from the only unit in the southern part of the country caused a slow voltage decline in that area. This continued to a point where synchronizing a new unit to replace the tripped one was impossible because voltages had declined to very low levels.

Lack of reactive power resources was also to blame for several New York City black-outs. In 1977 a New York disturbance of power was due to lack of reactive resources after two major transmission lines tripped because of system overloads [42]. The New York City Black-out of 1977 was localized to New York City and the immediate surroundings. The 1977 black-out was initiated when a lightning strike caused two 345 kV transmission lines to trip and an immediate loss of power from a 900 MW nuclear plant. Failure to start fast-start generation to replace power lost from the nuclear plant resulted in tripping the overloaded lines and a black-out occurred. The 2003 North East black-out caused the lights to go off in New York City due to lack of generation reactive power resources after tripping generation units in Ohio [44].

Sometimes a voltage collapse can occur due to lack of system reactive resources during a period where a drop of wind generation causes the system to become voltage unstable. This happened on February 26 2008 within the Electric Reliability Council of Texas (ERCOT) service area [46]. A decrease in wind generation in west Texas occurred simultaneously with an evening increase in electric demand. The grid frequency was negatively impacted when wind generation within the ERCOT area fell from 1,700 megawatts to 300 MW. The grid frequency also decreased due to an unexpected load increase from 31,200 MW to 35,612 MW. Lack of generation resources to meet the increased demand of load caused by the rapid decrease of wind generation within the ERCOT area caused system operators to curtail system loads by

interrupting power to large industrial power consumers for a short period of time. About 1,100 megawatts of load was interrupted within 10 minutes to maintain generation and load balance. This event lasted for three hours and voltage collapse was avoided by using system controls to decrease the demand and maintain stability.

Tokyo suffered from voltage black-out back in July of 1987 due to lack of reactive power resources [43]. During the hot summer day, system demand increased rapidly and the available reactive power resources like shunt capacitors were not enough to maintain proper voltages on the 500 kV system. After 15 to 20 minutes, the voltage started decaying to low values that the system protection relays disconnected parts of Tokyo's system to shed about 8,000 MW of load and maintain voltage stability.

2.1.2 Control and Protection Scheme Limitation Cases

Control systems can trigger black-outs due to error in reading system loading data, as was the case in the North East 2003 black-out [44]. On August 14 2003, a 3,500 MW power surge (towards Ontario, Canada) affected the transmission grid. Temperature in the northeast part of the USA and the southeast part of Canada soared to above 100 degree Fahrenheit. This high temperature caused system demand to increase due to the increase in air conditioner loads. An extremely high power demand and a sudden loss of a large generation unit in Ohio caused the system to overload high voltage transmission lines. The first of several 345 kV overhead transmission lines in northeast Ohio failed due to excessive sags and came in contact with a tree. System operators did not react to these cascading high voltage transmission line trips due to a software error which disabled their alarm system. The software error was caused by a bug in the power system control room alarm system which prevented system operating personnel from observing in real time any power system changes. The lack of alarms caused system operators to ignore tripping of several major 345 kV transmission lines. Voltage black-out occurred when the number of transmission lines tripped was large, and the system could not transport generated power from the plants to the load centers. Lack of generation due to lack of transmission lines caused voltages across the Northeast to drop below 0.75 p.u. at which point reactive power was insufficient to recover voltages across the system.

2.2 Definition of Voltage Stability and Voltage Collapse

Voltage stability definition is difficult since voltage stability means different things to different people [46] and [47]. Although voltage stability can be defined differently, all definitions consider system status, time frames (which varies from around a second to several tens of minutes), types of disturbance, the action of voltage control equipment, generator reactive power capabilities and reactive power control limits etc. The difference in definitions is due to the different approaches to the voltage instability phenomena. Voltage stability as described by [46] and [47] is the ability of a power system to maintain acceptable voltages at all buses in the power system under normal and contingency conditions. When voltage drops below a predetermined acceptable value, reactive power resources, including generators, try to provide the necessary reactive power to bring voltages to an acceptable level. When system equipment cannot meet the reactive power demand, the system may experience a progressive uncontrolled voltage decline and the system becomes voltage unstable.

Voltage collapse is the process by which the sequence of events accompanying voltage instability leads to a low unacceptable voltage profile *in a significant part* of the power system [47]. If the post-contingency voltage level in an area of the system becomes uncontrollable, then the power system reaches the collapse point where any additional reactive resources will drive the voltages lower. In reference [47], a typical voltage collapse scenario is described. Voltage collapse takes time to build. Systems usually reach the collapse point after a series of events during abnormal operating conditions with large generation units near load centers being out of service or operated at their maximum reactive power capabilities. Figure 2.1 presents a flow chart of events typically seen in a voltage collapse scenario.

Voltage stability can be classified into two categories: large-disturbance voltage stability and small-disturbance voltage stability. For systems to be classified as voltage stable under large disturbances, the system is able to control voltages to an acceptable level after a system fault, loss of large load, or loss of generation units. Voltage stability for large-disturbances can be studied using nonlinear time-domain simulations taking into consideration performance of devices such as ULTCs and generator field current limits during and after the large-disturbance. A gradual change in load demand or generation resources can be classified as a small-disturbance and may also cause voltage stability problems. The time scale for a voltage collapse to develop may vary from less than a second to several tens of minutes or even hours.

Voltage collapse analysis depends on the time it requires for an area of voltage decline to develop. Figure 2.2 shows the overlapping of the power system device actions during a voltage decline lasting 0.1 second to several minutes. The actions of load/power transfer increases, generators excitation limitations, generation change/AGC unit limitations, and behavior of on-load tap changers are often studied in steady-state voltage stability methods. When voltage stability is due to slow-development of low voltages, voltage stability can be studied using steady-state simulations at a given operating point.

Figure 2.1 Typical Scenario of Voltage Collapse

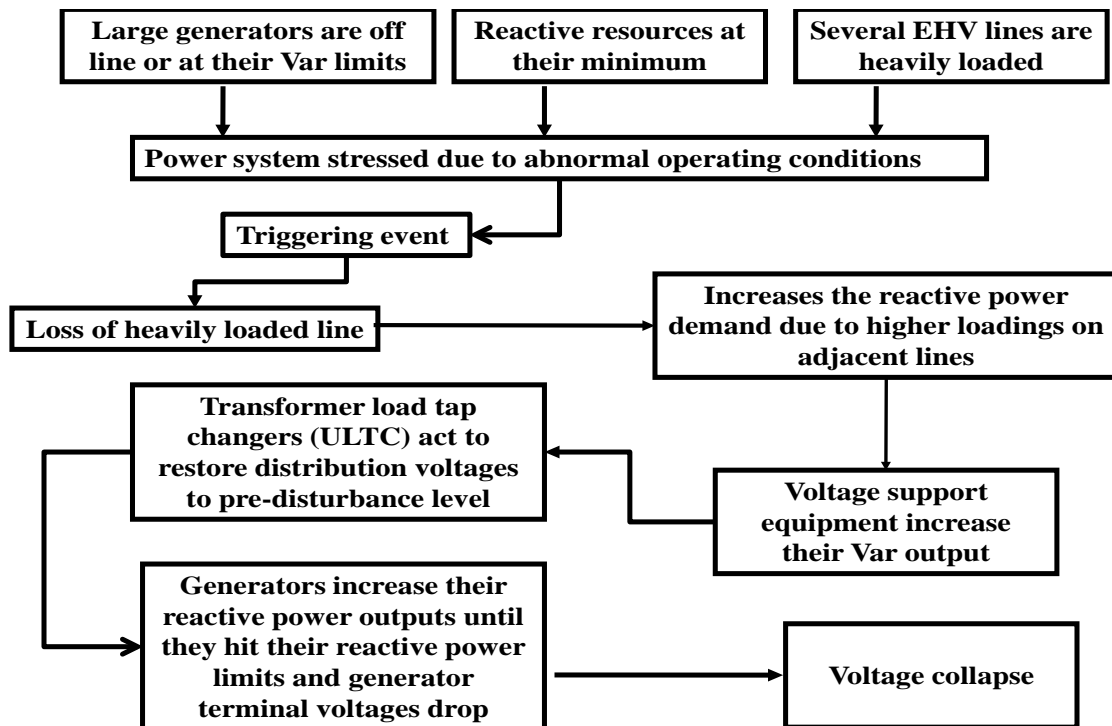
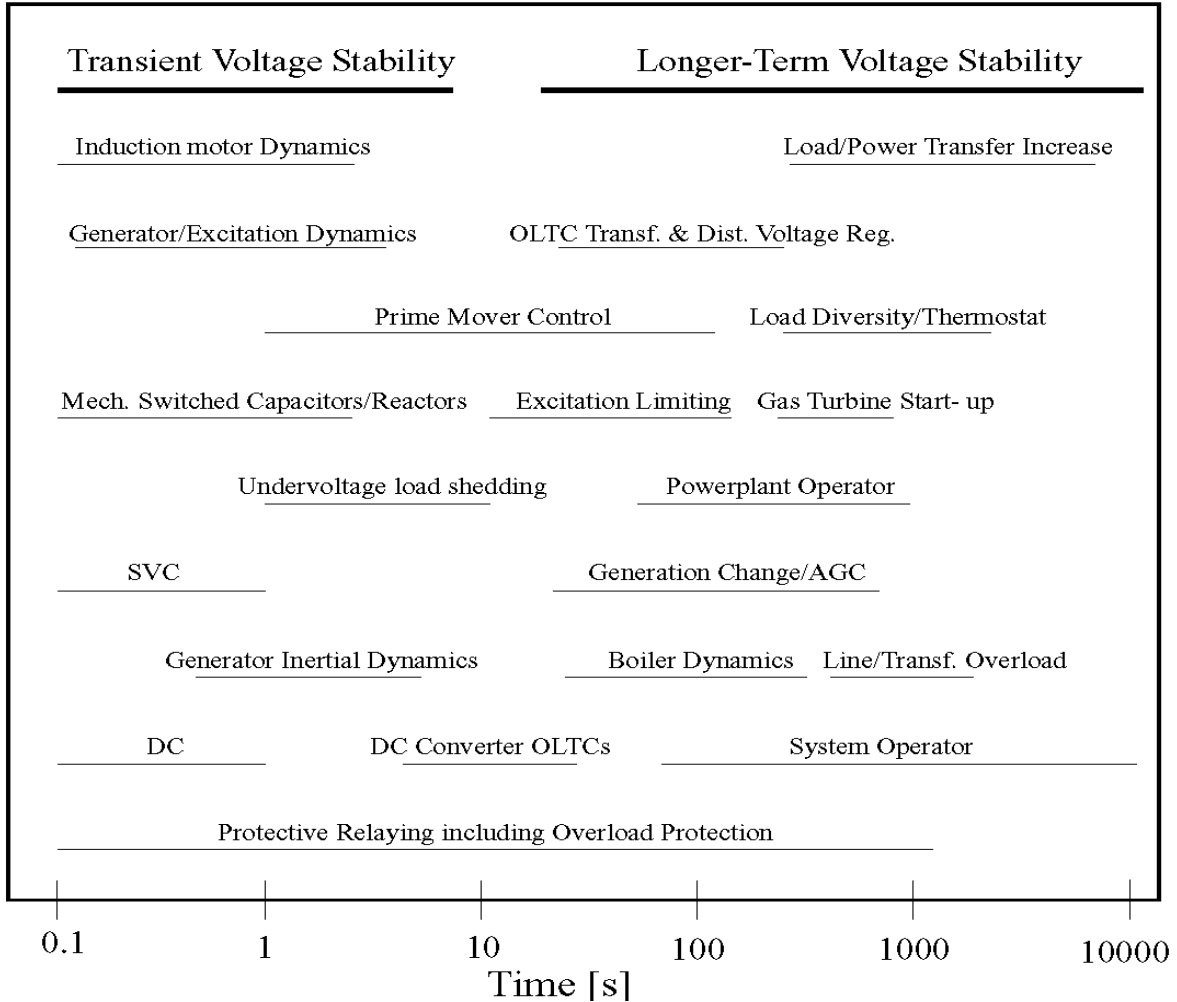


Figure 2.2 Voltage Stability Time Response [84]



2.3 Steady-State Voltage Stability Methods

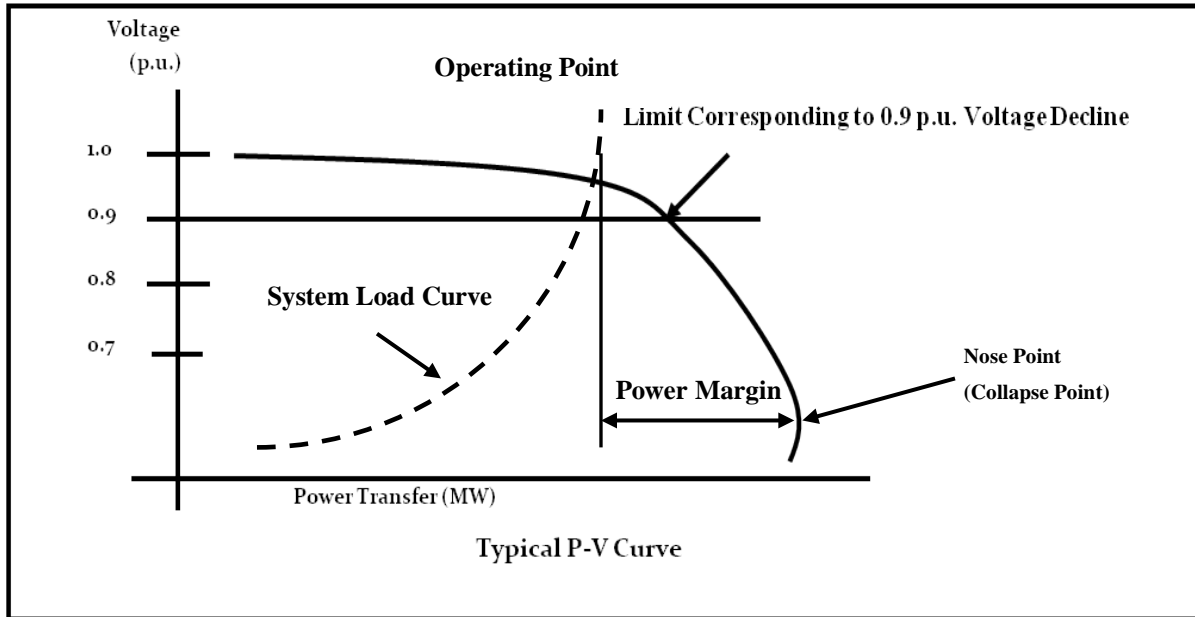
The ability of power systems to stay voltage stable during stressed conditions can be measured using steady-state voltage stability analytical methods. A number of steady-state voltage stability methods have been developed in the literature [46, 47, 48 – 50]. A brief discussion of the most popular steady-state voltage stability methods is discussed in the following sections.

2.3.1 The P-V Curve Method

The P-V curve method is used for measuring the active power vs. voltage relationship at a bus in a power system [46]. Figure 2.3 is an illustration of a typical P-V curve. The real power at a certain bus in the power system is shown on the horizontal axis and the bus voltage “V” is

shown on the vertical axis. The point where load real power intersects the P-V curve is called the operating point at the load bus.

Figure 2.3 P-V Curve Method



The maximum amount of power that can be sent to the receiving end is limited to a maximum power transfer capability indicated by the nose of the P-V curve. At the nose point, or sometimes referred to as the collapse point, the derivative of real power received with respect to the receiving end voltage is equal to zero. The horizontal axis can also be an indication of a power transfer limits. Figure 2.4 shows a simple three phase equivalent power system. The power-voltage relationship can be written as shown in the following equation [46] and [47].

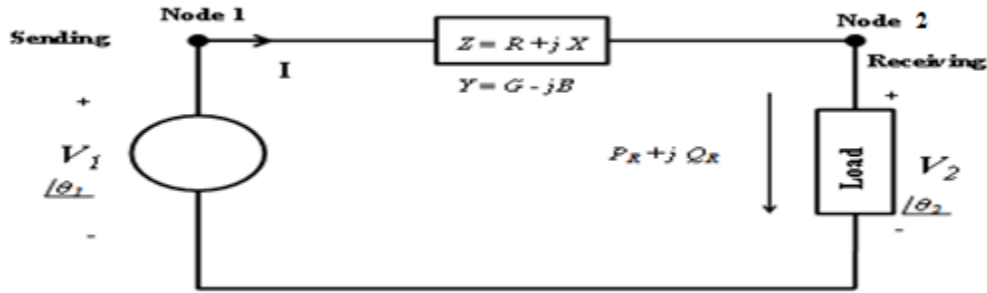
$$V_2 = \sqrt{a \pm \sqrt{a^2 - b}} \quad (2.1)$$

where,

$$a = \frac{V_1}{2} - R P_R - X Q_R$$

$$b = (P_R^2 + Q_R^2)(R + jX)$$

Figure 2.4 Single Phase Equivalent of Three Phase Power System



The collapse point, where maximum power is transferred from the sending end to the receiving end, can be calculated from Equation (2.1) by setting the derivative of P with respect to V_2 to zero ($\frac{dP}{dV} = 0$). If the power transfer to the load exceeds the collapse point transfer power, the receiving end voltage will decline uncontrollably and the system will become voltage unstable. At any operating point, the distance between that operating point and the collapse point is referred to as the power stability margin. When systems are evaluated for voltage stability margins during power transfers, some power margin needs to be reserved to accommodate for unexpected system changes.

2.3.2 The Q-V Curve Method

The Q-V method has an advantage over the P-V method. Standard power flow models will diverge when trying to solve near or below the voltage collapse point using the P-V curve method but they will reach a steady-state solution around the collapse point of Q-V curves [46, 47]. The Q-V curve method uses a fictitious synchronous condenser (a synchronous generator with $P_{generator} = 0$ and wide limits of reactive power) at the bus where the Q-V curves are to be generated [47]. Q-V curves are generated at any bus by setting a desired bus voltage magnitude and solving the power flow to the desired voltage value. The amount of reactive power generated by the condenser at the bus is the required reactive power to hold the voltage at the desired value. This process is repeated for a range of voltages and a Q-V curve at the bus can be plotted. For the simplified system shown in Figure 2.4 the following equations can be used to obtain Q-V curve at the receiving end.

$$P = V_1 V_2 B \sin \theta_{12} \quad (2.2)$$

$$Q = -V_2^2 B + V_1 V_2 B \sin \theta_{12} \quad (2.3)$$

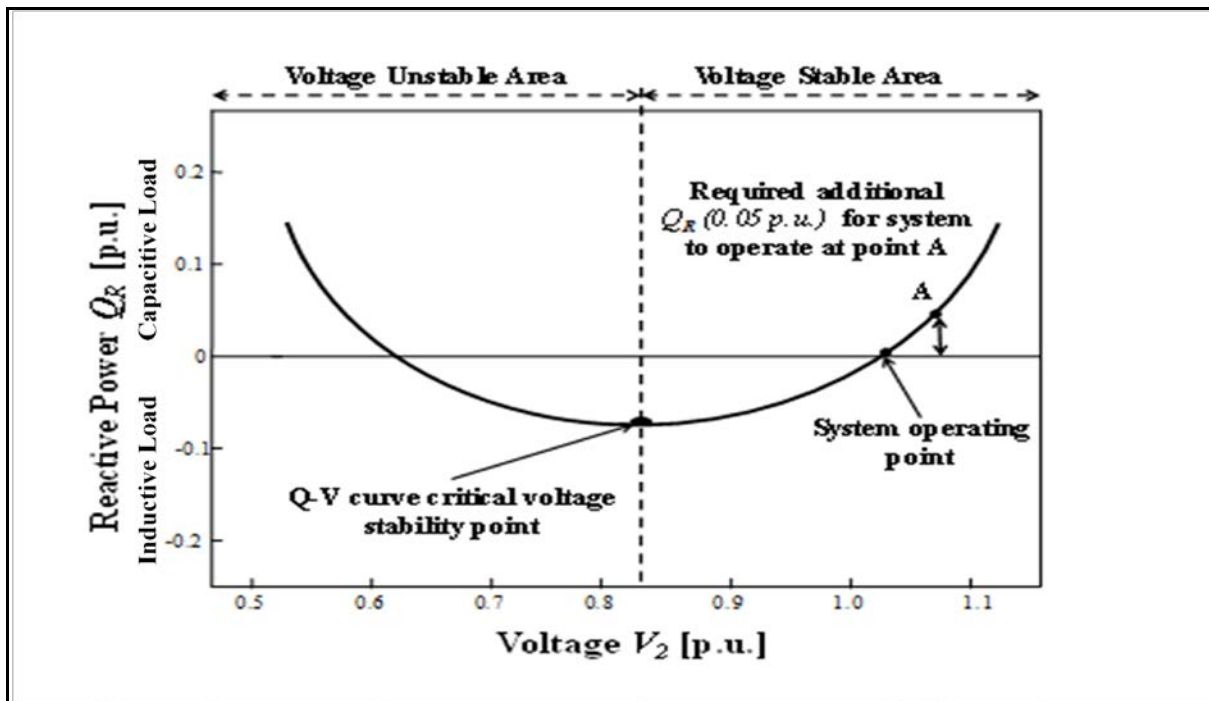
where,

$$\theta_{12} = \theta_1 - \theta_2$$

We assume V_1 magnitude is equal to 1.0, and for a given value of power transfer (P_R) and V_2 magnitude, compute θ_{12} from Equation (2.2) and then Q_R from Equation (2.3). This process is repeated for various values of V_2 to obtain a Q-V curve for the specific power transfer P_R .

Figure 2.5 shows a typical Q-V curve plot at the load bus in Figure 2.4. The curve is plotted for a specific system load. The load bus reaches the “0” Mvar point where the magnitude

Figure 2.5 Q-V Curve Method



of the receiving end voltage “ V_2 ” is approximately 1.02 p.u. The figure also shows that for the system to operate at a higher receiving end voltage at point “A” an additional reactive power of approximately 0.05 p.u. must be injected at the receiving end.

The bottom of the Q-V curve point shown in Figure 2.5, where the derivative dQ_R/dV_2 equals zero, represents the voltage stability limit. For stable operation, an increase of reactive

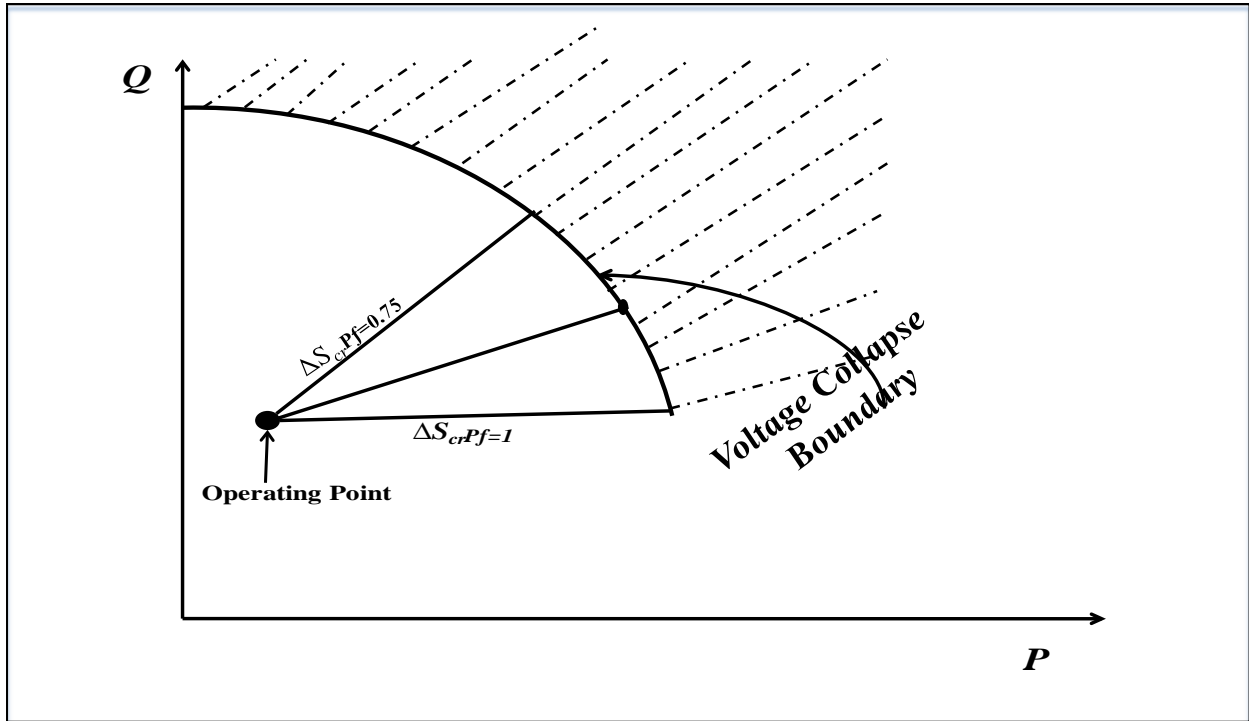
power Q results in an increase in receiving end voltage, that is, operation on the right side of the Q-V curve is stable. For an unstable operation, an increase of reactive power Q results in a decrease in receiving end voltage, i.e., operation on the left side of the Q-V curve. The bottom of the Q-V curve point also represents the largest load reactive power (VAR) increase for stable system [46].

2.3.3 The P-Q Curve Method

The maximum permissible loading of a power system can be determined using the previously mentioned P-V and Q-V curve methods. When the load is increased beyond the maximum loadability, the voltages will decay uncontrollably. These two methods are well known and have been used for many years [46]. However, the load voltage characteristics of the power *system* are not detailed in determining the voltage stability limit using either of these two traditional methods. The P-V curve method is based on changes in system load real power only. The reactive power of the system is often assumed constant while solving a series of power flow cases to relate bus voltages to load within a special region. The Q-V curve method assumes an infinite synchronous condenser with unlimited reactive power capability at a specific bus while solving a series of the power flow cases for specific bus voltages assuming real power of the system stays unchanged. The P-Q method is simply a combination of both the P-V and the Q-V methods. The P-Q curve method solves a series of power flow cases while the change in real and reactive power of the system is included.

The P-Q curve method [24] and [51] is a method in which the apparent power limits are determined by calculating a voltage stability boundary which separates stable from unstable operating points while considering both load dynamics and load power factors as shown in Figure 2.6.

Figure 2.6 P-Q Curve Method



For any given system operating point, the voltage stability margin of the system, with respect to P_{CR} and Q_{CR} , can be determined by calculating the distance from the existing operating point to the voltage stability boundary curve. As shown in Figure 2.6, the direction taken to reach the stability boundary depends on the system power factor. The distance between the operating point and the stability boundary point is called the apparent power margin (ΔS_{cr}). The “ ΔS_{cr} ” value can be used as the maximum limit of load increase that the power system can safely incorporate before reaching the collapse point.

To calculate the system voltage stability boundary, consider the equivalent power system shown in Figure 2.4 with a sending end source transferring power to a load at the receiving end through an equivalent transmission line impedance, Z , and an equivalent shunt capacitance on both ends, Y_c . Using generalized equivalent line constants and the distributed parameter A B C D model, the voltage Equation for the circuit can be written as

$$V_1 = A V_2 + B I_R \quad (2.4)$$

$$I_R = \frac{P_{CR} - jQ_{CR}}{V_2} \quad (2.5)$$

where $A = 1 + Z Y_c$ and $B = Z$. Substituting for I_R in Equation (2.4) results in,

$$V_1 = A V_2 + B \frac{P_{CR} - jQ_{CR}}{V_2} \quad (2.6)$$

For a given system equivalent load of $P_{CR} + jQ_{CR}$ and multiplying Equation (2.6) by V_2 , Equation (2.6) can be written as

$$A V_2^2 + B P_{CR} - j B Q_{CR} - V_1 V_2 = 0 \quad (2.7)$$

A and B can be written in rectangular form as follows

$$A = a_1 + j a_2 \text{ and } B = b_1 + j b_2$$

Substituting for A and B in Equation (2.7) results in

$$c_1 V_2^4 + (c_2 P_{CR} + c_3 Q_{CR} - V_1^2) V_2^2 + c_4 (P_{CR}^2 + Q_{CR}^2) = 0 \quad (2.8)$$

where

$$c_1 = a_1^2 + a_2^2, c_2 = 2(a_1 b_1 + a_2 b_2), c_3 = 2(a_1 b_2 - a_2 b_1) \text{ and } c_4 = b_1^2 + b_2^2$$

To solve Equation (2.8) assume $X = V_2^2$ then re-write the Equation into a quadratic one which can be solved for X and thus V_2

$$c_1 X^2 + (c_2 P_{CR} + c_3 Q_{CR} - V_1^2) X + c_4 (P_{CR}^2 + Q_{CR}^2) = 0 \quad (2.9)$$

Equation (2.9) is in the form of $aX^2 + bX + c = 0$, where $a = c_1$, $b = (c_2 P_{CR} + c_3 Q_{CR} - V_1^2)$, and $c = (P_{CR}^2 + Q_{CR}^2)$, and the magnitude of the receiving end voltage can be found by solving for X and taking the square root of X to find V_2 .

$$V_2 = \sqrt{X} \quad \text{and} \quad V_2 = \sqrt{X} = \frac{-b \pm \sqrt{b^2 - 4ac}}{2a} \quad (2.10)$$

For a given power factor, Equation (2.10) can be used to plot the P-V curve by varying P_{CR} for a given V_1 and a given Q_{CR} . The Q-V curve can also be plotted for a given P_{CR} and V_1 .

Voltage collapse occurs when system load exceeds certain limits. To calculate the voltage stability limits using the P-Q method, system load expressed as $S_L = P_{CR} + jQ_{CR}$ can be increased gradually until the discriminant of (2.9) becomes negative such that there is no real solution to the equation. This amount of load becomes the critical loading for the system. Any load value above the critical value will drive the power system to become voltage unstable.

2.4 Load Models for Voltage Stability Analysis in Power Systems with High Wind Penetration

In analyzing voltage instability, it is necessary to consider the network under various voltage profiles since voltage stability depends on the level of load currents [47, 121]. Power system loads can be classified as constant power like some types of motor loads, constant current, like televisions and clothes dryers, or constant impedance, like large agricultural water pumps. For steady-state voltage stability, loads can be modeled as constant power (voltage independent) when there are enough control devices like ULTCs (transformer Under-Load Tap Changers) which can keep system voltages close to their rated values. However, using constant power loads for voltage stability studies can give misleading results due to the assumption that loads are not sensitive to voltage changes [53]. In voltage stability studies, system voltages experience large variations where load voltage dependency must be taken into account for proper stability evaluations [54].

Voltage instability can be alleviated when the demand is reduced due to lower load values during low voltage periods. When voltage decline results in lower demand due to load

voltage dependency and a reduction in the current flowing results in lower reactive power losses (I^2X), voltage profiles can improve.

In large power systems, actual load types are generally difficult to determine. Actual loads can be very difficult to characterize due to variation in different parts of the power system. For suitable load models for voltage stability studies, load models must be accurate enough to correctly present load behavior when subjected to steady-state voltage variations. To consider voltage variation on load models, loads voltage dependency can be modeled at any bus using the exponential model given below [47].

$$P = P_0 \left(\frac{V}{V_0} \right)^\alpha \tag{2.11}$$

$$Q = Q_0 \left(\frac{V}{V_0} \right)^\beta$$

Where P_0 , Q_0 and V_0 are the initial operating conditions. The exponents α and β are specific to the load type and can be found in [47] and [55]. Table 2.1 shows some constants for α and β for some selected load types.

Table 2.1 Load Types α and β Constants [47] and [55]

Load Type	α	β
Incandescent lamps	1.54	0.00
Room air conditioner	0.50	2.50
Furnace fan	0.08	1.60
Battery charger	2.59	4.06
Electronic florescent	1.00	0.40
Small industrial motors	0.10	0.06
Large industrial motors	0.05	0.50
Conventional florescent	2.07	3.21
Agriculture water pumps	1.40	1.40

There are two empirical approaches to represent loads in the load flow models [56, 57, 58]. The most used power system load model approaches in large power systems are the measurement based load models and the component based load models. In the measurement load model approach, field measurements are taken of load response to sudden step voltage perturbation. These perturbations are caused by capacitor bank switching or changing distribution transformer tap ratios. The data is used to predict load behavior under different voltage levels. The disadvantage of the measurement, approach is that it is only valid for the time of measurement and it can't capture the type of load effect during actual voltage instability when voltages drop below 0.90 p.u. since the measurement approach only drops the bus voltage by 5% to 7%.

The component based load models (composite load models) are more suitable for large power systems when the dominant composite of load at each load bus can be determined. For this approach, each load bus can be composed of different load classes (Residential, Agriculture, Commercial, Industrial etc.). The power system can be divided into load characteristic zones where zone load characteristics are similar. In this approach, capacitor and reactor portions of the loads at each bus must be represented as constant impedance (Z), then the remaining load at each bus is split into Large Motors, Small Motors, Discharge Lighting, Resistive and others. For each load classification (Residential, Agriculture, Commercial and Industrial) a composition is obtained using load surveys in which each load classification is assigned a percentage of each component.

Load component modeling can normally be divided into four categories [52]. The first category is residential loads, which includes but is not limited to houses, apartments, lighting and home appliances, computers, television sets, etc. The second category is commercial loads such as small motors and discharge lighting. The third category is industrial loads which includes manufacturing facilities with large motors, lighting, and small motors, and the last category is Agriculture which includes irrigation and rural residential.

To properly model power system loads using the component based approach, a survey must be conducted for each load bus in the power system to determine the percentage of different load types on each load bus. A simple description of the component approach using the four categories is shown in Figure 2.8. The categorization of load types is based on the percentages of

four basic categories (residential, agricultural, commercial, industrial). Table 2.2 presents typical data which can be used in deriving the overall load model [53, 54].

Figure 2.7 Component Approach Load Model

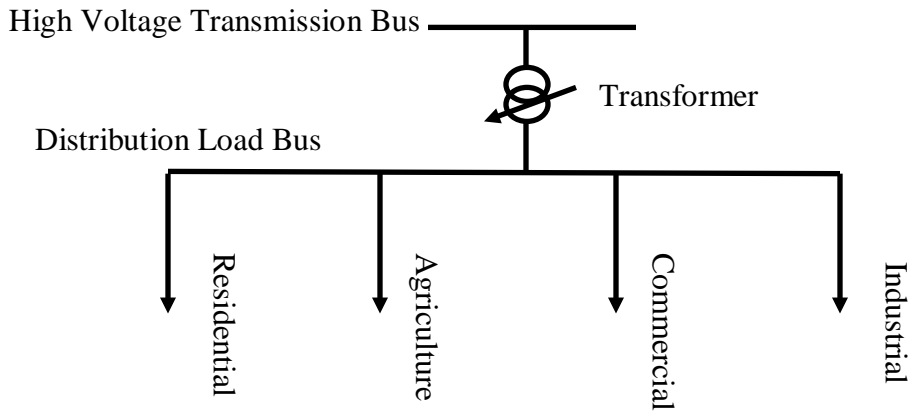


Table 2.2 Typical Load Composition for the Component Load Model [52] and [58]

Load Class	Load Composition (%)			
	Residential	Agriculture	Commercial	Industrial
Resistive	25	19	14	5
Small Motors	75	62	51	20
Large Motors	0	15	0	56
Discharge Lighting	0	4	35	19

For each load category, a system survey must be conducted to determine load mix for each category. A typical load model for a load at a bus can be represented in a polynomial ZIP model [55]. The ZIP model represents three types of loads. The “Z” represents a constant impedance load where the load changes as a square of the voltage change. This type of load will result in significant decrease in load demand during voltage decline periods. The “I” represents a constant current load where the load changes linearly with the voltage change. These loads also results in decreasing load demand during voltage decline periods. The “P” represents a constant power load where the load is not impacted by voltage changes and will not result in any

decreases in load demand during voltage decline periods. Equation (2.12) is a special case of the more general Equation (2.11).

$$P = P_0 \left[p_3 \left(\frac{V}{V_0} \right)^2 + p_2 \frac{V}{V_0} + p_1 \right] \quad Q = Q_0 \left[q_3 \left(\frac{V}{V_0} \right)^2 + q_2 \frac{V}{V_0} + q_1 \right] \quad (2.12)$$

In Equation 2.12, P_0 , Q_0 and V_0 are the nominal operating conditions, p_1 , p_2 , p_3 , q_1 , q_2 and q_3 are constant multiplying factors such that $p_1 + p_2 + p_3 = 1.0$ and $q_1 + q_2 + q_3 = 1.0$. Table 2.3 shows multiplying factors for each load mix type, and Table 2.4 shows power system load classifications based on their load type.

Table 2.3 Load Mixes Multiplying Factors

Load Mix Type	p_1	p_2	p_3	q_1	q_2	q_3	Effect on Voltage Instability
Constant Impedance (Z)	1	0	0	1	0	0	Good
Constant Current (I)	0	1	0	0	1	0	OK
Constant Power (P)	0	0	1	0	0	1	Bad

Table 2.4 Classifications of Power System Loads [52, 53]

Load Type	% Constant P	% Constant Z	% Constant I
Resistance heaters, water heaters, ranges	0	50	50
Heat pumps, air conditioning, refrigeration	15-35	20-40	45
Clothes dryers	0	0	100
Televisions	0	0	100
Incandescent lighting	45	35	20
Fluorescent lighting	0	50	50
Pumps, fans, small motors	40	40	20
Arc furnace	0	30	70
Large industrial motors	60	40	0
Large agricultural water pumps	0	75	25
Power plant auxiliaries	40	40	20

2.4.1 Load Modeling Impact on Power System Voltage Stability

Despite using survey data for obtaining the component load models, load models are not certain. The characteristics of actual loads make it impossible to eliminate uncertainties. Load component models are uncertain due to various reasons. Motor protections and controls which may disconnect or connect loads, voltage control equipment installed in the distribution system like voltage regulators and shunt capacitors which may result in variations in load voltage response, and variation of the nature of the load over time are some examples of causes for load model uncertainties.

To deal with the load component uncertainties, three options are considered. The first option is to assume all load categories are of the constant power type. This is the most conservative option when it comes to voltage stability studies, but it is recommended when there is a lack of available load type survey data or when a no-risk voltage stability measure is required. A second option is to use some load type mix based on previous system experiences and assumptions. However, voltage stability limits found using the second method should be followed by a sensitivity analysis in order to assess the effect of load type variations on system stability limits. A third option developed in this dissertation is to use the P-Q voltage stability method to create a buffer which can prevent the system from becoming voltage unstable due to model type uncertainties.

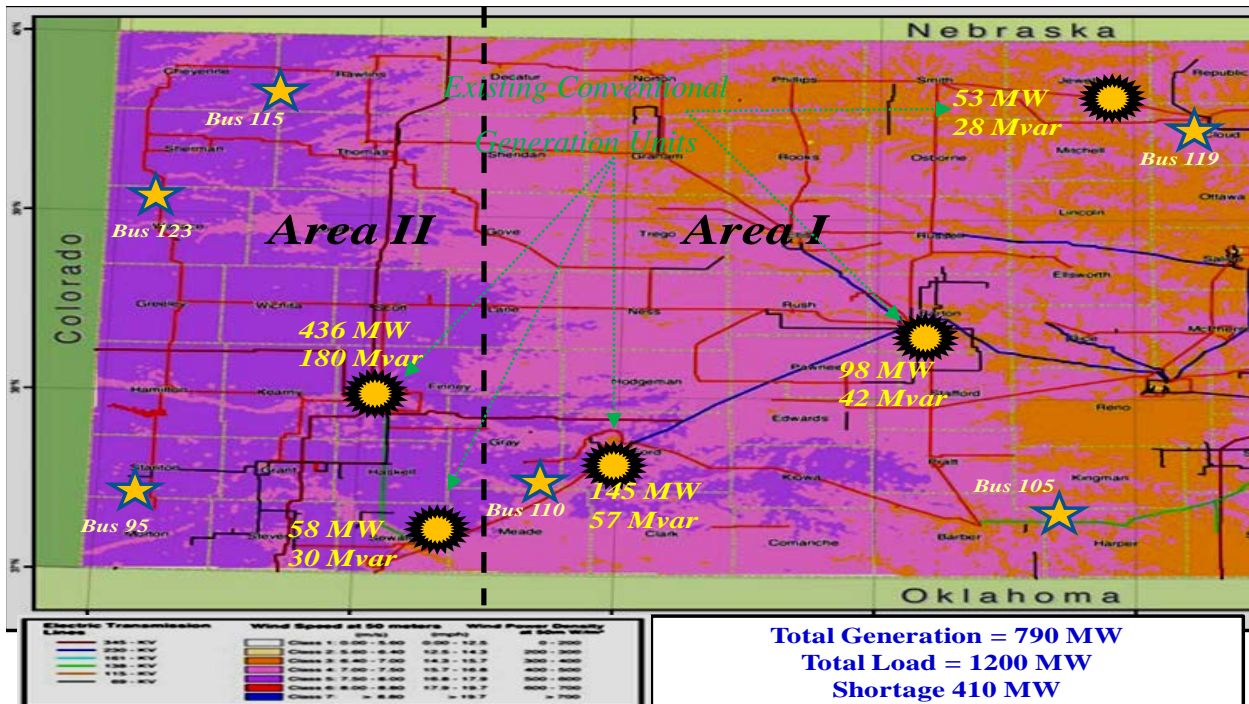
2.4.2 Case Studies for Load Modeling Impact on Power System Voltage Stability

In this dissertation the three steady-state voltage stability evaluation methods are applied to a real large power system to determine the impact of load model types. The western Kansas power system is used for this purpose. The western Kansas power system consists of two major areas as shown in Figure 2.8. The vertical black dotted line shown in the figure defines the boundaries between the two areas. Area I is a 156 bus system connected to the Eastern Electric Grid (EEG) with three transmission voltage levels, specifically 115 kV, 138 kV and 230 kV. Area II is a 144 bus system connected to the Eastern Electric Grid (EEG) with three transmission voltage levels, specifically 69 kV, 115 kV and 345 kV. The total miles of transmission lines serving loads in both areas exceeds 2,219 miles with 222 miles of 345 kV, 193 miles of 230 kV,

90 miles of 138 kV and 1,714 miles of 115 kV. The western Kansas areas I and II are part of the Southwest Power Pool (SPP) [26]. SPP is a Regional Transmission Organization (RTO), mandated by the Federal Energy Regulatory Corporation's (FERC) [59].

The western Kansas Area I, 2010 peak July load was 541 MW. This load was served from two gas steam units, two gas combustion turbine (CT) units and one coal steam unit. The Fort Dodge unit rated at 146.6 MW and the Great Bend unit rated at 98.7 MW serve the bulk of the western Kansas Area I loads. Several gas turbine units and a coal steam unit serve the balance of the load. 2010 peak July load for the western Kansas Area II was 659 MW. This load was served from a coal power plant located in Holcomb, Kansas. The Holcomb generation unit is rated for 387 MW (360 MW net maximum output power) which serves the bulk of western Kansas Area II loads. Several gas generation units, with the largest gas units located in the City of Garden City, Kansas, serve the balance of the load. A one-line diagram of the western Kansas power system and system configuration data are included in Appendix B.

Figure 2.8 Western Kansas Power System (Areas I & II)



2.4.2.1 Stability Limit Calculations for Constant Power (P), Constant Current (I), and Constant Impedance (Z) Load Types Using Different Stability Analysis Methods

In power systems, a composite load consisting of different proportions of constant power, constant current, and constant impedance loads represents the load mix for each load bus. The voltage stability limits calculated using P-V curve, Q-V curve and P-Q curve methods are all impacted by the components of each composite load. All three voltage stability methods have been applied to the western Kansas power system (Area I) to calculate voltage stability limits using the three load types (constant power (P), constant current (I) and constant impedance (Z)).

A composite load consisting of different percentages of load type components (ZIP) is considered a mixed load type. From Equation (2.12) and assuming $V_0 = 1$ p.u., we can represent a mix of load components by (2.13) and (2.14).

$$P_{CR} = P_o (p_1 + p_2 V_2 + p_3 V_2^2) \quad (2.13)$$

$$Q_{CR} = Q_o (q_1 + q_2 V_2 + q_3 V_2^2) \quad (2.14)$$

Here p_1, p_2, p_3 represent constant power (P), constant current (I) and constant impedance (Z) real power load type component percentages respectively, with $p_1 + p_2 + p_3 = 1.0$; q_1, q_2, q_3 represent constant power (P), constant current (I) and constant impedance (Z) reactive power load type component percentages respectively, with $q_1 + q_2 + q_3 = 1.0$. Receiving end voltage from Equation (2.9) with the mixed load from (2.13) and (2.14) becomes

$$\begin{aligned} c_1 V_2^4 + ((c_2 P_o (p_1 + p_2 V_2 + p_3 V_2^2)) + (c_3 (Q_o (q_1 + q_2 V_2 + q_3 V_2^2)) V_2^2) - V_1^2) V_2^2 \\ + c_4 \left((P_o (p_1 + p_2 V_2 + p_3 V_2^2))^2 + (Q_o (q_1 + q_2 V_2 + q_3 V_2^2))^2 \right) = 0 \end{aligned} \quad (2.15)$$

The condition of voltage instability in Equation (2.15) occurs when the discriminant ($b^2 - 4ac$) = 0 as shown previously in Equation (2.10). The solution for (2.15) is presented in [51]. For any given value of load real power P_{CR} , a corresponding reactive power Q_{CR} can be found.

Equation (2.15) shows that the stability boundary depends on several factors besides load mix percentages. Equation (2.15) also shows that transmission system equivalent impedance and capacitance (parameters c_1 , c_2 , c_3 , and c_4 included in Equation (2.8)) can also affect stability limits.

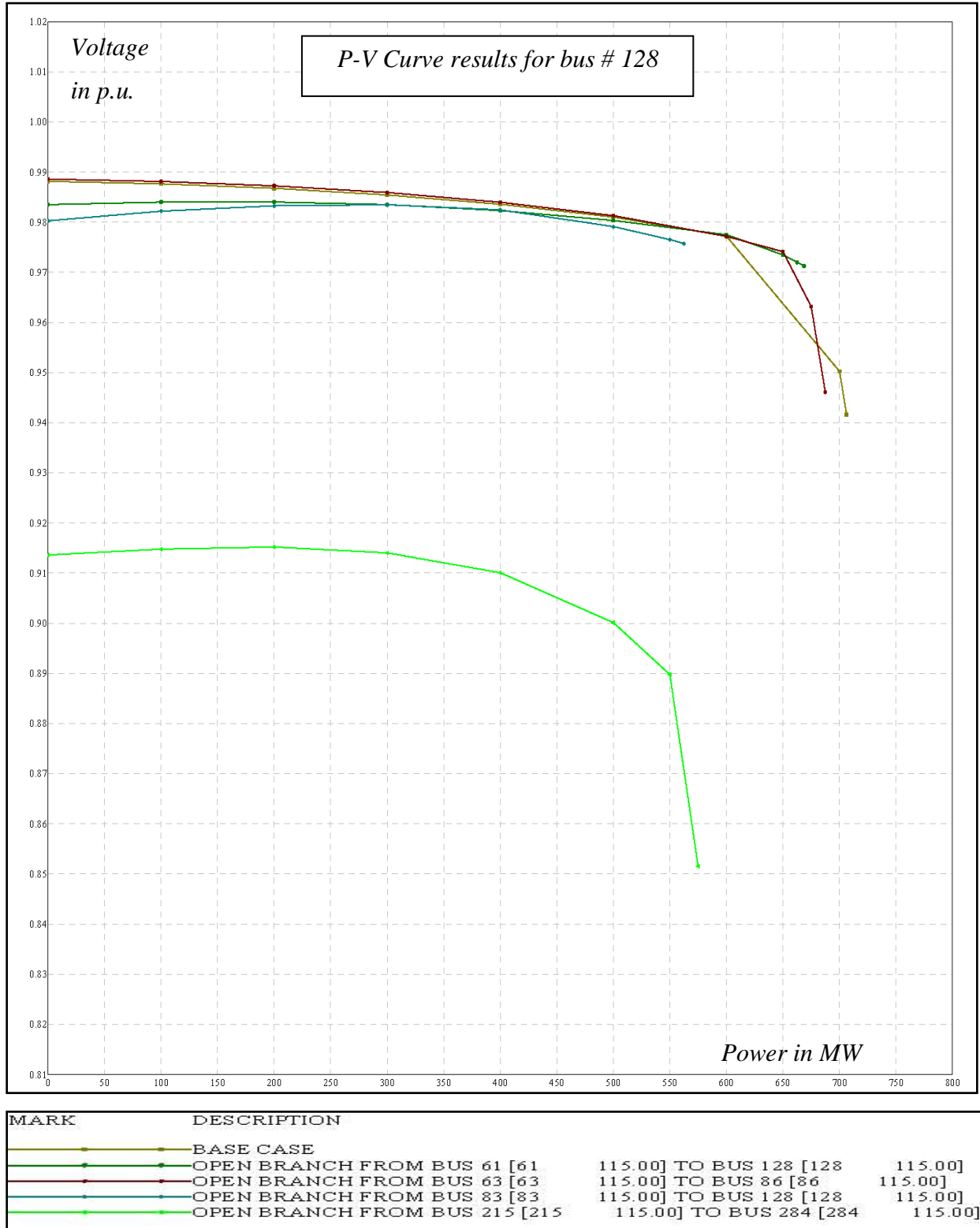
2.4.2.1.1 Stability Limit Calculations Using the P-V Curve Method for Calculating Voltage Stability Limits with Load Type Sensitivity

The P-V curve method was applied to the western Kansas Area I and II power system using the ZIP load modeling. Several 115 kV lines connect both areas. Applying the P-V curve method to the power system resulted in a maximum of 250 MW of power transfer from Area I to Area II in the western Kansas Power system assuming western Kansas load is only a constant power (P) load type. Curves are made for contingencies involving the outage of one major system component at a time (n-1 contingencies). Table 2.5 shows results of applying the P-V curve method for the base case with the associated most limiting contingencies in the power system. Actual P-V curve plots for each case are shown in Figure 2.9. Applying the P-V curve method to the western Kansas power system using constant current (I) and constant impedance (Z) load types are shown in Appendix C.

Table 2.5 Maximum Power Transfer Calculated Using the P-V Curve Method for Constant Power (P) Load Type Applied to the Western Kansas Power System (Area I to Area II Transfer)

P-V Curve Contingencies (Constant Power (P) Load Type)		
CON#	Max MW	Contingency Description
Base Case	706	Base Case
1	668	Open Branch from Bus 61 to Bus 128
2	687	Open Branch from Bus 63 to Bus 86
3	546	Open Branch from Bus 83 to Bus 128
4	575	Open Branch from Bus 215 to Bus 284

Figure 2.9 P-V Curves for Constant Power (P) Load Type in the Western Kansas Power System (Area I to Area II Transfer)



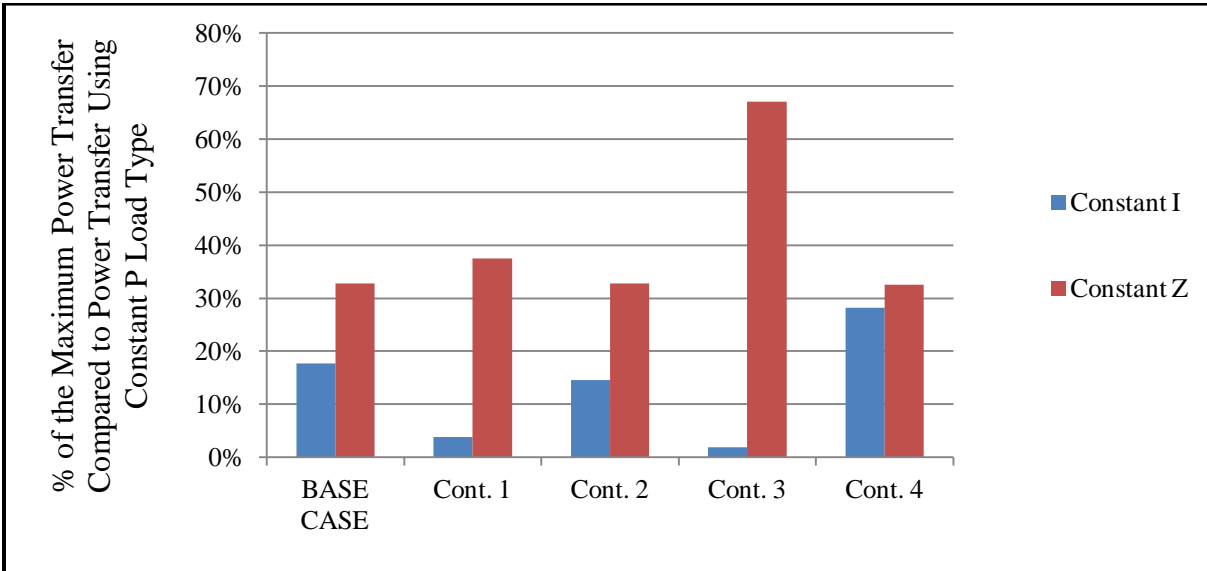
Due to lack of dependency on voltage level changes, the constant power (P) load type resulted in the lowest power transfers from Area I to Area II of the western Kansas power system as shown in Table 2.6. For normal operating conditions (base case), the maximum power transfer between the two areas was 938 MW when system loads are modeled as constant impedance (Z). Constant impedance load (Z) models also resulted in the highest power transfer between the two areas in the base case and for all power system contingencies considered. For the constant power (P) and constant impedance (Z) cases, the loss of the 115 kV transmission line between bus 215 and bus 284 resulted in the lowest power transfer between the two western Kansas areas. For the constant current (I) load type, the loss of the 115 kV transmission line between bus 83 and bus 128 resulted in the lowest power transfer between the two western Kansas areas.

For normal operating conditions, the “Z” load type resulted in 32.86% increase in maximum power transfer when compared to the constant power (P) load type. The constant current (I) load type resulted in 17.7% increase above the constant power (P) load type. A summary of maximum power transfer from western Kansas Area I to Area II as a percent of the constant power (P) maximum transfer limits are shown in Figure 2.10.

Table 2.6 Comparison of P-V Curves Based on Maximum Power Transfer for Voltage Sensitive Loads (ZIP) in the Western Kansas Power System (Area I)

Comparison of P-V Curves - Maximum Power Transfer for Voltage Sensitive Loads				
Case #	Contingency Descriptions	Load Type		
		Constant P	Constant I	Constant Z
	DESCRIPTION	MW		
Base Case	Base Case	706	831	938
Cont. 1	Open Branch from Bus 61 to Bus 128	668	694	919
Cont. 2	Open Branch from Bus 63 to Bus 86	687	788	913
Cont. 3	Open Branch from Bus 83 to Bus 128	546	556	913
Cont. 4	Open Branch from Bus 215 to Bus 284	575	738	763

Figure 2.10 Maximum Power Transfer from Area I to Area II in the Western Kansas Power System Using Constant Current (I) & Constant Impedance (Z) Load Types as a Percent of the Constant Power (P) Load Type



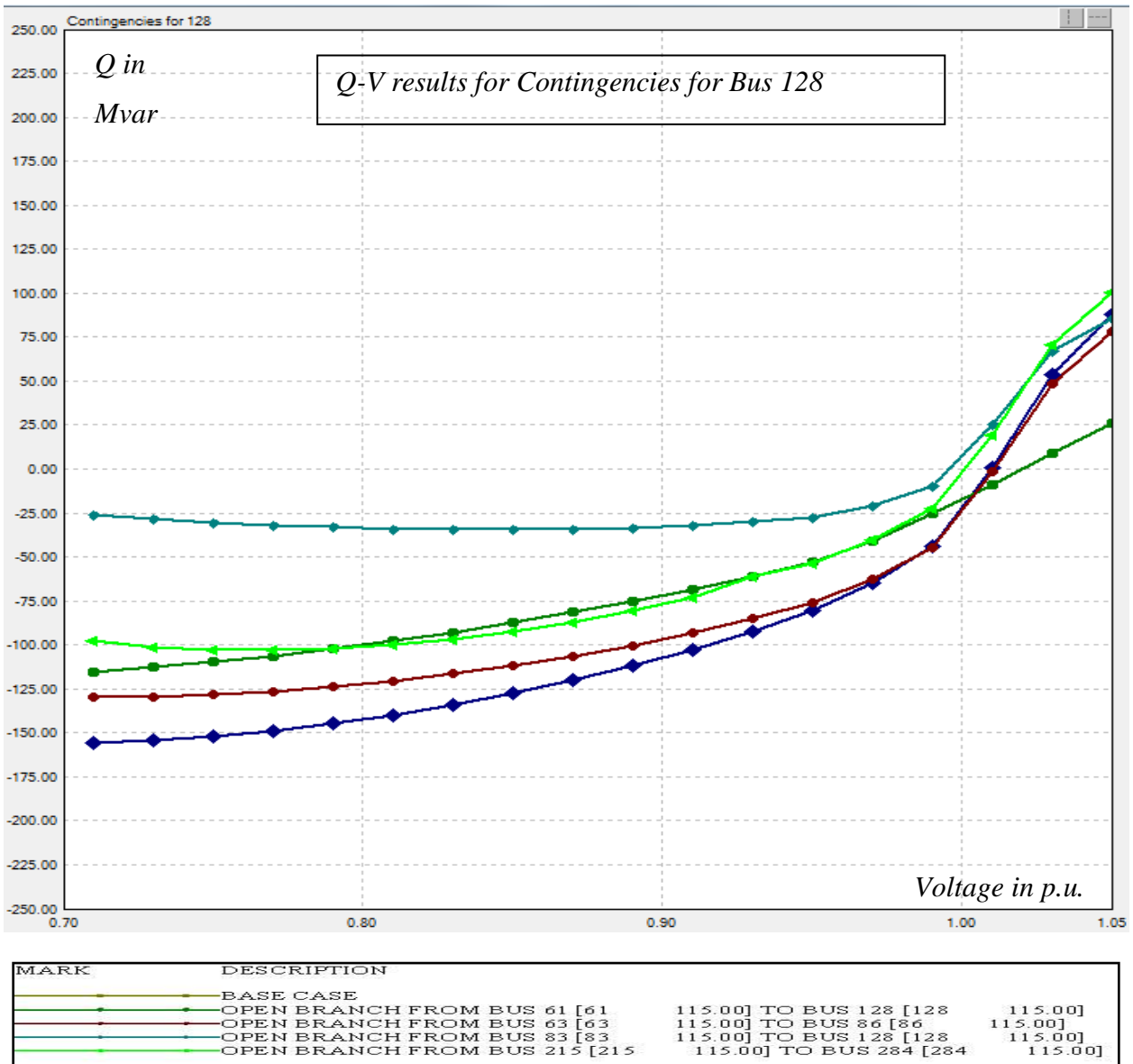
2.4.2.1.2 Stability Limit Calculations Using the Q-V Curve Method for Calculating Voltage Stability Limits with Load Type Sensitivity

The Q-V curve method application for stability limit calculations using only constant power load type resulted in a 34.36 Mvar of voltage stability margin in Area I limited by contingency 3 as shown in Table 2.7. This means only 34.36 Mvar of load could be added at this bus before the system goes unstable for this case. The actual Q-V curve plots for each case are shown in Figure 2.11.

Table 2.7 Voltage Stability Margins (VSMs) Obtained Using Q-V Curve Method for Constant Power (P) Load Type Applied to the Western Kansas Power System (Area I)

Q-V Contingencies (Constant Power (P) Load Type)			
CON#	Min MVAR	Max MVAR	DESCRIPTION
Base Case	-155.782	87.722	Base Case
1	-115.325	26.068	Open Branch from Bus 61 to Bus 128
2	-129.614	78.339	Open Branch from Bus 63 to Bus 86
3	-34.360	85.418	Open Branch from Bus 83 to Bus 128
4	-102.821	100.452	Open Branch from Bus 215 to Bus 284

Figure 2.11 Curves for Voltage Stability Margins Using Q-V Curve Method for Constant Power (P) Load Type Applied to the Western Kansas Power System (Area I)



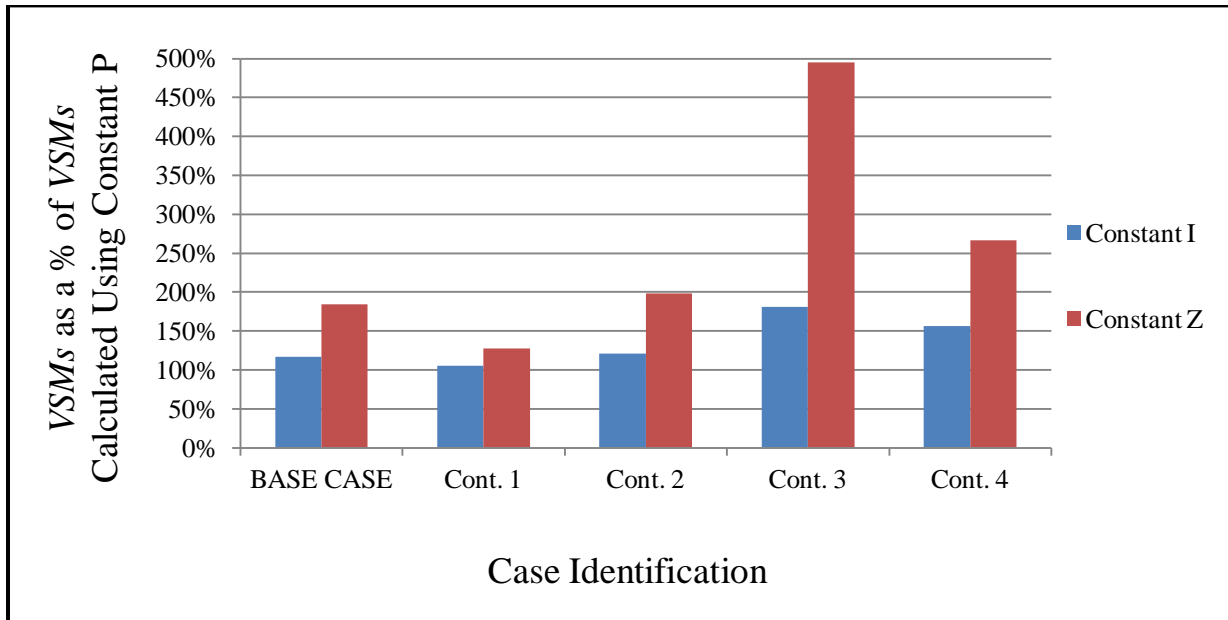
For normal operating conditions (base case), the *VSM* of 287 Mvar, obtained when system loads are modeled as constant impedance (Z), was the highest margin found. Under contingency conditions, the constant power (P), constant impedance (Z) and constant current (I) load types had their lowest *VSMs* when the 115 kV transmission line between bus 83 and bus 128 is out of service. The lowest *VSMs* were obtained when the system load was modeled as a constant power (P). Table 2.8 list *VSMs* calculated for different load types in the western Kansas

system, and Figure 2.12 is a graphical representation of *VSMs* calculated for constant current (I) and constant impedance (Z) as a percent of *VSMs* obtained using only constant power (P) load type.

Table 2.8 Comparison of Q-V Curves Based on Maximum Power Transfer for Voltage Sensitive Loads (ZIP) in the Western Kansas Power System (Area I)

Comparison of Q-V Curves - <i>VSMs</i> for Voltage Sensitive Loads				
Case #	Contingency Descriptions	Load Type		
	DESCRIPTION	Constant P	Constant I	Constant Z
		Magnitude of <i>VSMs</i> in Mvar		
Base Case	Base Case	156	182	287
Cont. 1	Open Branch from Bus 61 to Bus 128	115	121	147
Cont. 2	Open Branch from Bus 63 to Bus 86	130	156	258
Cont. 3	Open Branch from Bus 83 to Bus 128	34	62	170
Cont. 4	Open Branch from Bus 215 to Bus 284	103	161	274

Figure 2.12 *VSMs* Obtained Using Constant Current (I) & Constant Impedance (Z) Load Types as a Percent of *VSMs* Obtained Using Constant Power (P) Load Type in Area I of the Western Kansas Power System



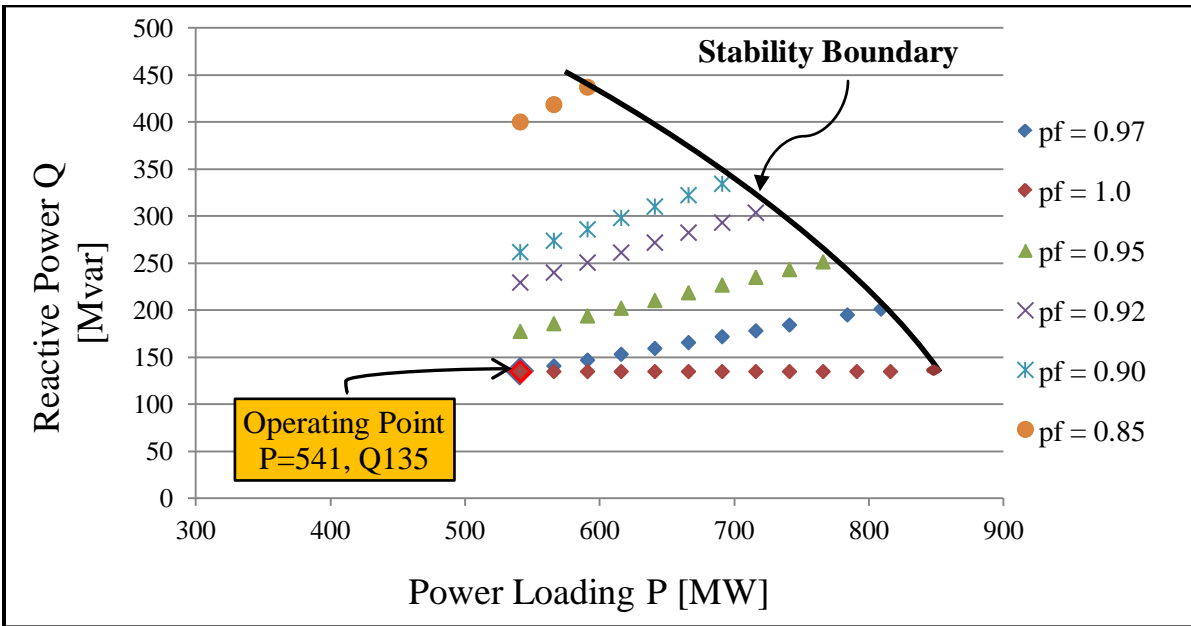
2.4.2.1.3 Stability Limit Calculations Using the P-Q Curve Method for Calculating Stability Limits with Load Type Sensitivity

The P-Q curve method can be used to calculate the apparent power margin (ΔS_{cr}) of the system in terms of P and Q for any given system operating point. The distance from the operating point to the voltage stability boundary curve is the apparent power margin (ΔS_{cr}) at a certain load power factor. Results of the analysis applied to the western Kansas power system Area I indicate that 231 MVA of additional load at 0.97 lagging power factor ($\Delta S_{crpf=0.97}$) can be added to the western Kansas power system before reaching the collapse point. The loads in Area II are also changed in equal percentage as Area I, assuming that the load will grow in both areas at the same level. Table 2.9 shows the stability limits calculated using the P-Q method for a range of power factors assuming all loads are 100% constant power (P) type. All the maximum P and Q values shown in the table were limited by Contingency 3 (opening the branch between bus 83 and bus 128). Any load increases above these values will result in an unstable system. Figure 2.13 shows the stability boundary curve where any operating point below the curve is considered stable and any operating point above the curve is considered unstable.

**Table 2.9 P-Q Curve Method Applied to the Western Kansas Power System (Area I)
Assuming Constant Power (P) Load (Opening the Branch between Bus 83 and Bus 128)**

P-Q Curve Method Analysis for Constant Power (P) Load Type											
Power Factor = 1.0				Power Factor = 0.97 Lagging				Power Factor = 0.95 Lagging			
P MW	Q Mvar	Solution Converge	Voltage Stability Status	P MW	Q Mvar	Solution Converge	Voltage Stability Status	P MW	Q Mvar	Solution Converge	Voltage Stability Status
541	0	Yes	Stable	541	135	Yes	Stable	541	178	Yes	Stable
566	0	Yes	Stable	566	141	Yes	Stable	566	186	Yes	Stable
591	0	Yes	Stable	591	147	Yes	Stable	591	194	Yes	Stable
616	0	Yes	Stable	616	153	Yes	Stable	616	202	Yes	Stable
641	0	Yes	Stable	641	160	Yes	Stable	641	211	Yes	Stable
666	0	Yes	Stable	666	166	Yes	Stable	666	219	Yes	Stable
691	0	Yes	Stable	691	172	Yes	Stable	691	227	Yes	Stable
716	0	Yes	Stable	716	178	Yes	Stable	716	235	Yes	Stable
741	0	Yes	Stable	741	185	Yes	Stable	741	243	Yes	Stable
766	0	Yes	Stable	784	191	Yes	Stable	743	244	Yes	Stable
791	0	Yes	Stable	791	197	No	Unstable	791	260	No	Unstable
816	0	Yes	Stable	816	203	No	Unstable	841	276	No	Unstable
841	0	Yes	Stable	841	209	No	Unstable	866	284	No	Unstable
886	0	No	Unstable	866	216	No	Unstable				
Power Factor = 0.92 Lagging				Power Factor = 0.90 Lagging				Power Factor = 0.85 Lagging			
P MW	Q Mvar	Solution Converge	Voltage Stability Status	P MW	Q Mvar	Solution Converge	Voltage Stability Status	P MW	Q Mvar	Solution Converge	Voltage Stability Status
541	230	Yes	Stable	541	262	Yes	Stable	541	334	Yes	Stable
566	240	Yes	Stable	566	274	Yes	Stable	566	349	Yes	Stable
591	251	Yes	Stable	591	286	Yes	Stable	591	365	Yes	Stable
616	261	Yes	Stable	616	298	Yes	Stable	616	380	No	Unstable
641	272	Yes	Stable	641	310	Yes	Stable	641	395	No	Unstable
666	283	Yes	Stable	666	323	Yes	Stable	666	411	No	Unstable
691	293	Yes	Stable	691	335	Yes	Stable	691	426	No	Unstable
716	304	Yes	Stable	716	347	Yes	Unstable	716	442	No	Unstable
741	315	No	Unstable	741	359	Yes	Unstable	741	457	No	Unstable
766	325	No	Unstable	766	371	Yes	Unstable	766	473	No	Unstable
791	336	No	Unstable	791	383	No	Unstable	791	488	No	Unstable
841	357	No	Unstable	841	407	No	Unstable	841	519	No	Unstable
866	368	No	Unstable	866	419	No	Unstable	866	534	No	Unstable

Figure 2.13 Stability Boundary Calculated in P-Q Curve Method for Constant Power (P) Load Type Applied to the Western Kansas Power System (Area I)



Results of stability limits with the P-Q method and three different load models are shown in Table 2.10. Load-type sensitivity impacts on the results above are noticeable when comparing results from different load models. The P-Q curve method resulted in lower sensitivity values to load type variations than the P-V and the Q-V load sensitivity results. This is due to the fact that the P-Q method incorporates changes in real and reactive power simultaneously while other methods only incorporate the real power change (P-V curve method) or the reactive power change (Q-V curve method) in the calculations of voltage stability limits. At 0.97 lagging power factor, the constant current (I) load type resulted in 38.91 MVA of additional apparent power, when compared to the constant power (P) load type, that the system can incorporate safely before reaching the stability boundary point. Also at 0.97 lagging power factor, modeling the western Kansas load as 100% constant impedance (Z) resulted in 73 MVA of additional apparent power (compared to constant power (P) load type) that the system can safely incorporate.

Table 2.10 P-Q Curve Method for Constant Current (I) & Constant Impedance (Z) Load Types Applied to the Western Kansas Power System

Stability Boundary Limits for (ZIP) Load Types for Most Constraining Contingency							
	Constant P	Constant I			Constant Z		
Load Power Factor	Stability Boundary Limit	Stability Boundary Limit	Change in Stability Boundary Limit (I - P)	Change in Stability Boundary Limit (I - P)	Stability Boundary Limit	Change in Stability Boundary Limit (Z - P)	Change in Stability Boundary Limit (Z - P)
	MVA	MVA	MVA	%	MVA	MVA	%
1.00	851.77	869.77	25.00	2.94%	896.58	44.81	5.26%
0.97	808.13	847.04	38.91	4.82%	881.13	73.00	9.03%
0.95	782.00	846.75	64.75	8.28%	868.34	86.34	11.04%
0.92	777.86	806.35	28.49	3.66%	833.54	55.68	7.16%
0.90	767.92	785.47	17.55	2.29%	816.20	48.28	6.29%
0.85	694.63	747.30	52.67	7.58%	735.52	40.89	5.89%

Table 2.11 Stability Margins for the Three Constant Load Models in Western Kansas

	Constant P		Constant I		Constant Z	
Load Power Factor	Stability Limits	Stability Margin	Stability Limits	Stability Margin	Stability Limits	Stability Margin
	MVA	MVA	MVA	MVA	MVA	MVA
1.00	851.77	294.18	869.77	312.18	896.58	338.99
0.97	808.13	250.54	847.04	289.45	881.13	323.54
0.95	782.00	224.41	846.75	289.16	868.34	310.75
0.92	777.86	220.27	806.35	248.76	833.54	275.95
0.90	767.92	210.33	785.47	227.88	816.20	258.61
0.85	694.63	137.04	747.30	189.71	735.52	177.93

Regardless of the load power factor used in the analysis, results of the P-Q curve analysis indicated that the constant power (P) load model was on the conservative side in predicting stability limits. Load models in constant current (I) or constant impedance (Z) resulted in much higher stability limits than the constant power (P) load models. Constant impedance (Z) load

models resulted in the largest distance between the operating point and the stability boundary curve (stability margins) as shown in Table 2.11. On an average and for all load power factors considered, the constant current load (I) models resulted in 4.93% higher stability limits than the constant power (P) load model while the constant impedance (Z) models resulted in 6.86% higher stability limits than the P load models.

2.4.3 Stability Boundaries Load-Type Buffer Analysis Using P-Q Curve Method

Power system loads are usually composed of combination of all load types, however, the uncertainties of load compositions necessitate load sensitivity analysis to make sure that the system stays stable for an expected change in the load mix. To address load type uncertainties, a load type sensitivity analysis is recommended in order to assess the effect of variations in load types on stability boundary calculations. This should include varying the mixed load percentages at the load buses while monitoring the changes in the stability boundaries. Results of the sensitivity analysis can be used to create a stability boundary buffer to insure system stability for any unexpected load mix changes.

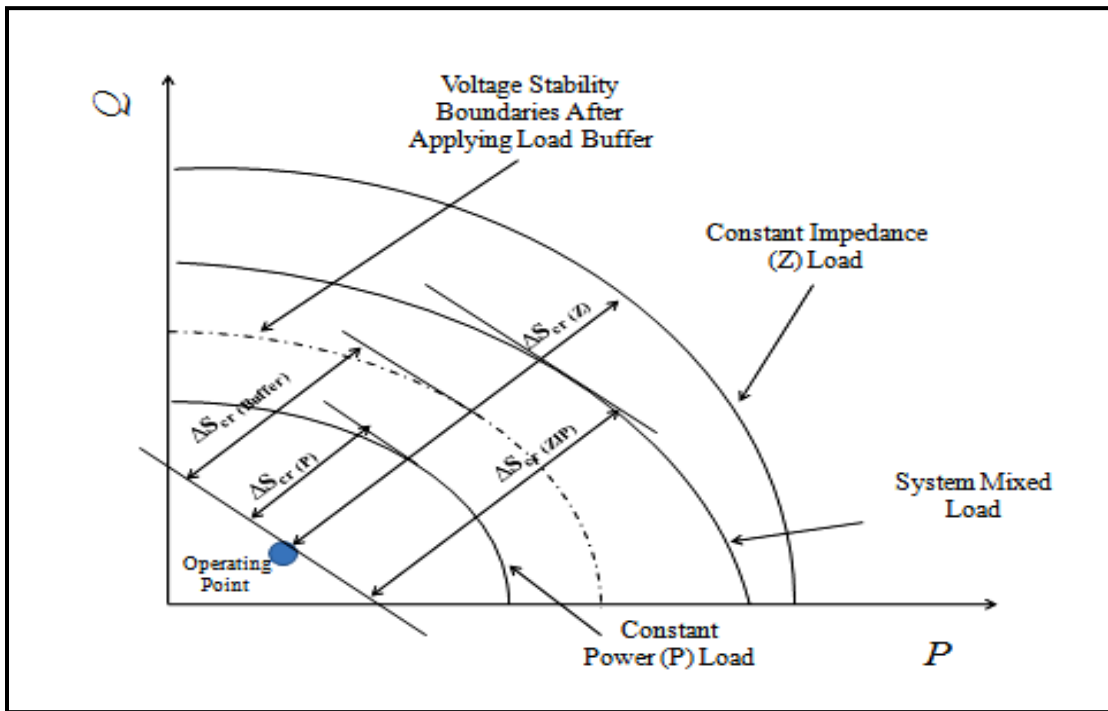
To assess power system sensitivity to load mix changes, a new stability boundary index S_i is introduced in this dissertation. The new index “ S_i ”, which varies from zero to 1, is a ratio of the change in stability boundary limits when system load mix percentages changes. High value of “ S_i ” indicates that the system is very sensitive to load mix changes, while a low value of “ S_i ” indicates that the system is not sensitive to load mix percentage changes.

Power system sensitivity to load mix percentage changes depends on the strength of the power system. The stability limit sensitivity to load mix changes also depends on the transmission line equivalent impedance and the load power factor as can be seen in Equations (2.9), (2.10) and (2.15). A power system with an “ S_i ” index value of 1, represents a system that is very sensitive to load mix changes. A power system with 0 “ S_i ” index value is a system with no sensitivity to load mix changes. However, the intent of this stability index factor is for a *relative* measure of load type changes for different load power factors on system stability boundaries. For a selected range of load power factor, the “ S_i ” index is used to determine at what load power factor a change in load type will impact stability boundary limits the most.

To calculate the “ S_i ” index, it is necessary to calculate the two extreme P-Q stability boundaries to determine the upper and lower limits of the stability region shown in Figure (2.14).

The lower stability limits will be determined using 100% constant power (P) load models. This type of load composition results in the lowest stability limits. The upper stability limits will be determined using 100% constant impedance (Z) load models. This type of load composition results in the highest stability limits. For a certain power factor, the variance between the upper and lower limits of the stability boundaries is the bandwidth where the system stability must be kept for safe operation. The larger the stability limit bandwidth, the more sensitive voltage stability limits are to load type changes. The equation for the stability sensitivity index “ S_i ” is shown in (2.16).

Figure 2.14 Illustration of the Use of the P-Q Stability Curve Method in Calculating Load Mix Sensitivity Index “ S_i ”



$$S_i = \frac{\Delta S_{cr(Z)} - \Delta S_{cr(P)}}{\Delta S_{cr(Z)}} \quad (2.16)$$

$\Delta S_{cr(Z)}$ is the apparent power distance from the system operating point to the stability limit curve calculated using 100% constant impedance (Z) load type. $\Delta S_{cr(P)}$ is the apparent power distance

from the system operating point to the stability limit curve calculated using 100% constant power (P) load type.

The sensitivity index “ S_i ” value can be used to determine stability buffer to avoid reaching voltage collapse caused by load uncertainties. Since an increase of constant power (P) load types produces the most negative impact on stability limits, it is recommended to increase the constant power (P) load percentage in the (ZIP) load mix to calculate the stability buffers. In systems with low sensitivity index values “ S_i ”, increases to the constant power (P) load type will result in small changes to the voltage stability limits. For systems with high sensitivity index values “ S_i ”, a significant increase in the constant power (P) load type in the composite load mix (ZIP) model will result in significant changes to the voltage stability limits.

System load mix calculations for each load bus can be explained using Figure 2.15 where each load bus component is divided into an equivalent (ZIP) model using Table (2.2). The following equations represent mathematical expressions for the (ZIP) equivalent load model for all load classes considered.

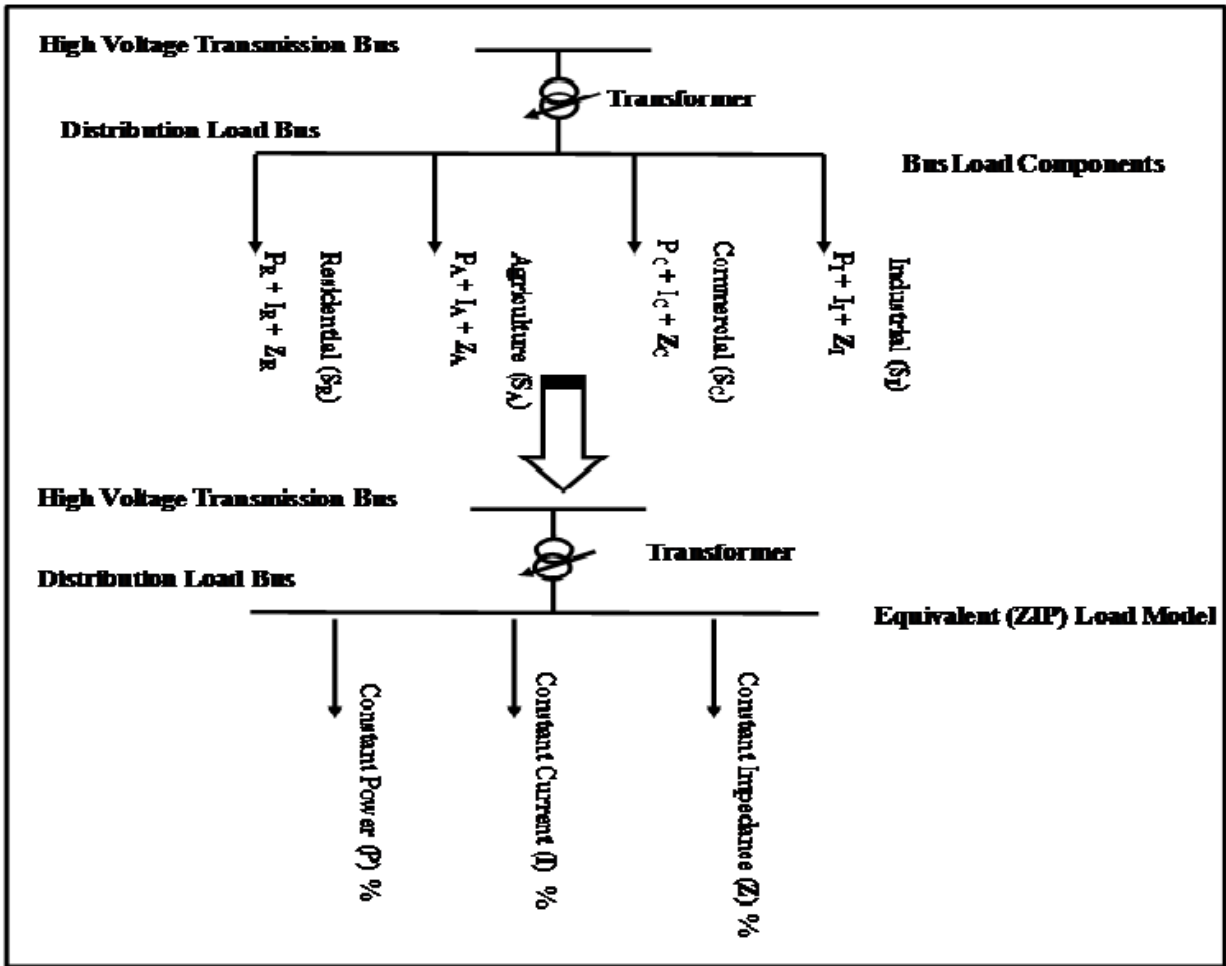
$$S_{Total} = S_{Residential} + S_{Agriculture} + S_{Commercial} + S_{Industrial} \quad (2.17)$$

Where, S_{Total} is the total apparent power at the load bus, $S_{Residential}$, $S_{Agriculture}$, $S_{Commercial}$ and $S_{Industrial}$ are the apparent power class components of residential, agriculture, commercial and industrial loads. Substituting for each apparent power load class in terms of constant power (P), constant current (I) and constant impedance (Z) using Table 2.4 and load class reference from Table 2.4 gives the following equations.

$$k_{Residential} = 25\% \text{ Resistive} + 75\% \text{ Small Motors}$$

$$k_{Residential} = 30\% (P) + 27.5\% (I) + 42.5\% (Z) \quad (2.18)$$

Figure 2.15 Equivalent (ZIP) Load Bus Model



$$k_{Agriculture} = 19\% \text{ Resistive} + 62\% \text{ Small Motors}$$

$$+ 15\% \text{ Large Motors} + 4\% \text{ Discharge Lighting}$$

$$k_{Agriculture} = 24.8\% (P) + 27.65\% (I) + 47.55\% (Z) \quad (2.19)$$

$$k_{Commercial} = 14\% \text{ Resistive} + 51\% \text{ Small Motors} + 35\% \text{ Discharge Lighting}$$

$$k_{Commercial} = 20.4\% (P) + 34.7\% (I) + 44.9\% (Z) \quad (2.20)$$

$$k_{Industrial} = 5\% \text{ Resistive} + 20\% \text{ Small Motors} + 56\% \text{ Large Motors} + 19\% \text{ Discharge Lighting}$$

$$k_{Industrial} = 41.6\% (P) + 16\% (I) + 42.4\% (Z) \quad (2.21)$$

Where $k_{Residential}$, $k_{Agriculture}$, $k_{Commercial}$ and $k_{Industrial}$ are the apparent power components' load class multipliers to convert load classes to ZIP load models. Results of load class multipliers are tabulated in Table (2.12).

Table 2.12 Load Class k -Factors Multiplier for Converting Load Classes to a ZIP Load Model

Load Classes	Load Class Multipliers to Convert Load Classes into a ZIP Load Model		
	Constant (P)	Constant (I)	Constant (Z)
Residential	30.00%	27.50%	42.50%
Agriculture	24.80%	27.65%	47.55%
Commercial	20.40%	34.70%	44.90%
Industrial	41.60%	16.00%	42.40%

To express the total load S_T in terms of the ZIP load mix model, multiply each apparent power load class by its ZIP percentage factors found in Equations (2.18), (2.19), (2.20) and (2.21) and Equation (2.17) can written as,

$$S_{Total} = k_{Residential} S_{Residential} + k_{Agriculture} S_{Agriculture} + k_{Commercial} S_{Commercial} + k_{Industrial} S_{Industrial}$$

$$\begin{aligned} S_{Total} = & S_{Residential} [(30\% (P) + 27.5\% (I) + 42.5\% (Z))] \\ & + S_{Agriculture} [(24.8\% (P) + 27.65\% (I) + 47.55\% (Z))] \\ & + S_{Commercial} [(20.4\% (P) + 34.7\% (I) + 44.9\% (Z))] \\ & + S_{Industrial} [(41.6\% (P) + 16\% (I) + 42.4\% (Z))] \end{aligned}$$

(2.22)

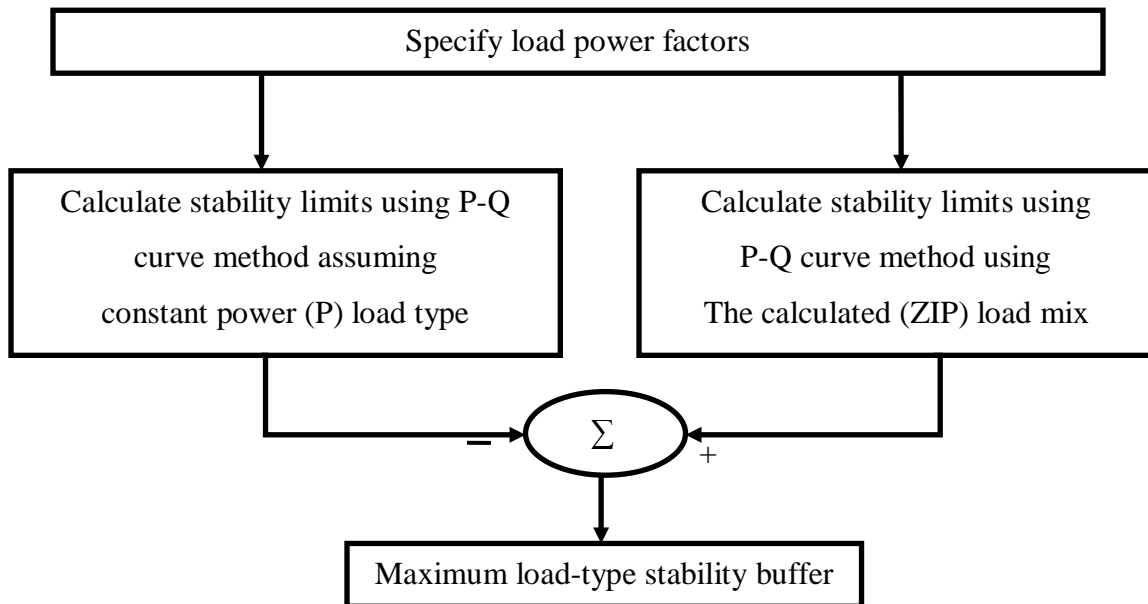
2.4.3.1 Case Study for the Application of Load Type Stability Buffer Calculations Applied to the Western Kansas Power System

When load mix data are not available, system transmission planners use a stability boundary safety margin of 3% to 5% to set buffer for stability limits calculated using only a

constant power (P) load mix type [60]. The stability buffer is needed to account for system uncertainties which may cause a system to become unstable. However, the 3% to 5% range of stability buffers (taken from the calculated mixed load stability boundary values), arbitrarily chosen assuming that it provides enough margin for systems to avoid instability due to load type sensitivities. This may or may not be so conservative that it exceeds the stability limits when calculated using only constant power (P) load type. A load composite mix model in conjunction with the P-Q curve method can be used to determine a more appropriate safety buffer for the power system taking into consideration its unique load mix. By using the P-Q curve method, a maximum load type stability buffer can be created for any system load power factor condition, and based on the accuracy of the load type data, an effective safety buffer can be determined.

For each expected operating power factor, the distance from the stability limit calculated using the mixed-load model to the stability limit calculated using the constant power (P) load model can be determined. This distance is the maximum system stability buffer for load type sensitivities since the stability limit calculated using only constant power (P) load model is the most conservative approach. The process of calculating the maximum load type stability margin buffer is summarized in the flow chart shown in Figure 2.16.

Figure 2.16 Maximum Voltage Stability Buffer Calculation Process for Uncertainties in Load Type Models



The need for calculating load type stability buffers for different system power factors is due to load power factor changes and the lack of exact data obtained from the load type survey which may not capture induction motor stalling at low voltages, thermostatic load recovery and load tap changers. This can be compensated for by using a load mix sensitivity analysis where load type percentages are changed to detect the impact on stability limit results. One of the main reasons for system power factors to change is when additional low power factor loads are switched on. During hot summer days, the system load power factor decreases when system voltages decline due to an increase in air conditioner and refrigeration equipment loads (which have low power factors [54]). It is recommended to calculate load type stability buffers for different system power factors to capture a range of operating points where the system, if stressed will stay stable.

The equivalent load mix components (composite load) for the western Kansas power system during the summer peak hour of 2010 are shown in Table 2.13. Using Table (2.12) and Equation (2.22), the system equivalent ZIP model can be calculated for each load bus.

Table 2.13 Load Types for the Summer Peak in Western Kansas Power System

Load Class Summer 2010 – Peak Hour	% of Total System Load (S_{Total})
Residential	32
Agriculture	28
Commercial	15
Industrial	25

The four load classes can be converted to a ZIP equivalent model as shown in the following equations followed by a summary of the results in Table 2.14.

$$ZIP \text{ Equivalent of Residential Load} = S_{Total} (32\%)(k_{Residential})$$

$$ZIP \text{ Equivalent of Residential Load} = S_{Total} (32\%)[(30\% (P) + 27.5\% (I) + 42.5\% (Z)]$$

$$ZIP \text{ Equivalent of Residential Load} = S_{Total} [(9.6\% (P) + 8.8\% (I) + 13.6\% (Z)] \quad (2.23)$$

$$\text{ZIP Equivalent of Agriculture Load} = S_{\text{Total}} (28\%)(k_{\text{Agriculture}})$$

$$\text{ZIP Equivalent of Agriculture Load} = S_{\text{Total}} (28\%)[(24.8\% (P) + 27.65\% (I) + 47.55\% (Z))]$$

$$\text{ZIP Equivalent of Agriculture Load} = S_{\text{Total}} [(6.944\% (P) + 7.742\% (I) + 13.314\% (Z))] \quad (2.24)$$

$$\text{ZIP Equivalent of Commercial Load} = S_{\text{Total}} (15\%)(k_{\text{Commercial}})$$

$$\text{ZIP Equivalent of Commercial Load} = S_{\text{Total}} (15\%)[(20.4\% (P) + 34.7\% (I) + 44.9\% (Z))]$$

$$\text{ZIP Equivalent of Commercial Load} = S_{\text{Total}} [(3.06\% (P) + 5.205\% (I) + 6.735\% (Z))] \quad (2.25)$$

$$\text{ZIP Equivalent of Industrial Load} = S_{\text{Total}} (25\%)(k_{\text{Industrial}})$$

$$\text{ZIP Equivalent of Industrial Load} = S_{\text{Total}} (25\%)[(41.6\% (P) + 16\% (I) + 42.4\% (Z))]$$

$$\text{ZIP Equivalent of Industrial Load} = S_{\text{Total}} [(10.40\% (P) + 4.00\% (I) + 10.60\% (Z))] \quad (2.26)$$

Table 2.14 Constant ZIP Model as a % of the Western Kansas Total Summer 2010 System Peak Load ($S_{\text{Total}} = 557.59$ MVA)

Load Class	Percent of the Total System Load “% of S_{Total} ”		
	Constant (P)	Constant (I)	Constant (Z)
Residential	9.60	8.80	13.60
Agriculture	6.94	7.74	13.31
Commercial	3.06	5.20	6.73
Industrial	10.40	4.00	10.60
Total Load in %	30.00	25.75	44.25
Total Load in MVA	167.30	143.56	246.73

Table 2.15 shows the stability boundaries for the western Kansas system (Area I) using the load composite mix equivalent (ZIP), the constant power (P) and the constant impedance (Z) load models for the summer 2010 peak hour. The stability margins calculated in the table are the distance from the operating point at a specific power factor to the stability boundary calculated using the P-Q curve method. Stability margins were highest using the constant impedance (Z) load models and at their lowest when loads were modeled as constant power (P). The ZIP load model resulted in stability boundary limits in between the two extreme boundary values. For a system power factor of 0.97 lagging, the highest stability margin of 323.5 MVA for a constant impedance (Z) load model, the lowest stability margin of 250.5 MVA for the constant power (P) load model and a stability margin of 301.7 MVA for the mixed-load model were found.

Table 2.15 Stability Limits for Constant Power (P), Constant Impedance (Z) and The ZIP Mixed Load Model Applied to the Western Kansas Power System Using The P-Q Curve Method

Load Power Factor	Constant P		Mixed Model		Constant Z	
	Stability Limit in MVA	Stability Margin in MVA	Stability Limit in MVA	Stability Margin in MVA	Stability Limit in MVA	Stability Margin in MVA
1.00	851.8	294.2	888.0	330.4	896.6	339.0
0.97	808.1	250.5	859.3	301.7	881.1	323.5
0.95	782.0	224.4	825.4	267.8	868.3	310.8
0.92	777.9	220.3	799.9	242.3	833.5	276.0
0.90	767.9	210.3	793.2	235.7	816.2	258.6
0.85	694.6	137.0	708.8	151.2	735.5	177.9

To provide recommendations on suitable load type stability buffers, the stability margins are plotted in Figure 2.17 and the variances of the stability margins calculated using constant power (P) load model from those calculated using the mixed-load model are shown in Table 2.15. The traditional 5% of stability safety buffer percent exceeds the most conservative stability boundary limits calculated using only constant power (P) load type for the four system power factors considered. This indicates that a 5% stability buffer is too aggressive and may unnecessarily limit system capabilities for adding new loads.

Figure 2.17 Stability Margins for the Three Different Load Models

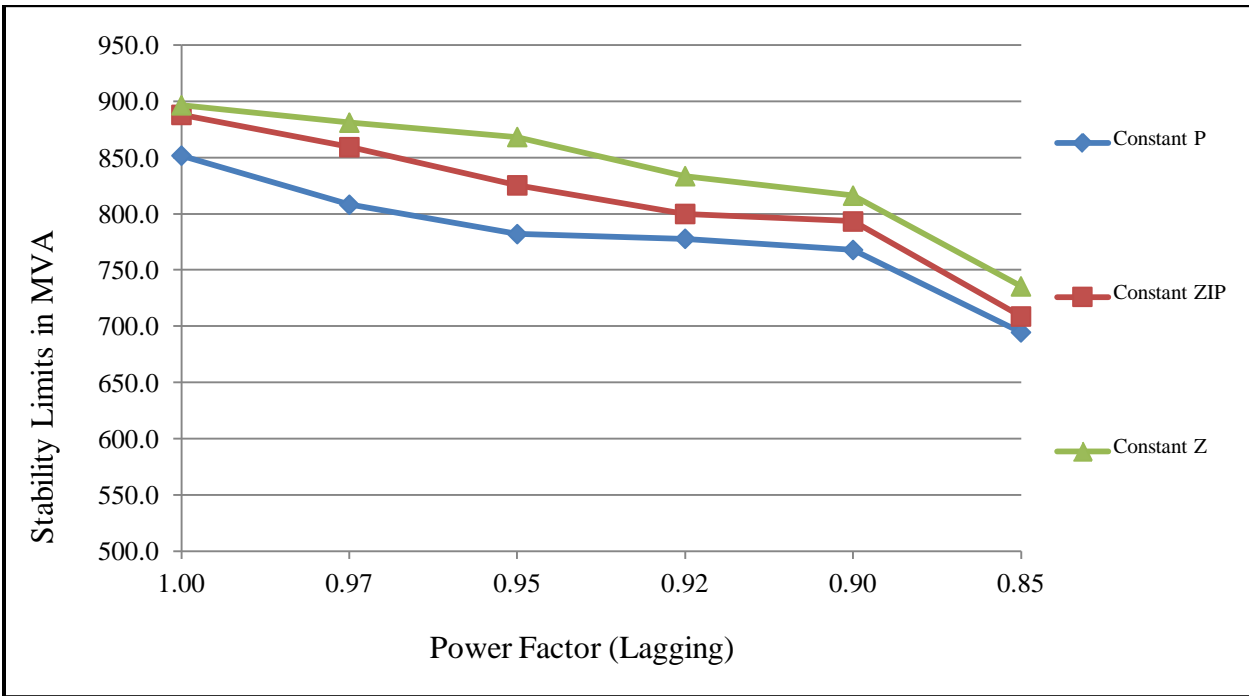


Table 2.16 Variances of Stability Boundary Limits between Constant Power (P) and ZIP Load Models for Determining Appropriate VSM Buffer

Maximum VSM Buffer “Variance of the Stability Boundary Limits Calculated Using the P-Q Curve Method for the Western Kansas Power System (Area I) for Different Load Types”				
Load Power Factor	Constant P VSM in MVA	Exact (ZIP) VSM in MVA	Max VSM Buffer in MVA	Maximum VSM Buffer as a % of Exact (ZIP) VSM
1.00	851.77	888.02	36.25	4.08%
0.97	808.13	859.28	51.15	5.95%
0.95	782.00	825.37	43.37	5.25%
0.92	777.86	799.93	22.06	2.76%
0.90	767.92	793.24	25.32	3.19%
0.85	694.63	708.75	14.12	1.99%

Since the increase of the constant power (P) component of the ZIP load mix has the most negative impact on system stability boundary limits, the stability buffer can be obtained by increasing the constant power (P) component in the ZIP model. To provide a guide to how much

the “P” component of the exact ZIP load model should be increased and at what load power factor should be calculated, the load type sensitivity index “ S_i ” is calculated using Equation (2.16) for each of the load power factors considered. The power factor, which produces the highest sensitivity index “ S_i ”, is the power factor for which the constant power (P) component is varied. Based on the results of system stability limits obtained for different load types in Table 2.15, the “ S_i ” indexes for all power factors are calculated and summarized in Table 2.17. The highest index value of 9.94% calculated is when the system load power factor was set at 0.95 lagging.

Table 2.17 Load Type Impact on Sensitivity Index " S_i " for the Range of Load Power Factors Considered

	Constant P	Constant Z	“ S_i ” Index Calculation	
Load Power Factor	Stability Limit in MVA	Stability Limit in MVA	Stability Limit Variance in MVA (Constant Z limit - Constant P limit)	“ S_i ” Index
1.00	851.8	896.6	44.8	5.00%
0.97	808.1	881.1	73.0	8.29%
0.95	782.0	868.3	86.3	9.94%
0.92	777.9	833.5	55.6	6.67%
0.90	767.9	816.2	48.3	5.92%
0.85	694.6	735.5	40.9	5.56%

To create a stability buffer, the constant power (P) component for the 0.95 power factor case is used as the basis for load mix sensitivity buffer determination analysis. The results shown in Table 2.18 are based on varying the constant power (P) load percentage in the total load mix ZIP model while calculating voltage stability boundary changes from the original mixed-load type percentages. From the list of the buffers calculated when the constant power (P) component doubled from 30% to 60%, the stability buffer was only at 2.629 % of the stability limit obtained when using the exact ZIP load model. For all other system load power factor cases, the stability buffer should be set at 2.629% of the limits calculated using the exact ZIP load model since the 0.95 load power factor resulted in the most stability boundary sensitive case for load type changes.

Table 2.18 Stability Boundary Buffer Calculations for Western Kansas (Area I) Power System

Stability Boundary Limits Calculated Using the P-Q Curve Method for the Western Kansas Power System (Area I) for Different Mixed-Load at 0.95 System Power Factor					
Buffer Case Identification	Constant P	Constant I	Constant Z	Stability Boundary Limit in MVA	VSM Buffer as a % of the Stability Margin for the Exact ZIP 0
	Components of ZIP Load Mix				
ZIP 0 (Exact ZIP)	30.004	25.747	44.249	825.40	0.00%
ZIP 1	40.000	22.070	37.930	821.08	0.523%
ZIP 2	50.000	18.392	31.608	814.30	1.345%
ZIP 3	60.000	14.713	25.287	803.70	2.629%
ZIP 4	70.000	11.035	18.965	797.70	3.356%
ZIP 5	80.000	7.357	12.643	792.10	4.034%
ZIP 6	90.000	3.678	6.322	784.39	4.968%
ZIP 7	100.00	0.000	0.000	782.00	5.212%

2.5 Conclusions

Black-outs caused by voltage instability are a real threat to the power grid. Several instances of major voltage black-outs worldwide have been attributed to voltage instability. Voltage instability occurs when power system reactive power generators cannot meet the reactive power demand. Voltage black-outs have other causes besides reactive power deficiencies. Control systems can trigger black-outs due to an error in reading system loading data just like what happened in the Northeast 2003 black-out incident. Load characteristics can also be a factor in triggering voltage instability. A sudden increase in load demand may drop system frequencies to levels where protection systems disconnect a main power source and leave the system with low resources to meet load demand. Voltage instability analysis depends on the time it requires for an area of voltage decline to develop. Voltage instability takes time to develop which makes it possible to study using steady-state simulation models.

A number of steady-state voltage stability analytical methods have been investigated and are used in this chapter to calculate voltage stability limits for the western Kansas (Area I) power system. Both the P-V and Q-V methods are reliable and produce close approximation to voltage

instability points. However, both methods only consider changes in the real power as it is with the P-V curve method or in the reactive power as it is in the Q-V curve method when calculating the instability points. This may make it difficult for finding the voltage instability points. A new P-Q curve method which considers the changes in both real and reactive power when calculating instability points is discussed in this chapter.

Regardless of which voltage stability method is used, voltage instability in large power systems is influenced by different factors. Load types, reactive power limits on generators, loss of circuit during contingencies and availability of switchable shunt devices. All these factors were addressed in this chapter and a load type sensitivity analysis was conducted to quantify their impact on voltage stability limits. Even though it has its own limitations, the composite load mix approach was used in this study using the western Kansas load survey data. The survey data neglects induction motor stalling at low voltages, thermostatic load recovery and load tap changers. This can be compensated for by using load mix sensitivity analysis where load type percentages are varied to detect the impact on the stability limit results found using the P-Q curve method.

Load types considered in this study are constant power (P), constant current (I) and constant impedance (Z). Regardless of which voltage stability method used, among the three different load types, the constant power (P) load type resulted in the lowest voltage stability limits. Modeling loads as constant power (P) type is the most conservative approach to calculating stability limits.

Results of applying all three steady-state stability methods were sensitive to load type models. The stability limits calculated using the P-Q curve method resulted in lower sensitivity to load type variations than the P-V and the Q-V load sensitivity results. This is due to the fact that the P-Q method incorporates changes in real and reactive power simultaneously. Using the P-Q curve method, the constant impedance (Z) load type carries the highest voltage stability limits at about 124% more than that of the constant power (P) (for a 0.97 load power factor). The constant current (I) load type has higher voltage stability limits than the constant power (P) load type but slightly lower than the constant impedance (Z) load type.

To address load uncertainties, a load type sensitivity analysis was performed using the P-Q curve method. A new stability boundary limit sensitivity factor was introduced to provide a relative measure of load type changes for different load power factors on system stability

boundaries. The sensitivity index was used to calculate a stability boundary buffer to avoid reaching voltage collapse due to load type uncertainties. Application for determining an effective stability buffer has been studied for the western Kansas power system (Area I). The stability buffer was calculated for the load power factor which has the highest sensitivity index. Load power factor of 0.95 lagging resulted in the highest sensitivity index value, and a buffer of 2.7% from the stability boundary limits obtained using the original mixed-load is recommended.

Chapter 3 - Application of Steady-State Voltage Stability Methods for Wind Integration in Western Kansas

Modeling of wind farms for wind integration studies depends on the purpose of the analysis. For analysis of the internal behavior of wind turbines within a wind farm, it is required that the wind farm be represented by a detailed model. It includes the modeling of all the wind turbines and the wind farm electrical network. Aggregating all wind turbines to an equivalent large wind turbine for wind integration studies of large-scale power systems is also possible. Wind aggregation is used to reduce the complexity of the wind farm model during simulations of a large power system. The equivalent large wind turbine is assumed to receive the same wind power as the wind incident on the group of wind turbines [35, 40].

However, if the terrain or other factors cause wind turbines inside the wind farm to experience different wind speeds, a new aggregation method must be used. In such a case, the differences in the incoming winds lead to output power deviations among the aggregated wind turbines, and therefore the wind incident on each wind turbine should be considered in the aggregation method.

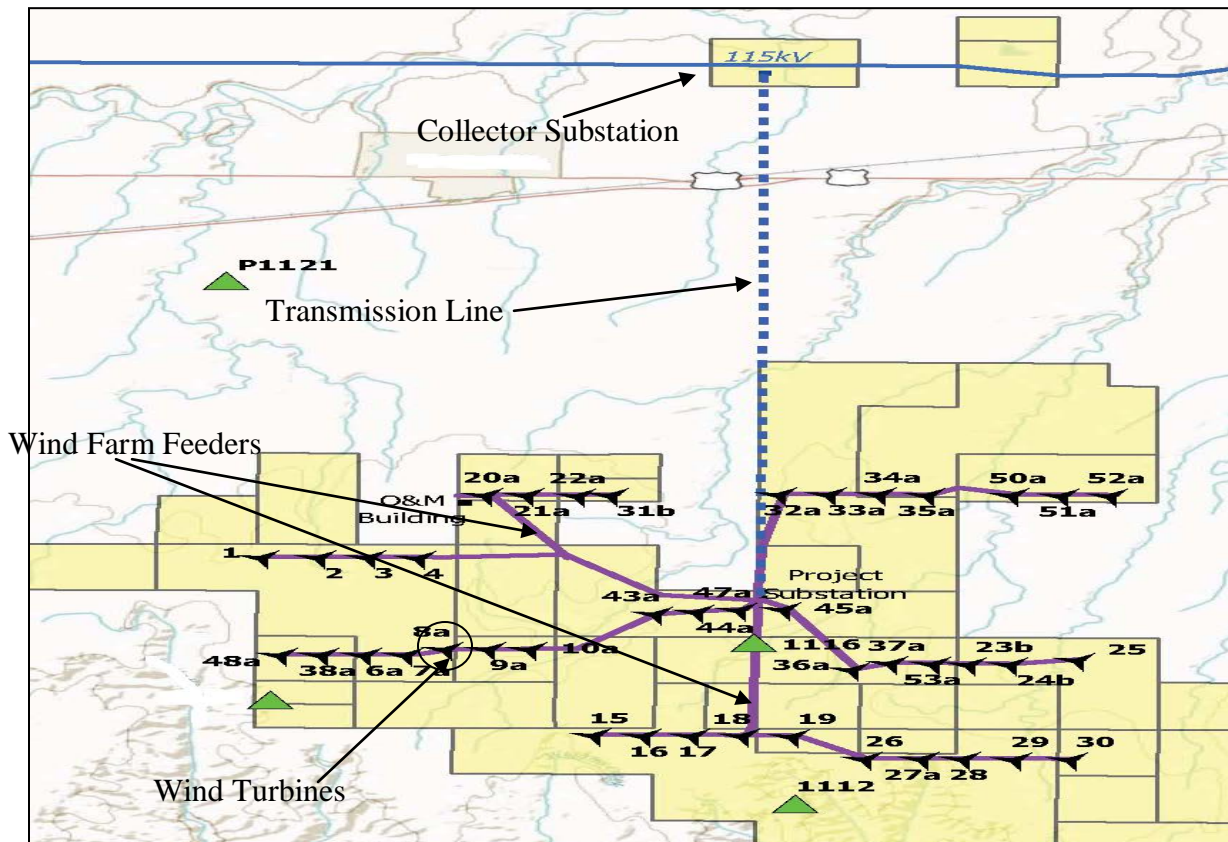
3.1 Wind Farm Aggregate Models for Steady-State Voltage Stability Analysis

In power system studies, it is simpler to represent a wind farm with tens or hundreds of wind turbines by one equivalent generator with suitable scaling and adjustment of the wind farm electrical and mechanical components [40, 61]. To study the impact of a wind farm on the grid, it is acceptable to aggregate all wind turbines inside the wind farm to a single large wind turbine at the point of common coupling with the grid [62]. The geographical spread of individual wind turbines inside a wind farm is necessary only for evaluating the wind farm internal dynamics [35]. However, some accuracy in modeling is lost when aggregating all wind turbines inside the wind farm into one large turbine [62]. Much more accurate results can be obtained by taking into account the number of wind turbine generators that are injecting currents into each branch inside the wind farm.

Wind turbines inside a wind farm are connected to each other in a string or “daisy chain” configuration with an example shown in Figure (3.1). Underground cables are most commonly used as trunk lines. Two or more wind turbines are connected via the trunk lines, which then

connect to one of the main wind farm feeders. The feeder circuits can be overhead lines or underground cables at the distribution voltage level (22 kV – 34.5 kV) [62 – 65, 67]. All feeders inside the wind farm connect to the collector substation which it connects to the transmission grid via a large transmission transformer.

Figure 3.1 Wind Farm Collector System Network



The “feeders” inside the wind farm have a smaller impedance value and a smaller shunt representation value compared to the “complete system” equivalent impedance. The equivalent shunt capacitance representing capacitance of the cables and overhead lines is also much smaller than the system equivalent capacitance. The pad mount transformer impedances connecting wind turbine generators to the major lines inside the wind farm can be significant. An aggregated impedance of these transformers can be assumed using the following equivalent impedance representation [62].

$$Z_{EQXFMR} = Z_{WTG_XFMR} / n_{turbine} \quad (3.1)$$

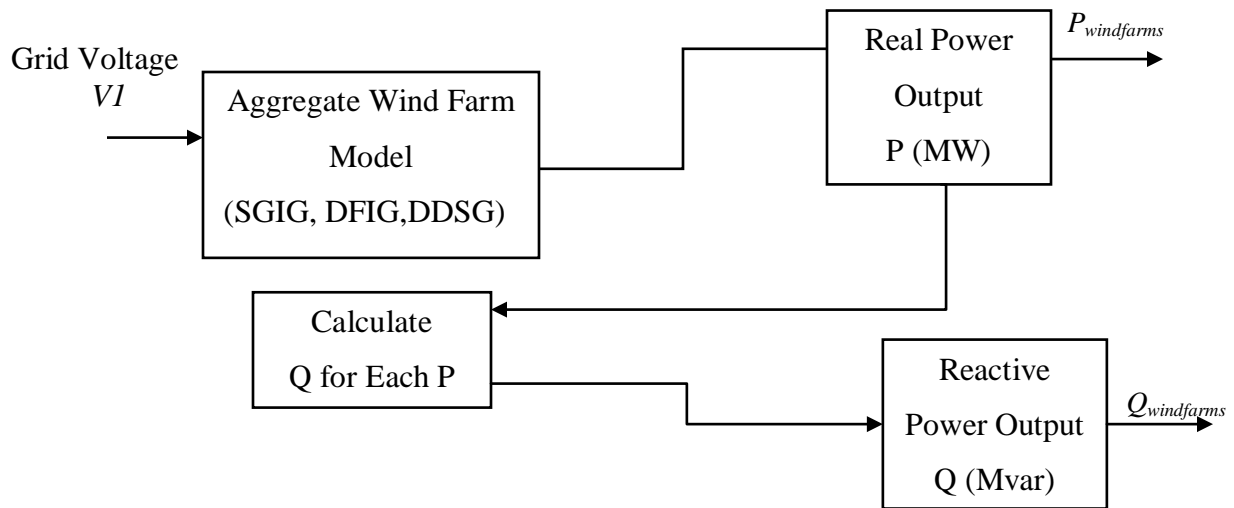
Where, Z_{EQXFMR} is the total wind farm equivalent transformer impedance, Z_{WTG_XFMR} is the individual wind turbine step-up transformer impedance and $n_{turbine}$ is the number of wind turbines inside the wind farm. The resulting equivalent impedance of the wind farm can be ignored for steady-state voltage stability studies since its impact on the bus voltage at the point of interconnection with the grid is negligible [62, 63].

3.2 Bus Type Models for Aggregated Wind Farms for Steady-State Stability Analysis

The focus for wind turbine models in power system steady-state studies is to capture turbine power conversion in terms of megawatt (P) and megavar (Q) power output for variable wind speed. The steady-state models of SCIG, DFIG and DDSG wind turbine generators have significant effect on voltage stability [64].

To model wind farms for steady-state power system studies, variations in wind speed within the wind farm are neglected [64]. All wind turbines in the wind farm (n parallel connected wind turbines) are assumed to produce same amount of active power. The output active and reactive power of each generator unit is calculated under different wind conditions. From these power calculations, the total active and reactive powers of the wind farm are calculated, as illustrated in Figure 3.2.

Figure 3.2 Flow Chart for Active (P) and Reactive (Q) Power Model for a Wind Farm



Wind Farms with SCIG wind turbine type are modeled as PQ buses. To calculate wind farm reactive power output for every wind speed, the generators' active power (P) is assumed and the reactive power (Q) is calculated by considering the steady-state model of the wind turbine used in the wind farm and represented in Equation (3.5). The real power (P) is calculated first from the wind speed by using the power curves, and it is assumed that the active power (P) calculated is constant for the calculation of the reactive power (Q) which is dependent only on the bus voltages.

Wind farms with DFIG wind turbine type can be modeled as PQ or PV buses, as they operate in either power factor control mode or voltage control mode. Since the inverters operate as regulated current sources which are both synchronized and phase locked to the bus voltage of the point of common coupling, the wind farm does not regulate bus voltage or bus frequency. The inverter responds only to the AC current commands generated by turbine power factor controller that are intended to maximize extraction of wind power from the available wind flow at the wind farm site. For this reason, a wind farm consisting of DFIG wind turbine type can be modeled as a simple PQ bus, with P a function of wind speed and Q at the point of common coupling set to maintain acceptable power factor [65]. However, DFIG can also be modeled as a PV bus (voltage control mode) at the point of common coupling with the reactive power (Q) limits applied. These limits are typically $\pm 30\%$ of the maximum active power of the wind farm.

Wind farms with DDSG type wind turbines can be modeled as PV or PQ buses depending on reactive power limit enforcement. When enforcing reactive power limits, DDSG wind farms convert from a PV to PQ buses. A summary of wind turbine generator types' steady-state model representations is shown in Table 3.1.

The way in which wind farms locally affect grid bus voltages depends on whether constant-speed or variable-speed turbines are used. The SCIGs are constant-speed turbines, which have a fixed relation between rotor speed, active power, reactive power, and terminal voltage with no control over the rotor voltage. Therefore, it cannot positively affect bus voltages using the reactive power that it receives from the grid. Additional voltage support equipment for generating reactive power would be necessary to allow for voltage control. On the other hand, DFIG and DDSG (variable-speed turbines) have the capability of varying reactive power to affect their terminal voltage by changing the rotor voltage to capture the optimal wind power over a wide range of rotor speed. However, the voltage control obtained using variable-speed

turbines is limited by the grid side convertor MVA rating and its controls. Table 3.1 shows a summary of voltage control per wind turbine type.

Table 3.1 Summary of Steady-State Models of SCIG, DFIG and DDSG Wind Turbine Generators

Wind Turbine Generator Types	PQ Bus	PV Bus	Voltage Control
SCIG	Conventional PQ model	None	Only possible with additional voltage support equipment
DFIG	Power factor control mode	Voltage control mode	Yes (limited to convertor MVA rating and controller)
DDSG	Operated at the maximum limits of the generator reactive power capability	Operated within the maximum limit bandwidth of the generator reactive power capability	Yes (limited to convertor MVA rating and controller)

3.3 Maximum Wind Penetration for Different Turbine Type Wind Farms in the Western Kansas Power System

The type of wind generator used in integrating wind power in power systems has significant effect on the level of wind penetration that a power system can safely incorporate in the generation mix. A one-bus wind injection study in the western Kansas power system is presented here to compare the impact of wind turbine type on maximum wind penetration. The wind is injected at bus number 105, shown in Figure 2.8, at the 115 kV voltage level. This bus is located in an area where future wind injection has been identified through the SPP Generation Interconnection (GI) process [27]. Wind is injected in increments and the P-Q curve method is used to calculate the maximum wind level that can be injected at three different power system

power factors before driving the system voltage unstable. Wind injection was increased in increments of 10 MW starting with “0” MW. Voltage stability boundary limits are calculated at each wind injection increment. Results of the P-Q analysis for three different load power factors and the three wind turbine types considered in this dissertation are summarized in Table 3.2. The maximum wind injection values in Table 3.2 are the maximum wind injections at Bus 105 which resulted in a voltage stable condition determined using the P-Q method. Detailed results of the calculations are shown in Tables 3.3, 3.4 and 3.5 for SCIG, DFIG, and DDSG types respectively.

Table 3.2 Stability Limits on Maximum Wind Injection from Bus 105

Wind Turbine Generator Type	Western Kansas Area I - Load Power Factor (Lagging Power Factors)		
	0.97	0.95	0.90
	Maximum Wind Injection from Bus 105 before Reaching the Collapse Point		
SCIG	100 MW	100 MW	90 MW
DFIG	150 MW	140 MW	120 MW
DDSG	160 MW	150 MW	140 MW

Table 3.3 Wind Injection Impact on Stability Boundaries Using SCIG Wind Turbine Type for the Western Kansas Power System (Area I) – P-Q Curve Method Results

SGIG Wind Farm P-Q Analysis							
ZIP Load Components for the 2010 Summer Peak Load Hour 17 (541 MW)				Most Limiting Contingency Opening the Branch between Bus 83 and Bus 128			
Constant Power (P)	30.00%	S_P	167.300 MVA				
Constant Current (I)	25.75%	S_I	143.563 MVA				
Constant Impedance (Z)	44.25%	S_Z	246.727 MVA				
Maximum Wind Injection - P-Q Curve Method Analysis							
Wind Injection from Bus 105	Iteration #	Wind Farm Power Output		Stability Limits			Voltage Stability
Load Power Factor		MW	Mvar	P (MW)	Q (Mvar)	Scr (MVA)	Results
0.97	1	0	0.00	800.638	200.659	825.40	Stable
0.97	2	10	-1.50	802.170	201.043	826.98	Stable
0.97	3	20	-3.00	807.534	202.387	832.51	Stable
0.97	4	30	-4.50	813.412	203.860	838.57	Stable
0.97	5	40	-6.00	796.893	199.720	821.54	Stable
0.97	6	50	-7.50	775.078	194.253	799.05	Stable
0.97	7	60	-9.00	730.022	182.961	752.60	Stable
0.97	8	70	-10.50	697.818	174.890	719.40	Stable
0.97	9	80	-12.00	610.033	152.889	628.90	Stable
0.97	10	90	-13.50	575.792	144.307	593.60	Stable
0.97	11	100	-15.00	571.931	143.340	589.62	Stable
0.97	12	105	-15.75	0.000	0.000	0.00	Unstable
0.95	1	0	0.00	784.130	257.731	825.40	Stable
0.95	2	10	-1.50	785.213	258.087	826.54	Stable
0.95	3	20	-3.00	788.994	259.330	830.52	Stable
0.95	4	30	-4.50	778.126	255.758	819.08	Stable
0.95	5	40	-6.00	734.967	241.572	773.65	Stable
0.95	6	50	-7.50	692.483	227.608	728.93	Stable
0.95	7	60	-9.00	658.844	216.552	693.52	Stable
0.95	8	70	-10.50	619.210	203.524	651.80	Stable
0.95	9	80	-12.00	570.085	187.378	600.09	Stable
0.95	10	90	-13.50	554.040	182.104	583.20	Stable
0.95	11	100	-15.00	535.629	176.053	563.82	Stable
0.95	12	105	-15.75	0.000	0.000	0.00	Unstable
0.90	1	0	0.00	742.860	359.784	825.40	Stable
0.90	2	10	-1.50	743.445	360.067	826.05	Stable
0.90	3	20	-3.00	742.788	359.749	825.32	Stable
0.90	4	30	-4.50	706.788	342.313	785.32	Stable
0.90	5	40	-6.00	650.250	314.930	722.50	Stable
0.90	6	50	-7.50	620.388	300.468	689.32	Stable
0.90	7	60	-9.00	592.020	286.728	657.80	Stable
0.90	8	70	-10.50	556.200	269.38	618.00	Stable
0.90	9	80	-12.00	523.485	253.535	581.65	Stable
0.90	10	90	-13.50	504.468	244.325	560.52	Stable
0.90	11	95	-15.00	0.000	0.000	0.00	Unstable

Table 3.4 Wind Injection Impact on Stability Boundaries Using DFIG Wind Turbine Type for the Western Kansas Power System (Area I) – P-Q Curve Method Results

DFIG Wind Farm P-Q Analysis							
ZIP Load Components for the 2010 Summer Peak Load Hour 17 (541 MW)				Most Limiting Contingency Opening the Branch between Bus 83 and Bus 128			
Constant Power (P)	30.00%	S_p	167.300 MVA				
Constant Current (I)	25.75%	S_I	143.563 MVA				
Constant Impedance (Z)	44.25%	S_Z	246.727 MVA				
Maximum Wind Injection - P-Q Curve Method Analysis							
Wind Injection from Bus 105	Iteration	Wind Farm Power Output		Stability Limits			Voltage Stability
Load Power Factor	#	MW	Mvar	P (MW)	Q (Mvar)	Scr (MVA)	Results
0.97	1	0	0.00	800.64	200.66	825.40	Stable
0.97	2	10	0.00	805.73	201.94	830.65	Stable
0.97	3	20	-0.08	810.15	203.04	835.21	Stable
0.97	4	30	-1.02	817.23	204.82	842.50	Stable
0.97	5	40	0.18	815.09	204.28	840.30	Stable
0.97	6	50	3.92	791.20	198.29	815.67	Stable
0.97	7	60	8.63	764.97	191.72	788.63	Stable
0.97	8	70	9.52	731.28	183.28	753.90	Stable
0.97	9	80	10.85	679.49	170.29	700.50	Stable
0.97	10	90	12.37	652.18	163.45	672.35	Stable
0.97	11	100	13.39	638.57	160.04	658.32	Stable
0.97	12	110	14.52	609.47	152.75	628.32	Stable
0.97	13	120	14.95	597.32	149.70	615.79	Stable
0.97	14	130	14.99	571.79	143.30	589.47	Stable
0.97	15	140	15.83	556.30	139.42	573.50	Stable
0.97	16	150	16.08	552.77	138.54	569.87	Stable
0.97	17	155	25.98	0.00	0.00	0.00	Unstable
0.95	1	0	0.00	784.13	257.73	825.40	Stable
0.95	2	10	0.00	788.06	259.02	829.54	Stable
0.95	3	20	0.00	792.92	260.62	834.65	Stable
0.95	4	30	0.38	798.02	262.30	840.02	Stable
0.95	5	40	0.52	796.14	261.68	838.04	Stable
0.95	6	50	4.62	769.50	252.92	810.00	Stable
0.95	7	60	8.69	730.55	240.12	769.00	Stable
0.95	8	70	9.83	706.14	232.10	743.30	Stable
0.95	9	80	11.08	644.40	211.81	678.32	Stable
0.95	10	90	12.88	624.44	205.24	657.30	Stable
0.95	11	100	13.59	607.25	199.59	639.21	Stable
0.95	12	110	14.87	586.39	192.74	617.25	Stable
0.95	13	120	15.08	575.07	189.02	605.34	Stable
0.95	14	130	15.44	548.45	180.27	577.32	Stable
0.95	15	140	16.02	541.24	177.90	569.73	Stable
0.95	16	150	19.55	0.00	0.00	0.00	Unstable

Wind Injection from Bus 105	Iteration	Wind Farm Power Output		Stability Limits			Stability Limits
Load Power Factor	#	MW	Mvar	P (MW)	Q (Mvar)	Scr (MVA)	Results
0.90	1	0	0.00	742.86	359.78	825.40	Stable
0.90	2	10	2.04	744.46	360.56	827.18	Stable
0.90	3	20	2.54	741.55	359.15	823.94	Stable
0.90	4	30	2.55	738.69	357.77	820.77	Stable
0.90	5	40	2.67	732.19	354.61	813.54	Stable
0.90	6	50	5.24	722.28	349.81	802.53	Stable
0.90	7	60	7.55	676.93	327.85	752.14	Stable
0.90	8	70	13.81	660.31	319.80	733.68	Stable
0.90	9	80	15.22	605.79	293.40	673.10	Stable
0.90	10	90	17.62	580.05	280.93	644.50	Stable
0.90	11	100	20.54	566.09	274.17	628.99	Stable
0.90	12	110	22.00	546.45	264.66	607.17	Stable
0.90	13	120	24.35	537.03	260.10	596.70	Stable
0.90	14	130	27.73	0.00	0.00	0.00	Unstable

Table 3.5 Wind Injection Impact on Stability Boundaries Using DDSG Wind Turbine Type for the Western Kansas Power System (Area I) – P-Q Curve Method Results

DDSG Wind Farm P-Q Analysis							
ZIP Load Components for the 2010 Summer Peak Load Hour 17 (541 MW)				Most Limiting Contingency Opening the Branch between Bus 83 and Bus 128			
Constant Power (P)	30.00%	S_p	167.300 MVA				
Constant Current (I)	25.75%	S_I	143.563 MVA				
Constant Impedance (Z)	44.25%	S_Z	246.727 MVA				
Maximum Wind Injection - P-Q Curve Method Analysis							
Wind Injection from Bus 105	Iteration #	Wind Farm Power Output		Stability Limits			Voltage Stability
Load Power Factor		MW	Mvar	P (MW)	Q (Mvar)	Scr (MVA)	Results
0.97	1	0	0.00	800.64	200.66	825.40	Stable
0.97	2	10	0.00	806.87	202.22	831.82	Stable
0.97	3	20	-0.08	814.04	204.02	839.22	Stable
0.97	4	30	-1.02	823.20	206.31	848.66	Stable
0.97	5	40	0.18	824.60	206.66	850.10	Stable
0.97	6	50	3.92	825.35	206.85	850.88	Stable
0.97	7	60	8.63	825.79	206.96	851.33	Stable
0.97	8	70	9.52	824.76	206.70	850.27	Stable
0.97	9	80	10.85	819.17	205.30	844.51	Stable
0.97	10	90	12.37	817.23	204.82	842.51	Stable
0.97	11	100	13.39	813.23	203.81	838.38	Stable
0.97	12	110	14.52	797.01	199.75	821.66	Stable
0.97	13	120	14.95	779.64	195.40	803.75	Stable
0.97	14	130	14.99	764.87	191.70	788.53	Stable
0.97	15	140	15.83	736.18	184.50	758.95	Stable
0.97	16	150	16.08	699.37	175.28	721.00	Stable
0.97	17	160	25.98	666.68	167.09	687.30	Stable
0.97	18	170	29.37	0.00	0.00	0.00	Unstable
0.95	1	0	0.00	784.13	257.73	825.40	Stable
0.95	2	10	0.00	788.73	259.24	830.24	Stable
0.95	3	20	0.00	796.11	261.67	838.01	Stable
0.95	4	30	0.38	801.34	263.39	843.52	Stable
0.95	5	40	0.52	806.08	264.94	848.50	Stable

Wind Injection from Bus 105	Iteration	Wind Farm Power Output		Stability Limits			Stability Limits
Load Power Factor	#	MW	Mvar	P (MW)	Q (Mvar)	Scr (MVA)	Results
0.95	6	50	4.62	806.17	264.98	848.60	Stable
0.95	7	60	8.69	808.45	265.72	851.00	Stable
0.95	8	70	9.83	804.85	264.54	847.21	Stable
0.95	9	80	11.08	780.35	256.49	821.42	Stable
0.95	10	90	12.88	764.10	251.15	804.32	Stable
0.95	11	100	13.59	759.24	249.55	799.20	Stable
0.95	12	110	14.87	750.70	246.74	790.21	Stable
0.95	13	120	15.08	745.97	245.19	785.23	Stable
0.95	14	130	15.44	713.64	234.56	751.20	Stable
0.95	15	140	16.02	675.81	222.13	711.38	Stable
0.95	16	150	19.55	654.79	215.22	689.25	Stable
0.95	17	160	27.68	0.00	0.00	0.00	Unstable
0.90	1	0	2.04	742.86	359.78	825.40	Stable
0.90	2	10	2.54	739.94	358.37	822.15	Stable
0.90	3	20	2.55	738.51	357.68	820.57	Stable
0.90	4	30	2.67	734.08	355.53	815.64	Stable
0.90	5	40	5.24	730.21	353.65	811.34	Stable
0.90	6	50	7.55	723.91	350.60	804.34	Stable
0.90	7	60	13.81	719.10	348.28	799.00	Stable
0.90	8	70	15.22	714.60	346.10	794.00	Stable
0.90	9	80	17.62	713.25	345.44	792.50	Stable
0.90	10	90	20.54	700.52	339.27	778.35	Stable
0.90	11	100	22.00	698.31	338.21	775.90	Stable
0.90	12	110	24.35	689.24	333.81	765.82	Stable
0.90	13	120	27.73	667.80	323.43	742.00	Stable
0.90	14	130	28.10	643.50	311.66	715.00	Stable
0.90	15	140	28.25	623.12	301.79	692.35	Stable
0.90	16	150	30.25	0.00	0.00	0.00	Unstable

For the SCIG type turbines, voltage stability boundaries calculated for wind injections at Bus 105 not only depended on the wind turbine type used but also on the system load power factor. As system load power factor decreased from 0.97 to 0.90 lagging, increases in wind injections resulted in reductions to the system active and reactive power voltage stability

boundaries as shown Figure 3.3. At a 0.90 system load power factor, increasing wind injection from 0 MW to 40 MW caused a stability boundary decrease of 12.5%. For a system power factor of 0.97, the increase of 0 MW to 40 MW caused the stability boundary limit to decrease by only 0.48%.

Figure 3.3 shows that system power factor has significant impact on how fast the voltage stability limit boundary decreases for any additional wind injected in the system. The higher the power factor the less sensitive the system is to higher wind penetrations until wind penetration exceeds 70 MW where the system power factor has less of an impact on voltage stability boundaries. The same conclusion can be drawn from Figure 3.4, which shows the change in the system stability boundaries (the change from the zero wind injection case expressed in apparent power in MVA) for each system power factor caused by increasing wind injections at Bus 105.

As wind injection at Bus 105 increased using DFIG wind turbine type and with system load power factor decreased from 0.97 to 0.90 lagging, the system active and reactive power voltage stability boundaries decreased. A graphical representation of the effect of increasing wind injection at Bus 105 on active and reactive voltage stability boundaries is shown in Figure 3.5. This figure shows that the system power factor had less of an impact on the changes in voltage stability boundaries for increasing wind penetration with this generator type. At 0.90 system load power factor, increasing wind injection from 0 MW to 40 MW caused the stability boundary decrease of less than 1%. Only when wind injection increased above 60 MW, did the system voltage stability boundaries decrease significantly. It was also noticed that the decrease in voltage stability boundary was not as rapid as in the case of SCIG type. This is due to the fact that DFIG has the ability to control power factor at the point of interconnection.

Figures 3.4, 3.6, and 3.8 shows the stability boundary limits for changes in the power system load power factors for each wind turbine type. In Figure 3.4, and regardless of the load power factor, increasing wind injection from Bus 105 resulted in rapid decrease in the stability boundaries. At a load power factor of 0.97 lagging, a maximum of only 100 MW can be injected at Bus 105 using SCIG. The decrease in the voltage stability boundaries when using DFIG or DDSG wind turbine types was less rapid than the case when using SCIG type of wind turbines, which led to much higher maximum wind injections at Bus 105. At load power factor of 0.97 lagging, using DFIG wind type resulted in a maximum of 150 MW of wind injection at Bus 105. A maximum of 160 MW was obtained using DDSG for the same load power factor.

Figure 3.3 Stability Boundaries for Increasing Wind Injection at Bus 105 Using SCIG Wind Turbine Type for the Western Kansas Power System (Area I) - P-Q Curve Method Results

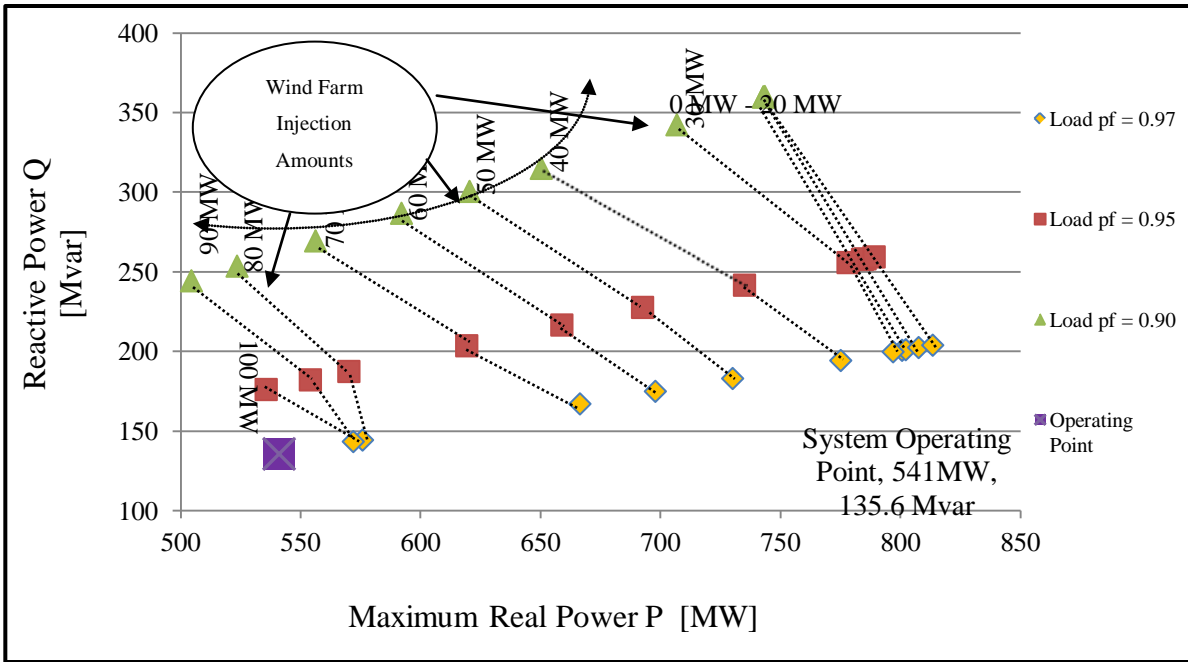


Figure 3.4 Stability Boundary Limits in MVA for Increasing Wind Injection at Bus 105 Using SCIG Wind Turbine Type for the Western Kansas Power System (Area I) - P-Q Curve Method Results

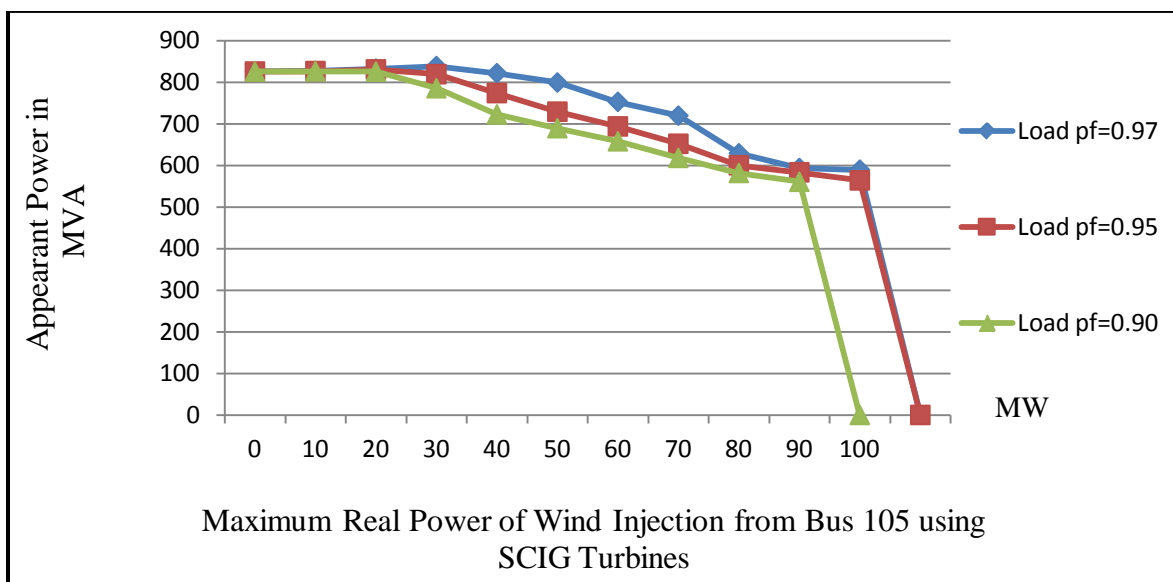


Figure 3.5 Wind Injection Impact on Stability Boundaries Using DFIG Wind Turbine Type for the Western Kansas Power System (Area I) – P-Q Curve Method Results

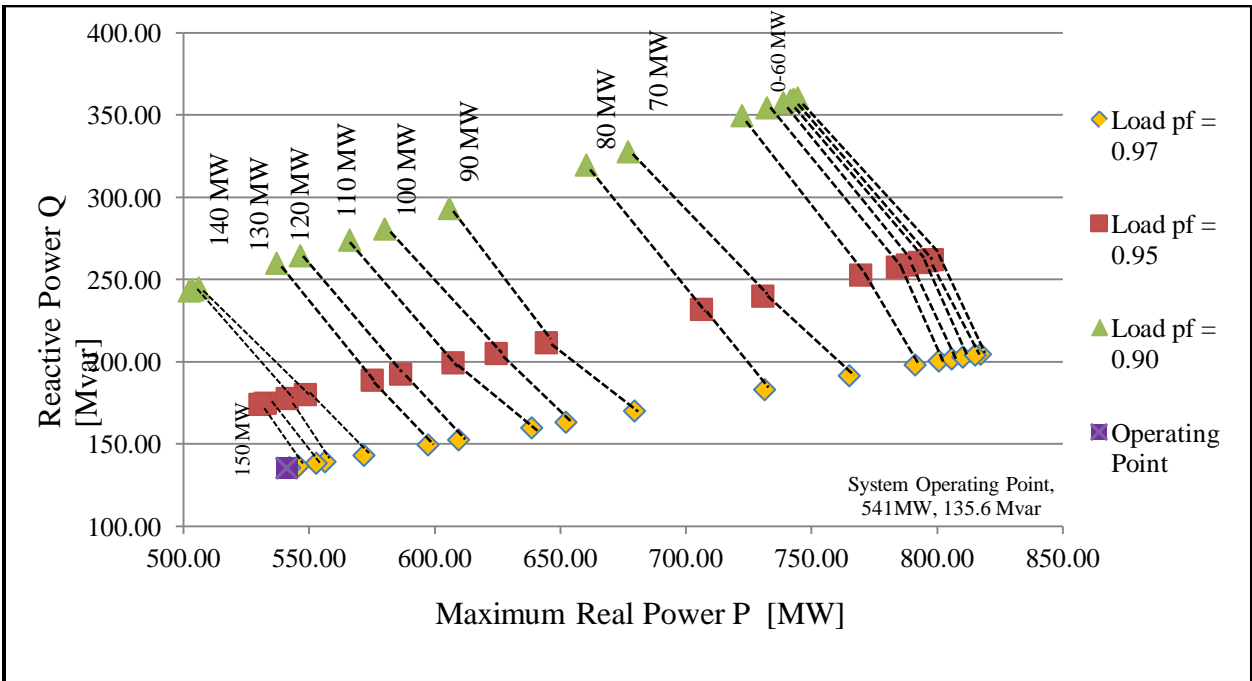


Figure 3.6 Stability Boundary Limits for Increasing Wind Injection at Bus 105 Using DFIG Wind Turbine Type for the Western Kansas Power System (Area I) - P-Q Curve Method Results

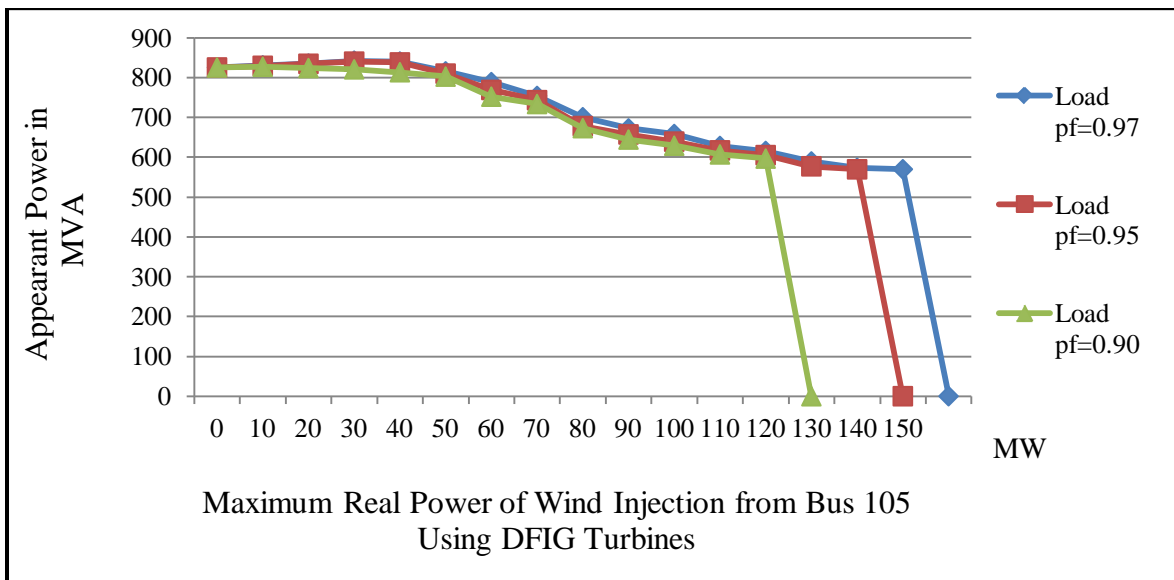


Figure 3.7 Wind Injection Impact on Stability Boundaries Using DDSG Wind Turbine Type for the Western Kansas Power System (Area I) – P-Q Curve Method Results

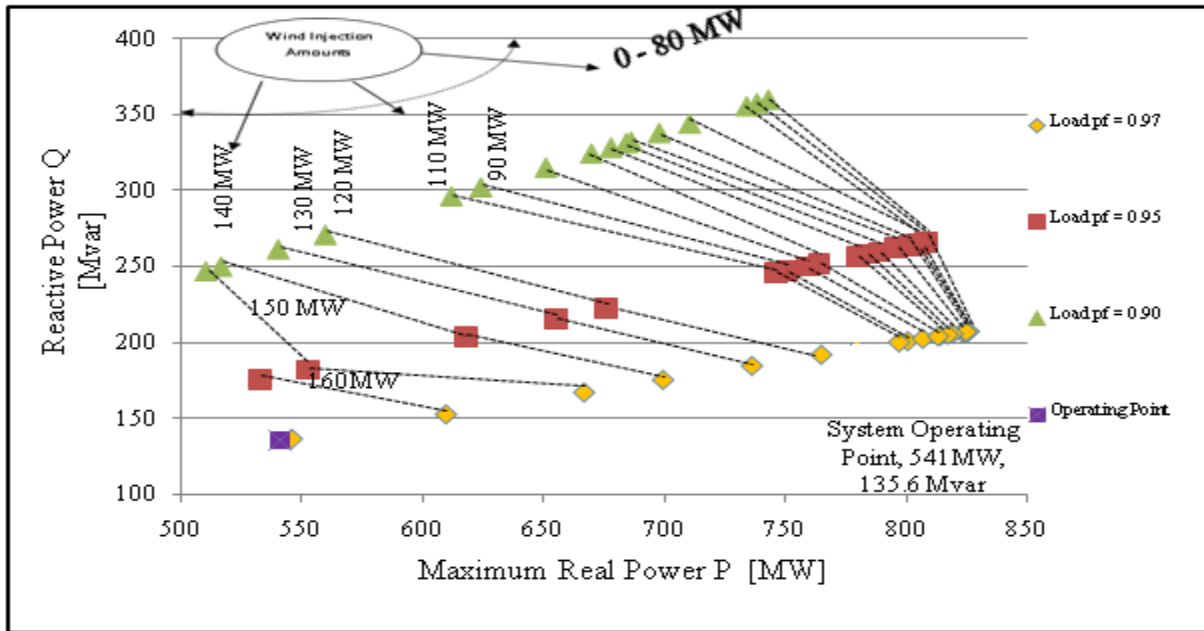
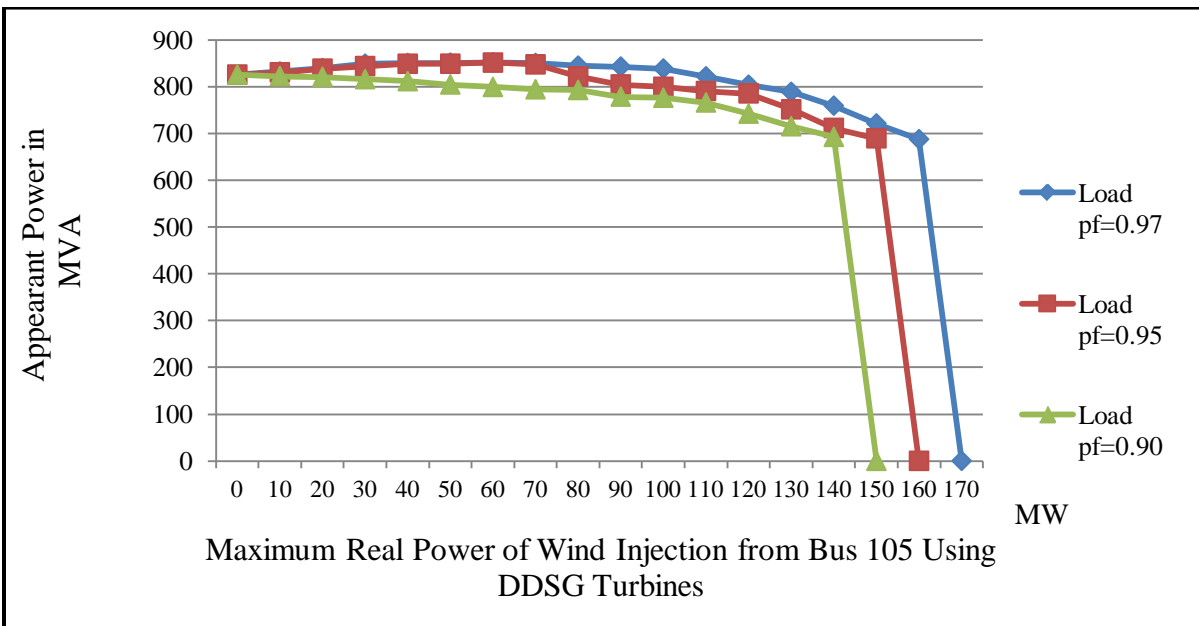


Figure 3.8 Stability Boundary Limits for Increasing Wind Injection at Bus 105 Using DDSG Wind Turbine Type for the Western Kansas Power System (Area I) - P-Q Curve Method Results



3.5 Conclusions

Levels of wind power penetration in power systems depend on the strength of the power system and the type of wind turbine used in the wind power integration. Three wind turbine types have been investigated and the turbine type impact on maximum wind penetration in the western Kansas power system has been evaluated. The three wind turbine types investigated are the Squirrel-Cage Induction Generators (SCIG), the Doubly-Fed Induction Generator (DFIG) and the Direct-Drive Synchronous Generators (DDSG). These are the most popular types of wind turbine in the market today. SCIG is a fixed speed turbine, which is the cheapest turbine among the three types. The biggest disadvantage of SCIG wind turbine type is that it does not have the capability of controlling its own power factor. It actually relies on the power system to provide its needed reactive power for it to produce power. The DFIG and DDSG wind turbine types are variable-speed turbines and have same reactive power control capabilities using AC-DC-AC converters. The convertors that decouple these type of turbines from the power system enable them to vary active and reactive power to maintain high power factor at the point of interconnection with the grid. However, DFIG and DDSG wind turbine types are very costly when compared to SCIG.

Wind farms, which consist of tens or hundreds of wind turbines, can be modeled as an aggregate wind turbine for system analysis that focuses on the power system external to the wind farm. Wind turbines within a wind farm can be aggregated to an equivalent large wind turbine which reduces the complexity of the wind farm during voltage stability simulations of large power systems. The equivalent large wind turbine receives the same wind power as the wind incident on the group of wind turbines.

Voltage stability boundaries calculated for each type of wind turbine confirmed that the lowest wind penetration obtained is when the wind farm in the power system consists of SCIG type wind turbines. At 0.97 lagging power factor, the western Kansas power system was able to safely integrate a maximum of 100 MW when wind injected from a wind farm consisting of only type SCIG wind turbines. The other two types of wind turbines resulted in much higher wind penetration levels. For the DFIG type wind turbines, a maximum wind injection of 150 MW was safely integrated in the power system, and using the DDSG type wind turbines in the wind injection from the wind farm resulted in integrating a maximum of 160 MW. The ability to

produce reactive power using DFIG or DDSG wind turbine types enabled the higher values of wind penetration in the western Kansas power system.

Chapter 4 - Voltage Stability Based Calculations of the Maximum Wind Penetration Using Voltage Stability Iterative Methods

Voltage stability is characterized by a slow decrease in voltage levels at one or more buses in the power system. Both static and dynamic approaches can be used to study voltage stability limits. Dynamic analysis is recommended when studying fast voltage collapse situations. However, dynamic analysis is time consuming and requires detailed dynamic models of all components in the power system which may have an influence on voltage stability. Since in most cases, voltage collapses are usually slow in progress, voltage stability analysis can be effectively analyzed using a static approach instead of dynamic. This will save time and allow the system planner to use readily available steady-state power flow models to conduct voltage stability studies.

Several references have shown that an increase in wind penetration results in greater demand on reactive power, which if not met by the existing power system may, lead to voltage instability [50, 66, 67]. With the increase of wind generation penetration in power systems and their reactive power demand, voltage stability constraints have become one of the most limiting factors in increasing wind penetration in power systems. Based on new wind farm locations, sizes, and wind turbine types, voltage stability margins are impacted even if the existing power systems can incorporate a certain amount of wind generation before reaching voltage collapse [67].

The size of a new wind farm connected to the power system has an impact on the allowed size of any future wind farm in the power system. One of the most significant factors in increasing wind penetration in power systems is the maximum size of newly installed wind farms. Within a power system, wind penetration can be maximized by placing new larger wind farms in areas where the transmission system is strong and has high voltage stability margins. Power system voltage stability margins are impacted by new wind farm installation locations.

Power system wind penetration levels depend on the available *VSMs* of the existing power system [67, 68]. To maximize wind penetration level in a power system, newly installed wind farms which result in less negative impact on voltage stability margins must be sized larger than other wind farms which result in high negative impact on *VSMs*. In sizing new wind farms, the use of the hourly analysis is necessary due to wind power output fluctuations during the day.

Wind power outputs tend to be at a maximum during early morning and late evening hours and at a minimum during the afternoon hours. Hourly analysis is also necessary since hourly load types changes during the day [69]. Hourly load type changes must be identified and properly modeled in the seasonal base case for every hour of the day since load type changes can significantly impact the location of the voltage collapse point, which may in turn limit maximum sizes of new wind farms. As discussed earlier, using constant power (P) load type models when calculating voltage collapse point can result in conservative voltage stability limit [70].

Two new iterative methods for sizing new wind farms are presented. The proposed methods are then applied to determine the maximum size of three widely separated wind farms (about 60 miles apart) which are proposed for installation on the western Kansas power system Area I. The findings and analysis are presented and followed by a comparison between the methods.

4.1 Impact of Load Modeling on Voltage Stability Assessment for Power Systems with High Wind Penetration

Even when only static models are used, load levels and load models are known to have profound impacts on voltage stability calculations. Heavy loading conditions have the most negative impact on voltage stability margins [71, 72]. As shown previously, voltage stability margins are also sensitive to load mix with respect to constant power (P), constant current (I) and constant impedance (Z) loads. Therefore, power system load types must be accurately modeled when calculating voltage stability margins. Since voltage stability margins calculated using constant power (P) tend to be conservative estimates of voltage collapse point, it may limit the maximum size of new wind farms allowed to connect to the power system. Also, large voltage stability buffers, which may be as high as 5%, may limit wind farm maximum sizes. Voltage stability buffer calculation method developed in this dissertation can be used to determine more realistic load type buffer that has minimum impact on maximum wind farm sizes.

Power systems with a high concentration of fast response dynamic loads like induction motors require detailed load dynamics to calculate voltage stability margins [55], however, the overall composite load in a typical power system exhibits slow dynamic characteristics which enable transmission planners to use steady-state load flow analysis for any kind of contingencies.

For all load types in a power system, it is generally acceptable to calculate voltage stability margins using static load modeling since voltage collapse is a relatively slow process [73].

Power system loads are voltage sensitive and their response to voltage fluctuation must be modeled when calculating voltage stability. When voltage drops below 0.90 per unit (pu) on a load bus, load dynamics have significant impact on collapse point calculations even for slow occurring voltage collapse. The 0.90 p.u. voltage limit is based on power systems voltage controls which keep loads constant; however, when systems experience lower than a 0.90 p.u. voltage level, loads are no longer constant [74]. Load dynamics impact on *VSMs* are not very significant when limiting the power system to voltages above 0.90 p.u. when calculating *VSMs* [55, 74]. To enforce the assumption, power system is considered voltage unstable when any load bus voltage drops below 0.90 p.u. or reaches voltage collapse point which ever happens first.

4.2 Voltage Stability Based Methods for Determining Maximum Wind Farm Sizes

Two new iterative methods have been developed to optimally determine the size of new wind farms in an interconnected power system. Wind farm size is the maximum power that a wind farm can produce based on its rated power. The main difference between the two methods is how each wind farm maximum size is incremented during each iterative step. All new wind farm power outputs are increased from zero MW to a final maximum MW value based on their impact on *VSMs*.

In Method I, all new wind farms are simultaneously incremented until reaching voltage instability or until any bus voltage drops below a pre-defined value (0.90 p.u.). In Method II, only one wind farm power output is incremented at the end of each iterative step until reaching voltage instability or voltage drops below a pre-defined value (0.90 pu). Thus, Method II allows different sizes of wind farms between sites while Method I does not. In every iterative step, both methods uses hourly peak loads, hourly load types and maximum wind farm power outputs as input in the base load flow case.

Available power system models with large interconnected systems of many buses are used for wind integration studies with some modifications. The following steps can be used to modify large base case load-flow models for wind integration studies.

1. Specify new wind farm injection sites.

2. Specify applied terminal voltage where wind injection site collector substation will be connected to the grid.
3. Specify the power factor at the point of interconnection for every new wind injection site, and then calculate reactive power output “ Q_{out} ” in Mvar for each wind injection site for every possible output power “ P_{out} ”.
4. Specify seasonal base load flow case to be used in the analysis, then solve the load flow case.
5. Model and connect all new wind farms to the power system at their proposed point of interconnection.
6. Set all new wind connection points to generate zero MW of real power with their corresponding Q_{out} Mvar and then solve the load flow case.
7. Solve the new base power flow case with new wind farms modeled. Verify that the new base power flow case is voltage stable under normal operating conditions.
8. Perform contingency analysis to determine if the new base power flow case is voltage stable under contingencies. Verify that the new base case is voltage stable under contingency conditions.
9. Determine the power increment “ ΔP ” in MW by which wind farm power output will be increased.

The new methods for maximizing wind penetration are described next.

4.2.1 Method I: Simultaneous Wind Farm Power Output Incremental Increase

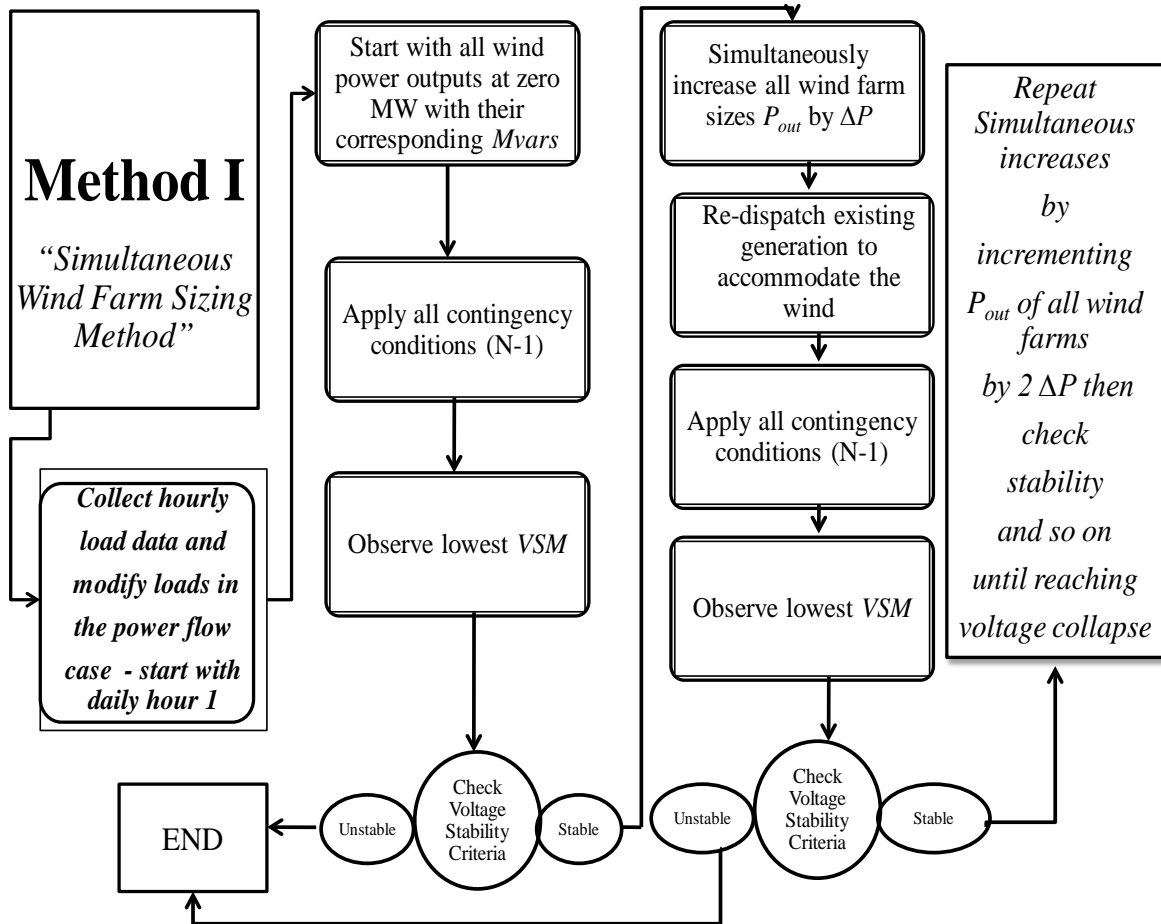
This method calculates maximum wind farm size for each new wind farm by simultaneously increasing new wind farms maximum power outputs in equal increments. Each proposed wind farm’s power output is incremented (starting from zero MW output) in steps until reaching voltage instability or voltage drops below a pre-determined value (0.90 p.u.). The steps for this calculation method are listed below.

1. Start with the new voltage stable power flow case modified using the steps above.
2. List and sort all seasonal hourly peak loads in 24 different groups with each group representing a daily hour starting with hour 1 to hour 24. Each daily hour represents all maximum system peak loads occurring in that hour for all the days in the study season.

3. In each daily hour, sort all seasonal peak load data. Only the maximum load value for each daily hour is needed to create 24 different power flows. Each of the 24 daily hour power flows represent a power flow with total system load equal to the maximum load observed for that hour during the season.
4. Specify the daily hour of the season to analyze for the maximum sizes of all new wind farms (from hour 1 to hour 24). Start with daily hour 1.
5. In the load flow case, scale all loads in power flow case in Step 1 to equal the maximum load of the daily hour specified in Step 4. This will result in the worst *VSM* values when compared with the same wind penetration at a lower load levels.
6. For the daily hour specified in Step 4, modify the power flow load flow model to account for load model characteristics by entering the percent of load with constant power (P), constant current (I) and constant impedance (Z) into the power flow model. This step is necessary to include load voltage dependent characteristics in the load flow model for any specific daily hour.
7. Calculate new wind farm sizes by simultaneously increasing all wind farms sizes by ΔP . Set new power outputs of each new wind farm to equal to $P_0 + \Delta P$.
8. Re-dispatch existing generation based on a pre-defined generation schedule to accommodate the new wind generation level assuming wind farm power outputs are at their maximum outputs.
9. With the new maximum power outputs of all wind farms, perform contingency power flow analysis to calculate voltage stability margin (*VSM*) at the weakest point in the power system.
10. If the *VSM* of the weakest bus is voltage stable, then repeat steps 7 through 9. Otherwise, go to step 11.
11. Power system is voltage unstable. The maximum size of each new wind farm is equal to the maximum size found in Step 7; just before the last iteration at which the power system reached voltage instability.
12. Repeat Steps 4 through 11 for all remaining season daily hours; hours 2 through 24.
13. END.

The flow chart shown in Figure 4.1 illustrates the 13 steps describing Method I.

Figure 4.1 Sizing Wind Farms Using Method I – Simultaneous Increase of Wind Farms’ Power Outputs



4.2.2 Method II: Independent Wind Farm Power Output Incremental Increase

This method calculates maximum wind farm size for each new wind farm independently by using iterative steps for incrementing each new wind farm size from zero to a maximum value. At each iterative step, each new wind farm power output is incremented by “ ΔP ” in MW while holding all other wind farm sizes at their current sizes. The impact of incrementing each wind farm’s size on VSMs is compared in each iterative step. At the end of each iterative step, the size of the incremented wind farm which resulted in the least negative impact on VSMs is increased. The new size of this wind farm will be increased by “ ΔP ” MW, and it will be used in the next iterative step as an initial value. All other wind farm sizes remain constant at their

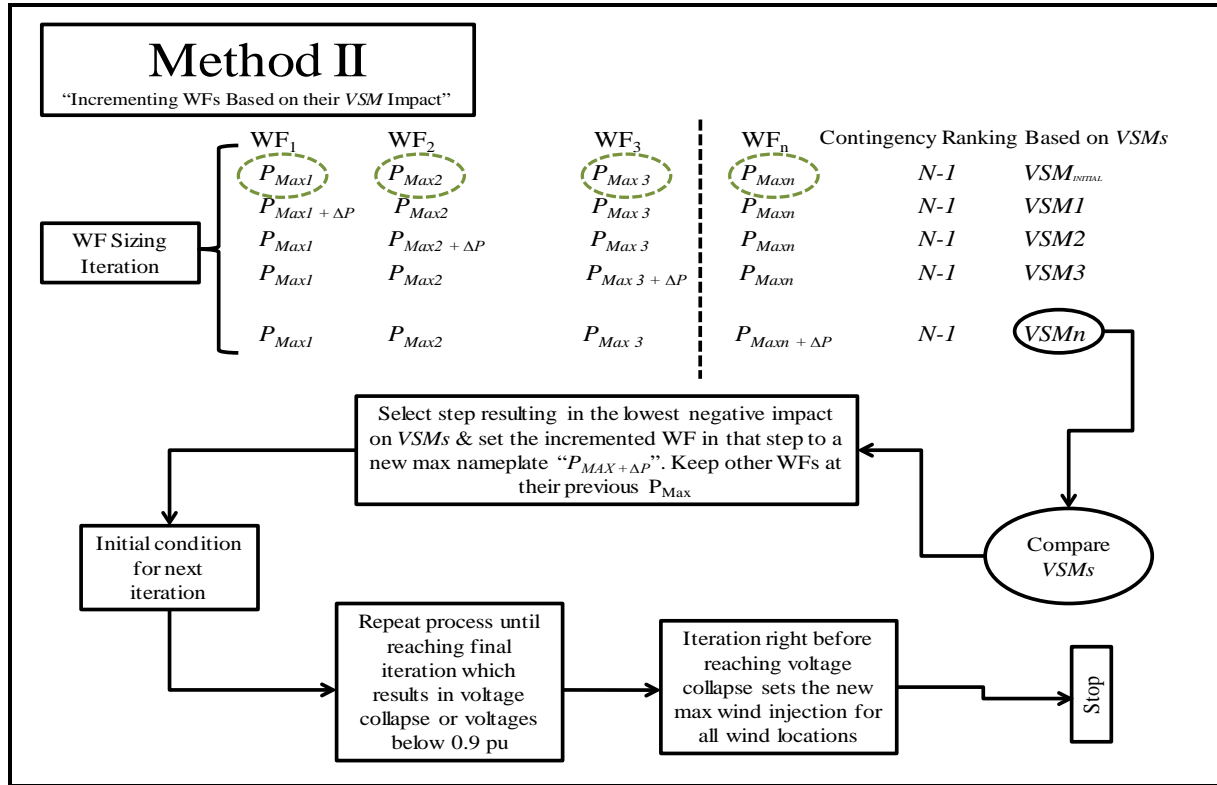
current maximum sizes. Iterative steps are repeated until a new wind farm size increment results in voltage instability or voltage drops below a pre-determined value (0.90 pu). Steps for this calculation method are listed below.

1. Start with the new voltage stable power flow case created in Section 4.2. .
2. List all hourly peak loads in 24 different groups (24 daily hours). Each group contains all maximum system peak load that occurred in that hour for all the days in the study season.
3. In each group, sort all seasonal peak load data. Only the maximum peak load that occurred in each daily hour is used in the modified load flow model to calculate *VSMs*. The maximum load observed for each daily hour is the amount of load that will result in the lowest *VSM*, since lack of reactive power in weak power system is the main cause to voltage instability [67, 68, 75].
4. Specify the daily hour of the season to analyze for the maximum sizes of all new wind farms (from daily hour 1 to daily hour 24) starting with daily hour 1.
5. Scale all loads from Step 1 in the same proportion to equal the maximum peak load that occurred in that daily hour as specified in Step 3. This is the highest load level seen for this daily hour during the season. Highest load level observed is used since it will result in the worst *VSM* values when compared to lower load levels (conservative approach).
6. Modify the power flow load model for each hour to account for load model characteristics by entering the percent of loads as a (ZIP) load composite mix. This step is necessary to include load voltage dependent characteristics in the load flow model for the specified daily hour.
7. Start iterative steps by increasing wind power output of one new wind farm by an increment of “ ΔP ” in MW while keeping all other new wind farm power outputs at their previous maximum outputs.
8. Re-dispatch existing conventional generation based on a pre-defined generation schedule to accommodate the new wind generation level, assuming wind farm power outputs are at their maximum outputs (at their maximum rated power).
9. Perform N-1 contingency power flow analysis to calculate the *VSM* at the weakest point in the power system. The N-1 contingency is the loss of single transmission line due to power system disturbance.
10. Record the lowest *VSM* calculated in Step 9.

11. Repeat Steps 3 through 10 for all other new wind farms by increasing their power outputs by ΔP MW.
12. Compare *VSMs* resulting from incrementing each wind farm.
13. Increase the size of the wind farm which resulted in the highest *VSM* (the wind farm which resulted in the least impact on *VSMs*). All other wind farms remain at their previous sizes.
14. Repeat Steps 7 through 13 until the power system reaches voltage collapse or a voltage drops below the pre-defined value of 0.90 pu. The iterative step right before reaching voltage collapse sets the final wind farm sizes.
15. Repeat Steps 4 through 14 for all remaining hours; daily hours 2 through 24.
16. End

The flow chart shown in Figure 4.2 illustrates the 13 steps describing Method II.

Figure 4.2 Sizing Wind Farms Using Method II - Wind Farm Power Output Increases Based on their VSM Impacts



4.3 Simulation Model Formulation & Results

The two methods described in Section 4.2 are applied to the western Kansas power system (Area I). Following is the detailed simulation model formulation followed by the results of the analysis using the two wind farm sizing methods.

4.3.1 Simulation Model Formulation

The proposed Wind farm sizing methods have been applied to the western Kansas power system (Area I) as shown in Figure 2.8. Three new wind farms in three widely separated locations within the western Kansas power system are being studied for optimal sizes. All three wind farms are located in regions with similar wind class (Class 5) and similar transmission interconnection facilities at 115 kV. New wind farms are connected to the grid at 115-kV voltage and are modeled as PQ buses at the point of interconnection with a fixed power factor bandwidth of leading/lagging 0.95. VSM calculations were generated using the Southwest Power Pool (SPP) summer 2010 power flow model which was modified to incorporate the new wind farms. The

worst contingency for *VSMs* in Area I is when the 115 kV transmission line from Bus 83 to Bus 128 is out of service. All calculations presented next are based on this contingency.

The SPP 2010 base summer model showed all load types as constant power loads (P). Modifications to the load type in the base case were necessary even though the voltage stability criteria used for this analysis does not allow for load bus voltages to fall below 0.90 pu. Load levels are still impacted by any voltage level changes; however, their dynamic representation is not necessary due to the 0.90 pu limit imposed on voltage stability calculations.

Representing loads in the power flow models only as constant power (P) load type will result in conservative limits on voltage stability calculations [47]. Load types in the SPP base model have been modified based on data collected by Sunflower Electric Power Corporation in western Kansas for Area I. Tables 4.1 and 4.2 show typical load types as a percent of the total loads. Tables 4.1 and 4.2 also show the composite of loads in the western Kansas power system, which consist of Residential, Agriculture, Commercial, and Industrial components.

Table 4.1 Load Types and Load Characteristics for the July 2010 (Daily Hours 1 through 15 and Daily Hours 21 Through 24)

Load Type Hours 1-15 & 21-24 Summer Season	% of Total System Load	Constant Power P	Constant Current I	Constant Impedance Z
Residential	28	23	42	35
Agriculture	45	75	15	10
Commercial	11	50	33	17
Industrial	16	80	12	8

Table 4.2 Load Types and Load Characteristics for July 2010 (Daily Hours 16 Through 20)

Load Type Hours 16-20 Summer Season	% of Total System Load	Constant Power P	Constant Current I	Constant Impedance Z
Residential	32	20	53	27
Agriculture	28	68	25	7
Commercial	15	20	57	23
Industrial	25	50	27	23

4.3.2 Simulation Results

The two voltage stability optimization methods were applied to determine optimal sizes for three proposed wind farms in the western Kansas Region. New wind farms are located about 120 miles apart but with similar wind patterns and similar grid interconnection facility ratings. All new wind farm generation sinks in the western Kansas power system.

In weak power systems, the most limiting condition for maximum wind farm sizes is during heavy loading hours. For each daily hour, only the hour with the highest load level is necessary for calculating *VSM* limits on wind farm sizes. Therefore, an hourly approach was applied to determine optimal wind farm sizes for each hour of summer days (month of July 2010) using the maximum loading conditions for each daily hour. Both new methods have been applied to 24 new load flow models with each load flow represent a daily hour with the maximum load observed for that daily hour.

Western Kansas load peaks in the afternoon hours (4 pm – 8 pm) as shown in Figure 4.3. For the base case with no new wind injection, heavier loading conditions during the afternoon hours resulted in lower *VSMs* than other hours of the day as can be seen from Table 4.3 and Figure 4.4.

Figure 4.3 “2010” July Peak MW Load for the Western Kansas Power System (Area I)

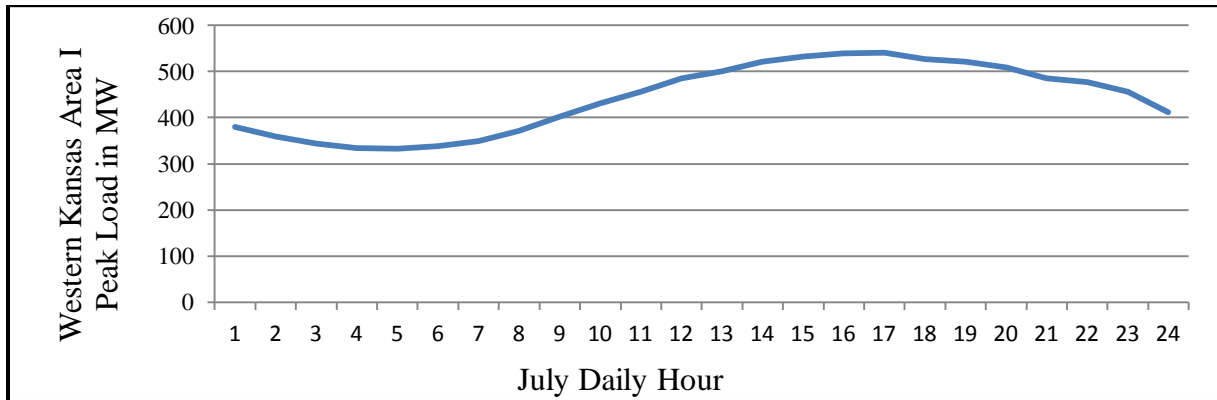
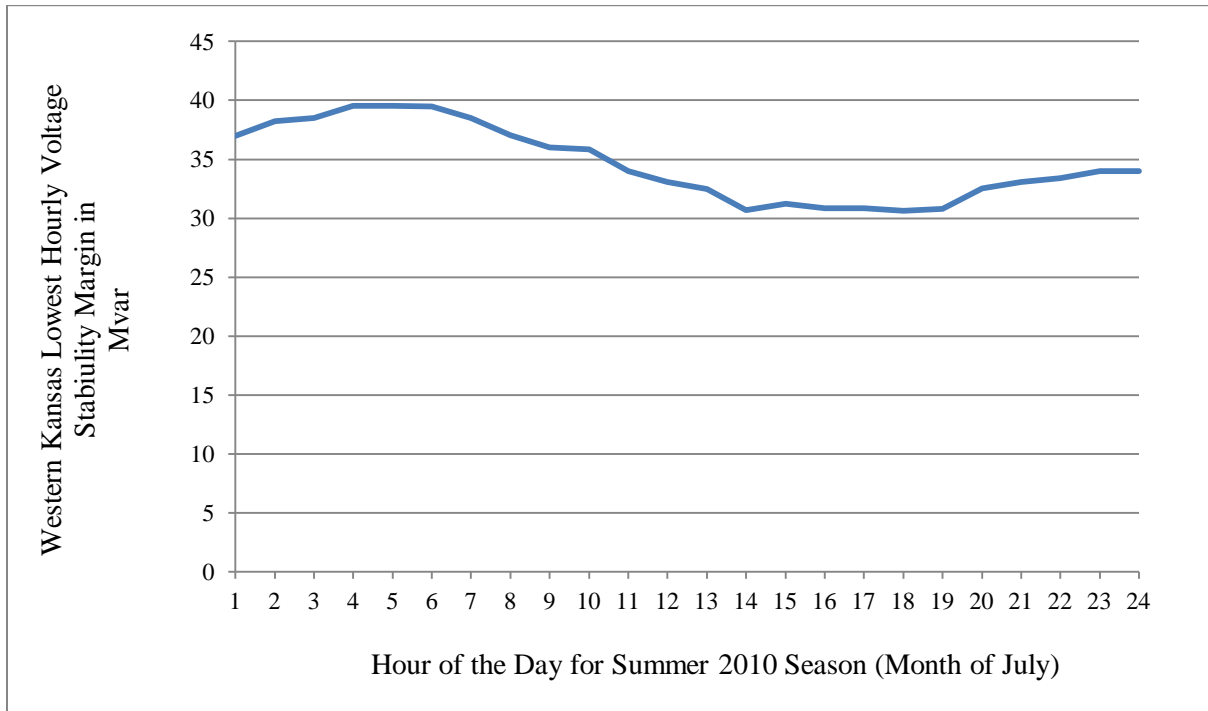


Table 4.3 July 2010 Peak Load in MW and the Hourly VSMs in Mvars before Wind

Injections

Hour of the Day for Summer July 2010	Max Western Kansas Hour Peak Load in MW	Lowest VSM Calculated in Mvar for the Worst Contingency Without Wind Injection
1 (12 am – 1 am)	380	36.98
2 (1 am – 2 am)	359	38.23
3 (2 am – 3 am)	344	38.51
4 (3 am – 4 am)	334	39.53
5 (4 am – 5 am)	332	39.55
6 (5 am – 6 am)	338	39.50
7 (6 am – 7 am)	349	38.52
8 (7 am – 8 am)	371	37.05
9 (8 am – 9 am)	402	36.02
10 (9 am – 10 am)	431	35.85
11 (10 am – 11 am)	456	34.01
12 (11 am – 12 pm)	485	33.09
13 (12 pm – 1 pm)	501	32.45
14 (1 pm – 2 pm)	522	30.68
15 (2 pm – 3 pm)	533	31.20
16 (3 pm – 4 pm)	540	30.85
17 (4 pm – 5 pm)	541	30.84
18 (5 pm – 6 pm)	527	30.65
19 (6 pm – 7 pm)	522	30.79
20 (7 pm – 8 pm)	509	32.55
21 (8 pm – 9 pm)	485	33.09
22 (9 pm – 10 pm)	477	33.42
23 (10 pm – 11 pm)	456	34.01
24 (11 pm – 12 am)	412	34.02

Figure 4.4 Lowest Hourly VSMs in Mvar for July 2010 (Month of July)



Results for determining maximum wind farm sizes for each daily hour for the 2010 summer season using Methods I and II are shown in Tables 4.4 and 4.5 for the three different turbine types. In Method I, all three wind farm's maximum sizes were increased by 10 MW increments until reaching the collapse point. Applying Method I to determine maximum wind farm sizes resulted in equal wind farm sizes for all three wind farms due to the application of uniform equal increases for all wind farms during each iterative step. Method II resulted in higher total wind penetration and for all daily hours. In each iterative step, wind farm maximum sizes were incremented by 10 MW while observing the impact on *VSMs*. After every size increase iteration, the wind farm which resulted in the lowest negative impact on *VSM* after each increase was selected and its size was increased by the incremented amount. The application of Method II for the heaviest loading hour (hour 17 (4 pm – 5 pm)) is shown in Table 4.7 for illustration purposes.

Table 4.4 Maximum Wind Penetration in MW for Each Daily Hour During the Summer 2010 for Three Wind Turbine Types Using Method I (Simultaneously Increasing All Wind Injection Sites Until Reaching the Collapse Point)

Daily Hour	Peak Load MW	Total Wind Injection In MW Using SCIG Type with Additional Shunt Capacitors	Total Wind Injection In MW Using DFIG Type	Total Wind Injection In MW Using DDSG Type
1	380	240	270	285
2	359	240	270	285
3	344	240	270	285
4	334	240	270	285
5	332	240	270	285
6	338	240	270	285
7	349	240	270	285
8	371	240	270	285
9	402	240	255	285
10	431	225	240	285
11	456	225	240	285
12	485	225	240	255
13	501	225	240	255
14	522	210	240	255
15	533	210	240	255
16	540	210	240	255
17	541	210	240	255
18	527	210	240	255
19	522	210	240	255
20	509	210	240	255
21	485	225	240	285
22	477	225	240	285
23	456	225	240	285
24	412	240	255	285

Table 4.5 Maximum Hourly Wind Penetration Using Method II

Hour	Peak 2010 Load MW	Total Maximum Combined Wind Farm Sizes for SCIG Type with Additional Shunt Capacitors MW	Total Maximum Combined Wind Farm Sizes for DFIG Type MW	Total Maximum Combined Wind Farm Sizes for DDSG Type MW
1	380	260	280	300
2	359	260	280	300
3	344	260	280	300
4	334	260	280	300
5	332	260	280	300
6	338	260	280	300
7	349	260	280	300
8	371	260	280	300
9	402	260	280	300
10	431	260	280	300
11	456	260	280	300
12	485	260	280	300
13	501	260	270	300
14	522	250	260	300
15	533	250	260	290
16	540	250	260	290
17	541	250	260	290
18	527	250	260	300
19	522	250	260	300
20	509	260	270	300
21	485	260	280	300
22	477	260	280	300
23	456	260	280	300
24	412	260	280	300

At low levels of wind penetration, *VSMs* are not significantly impacted by adding small amounts of wind generation since the available reactive power support from existing conventional generators in the power system has not changed and the wind resources are closer to the loads. However, as can be seen in iterations number 24 and higher in Table 4.7, when wind penetration became significantly higher, *VSMs* decreased for every increase in wind farm size due to the reduction in system reactive power. Wind generators which provide limited reactive power replaced conventional generators capable of providing more reactive power.

Table 4.6 Iterative Steps for Calculating Maximum Wind Farm Sizes for the SCIG, DFIG and DDSG Wind Turbine Types Using Method II for Daily Hour “4 pm – 5 pm” for the Contingency of Losing the 115 kV Transmission Line from Bus 83 to Bus 128

Iteration Number	WF 1	WF 2	WF 3	Lowest Voltage Stability Margin Observed in Mvar			Comments
	Bus 105	Bus 110	Bus 119	SGIG Wind Turbine with Shunt Capacitors	DFIG Wind Turbine	DDSG Wind Turbine	
	Max Wind Farm Sizes in MW						
BASE CASE	0	0	0	23.84	30.84	30.84	No Wind Injection
Iteration 1	10	0	0	30.25	30.99	31.05	Increase WF 1
	0	10	0	29.95	30.97	30.99	Increase WF 2
	0	0	10	29.22	30.15	30.83	Increase WF 3
Result 1	10	0	0	29.25	30.99	31.05	Set WF 1 to 10 MW
Iteration 2	20	0	0	30.03	31.08	31.11	Increase WF 1
	10	10	0	29.90	30.53	30.97	Increase WF 2
	10	0	10	29.87	30.01	30.33	Increase WF 3
Result 2	20	0	0	30.03	31.08	31.11	Set WF 1 to 20 MW
.....
Result 23	90	60	80	19.50	20.32	21.05	Results of Iteration #23
Iteration 24	100	60	80	18.65	20.23	20.92	Increase WF 1
	90	70	80	18.08	18.35	20.86	Increase WF 2
	90	60	90	18.12	19.25	20.55	Increase WF 3
Result 24	100	60	80	18.65	20.23	20.92	Set WF 1 to 100 MW
Iteration 25	110	60	80	17.32	18.33	19.04	Increase WF 1

	100	70	80	16.24	17.54	18.67	Increase WF 2
	100	60	90	16.54	17.33	18.54	Increase WF 3
Result 25	110	60	80	17.32	18.33	19.04	Max Limit on SCIG Type
Iteration 26	120	60	80	Unstable	12.57	13.84	Increase WF 1
	110	70	80	Unstable	12.67	14.35	Increase WF 2
	110	60	90	Unstable	11.23	14.22	Increase WF 3
Result 26	110	70	80	Unstable	12.67	14.35	Max Limit on DFIG Type
Iteration 27	120	70	80	Unstable	Unstable	13.25	Increase WF 1
	110	80	80	Unstable	Unstable	12.54	Increase WF 2
	110	70	90	Unstable	Unstable	12.85	Increase WF 3
Results 27	120	70	80	Unstable	Unstable	13.25	Set WF 1 to 120 MW
Iteration 28	130	70	80	Unstable	Unstable	11.39	Increase WF 1
	120	80	80	Unstable	Unstable	11.22	Increase WF 2
	120	70	90	Unstable	Unstable	12.08	Set WF 3 to 90 MW
Results 28	120	70	90	Unstable	Unstable	12.08	Increase WF 1
Iteration 29	130	70	90	Unstable	Unstable	10.25	Increase WF 2
	120	80	90	Unstable	Unstable	8.37	Increase WF 3
	120	70	100	Unstable	Unstable	10.85	Max Limit on DFIG Type
Iteration 30	130	70	100	Unstable	Unstable	Unstable	Increase WF 1
	120	80	100	Unstable	Unstable	Unstable	Increase WF 2
	120	70	110	Unstable	Unstable	Unstable	Increase WF 3
TOTAL COMBINED WIND FARM MAX SIZES				250 MW	260 MW	290 MW	Summary

The decrease in *VSMs* was dependent on the location of the new wind farm and the type of turbine used in the wind farms. Location 3 was the best location to inject additional wind during high wind penetration cases. Method II resulted in higher wind penetration levels than Method I for all the daily hours studied by an average of 13.7% for all the types of wind turbine generators considered.

Results of applying both methods indicated that the effect of voltage stability limits on maximum wind farm sizes is highly dependent on the type of wind turbine used at each new wind farm location. Also, the degree to which wind turbine type impacted the maximum wind farm sizes was dependant on the method used to increase wind farm sizes. Results of the analysis indicated that maximum wind farm sizes were less sensitive to the type of wind turbine used in each wind farm when sizing new wind farms using Method II. Sizing new wind farms based on each individual wind farm's impact on system *VSMs* allowed for maximum use of available systems *VSMs* and resulted in better reduction in *VSMs* after each incremental increase in wind farm sizes.

When Method II was applied to determine maximum wind farm sizes using DFIG type or DDSG type turbines in new wind farms, the combined wind farm sizes for all three wind farms was at least 4% higher than the combined sizes found using SCIG type even when shunt capacitors are added to provide the SCIGs with reactive power. This is due to the fact that the DFIG and DDSG wind turbine types operate in power factor controlled mode and do not consume reactive power, which yielded higher voltage stability margins when compared to the SCIG type which consumes reactive power that may exceed the Mvar size of the shunt capacitor banks. The use of DDSG type in new wind farms allowed for a minimum of 11.5% increase in the combined maximum wind farm sizes when compared to the DFIG type using Method II. This is due to the fact that the reactive power capability of the DFIG type is less than that of the DDSG type. The DDSG wind turbine type uses full rated power converters with available reactive power that is much higher than the reactive power available from converters used in DFIG type which are only rated for 20 to 25% of their maximum real power output.

4.4 Conclusions

This chapter presents a new approach for determining the maximum size of new wind farms that can be injected in power systems without reaching voltage instability. Not relying on a

voltage stability based approach for determining maximum sizes of new wind farms could limit future wind integration due to the reduction in voltage stability margins in other parts of the power system.

To maximize wind penetration in power systems, new wind farm maximum sizes should be decided using Method II. Method II resulted in higher wind penetration than Method I for all hours studied. The new method uses a steady-state power flow models with potential new wind farm sites included.

The new methods presented in this chapter give wind farm developers and utility planners a tool to determine the maximum wind farm sizes which are safe, in the voltage stability point view, while maximizing total system wind penetration level. This new approach can be applied to any number of proposed wind farms in any weak power system.

Chapter 5 - Methods for Assessing System Impact of Increasing Wind Farm Sizes Above Their Maximum Limits

Maximum wind penetration levels depend on the available *VSMs* of the existing power system [76]. To maximize wind penetration levels in a power system, new wind farms which result in less negative impact on *VSMs* must be sized larger than wind farms which result in more negative impact on *VSMs*. Limiting the maximum size of wind farms based on the assumption that high wind speed occurs simultaneously with peak loading conditions may not result in maximizing wind penetration levels [50, 67]. The wind speed threshold which is required for a wind farm to produce at its maximum power output may never occur during peak loading conditions.

In the previous chapter, wind farms were sized to maximize wind farm sizes based on their impact on *VSMs*. Wind farms with lowest negative impact on *VSMs* were sized larger than the others. In calculating maximum voltage stable wind farm sizes, it was assumed that wind resources would be available during peak loading hours to produce power concurrent with peak load. Although this approach provide wind farm sizes which are voltage stable for all times under all conditions, it is a conservative approach since it limits wind farms to a maximum power output based on wind speed assumptions at the wind farm sites, which may not occur during worst voltage stability conditions.

Wind farm sizes can be increased above the maximum sizes found in the previous chapter by considering actual wind speed levels during peak loading conditions, with the option of curtailing wind generation under certain conditions based on voltage stability margins. During wind curtailment, some of the turbines within a wind farm must shut down (disconnected) to mitigate voltage instability conditions. It is assumed that if the wind speed during peak loading conditions exceeded the expected maximum speed, wind power generated will be curtailed to prevent voltage collapse. In the area studied in this chapter (western Kansas, Area I), wind power outputs tend to be at their maximum during early morning and late evening hours and at their minimum during the afternoon hours when the area loads are at their peak [31, 77].

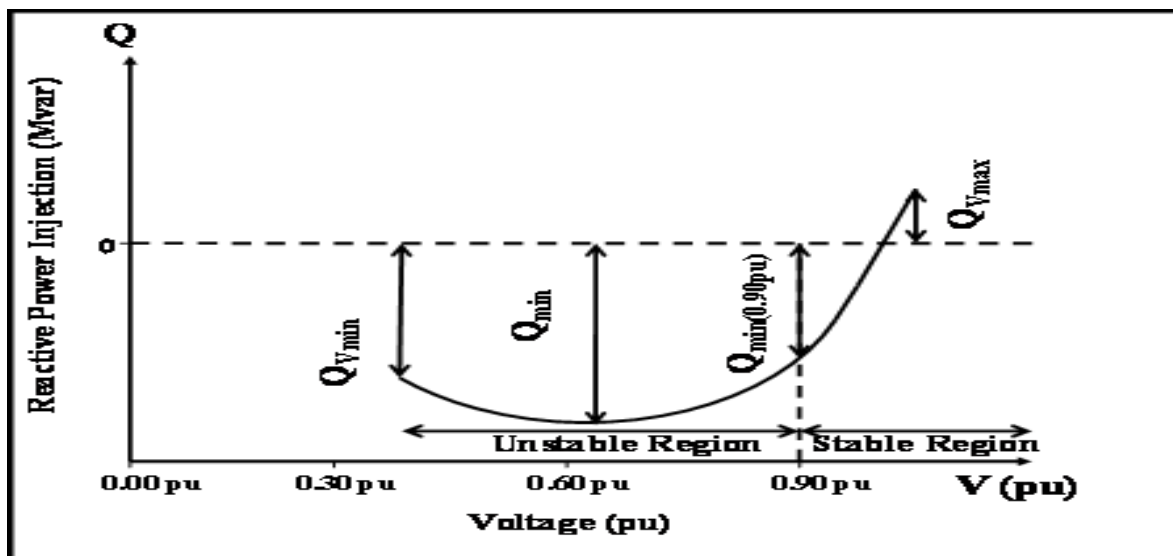
This chapter presents a new practical approach for assessing the impact of increasing wind penetration by combining system *VSMs*, load patterns and available wind resources at the wind generation sites. A brief presentation of the steady-state voltage stability technique “Q-V

Curve Method” and voltage stability criteria are discussed in Section 5.1. In Section 5.2, a voltage stability strength index based on the *EVSM* concept is introduced. The new index provides a quantitative measure to the impact of increasing wind penetration on system voltage stability. Detailed steps of a new wind farm sizing method which can be used to assess the impact of increasing wind farm sizes on system voltage stability are also presented in Section 5.2. In Section 5.3, the proposed method is applied to one of the wind farms in western Kansas. The impact of increasing the wind farm size on western Kansas voltage stability and the expected number of curtailment hours are discussed in Section 5.3 or in chapter conclusions presented in Section 5.4.

5.1 Voltage Stability Assessment Criteria

A power system experiences a state of voltage instability when there is a progressive or uncontrollable decrease in voltage level after a disturbance, increase in load demand, or change in operating condition. For a voltage stable system, an increase in reactive power “Q” will result in an increase in bus voltage “V”. For a voltage unstable system, an increase in reactive power “Q” results in a decrease in bus voltage “V” [47]. Figure 5.1 shows the stable region considered by this voltage stability criterion. Only steady-state load level changes for voltage fluctuation is considered in calculating *VSMs*.

Figure 5.1 Q-V Curve Stability Regions per Criteria



The Q-V curve method used for calculating voltage stability margins has several advantages over other static voltage stability analysis tools especially when lack of reactive power “Q” causes power systems to reach the collapse point. For this chapter, and to comply with the local utility criteria that no bus voltages should drop below 0.90 p.u., voltage stability margin is defined as the lesser of the reactive power Mvar distance measured from the operating point to the bottom of the Q-V curve (Q min) or from the point where bus voltage drops below the 0.90 p.u. as shown in Figure 5.1 [46].

5.2 New Expected Voltage Stability Method for Assessing the Voltage Stability Impact of Wind Farm Sizes on Weak Power Systems

Several references have shown that an increase in wind penetration results in greater demand on reactive power, which if not met by the existing power system, may lead to voltage instability [41, 66, 78, 79]. With the increase of wind generation penetration in power systems and their reactive power demand, voltage stability limitations are becoming the most limiting factor in increasing wind generation penetration in weak power systems.

The use of the Expected Voltage Stability Margin (*EVSM*) in conducting power system voltage stability analysis under a variety of system configurations and load conditions has been documented [80] and [81]. The *EVSM* can be used to provide an average system voltage stability measure with unpredictable generation resources like wind generation. The *EVSM* incorporates both *VSMs* and the probabilistic nature of wind speed. The *EVSM* is calculated as the sum of voltage stability margins for each wind speed multiplied by the probability of its occurrence as the following equation describes:

$$EVSM = \sum_{i=1}^n VSM (V_wind) * Probability (V_wind) \quad (5.1)$$

Where *VSM* (*V_wind*) is the voltage stability margin calculated at wind speed *V_wind* measured at the wind farm site, *Probability* (*V_wind*) is the probability of occurrence of that wind speed, and “n” is the number of different wind speed intervals which are included in the *EVSM* calculations.

To assess the impact of increasing the size of wind farms on voltage stability, a new Expected Voltage Stability Index L_i is introduced. The new index provides a quantitative

measure of changes to system voltage stability margins for increasing wind penetration. Large values of L_i indicate that the system is closer to becoming unstable for any system parameter changes like load, power factor etc. A lower value of index L_i indicates that the system is strong and system $VSMs$ are not significantly impacted by the change in wind farm sizes. The stability index “ L_i ” is calculated by subtracting the system’s final $EVSM$ from the system’s initial $EVSM$ and dividing by system’s initial $EVSM$. The L_i index can be expressed as follows.

$$L_i = \frac{EVSM_b - EVSM_a}{EVSM_b} \quad (5.2)$$

Where, $EVSM_b$ is the system expected voltage stability margin before the increase in wind farm size and $EVSM_a$ is the system Expected Voltage Stability Margin after the increase in wind farm size. The L_i index has values between “0” and “1”, with “0” indicating that the expected system voltage stability margins are not impacted by the increase in wind farm size and with larger values indicating that the system is voltage unstable for any increase in wind farm sizes.

5.2.1 Details of the New Expected Voltage Stability Method

Following are the steps describing a new method for assessing the impact of increasing wind farm sizes to values above their maximum voltage stable limit.

- Step 1: From the available seasonal load flow cases, select the peak load power flow case as the base case before wind injection. The peak load flow case is the case which includes the peak load month. Then compute $VSMs$ before the addition of new wind generation. The peak load power flow case is selected since it results in the lowest $VSMs$.
- Step 2: Specify the wind farm injection site and the type of wind turbines to be used (SCIG, DFIG or DDSG). Construct the wind farm power curve (wind speed versus active power and wind speed versus reactive power) based on the wind turbines’ manufacturers data and reference [60].
- Step 3: Specify terminal voltage at the wind injection site where collector substation will be connected to the grid.
- Step 4: Specify power factor at the point of interconnection (POI) for the new wind injection site. This sets the minimum (Q_{min}) and maximum (Q_{max}) reactive power capability of the

wind farm. If the wind farm cannot meet the required reactive power (calculated in Step 2) for the specified power factor, additional reactive power equipment is assumed to be installed to meet the power factor requirement at the POI.

Step 5: Power outputs of the wind farm are divided into several intervals with each interval representing a range of power output levels that the wind farm will produce.

Step 6: Collect wind speed data at the wind farm site for the peak load month. Considering the lowest voltage stability margin scenario of maximum wind occurring simultaneously with maximum load, use the maximum of 3 years' hourly wind speed data at the wind farm site to calculate the number of hours for each wind farm power output interval. For each wind " P_{out} " interval, the number of hours the wind farm produces power within that range is then calculated. Calculate the probability of each " P_{out} " interval by dividing the number of hours the output of the wind farm is within the power interval by the total number of hours in the peak month.

Step 7: Identify the peak month to analyze. Divide the peak month into 24 daily hours with each hour of the day repeating 30 or 31 times during the peak month depending on which month the peak load occurred. For example, hour-one of the peak month of July represents hour 12 am to 1 am. This hour repeats 31 times in the month of July. Collect hourly wind speed data for the month of July for the last 3 years. Only the maximum wind speed observed for each daily hour is used in the calculations which results in a total of 93 maximum wind speed data points for each hour for the whole month of July. From the 93 wind speed data points, select the highest wind speed value for each hour of the day. So, only one wind speed value per daily hour is selected. The maximum observed wind speed value is selected because it will result in the lowest *VSM*.

Step 8: From the peak load flow case including the wind farm, build 24 different load flow models to represent the month in a 24 hour period. Each load flow model represents a daily hour with its corresponding maximum wind speed observed in the last 3 years.

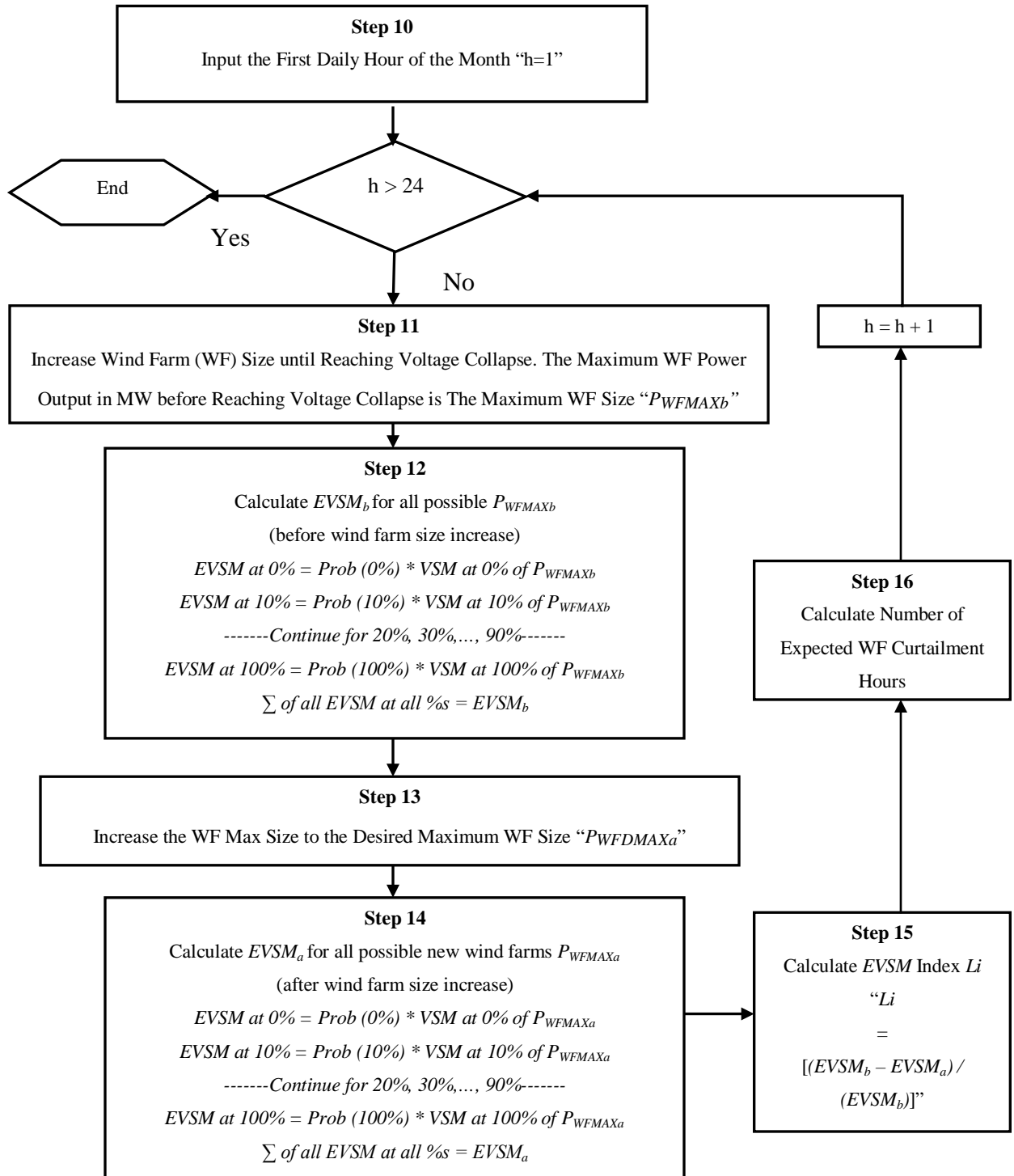
Step 9: Set peak loads in each of the 24 models built to equal the peak load for each daily hour. For example, load flow for hour-one of the peak month has a total peak load equal to the maximum monthly load observed for that hour.

Step 10: Select hour of the day to analyze starting with hour-one (12 am and 1 am).

- Step 11: Gradually increase the wind farm size in the load flow model until reaching voltage collapse. The wind farm size right before reaching the collapse point is the maximum size limit “ P_{WFMAXb} ” at which no wind curtailment is expected. Repeat for each of the next 23 daily hours.
- Step 12: Calculate $EVSMs$ as a function of wind speed for the maximum size found in Step 11. Vary the wind farm power output from 0 MW to the maximum size “ P_{WFMAXb} ” in increments equal to 10% of the new maximum size. For each incremental change, calculate $VSMs$ then multiply each value by the probability of that power output. The sum of all $VSMs$ is the system $EVSM_b$.
- Step 13: Increase the wind farm maximum size found in Step 11 to a desired maximum size “ P_{WFDMAX} ”.
- Step 14: Calculate $EVSMs$ as a function of wind speed for the desired maximum wind farm size “ P_{WFDMAX} ”. Vary the wind farm power output from 0 MW to up to the P_{WFDMAX} using interval ranges specified in Step 5. Calculate the $VSMs$ for each interval; then multiply $VSMs$ for each of the wind farm power intervals by the probability of that interval. The sum of all $EVSMs$ for all levels of wind farm power output is the new system $EVSM_a$ for the new size of the wind farm.
- Step 15: Calculate system $EVSM$ Index L_i as shown in Equation (5.2).
- Step 16: Calculate the expected curtailment hours (hours of expected voltage instability) for the wind farm based on wind farm power output probabilities.
- Step 17: Repeat steps 10 through 17 for all remaining daily hours; hours 2 through 24.
- Step 18: END.

The flow chart shown in Figure 5.2 provides a description of Steps 10 through 18. The closed loop is needed for repeating the analysis for the rest of the daily hours as described in Step 17. Due to their simplicity and the ease of following, Steps 1 through 9 are not included in the flow chart.

Figure 5.2 Flow Chart for Calculating EVSMs and the Number of Expected Curtailment Hours



5.3 Simulation Model Formulation and Results

To investigate the impact of increasing wind farm sizes above their maximum limits, the methods presented in the previous section are applied to a wind farm in western Kansas which is modeled as a type DFIG turbine. The DFIG type is used since it has the capability of producing or absorbing reactive power which makes it more suitable (less curtailment hours) for applications where its maximum size increases above its voltage stable limit size.

5.3.1 Simulation Model Formulation

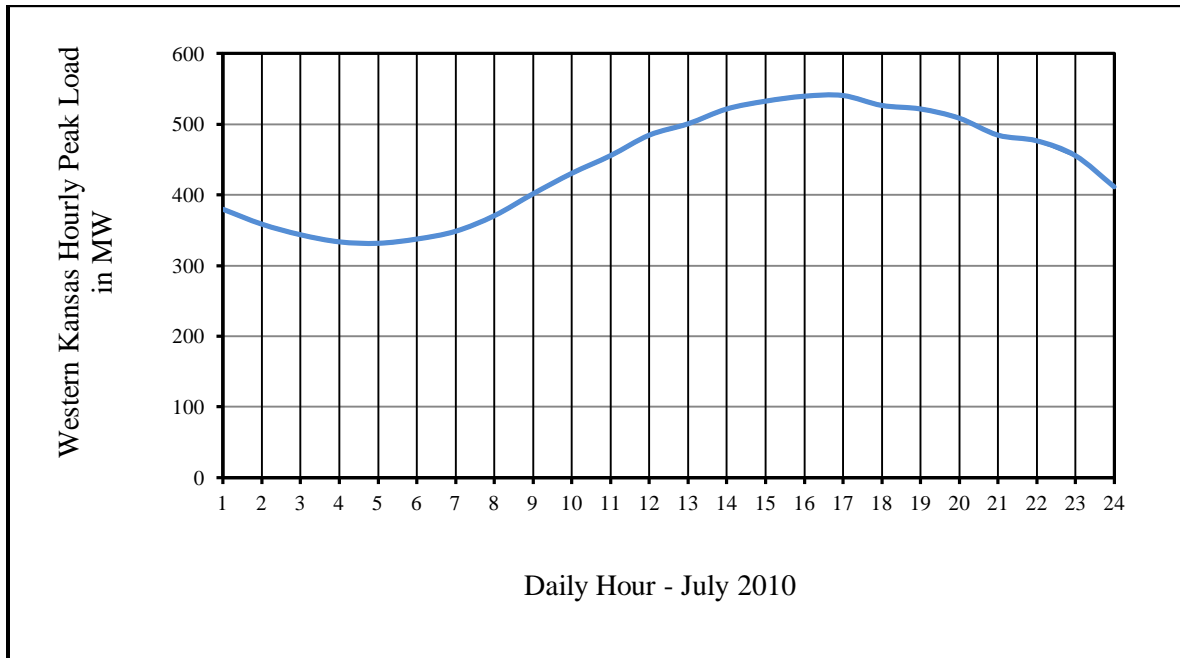
The western Kansas 2010 peak July load was 541 MW. Load types in the SPP base model have been modified based on data collected for loads in the western Kansas Area I as discussed in Chapter 4.

The proposed system impact assessment method has been applied to a single wind farm in western Kansas “Bus 105 in Area I” without considering any system contingencies. The wind farm is connected to the 115 kV transmission system at the point of interconnection (POI) with the local utility (Sunflower Electric Power Corporation). All of its DFIG wind turbines are aggregated at the POI. All of the wind farm generation output is absorbed in the western Kansas power system. *VSM* calculations were generated using the Southwest Power Pool (SPP) summer 2010 load flow model which was modified to incorporate the wind farm under study. The PSS/E software package, version 32 was used for load flow analysis and to generate Q-V curves needed to calculate the *VSMs* [82].

5.3.2 Simulation Results

For the month of July 2010, western Kansas loads are at their highest values during the afternoon hours (4 pm – 8 pm) as shown in Figure 5.3. Most of the load is irrigation, small commercial, and residential.

Figure 5.3 Western Kansas Maximum Hourly Peak Load for the Month of July 2010



VSMs are calculated for the base case with no wind injection. A summary of the results is shown in Table 4.4 in Chapter 4. The power system was voltage stable for all the daily hours of the July month. As expected, heavier loading conditions during the afternoon hours resulted in lower *VSMs*. Low reactive power margins during heavy loading conditions indicates that the system is stressed.

Simulation results indicated that increasing wind injections in the western Kansas power system resulted in reductions in *VSMs* for all of the July daily hours. The maximum wind injection values shown in Table 5.1 are the maximum sizes of the wind farm that can safely be injected into the power system without resulting in voltage instability for any daily hour. Using the Q-V method and the voltage stability criteria in Section 5.1, the maximum size of the wind farm during these daily hours is referred to as the voltage stable wind farm size. For the heaviest loading hour (hour 17), a maximum of 145 MW of wind injection was possible before a less than 0.90 p.u. load bus voltage occurred (voltage unstable by the criteria). If the wind farm maximum size does not exceed the 145 MW, there will be no wind curtailment hours expected. From Table 5.1, daily hours 13 through 20 had a maximum wind farm size limit of 145 MW while the rest of the daily hours had a maximum wind farm size of higher than 145 MW.

Table 5.1 Maximum Wind Injections in MW from the Wind Farm Site Using DFIG Wind Turbine Type before Reaching the Collapse Point Using the Q-V Curve Method

Daily Hours for July 2010	Peak Load MW	Max MW Limits of Wind Injection at the Wind Farm Site
1 (12 am – 1 am)	380	180
2 (1 am – 2 am)	359	180
3 (2 am – 3 am)	344	185
4 (3 am – 4 am)	334	185
5 (4 am – 5 am)	332	185
6 (5 am – 6 am)	338	185
7 (6 am – 7 am)	349	185
8 (7 am – 8 am)	371	180
9 (8 am – 9 am)	402	170
10 (9 am – 10 am)	431	170
11 (10 am – 11 am)	456	150
12 (11 am – 12 pm)	485	150
13 (12 pm – 1 pm)	501	145
14 (1 pm – 2 pm)	522	145
15 (2 pm – 3 pm)	533	145
16 (3 pm – 4 pm)	540	145
17 (4 pm – 5 pm)	541	145
18 (5 pm – 6 pm)	527	145
19 (6 pm – 7 pm)	522	145
20 (7 pm – 8 pm)	509	145
21 (8 pm – 9 pm)	485	150
22 (9 pm – 10 pm)	477	150
23 (10 pm – 11 pm)	456	150
24 (11 pm – 12 am)	412	165

Limiting the maximum wind farm size to 145 MW did not provide for maximization of wind energy penetration since most of the monthly hours (67% of the monthly hours) allowed for higher wind injection values. As it can be seen in Table 5.1, the 145 MW maximum wind injection limit for the system to stay voltage stable is only required to be met for 248 hours (daily hours 13 through 20) out of the 744 hours of the month of July. As per the wind speed data collected for this wind farm location, wind speed was not high enough for all of the 248 hours (the heavy loading hours; hours 13 through 20) to produce the full wind farm rated power. The wind farm did not produce its maximum power output during these hours. Hence, if the wind farm size is increased above the 145 MW limit (safe voltage stability limit), voltage instability may not occur if the available wind speed at the wind farm site was not high enough to make the wind farm produce more than 145 MW during these 248 peak loading hours.

To evaluate the impact on *VSMs* and *EVSMs* of increasing the wind farm size above the 145 MW voltage stable size, three new sizes were analyzed. The new sizes used in the load flow models are 150 MW, 175 MW and 200 MW. The details of calculating *EVSM* for a wind farm size of 150 MW during the heaviest loading hour (hour 17) is shown in Table 5.2. *EVSMs* were calculated by multiplying the probability of the power output by the *VSM* which corresponds to that value of the power output. As an example, for the 150 MW case shown in Table 5.2, at 40% of the maximum size, the wind farm power output is equal to 60 MW which resulted in a *VSM* of 29.05 Mvar with probability of 0.064516129 as found in Table 5.3. The *EVSM* at this power output level is equal to the product of the *VSM* times the probability for the 40% of the maximum size of the wind farm (60 MW output) as shown in the following equation.

$$EVSM_{40\% \text{ of max size}} = 29.05 * 0.064516129 = 1.87 \text{ Mvar} \quad (5.3)$$

The total system *EVSM_a* for daily hour 17 when the wind farm size increased to 150 MW is then calculated by accumulating all of the expected voltage stability margins over the entire set of wind power outputs. The total system *EVSM* after increasing the wind farm maximum size from 145 MW to 150 MW is 20.25 Mvar; a reduction of 9.26% in expected voltage stability margin.

Table 5.2 EVSM Calculations for 150 MW Wind Farm in Western Kansas for Daily Hour 17 in the Month of July 2010

Wind Farm Maximum Size "Rated Power" = 150 MW			
Wind Farm P_{OUT} in MW	% of Rated Power	VSM_{150} Mvar	$EVSM_{150}$ Mvar
0	0%	29.01	1.87
15	10%	29.59	0.95
30	20%	29.71	2.88
45	30%	29.76	2.88
60	40%	29.05	1.87
75	50%	28.32	1.83
90	60%	28.05	0.90
105	70%	28.02	0.90
120	80%	26.28	2.54
135	90%	18.78	3.63
150	100%	0.00	0.00
		System $EVSM_a$	20.25
Expected # of Curtailment hrs	7		

Table 5.3 Expected Wind Farm Power Outputs and their Probabilities as a % of the Maximum DFIG’s Size at the Wind Farm Site for Daily Hour 17 (4 pm – 5 pm) for the Month of July 2010

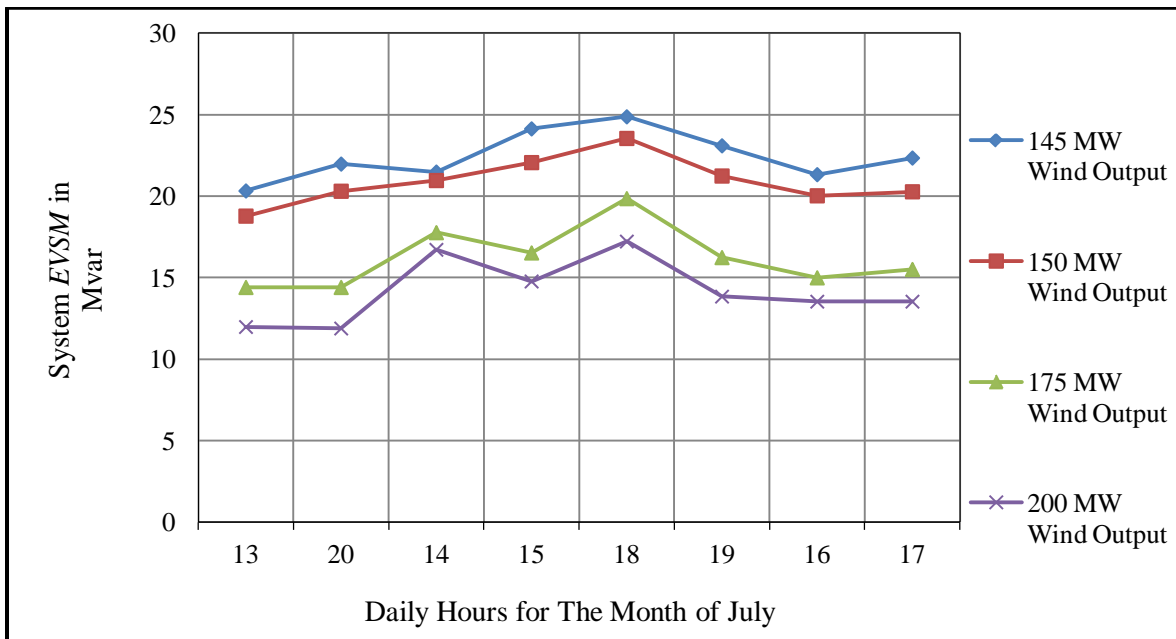
Wind Power Output of DFIG Wind Farm in Western Kansas		
Daily Hour 17 (4 pm- 5 pm) of the Month of July		Probability
% of Rated Power	Number of Hours Observed	
0.00%	6	0.193548387
10.00%	1	0.032258065
20.00%	2	0.064516129
30.00%	1	0.032258065
40.00%	2	0.064516129
50.00%	1	0.032258065
60.00%	1	0.032258065
70.00%	1	0.032258065
80.00%	3	0.096774195
90% - 95%	6	0.193548387
96% - 100%	7	0.225806452
TOTAL	31	1.000000000

For the heavy loading hours with possible voltage instability, hourly wind power curtailments may occur when the wind farm power output exceeds the voltage stable limit of 145 MW. During these hours, any time the wind farm produces more than the maximum voltage stable size limit (145 MW which is a hard limit for a secured stable system); a power output control mechanism is assumed to operate by disconnecting wind turbines inside the wind farm to reduce the wind farm power output for protecting the system from reaching the voltage collapse point. This type of control mechanism is referred to as a special protection scheme (SPS) [83]. SPS schemes can be designed to detect one or more predetermined system conditions that have high probability of causing voltage collapse. Some wind turbines inside the wind farm are then disconnected to prevent the wind farm power output from exceeding a predetermined value. Table 5.4 shows the amount of wind farm power output that must be curtailed to prevent voltage collapse for each wind farm rated size. Curtailment only occurs when there is a voltage

instability risk. The amount of wind farm power output to be curtailed when wind farm produce its rated power during heavy loading conditions.

The *EVSMs* calculated for daily hours 13 through 20 are shown in Table 5.5. Graphical representations of these results are shown in Figure 5.4. All *EVSMs* were lower for the increase in the wind farm maximum size. Regardless of the daily hour analyzed, the case with the 200 MW of maximum wind farm size resulted in the lowest *EVSMs*.

Figure 5.4 Impact of Increasing Wind Farm Sizes on Western Kansas System *EVSMs* for Each of the Heavy Loading Hours for the Month of July 2010



The impact of size increases on the number of expected curtailment hours and on system *EVSMs* for the three wind farm size increase cases are shown in Table 5.5. A graphical representation of the expected curtailment hours for each case is shown in Figure 5.5. Only hours 13 through 20 (heaviest loading hours of July) are analyzed since they were the only daily hours that resulted in possible wind curtailments.

Table 5.4 Wind Farm Power Output Curtailment Limits for Voltage Stability

Case	Maximum Wind Farm Rated Power (Size of the Wind Farm)	Maximum Amount of Wind Farm Power Output to be Curtailed when the Wind Farm Produces its Maximum Rated Power During Heavy Loading Conditions
Case 1	145 MW	0 MW
Case 2	150 MW	5 MW
Case 3	175 MW	30 MW
Case 4	200 MW	55 MW

For larger than 145 MW rated wind farm size (wind farm rated more than 145 MW), the number of curtailment hours was determined by counting the number of hours the wind profile at the location of the wind farm allows it to produce more than 145 MW. Table 5.4 lists the percentages of the rated power at which the wind farm power output is expected to be curtailed for all of the four wind increase cases.

The number of expected curtailment hours increased as the wind farm maximum sizes increased. Increasing the wind farm size from 145 MW to 150 MW resulted in 60 hours of curtailments. In Case 3, possible curtailment hours increased to 124 as wind farm rated power increased from 145 MW to 175 MW. In Case 4, possible curtailment hours increased to 134 as wind farm rated power increased from 145 MW to 200 MW. The increase in the number of curtailment hours as wind injection from the wind farm increases is due to lower system voltage stability margins at higher wind injections.

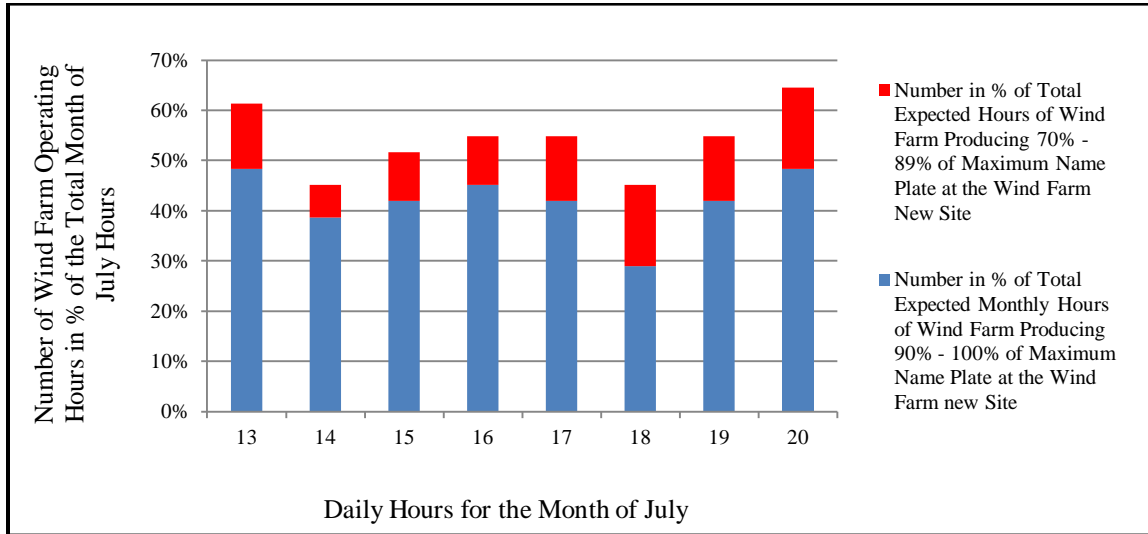
The increase in the number of possible curtailment hours did not show a significant change between Cases 3 and 4 due to having a low number of wind farm operating hours when the wind farm produces between 73% and 83% of its maximum size. This is in agreement with the findings of reference [66] which indicated that wind farms mostly operate at their highest or near highest outputs or at their lowest or near their lowest output due to their power vs wind speed relationship.

Table 5.5 Summary of the Impact of Increasing Wind Farm Size on System EVSMs and Expected Curtailment Hours for the Heavy Loading Hours in the Month of July 2010

The Western Kansas Wind Farm Maximum Power Output Cases									
Cases		Case 1 145 MW		Case 2 150 MW		Case 3 175 MW		Case 4 200 MW	
Daily Hours / Peak Load		# of Curtailed Hours / EVSM		# of Curtailed Hours / EVSM		# of Curtailed Hours / EVSM		# of Curtailed Hours / EVSM	
Hr	MW	Hrs	Mvar	Hrs	Mvar	Hrs	Mvar	Hrs	Mvar
13	501	0	20.3	10	18.8	18	14.4	19	2.0
20	509	0	22.0	8	20.3	18	14.4	20	1.9
14	522	0	21.5	8	21.0	13	17.7	14	6.7
15	533	0	24.1	6	22.1	15	16.5	16	4.8
18	527	0	24.9	7	22.2	12	19.8	14	7.2
19	522	0	23.1	7	21.2	16	16.2	17	3.8
16	540	0	21.3	7	20.0	16	15.0	17	3.5
17	541	0	22.3	7	20.3	16	15.5	17	3.5
Total # of Expected Curtailed Hours		0 hr		60 hr		124 hr		134 hr	
Average EVSMs in Mvar for Daily Hours (13 – 20)		22.4		20.7		16.2		4.2	
Curtailment Hours as a % of the Total July Hours				24.19%		50.00%		54.03%	

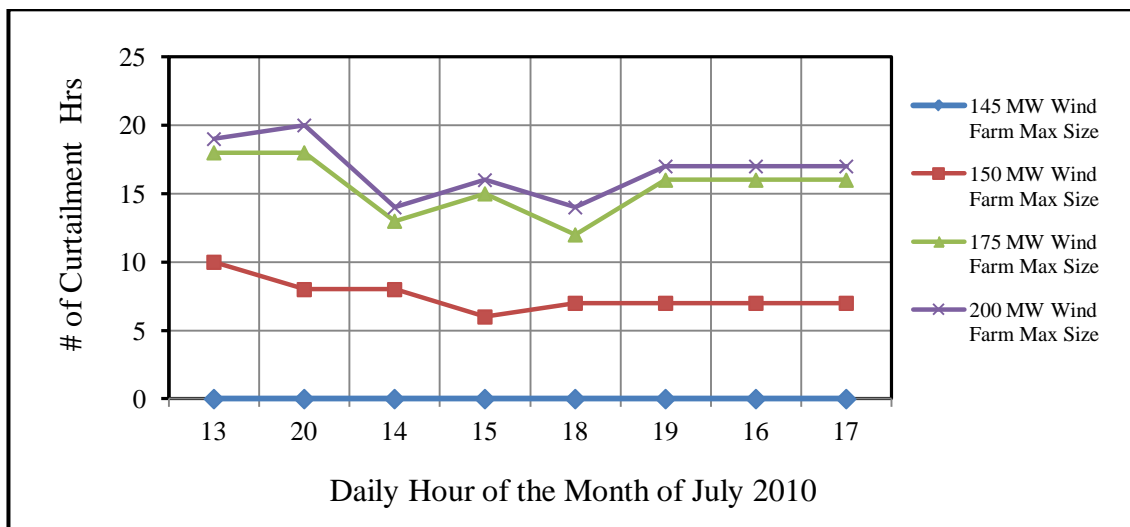
The clustering of the wind production hours in the range of 90% to 100% of the Rated power can be explained using the characteristics of the DFIG power curve in which the range of wind speed that produces wind power above 90% is about 57% of the total wind speed-power generation range. The number of hours a wind turbine operates in constant maximum power output mode of 100% of the Rated power is usually obtained when wind speeds are in a wide range of 15 to 25 m/s [66].

Figure 5.5 Number of Wind Farm Operating Hours as a Percent of the Total “744” July Hours for the Selected Heavy Loading Hours at Bus 105 in Western Kansas



EVSM index L_i was calculated for all of the three wind farm size increase cases as listed in Table 5.6. As the wind farm size increases, the L_i index increases. This indicates that system voltage stability margins became lower as more wind is injected into the system.

Figure 5.6 Number of Expected Curtailment Hours for Each Maximum Wind Farm Size Case for the Heavy Loading Hours in the Month of July



The highest L_i was found in Case 4 at daily hour 20 for which the system was at its lowest stability point. The change in the *EVSM* index L_i between Cases 3 and 4 was much less than the change from Case 2 to Cases 3 and 4. This indicates that increasing the wind farm size above the 150 MW causes the power system to become less voltage stable. The 200 MW wind farm size resulted in the highest L_i index value which is the worst case among the four cases analyzed. The average L_i Index for the 200 MW case reached 0.3687 which is 4.36 times higher than the average L_i index calculated for the 150 MW case (Case 2). As shown in Table 5.6 the *EVSMs* did predict the daily hour with the worst stability while incorporating wind speed patterns in their calculated values. In Case 4, the worst *EVSM* calculated was for daily hour 20 at 11.9 Mvar with *EVSM* index L_i of 0.459 which was the worst value for all of the cases studied.

Table 5.6 Expected Voltage Stability Index L_i for Changes in the Wind Farm Maximum Size During the Heavy Loading Hours

July 2010	Case 1 145 MW	Case 2 150 MW		Case 3 175 MW		Case 4 200 MW	
Daily Hour	<i>EVSM</i> Mvar	<i>EVSM</i> Mvar	L_i	<i>EVSM</i> Mvar	L_i	<i>EVSM</i> Mvar	L_i
13	20.3	18.8	0.074	14.4	0.291	12.0	0.409
20	22.0	20.3	0.077	14.4	0.345	11.9	0.459
14	21.5	21.0	0.023	17.7	0.177	16.7	0.223
15	24.1	22.1	0.083	16.5	0.315	14.8	0.386
18	24.9	22.2	0.108	19.8	0.205	17.2	0.309
19	23.1	21.2	0.082	16.2	0.299	13.8	0.403
16	21.3	20.0	0.061	15.0	0.296	13.5	0.366
17	22.3	20.3	0.090	15.5	0.305	13.5	0.395
Average	22.44	20.74	0.075	16.19	0.279	14.17	0.369

5.4 Conclusions

This chapter presents a new voltage stability based method for assessing the impact of wind farm maximum sizes on system expected voltage stability margins and the expected

number of curtailment hours. A new voltage stability based method was presented in this chapter to assess the impact of increasing wind farm maximum size above the voltage stability size limit. Increasing the wind farm size above this value may require curtailment of wind farm power output to prevent voltage collapse. Increasing the wind farm size from 145 MW to 200 MW resulted in 134 hours of curtailment which is about 18% of the month of July total hours. Increasing the wind farm size from 145 MW to smaller values than the 200 MW resulted in fewer curtailment hours.

The new method evaluates the voltage stability risk of increasing the wind farm size above the voltage stable limit. It evaluates that risk by incorporating the probabilistic nature of wind into the voltage stability margin calculations. The Expected Voltage Stability Margin (*EVSM*) incorporates wind speed, wind farm probable power outputs and voltage stability margins using a voltage stability Index, L_i . Simulation results showed that the stability index can predict the daily hour with the highest voltage stability risk.

It has been demonstrated that increasing the size of a wind farm above the voltage stable size limit can increase wind penetration. However, depending on wind speed patterns and the availability of reactive power, the maximum power output of the wind farm may be limited (curtailed) to keep the power system from reaching voltage collapse. Results of the analysis also indicated that the western Kansas power system “*EVSMs*” decreased for an increase in wind farm sizes. Wind farms that are sized above the voltage stable size experienced an increase in curtailment hours as the system *EVSMs* became lower.

Increasing the wind farm size from 145 MW to 200 MW resulted in a 62.5% reduction in average *EVSM*. The lower the value of *EVSM*, the higher the risk of instability and the higher the number of curtailment hours expected. The reduction in *EVSMs* results in the system operating closer to the voltage collapse point.

Depending on the number of expected wind power curtailment hours, the assessment method presented in this chapter can be used to properly evaluate if a size increase will result in higher injection of wind energy. Depending on the calculated stability index L_i for a power system, a wind farm size increase can be assessed to determine it will produce higher wind energy with minimal curtailment hours. Increasing wind farm sizes in power systems with high values of L_i may not necessarily result in higher wind energy productions due to a large number of wind power curtailment hours.

Chapter 6 - Effective Wind Farm Sizing Using Modes of Voltage Instability

As wind penetration increases in a weak power system, the system operating point may start drifting toward a set of voltage unstable operating points. If wind penetration exceeds a certain threshold, the system may become unstable. Voltage stability modal analysis can be used to pre-determine locations (buses) that are more strongly connected to system voltage instability for any wind penetration level.

In this chapter, a method is developed to increase wind penetration level by placing new wind generation at strong wind injection buses. This method provides a comprehensive methodology for the identification of system voltage stability weaknesses for each wind penetration level. The method incorporates modal analysis [47] as well as the traditional voltage stability method (Q-V curve) in sizing and placing new wind farms.

6.1 Q-V Modal Analysis Method

Voltage stability assessment using Q-V modal analysis has been described in [46, 47, 84]. The most generally used algorithm to solve the power flow program is the Newton-Raphson method which involves iteration using the first term of a Taylor expansion of the equation to be solved [84]. The Newton-Raphson method solves the partitioned matrix equation shown below.

$$J \begin{bmatrix} \Delta\theta \\ \Delta V \end{bmatrix} = \begin{bmatrix} \Delta P \\ \Delta Q \end{bmatrix} \quad (6.1)$$

Where ΔP is vector of the changes in real power and ΔQ is the changes in reactive power, ΔV is vector of which the unknown voltage magnitudes, the voltage angles are denoted by $\Delta\theta$, and J is the Jacobian matrix consisting of partial derivative terms. By expanding the Jacobian matrix, a full matrix equation can written for the general algorithm to solve power flow as shown in Equation (6.2).

$$\begin{bmatrix} \Delta P \\ \Delta Q \end{bmatrix} = \begin{bmatrix} J_{P\theta} & J_{PV} \\ J_{Q\theta} & J_{QV} \end{bmatrix} \begin{bmatrix} \Delta\theta \\ \Delta V \end{bmatrix} \quad (6.2)$$

When the focus in solving the power flow is on reactive power solutions, ΔP is set to zero and Equation (6.2) can be written as

$$\Delta P = J_{P\theta} \Delta\theta + J_{PV} \Delta V = 0 \quad (6.3)$$

Solving for $\Delta\theta$,

$$\Delta\theta = - J_{P\theta}^{-1} J_{PV} \Delta V \quad (6.4)$$

From Equation (6.2), solving for ΔQ and substituting for $\Delta\theta$, gives

$$\Delta Q = [J_{QV} - J_{Q\theta} J_{P\theta}^{-1} J_{PV}] \Delta V = J_R \Delta V \quad (6.5)$$

$$J_R = [J_{QV} - J_{Q\theta} J_{P\theta}^{-1} J_{PV}] \quad (6.6)$$

From Equation (6.5),

$$\Delta V = J_R^{-1} \Delta Q \quad (6.7)$$

The modes of instability can be defined by the eigenvalues and eigenvectors of J_R [83, 84]. Assuming $J_R = \zeta \lambda \eta$, where, ζ is the right eigenvector matrix of J_R , λ is the diagonal eigenvalue matrix of J_R , η is the left eigenvector matrix of J_R . Taking the inverse of both sides for J_R results in

$$J_R^{-1} = \zeta \lambda^{-1} \eta \quad (6.8)$$

Substituting for J_R^{-1} from Equation (6.8) in Equation (6.7) results in,

$$\Delta V = \zeta \lambda^{-1} \eta \Delta Q \quad (6.9)$$

Noting that $\eta = \zeta^{-1}$, and pre-multiplying both sides by η

$$\eta \Delta V = \lambda^{-1} \eta \Delta Q \quad (6.10)$$

Equation (6.10) can be written

$$\Delta V = \sum_i \frac{\xi_i \eta_i}{\lambda_i} \Delta Q \quad (6.11)$$

Where i corresponds to each i^{th} mode of stability, i.e. λ_i is the i^{th} eigenvalue of J_R , ξ_i the i^{th} column right eigenvector of J_R , and η_i the i^{th} row left eigenvector of J_R . Modal voltages ΔV_{mi} 's (elements of vector ΔV) and reactive power flows ΔQ_{mi} 's (elements of vector ΔQ) are defined using $\Delta V_m = \eta \Delta V$ and $\Delta Q_m = \eta \Delta Q$ and using Equation 6.10 gives

$$\Delta V_{mi} = \frac{1}{\lambda_i} \Delta Q_{mi} \quad (6.12)$$

The relationship between the eigenvalues λ_i and voltage stability can be seen from Equation (6.12). The sensitivity of V-Q at each bus in the system is related to the eigenvalues of the system. If λ_i is positive, the system is voltage stable since changes in system reactive power result in positive changes in modal voltage. When λ_i magnitude becomes close to zero, any changes in reactive power produce large changes in modal voltage and thus in bus voltage. If the magnitude of λ_i is equal to zero, the system is on the verge of voltage instability and voltage collapses may occur. If λ_i is negative, the system is voltage unstable since changes in system reactive power result in negative changes in modal voltage.

One of the advantages of using modal analysis for voltage stability studies is the key mechanics that this analysis provides about the system during stressed periods. The participation factor of any bus in the system in modes of instability can be used to determine which bus, branch or generator in the power system contributes heavily to system modes of instability. Buses with large participation in the modes of instability “ λ_i ” correspond to the most critical system buses. Bus participation factor for bus j can be written as [84]:

$$P_{ji} = \xi_{ji} \eta_{ji} \quad (6.13)$$

The magnitude of P_{ji} determines if bus j contributes significantly to the i^{th} mode of instability, λ_i .

6.2 Developing a Q-V Modal Method for Increasing Wind Penetration in Weak Power Systems

As wind penetration increases in weak power systems, Q-V modal analysis can be used to determine which areas in the power system are most vulnerable to voltage stability problems and to evaluate wind injection buses for their impact on voltage stability margins. Q-V modal analysis is best suited for power systems which are operated near the voltage collapse point. When the power system is stressed and reactive power support is needed to allow for more wind penetrations, Q-V modal analysis can predict the best sites for installing new reactive power compensation equipment to increase *VSMs*. Hence QV/modal analysis allows for increases in wind penetration.

6.2.1 Development of a Systematic Voltage Stability Procedure for Increasing Wind Penetration in Weak Power Systems

A systematic voltage stability procedure for increasing wind penetration in weak power systems using modal analysis and Q-V voltage stability methods should involve the following six steps:

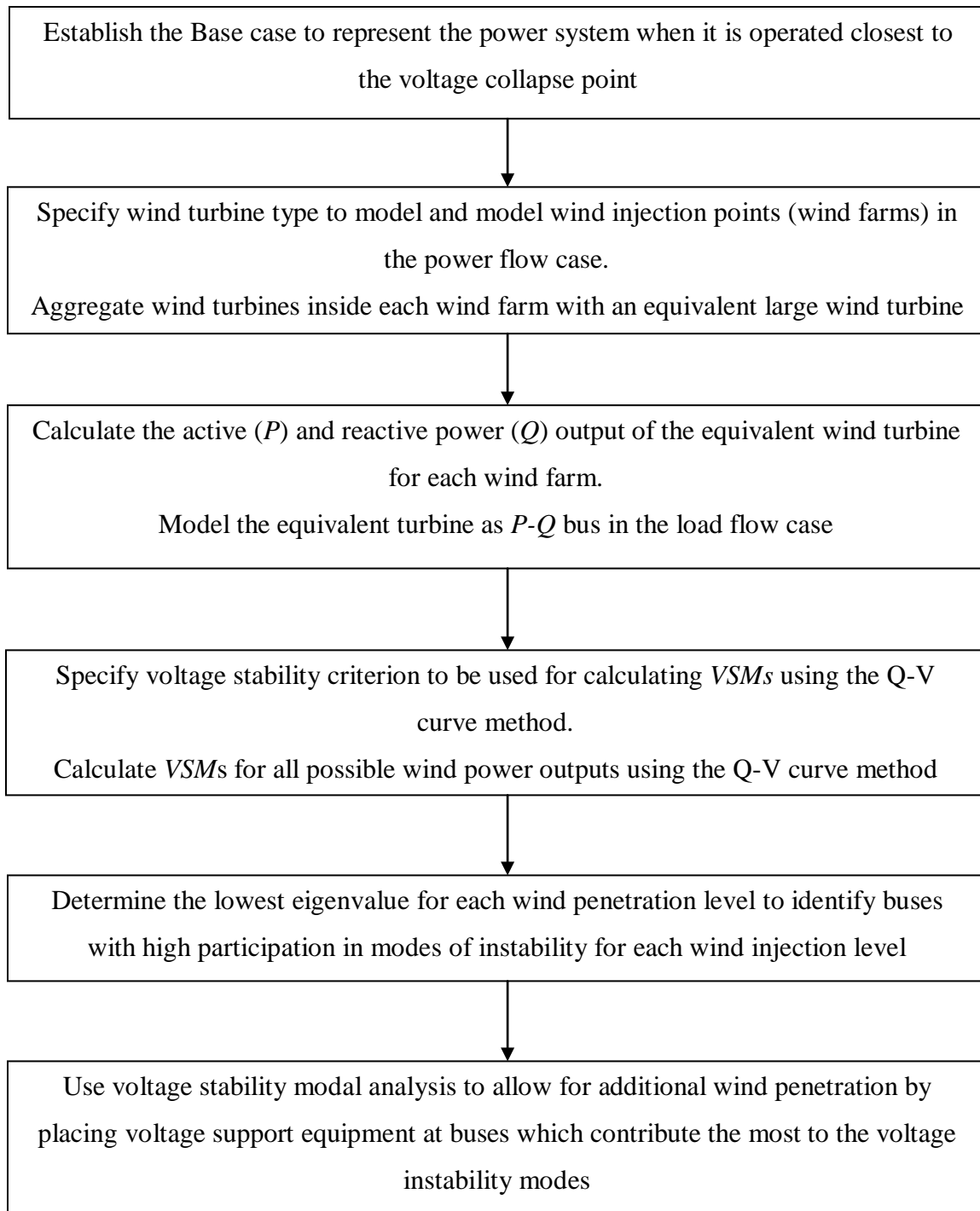
1. Establishment of the base case for voltage stability assessment. Voltage stability assessment depends on how voltage control devices are modeled and how many details of the study area are represented [84]. The base case is selected to represent the system when it's operating nearest the voltage collapse point (lowest *VSM*). In a weak power system, this operating point traditionally occurs during the summer season at peak loading conditions.
2. Determine the type of turbines to be used in modeling new wind farms. Aggregate all wind turbines inside each wind farm as single wind turbine unit having an MVA rating equal to the summation of the MVA rating of the individual units at the point of interconnection (POI) with the transmission grid [49].
3. Develop the active power vs wind speed curve for the equivalent wind turbine unit. Also, develop the reactive power capability of the equivalent wind turbine to calculate the

amount of reactive power that the equivalent wind turbine can produce or absorb at each level of wind power output [39].

4. Specify system voltage stability criterion. In wind integration studies, the voltage stability criterion must define a *VSM* threshold that is sufficient for the base case and wind injection cases. The *VSM* threshold can be at or near zero if it is assumed that wind curtailment may need to be employed for critical conditions using special protection schemes or any other means. Calculate system *VSMs* for the base case and for all of the possible wind power outputs generated from the pre-selected wind injection locations. *VSMs* can be calculated using the Q-V curve method at the weak buses identified by the modal analysis.
5. The lowest eigenvalue (least stable mode) for each wind penetration level must be determined to evaluate system stability and to identify buses in the system with most contribution to voltage instability modes (weak buses). The lowest eigenvalues for each wind penetration level must be calculated since different penetration levels can result in different minimum eigenvalues. Modes of instability can change from the no wind injection case to the case with high wind penetration. If increasing wind penetration causes the system to reach the collapse point, the minimum eigenvalue at the collapse point may be different from the minimum at the no wind injection case. While increasing wind injections, several system eigenvalues must be tracked since a new minimum eigenvalue, which did not show in the no-wind case, may suddenly appear and take control. Therefore, tracking only one eigenvalue can be misleading.
6. Use modal analysis to locate and size voltage support equipment to enhance the system to meet the voltage stability criterion for high wind penetration level cases or to increase wind penetration levels to meet the desired values. Voltage support equipment must be sized and located at buses with highest positive impact (largest bus participation factors) on system voltage stability margins.

The flow chart shown in Figure 6.1 illustrates the proposed voltage stability procedure.

Figure 6.1 Systematic Voltage Stability Procedure for Assessing Weak Power Systems with High Wind Penetration Using Modal Analysis and the Q-V Voltage Stability Method



6.2.2 Voltage Stability Method for Increasing Wind Penetration Using Modes of Instability

A new method has been developed and presented in this section for maximizing wind farm sizes in weak power systems using modes of voltage instability. The new method uses the systematic procedure for comprehensive voltage stability assessment of weak power systems introduced in the previous section. The new method incorporates modal analysis as well as a traditional voltage stability method (Q-V curve) in sizing and placing new wind farms. The effect of wind penetration on system voltage stability can be evaluated using the sensitivity of the reduced system Jacobian eigenvalues with respect to variations in system wind penetration as described earlier in Section 6.1.

The proposed method is summarized in the following steps. Application of this method to the western Kansas power system is shown in the next section.

1. From the available seasonal load flow cases, select the peak load power flow case as the base case before wind injection. The peak load power flow case is the case which includes the peak load month.
2. Specify wind injection buses and maximum wind injection desired (PD_{wind}). Wind is to be injected from these buses based on their contribution to voltage instability modes and their available *VSMs*.
3. Rank all of the proposed wind injection buses based on their contribution to voltage instability modes using modal analysis. Apply modal analysis to calculate bus participation factors (from the eigenvectors) for the least stable mode for each wind penetration level. Use the results of the modal analysis to determine which of the proposed wind injection buses has high contribution to modes of instability (weak buses for wind injection). Buses with low contribution to modes of instability are considered strong wind injection buses. A strong wind injection bus has a participation value of near zero.
4. Perform the Q-V curve analysis to compute *VSMs* at the buses identified as weak and at the buses identified as strong for wind injection. This analysis is required to verify modal analysis results.
5. Compare the wind injection bus ranking results found in (3) and (4), and select strong buses to install new wind farms. Only buses with high ranking in both methods are

selected. A wind injection bus which has a high ranking in the Q-V curve method but low ranking in the modal method will not be selected as a strong wind injection bus. This indicates that the modal QV analysis found a *local minimum* not the actual collapse point. The local minimum found is due to the nonlinearities encountered in loading (stressing) the system from the initial operating point to the collapse point which depends on the initial direction chosen for loading the system. This can be prevented by using the left eigenvectors corresponding to the minimum eigenvalue of the Jacobian at the system operating point for the initial direction of loading the system [84].

6. Specify the type of wind turbine to be used (SCIG, DFIG or DDSG) in the analysis then construct the wind farm power curve for each wind injection bus. A wind farm power curve (wind speed versus active power and wind active power output versus reactive power) is generated based on the wind turbine manufacturer data.
7. Simultaneously increase wind farm sizes at the strong buses in increments. For each incremental increase in wind generation, perform modal and Q-V curve analysis to determine if significant change has occurred to the voltage instability modes. If there are no significant changes, continue increasing the wind generation until reaching the collapse point. The maximum wind generation level right before reaching the collapse point sets the maximum size of the wind farms (P_{wind0}) before any system enhancements.
8. If the desired wind generation level has not been reached due to voltage collapse, a further increase of the wind farm maximum sizes can be achieved by installing voltage support equipment like Static Var Compensators (SVCs). Wind farm maximum sizes are increased in increments while adding SVCs as necessary to prevent voltage instability. SVCs are placed at buses based on the modal analysis results found in Step (7). The effectiveness of an SVC location is evaluated according to the calculated improvement in systems' *VSMs*. Different SVC locations yield different *VSM* improvement [63].
9. After adding the first set of SVCs in step (8), increase wind farm maximum sizes until reaching the desired wind penetration level or the collapse point. If the collapse point occurred before reaching the desired penetration level, a second set of SVCs is placed at the weakest bus found using modal analysis. The second set of SVCs is determined by performing modal analysis near the collapse point to identify best buses for the second set

of SVCs. Depending on the desired wind penetration level, Steps (7) and (8) may be repeated until reaching the desired wind penetration.

The process involved in sizing new wind farms based on critical modes of voltage instability for Steps (1) through (7) is shown in Figure 6.2. A second flow chart is shown in Figure 6.3 for Steps (8) and (9). These steps are necessary when the desired maximum wind injection level cannot be reached without the installation of additional voltage support equipment.

Figure 6.2 Process for Calculating Maximum Wind Injection Using Modal Analysis

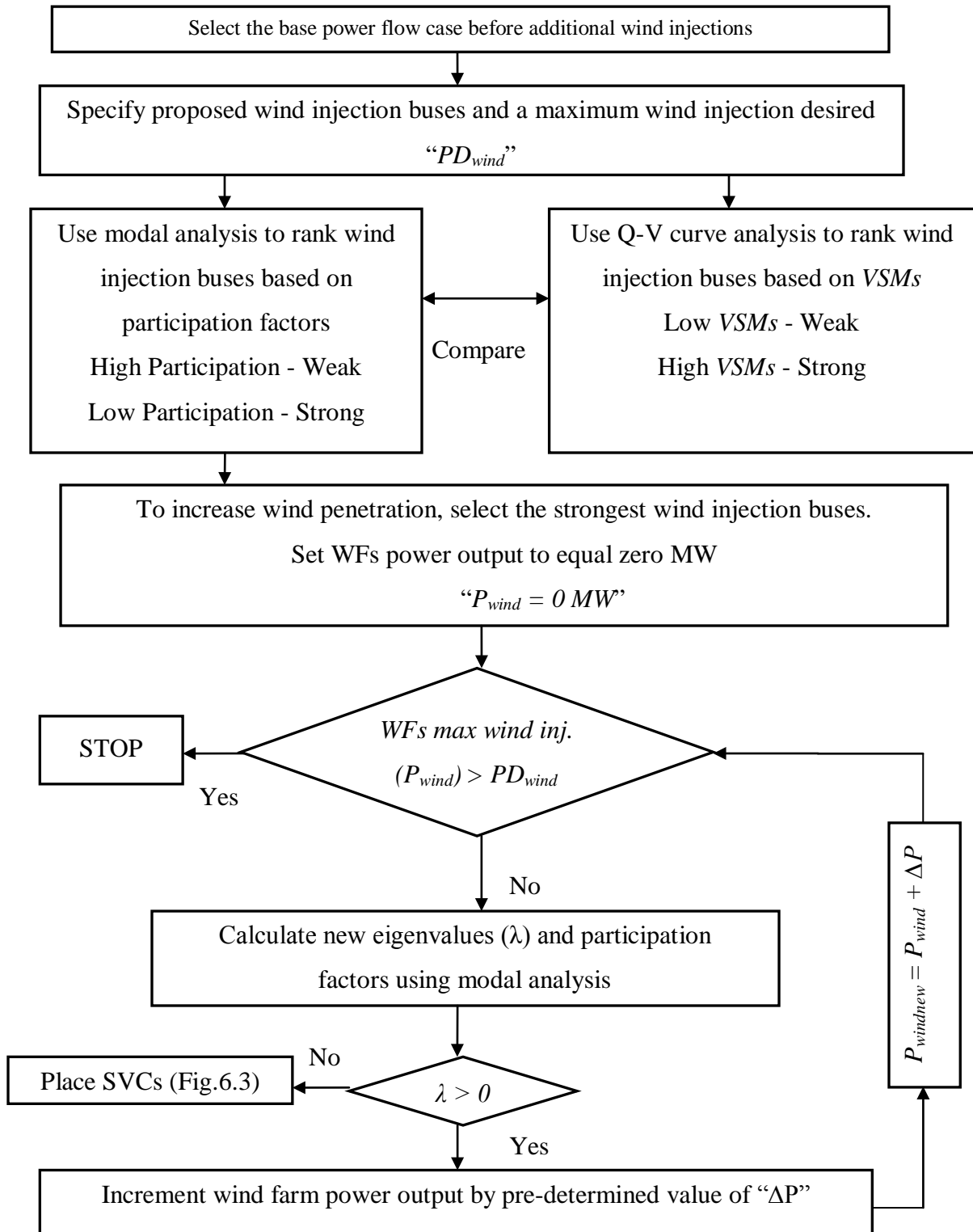
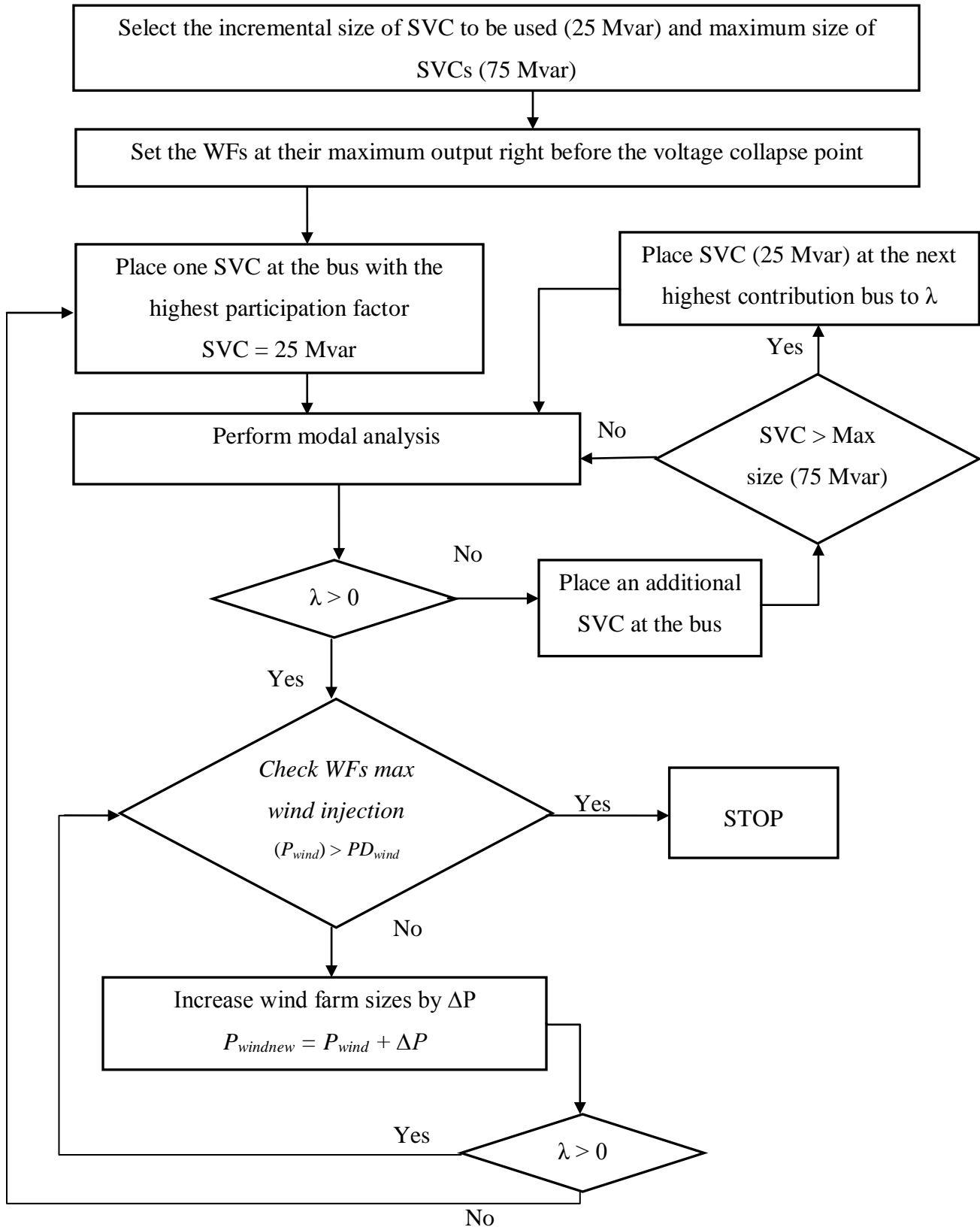


Figure 6.3 Locating New SVCs for Increasing Wind Penetration



6.3 Simulation and Performance Using Simultaneous Increase of Wind Farms' Power Outputs

The proposed method for sizing wind farms was applied to the power system in western Kansas with combined areas I and II. The combined area has a July peak load of 1,200 MW, which occurred in hour 17 (4 pm – 5pm). Results of the modal analysis are shown in the next sections. The study identifies six possible buses for wind power injection in the western Kansas power system. All six locations have similar transmission connection facilities at the 115 kV voltage level. The six buses are referred to in this study by their bus numbers, which are 95, 105, 110, 115, 119 and 123. These six locations are located far from each other. All of the wind generation output is absorbed in the combined western Kansas power system. To compare the results from this method with previously presented methods, Method I presented in Chapter 4 was also applied to the power system in western Kansas with combined areas I and II.

Calculations of system *VSMs* are generated using the Southwest Power Pool (SPP) Summer 2010 load flow model using the western Kansas ZIP load model shown in Table 2.14. The SPP model has been modified to incorporate the new wind farms under study. The PSS/E software package, version 32 has been used for load flow analysis and to generate the Q-V curves for the calculation of systems' *VSMs* [82]. For the modal analysis calculations, the PSS/E SPP model was converted to a model in Matlab [85].

The six wind generation buses were ranked using the modal analysis method and the Q-V curve method. In the modal analysis method, buses were ranked based on their contribution to the voltage instability modes before and after wind injections. The participation factors of each of the wind injection buses indicates their participation to the most critical voltage instability mode. Buses with high participation in instability modes are referred to as weak buses while buses with low participation to the instability modes are referred to as strong buses.

In the Q-V curve method, buses were ranked based on their impact on *VSMs* before and after wind injections. The system *VSMs* are used as a measure to how strong the system is for wind injections from the six wind buses and ranked accordingly. Buses with wind injections that cause the system *VSMs* to drop are considered weak buses for injections. Buses that do not negatively impact *VSM* are considered strong wind injection buses.

For the combined western Kansas power system, additional N-1 (transmission line outages) contingencies were monitored by adding contingencies in Area II, and a new most

limiting contingency appeared. Losing the 345 kV transmission line from Bus 285 to Bus 298 had significantly reduced the available amounts of *VSMs* when compared to the to the limiting contingency used in previous chapters (Area I contingencies). All analysis followed in this chapter and Chapter 7 uses the loss of the line from Bus 285 to Bus 298 as the most limiting contingency.

6.3.1 Case I: Base Case - No Wind Injection

Modal analysis was performed on the 2010 peak July load case before injecting any new wind to determine best buses for wind injecting based on bus participation factors. Results of the modal analysis indicated that the system is voltage stable with the most critical eigenvalue > 0 ($\lambda_0 = 0.1706$), and the highest participation factor for that mode at bus number 95. Due to its high participation in the mode of instability “ λ_0 ”, bus 95 is considered a weak bus for wind injection. Normalized bus participation factors in λ_0 are shown in Figure 6.4 and a list of the normalized participation factors is shown in Table 6.1. Since buses 105, 110 and 119 had very low participation in λ_0 , they are considered strong buses for wind injections. However, buses 95, 115 and 123 have significantly high participation in λ_0 , and they are considered weak buses for wind injections.

As shown in Table 6.1 and with no wind injections, results of the classification of the six buses as strong or weak for wind injections obtained using modal analysis and using Q-V curve method are identical. Buses which were classified as strong buses in the modal analysis were also classified as strong buses in the Q-V curve analysis since they have high *VSMs*. Similarly, buses classified as weak buses in the modal analysis also were classified as weak buses in the Q-V curve analysis.

Figure 6.4 Participation Factors for Mode of Instability without Any Wind Injection

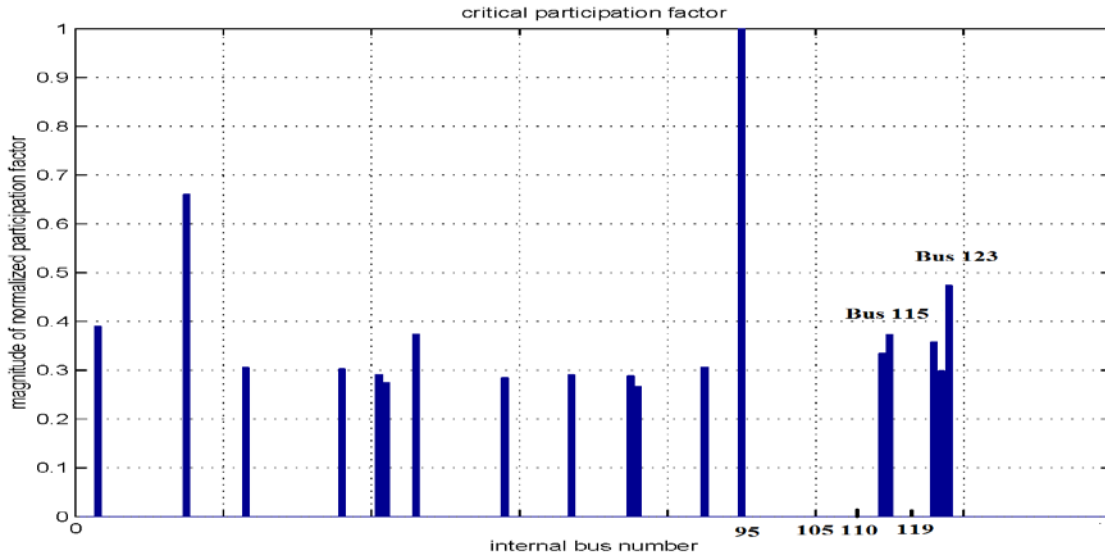


Table 6.1 Ranking & Classification of the Proposed Wind Injection Buses before Wind Injection Using Modal Analysis

Before Wind Injection Case	Modal Analysis Critical Eigenvalue of $\lambda_0 = 0.170651376$		Wind Injection Bus Classification	Q-V Curve Analysis at the Injection Bus	
	Bus Number	Normalized Participation Factors		VSM in Mvar at the Bus	Rank
	Rank				
	1	0.000	Strong	60.5	1
	2	0.000	Strong	45.3	2
	3	0.000	Strong	38.9	3
	4	0.380	Weak	23.5	5
	5	0.470	Weak	24.9	4
	6	1.000	Weak	10.8	6

6.3.2 Maximum Wind Penetration Using SCIG Wind Turbine Type

Maximum wind penetration and the impact on modes of voltage instability of connecting wind turbines that use Squirrel Cage Induction Generators (SCIGs) to generate power is analyzed in this section. The SCIG type generator consumes reactive power for magnetic excitation. The required reactive power consumption by SCIGs cannot be regulated by itself. Power factor of systems which have SCIG type wind turbines connected to it decrease if operated without reactive power compensation by additional devices like shunt capacitors. Power system voltage stability margins and system voltage stability eigenvalues are negatively impacted by this type of wind turbine. It is assumed that for the SCIG, the maximum wind penetration calculated in this chapter is based on consuming the needed reactive power directly from the power system (no additional shunt capacitors are installed).

6.3.2.1 Case II: Maximum Wind Penetration from Individual Bus Wind Injection Using SCIG Wind Type Turbines

Wind power was injected from each of the six wind injection buses individually to determine the maximum wind injection level which can be safely injected from each wind injection bus. Only one individual wind injection bus is assumed to produce wind power for this analysis with all other wind buses disconnected (not installed). Other buses are assumed to produce zero MW during this analysis. The maximum wind injection from each bus using SCIG wind turbine type is shown in Table 6.2. These wind injection values are limited by voltage stability constraints, that if exceeded, cause the system to become voltage unstable. In Table 6.2, buses are ranked based on the maximum value of wind injection in “MW”. Buses are also classified as weak or strong buses for wind injections based on the maximum wind injection values obtained. A “weak bus” is not a good location for wind injections. Injecting wind from the weak buses does not minimize the negative impact on voltage stability margins and the negative impact on the system modal eigenvalues. A “strong bus” is a good location for wind injections. Injecting wind from the strong buses minimizes the negative impact on voltage stability margins and modal eigenvalues of the system.

Table 6.2 Maximum Wind Injected Separately From Each Individual Bus before Reaching the Collapse Point Using SCIG Wind Turbine Type

Bus Number	Max Wind Injection in MW P_{wind0}	Rank Based on Max Wind Injection	Bus Wind Injection Classification Using Modal Analysis
105	106	1	Strong
119	80	2	Strong
110	66	3	Strong
115	60	4	Weak
123	52	5	Weak
95	33	6	Weak

Calculated results for the maximum wind injections from each of the six buses indicate that bus ranking and bus classifications of weak and strong buses identified using DFIG wind turbine type in previous sections stayed the same when wind is injected using the SCIG wind turbine type. For the SCIG wind turbine type, Buses 95, 115, and 123 are considered weak while buses 105, 110, and 119 are considered strong buses for wind injections. Using SCIG wind turbine type, Bus 105 resulted in the highest wind injection of 105 MW.

Modal analysis indicates that the impact of increasing wind injections using SCIG type wind turbines is dependent on the contribution of the wind injection bus to modes of voltage instability. As it can be observed in Figure 6.5, the system eigenvalues were very sensitive to increasing wind injections from the weak buses. The system eigenvalues decreased rapidly when wind injection increased from bus 95 which is the weakest bus. However, when wind injection increased from the strong buses using SCIG wind turbine type, system eigenvalues stayed practically unchanged until the system reached the voltage collapse point as shown in Figure 6.6. Increasing wind injections using SCIG wind turbine type can reduce or even deplete reactive power in the system which results in reducing system eigenvalues. Power system eigenvalues decreased and the system became less voltage stable when wind was injected from the weak buses. The initial increase in system eigenvalues for wind injections from Bus 123 is a result of having a load close to that bus. When wind injection increased above the load value, and power has to travel further to a load point, eigenvalues decreased.

Figure 6.5 Impact on System Eigenvalues for Increasing Wind Injections From Each of the Weak Buses Individually Using SCIG Wind Turbine Type

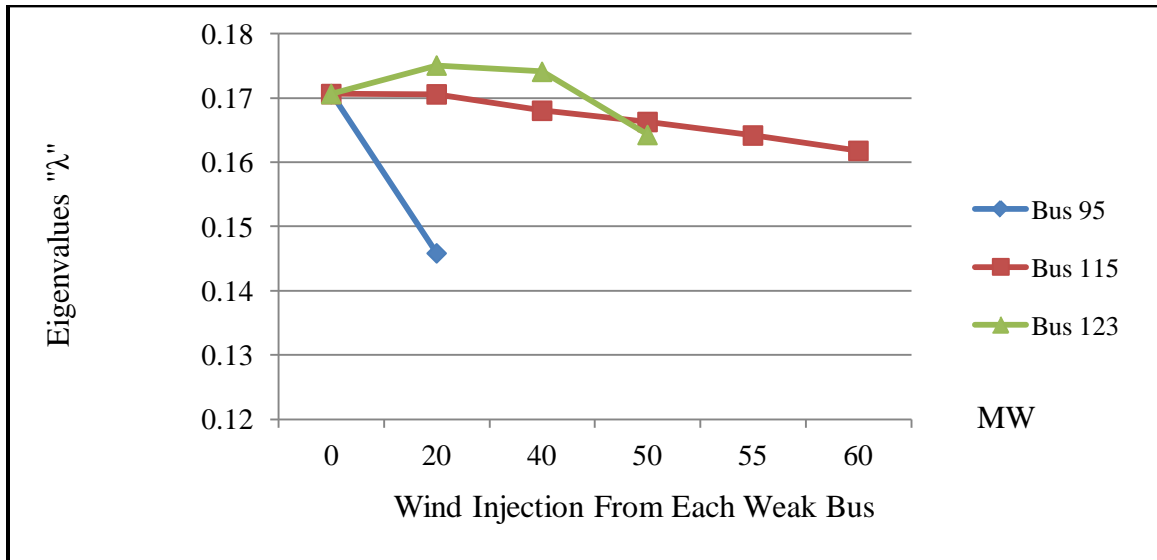
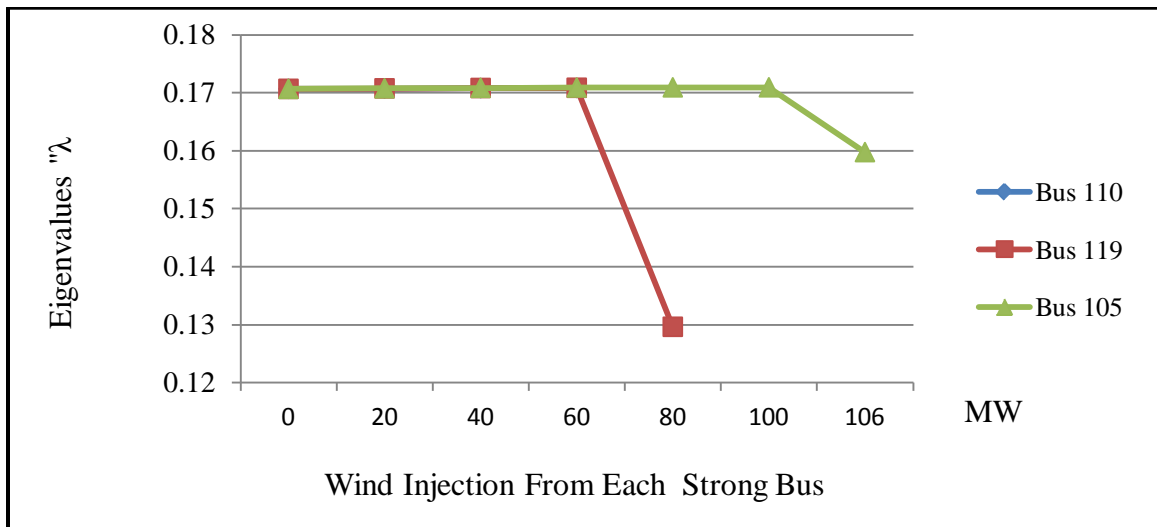


Figure 6.6 Impact on System Eigenvalues for Increasing Wind Injections From Each of the Strong Buses Individually Using SCIG Wind Turbine Type



Bus participation factors were impacted by the location of wind power injections. Table 6.3 shows buses which have the highest participation factors in modes of voltage instability as wind power injections increased from the six buses using SCIG wind turbine type. Injecting wind power from the weak buses indicated that Bus 95 has the highest contribution to modes of instability regardless of the wind turbine power outputs. In the cases of injecting wind power

from the weak buses, Bus 95's contribution to modes of instability became stronger as wind injection increase as shown in the figures in Appendix D. For wind injection increases from the strong buses, Bus 95 had the highest participation in modes of instability up until wind injection approached the maximum allowed values (near the collapse point). Here Bus 95 participation to modes of instability decreased and the buses where the wind was injected became the highest participating buses in modes of instability. This observation is important and it indicates that at or near maximum wind injections, additional voltage control equipment like SVCs needs to be installed at the wind injection bus when wind is injected from strong buses. However, when wind is injected from weak buses, SVCs are best located at buses other than the wind injection buses.

Table 6.3 Impact of Gradual Increases of Wind Penetration from Each Individual Bus on System Eigenvalues and Bus Normalized Participation Factors Using SCIG Wind Turbine Type

Bus Number Where Wind is Injected From	Wind Injection at the Bus in MW	Bus with Highest Participation Factor
95	0 - 33	95
115	0 - 60	95
123	0 - 52	95
110	0 - 60	95
	61 - 66	110
119	0 - 78	95
	79 - 80	119
105	0 - 100	95
	101 - 106	105

6.3.2.2 Case III: Maximum Wind Penetration from 3-Combined Bus for Wind Injections Using SCIG Wind Turbine Type

Simulation results indicate that injecting wind power from different buses simultaneously into the power system results in higher wind penetration values than injecting the wind from each of the wind injection buses separately. In this section, maximum wind penetration was calculated using two wind injection bus combinations. The first combination is a weak bus combination where wind was equally and simultaneously injected from all of the three weak buses (Bus 95, 115 and 123) in increments of 10 MW at each weak wind injection bus until reaching the voltage collapse point. Results of the modal analysis indicated that a maximum of 90 MW of wind power injection using SCIG wind turbine type was possible. The maximum combined weak bus wind injection of 90 MW was 16 MW lower than the maximum obtained using only the best strong bus for wind injections (Bus 105).

The second combination of buses for wind injection was the strong bus combination which includes buses 105, 110 and 119. Injecting wind power equally and simultaneously at these strong buses resulted in a maximum wind injection of 180 MW using SCIG wind turbine type. The combined strong bus maximum wind injection was 74 MW higher than the maximum wind injection obtained using the single strongest bus (bus 105). Maximum wind penetration obtained using the strong bus combination was 15% which is 7.5% higher wind penetration than the weak bus combination used for wind injections.

Similar to the finding from single bus wind injections, for the weak bus wind injection combination, and as the combined wind injection increased from zero to the maximum value of 90 MW, Bus 95 had the highest participation factor to modes of instability as shown in Figure 6.7 and Appendix D. For the strong bus wind injection combination, Bus 95 was the highest participation bus until the output of the combined strong buses became close to the maximum value of 180 MW, then Bus 110 became the highest participating bus as shown in Figure 6.18 and Appendix D. This observation is important, and it indicates that at or near maximum wind injections, additional voltage control equipment like SVCs needs to be installed at the wind injection bus when wind is injected from strong buses. However, when wind is injected from weak buses, SVCs are best located at buses other than the wind injection buses.

Figure 6.7 Normalized Bus Participation Factor to the Most Critical Mode of Voltage Instability for the Combined Weak Bus Wind Injection of 90 MW Using SCIG Wind Turbine Type

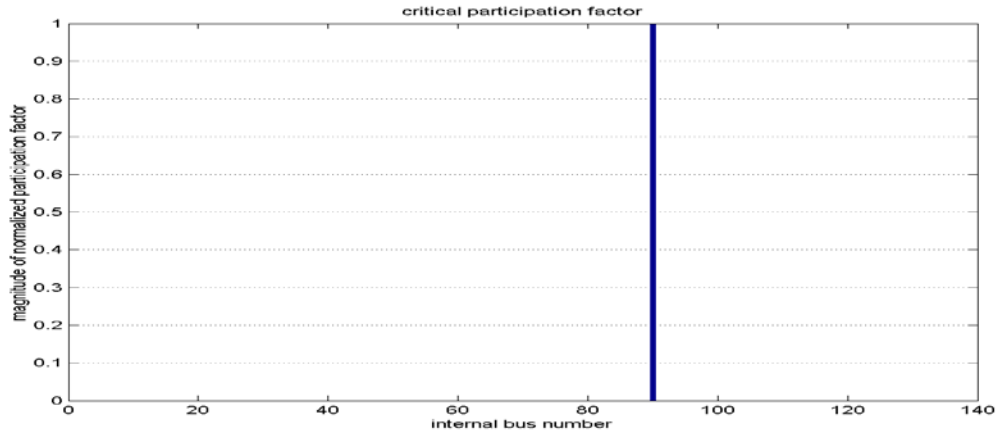
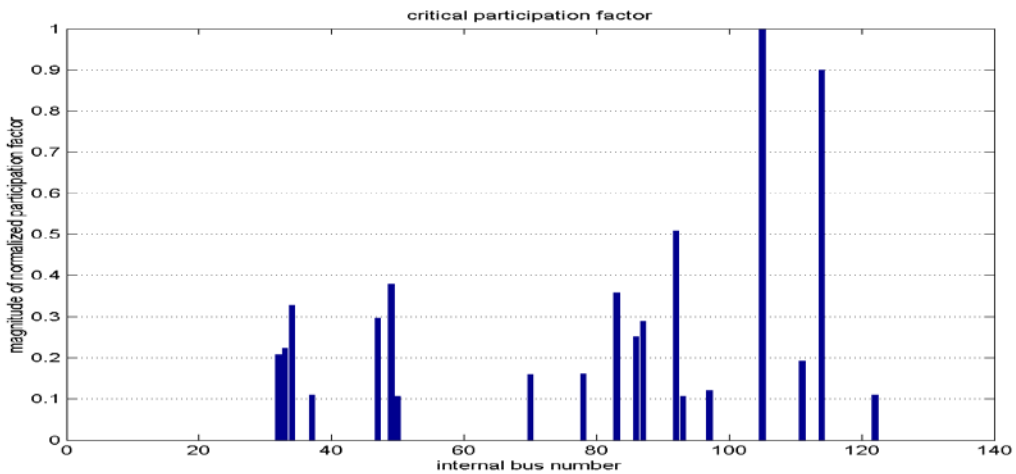


Figure 6.8 Normalized Bus Participation Factor to the Most Critical Mode of Voltage Instability for the Combined Strong Bus Wind Injection of 180 MW Using SCIG Wind Turbine Type



6.3.3 Maximum Wind Penetration Using DFIG Wind Turbine Type

Maximum wind penetration and the impact on modes of voltage instability of connecting wind turbines that use Doubly-Fed Induction Generators (DFIGs) to generate power is analyzed in this section. The required reactive power consumption by DFIGs can be regulated by itself. Power factor of systems which have DFIG type wind turbines connected to can be controlled without additional reactive power compensation. Power system voltage stability margins and

system voltage stability eigenvalues are impacted by this type of wind turbine but to a lesser degree than the SCIG type turbines.

In order to assess the impact of wind injections, modal analysis was performed each time wind injection was increased at each bus individually or as a group of buses. For each operating point, the eigenvalues of the reduced Jacobian matrix were generated to obtain the proximity to voltage instability. The bus participation factors were then calculated for the most critical voltage instability mode to identify buses with highest contribution to the instability mode. In order to verify the modal analysis results, the Q-V curves were also generated at those buses. Buses with high *VSMs* are considered strong buses for wind injections while buses with low *VSMs* are considered weak buses for wind injection.

6.3.3.1 Case II: Maximum Wind Penetration from Individual Bus Wind Injection Using DFIG Wind Turbine Type

In this case wind was injected from each of the six buses separately. This is done to verify that ranking buses based on the maximum amount of wind injections from each bus is consistent with the bus ranking for wind injection obtained using modal analysis and the Q-V curve method. The steps can be assumed as follows.

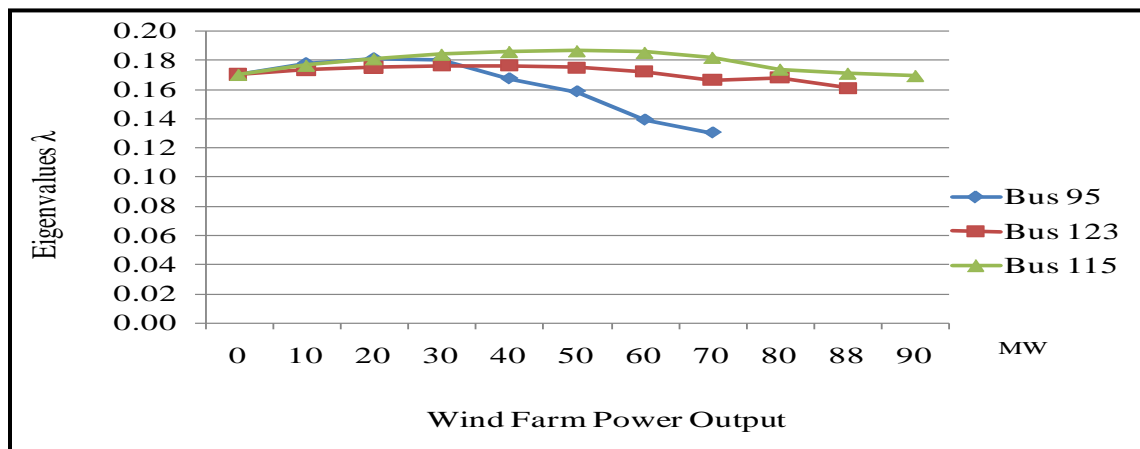
1. Calculations for the maximum wind injection levels from each bus. The maximum wind injections per bus are calculated, and a summary of the results is shown in Table 6.4. Wind was injected from each bus in increments until reaching the collapse point. To determine the maximum wind injection right before reaching the collapse point, the wind injection value at which the system collapsed was reduced by 1 MW increments and power flow is solved repeatedly until reaching a stable solution. The first maximum wind injection value at which the system reaches a stable solution is the maximum value of wind injection reported in Table 6.4. Buses which were classified by the modal and the Q-V analysis as weak buses resulted in significantly lower maximum wind injections. The highest wind injection was 156 MW from Bus 105 and the lowest was 45 MW from Bus 95.

Table 6.4 Maximum Wind Injection from Each Individual Bus in MW Using DFIG Wind Turbine Type Before Reaching the Voltage Collapse Point

Bus Number	Max Wind Injection in MW P_{wind0}	Rank Based on Max Wind Injection	Bus Wind Injection Classification Using Q-V Curve and Modal Analysis
105	156	1	Strong
119	131	2	Strong
110	109	3	Strong
115	88	4	Weak
123	83	5	Weak
95	45	6	Weak

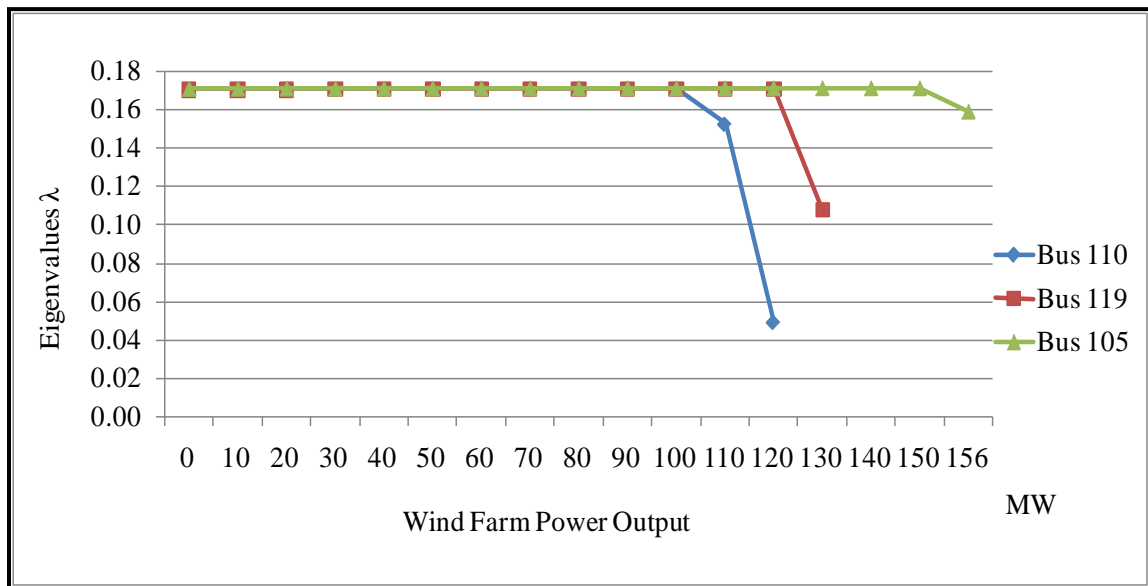
2. Calculations of the eigenvalues using modal analysis. For every wind injection level, modal analysis was performed after each wind increase, and modes of voltage instability (eigenvalues) were determined to evaluate if the system stays voltage stable after each wind injection increase. Results of the modal analysis of the impact on system eigenvalues, after each increase of wind generation from the weak buses, are shown in Figure 6.9.

Figure 6.9 The Impact on Eigenvalues of Increasing Wind Injection from Each of the Weak Buses Using DFIG Wind Turbine Type



Results show that system eigenvalues were very sensitive to the amount of wind injected from the weak buses. When the weak buses' wind injection level decreased to lower than 2/3 of the maximum wind injection values shown in Table 6.4, the system eigenvalues became more positive and hence the system voltage stability improved. This is due to the fact that at low wind penetration the reactive power required to deliver the small amount of wind to the load was available and system was strong enough to absorb these wind levels. However, when the wind injected levels exceeded 2/3 of the maximum wind injection limit, system critical eigenvalues decreased and the system became less stable. This is due to lack of reactive power support when the wind injection from the weak buses became high. Increasing wind injection from the strong buses had no significant impact on the system critical eigenvalues. System eigenvalues were not sensitive to increasing wind injection from these buses until the system was operated very close to the collapse point as shown in Figure 6.10.

Figure 6.10 The Impact on Eigenvalues of Increasing Wind Injection from Each of the Strong Buses Using DFIG Wind Turbine Type



3. Calculations of the bus participation factors in modes of instability. Table 6.5 shows the largest system participation factors found using eigenvectors for all the selected buses as wind injection gradually increased from each wind injection bus. From the results shown in

Table 6.3, as wind injections increased from each of the weak buses, the bus with the most contribution to modes of instability did not change. For all three weak buses, Bus 95 had the most participation to modes of instability regardless of which weak bus the wind was injected from. For all three strong buses, Bus 95 had the highest participation until the system was operated very close to collapse point. At that point, system reactive power was depleted and any additional wind injections from any of the strong buses resulted in changing the most participating bus from bus 95 to the bus where the additional wind was injected from. In other words, the large wind farm made the bus where it was located a weak bus.

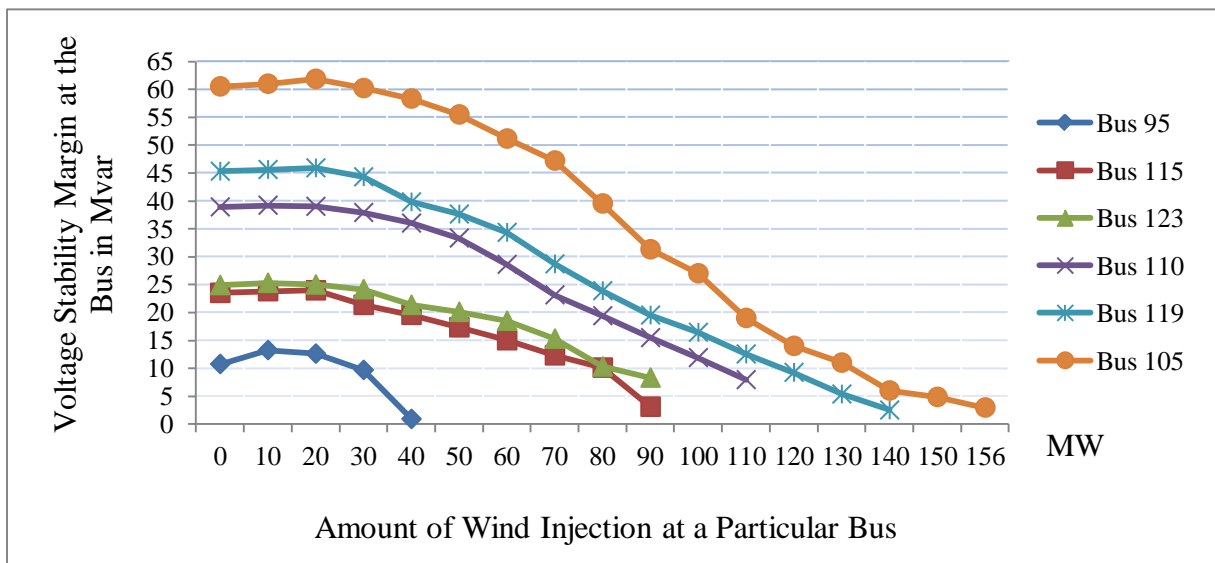
Table 6.5 Bus Participation Factors for all Six Buses as Wind Injection Gradually Increased from Each Bus Individually Using DFIG Wind Turbine Type

Bus Number Where Wind is Injected From	Amount of Wind Injection at the Bus MW	Bus- Highest Participation Factor
95	0 - 45	95
115	0 - 88	95
123	0 - 83	95
110	0 - 100	95
	101 - 109	110
119	0 - 120	95
	121 - 131	119
105	0 - 150	95
	151 - 156	105

4. Calculation of the impact of increasing wind injections on VSMs using Q-V curve method. Results of the Q-V curve analysis showed that the “Bus” VSMs are impacted by increases in wind injection from both weak and strong buses. VSMs at the wind injection bus versus wind injection levels from all of the locations considered in this study are shown in Figure 6.11. From this figure, the Q-V curve bus ranking was exactly the same as the modal

analysis ranking shown in Table 6.1. Bus *VSMs* were sensitive to the amount of wind injected from each of the weak buses. The slight increase in *VSMs* at lower wind injection levels is expected since some small system loads are located close to these wind injection buses and system reactive power was sufficient to supply system loads.

Figure 6.11 The Impact on the “Q-V” Voltage Stability Margins (*VSMs*) of Increasing Wind Injections Using DFIG Wind Turbine Type



6.3.3.2 Case III: Maximum Wind Penetration from 3-Combined Bus for Wind Injections Using DFIG Wind Turbine Type

Combined wind injection from the top three ranked buses (strong buses) and the lower three buses (weak buses) has been investigated. Results of the analysis indicate that the combined wind injection from the three strong buses exceeded the combined wind injection from the weak buses by 148% (192 MW).

Several combinations of wind injections have been analyzed using modal analysis to calculate maximum wind injection possible before reaching the voltage collapse point. For each combination, wind power was equally injected from each bus in the combination. The simultaneous wind farm size increase is very similar to what was presented in Chapter 4 (Method I). Wind injection from each wind farm can be increased individually similar to what was

presented in Chapter 4 (Method II) for increases in wind penetration. Method II is discussed in the next chapter. Table 6.6 shows each combination of wind injections and their maximum wind injection values “ P_{wind0} ” allowed before reaching the collapse point.

Table 6.6 Maximum Wind Injections in MW for Case III with DFIG

Case III Scenario	Combined Buses Bus Numbers	Max Wind Injection P_{wind0} in MW
Strong Bus Combinations	105-110-119	321
	110-119	224
	105-119	220
	105-110	216
Weak Bus Combinations	95-115-123	129
	115-123	134
	95-123	84
	95-115	90

For all of the combinations considered, strong bus combinations resulted in significantly higher wind injections than weak bus combinations. For the strong bus combinations, the highest wind injection was 321 MW using all three strong buses. But for the weak bus combinations, injecting wind from two buses (Bus 115 and Bus 123) resulted in higher wind injection than the combination of three weak buses. Including Bus 95, which had the most participation in modes of instability, caused voltage stability limits to decrease more rapidly for wind injection increases from these buses.

The impact on system eigenvalues “ λ ” of increasing wind injections from the combined three strong buses and the combined three weak buses are shown in Figure 6.12. System eigenvalues were not sensitive to wind increases from the combined strong buses. Only at a wind injection exceeding 300 MW, were the system eigenvalues negatively impacted and moved closer to zero where the system became less voltage stable. For the combination of weak bus injections, eigenvalues were very sensitive to wind increases. At a combined wind injection less than 90 MW, system eigenvalues are improved and moved away from zero without noticing any

deficiencies in reactive resources. However, as shown in Figure 6.12, when wind injection increased above 90 MW, the system eigenvalues became smaller due to lack of reactive power support during heavier wind penetrations.

The impact of the combined wind injections on *VSMs* has been analyzed the three strong and three weak buses using the Q-V curve method. Wind injection increases using the three strong buses had no significant impact on *VSMs* until the combined strong bus wind injection exceeded 300 MW, as indicated by the results of the Q-V curve analysis shown in Figure 6.13. *VSMs* were significantly impacted when the combined weak bus wind injection exceeded 60 MW as shown in this figure. This confirms the maximum wind injection results found using modal analysis for the combined wind injection scenarios.

Figure 6.12 Impact on System Eigenvalues of Increasing Wind Injections from the Combined Strong and the Weak Buses Using Modal Analysis for DFIG

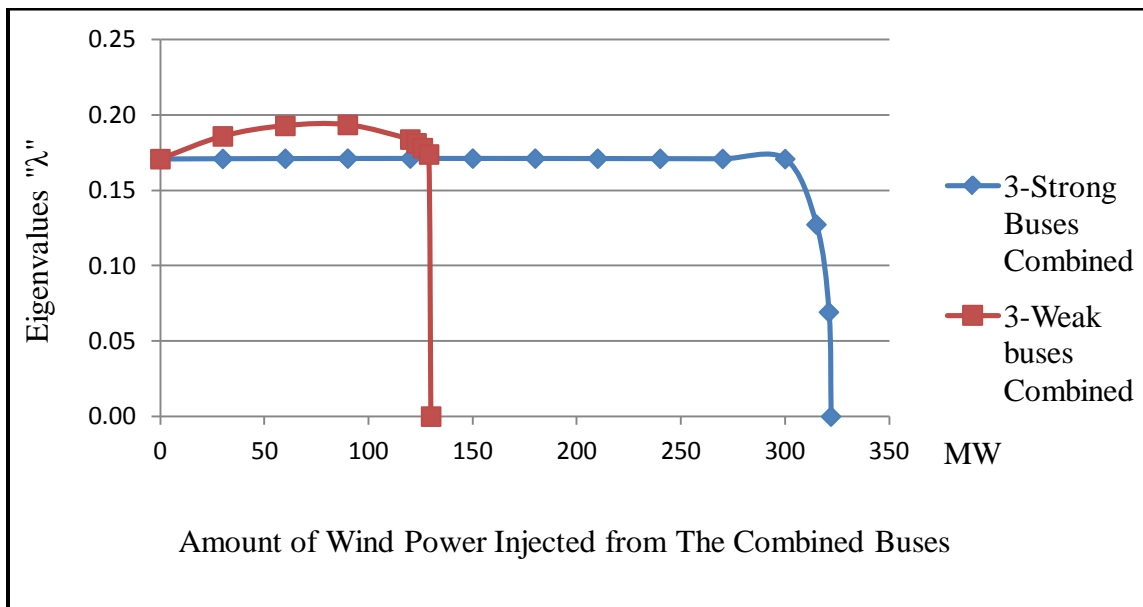
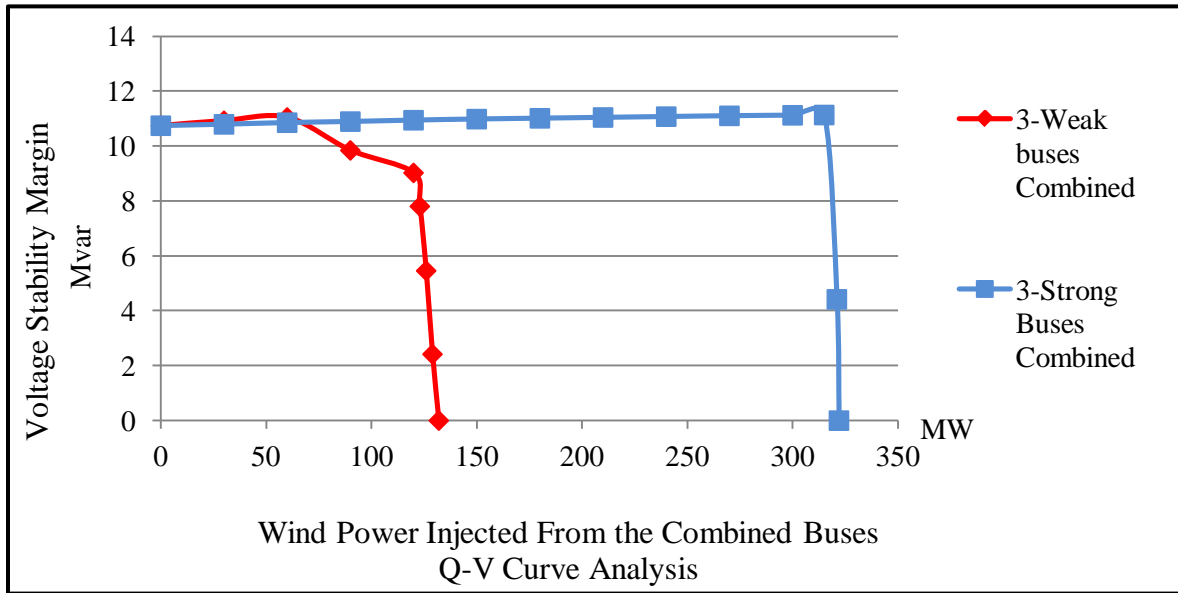


Figure 6.13 The Impact of Increasing Wind Injection from the Combined Weak and Strong Buses on Voltage Stability Margins (VSMs) Using the Q-V Curve Method for DFIG



6.3.4 Maximum Wind Penetration Using DDSG Wind Turbine Type

Maximum wind penetration and the impact on modes of voltage instability of connecting wind turbines that use direct-drive synchronous generators (DDSG) to generate power is analyzed in this section. When wind resources are available, the DDSG generator behaves like a conventional generator. The required reactive power consumption by a DDSG can be regulated by itself. Power factor of systems which contain DDSG wind turbines can be controlled, and the DDSG can supply the grid with reactive power. However, this type of wind turbine may negatively impact system voltage stability margins and system voltage stability eigenvalues if it located in areas far from loads in weak power systems.

6.3.4.1 Case II: Maximum Wind Penetration from Individual Bus Wind Injection Using DDSG Wind Turbine Type

Wind power was injected from each of the six wind injection buses to determine the maximum wind injection in “MW” which can safely be injected from each wind injection bus individually. In Table 6.7, buses are ranked based on the maximum value of wind injection in “MW” which can be safely injected in the power system. Buses are also classified as weak or

strong buses for wind injections based on the maximum wind injection values obtained. Injecting wind from the strong buses minimizes the negative impact on voltage stability margins and the modal eigenvalues of the system.

Calculated results for the maximum wind injections from each of the six buses indicated that bus ranking and bus classifications of weak and strong buses identified using DFIG or SCIG wind turbine types in previous sections stayed the same when wind is injected using DDSG turbines. For the DDSG, Buses 95, 115, and 123 are considered weak while Buses 105, 110, and 119 are considered strong buses for wind injections as shown in Table 6.7. Using DDSG type wind turbines for wind injection, Bus 105 resulted in the highest wind penetration at 165 MW.

As can be observed in Figure 6.14, system eigenvalues were sensitive to increasing wind injections from the weak buses. The system eigenvalues decreased rapidly when wind injection increased from Bus 95 which is the weakest bus. However, when wind injection increased from the strong buses, system eigenvalues stayed practically unchanged until the system reached the voltage collapse point as shown in Figure 6.15.

Table 6.7 Maximum Wind Injected Separately from Each Individual Bus Before Reaching the Collapse Point Using DDSG Wind Turbine Type

Bus Number	Max Wind Injection in MW P_{wind0}	Rank Based on Max Wind Injection	Bus Wind Injection Classification Using Modal Analysis
105	165	1	Strong
119	135	2	Strong
110	120	3	Strong
115	100	4	Weak
123	100	5	Weak
95	57	6	Weak

Figure 6.14 Impact on System Eigenvalues for Increasing Wind Injections from Each of the Weak Buses Individually Using DDSG Wind Turbine Type

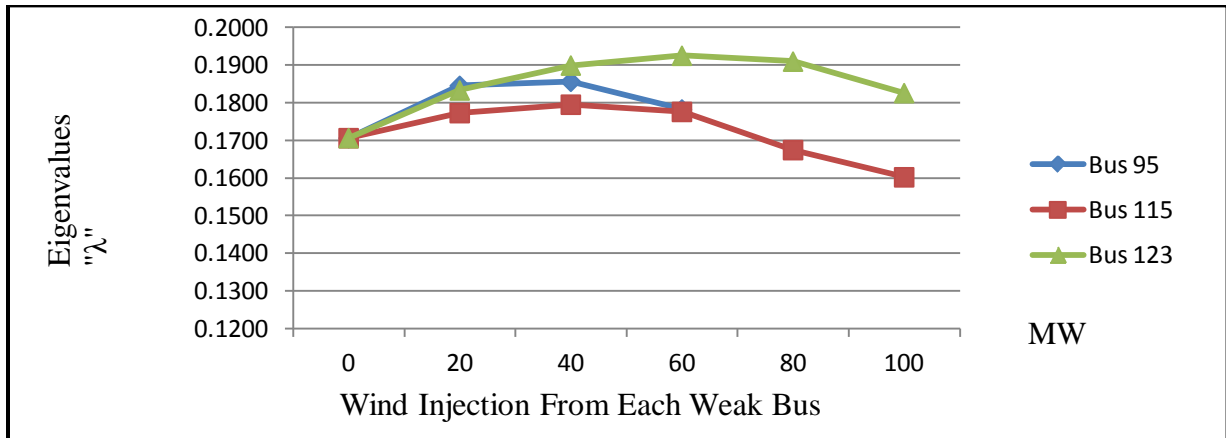
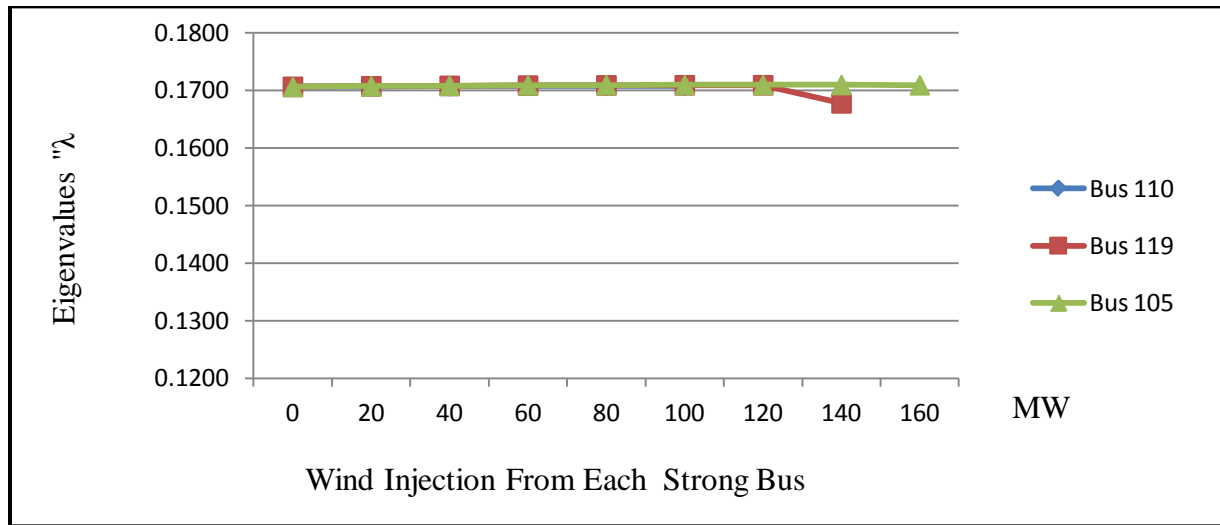


Figure 6.15 Impact on System Eigenvalues for Increasing Wind Injections from Each of the Strong Buses Individually Using DDSG Wind Turbine Type



Bus participation factors were impacted again by the location of wind power injections. Table 6.8 shows buses which have the highest participation factors to modes of voltage instability as wind power injections increased from the six buses using DDSG wind turbine type. Injecting wind power from the weak buses indicated that Bus 95 has the highest contribution to modes of instability regardless of the wind turbine power outputs. In the cases of injecting wind power from the weak buses, Bus 95's contribution to modes of instability became stronger as wind injection increased as shown in figures in Appendix D. For wind injection increases from

the strong buses, Bus 95 had the highest participation to modes of instability. When wind was injected from Bus 110 (strong bus), the Bus 95 participation factor decreased. When wind injection from Bus 110 increased above 110 MW, Bus 110 (where the wind was injected) became the highest participation bus in modes of instability.

Table 6.8 Impact of Gradual Increases of Wind Penetration from Each Individual Bus on System Eigenvalues and Bus Normalized Participation Factors Using DDSG Wind Turbine Type

Bus Number Where Wind is Injected From	Wind Injection at the Bus MW	Bus- Highest Participation Factor
95	0 – 20	95
	21 - 57	95
115	0 - 100	95
123	0 - 100	95
110	0 - 109	95
	110 - 120	110
119	0 - 135	95
105	0 - 165	95

6.3.4.2 Case III: Maximum Wind Penetration from 3-Bus Combination for Wind Injections Using DDSG Wind Turbine Type

Simulation results indicate that injecting wind power from different buses simultaneously into the power system results in higher wind penetration values than injecting the wind from each of the wind injection buses separately. In this section, maximum wind penetration was calculated using the two wind injection bus combinations used previously in 10 MW per wind farm increments. Results of the modal analysis indicate a maximum of 150 MW of wind power injection using DDSG wind turbine type is possible. The maximum combined weak bus wind injection of 150 MW was 15 MW lower than the maximum obtained using only the best strong

bus for wind injections (Bus 105). The 150 MW result of the combined weak bus injection is only 12.5% of wind penetration during peak loading condition of 1,200 MW.

The second combination of buses for wind injection was the strong bus combination which includes buses 105, 110 and 119. Injecting wind power equally and simultaneously from these strong buses resulted in a maximum wind injection of 350 MW using DDSG wind turbine type. The combined strong bus maximum wind injection was 185 MW higher than the maximum wind injection obtained using the single strongest bus. Maximum wind penetration obtained using the strong bus combination was 29.17% which is 16.67% higher wind penetration than the weak bus combination used for wind injections.

The impact on bus participation for this case is shown in Figures 6.16 and 6.17. For the weak bus contribution, Bus 95 had the highest participation factor to modes of instability regardless of the output wind power injected from the combined weak buses. Bus participation factors for every incremented power output of the combined weak buses are shown in Figure 6.16 and Appendix D. Also for the strong bus wind injection combination, bus 95 had the highest participation factor to modes of instability regardless of the output wind power injected from the combined weak buses. Bus participation factors for the incremented power output of the combined weak buses are shown in Figure 6.17 and Appendix D.

Figure 6.16 Combined Weak Buses Wind Injection of 150 MW on System Bus Normalized Participation Factors Using DDSG Wind Turbine Type

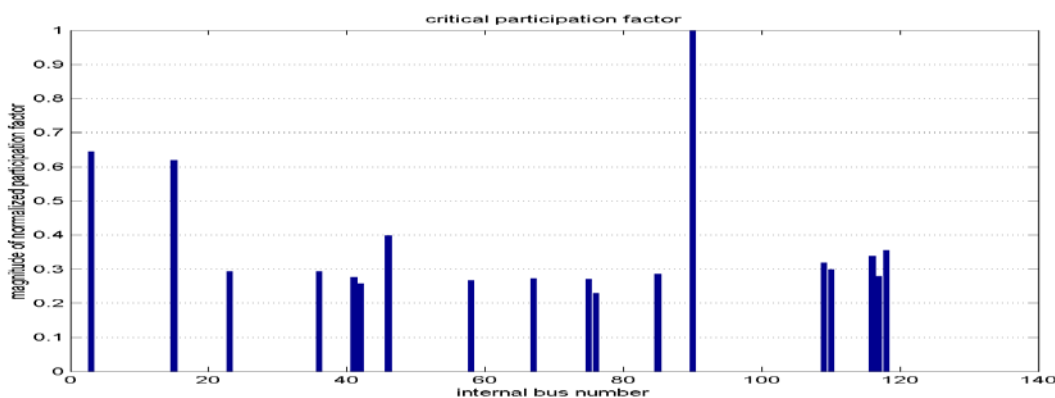
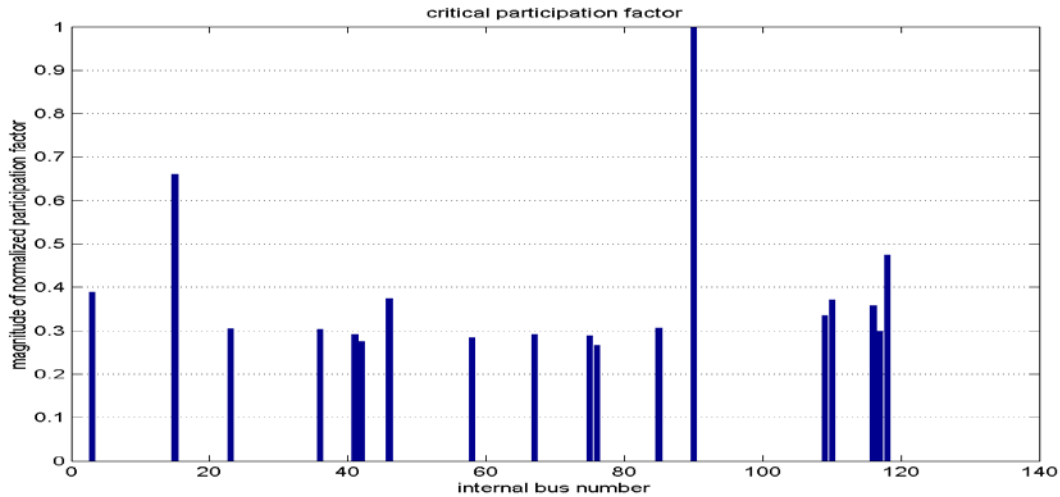


Figure 6.17 Combined Strong Buses Wind Injection of 350 MW on System Bus Normalized Participation Factors Using DDSG Wind Turbine Type



6.3.5 Comparison of the Impact of Using Three Different Types of Wind Generators on Maximum Wind Penetrations and on System Critical Eigenvalues

Regardless if the wind power injected into the power system is from a single location or multiple locations, maximum wind penetration level largely depends on the type of wind turbine used in the injections. Each wind turbine type has its own characteristics which impact the system voltage stability margins and critical eigenvalues. All three types of wind turbines used negatively impacted voltage stability margins and system eigenvalues. The impact was more noticeable when the wind penetration became high (above 10% of the peak load). Wind resources in the area studied are located far from load centers, and the transmission network connecting new wind power to the load is a weak system with lack of reactive power support. Using some types of wind turbine like the SCIG type, which consumes large amounts of reactive power, can deplete reactive resources and may cause these sources to reach their maximum reactive power limits making the system voltage unstable. Even using the DFIG and DDSG wind turbine types, which provide limited reactive power support to the grid, may deplete available reactive power margins due to the long distances between wind injection buses and load centers. In the power system studied, single bus injections resulted in lower maximum wind penetration when compared to combined three-bus injections. This is due to the fact that multiple wind

injection points result in less reactive power losses to flow in the system as line loadings are not as high as the single bus injection cases.

In the single bus injections, Bus 105 resulted in the maximum wind injection level regardless of the type of wind turbine used. One of the reasons is that Bus 105 is close to a large load center of 45 MW. Thus the first 45 MW of wind power injection from this bus doesn't have to travel far to reach a load. On the other hand, Bus 95 had the lowest wind injection levels for the single bus wind injection cases regardless of the type of wind turbine used. The maximum wind penetration obtained using bus 105 was 13.75% of the peak load using DDSG, while the lowest was at 2.08% when wind injected from Bus 95 using SCIG. Maximum wind penetrations from each single bus injection are shown in Table 6.9.

In the combined wind injection cases, the combined bus injections from the strong buses resulted in higher wind penetrations than the maximum penetration obtained using combined weak bus injections as shown in Table 6.9 and Table 6.10. The highest penetration level was 29.17% of peak load when injecting wind power from the combined strong buses using DDSG wind turbine type. As expected the lowest wind penetration level was 7.5% of peak load when injecting wind power from the combined weak buses using SCIG wind turbine type.

System modes of stability were also impacted by the type of wind turbine used. When injecting wind power from the weak buses, system eigenvalues were positively impacted at low wind output levels. But as wind generation increased from the weak buses, system critical eigenvalues decreased. At low levels of wind penetration, the system eigenvalues increased due to the locations of the weak buses. The three weak buses are located near small loads and adding wind injection at these locations actually improved voltage stability margins initially. But when the wind injection from these buses increased to higher levels, voltage stability margins decreased rapidly due to depleting available system reactive resources, and hence the systems' eigenvalues decreased.

When injecting wind power from the strong buses, system eigenvalues did not change significantly. The power system critical eigenvalues were not sensitive to the amount of wind power injected from these strong buses until the high wind penetration caused system to operate near the collapse point where system eigenvalues decreased rapidly.

Table 6.9 Comparison of Maximum Wind Penetration Using the Weak Buses for Each Wind Turbine Type

Weak Buses - High Contribution to Modes of Instability						
Individual Strong Bus Injection	Max Wind Injection in MW for Each Wind Turbine Type			Max Wind Penetration as a Percent of Maximum Load		
Bus Number	SCIG	DFIG	DDSG	SCIG	DFIG	DDSG
95	33	45	57	2.75%	3.75%	4.75%
115	60	88	100	5.00%	7.33%	8.33%
123	52	83	100	4.33%	6.92%	8.33%
Combined Weak Bus Injection Buses 95-115-123	90	129	150	7.50%	10.75%	12.50%

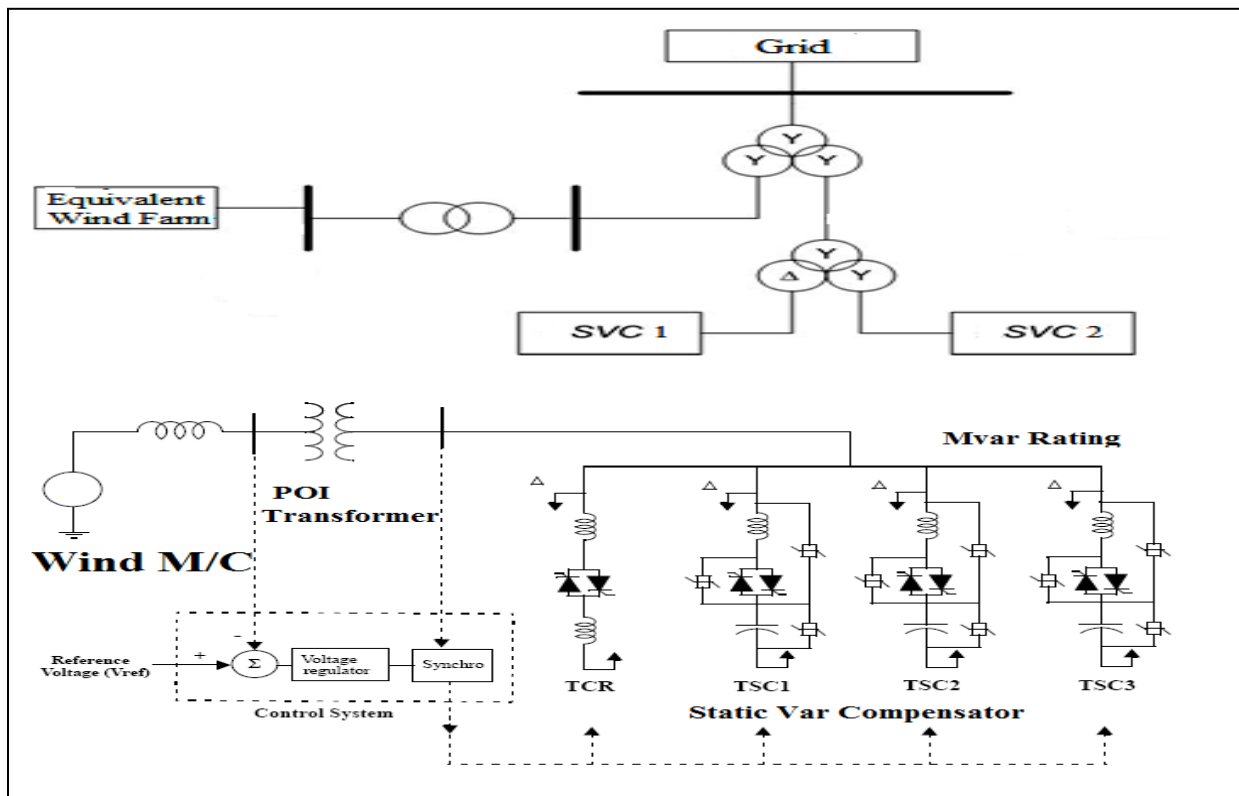
Table 6.10 Comparison of Maximum Wind Penetration Using the Strong Buses for Each Wind Turbine Type

Strong Buses - Low Contribution to Modes of Instability						
Individual Strong Bus Injection	Max Wind Injection in MW for Each Wind Turbine Type			Max Wind Penetration as a Percent of Maximum Load		
Bus Number	SCIG	DFIG	DDSG	SCIG	DFIG	DDSG
105	106	156	165	8.83%	13.00%	13.75%
110	66	109	120	5.50%	9.08%	10.00%
119	80	131	135	6.67%	10.92%	11.25%
Combined Strong Bus Injection Buses 105-110-119	180	321	350	15.00%	26.75%	29.17%

6.4 Increasing Wind Penetration by Placing SVCs Using the Different Types of Wind Turbines for the 3-Strong Bus Combination

The Static VAR Compensator (SVC) has been described as a solution to control the reactive power of a wind farm [115]. The power system with these types of compensators is shown in Figure 6.18. The SVCs can provide or absorb reactive power for the wind farm under different operating conditions to control bus voltages at the grid level. Using built-in reactors, SVCs can also prevent over voltage under islanding conditions.

Figure 6.18 SVCs Connected to an Equivalent Wind Farm for Voltage Support [115]



Modal analysis was used to determine the best location for adding shunt compensation (SVCs) to increase wind penetration to 410 MW from the 3-strong bus combination. Two options have been developed to locate new SVCs for increasing wind penetration. The first option (Option I) is to place SVCs only at the wind injection sites which have the highest contribution to instability modes. Placing SVCs at the wind farm bus is the current practice used in the industry to prevent disconnecting the wind farm from the grid during system disturbances

[27]. The second option (Option II) is to place SVCs at system buses with the highest contribution factors to modes of instability. This option does not limit the installation to only the wind injection sites. Placing SVCs at system buses can also provide for protection against disconnecting the wind farm from the grid during disturbances [48, 50].

Wind injection was increased simultaneously from each of the 3-strong bus combinations in increments of 10 MW. SVCs were placed at buses in the power system in 25 Mvar increments with a maximum of 75 Mvar allowed at each bus. The maximum size of 75 Mvar is necessary to eliminate the risk of voltage collapse if a very large SVC becomes unavailable during normal or contingency conditions.

6.4.1 Increasing Wind Penetration Using SVC Placement for the Combined 3-Strong Bus Combination Using SCIG Wind Type Turbines

Option I & II were applied to the western Kansas power system using the 3-strong bus combination equipped with SCIG wind type turbines. Modal analysis was used to determine the number and location of SVCs needed to be added to the power system to allow for 410 MW of wind injection from the 3-strong bus combination.

Option I, which was described in an earlier section, was used to determine location and size of SVCs needed to allow for 410 MW of wind injection. Table 6.11 shows that a total of 225 Mvar of SVCs were not sufficient to allow for a wind penetration level of 410 MW. By limiting the SVC installations to only the wind farm buses, a maximum of 300 MW of wind injection was possible without exceeding the 75 Mvar SVC size limit.

Option II, which was described in an earlier section, was used to determine location and size of SVCs needed. Table 6.12 shows that a total of 300 Mvar of SVCs were needed to allow for a wind penetration level of 410 MW. To reach this level, four SVCs with 75 Mvar each were necessary as shown in Figure 6.19. Two of the SVCs were needed at wind injection buses (Bus 110 and Bus 119) and two were needed at non wind injection buses; Bus 8 and Bus 95.

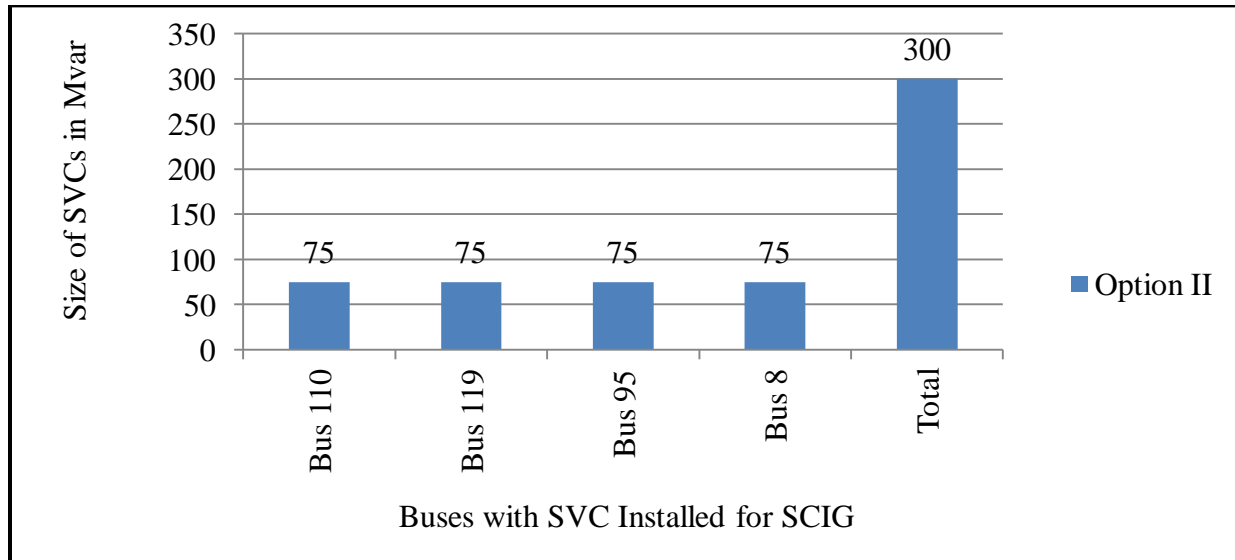
Table 6.11 Placement of SVCs to Increase Wind Penetration from Strong Buses Using SCIG Wind Turbine Type Using Option I

Iteration	Total Wind Injection	Eigenvalue	Highest Participation Factors	Installed SVC in Mvar			
	MW		Bus Number	Bus 105	Bus 110	Bus 119	Total SVC
Starting Point	180	0.1709	110	0	0	0	0
1	210	Unstable		0	0	0	0
2	210	Unstable		0	25	0	25
3	210	Unstable		0	50	0	50
4	210	Unstable		0	75	0	75
5	210	Unstable		25	75	0	100
6	210	Unstable		50	75	0	125
7	210	Unstable		75	75	0	150
8	210	Unstable		75	75	25	175
9	210	0.1651	110	75	75	50	200
1	240	0.1510	119	75	75	50	200
1	270	Unstable		75	75	50	200
2	270	0.1531	119	75	75	75	225
1	300	Unstable		75	75	75	225

Table 6.12 Placement of SVCs to Increase Wind Penetration from Strong Buses Using SCIG Wind Turbine Type Using Option II

Iteration Number	Total Wind Injection MW	Eigenvalues λ	Highest Participation Factors Bus Number	Size of Installed SVCs in Mvar During Each Iteration				Total SVCs in Mvar
				Bus Number				
			8	95	110	119	0	
Starting Point	180	0.1709	110	0	0	0	0	0
0	210	0.0000		0	0	0	0	0
1	210	0.1708	95	0	0	25	0	25
0	240	0.0000		0	0	25	0	25
1	240	0.0000		0	25	25	0	50
2	240	0.0000		0	50	25	0	75
3	240	0.1705	8	0	75	25	0	100
0	270	0.0000		0	75	25	0	100
1	270	0.0000		25	75	25	0	125
2	270	0.0000		50	75	25	0	150
3	270	0.1705	110	75	75	25	0	175
0	300	0.0000		75	75	25	0	175
1	300	0.0000		75	75	50	0	200
2	300	0.1802	119	75	75	75	0	225
0	330	0.0000		75	75	75	0	225
1	330	0.1706	119	75	75	75	25	250
0	360	0.0000		75	75	75	25	250
1	360	0.1705	119	75	75	75	50	275
0	390	0.0000		75	75	75	50	275
1	390	0.1710	119	75	75	75	75	300
0	410	0.1701	110	75	75	75	75	300

Figure 6.19 Using Option II for SVC Placement s for Reaching 410 MW of Total Wind Injection Using SCIG Wind Type Turbines



6.4.2 Increasing Wind Penetration Using SVC Placement for the 3-Strong Bus Combination Using DFIG Wind Type Turbines

Modal analysis process and results for the first SVC placement option (Option I) are shown in Table 6.13. After adding the first 25 Mvar SVC at Bus 119 in Iteration 1, modal analysis resulted in an unstable solution. In the second iteration, a second 25 Mvar SVC was added to Bus 119 but modal analysis still resulted in unstable solution. It took 6 iterations of adding 25 Mvar SVCs to wind injection buses before modal analysis resulted in a stable solution for the first increase of wind injections with a total of 125 Mvar of SVCs for an increase of maximum wind injection power from 321 MW to 330 MW. Steps are repeated for the next increase of wind injections from 300 MW to 360 MW. To reach the desired maximum wind injection of “ $PD_{wind} = 410$ MW”, required the installation of 225 Mvar of SVCs as shown in Table 6.13.

The second option for locating new SVCs was to place new SVCs at the buses with the highest participation factor to modes of instability regardless of whether they were a wind injection buses or not. Table 6.20 is a summary of the modal analysis used to place new SVCs to reach the 410 MW of wind injection using Option II.

Table 6.13 Locating SVCs to Increase Wind Penetration for DFIG Wind Turbine Type Using Option I

Iteration	Total Wind Injection	Eigenvalue	Highest Participation Factors	Installed SVC in Mvar			
				Bus 105	Bus 110	Bus 119	Total SVC
Starting Point	321	0.003	119	0	0	0	0
1	330	Unstable		0	0	0	0
2	330	Unstable		0	0	25	25
3	330	Unstable		0	0	50	50
4	330	Unstable		0	0	75	75
6	330	Unstable		25	0	75	100
7	330	0.153	110	25	25	75	125
1	360	Unstable		25	25	75	125
2	360	0.143	119	25	50	75	150
1	390	Unstable		25	50	75	150
2	390	Unstable		25	50	100	175
3	390	0.140	110	25	50	125	200
1	410	Unstable		25	50	125	200
2	410	0.157	119	25	75	125	225

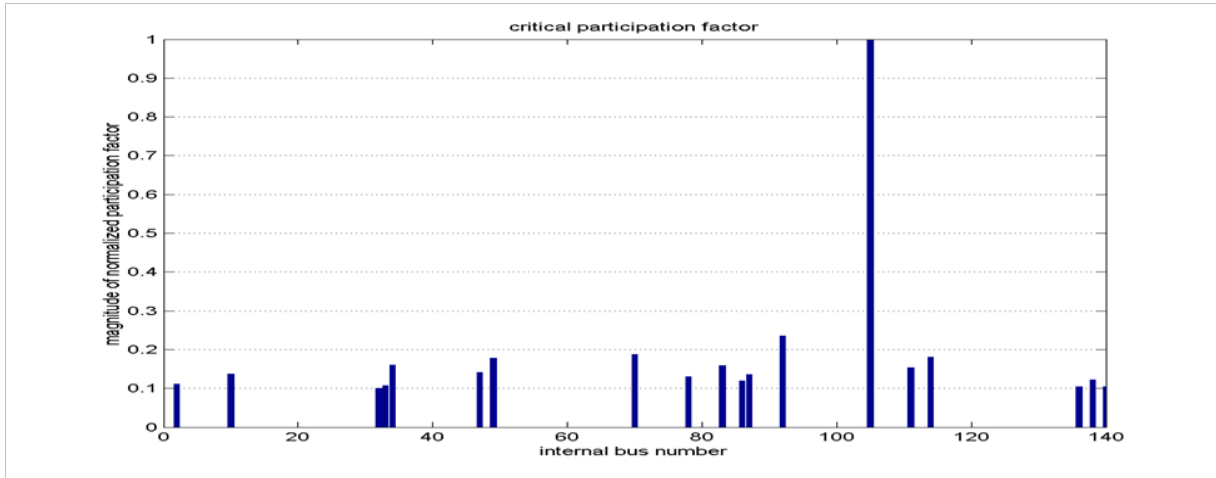
Starting with a combined wind injection from the strong buses at 321 MW, the modal analysis indicated that Bus 119 had the highest contribution to the critical mode of instability ($\lambda = 0.003$). The system became voltage unstable when the combined wind injection increased from 321 MW to 330 MW. Using Option II, where SVCs were placed at the bus with the highest participation factor, thus a 25 Mvar SVC was placed at Bus 119. This resulted in increasing wind penetration by 9 MW while maintaining system voltage stability.

Table 6.14 Locating new SVCs to Increase Wind Penetration for DFIG Wind Turbine Type Using Option II

Iteration	Total Wind Injection	Eigenvalues	Highest Participation Factors	Size of Installed SVCs in Mvar During Each Iteration				Total SVCs in Mvar
				Bus Number				
Number	MW	λ	Bus Number	95	97	110	119	0
Starting Point	321	0.003	119	0	0	0	0	0
0	330	Unstable		0	0	0	0	0
1	330	0.099	110	0	0	0	25	25
0	360	Unstable		0	0	0	25	25
1	360	Unstable		0	0	25	25	50
2	360	Unstable		0	0	50	25	75
3	360	0.089	95	0	0	75	25	100
0	390	Unstable		0	0	75	25	100
1	390	0.008	97	25	0	75	25	125
0	410	Unstable		25	0	75	25	125
1	410	0.072	110	25	25	75	25	150

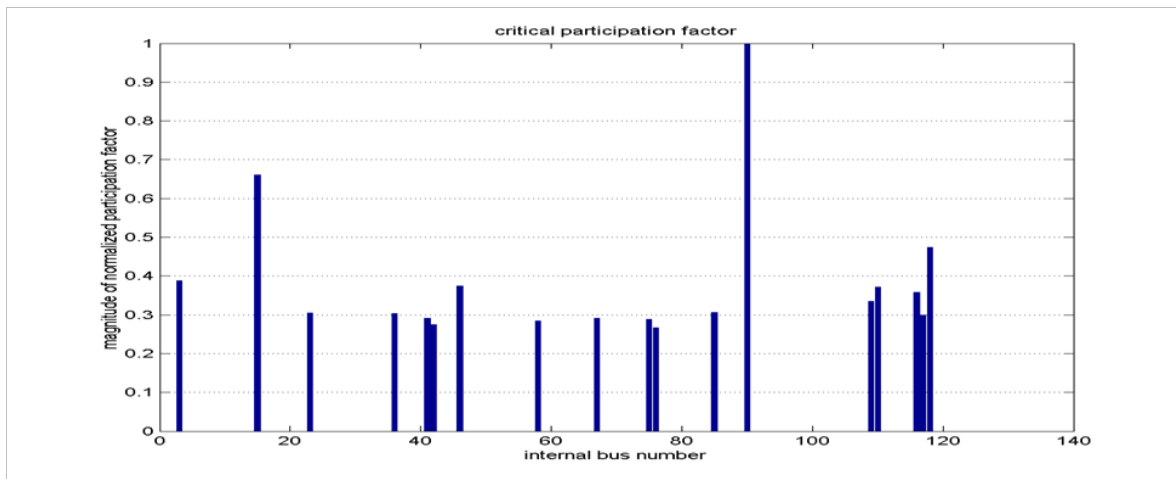
Increasing wind injection from 330 MW to 360 MW resulted in a voltage unstable condition even with the addition of the SVC at Bus 119. To avoid reaching the collapse point, a second SVC at the most participating bus in the mode of instability is used. As shown in Figure 6.20, at 330 MW of combined wind injection and with the SVC at bus 119, the most participating bus in modes of instability was Bus 110. Installing a total of 75 Mvar of SVCs at bus 110 was necessary to avoid voltage collapse when the combined wind injection level reached 360 MW.

Figure 6.20 Normalized Participation Factors for Combined Strong Bus Wind Injection of 330 MW



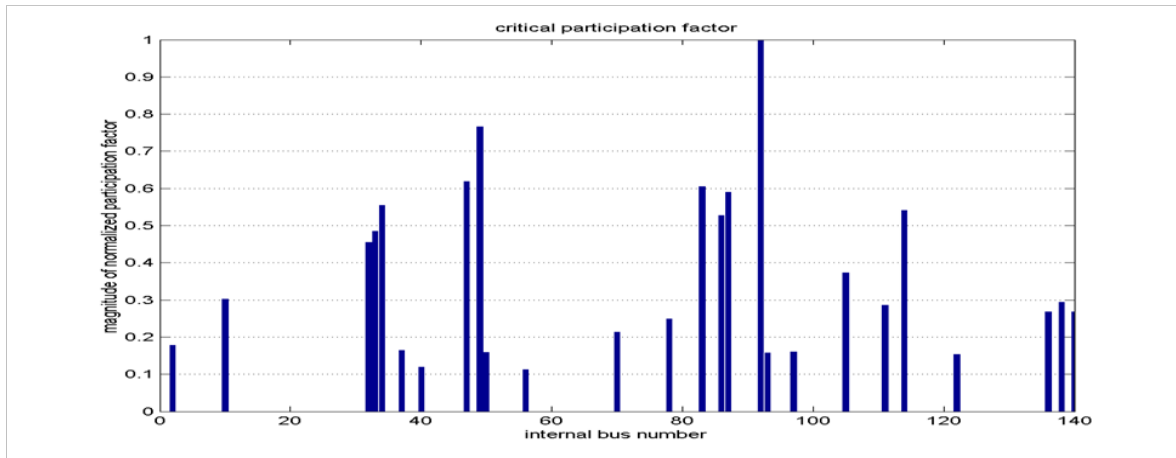
Increasing wind injection from 360 MW to 390 MW resulted in a voltage unstable condition even with the total addition of 100 Mvar of SVCs at Buses 110 and 119. To avoid reaching the collapse point, a third placement of SVC at the most participating bus in the mode of instability was used. As shown in Figure 6.21, at 360 MW of combined wind injection and with the SVCs at Buses 110 and 119, the most participating bus in modes of instability was bus 95. Installing a 25 Mvar of SVCs at bus 95 was sufficient to avoid voltage collapse when the combined wind injection level reached 390 MW.

Figure 6.21 Normalized Participation Factors for Combined Strong Bus Wind Injection of 360 MW



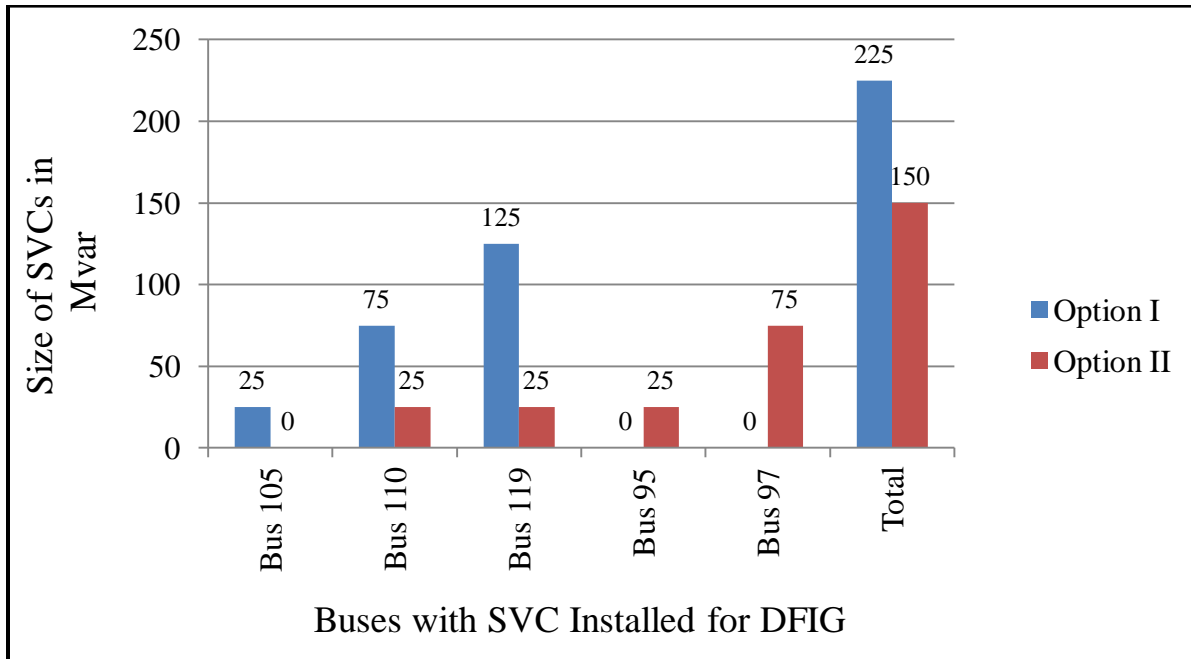
Increasing wind injection from 390 MW to 410 MW resulted in a voltage unstable condition even with the total addition of 125 Mvar of SVCs at Buses 95, 110 and 119. To avoid reaching the collapse point, a fourth placement of SVC at the most participating bus in the mode of instability is used. As shown in Figure 6.22, at 390 MW of combined wind injection and with the SVCs at Buses 95, 110 and 119, the most participating bus in modes of instability was bus 97. Installing a 25 Mvar of SVCs at Bus 97 was sufficient to avoid voltage collapse when the combined wind injection level reached 410 MW.

Figure 6.22 Normalized Participation Factors for Combined Strong Bus Wind Injection of 390 MW



Comparing the two options for placing SVCs to reach the 410 MW of total wind injection, Option II required 75 Mvar less than Option I. The amount of SVCs required to reach the 410 MW of wind penetration using both options are compared in Figure 6.23. The comparison indicates that placing SVCs at buses with the highest contribution to modes of instability regardless of whether if they are wind injection buses or not will result in a reduced amount of SVCs (75 Mvar less) for achieving the desired maximum wind injection level.

Figure 6.23 Comparison of the Amount of the Reactive Power Installed (SVCs) Using the Two SVC Placement Options for Reaching 410 MW of Total Wind Injection Using DFIG Wind Type Turbines



6.4.3 Increasing Wind Penetration Using SVC Placement for the 3-Strong Bus Combination Using DDSG Wind Type Turbines

Option I & II were applied to the western Kansas power system using the 3-strong bus combination equipped with DDSG wind type turbines. Modal analysis was used to determine the number and location of SVCs needed to be added to the power system to allow for 410 MW of wind injection from the 3-strong bus combination.

Option I was used to determine location and size of SVCs needed to allow for 410 MW of wind injection. Table 6.15 shows that a total of 150 Mvar of SVCs were sufficient to allow for a wind penetration level of 410 MW. One 75 Mvar SVC at Bus 105 and at Bus 110 was necessary to allow for a 410 MW of wind penetration.

Option II was used to determine location and size of SVCs needed. Table 6.16 shows that a total of 100 Mvar of SVCs were needed to allow for a wind penetration level of 410 MW. To reach this level, two SVCs were necessary. A 75 Mvar SVC was needed at Bus 95 and a 25 Mvar was needed at Bus 8. The amount of SVCs required to reach the 410 MW of wind

penetration using both options are compared in Figure 6.24. The comparison indicates that placing SVCs at buses with the highest contribution to modes of instability regardless of whether if they are wind injection buses or not will result in a reduced amount of SVCs (50 Mvar less) for achieving the desired maximum wind injection level.

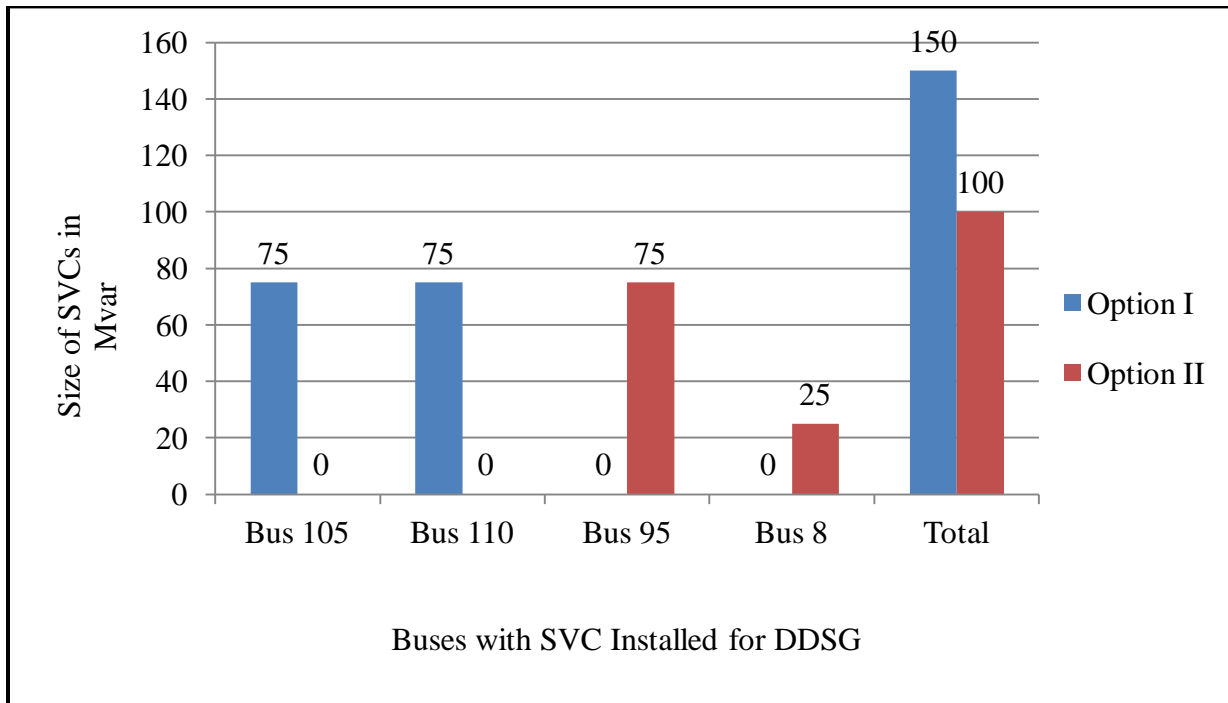
Table 6.15 Placement of SVCs to Increase Wind Penetration from Strong Buses Using DDSG Wind Turbine Type Using Option I

Iteration	Total Wind Injection	Eigenvalue	Highest Participation Factors	Installed SVC in Mvar			
Number	MW	λ	Bus Number	Bus 105	Bus 110	Bus 119	Total SVC
Starting Point	350	0.1707	110	0	0	0	0
1	380	Unstable		0	0	0	0
2	380	Unstable		0	25	0	25
3	380	Unstable		0	50	0	50
4	380	Unstable		0	75	0	75
5	380	0.1683	105	25	75	0	100
1	410	Unstable		25	75	0	100
2	410	Unstable		50	75	0	125
3	410	0.1705	119	75	75	0	150

Table 6.16 Placement of SVCs to Increase Wind Penetration from Strong Buses Using DDSG Wind Turbine Type Using Option II

Iteration Number	Total Wind Injection	Eigenvalues	Highest Participation Factors	Size of Installed SVCs in Mvar During Each Iteration Bus Number		Total SVCs in Mvar
	MW	λ	Bus Number	8	95	0
Starting Point	350	0.1707	95	0	0	0
0	380	0.0000		0	0	0
1	380	0.0000		0	25	25
2	380	0.0000		0	50	50
3	380	0.1706	8	0	75	75
0	410	0.0000		0	75	75
1	410	0.1760	119	25	75	100

Figure 6.24 Comparison of the Amount of the Reactive Power Installed (SVCs) Using the Two SVC Placement Options for Reaching 410 MW of Total Wind Injection Using DDSG Wind Type Turbines

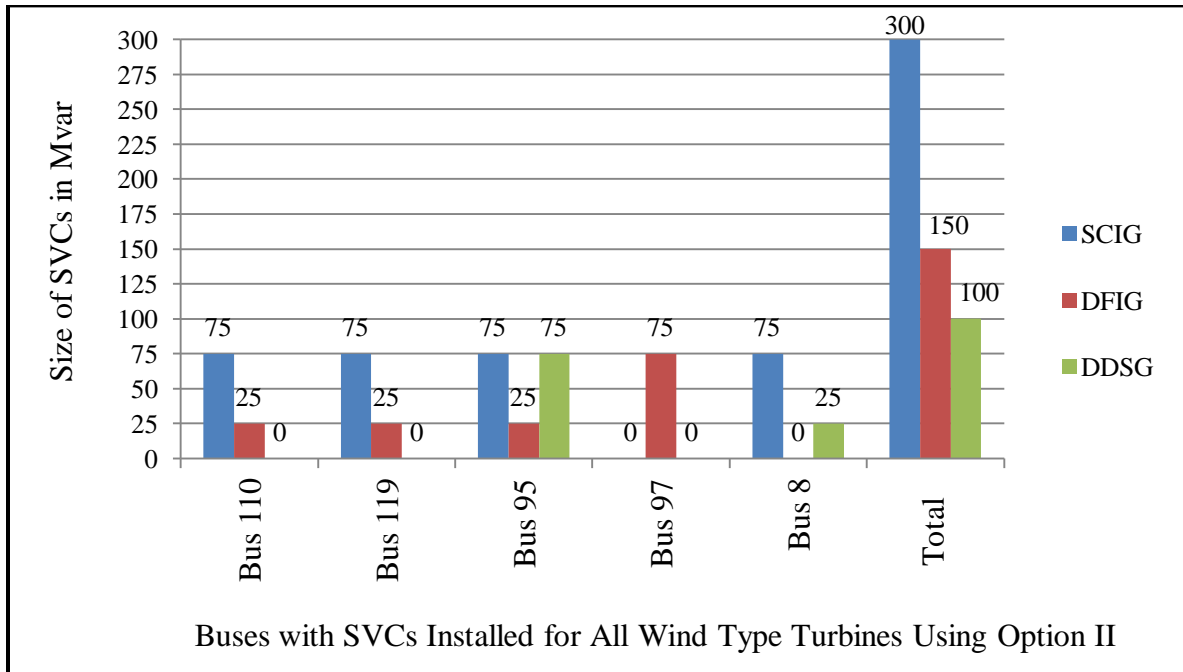


6.5 Comparison of the Amount of SVCs Required for Reaching 410 MW of Wind Power Injection Using Different Wind Turbine Types for the 3-Strong Bus Combination Using Option II

Installing SVCs at buses in the system with high contribution to modes of instability increased wind penetration regardless of the type of wind turbine used. To reach the desired wind power penetration of 410 MW from the combined strong buses, SVCs were necessary in all of the cases for the three-wind turbine types considered. However, the number and the total size of SVCs required varied significantly depending on the type of wind turbine used. Using Option II to place SVCs (which resulted in the lowest amount required to reach the 410 MW of wind injection), the SCIG wind type turbines, required 300 Mvar. The DFIG and the DDSG required significantly less SVCs to reach the 410 MW due to their ability to provide reactive power to themselves and to the power system. Only a 150 Mvar of SVCs was required for the DFIG type, and a 100 Mvar was sufficient for the DDSG type.

As far as the locations of the SVCs, Bus 95 was identified as a bus for installing SVCs for all types since Bus 95 had the highest participation in modes of instability regardless of the type of turbine used. Buses 110 and 119 were identified for SVC installations when wind is injected from SCIG and DFIG types. Bus 97 was identified for SVC installation only when wind is injected from DFIG type and Bus 8 was identified when wind was injected using SCIG and DDSG types.

Figure 6.25 Comparison of the Required Number and Size of SVCs for Each Type of Wind Turbine Using Option II for Reaching a Total Combined Bus Wind Injection of 410 MW



6.6 Load Model Sensitivity Impact on Maximum Wind Penetration for the 3-Weak & the 3-Strong Bus Wind Combinations

Load types can impact the amount of wind penetration in power systems. Constant power (P) load types can negatively impact the maximum amount of wind penetration allowed before reaching the collapse point. All wind penetration levels calculated in this chapter were based on known western Kansas load mix which consist of 30% of constant power (P), 27.5% of constant current (I), and 42.5% of constant impedance (Z) as shown in Table 2.12. Due to load mix uncertainties, a load sensitivity analysis is presented her to determine a suitable wind penetration voltage stability buffer. Detailed derivation of the calculation of voltage stability buffer are derived in Chapter 3 of this dissertation.

Voltage stability buffer is calculated for the 3-Strong bus combination and the 3-weak bus combination to provide for a comparison in the buffer amount needed when wind is injected from weak versus strong buses.

Following is an example of the buffer calculation for the 3-Strong bus combination using DFIG type turbines. The 3-Strong bus combination consists of Bus 105, Bus 110, and Bus 119 in

the western Kansas power system. In previous section, the DFIG type wind turbines used in the 3-strong bus combination resulted in a maximum size of 321 MW limited by voltage stability boundaries as shown in Table 6.10. This maximum size was based on the exact ZIP load mix (actual load mix) calculated in Chapter 3. Table 6.17 shows the impact on the maximum size allowed when the power system load-type mix changes to a 100% constant power (P) versus the exact ZIP load mix. The highest reduction (variance) in the maximum size of the 3-Strong bus combination of 28 MW occurred when the system power factor drops to 0.92 lagging. Regardless of the load power factor, the impact of increasing the constant power (P) component in the ZIP load mix is a reduction in the maximum allowed size for system to stay voltage stable.

Table 6.17 Maximum Size for the 3-Strong Bus Based on Load-Type for DFIG - Constant Power (P) Versus Exact (ZIP) Load Mix

“3-Strong Bus Combination Total Size Variance Based on the Stability Boundary Limits Calculated Using the P-Q Curve Method for the Western Kansas Power System for Different Load Types”				
Load Power Factor	Constant P	Exact (ZIP)	Max Size Variance in MW	Maximum VSM Buffer Wind Injection Buffer as a % of Exact (ZIP) Size
	Total Size in MW	Total Size in MW		
1.00	308	333	25	7.51%
0.97	298	321	23	7.17%
0.95	290	315	25	7.94%
0.92	282	310	28	9.03%
0.90	281	305	24	7.87%
0.85	279	300	21	7.00%

Since the increase of the constant power (P) component of the ZIP load mix has the most negative impact on system stability boundary limits, the stability buffer is obtained by increasing the constant power (P) component in the ZIP model. The sensitivity index “ S_i ” shown in Equation 2.16 can be used to determine at what load power factor the buffer should be calculated. The “ S_i ” indexes for all possible load power factors are calculated and summarized in Table 6.18. The highest index value of 94.12% calculated is when the system load power factor

was set at 0.97 lagging. i.e. the system is most sensitive to load type changes when the load power factor is at 0.97 lagging.

Table 6.18 Sensitivity Index “ S_i ” for Different Load Power Factors for the 3-Strong Bus Combination with DFIG at the Maximum Wind Sizes of the Constant P Model

Load Power Factor	Maximum Wind Injection Based on 100% Constant P MW	Constant P	Exact (ZIP)	Constant Z	“ S_i ” Index Calculation	
		Stability Limit in MVA	Stability Limit in MVA	Stability Limit in MVA	Stability Limit Variance in MVA (Constant Z limit - Constant P limit)	“ S_i ” Index [VSM Cont. Z – VSM Const P] / [VSM Const Z]
1.00	308	2.12	19.23	22.33	20.21	90.51%
0.97	298	1.27	17.55	21.61	20.34	94.12%
0.95	290	1.54	14.73	17.24	15.70	91.07%
0.92	282	1.88	10.47	12.41	10.53	84.85%
0.90	281	2.03	6.88	8.19	6.16	75.21%
0.85	279	0.47	4.17	4.88	4.41	90.37%

To create a stability buffer, the constant power (P) component for the 0.97 power factor case is used as the basis for load mix sensitivity buffer determination analysis. The results shown in Table 6.19 are based on varying the constant power (P) load percentage in the total load mix ZIP model while calculating voltage stability boundary changes from the original mixed-load type percentages. From the list of the buffers calculated when the constant power (P) component doubled to 60% (from 30% to 60%), the stability buffer was only at 3.12 % of the stability limit obtained when using the exact ZIP load model. For all other system load power factor cases, the stability buffer should be set at 3.12% of the limits calculated using the exact ZIP load model since the 0.97 load power factor case resulted in the most stability boundary sensitive case for load type changes. The 3-Strong bus combination the maximum size should be limited to 311 MW instead of 321 MW if a buffer of 3.12% is to be used.

Table 6.19 Load-Type Voltage Stability Buffer for the 3-Strong Bus Combination with DFIG

	Constant P	Constant I	Constant Z		Maximum Wind Injection Before Reaching the Collapse Point “Maximum Wind Injection as a Percent of the Maximum Wind Injection Found Using the Exact ZIP 0 Load Mix”
Buffer Case	Components of ZIP Load Mix			Maximum Wind Penetration Level in MW	
ZIP 0	30.004	25.747	44.249	321	0.00%
ZIP 1	40.000	22.070	37.930	317	1.25%
ZIP 2	50.000	18.392	31.608	315	1.87%
ZIP 3	60.000	14.713	25.287	311	3.12%
ZIP 4	70.000	11.035	18.965	305	4.98%
ZIP 5	80.000	7.357	12.643	303	5.61%
ZIP 6	90.000	3.678	6.322	299	6.85%
ZIP 7	100.000	0.000	0.000	298	7.17%

Similar calculations have been completed for the 3-Weak bus combination using the three types of wind turbine. Results are summarized in Table 6.20 and Table 6.21. For both of the 3-Bus combinations, using SCIG type turbines resulted in the largest voltage stability buffer percent. Whereas, the DDSG type turbines resulted in the lowest voltage stability buffer percent. Regardless of the type of turbine used, the 3-Strong bus combination case was less sensitive to increasing the constant power (P) component in the load mix. For a constant power (P) component of 60% in the ZIP load mix, the buffer percent was approximately half of that of the 3-Weak bus combination.

Table 6.20 Load-Type Voltage Stability Buffer for the 3-Weak Bus Combination for Different Type of Turbines

3-Weak Bus Combination - Bus 95, Bus 115, and Bus 123					
Wind Type Turbines	Exact ZIP Load Mix Max 3-Weak Bus Combination Size MW	All (100%) Constant (P) Max 3-Weak Bus Combination Size MW	Double (60%) Constant (P) Max 3-Weak Bus Combination Size MW	Buffer at 60% Constant (P) Max 3-Weak Bus Size as % of Exact ZIP Max Size	Controlling Load pf S_i Index
SCIG	90	78	84	7.21%	0.95
DFIG	129	117	123	4.52%	0.97
DDSG	150	140	147	2.13%	0.97

Table 6.21 Load-Type Voltage Stability Buffer for the 3-Strong Bus Combination for Different Type of Turbines

3-Strong Bus Combination - Bus 105, Bus 110, and Bus 119					
Wind Type Turbines	Exact ZIP Load Mix Max 3-Strong Bus Combination Size MW	All (100%) Constant (P) Max 3-Strong Bus Combination Size MW	Double (60%) Constant (P) Max 3-Strong Bus Combination Size MW	Buffer at 60% Constant (P) Max 3-Strong Bus Size as % of Exact ZIP Max Size	Controlling Load pf S_i Index
SCIG	180	160	172	4.38%	0.95
DFIG	321	298	311	3.12%	0.97
DDSG	350	333	345	1.30%	0.97

6.7 Conclusions

Wind penetration in weak power systems is closely related to the available voltage stability margins. Current wind farm sizing methods, do not include the impact of new wind generation on system *VSMs*. Installing wind generation in one area may negatively impact *VSMs* in other areas of the power system. Buses with high *VSMs* before wind injection may become

weak buses after injecting wind power in other areas of the system. It was shown in this chapter that if new wind farms are placed at buses with low contribution to modes of instability, system wind penetration could be increased without using additional voltage support equipment. The methods developed in this chapter use modal and Q-V curve voltage stability analysis for the identification of strong and weak wind injection buses. These methods proved to be both theoretically sound and validated with practical application to a real power system. Applying the proposed methods enabled the power system to incorporate a maximum of 321 MW of wind power injection during the peak loading month.

Modal analysis indicates that the impact of increasing wind injections using any of the three wind turbine types on the system eigenvalues is dependent on the contribution of the wind injection bus to modes of voltage instability. The sensitivity of bus voltages to changes in system reactive power is related to the eigenvalues of the system. When system's eigenvalues are relatively large and positive, changes in system reactive power do not significantly impact bus voltages. The power system eigenvalues were very sensitive to increasing wind injections from buses with high contribution to modes of instability. The system eigenvalues decreased rapidly when wind injection increased above a total of 100 MW from the combined weak wind injection buses. When wind power from DFIGs increased from the combined strong wind injection buses, system eigenvalues stayed practically unchanged. However, when the total wind injection exceeded 300 MW, bus voltages decreased rapidly due to lower system eigenvalues.

To further increase wind penetration in weak power systems, dynamic reactive power sources such as Static Var Compensators (SVCs) proved to be very effective if installed at locations with highest contribution to modes of voltage instability. Results of the analysis indicated that placing SVCs at buses with high contribution to modes of instability (weak buses) provided the largest level of wind penetration regardless of the type of wind turbine used. To allow for a 410 MW of wind injection in the western Kansas power system using DFIGs, a total of 150 Mvar of SVCs were required when the SVCs placed at the buses with the highest contribution to modes of instability. A total of 225 Mvar of SVCs were required for a 410 MW of wind injection when placing SVCs only at the wind injection buses.

For both of the 3-Bus combinations, using SCIG type turbines resulted in the largest voltage stability buffer percent. Whereas, the DDSG type turbines resulted in the lowest voltage stability buffer percent. Regardless of the type of turbine used, the 3-Strong bus combination

case was less sensitive to increasing the constant power (P) component of the load mix. For the same type of wind turbine, a constant power (P) component of 60% in the ZIP load mix, the buffer percent was approximately half of that of the 3-Weak bus combination.

Chapter 7 - Increasing Wind Farm Sizes Using Iterative Modal Voltage Stability Method

In the previous chapter, the maximum voltage stable size of the combined 3-bus wind injection calculations were based on simultaneous increase of their outputs until reaching the collapse point. This is similar to Method I developed in Chapter 4 for maximizing wind farm sizes. To further increase wind penetration levels, without using the SVC, a voltage stability sizing method based on modes of voltage instability is developed and tested in the next sections. The wind farm sizing method (Method II), which was developed in Chapter 4, is used in this chapter as the basis to develop a new iterative modal voltage stability method for sizing wind farms based on system eigenvalues and bus participation factor in the modes of instability. The new method is applied to the western Kansas power system (combined Areas I and II), and the results are compared with Method II of Chapter 4 based on voltage stability margins. The application of all of the sizing methods to follow is for the daily hour 17 (4 pm – 5 pm), heaviest loading hour in the summer, in the month of July with peak load of 1,200 MW. Wind is injected from either the 3-Weak Bus or the 3-Strong Bus combinations used in the previous chapter.

7.1 Increasing Wind Penetration Using the Iterative Voltage Stability Margins (*VSM*) Method (Method II) for the Combined Bus Wind Injection Cases

This method calculates maximum wind farm sizes for each new wind farm independently using iterative steps (as derived in Chapter 4) for incrementing each new wind farm size from zero to a maximum value. At each iterative step, each new wind farm power output is incremented by 10 MW while holding all other wind farm sizes at their current sizes. The impact of incrementing each wind farm's size on *VSMs* is compared in each iterative step. For each wind farm size increase, the most severe single contingency is used to calculate *VSMs*. At the end of each iterative step, the size of the incremented wind farm which resulted in the least negative impact on *VSMs*, highest *VSM*, is increased and set as an initial condition for the next iteration. All other wind farm sizes remain constant at their current maximum sizes. Iterative steps are repeated until a new wind farm size increment results in voltage instability. Results of

applying this method to the 3-Weak Bus and the 3-Strong Bus wind injection bus combinations are shown in Tables 7.1 and 7.2 respectively.

Table 7.1 Iterative Steps for Calculating Maximum Wind Injections for the 3-Weak Bus Combination Using the “Q-V” Method (Method II)

Iteration Number	Bus 95	Bus 115	Bus 123	Lowest System <i>VSM</i> in <i>Mvar</i>			Total MW
	Max Wind Farm Sizes in MW			SGIG Wind Turbine	DFIG Wind Turbine	DDSG Wind Turbine	
BASE CASE	0	0	0	10.80	10.80	10.80	No Wind Injection
Iteration 1	10	0	0	10.62	10.98	10.99	
	0	10	0	10.81	11.13	11.13	
	0	0	10	10.81	11.33	11.32	Best
Result 1	0	0	10	10.81	11.33	11.32	10 MW
Iteration 2	10	0	10	10.78	11.35	11.37	Best
	0	10	10	10.23	11.22	11.24	
	0	0	20	10.43	11.31	11.33	
Result 2	10	0	10	10.78	11.35	11.37	20 MW
.....
Result 8	10	40	30	9.37	9.48	10.12	80 MW
Iteration 9	20	40	30	9.01	9.33	9.85	
	10	50	30	9.12	9.10	9.33	
	10	40	40	9.15	9.45	9.91	Best
Result 9	10	40	40	9.15	9.45	9.91	90 MW
Iteration 10	20	40	40	8.65	9.13	9.38	

	10	50	40	8.95	8.99	9.35	Best
	10	40	50	8.90	8.92	9.34	
Result 10	20	40	40	8.95	8.99	9.35	100 MW
Iteration 11	30	40	40	Unstable	7.38	8.39	
	20	50	40	Unstable	7.82	8.53	Best
	20	40	50	Unstable	7.77	8.23	
Result 11	20	50	40	Unstable	7.82	8.53	110 MW
Iteration 12	30	50	40	Unstable	7.53	8.12	
	20	60	40	Unstable	7.48	7.95	
	20	50	50	Unstable	7.62	8.27	Best
Results 12	20	50	50	Unstable	7.62	8.27	120 MW
Iteration 13	30	50	50	Unstable	6.89	8.00	
	20	60	50	Unstable	7.12	7.81	
	20	50	60	Unstable	7.25	8.11	Best
Results 13	20	50	60	Unstable	7.25	8.11	130 MW
Iteration 14	30	50	60	Unstable	7.02	7.83	
	20	60	60	Unstable	7.09	7.89	Best
	20	50	70	Unstable	6.87	7.81	
Results 14	20	60	60	Unstable	7.09	7.89	140 MW
Iteration 15	30	60	60	Unstable	7.0	7.58	Best
	20	70	60	Unstable	6.73	7.19	
	20	60	70	Unstable	6.78	7.28	
Results 15	30	60	60	Unstable	7.0	7.58	150 MW

Iteration 16	40	60	60	Unstable	Unstable	7.24	
	30	70	60	Unstable	Unstable	7.09	
	30	60	70	Unstable	Unstable	7.31	Best
Result 16	30	60	70	Unstable	Unstable	7.31	160 MW
Iteration 17	40	60	70	Unstable	Unstable	Unstable	
	30	70	70	Unstable	Unstable	Unstable	
	30	60	80	Unstable	Unstable	Unstable	
Total Combined 3-Weak Bus Combination				100 MW	150 MW	160 MW	

Table 7.2 Iterative Steps for Calculating Maximum Wind Injections for the 3-Strong Bus Combination Using the “Q-V” Method (Method II)

Iteration Number	Bus105	Bus 110	Bus 119	Lowest System VSM in Mvar			Total MW
	Max Wind Farm Sizes in MW			SGIG Wind Turbine	DFIG Wind Turbine	DDSG Wind Turbine	
BASE CASE	0	0	0	10.80	10.80	10.80	No Wind Injection
Iteration 1	10	0	0	11.19	11.35	11.54	Best
	0	10	0	11.10	11.28	11.52	
	0	0	10	11.09	11.33	11.52	
Result 1	10	0	0	11.19	11.35	11.54	10 MW
Iteration 2	20	0	0	11.21	11.42	11.68	Best
	10	10	0	11.21	11.37	11.55	
	10	0	10	11.20	11.35	11.52	
Result 2	20	0	0	11.21	11.42	11.68	20 MW
.....

Result 16	70	40	50	9.29	9.84	10.83	160 MW
Iteration 17	80	40	50	9.05	9.73	10.22	
	70	50	50	9.11	9.79	10.66	Best
	70	40	60	8.93	9.66	10.17	
Result 17	70	50	50	9.11	9.79	10.66	170 MW
Iteration 18	80	50	50	8.38	8.99	9.75	
	70	60	50	8.18	8.84	9.18	
	70	50	60	8.66	9.22	9.93	Best
Result 18	70	50	60	8.66	9.22	9.93	180 MW
Iteration 19	80	50	60	7.54	7.91	9.25	
	70	60	60	8.49	9.00	9.55	Best
	70	50	70	7.58	7.95	9.37	
Result 19	70	60	60	8.49	9.00	9.55	190 MW
Iteration 20	80	60	60	Unstable	7.62	8.36	Best
	70	70	60	Unstable	7.08	8.08	
	70	60	70	Unstable	7.11	8.27	
Results 20	80	60	60	Unstable	7.62	8.36	200 MW
.....
Iteration 32	120	100	100	Unstable	6.38	6.74	Best
	110	110	100	Unstable	5.17	6.57	
	110	100	110	Unstable	5.20	6.63	
Results 32	120	100	100	Unstable	5.20	6.63	320 MW
Iteration 33	130	100	100	Unstable	5.12	6.42	Best

	120	110	100	Unstable	4.98	6.35	
	120	100	110	Unstable	4.77	6.31	
Results 33	130	100	100	Unstable	5.12	6.42	330 MW
Iteration 34	140	100	100	Unstable	Unstable	6.24	Best
	130	110	100	Unstable	Unstable	6.21	
	130	100	110	Unstable	Unstable	6.21	
Results 34	140	100	100	Unstable	Unstable	6.24	340 MW
Iteration 35	150	100	100	Unstable	Unstable	4.87	
	140	110	100	Unstable	Unstable	4.33	
	140	100	110	Unstable	Unstable	4.89	Best
Results 35	140	100	110	Unstable	Unstable	4.89	350 MW
Iteration 36	150	100	110	Unstable	Unstable	3.83	
	140	110	110	Unstable	Unstable	4.08	
	140	100	120	Unstable	Unstable	4.28	Best
Results 36	140	100	120	Unstable	Unstable	4.28	360 MW
	150	100	120	Unstable	Unstable	Unstable	
	140	110	120	Unstable	Unstable	Unstable	
	140	100	130	Unstable	Unstable	Unstable	
Total Combined 3-Strong Bus Combination					190 MW	330 MW	360 MW

In the case of the 3-Weak Bus combination, Method II resulted in maximum combined weak bus wind injections of 100 MW, 150 MW, and 160 MW for the SCIG, DFIG, and DDSG respectively. While in the case of the 3-Strong Bus combination, Method II resulted in a

maximum combined strong bus wind injection of 190 MW, 330 MW, and 360 MW for the SCIG, DFIG, and DDSG respectively.

7.2 Iterative Method (Method III) for Increasing Wind Penetration Using Modal Analysis of Voltage Instability for the Combined Bus Wind Injection Cases

Some modifications to Method II had to be made to allow for using system eigenvalues, given in Equation 6.12 " λ_i ", and wind injection bus participation factors, given in Equation 6.13 " P_{ji} ", as determining factors for which wind injection bus is set to increase after each step increase in each wind farm sizing iteration. This method (Method III) calculates maximum wind farm size for each new wind farm independently by using iterative steps for incrementing each wind injection bus from zero to a maximum value. Modal analysis is applied after each increment to determine proximity to instability and which buses participate in each mode of instability. At each iterative step and for each wind injection level, each bus power output is incremented by 10 MW while holding all other buses at their current maximum outputs. After every bus increment, system eigenvalues are calculated, as are the associated bus participation factors for all wind injection buses. At the end of each iterative step, the size of the incremented bus, which resulted in the highest system eigenvalue, is used to select the bus with the smallest participation factor. Wind injection from the bus with the smallest participation factor is set to increase its size by 10 MW and is used as an initial condition for the next iteration. All other wind injection bus sizes remain constant at their current maximum sizes for the next iteration. Iterative steps are repeated until all wind injection bus increments result in voltage instability, indicated by a negative value for the smallest system eigenvalue. Results of applying this method to the 3-Weak Bus and the 3-Strong Bus wind injection combinations are shown in Tables 7.3 and 7.4 respectively.

Table 7.3 Iterative Steps for Calculating Maximum Wind Injections for the 3-Weak Bus Combination Using the “Bus Participation Factor” Method (Method III)

Iteration #	Max Wind Farm Sizes in MW			Normalized Participation Factor for Bus 95	Normalized Participation Factor for Bus 115	Normalized Participation Factor for Bus 123	Increase the Bus with the Lowest Participation Factor	System Eigenvalues
	Bus 95	Bus 115	Bus 123	SCIG Type Turbines			Comments	
BASE CASE	0	0	0	1.00	0.52	0.44	No Wind Injection	0.1706
Initial Condition	10	10	10	1.00	0.51	0.42		0.1733
Iteration 1	20	10	10	1.00	0.51	0.42	Increase Bus 95	0.1712
	10	20	10	1.00	0.57	0.42	Increase Bus 115	0.1711
	10	10	20	1.00	0.53	0.51	Increase Bus 123	0.1730
Select the Iteration with the Largest Eigenvalue								
Result 1	10	10	20	1.00	0.53	0.51	Increase Bus 123	0.1730
Iteration 2	10	10	30	1.00	0.48	0.73	Increase Bus 115	0.1725
Iteration 3	10	20	30	0.73	0.210	1.00	Increase Bus 115	0.1719
Iteration 4	10	30	30	0.33	0.77	1.00	Increase Bus 95	0.1702
Iteration 5	20	30	30	1.00	0.57	0.67	Increase Bus 115	0.1651
Iteration 6	20	40	30	0.81	1.00	0.34	Increase Bus 123	0.1513
Iteration 7	20	40	40	0.62	0.23	0.53	Increase Bus 115	0.1431
Iteration 8	20	50	40	Unstable	Unstable	Unstable	END Total = 100 MW	
	Bus 95	Bus 115	Bus 123	DFIG Type Turbines			Comments	
BASE CASE	0	0	0	1.00	0.52	0.44	No Wind Injection	0.1706
Initial Condition	10	10	10	1.00	0.42	0.57		0.1733

Iteration 1	20	10	10	1.00	0.51	0.42	Increase Bus 95	0.1709
	10	20	10	1.00	0.57	0.42	Increase Bus 115	0.1714
	10	10	20	1.00	0.51	0.53	Increase Bus 123	0.1681
Select the Iteration with the Largest Eigenvalue								
Result 1	10	20	10	1.00	0.68	0.42	Increase Bus 123	0.1714
Iteration 2	10	20	20	1.00	0.48	0.73	Increase Bus 115	0.1732
Iteration 3	10	30	20	0.87	1.00	0.63	Increase Bus 123	0.1738
Iteration 4	10	30	30	0.73	1.00	0.55	Increase Bus 123	0.1734
Iteration 5	10	30	40	0.79	1.00	0.77	Increase Bus 123	0.1712
Iteration 6	10	30	50	0.38	0.72	1.00	Increase Bus 95	0.1693
Iteration 7	20	30	50	1.00	0.68	0.60	Increase Bus 123	0.1638
Iteration 8	20	30	60	0.63	0.29	1.00	Increase Bus 115	0.1630
Iteration 9	20	40	60	0.35	1.00	0.62	Increase Bus 95	0.1623
Iteration 10	30	40	60	1.00	0.48	0.52	Increase Bus 115	0.1620
Iteration 11	30	50	60	0.89	0.22	0.47	Increase Bus 115	0.1587
Iteration 12	30	60	60	0.71	0.57	0.62	Increase Bus 115	0.1509
Iteration 13	30	70	60	0.67	0.66	0.31	Increase Bus 123	0.1422
Iteration 14	30	70	70	Unstable	Unstable	Unstable	END Total = 160 MW	
	Bus 95	Bus 115	Bus 123	DDSG Type Turbines			Comments	
BASE CASE	0	0	0	1.00	0.52	0.44	No Wind Injection	0.1706
Initial Condition	10	10	10	1.00	0.32	0.42		
Iteration 1	20	10	10	1.00	0.51	0.42	Increase Bus 95	0.1709

	10	20	10	1.00	0.57	0.42	Increase Bus 115	0.1714
	10	10	20	1.00	0.51	0.53	Increase Bus 123	0.1681
Select the Iteration with the Largest Eigenvalue								
Result 1	10	20	10	1.00	0.38	0.35	Increase Bus 123	0.1714
Iteration 2	10	20	20	1.00	0.48	0.73	Increase Bus 115	0.1733
Iteration 3	10	30	20	1.00	0.67	0.34	Increase Bus 123	0.1740
Iteration 4	10	30	30	1.00	0.63	0.42	Increase Bus 123	0.1738
Iteration 5	10	30	40	1.00	0.58	0.45	Increase Bus 123	0.1700
Iteration 6	10	30	50	1.00	0.47	0.41	Increase Bus 123	0.1699
Iteration 7	10	40	60	0.78	0.21	0.53	Increase Bus 115	0.1676
Iteration 8	10	50	60	0.73	0.32	0.71	Increase Bus 115	0.1667
Iteration 9	10	60	60	0.51	0.28	0.63	Increase Bus 115	0.1624
Iteration 10	10	70	60	0.43	1.00	0.75	Increase Bus 95	0.1629
Iteration 11	20	70	60	0.51	1.00	0.67	Increase Bus 95	0.1591
Iteration 12	30	70	60	0.57	0.48	0.37	Increase Bus 123	0.1519
Iteration 13	30	70	70	0.52	0.38	0.58	Increase Bus 115	0.1453
Iteration 14	30	80	70	Unstable	Unstable	Unstable	END Total = 170 MW	
				SCIG	DFIG	DDSG		
Total Combined 3-Weak Bus Combination				100 MW	160 MW	170 MW		

Table 7.4 Iterative Steps for Calculating Maximum Wind Injections for the 3-Strong Bus Combination Using the “Bus Participation Factor” Method (Method III)

Iteration #	Max Wind Farm Sizes in MW			Normalized Participation Factor for Bus 105	Normalized Participation Factor for Bus 110	Normalized Participation Factor for Bus 119	Increase the Bus with the Lowest Participation Factor	
	Bus 105	Bus 110	Bus 119	SCIG Type Turbines			Comments	
BASE CASE	0	0	0	0.011	0.020	0.013	No Wind Injection	0.1706
Initial Condition	10	10	10	0.016	0.025	0.018		0.1723
Iteration 1	20	10	10	0.016	0.025	0.017	Increase Bus 105	0.1732
	10	20	10	0.016	0.024	0.019	Increase Bus 110	0.1711
	10	10	20	0.016	0.025	0.023	Increase Bus 119	0.1730
Select the Iteration with the Largest Eigenvalue								
Result 1	20	10	10	0.015	0.023	0.016	Increase Bus 105	0.1732
-----	-----	-----	-----	-----	-----	-----	-----	
Iteration 16	80	30	60	0.298	0.290	0.136	Increase Bus 119	0.1628
Iteration 17	80	30	70	0.296	0.203	0.284	Increase Bus 110	0.1602
Iteration 18	80	40	70	0.290	0.216	0.283	Increase Bus 110	0.1535
Iteration 19	80	50	70	0.213	0.438	0.311	Increase Bus 105	0.1453
Iteration 20	90	50	70	Unstable	Unstable	Unstable	END Total = 200 MW	
	Bus 105	Bus 110	Bus 119	DFIG Type Turbines			Comments	
BASE CASE	0	0	0	0.011	0.020	0.013	No Wind Injection	0.1706
Initial Condition	10	10	10	0.014	0.023	0.016		0.1725
Iteration 1	20	10	10	0.015	0.023	0.016	Increase Bus 105	0.1738

	10	20	10	0.014	0.022	0.017	Increase Bus 110	0.1729
	10	10	20	0.014	0.022	0.019	Increase Bus 119	0.1733
Select the Iteration with the Largest Eigenvalue								
Result 1	20	10	10	0.015	0.020	0.013	Increase Bus 105	0.1738
-----	-----	-----	-----	-----	-----	-----	-----	
Iteration 28	130	70	110	0.293	0.285	0.131	Increase Bus 119	0.1627
Iteration 29	130	70	120	0.299	0.214	0.314	Increase Bus 110	0.1533
Iteration 30	130	80	120	0.233	0.462	0.277	Increase Bus 110	0.1422
Iteration 31	130	90	120	Unstable	Unstable	Unstable	END Total = 330MW	
	Bus 105	Bus 110	Bus 119	DDSG Type Turbines			Comments	
BASE CASE	0	0	0	0.011	0.020	0.013	No Wind Injection	0.1706
Initial Condition	10	10	10	0.014	0.023	0.016		0.1727
Iteration 1	20	10	10	0.015	0.023	0.016	Increase Bus 105	0.1739
	10	20	10	0.014	0.022	0.017	Increase Bus 110	0.1729
	10	10	20	0.014	0.022	0.019	Increase Bus 119	0.1735
Select the Iteration with the Largest Eigenvalue								
Result 1	20	10	10	0.017	0.023	0.018	Increase Bus 105	0.1739
-----	-----	-----	-----	-----	-----	-----	-----	
Iteration 31	140	90	110	0.160	0.213	0.331	Increase Bus 105	0.1698
Iteration 32	150	90	110	0.310	0.384	0.244	Increase Bus 119	0.1537
Iteration 33	150	90	120	0.353	0.187	0.284	Increase Bus 110	0.1483
Iteration 34	150	100	120	Unstable	Unstable	Unstable	END Total = 360 MW	

Iteration 35	150	110	120	Unstable	Unstable	Unstable	END Total = 370 MW	
				SCIG	DFIG	DDSG		
Total Combined 3-Strong Bus Combination				200 MW	330 MW	360 MW		

In the case of the 3-Weak Bus combination, Method III resulted in maximum combined wind injections of 100 MW, 160 MW, and 170 MW for the SCIG, DFIG, and DDSG respectively. While in the case of the 3-Strong Bus combination, Method III resulted in maximum combined wind injections of 200 MW, 330 MW, and 360 MW for the SCIG, DFIG, and DDSG respectively.

7.3 Conclusions

Three different wind farm-sizing methods have been investigated for the combined weak and strong wind injection cases in the combined western Kansas power system (Area I and Area II). The first sizing method (Method I), calculates the maximum wind farm size at each wind injection bus by equally increasing wind power output at each bus simultaneously. Method II uses the impact of increasing wind penetration on system's *VSMs* to select which wind injection bus output is increased for each iterative step. The wind injection bus which has the lowest negative impact on *VSMs* is sized larger than the others. Method III uses a similar approach to Method II however, the impact on system's eigenvalues and bus participation factors determines which wind injection bus size is selected to increase. Wind injection buses which have small impact on system eigenvalues and have less participation factor in modes of instability are sized larger than the others. However, when incrementing the bus with lowest participation in modes of instability results in low system eigenvalues, that bus is no longer the bus selected to increment its size in the next step.

To test these methods for increasing wind farm sizes, the 3-Weak Bus and the 3-Strong Bus wind injection bus combinations used in Chapter 6 were used. Applying these sizing methods to these two wind injection combinations resulted in increases to wind penetration when compared to the method used in Chapter 6 (Method I). Table 7.5 and Figures 7.1 and 7.2 shows the maximum wind injections from the 3-Weak Bus and the 3-Strong Bus combinations obtained

using each sizing method. When compared to Method I, Methods II and III resulted in larger amounts of wind injections regardless of the wind turbine type used or the wind injection combination. This is because in Methods II and III, wind injection buses are sized based on their impact on voltage stability whereas in Method I all buses are sized equally regardless of their impact on voltage stability. In Methods II and III, buses with low impact on voltage stability are sized larger than the others.

Method III resulted in slightly higher wind injections than Method II for some wind turbine types. For the 3-Weak Bus combination, Method III exceeded Method II by 10 MW when using DFIG or DDSG wind turbine types. However, the two methods resulted in equal amount of wind injection when using SCIG wind turbine type. For the 3-Strong Bus combination, Method III exceeded Method II by 10 MW only when using SCIG wind turbine type. However, the two methods resulted in equal amount of wind injection when using DFIG or DDSG wind turbine types. Table 7.6 shows the individual machine values for the various cases.

For the 3-Weak Bus combination, the maximum wind penetration obtained using Method I was 12.50% based on the peak load of 1,200 MW using DDSG wind turbine type. Methods II and III resulted in maximum wind penetration of 13.33% and 14.17% respectively using DDSG wind turbine type. For the 3-Strong bus combination, the maximum wind penetration obtained using Method I was 29.17% based on the peak load of 1,200 MW using DDSG wind turbine type. Methods II and III resulted in the same maximum wind penetration of 30.00% using DDSG wind turbine type.

The iterative process used in Methods II and III allowed for higher wind injections than those obtained using Method I. Methods II and III, in which each bus (wind farm) is sized based on its impact on voltage stability, produce higher wind penetration than Method I. However, even though Methods II and III use similar iterative processes for sizing wind farms, Method III is proven a better option when it comes to maximizing wind penetration. Method III uses the modal analysis method (bus participation factors and system eigenvalues) instead of the system *VSMs* for determining wind farm sizes. The modal analysis is more accurate in predicting voltage instability when compared to other static voltage stability methods [84]. At high wind levels, and when the system is stressed, modal analysis is a better measure of voltage instability than any other static method (Q-V curve, P-Q method or P-V curve) because of its ability to predict which bus wind injection increase will affect system eigenvalues.

Results of the *VSMs* obtained using the static voltage stability methods are slightly more conservative than the modal method especially near the collapse point. Power system nonlinearities are not considered when calculating voltage collapse points using the static methods. The power flow models used to calculate *VSMs* in PSS/E, which use the entire Eastern power system, provide the maximum loadability to instability point by stressing the system until reaching the collapse point assuming linear system models (first order). Modal voltage stability analysis used to calculate system eigenvalues using Matlab, which uses a reduced equivalent model, does not provide the maximum loadability to instability point. The reduced power flow models include the detailed western Kansas power system and the Thevenin equivalents of the rest of the eastern power system. Using the reduced power flow model can result in some small error when predicting the collapse point due to not accounting for all possible eigenvalues that may appear in the part of the power system that has been reduced.

Table 7.5 Summary of the Maximum Amount of Wind Injection from the 3-Weak and the 3-Strong Buses Obtained from Each Sizing Method

Sizing Method	Type of Wind Injection Increases	Size Wind Farms Based on Value of	3-Weak Wind Injection Bus Combination			3-Strong Wind Injection Bus Combination		
			SCIG	DFIG	DDSG	SCIG	DFIG	DDSG
Method I	Steps Simultaneous Increments	System Collapse Point	90	129	150	180	321	350
Method II	Iterative Individual Increments	Voltage Stability Margins	100	150	160	190	330	360
Method III	Iterative Individual Increments	Eigenvalues & Bus Participation	100	160	170	200	330	360

Figure 7.1 Combined Wind Power Output for the 3-Weak Bus Combined Using Different Methods

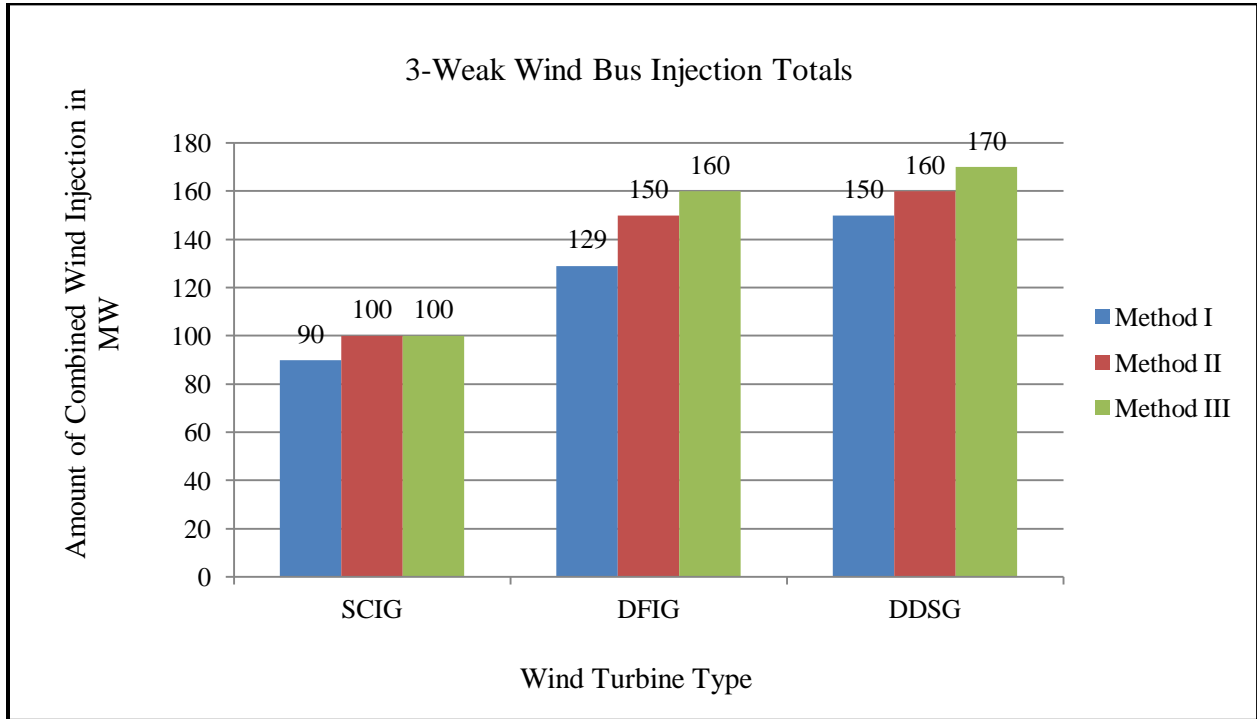


Figure 7.2 Combined Wind Power Output for the 3-Strong Bus Combined Using Different Methods

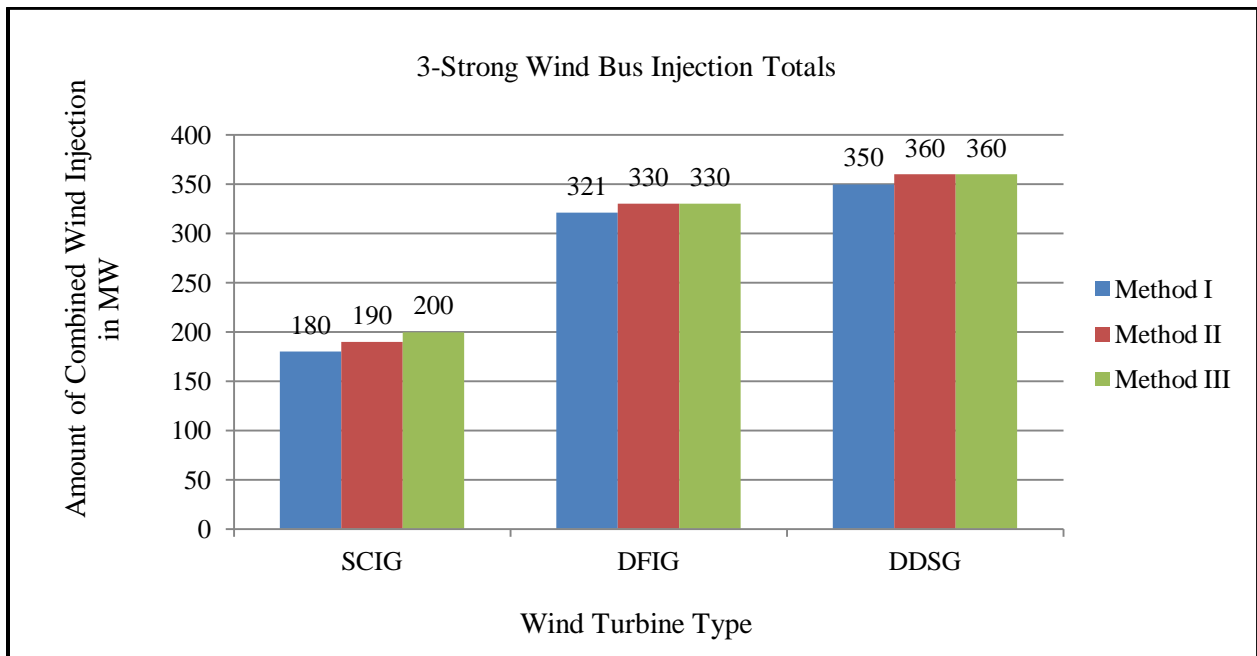


Table 7.6 Summary of the Maximum Amount of Wind Injection from each of the 3-Weak and the 3-Strong Buses Obtained from Each Sizing Method

SCIG	3-Weak Wind Injection Bus Combination in MW				3-Strong Wind Injection Bus Combination in MW			
	Bus 95	Bus 115	Bus 123	Total	Bus 105	Bus 110	Bus 119	Total
Method I	30	30	30	90	60	60	60	180
Method II	20	40	40	100	70	60	60	190
Method III	20	40	40	100	80	50	70	200
DFIG	3-Weak Wind Injection Bus Combination in MW				3-Strong Wind Injection Bus Combination in MW			
	Bus 95	Bus 115	Bus 123	Total	Bus 105	Bus 110	Bus 119	Total
Method I	43	43	43	129	107	107	107	321
Method II	30	60	60	150	130	100	100	330
Method III	30	70	60	160	130	80	120	330
DDSG	3-Weak Wind Injection Bus Combination in MW				3-Strong Wind Injection Bus Combination in MW			
	Bus 95	Bus 115	Bus 123	Total	Bus 105	Bus 110	Bus 119	Total
Method I	50	50	50	150	117	117	117	351
Method II	30	60	70	160	140	100	120	360
Method III	30	70	70	170	150	90	120	360

Chapter 8 - Conclusions and Future Work

Wind power is one of the major components of renewable energy worldwide. Global wind power installations increased by 22.5% between 2009 and 2010 bringing the total installed capacity to 194,400 MW [7]. Wind power installation in the US is expected to become a major portion of the generation mix by the year 2020. The state of Kansas is ranked as one of the most attractive regions for installing big portions of the needed wind energy to achieve a 20% of the total US generation mix from wind resources by 2020.

Steady-state voltage stability analytical methods (P-V, Q-V and P-Q) have been used for calculating voltage stability limits for the western Kansas power system. Both the P-V and Q-V methods are reliable and produced good approximations to voltage instability points. The Q-V curve method is best used when system reactive power is the point of interest. The P-V curve method only considers changes in the real power while the Q-V method only considers changes in reactive power. A better method for calculating voltage stability limits is the P-Q curve method, applied in this work, which considers changes to both real and reactive power when calculating instability points.

Voltage instability in large power systems is influenced by power system load types. Load types considered in this dissertation are constant power (P), constant current (I) and constant impedance (Z) and combinations of these. Regardless of which voltage stability method is used, among the three different load types, the constant power (P) load type resulted in the lowest voltage stability boundary limits. Modeling loads as constant power (P) type is the most conservative approach to calculating stability limits since at lower voltage levels this type of load is a constant load. Other load types are voltage dependant and their magnitudes decrease as load bus voltages decrease. The reduction in power system load magnitudes during low voltage conditions (stressed power system) improves system voltage profiles. Voltage stability boundaries calculated using a composite mix load type must be followed by a sensitivity analysis to consider changes to the load mix. A new voltage stability load type index was introduced to calculate a voltage stability buffer that can be used to create a safety margin for systems to stay stable even when the power system load composition changes.

Three wind turbine types have been investigated for their effect on maximum wind penetration in western Kansas power system. SCIG, DFIG and DDSG are the three most popular

types of wind turbines in the market today. SCIG is a fixed speed turbine, which is the cheapest turbine among the three types. This type of turbine does not have the capability of controlling its power factor and it does absorb reactive power from the grid. The DFIG and DDSG wind turbine types are variable-speed turbines and have reactive power control capabilities using AC-DC-AC converters. These types of convertors have the ability to produce active and reactive power.

Voltage stability issues are a main challenge to further increase wind penetrations especially in weak power systems. Reactive power system limitations can limit wind penetration levels due to lack of reactive power resources. To increase wind penetrations using the existing power system available reactive power resources, several voltage stability methods developed in this dissertation proved to be very effective in increasing wind penetration levels in weak power systems.

Two new voltage stability based iterative methods are developed and implemented to determine the maximum wind penetration level in weak power systems. In each method, wind power for new wind farm sites are increased in increments until reaching the collapse point. To maximize wind farm sizes, wind farm maximum sizes are evaluated based on their impact on voltage stability margins (*VSMs*). Wind farms which result in low negative impact on system *VSMs*, are sized larger than other wind farms. This new approach gives wind farm developers and utility planners a tool to determine the maximum wind farm sizes which are safe, in the voltage stability point view, while maximizing total system wind penetration level. This new approach can be applied to any number of proposed wind farms in any power system.

A new voltage stability based method was presented in this dissertation to assess the impact of increasing wind farm maximum size above the voltage stability size limit. Increasing the wind farm size above this value required curtailment of wind farm power output under certain conditions to prevent voltage collapse. The new method evaluates the voltage stability risk of increasing the wind farm size above the voltage stable limit. It evaluates that risk by incorporating the probabilistic nature of wind into the voltage stability margin calculations. The Expected Voltage Stability Margin (*EVSM*) incorporates wind speed, wind farm probable power outputs and voltage stability margins for each of the wind farm using a voltage stability index, L_i .

It has been demonstrated that increasing the size of a wind farm above the voltage stable size limit can increase wind penetration. However, depending on wind speed patterns and the availability of reactive power, the maximum power output of the wind farm may be limited

(curtailed) to keep the power system from reaching voltage collapse. Results of the analysis also indicated that system *EVSMs* decreased for an increase in wind farm sizes. Wind farms that are sized above the voltage stable size experienced an increase in curtailment hours as the system *EVSMs* became lower.

Modal analysis was effectively used in maximizing wind penetration levels in weak power systems by identifying best locations to inject wind power. When new wind farms are placed at buses with low contribution to modes of instability, system wind penetration can be increased without using additional voltage support equipment.

Two options have been developed for increasing wind penetration levels by placing voltage support equipment like SVCs at specific buses that enable the system to incorporate further increases to wind farm maximum sizes. The location of SVCs was key to increasing wind penetration. Placing SVCs at the weakest buses in the system instead of the wind generation buses provided the most wind penetration.

In Chapter 7, a new wind farm sizing method, based on modal voltage stability analysis, has been developed and compared to the other wind farm sizing methods developed in Chapter 4. This method uses system eigenvalues and the associated bus participation factors to maximize wind injections from buses with low contribution to modes of voltage instability. Results of applying this method to the 3-Weak Bus and the 3-Strong Bus wind injection combinations indicated that this method increases wind penetration when compared to the other methods.

In future work, additional research needs to focus on using real-time voltage stability to determine maximum wind penetration using certain limits for *VSMs* which must be kept under normal or emergency conditions. When the system is stressed, wind farms have to be controlled to maintain voltage stability of the system. When wind speed allows it, wind farms' maximum capacity can be injected into the system, however, a control mechanism must be used during certain conditions such that wind farms which contribute more to voltage instability modes are curtailed to allow for maximization of wind penetration and to prevent the system from reaching the collapse point.

The application of the voltage stability methods described in this dissertation is limited to power systems where wind injections are absorbed (sink) in the area of the power system where wind is injected. Sizing wind farms based on maximizing wind power transfer between two regions could be an interesting research topic. Future research is needed to expand on the

methods developed in this dissertation for maximizing wind penetration in power systems where wind resources are poor and the system depends on other rich wind power areas to supply their need of wind power. Several states in the US that have a need to incorporate high levels of wind energy in their portfolio, rely on other states like Kansas to fulfill their need, since feasible wind resources are not available in these states. Maximizing wind penetration in areas far from wind energy resources requires the development of new methods or reconsideration of assumptions in these methods to determine best system upgrades needed for maximizing wind power transfers from one area of the power system to another.

The voltage stability based methods developed in this research are specific for weak power systems where lack of available reactive power capacity during peak loading conditions resulted in the lowest voltage stability margins. Results of the wind integration analysis in weak power systems like the western Kansas system indicated that the lowest voltage stability margin of the system happens when maximum wind power output occurs simultaneously with maximum peak loading conditions. The voltage stability methods developed in this dissertation can be modified to incorporate additional steps to make them useful for calculating maximum wind farm sizes in strong power systems where lowest voltage stability margins may not happen when maximum wind power outputs occur simultaneously with maximum peak loading conditions.

References

- [1] A. A. Tamimi, A. Pahwa, S. Starrett and N. Williams, “Maximizing Wind Penetration Using Voltage Stability Based Methods for Sizing and Locating New Wind Farms in Power System”, *2010 IEEE/PES General Meeting*, Paper 20105590060, Minneapolis, July 2010.
- [2] A. A. Tamimi, A. Pahwa and S. Starrett, “Method for Assessing System Impact of Increasing Wind Farm Sizes Above Their Maximum Limits”, Accepted for Presentation in the *2011 IEEE/PES General Meeting*, Detroit, July 2011.
- [3] A. A. Tamimi, A. Pahwa and S. Starrett, “Effective Wind Farm Sizing Method in Weak Power Systems Using Critical Modes of Voltage Instability”, Under Review for *IEEE Trans. on Power Systems* August 2011.
- [4] Renewable Energy Policy Network for the 21st Century Report (REN21), *Renewables 2010 Global Status Report*, pp. 15-16. Available at <http://www.ren21.net> as retrieved on April 19, 2011 at 2:15:18 GMT.
- [5] Renewable Energy Policy Network for the 21st Century (REN21). , *Renewables 2008 Global Status Report*, pp. 51. Available at <http://www.ren21.net> as retrieved on April 19, 2011 at 3:22:01 GMT.
- [6] Lars Kroldrup, “Gains in Global Wind Capacity Reported Green Inc.”, February 15, 2010. Available at <http://www.ren21.net> as retrieved on April 19, 2011 at 3:13:20 GMT.
- [7] Renewable Energy Policy Network for the 21st Century (REN21) , *Renewables 2009 Global Status Report*, pp. 9. Available at <http://www.ren21.net> as retrieved on April 21, 2011 at 4:13:20 GMT.
- [8] J. Russell, “Record Growth in Photovoltaic Capacity and Momentum Builds for Concentrating Solar Power *Vital Signs*,” June 03, 2010. http://www.energy.ca.gov/sitingcases/genesis_solar/documents/others/testimony_central_biological_diversity/exhibits/Exh.%20822.%2003-june10_WorldwatchInstitute_PVindustry.pdf as retrieved on April 05, 2011 at 1:21:08 GMT.
- [9] “Renewable Energy Policy Network for the 21st Century (REN21), *Renewables 2009 Global Status Report*, pp. 12. Available at <http://www.ren21.net> as retrieved on April 05, 2011 at 1:33:04 GMT.

- [10] “Renewable Energy Policy Network for the 21st Century (REN21) , *Renewables 2009 Global Status Report*, pp. 15. Available at <http://www.ren21.net> as retrieved on April 03, 2011 at 4:01:44 GMT.
- [11] “World's Largest Photovoltaic Power Plants”. March 4, 2008. Available at <http://www.pvresources.com/en/top50pv.php> as retrieved on April 01, 2011 at 4:23:17 GMT.
- [12] Solar Trough Power Plants. May 15, 2006. Available at http://www.osti.gov/cgi-bin/rd_accomplishments/redirect.cgi.pdf as retrieved on may 14, 2011 at 1=2:01:55 GMT.
- [13] I. Castano, “America and Brazil Intersect on Ethanol,” January 13, 2010. Available at <http://www.renewableenergyworld.com/rea/home> as retrieved on May 12, 2011 at 3:71:13 GMT.
- [14] “World Energy Assessment (2001)”. Renewable Energy Technologies 2001, pp. 221. Available at <http://www.undp.org/energy/activities/wea/drafts-frame.html> as retrieved on April 05, 2011 at 3:41:71 GMT.
- [15] United Nations Environment Program, “Global Trends in Sustainable Energy Investment 2007: Analysis of Trends and Issues in the Financing of Renewable Energy and Energy Efficiency in OECD and Developing Countries,” pp. 3. Available at http://sefi.unep.org/fileadmin/media/sefi/docs/publications/SEFI_Investment_Report_2007.pdf as retrieved on April 05, 2011 at 3:41:71 GMT.
- [16] Clean Edge (2009). “Clean Energy Trends 2009,” pp. 1-4. Available at <http://www.cleandedge.com/reports/pdf/Trends2009.pdf> as retrieved on March 13, 2010 at 4:05:53 GMT
- [17] Renewables Global Status Report 2009 Update. Available at http://www.ren21.net/pdf/RE_GSR_2009_Update.pdf as retrieved on December 15, 2010 at 3:58:13 GMT.
- [18] “Renewable Energy into the Mainstream,” pp. 9. Available at http://en.wikipedia.org/wiki/Renewable_energy#cite_note-chinawind-39 as retrieved on Nov 14, 2010 at 4:32:52 GMT
- [19] Renewable Energy Policy Network for the 21st Century Report (REN21), “*Renewables 2010 Global Status Report*,” pp. 53. Available at <http://www.ren21.net> as retrieved on April 19, 2011 at 2:19:22 GMT.

- [20] Wald, Matthew L. "China's Galloping Wind Market," *The New York Times*. January 2011. Available at <http://green.blogs.nytimes.com/2011/01/11/chinas-galloping-wind-market/> as retrieved on November 10, 2010 at 4:43:28 GMT.
- [21] L. Barroso, H. Rudnick, F. Sensfuss and P. Linares, "The Green Effect," *IEEE Power & Energy for Electric Power Professionals*. Volume 8, Number 5, September/October 2010, pp. 23-27.
- [22] F. Katiraei and J. Aguero, "Integration Challenges", *IEEE Power & Energy for Electric Power Professionals*. Volume 9, Number 3, May/June 2011, pp. 69-70.
- [23] Energy Information Administration. Renewable Potential Map for the State of Kansas. May 2008. Available at http://www.eia.doe.gov/emeu/reps/remap/w_n_c.html
- [24] M.H Haque, "Determination of Steady-State Voltage Stability Limit Using P-Q curve", *IEEE Power Eng. Rev*, April 2002, pp. 71.
- [25] Xi Lua, Michael B. McElroy and J. Kiviluomac, "Global Potential for Wind-Generated Electricity," February 2009. Available at <http://www.pnas.org/content/106/27/10933.full.pdf> as retrieved on November 17, 2009 at 1:13:51 GMT.
- [26] Southwest Power Pool available at <http://www.spp.org/>.
- [27] Southwest Power Pool Large Generation Interconnection Study. June 2010. Available at <http://sppoasis.spp.org/documents/swpp/transmission/GENInterPAGE.cfm>.
- [28] "Eastern Wind Integration and Transmission Study," *National Renewable Energy Laboratory (NREL)*, May 2010. Available at <http://www.nrel.gov/wind/integrationdatasets/eastern/methodology.html>.
- [29] AWS True Power available at <http://www.awstruepower.com>.
- [30] Suzlon S64-1,250 kW and S66-1,250 kW. Available at <http://www.suzlon.com>.
- [31] Kansas Energy Information Network. Available at http://www.kansasenergy.org/wind_resources.htm as retrieved on November 10, 2010 at 4:43:28 GMT
- [32] J. Manwell, J. McGowan, and A. Rogers, *Wind Energy Explained Reference Book*, John Wiley & Sons, 2002.
- [33] Wind Turbine Components. Available at <http://windeis.anl.gov/guide/basics/turbine.html> as retrieved on October 15, 2010 at 1:23:05 GMT.

- [34] J. Slootweg and W. Kling, “*Is The Answer Blowing in The Wind?*,” *Power and Energy Magazine, IEEE* Volume: 1 , Issue: 6, Publication Year: 2003 , pp 26 – 33.
- [35] Saad-Saoud Z., Jenkins N. “Simple Wind Farm Dynamic Model”, *IEEE Proceedings on Generation, Transmission & Distribution*, Vol. 142, No. 5, September 1995, pages 545- 548.
- [36] T. Ackermann, “Wind Power in Power Systems”, John Wiley & Sons, 2005, pp. 337 – 339.
- [37] Danish Wind Industry Association. Guide Tour Available at <http://www.windpower.org> as retrieved on October 5, 2010 at 3:33:17 GMT.
- [38] S. Heier, *Grid Integration of Wind Energy Conversion Systems Reference Book*, John Wiley & Sons, 2005, pp. 421 – 429.
- [39] Hoeijmakers, M. J., “Synchronous Machine with Rectifier for Wind Turbines”, *IEA 21th Meeting of Experts – Electrical Systems for Wind Turbines with Constant and Variable Speed*, Göteborg, Sweden, October 7-8, 1991, p. 51-61.
- [40] Y. A. Kazachkov, J. W. Feltes, R. Zavadil “Modeling Wind farms for Power System Stability Studies”, *2003 IEEE/PES General Meeting*, Paper Print ISBN: 0-7803-7989-6, July 2003.
- [41] Z. Chen, “Characteristics of Induction Generators and Power System Stability”, *ICEMS 2005 Proceedings of the Eighth International Conference on Electrical Machines and Systems*, Vol. 2, June 2006, pp. 91 – 99.
- [42] North East Black-out. Available at http://en.wikipedia.org/wiki/Northeast_Blackout_of_1977 as retrieved on March 10, 2010 at 3:37:19 GMT.
- [43] A. Kurita, T. Sakurai, “The Power System Failure on July 23, 1987 in Tokyo,” *Proc. 27th conf. on Decision and Control*, Austin, Texas, 1988, pp. 2093-2097.
- [44] North East Black-out. Available at http://en.wikipedia.org/wiki/Northeast_Blackout_of_2003 as retrieved on March 10, 2010 at 3:52:34 GMT.
- [45] R. van den Damme, “The Incident of August 4th 1982 of the Belgian Electricity System”, Intercom, September 12, 1983.

- [46] P. Kundur and G. K. Morison, "A Review of Definitions and Classification of Stability Problems in Today's Power Systems," *Presented at IEEE/PES Panel on Stability Terms and Definitions*, New York, February 1997.
- [47] C. W Taylor, "Maybe I can't Define Stability, but I know it when I See it," *Presented at IEEE/PES panel on Stability Terms and Definitions*, New York, February, 1997.
- [48] IEEE Working Group of Voltage Stability, "Suggested Techniques for Voltage Stability Analysis," *IEEE Publication No. 93TH0620-5PWR*, 1993.
- [49] A.Yokoyama and T. Kumano, "Static Voltage Stability Index Using Multiple Load-Flow Solutions," Translated from *Denki Cakkai Ronbunehi*, Vol. IIOB, No. 11, November 1990, pp. 870-879. Available at <http://onlinelibrary.wiley.com/doi/10.1002/ej.4391110308/abstract> as retrieved on May 23, 2011 at 3:51:23 GMT.
- [50] Usaola J. "Transient Stability Studies in Grid with Great Wind Power Generation and Modeling Issues and Operation Requirements," *IEEE Power Engineering Society General Meeting*, Vol. 3, 2003, pp. 1534–41.
- [51] IEEE/PES Power System Stability Subcommittee, "Voltage Stability Assessment: Concepts, Practices and Tools, special publication," Aug. 2003.
- [52] Wang Qi; Zhang Wen-Chao; Tang Yong; Zhao Bing; Qiu Li-Ping; Gao Xun; Shao Guang-Hui; XiongWei-Hong; ShiKe-Qin, "A New Load Survey Method and its Application in Component Based Load Modeling", *Power System Technology (POWERCON)*, 2010 International Conference on 24-28 October 2010.
- [53] K. Morison, H. Hamadani, L. Wang, "Load Modeling for Voltage Stability Studies," *IEEE Power Engineering Society General Meeting 2006*, October 29 – November 1, 2006, pp. 564 – 568.
- [54] W. W. Price, K. A. Wirgau, A. Murdoch, J. V. Mitsche, E. Vaahedi, and M. A. Elkady, "Load Modeling for Power Flow and Transient Stability Computer Studies," *IEEE Transactions on Power Systems*, Vol. 3, No. 1, February 1988, pp. 180 – 187.
- [55] EPRI Project 849-7 Final Report EL-5003, "Load Modeling for Power Flow and Transient Stability Computer Studies", January 1987.
- [56] EPRI Project RP3578-01 Final Report TR-105214, "Assessment of Voltage Stability Methods and Tools," October 1995.

- [57] W. Xu and Y. Mansour, "Voltage stability Analysis Using Generic Dynamic Load Models," *IEEE Transactions on Power Systems*, Vol. 9, No. 1, February 1994, pp. 479 – 493.
- [58] N. Dizdarevic, S. Tesnjak and G. Anderson, "Composite Load Sensitivity in Voltage Stability Problem Solved by Unified Power Flow Controller," *14th Annual Power System Computation Conference*, Sevilla, Session 38, No. 4, June 2002, pp. 24 – 28.
- [59] The Federal Energy Regulatory Corporation's (FERC) available at <http://www.ferc.gov>.
- [60] S.K. Salman, A.L.J. Teo, "Windmill Modeling Consideration and Factors Influencing the Stability of A grid-connected Wind Power Based Embedded Generator", *IEEE Transactions on Power Systems*, Vol. 18, Issue 2, May 2003 Pages: 793-802.
- [61] E. Muljadi and C. Butterfield, "Wind Farm Power System Model Development," National Renewable Energy Laboratory (NREL), *Colorado, Tech. Rep.* Available at http://www.nrel.gov/wind/systemsintegration/pdfs/2004/muljadi_wind_farm_power_system_model.pdf as retrieved on May 27, 2011 at 5:24:15 GMT.
- [62] Akhmatov V, Knudsen H., "An Aggregated Model of a Grid-Connected, Large-Scale, Offshore Wind Farm for Power Stability Investigations," *IEEE Electric Power Energy Systems*, Vol. 24, 2002, pp. 709 – 717.
- [63] Sloomweg JG, Kling WL. "Aggregated Modeling of Wind Parks in Power System Dynamics Simulations," *IEEE Power Tech Conference*, Vol. 3, 2003, pp. 626 – 631.
- [64] Feijoo, A. and Cidras, J., "Corrections to "Modeling of Wind Farms in the Load Flow Analysis", *IEEE Transactions on Power Systems*, Vol. 16, No. 4, Nov. 2001, pp. 955 -955.
- [65] V. Akhmatov, "An Aggregated Model of a Large Wind Farm with Variable-Speed Wind Turbines Equipped with Doubly-Fed Induction Generators," *Journal of the Wind Engineering*, Vol. 28, No. 4, 2004, pp. 479-486.
- [66] G. Coat and M. Al-Dabbagh, "Effect of Steady-State Wind Turbine generator Models on Power Flow Convergence and Voltage Stability", Available at <http://itee.uq.edu.au/~aupec/aupec05/AUPEC2005/Volume1/S113.pdf> as retrieved on December 15, 2010 at 2:21:17 GMT.
- [67] C. Chompoo-inwai and P.Fuangfoo, "System Impact Study for the Interconnection of Wind Generation and Utility System", *IEEE transactions on Industry Applications*, Vol. 41, No.1, February 2005.

- [68] SPP (Southwest Power Pool) the 2010 Wind Integration Study Report. Available at http://www.uwig.org/CRA_SPP_WITF_Wind_Integration_Study_Final_Report.pdf as retrieved on October 13, 2010 at 5:01:43 GMT.
- [69] D. J. Hill, I. A. Hiskens and D. Popovic, "Load Recovery in Voltage Stability Analysis and Control," *International Journal of Electrical Power & Energy Systems*, Vol. 22, Issue 4, May 2000, pp. 291-301.
- [70] C. Concordia and S. Ihara: "Load Representation in Power System Stability Studies," *IEEE Transactions on Power Apparatus and Systems*, Vol. PAS-101, No.4, April 1982.
- [71] J. Falk Christensen, M. Stubbe, A. W. Grainger, J. Verseille and G. Santagostino, "Planning Against Voltage Collapse", Cigré Report SC 38- 01 TF03, 1986, pp. 102 – 108.
- [72] K. Lindén and I. Segerqvist, "Modeling of Load Devices and Studying Load/System Characteristics," Technical Report No. 131L, ISBN 91-7197-038-X, Chalmers University of Technology, Sweden, 1993.
- [73] K. Morison, H. Hamdani, L. Wang, "Practical Issues in Load Modeling for Voltage Stability Studies," *IEEE Power Engineering Society General Meeting*, 13-17 July 2003, Vol. 3.
- [74] T.J.Overbye, "Effects of Load Modeling on Analysis of Power System Voltage Stability," *International Journal of Electrical Power and Energy Systems*, Vol. 16, No.5, 1994, pp. 47 – 52.
- [75] N. Flatabpr, R. Ognedal, and T. Carlsen, "Voltage Stability Condition in a Power Transmission System Calculated by Sensitivity Methods," *IEEE Transactions on Power Systems*, Vol. 5, No. 4, pp. 1286-1293. November 1990.
- [76] H.K. Clark, "New challenge: Voltage stability," *IEEE Power Eng. Rev.*, Vol. 10, 1990, pp. 33.
- [77] M. K. Pal, "Voltage Stability Conditions Considering Load Characteristics", *IEEE Transactions on Power Systems*, Vol. 7, No. 1, 1992, pp. 243-249.
- [78] E. N. Hinrichsen and P. J. Nolan, "Dynamics and Stability of Wind Turbine Generators," *IEEE Transactions on Power App. Syst.*, Vol. PAS-101, No. 8, August 1982, pp. 2640-2648.
- [79] Ledesma P, Usaola J, Rodríguez JL, "Transient stability of a Fixed Speed Wind Farm," *Renewable Energy 2003*; Vol. 28, pp. 1341–55.

- [80] “Transmission Reliability Evaluation of Large-Scale Systems (TRELSS)”, *EPRI Research Project 3833-1*, Final Report, October 1994.
- [81] Southwest Power Pool (SPP) Voltage Stability Criteria available at <http://www.spp.org>.
- [82] PSS/E Program - version 31, Siemens Power Transmission & Distribution, Inc., Power Technologies International (PTI). Available at <http://www.pti-us.com/pti/software/psse.com>.
- [83] T. Alzahawi, M. S. Sachdev and G. Ramakrishna, “A Special Protection Scheme for Voltage Stability Prevention”, *2005 Canada Conference on Electrical and Computer Engineering*, January 2006, pp. 545 – 546.
- [84] P. Kundur: *Power System Stability and Control*, New York: McGraw-Hill, 1994.
- [85] “Matlab” The MathWorks, Inc. available at <http://www.mathworks.com>.
- [86] Sørensen P, Anca H, Janosi L, Bech J, Bak-Jensen B., “Simulation of Interaction between Wind Farm and Power System,” *Risø National Laboratory*, December 2001. Available at <http://www.risoe.dk/rispubl/VEA/ris-r-1281.htm> as retrieved on December 11, 2010 at 3:31:15 GMT.
- [87] Tapia A, Tapia G, Ostolaza JX, Saenz JR, Criado R, Berasategui JL, “Reactive Power Control of a Wind Farm Made up with Doubly Fed Induction Generators (I) and (II),” *IEEE Porto Power Tech Conference*, Vol. 4, August 2001, pp. 1 – 6.
- [88] N. T. Linh, T. T. Chuong, “Voltage Stability Analysis of Grids Connected Wind Generators”, *ICIEA 2009. 4th IEEE Conference*, May 2009, pp. 2657 – 2660.
- [89] Sustainable Development Commission. “Wind power in the UK,” June 2010. Available at <http://www.sd-commission.org.uk> as retrieved on October 6, 2010 at 0:35:27 GMT.
- [90] Stavrakakis GS, Kariniotakis G., “A General Simulation Algorithm for the Accurate Assessment of Isolated Diesel-Wind Turbines Systems Interaction. Part I: A general multimachine power system model,” *IEEE Transactions on Energy Conversion*, Vol. 11, No. 2, April 1995, pp.577–83.
- [91] J. L. Rodriguez-Amenedo, “Automatic Generation Control of a Wind Farm with Variable Speed Wind Turbines,” *IEEE Transactions on Energy Conversion*, Vol. 17, No. 2, June 2002.
- [92] Clipper Wind Power Liberty Series. Available at http://www.bwea.com/pdf/28proceedings/Thurs_Carron_Still.pdf as retrieved on April 15, 2011 at 1:11:12 GMT.

- [93] Chen, H., Zhang, C., and Zhao, X., “Research on the Switched Reluctance Wind Generator System”, *IEEE International Conference on Systems, Man, and Cybernetics*, 2001, vol. 3, Oct. 2001, pp. 1936 -1941.
- [94] Qixue, Z., Xiangheng, W., Xuezhong, Z., and Diji, L., “Small Single-Phase Switched Reluctance Generator for Wind Power Generation”, *ICEMS 2001. Proceedings of the Fifth International Conference on Electrical Machines and Systems*, 2001, vol. 2, 18-20 Aug. 2001, pp. 1003 -1006.
- [95] E. Muljadi, A. Ellis, J. Mechenbier, J. Hochheimer, R. Young, N. Miller, R. Delmerico, R. Zavadil and J. C. Smith, “Equivalencing The Collector System Of A Large Wind Power Plant,” *IEEE Power Engineering Society General Meeting, 2006*. IEEE Digital Object Identifier: 10.1109/PES.2006.1708945, July 2006.
- [96] Feijoo, A.E. and Cidras, J., “Modeling of the Wind Farms in the Load Flow Analysis,” *IEEE Transactions on Power Systems*, Volume: 15, Issue:1 , February 2000, pp. 110 – 114.
- [97] Akhmatov V, Knudsen H, Nielsen AH, Pedersen JK, Poulsen NK, “Modeling and Transient Stability of Large Wind Farms,” *IEEE Electric Power Energy Systems*, Vol. 25, 2003, pp. 123–44.
- [98] Rodriguez JL, Arnalte S, Burgos JC., “Automatic Generation Control of a Wind Farm with Variable Speed Wind Turbines,” *IEEE Transactions on Energy Conversion* Vol. 17, July 2002, pp. 279 – 284.
- [99] Fernandez LM, Saenz JR, Jurado F., “Dynamic Models of Wind Farms with Fixed Speed Wind Turbines,” *Renewable Energy 2006 Conference, Makuhari Messe, Chiba, Japan*, Vol. 31, Section 8, 2006, pp. 1203–30.
- [100] Feijoo, A.E. and Cidras, J., “Modeling of Wind Farms in the Load Flow Analysis”, *IEEE Transactions on Power Systems*, vol. 15, no. 1, Feb. 2000, pp. 110 -115.
- [101] Fuerte-Esquivel, C.R., Tovar-Hernandez, J.H., Gutierrez-Alcaraz, G., Cisneros-Torres, F., Feijoo, A.E., and Cidras, J., “Discussion of Modeling of Wind Farms in the Load Flow Analysis,” *IEEE Transactions on Power Systems*, Vol. 16, No. 4, Nov. 2001, pp. 951 -952.
- [102] Feijoo, A.E. and Cidras, J., “Modeling of Wind Farms in the Load Flow Analysis,” *IEEE Transactions on Power Systems*, Vol. 15, Issue 1, 2000, pp. 110 - 115.

- [103] 2.5 MW Clipper Liberty Synchronous Wind Turbine. Available at http://www.clipperwind.com/pdf/Liberty_Brochure_2010.pdf as retrieved on December 10, 2010 at 4:10:43 GMT.
- [104] IEEE Committee Report, "Voltage Stability of Power Systems: Concepts, analytical tools and industrial experiences," *IEEE Publication* No. 90TH0358-2-PWR, New York, 1990.
- [105] R.K. Gupta, Z.A. Alaywan, R.B. Stuart, and T.A. Reece, "Steady State Voltage Instability Operations Perspective," *IEEE Transactions on Power Systems*, Vol. 5, 1990, pp. 1345.
- [106] C. Taylor, *Power System Voltage Stability*, McGraw-Hill, 1994.
- [107] T.V. Cutsem, Cioastas V., "Voltage Stability of Electric Power System," Massachusetts: Kluwer Academic Publisher, 1998.
- [108] P. Kessel, and H. Glavitch, "Estimating the Voltage Stability of a Power System," *IEEE Transactions on Power Delivery*, Vol. 1, No. 3, July 1986, pp. 346- 354.
- [109] K. Ramalingam and C. S. Indulkar, "Determination of Steady State Voltage Stability Limit Using PQ curves for Voltage Sensitive Loads," *Power System Technology and IEEE Power India Conference*, October 2008, pp. 12 – 15.
- [110] "System Innovations," *General Electric Publication*, Vol. 4, No. 3, December 1990.
- [111] Hau W, James D., Vijay V., "Risk Based Voltage Security Assessment," *IEEE Transactions on Power Systems*, Vol. 15, Issue 4, 2000, pp. 1247 – 1254.
- [112] C. Lemaitre, J.P. Paul, J.M. Tesson, Y. Harmand, and Y.S. Zhao, "An Indicator of the Risk of Voltage Profile Instability for Real-Time Control Applications," *IEEE Transactions on Power Systems*, Vol. 5, No. 1, February 1990, pp. 154-161.
- [113] T. Van Cutsem, "A Method to Compute Reactive Power Margins with Respect to Voltage Collapse," *IEEE Transactions on Power Systems*, Vol. 6, No. 2, February 1991, pp. 145-156.
- [114] F.L. Alvarado, and T.H. Jung, "Direct Detection of Voltage Collapse Conditions," *Proceedings: Bulk Power System Voltage Phenomena – Voltage Stability and Security*, EPRI EL-6183, January 1989, pp. 523- 538.
- [115] G. K. Morison, B. Gao and P. Kundur, "Voltage Stability Analysis Using Static and Dynamic Approaches", *IEEE transactions on Power Systems*, Vol. PS-8, No. 3, August 1993, pp. 121 – 129.

- [116] Cigré Task Force 38-02-10, “Modeling of Voltage collapse Including Dynamic Phenomena”, 1993. Available at https://www.ntnu.no/c/document_library/get_file?uuid=3ed8189e-108a-4b3c-9e4cf59ac3e as retrieved on September 9, 2010 at 2:52:59 GMT.
- [117] P.A. Lof, T. Smed, G. Andersson and D. J. Hill, “Fast Calculation of a Voltage Stability Index,” *IEEE Transactions on Power Systems*, Vol. 7, No. 1, 1992, pp. 54 - 64.
- [118] R. A. Schlueter, K. B. Kilani and U. Ahn, “Impact of Modeling Accuracy on Type, Kind, and Class of Stability Problems in A Power System Model”, *International Journal of Electrical Power & Energy Systems*, Vol. 22, Issue 4, May 2000, pp. 182 -191.
- [119] Y. Harmand, M. Trotignon, J. F. Lesigne, J. M. Tesson, C. Lemaitre and F. Bourgin, “Analysis of a Voltage Collapse-Incident and Proposal for a Time-Based Hierarchical Containment Scheme,” *IEEE Transactions on Power Systems*, Vol. 12, No. 4, November 1997, pp. 1555 – 1560.
- [120] Saad-Saoud, Z. and Jenkins, N., “The Application of Advanced Static VAR Compensators to Wind Farms”, *IEE Colloquium on Power Electronics for Renewable Energy* (Digest No: 1997/170), 16, June 1997, pp. 6/1 -6/5.
- [121] A Tiranuchit and R.J. Thomas, "A Posturing Strategy Against Voltage Instabilities in Electric Power Systems," *IEEE Transactions on Power Systems*, Vol. 3, 1988, pp. 87.
- [122] CIGRE Task Force 38-01-03, “Planning against Voltage Collapse”, *Electra*, No. 111, March 1987, pp. 55-75.
- [123] G. le Dous, J. Daalder and D. Karlsson, “Dynamic Load Measurement in a Transmission System,” *International Power Engineering Conference 1997*, Singapore, 1997, pp. 74-79.
- [124] K. Ramalingam and C. S. Indulkar, “Voltage Collapse Due to Load Variation in Compensated Transmission Lines,” *International Journal of Power and Energy Systems*, Vol. 19, No.3, 1999, pp. 218.
- [125] IEEE Committee Report, “Bibliography on Load Models for Power Flow and Dynamic Performance Simulation,” *IEEE Transactions on Power Systems*, Vol.10, No.4, Feb 1995, pp. 523.
- [126] Hua L., H. Yoshida, H. Chiiang, Y. Fukuyama, Y. Nakanishi, “The Generation of ZIP-V Curves for Tracing Power System Steady State Stationary Behavior Due to Load and

Generation Variations,” *IEEE Power Engineering Society General Meeting*, Winter Meeting 1999.

- [127] “The National Electric Reliability Study, Final Report,” U.S. Dept. of Energy, Washington, DC, DOE/EP-0004, Dist. Category UC-97C, Apr. 1981.
- [128] Electric Reliability Council of Texas (ERCOT) available at <http://www.ercot.com>.
- [129] Cigre Task Force 38-02-08, “Long Term Dynamics Phase II,” Final Report, 1995.
- [130] J. A. Momoh, Y. V. Makarov and M. Elfayoumy, “On Computing the Expected Voltage Stability Margin”, *Proceedings of Large Engineering Systems Conference on Power Engineering* Available at: <http://docs.google.com/viewerciteseerx.ist.psu.edu/> as retrieved on September 23, 2010 at 2:32:21 GMT.
- [131] “Global Wind Energy Markets Continue to Boom”, 2006. Available at http://www.gwec.net/uploads/media/07-02_PR_Global_Statistics_2006.pdf as retrieved on January 16, 2011 at 1:28:53 GMT.

Appendix A – Month of July Maximum Power Output Based on the Maximum Hourly Wind Speed Data Occurred from 2005 – 2007 for the Selected Six Wind Farms in Western Kansas Using SCIG Wind Turbine Type Manufactured by Suzlone “S64-1,250 kW”

Figure A.1 Suzlon S-64 Manufacture Data Sheet

MODEL	S64-1.25 MW
OPERATING DATA	
Rated Power	1,250 kW
Cut-in wind speed	3.5 m/sec (7.8293 mph)
Rated wind speed	14 m/sec (31.3170 mph)
Cut-off wind speed	25 m/sec (55.9230 mph)
Survival wind speed	59.5 m/sec (133.0980 mph)
ROTOR	
Type	3 blades, Upwind / Horizontal axis
Diameter	64 m (209.9740 ft)
Rotational speed at rated power	13.5 to 20.3 rpm
Rotor blade material	Epoxy bonded fiber glass
Swept area	3217 m ²
Power regulation	Active pitch regulated
GEARBOX	
Type	1 Planetary stage / 2 helical stages
Ratio	1 : 74.9
Normal load	1390 kW
Type of cooling	Forced oil cooling lubrication system
GENERATOR	
Type	Dual speed induction generator (asynchronous)
Speed at rated power	1006/1506 rpm 1007/1509 rpm
Rated power	300/1250 kW 250/1250 kW
Rated voltage	690 V AC (phase to phase)
Frequency	60 Hz
Insulation	Class H
Enclosure	IP 56
Cooling system	Air cooled
TOWER	
Type	Lattice tower (hot dip galvanized)
Tower height	54 m / 63 m / 72 m (variable as per requirement)
Hub height (including foundation)	Approximately 56.5 m / 65 m / 74.5 m (variable as per requirement)
BREAKING SYSTEM	
Aerodynamic breaking	3 Independent systems with blade pitching
Mechanical breaking	Hydraulic fail safe disk break system
YAW SYSTEM	
Type	Active electrical yaw motor
Bearing	Polyamide slide bearing with gear ring & automatic greasing system
Protection	Cable twist sensor, proximity sensor
PITCH SYSTEM	
Type	3 Independent blade pitch control with battery backup for each blade
Operating range	-5° to +90°
Resolution	0.1° to 10°

CONTROLLER	Suzlon Control System with following salient features
	Park slave
	Power output control / limitation
	Reactive power control
	Grid measurement
	Low voltage ride through (LVRT)
	Weather measurement
	Time synchronization
	Statistics
Wind Class	II
Certification& Standards	GL (T-GL-003A-2007)
Quality System	ISO 9001:2000

Figure A.2 Suzlon S-64-1,250 kW Manufacture Wind Speed vs. Power Output Characteristic

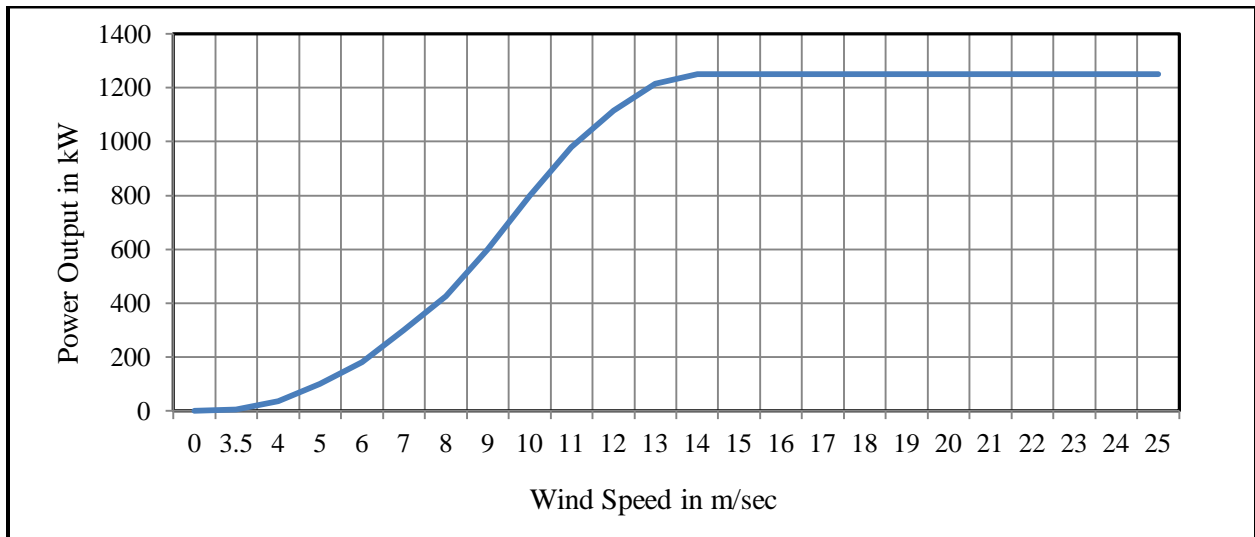


Table A.1 The Maximum Hourly Power Output of Six Wind Farms in Western Kansas Using Suzlon S64 Wind Turbine Type [46]

The Maximum Hourly Power Output of the Six Wind Farms in Western Kansas as a Fraction of Maximum Wind Farm Rated Power Calculated Based on Maximum Wind Speed Data for 2005-2007 using the SCIG Type Manufactured by Suzlon S64 Wind Turbine Type							
Month	Hour	Bus 95	Bus 105	Bus 110	Bus 115	Bus 119	Bus 123
7	0	0.40709172	0.711418779	0.211401859	0.201509637	0.398490698	0.385982539
7	1	0.128238467	0.597952557	0.129948814	0.156355304	0.192563401	0.241011709
7	2	0.011284471	0.419770903	0.177191058	0.101698342	0.220604793	0.186109914
7	3	0.029519407	0.224241604	0.198683798	0.066787977	0.244021768	0.152650911
7	4	0.111640823	0.182992093	0.161887601	0.183582693	0.204680714	0.168956785
7	5	0.310684131	0.146613151	0.094223336	0.295828279	0.442697442	0.258009268
7	6	0.042938778	0.284913262	0.087511752	0.096947028	0.346094043	0.171680973
7	7	0.004574786	0.177339827	0.128068526	0.127746327	0.164227119	0.120391317
7	8	0.003226428	0.055004359	0.128094641	0.336399784	0.067355638	0.11801617
7	9	0.04321166	0.032515559	0.286012744	0.02672193	0.099364645	0.097565308
7	10	0.112154483	0.030952166	0.394286013	0.04346947	0.168824728	0.149937372
7	11	0.140534207	0.023796639	0.461297399	0.101058094	0.279596268	0.201256521
7	12	0.24893255	0.069195153	0.557296563	0.080974525	0.292008471	0.249681453
7	13	0.251388488	0.15406933	0.319492322	0.038515973	0.227105785	0.19811438
7	14	0.256043533	0.210306365	0.3597096	0.047176169	0.251340411	0.224915215
7	15	0.22365084	0.264754517	0.415413141	0.044008626	0.205029221	0.230571269
7	16	0.191916273	0.333183007	0.54288102	0.023756571	0.216570157	0.261661406
7	17	0.194934027	0.378190674	0.642980257	0.013007144	0.207321323	0.287286685
7	18	0.173247937	0.426340158	0.775436122	0.002055533	0.167283256	0.308872601
7	19	0.168962085	0.266272812	0.830539016	0.000101092	0.219921184	0.297159238
7	20	0.252672638	0.567346141	0.79191476	0.029047041	0.402002574	0.408596631
7	21	0.403078751	0.844833288	0.439987465	0.210338321	0.537115972	0.487070759
7	22	0.529712029	0.83325817	0.525880079	0.331951746	0.703903276	0.58494106
7	23	0.671273556	0.886172995	0.668860336	0.489756032	0.839271353	0.711066854
7	0	0.784615879	0.715071706	0.619032696	0.531237364	0.78482387	0.686956303
7	1	0.805435166	0.582664382	0.555285699	0.539863863	0.88253981	0.673157784
7	2	0.802642139	0.613060341	0.453384519	0.662724087	0.923194467	0.691001111
7	3	0.775498411	0.691771143	0.564948292	0.68300984	0.883035762	0.71965269
7	4	0.801117211	0.524157422	0.576752324	0.639439278	0.79105678	0.666504603
7	5	0.736428136	0.549953399	0.379452627	0.457676237	0.825331081	0.589768296
7	6	0.391184308	0.234629145	0.373524496	0.258727591	0.524422283	0.356497565
7	7	0.255064368	0.136360903	0.513971587	0.1798086	0.438890676	0.304819227
7	8	0.543789528	0.157090887	0.484252585	0.357325785	0.430995657	0.394690889
7	9	0.642604899	0.377393945	0.607750966	0.366019679	0.5871401	0.516181918
7	10	0.665848021	0.693710351	0.693748041	0.423776789	0.48116723	0.591650087
7	11	0.661947414	0.705090045	0.734043664	0.536123467	0.438488553	0.615138629
7	12	0.674837073	0.655286973	0.732502873	0.46933549	0.348707844	0.576134051
7	13	0.572153199	0.743483359	0.796067064	0.367131689	0.315090344	0.558785131
7	14	0.432822884	0.64712426	0.690326961	0.249090174	0.267545976	0.457382051
7	15	0.446322514	0.4324885	0.524522093	0.212528643	0.230765106	0.369325371

7	16	0.463160936	0.246294459	0.369084926	0.18830031	0.325840438	0.318536214
7	17	0.623438955	0.220799134	0.319857934	0.233690524	0.460591925	0.371675694
7	18	0.735176089	0.317488951	0.353781469	0.402614908	0.594271085	0.4806665
7	19	0.639410575	0.412089234	0.357594276	0.503336029	0.644817972	0.511449617
7	20	0.773363511	0.420552599	0.663141126	0.658242351	0.755562704	0.654172458
7	21	0.879209605	0.680767265	0.856366865	0.810722469	0.921237467	0.829660734
7	22	0.87779704	0.796578576	0.891961767	0.872927618	0.920124926	0.871877986
7	23	0.924219076	0.841886895	0.913219471	0.916026419	0.91736368	0.902543108
7	0	0.939002857	0.918568293	0.954951426	0.891562205	0.898879417	0.92059284
7	1	0.948714244	0.946559033	0.953802361	0.839297749	0.914414777	0.920557633
7	2	0.956162317	0.919530381	0.959155959	0.814462866	0.906908477	0.911244
7	3	0.910703393	0.951068819	0.959521571	0.863660871	0.915473701	0.920085671
7	4	0.907075669	0.958915847	0.950590202	0.834613829	0.894415849	0.909122279
7	5	0.883029953	0.951083852	0.722474668	0.712865615	0.888370597	0.831564937
7	6	0.81135831	0.935765611	0.289329364	0.438772072	0.888196343	0.67268434
7	7	0.854200777	0.905550044	0.169356524	0.440894999	0.931384376	0.660277344
7	8	0.686651257	0.7454376	0.09618197	0.552938401	0.90708273	0.597658392
7	9	0.507367813	0.471693575	0.023477489	0.778844858	0.898919629	0.536060673
7	10	0.40495682	0.194537146	0.014990076	0.809913735	0.904107018	0.465700959
7	11	0.43142637	0.066850065	0.03170375	0.893516646	0.806458099	0.445990986
7	12	0.258900767	0.028351523	0.057348793	0.810149616	0.721073937	0.375164927
7	13	0.338614402	0.017753525	0.102371252	0.766949724	0.740952228	0.393328226
7	14	0.704838037	0.007335919	0.105766217	0.918958081	0.623357997	0.47205125
7	15	0.569392276	0.028471784	0.124908597	0.953902143	0.408101442	0.416955248
7	16	0.790747697	0.06630889	0.230387548	0.825077504	0.459720658	0.474448459
7	17	0.606969726	0.221430504	0.408492636	0.754144763	0.342930674	0.466793661
7	18	0.68172333	0.566414119	0.479369059	0.573898099	0.451999893	0.5506809
7	19	0.718594497	0.805282463	0.627598454	0.914139372	0.370771004	0.687277158
7	20	0.802915021	0.755584619	0.597278805	0.702689042	0.26155434	0.624004365
7	21	0.880365341	0.785078621	0.691841638	0.640618682	0.505589513	0.700698759
7	22	0.576310636	0.710862572	0.504517915	0.747337916	0.318039247	0.571413657
7	23	0.490417028	0.825817023	0.874856367	0.110088961	0.238123961	0.507860668
7	0	0.10777232	0.795030216	0.705343153	0.047344656	0.471342019	0.425366473
7	1	0.025297762	0.575719311	0.420636164	0.266680146	0.367621039	0.331190884
7	2	0	0.431330988	0.179645879	0.157837984	0.11099941	0.175962852
7	3	0.010626344	0.364646282	0.094484488	0.128588759	0.031191357	0.125907446
7	4	0.027191884	0.19387571	0.049697065	0.255458957	0.01021393	0.107287509
7	5	0.039295001	0.059559244	0.000705108	0.044985847	0	0.02890904
7	6	0.001797811	0.074636962	0.016400292	0.01071573	0	0.020710159
7	7	0.00478346	0.019662668	0.018254466	0.000438064	0	0.008627732
7	8	0.03971235	0.002735937	0.071973258	0	0	0.022884309
7	9	0.011798132	0.00935029	0.129818239	0	0	0.030193332
7	10	0	0.021707104	0.053170375	0.000808734	9.38287E-05	0.015156009
7	11	0.003531414	0.017663329	0.018332811	3.36973E-05	0.029917967	0.013895844
7	12	0.012006806	0.043654731	0.016792019	0.000707643	0.024140797	0.019460399
7	13	0.008668015	0.028201197	0.015303458	0.000505459	0.02574929	0.015685484
7	14	0.008009888	0.077688584	0.035464327	0.007581884	0.013162833	0.028381503
7	15	0.181434396	0.051441628	0.022850726	0.002796873	0.011044984	0.053913721

7	16	0.679909467	0.135924957	0.038937637	0.012333199	0.055251729	0.184471398
7	17	0.655013002	0.185307116	0.098245064	0.095093678	0.090477722	0.224827317
7	18	0.302995281	0.177084273	0.373681187	0.176742149	0.51801512	0.309703602
7	19	0.261838261	0.212335769	0.441998329	0.220919261	0.744799206	0.376378165
7	20	0.537545347	0.264544061	0.412723284	0.054151503	0.76906064	0.407604967
7	21	0.341744518	0.510147019	0.322861172	0.103787572	0.137338481	0.283175752
7	22	0.176153328	0.680436547	0.393528674	0.086264995	0.307275749	0.328731859
7	23	0.280041093	0.611887797	0.375352554	0.10456261	0.262184333	0.326805677
7	0	0.340877717	0.733125883	0.459286535	0.141292627	0.222534985	0.379423549
7	1	0.319913962	0.621628935	0.20139977	0.134047715	0.330719532	0.321541983
7	2	0.339304633	0.456931541	0.156037815	0.261928831	0.308696585	0.304579881
7	3	0.198866737	0.432789152	0.159354434	0.333670306	0.363827677	0.297701661
7	4	0.33373463	0.43157151	0.116186149	0.303544952	0.405407217	0.318088892
7	5	0.093293525	0.296758967	0.291052961	0.338219437	0.303482387	0.264561455
7	6	0.053613278	0.1434563	0.703802361	0.219470279	0.049206477	0.233909739
7	7	0.010770811	0.137232795	0.518332811	0.100148268	0	0.153296937
7	8	0.005329224	0.038588738	0.132351405	0.00185335	0.053549408	0.046334425
7	9	0.021397156	0.144222964	0.017027055	0	0.099833789	0.056496193
7	10	0.035394395	0.120877304	0.068108221	0.001887047	0.17705485	0.080664363
7	11	0.01887701	0.096990469	0.058994046	0.001010918	0.128518578	0.060878204
7	12	0.004879771	0.050254051	0.113548522	0.000235881	0.061484639	0.046080573
7	13	0.003724036	0.09360813	0.262300219	0.011794042	0.139255268	0.102136339
7	14	0.041173071	0.176979045	0.73534942	0.042155277	0.166948153	0.232520993
7	15	0.074898071	0.2735486	0.468583516	0.049602372	0.290480403	0.231422593
7	16	0.149057755	0.411803614	0.337172255	0.067765197	0.705069433	0.334173651
7	17	0.238434621	0.260590481	0.36879766	0.064193288	0.702696906	0.326942591
7	18	0.339063854	0.373891344	0.501149065	0.058700634	0.314648008	0.317490581
7	19	0.412019648	0.756200956	0.462054737	0.031877612	0.253860383	0.383202667
7	20	0.579970465	0.862316226	0.385354643	0.059003909	0.330062731	0.443341595
7	21	0.487126393	0.918463065	0.846208085	0.164341555	0.604350973	0.604098014
7	22	0.436370349	0.896455308	0.891282774	0.460978569	0.75577717	0.688172834
7	23	0.267135382	0.615480593	0.919931056	0.563957407	0.833655032	0.640031894
7	0	0.366063116	0.429271519	0.88237752	0.501819652	0.840987078	0.604103777
7	1	0.552874892	0.57588467	0.612373342	0.476883677	0.861495362	0.615902388
7	2	0.645413978	0.651333393	0.696124517	0.379599677	0.796364806	0.633767274
7	3	0.562650486	0.440320495	0.442050559	0.200936784	0.659495469	0.461090759
7	4	0.420061639	0.348982292	0.214770709	0.37302871	0.460364056	0.363441481
7	5	0.315483643	0.322494814	0.08816463	0.423978973	0.364658731	0.302956158
7	6	0.410944172	0.746565046	0.014911731	0.339061868	0.310881454	0.364472854
7	7	0.198529648	0.79408316	0	0.170777733	0.638571658	0.36039244
7	8	0.56797971	0.757538859	0	0.558970212	0.851951638	0.547288084
7	9	0.603470416	0.744265055	0.00010446	0.476142337	0.683247547	0.501445963
7	10	0.458136698	0.4570969	7.83453E-05	0.469773554	0.45744196	0.368505492
7	11	0.49282481	0.23247948	0.003760577	0.627982208	0.236502064	0.318709828
7	12	0.557369418	0.077508193	0.055076778	0.446050681	0.199560345	0.267113083
7	13	0.405245754	0.035266528	0.11992061	0.400323494	0.199774811	0.232106239
7	14	0.360252336	0.08122125	0.183850413	0.337242216	0.317449467	0.256003136
7	15	0.327169412	0.140885722	0.17306487	0.215965764	0.34148303	0.239713759

7	16	0.270409965	0.232524578	0.215736969	0.125825583	0.330598896	0.235019198
7	17	0.215737263	0.351658098	0.254805181	0.070865346	0.321725377	0.242958253
7	18	0.271469389	0.672815009	0.60863888	0.060992047	0.489303523	0.42064377
7	19	0.243073614	0.738357235	0.703227828	0.03177652	0.643249692	0.471936978
7	20	0.282127837	0.810077869	0.801681813	0.01539965	0.4804166	0.477940754
7	21	0.372034415	0.819653648	0.744985898	0.06699016	0.573226637	0.515378152
7	22	0.401906963	0.813490274	0.691005954	0.158882599	0.507492896	0.514555737
7	23	0.516292658	0.759237545	0.514885616	0.356517051	0.676733151	0.564733204
7	0	0.553388552	0.608174739	0.613104565	0.534910365	0.754074849	0.612730614
7	1	0.565186683	0.314602688	0.550767784	0.423305028	0.81214144	0.533200725
7	2	0.608398343	0.01491236	0.346155855	0.184155547	0.729679374	0.376660296
7	3	0.647934123	0.006133309	0.415491486	0.106483354	0.766607689	0.388529992
7	4	0.475601143	0.45141457	0.426015878	0.061463809	0.628599003	0.40861888
7	5	0.458537995	0.35660383	0.46503186	0.246293301	0.52529355	0.410352107
7	6	0.781244984	0.163103936	0.431917894	0.598800377	0.775910139	0.550195466
7	7	0.826928633	0.030290731	0.292750444	0.539931258	0.749852555	0.487950724
7	8	0.744759061	0.018790776	0.251462446	0.775576223	0.733687202	0.504855142
7	9	0.82442454	0.042572382	0.402198893	0.762366896	0.739357139	0.55418397
7	10	0.771212559	0.022849584	0.306016923	0.73756571	0.662685647	0.500066084
7	11	0.430350894	0.012236553	0.18776768	0.681661949	0.489531392	0.360309694
7	12	0.264262095	0.033853462	0.18317142	0.484465561	0.485228674	0.290196242
7	13	0.205303541	0.090812062	0.195079912	0.329323359	0.497882151	0.263680205
7	14	0.29906257	0.10984336	0.183119189	0.299164308	0.623827141	0.303003314
7	15	0.510016373	0.109196957	0.264728925	0.358134519	0.70917109	0.390249573
7	16	0.546020739	0.076470942	0.267523242	0.325178595	0.634778296	0.369994363
7	17	0.571607435	0.04881092	0.243575682	0.317124949	0.534220685	0.343067934
7	18	0.356608559	0.01864045	0.354173195	0.312272543	0.604216932	0.329182336
7	19	0.319592924	0.127296233	0.442834012	0.23460035	0.709908316	0.366846367
7	20	0.390574336	0.434202219	0.538833177	0.281068877	0.792477615	0.487431245
7	21	0.335484285	0.610895644	0.446568474	0.445208249	0.790560828	0.525743496
7	22	0.523965456	0.740281411	0.609135067	0.515500741	0.887365289	0.655249593
7	23	0.69692446	0.826673882	0.63227306	0.555398302	0.739464372	0.690146815
7	0	0.697117082	0.87237305	0.586937219	0.63805769	0.761795614	0.711256131
7	1	0.660839834	0.780689095	0.767366552	0.501516377	0.837247333	0.709531838
7	2	0.711242737	0.72805989	0.731301577	0.416026419	0.777277358	0.672781596
7	3	0.586583839	0.65527194	0.624908597	0.30566788	0.691973621	0.572881175
7	4	0.588959517	0.529990078	0.574532539	0.280866694	0.602018659	0.515273497
7	5	0.431731356	0.619614564	0.514441659	0.247000944	0.480228942	0.458603493
7	6	0.431731356	0.515874448	0.474093805	0.226378218	0.670781728	0.463771911
7	7	0.505971299	0.407323893	0.485845607	0.256469875	0.562744625	0.44367106
7	8	0.619682815	0.493325516	0.462211428	0.351192883	0.517639805	0.488810489
7	9	0.619843334	0.519196657	0.429619764	0.347755762	0.676264007	0.518535905
7	10	0.572024784	0.485388293	0.439856889	0.426539965	0.73851268	0.532464522
7	11	0.489855212	0.447716545	0.437558759	0.408174956	0.676920809	0.492045256
7	12	0.477382902	0.430263672	0.373498381	0.339499933	0.615302129	0.447189403
7	13	0.530065171	0.350440456	0.360989241	0.347317698	0.595276393	0.436817791
7	14	0.48659668	0.347990139	0.291000731	0.316181426	0.589298161	0.406213427
7	15	0.390076728	0.395613481	0.305076778	0.273655479	0.571631548	0.387210803

7	16	0.351985618	0.541384805	0.38242975	0.191265669	0.530346898	0.399482548
7	17	0.374971909	0.519121494	0.558628434	0.196623534	0.491823495	0.428233773
7	18	0.500738386	0.624560296	0.697482503	0.256537269	0.625060318	0.540875755
7	19	0.577691098	0.753134301	0.799383683	0.372759132	0.671103426	0.634814328
7	20	0.612908922	0.816662157	0.798783036	0.439075347	0.810801029	0.695646098
7	21	0.711916915	0.908331078	0.682126815	0.631756301	0.877151359	0.762256494
7	22	0.789367235	0.910465711	0.818264912	0.815777059	0.841550051	0.835084993
7	23	0.729493724	0.662171913	0.823879662	0.643145977	0.67405233	0.706548721
7	0	0.776333109	0.655858212	0.808706779	0.584546435	0.635783604	0.692245628
7	1	0.811968281	0.697378311	0.799383683	0.71687559	0.641440137	0.733409201
7	2	0.845436451	0.832686931	0.76817612	0.711248147	0.822167712	0.795943072
7	3	0.895582523	0.835482998	0.722109057	0.571337107	0.821510911	0.769204519
7	4	0.871970208	0.854784883	0.699519482	0.592903356	0.862674924	0.776370571
7	5	0.778981669	0.85470972	0.667606811	0.562373635	0.788483191	0.730431005
7	6	0.678175864	0.84002285	0.643084717	0.484802534	0.606120315	0.650441256
7	7	0.67002151	0.687637173	0.76133396	0.425090983	0.389375905	0.586691906
7	8	0.629025009	0.684916268	0.771780006	0.386676102	0.417953461	0.578070169
7	9	0.741596841	0.806259583	0.746004387	0.429977086	0.541726985	0.653112977
7	10	0.745866641	0.921529719	0.754935757	0.488846206	0.643651815	0.710966028
7	11	0.693585669	0.933630979	0.769377416	0.452116188	0.707348131	0.711211677
7	12	0.708433658	0.905144163	0.835605348	0.415925327	0.718728218	0.716767343
7	13	0.780972102	0.903986651	0.888592918	0.50037067	0.759436491	0.766671766
7	14	0.792015795	0.911938907	0.895252272	0.517926944	0.84239451	0.791905686
7	15	0.815820733	0.889044226	0.911887601	0.520285753	0.90182832	0.807773326
7	16	0.787280491	0.89262199	0.940039695	0.428157434	0.915473701	0.792714662
7	17	0.78445536	0.899882746	0.933145305	0.395639574	0.910943113	0.784813219
7	18	0.892307939	0.934908752	0.939726314	0.478063081	0.939064929	0.836814203
7	19	0.805948827	0.918929076	0.916457746	0.538246394	0.964103801	0.828737169
7	20	0.803958394	0.928790475	0.845842474	0.696286562	0.966436116	0.848262804
7	21	0.765225208	0.760650612	0.879974929	0.811531204	0.96644952	0.836766295
7	22	0.897300074	0.658879769	0.911965946	0.761928831	0.951168838	0.836248692
7	23	0.892388199	0.836204564	0.929045231	0.668385227	0.930178007	0.851240246
7	0	0.843959678	0.90288927	0.920792855	0.599272139	0.88883974	0.831150736
7	1	0.808404764	0.931195695	0.902329468	0.538280092	0.856133719	0.807268748
7	2	0.716957206	0.961155708	0.895226157	0.488138563	0.797933087	0.771882144
7	3	0.769655527	0.932323141	0.90274731	0.488239655	0.672256179	0.753044362
7	4	0.755995377	0.939779321	0.923482712	0.477389136	0.767237682	0.772776846
7	5	0.641561527	0.919515348	0.881855218	0.334344251	0.551927511	0.665840771
7	6	0.634980256	0.896876221	0.848741251	0.218459361	0.616682752	0.643147968
7	7	0.548203795	0.860587475	0.841115638	0.141393719	0.529194145	0.584098954
7	8	0.36370349	0.860016235	0.861616003	0.085018197	0.495362179	0.533143221
7	9	0.411008379	0.717837708	0.874020683	0.153389945	0.539501903	0.539151724
7	10	0.564801438	0.255043444	0.912462133	0.262569079	0.607527747	0.520480768
7	11	0.681322033	0.749691831	0.947482503	0.322381723	0.673918289	0.674959276
7	12	0.623968667	0.780042693	0.944165883	0.28534843	0.641306096	0.654966354
7	13	0.664467559	0.754757824	0.938707824	0.2857191	0.64823602	0.658377665
7	14	0.672381136	0.736613451	0.949989554	0.300411107	0.69011045	0.669901139
7	15	0.608398343	0.694281591	0.960252794	0.288617064	0.650876629	0.640485284

7	16	0.557112588	0.756306184	0.937193147	0.254111066	0.629322825	0.626809162
7	17	0.486131176	0.715222032	0.905149901	0.203261895	0.596710632	0.581295127
7	18	0.469790362	0.884158624	0.876188238	0.155883542	0.697415688	0.616687291
7	19	0.458698514	0.934081958	0.901049828	0.1194568	0.603922042	0.603441828
7	20	0.526742432	0.718018099	0.890786587	0.233387249	0.688461745	0.611479222
7	21	0.540643359	0.605228346	0.804998433	0.69224289	0.667913249	0.662205255
7	22	0.580500177	0.67116142	0.727958843	0.721020353	0.763524744	0.692833107
7	23	0.717390606	0.816707255	0.808732895	0.343644696	0.76524047	0.690343184
7	0	0.636729911	0.698400529	0.854747728	0.406085726	0.76906064	0.673004907
7	1	0.528171049	0.748609483	0.76817612	0.536224559	0.679909924	0.652218227
7	2	0.50743202	0.792850486	0.557374909	0.463135193	0.573186424	0.578795806
7	3	0.474220681	0.794413878	0.70706675	0.296535921	0.448461209	0.544139688
7	4	0.566342419	0.781395629	0.509584247	0.23473514	0.453863064	0.5091841
7	5	0.465970015	0.507561408	0.200433511	0.094588219	0.429266527	0.339563936
7	6	0.201210312	0.363969814	0.275749504	0.013579997	0.284596	0.227821126
7	7	0.070082507	0.122200174	0.181186671	0	0.078092327	0.090312336
7	8	0.044592122	0.333964703	0.171863575	0	0.089566243	0.127997329
7	9	0.04987319	0.252097051	0.276402382	0.000404367	0.150635355	0.145882469
7	10	0.024447013	0.145515769	0.180037606	0.000505459	0.146560506	0.099413271
7	11	0.005778677	0.071209525	0.119633344	6.73945E-05	0.145099458	0.06835768
7	12	0.000192623	0.024443041	0.05100282	0	0.108827945	0.036893286
7	13	0.004093229	0.019241755	0.010576622	0.004785011	0.103640555	0.028467435
7	14	0.08163986	0.017513003	0.007547268	0.026789325	0.10244759	0.047187409
7	15	0.024864362	0.016776405	0.022145618	0.004380644	0.076229157	0.028879237
7	16	0.094818453	0.040618141	0.03389742	0.003234937	0.12669562	0.059852914
7	17	0.706587691	0.064805628	0.030868066	0.00566114	0.103077583	0.182200022
7	18	0.256862179	0.179279036	0.206100491	0	0.497077905	0.227863922
7	19	0.073068156	0.387676257	0.249477698	0.04606416	0.349646132	0.221186481
7	20	0.326366818	0.678752894	0.245717121	0.003066451	0.49174307	0.349129271
7	21	0.204420688	0.627431526	0.410033427	3.36973E-05	0.716516541	0.391687176
7	22	0.118238146	0.567691891	0.341115638	0.071101227	0.521754866	0.323980353
7	23	0.061896048	0.680120862	0.237725896	0.123331985	0.493070077	0.319228974
7	0	0.06558798	0.653783711	0.164812493	0.040504111	0.538375958	0.292612851
7	1	0.023018395	0.564459878	0.170792855	0.014860493	0.314339714	0.217494267
7	2	0.000208674	0.684991431	0.111616003	0.005526351	0.287022144	0.217872921
7	3	0.032055604	0.735546135	0.144938891	0.021936919	0.331068039	0.253109117
7	4	0.083341359	0.560070353	0.09842787	0.010378757	0.275869927	0.205617653
7	5	0.120501461	0.27813355	0.033401233	0	0.247399603	0.135887169
7	6	0.115316704	0.120847239	0.0305808	0.008525408	0.180459493	0.091145929
7	7	0.035843847	0.029899883	0.004961872	0.057352743	0.056444695	0.036900608
7	8	0.033243443	0.050464508	0.221064452	0.01563553	0.010924347	0.066266456
7	9	0.149009599	0.082093142	0.178131202	0.046097857	0.064956303	0.104057621
7	10	0.200568237	0.028922762	0.246970647	0.071707777	0.094565975	0.12854708
7	11	0.140694725	0.00435946	0.075786065	0.060183313	0.119403785	0.08008547
7	12	0.079440753	0.007471213	0.010628852	0.021936919	0.098118063	0.04351916
7	13	0.078413432	0.010116954	0.128251332	0.019780294	0.080732937	0.06345899
7	14	0.053950368	0.008132648	0.274365403	0.008323224	0.024395475	0.073833423
7	15	0.170037561	0.012401912	0.012535255	0.108707373	0.015361107	0.063808642

7	16	0.49837876	0.00717056	0.139898673	0.720851867	0.041861026	0.281632177
7	17	0.138816655	0.024578335	0.111328737	0.624679876	0.581738245	0.29622837
7	18	0.095251854	0.645109888	0.134545075	0.84199353	0.360061123	0.415392294
7	19	0.326880478	0.888848802	0.123890108	0.438805769	0.145943917	0.384873815
7	20	0.266477254	0.437704819	0.22861172	0.212124276	0.107554555	0.250494525
7	21	0.117098462	0.424806831	0.322756712	0.267758458	0.111133451	0.248710783
7	22	0.082185624	0.283500195	0.139924788	0.205384823	0.009905635	0.144180213
7	23	0.056952069	0.357295331	0.003107699	0.179909691	0.014664093	0.122385777
7	0	0.017368134	0.278569496	0.026062885	0.251415285	0.103573535	0.135397867
7	1	0.003194324	0.145019693	0.009767053	0.145268904	0.152324272	0.091114849
7	2	0.011926547	0.101154505	0.000182806	0.075144898	0.067141172	0.051109986
7	3	0.004045074	0.006990169	0.001044605	0.070460979	0.022706557	0.021049477
7	4	0.000272882	0.00057124	0	0.043132498	0.00329741	0.009454806
7	5	0.000337089	0.002841165	0.012535255	0.03669632	0.01524047	0.01353006
7	6	0.055844489	0.071480112	0.055520735	0.226176035	0.000670205	0.081938315
7	7	0.082249831	0.073058537	0.078737073	0.170339668	0.000187657	0.080914553
7	8	0.127098783	0.023601215	0.122662697	0.05381453	0.017921291	0.069019703
7	9	0.11340653	0.065527194	0.126788885	0.103113627	0.018805962	0.08552844
7	10	0.089039777	0.105153182	0.086754413	0.1416296	0.018725538	0.088260502
7	11	0.11929757	0.20878807	0.095085135	0.209832862	0.085102675	0.143621262
7	12	0.227968795	0.195814918	0.09051499	0.214752662	0.126856469	0.171181567
7	13	0.264021317	0.123042001	0.059516348	0.185604529	0.140582274	0.154553294
7	14	0.231275482	0.316752353	0.080486786	0.124107023	0.167444105	0.18401315
7	15	0.178866095	0.214139683	0.094876214	0.07487532	0.160165675	0.144584598
7	16	0.126199878	0.227473618	0.060795989	0.170541852	0.130435365	0.14308934
7	17	0.121127484	0.02265416	0.068839444	0.098160129	0.10326524	0.082809292
7	18	0.205769046	0.132662878	0.143241408	0.147459226	0.023845906	0.130595693
7	19	0.191531028	0.21033643	0.22048992	0.062710608	0.017117045	0.140437006
7	20	0.165398568	0.246775503	0.259636478	0.0628117	0.016621093	0.150248668
7	21	0.163777328	0.429587204	0.327535778	0.029653592	0.029609672	0.196032715
7	22	0.184291631	0.203376327	0.430350987	0.086130206	0.03302772	0.187435374
7	23	0.09581367	0.372478278	0.497910791	0.153861706	0.04135167	0.232283223
7	0	0.06080452	0.302411232	0.400658101	0.161342499	0.059956571	0.197034585
7	1	0.053276189	0.228931782	0.333019952	0.159455452	0.057101496	0.166356974
7	2	0.02032168	0.098403536	0.200302935	0.121141663	0.0159911	0.091232183
7	3	0.019438826	0.064384715	0.171863575	0.048928427	0.009101389	0.062743386
7	4	0.009631128	0.073810168	0.177399979	0.020589028	0.017653209	0.059816702
7	5	0	0.054598479	0.137522198	0.005863324	0.053830894	0.050362979
7	6	0.000465505	0.061002375	0.050114907	0.028474188	0.03077583	0.034166561
7	7	0.033339754	0.041745588	0.028648282	0.015804017	0.048281593	0.033563847
7	8	0.090596809	0.021015604	0.085814269	0.022644561	0.08795775	0.061605799
7	9	0.035233876	0.142028201	0.144521049	0.022206497	0.095115543	0.087821033
7	10	0.012616777	0.15464057	0.065888436	0.000640248	0.065251193	0.059807445
7	11	0.017817586	0.067601696	0.030920297	0.002527295	0.035815774	0.03093653
7	12	0.012825452	0.021827365	0.007938995	0.006907939	0.019838078	0.013867566
7	13	0.011942598	0.011214335	0.001671367	0.01860089	0.015428127	0.011771464
7	14	0.036389611	0.039265205	0.007129427	0.024396819	0.043053992	0.030047011
7	15	0.077546631	0.047984126	0.010524392	0.028440491	0.094177256	0.051734579

7	16	0.040418633	0.129415832	0.027525332	0.007615582	0.104377781	0.061870632
7	17	0.031959292	0.206427949	0.051237856	0.005930718	0.124979894	0.084107142
7	18	0.046357829	0.208863233	0.17204638	0.001347891	0.240509892	0.133825045
7	19	0.100356352	0.291317158	0.248171942	0.002055533	0.439802155	0.216340628
7	20	0.144755851	0.279306094	0.418102998	0.001280496	0.341214948	0.236932077
7	21	0.096792834	0.350966598	0.399900763	0.000471762	0.314245885	0.232475568
7	22	0.046438088	0.669567962	0.393398099	0.066181426	0.285065144	0.292130144
7	23	0.01435038	0.574907549	0.470098193	0.133070495	0.252265294	0.288938382
7	0	0	0.285725023	0.302543612	0.244608438	0.320827301	0.230740875
7	1	0.009727439	0.23889841	0.216363731	0.205991374	0.298469251	0.193890041
7	2	0.109843013	0.307071345	0.173926669	0.098059038	0.164964345	0.170772882
7	3	0.145638704	0.243212772	0.167162854	0.062306241	0.067127768	0.137089668
7	4	0.123117917	0.137578545	0.113365716	0.052668823	0.025869927	0.090520186
7	5	0.104064336	0.096870208	0.142666876	0.033360291	0.002788054	0.075949953
7	6	0.056117371	0.132783139	0.165804868	0.003774094	0.008860115	0.073467917
7	7	0.008298822	0.062325246	0.054554476	0	0.004557396	0.025947188
7	8	0	0.048299811	0.020839862	0	0.000616589	0.013951252
7	9	0	0.043053426	0.022380654	0	0.000147445	0.013116305
7	10	0	0.014160729	0.037292385	0	0.001058924	0.010502408
7	11	0	0.004419591	0.046850517	0.004212158	0.010830518	0.013262557
7	12	0.078060291	1.50326E-05	0.008513528	0.006739453	0.00225189	0.019116039
7	13	0.078894989	0.026562641	7.83453E-05	0.009334142	0.018779154	0.026729854
7	14	0.065363254	0.132392291	0.002272015	0.004212158	0.070612836	0.054970511
7	15	0.121288003	0.09992183	0.009453672	0.016410567	0.046766929	0.0587682
7	16	0.005505795	0.106716575	0.013605975	0.010648335	0.041995067	0.035694349
7	17	0.00085075	0.151769339	0.013814896	0.008997169	0.048375422	0.044761515
7	18	0.044945263	0.172845074	0.044970229	0.00037067	0.121012278	0.076828703
7	19	0.060708209	0.219280839	0.082288729	0.000640248	0.165540722	0.105691749
7	20	0.064030948	0.287168155	0.160477384	0.051320933	0.222307115	0.157060907
7	21	0.151112395	0.2805989	0.361642118	0.060722469	0.278510536	0.226517284
7	22	0.193264631	0.340158143	0.594823984	0.060857258	0.272706557	0.292362115
7	23	0.162091881	0.357505788	0.529040008	0.062339938	0.209935124	0.264182548
7	0	0.1558477	0.43713358	0.587668442	0.063216067	0.115302129	0.271833584
7	1	0.166104851	0.720498482	0.538336989	0.0135463	0.094204064	0.306538137
7	2	0.225095509	0.622606055	0.433014729	0.005930718	0.092863653	0.275902133
7	3	0.328020161	0.471648477	0.33709391	0.007548187	0.055493003	0.239960748
7	4	0.317313557	0.28341	0.284733104	0.044143416	0.060318482	0.197983712
7	5	0.227358824	0.242461141	0.205212577	0.061396415	0.046002895	0.15648637
7	6	0.259253909	0.458434804	0.18108221	0.060183313	0.128733044	0.217537456
7	7	0.128190311	0.3509215	0.137417737	0.039493193	0.056216825	0.142447913
7	8	0.07037144	0.322284357	0.154862634	0.019005257	0.049622004	0.123229139
7	9	0.071591383	0.523495986	0.320563042	0.064260682	0.118197416	0.219621702
7	10	0.094818453	0.668079733	0.498642014	0.064429168	0.153758512	0.295945576
7	11	0.09897589	0.60456691	0.583698945	0.082996361	0.195083374	0.313064296
7	12	0.118125783	0.499233336	0.57468923	0.133171586	0.246206638	0.314285315
7	13	0.201916594	0.493971919	0.512430795	0.381587815	0.267934695	0.371568364
7	14	0.308854217	0.435840774	0.593074271	0.371613425	0.230148518	0.387906241
7	15	0.325419757	0.339346382	0.442938473	0.088522712	0.242600933	0.287765651

7	16	0.279912678	0.264303539	0.316854695	0.0628117	0.264342395	0.237645001
7	17	0.295868246	0.397687983	0.333437794	0.053410163	0.376266688	0.291334175
7	18	0.553549071	0.710186104	0.58495247	0.098463405	0.640206959	0.517471602
7	19	0.653423866	0.855521482	0.647472057	0.11551422	0.810546351	0.616495595
7	20	0.706764262	0.891554674	0.727854382	0.323864402	0.884630851	0.706933714
7	21	0.71716588	0.928640149	0.788258644	0.475030328	0.924682323	0.766755465
7	22	0.7907798	0.944138781	0.902146662	0.595498046	0.878853681	0.822283394
7	23	0.802481621	0.938591744	0.938472788	0.641966572	0.887432309	0.841789007
7	0	0.740055861	0.942440095	0.944531495	0.596475266	0.745817919	0.793864127
7	1	0.707021092	0.928685247	0.937428183	0.559138698	0.735161654	0.773486975
7	2	0.865260522	0.927422507	0.906690693	0.465965764	0.874644791	0.807996855
7	3	0.876898135	0.962568774	0.91504753	0.577065642	0.880368345	0.842389685
7	4	0.853189508	0.957788401	0.907526376	0.477355439	0.882459386	0.815663822
7	5	0.77215962	0.929030997	0.856027369	0.529316619	0.873250764	0.791957074
7	6	0.805499374	0.931676739	0.871774783	0.5135463	0.875516058	0.799602651
7	7	0.821214164	0.907203632	0.841141753	0.513748484	0.823561739	0.781373954
7	8	0.771790427	0.749827125	0.751828058	0.502628387	0.837997963	0.722814392
7	9	0.719332884	0.563648116	0.523059647	0.518398706	0.900474505	0.644982772
7	10	0.830219269	0.413231713	0.260576622	0.548490363	0.905688703	0.591641334
7	11	0.920832129	0.48158504	0.19236394	0.556341825	0.888732508	0.607971088
7	12	0.939853607	0.536258681	0.165752638	0.709529586	0.938166854	0.657912273
7	13	0.916594433	0.451279276	0.059176852	0.752560992	0.909843976	0.617891106
7	14	0.88710713	0.452722408	0.027995404	0.771330368	0.81866924	0.59156491
7	15	0.875276895	0.421755209	0.009636478	0.64580806	0.66961557	0.524418442
7	16	0.778660631	0.396470341	0.001044605	0.60985308	0.64709667	0.486625065
7	17	0.789736428	0.499729413	0.013605975	0.579154873	0.808240845	0.538093507
7	18	0.815098398	0.872673702	0.633004283	0.56453026	0.861696424	0.749400613
7	19	0.720905968	0.405775533	0.692860127	0.512569079	0.863224492	0.63906704
7	20	0.757006645	0.809807282	0.480126397	0.487700499	0.889362501	0.684800665
7	21	0.692526245	0.797600794	0.792463178	0.712124276	0.932818616	0.785506621
7	22	0.781325243	0.608159707	0.839574846	0.799096913	0.926947617	0.791020865
7	23	0.790025362	0.143591594	0.751619137	0.767522577	0.765682805	0.643688295
7	0	0.690600019	0.19909203	0.610623629	0.719234398	0.124765428	0.468863101
7	1	0.479726476	0.176482968	0.382246945	0.778170913	0.072140904	0.377753641
7	2	0.298982311	0.217702414	0.44241617	0.671047311	0.099713152	0.345972272
7	3	0.093919548	0.397552689	0.2284028	0.449791077	0.337233928	0.301380008
7	4	0.438489197	0.438982592	0.255196908	0.265972503	0.250576377	0.329843515
7	5	0.603309898	0.435134241	0.229029562	0.121748214	0.164240523	0.310692488
7	6	0.780153456	0.809596825	0.168129113	0.028474188	0.32183261	0.421637238
7	7	0.685800507	0.868239079	0.128120756	3.36973E-05	0.319192	0.400277208
7	8	0.524559376	0.512612369	0.03159929	0.021296671	0.080183368	0.234050215
7	9	0.350557	0.197483539	0.036665622	0.000235881	0.073776205	0.131743649
7	10	0.203794664	0.066323923	0.030763606	0.000606551	0.063307597	0.072959268
7	11	0.094240586	0.018805809	0.013814896	0.000943523	0.042276554	0.034016273
7	12	0.05602106	0.027194011	0.016765904	0.041144359	0.135435097	0.055312086
7	13	0.168480529	0.000165359	0.017758278	0.025946893	0.157551874	0.073980587
7	14	0.115429067	0	0.017340437	0.146751584	0.41811431	0.139527079
7	15	0.057337314	0.023315595	0.011882378	0.276149077	0.274985255	0.128733924

7	16	0.089360814	0.042361925	0.021806121	0.19433212	0.007412471	0.07105469
7	17	0.061783685	0.100944049	0.049958216	0.304387384	0.014181545	0.106250976
7	18	0.116520595	0.280117856	0.132508096	0.529518803	0.032143049	0.21816168
7	19	0.290073518	0.329605243	0.029588426	0.524531608	0.043925259	0.243544811
7	20	0.473402035	0.348531313	0.033688499	0.4975401	0.080143156	0.286661021
7	21	0.320572089	0.340954872	0.331792542	0.516309476	0.125770736	0.327079943
7	22	0.276573887	0.25513364	0.712159198	0.510075482	0.178475685	0.386483578
7	23	0.17480497	0.077282703	0.355975138	0.376398436	0.15887888	0.228668026
7	0	0.182654339	0.162201978	0.319857934	0.37660062	0.353050775	0.278873129
7	1	0.314119233	0.217101109	0.412096521	0.237498315	0.335612032	0.303285442
7	2	0.196812097	0.162758185	0.189543508	0.056341825	0.587582435	0.23860761
7	3	0.204661466	0.167267971	0.127389533	0.119557892	0.620476114	0.247870595
7	4	0.302931073	0.079838249	0.077849159	0.242721391	0.625743928	0.26581676
7	5	0.321374683	0.059694537	0.13227306	0.215325516	0.653342984	0.276402156
7	6	0.341969245	0.393298458	0.202000418	0.366356652	0.570599432	0.374844841
7	7	0.32339722	0.380385436	0.204324663	0.317765197	0.403503834	0.32587527
7	8	0.332883881	0.165268633	0.083072182	0.347216606	0.344498954	0.254588051
7	9	0.311229895	0.281966868	0.049592604	0.414847014	0.354458206	0.282418918
7	10	0.333766734	0.177941132	0.016452523	0.506335086	0.587032867	0.324305668
7	11	0.496629105	0.318932083	0.065522825	0.582356113	0.628143263	0.418316678
7	12	0.638800604	0.69915216	0.30779275	0.689007953	0.384349365	0.543820566
7	13	0.767697197	0.741123237	0.509114175	0.75923305	0.554594928	0.666352518
7	14	0.737391249	0.642343886	0.503394965	0.621815609	0.462267439	0.593442629
7	15	0.774101897	0.411923875	0.310743758	0.522374983	0.396319232	0.483092749
7	16	0.767873768	0.213974324	0.16846861	0.607426877	0.511594553	0.453867626
7	17	0.787232335	0.251736268	0.127702914	0.715089635	0.651841724	0.506720575
7	18	0.804038653	0.377318782	0.321111459	0.73928427	0.838453702	0.616041373
7	19	0.801422197	0.414734975	0.481954455	0.74150829	0.910661627	0.670056309
7	20	0.866335998	0.678001263	0.884936801	0.806173339	0.918127714	0.830715023
7	21	0.909595814	0.88734554	0.923221561	0.890753471	0.902873841	0.902758045
7	22	0.946820123	0.902528487	0.919121488	0.893213371	0.907297196	0.913796133
7	23	0.922806511	0.875890683	0.883735506	0.825279687	0.922993405	0.886141158
7	0	0.875951074	0.857716244	0.921419618	0.800478501	0.860945794	0.863302246
7	1	0.870429227	0.764438832	0.893685365	0.778137215	0.814540775	0.824246283
7	2	0.868246172	0.807807943	0.878486368	0.796232646	0.858425822	0.84183979
7	3	0.892645029	0.826839241	0.78394965	0.694803882	0.819312637	0.803510088
7	4	0.897203763	0.780749226	0.67862739	0.683548996	0.809058496	0.769837574
7	5	0.844970946	0.679399296	0.552178001	0.679572719	0.836121388	0.71844847
7	6	0.891071945	0.368178948	0.518593962	0.773588085	0.831483567	0.676583301
7	7	0.841712415	0.167944439	0.433902643	0.757244912	0.717562061	0.583673294
7	8	0.762095091	0.203406392	0.281233678	0.772543469	0.649241328	0.533703992
7	9	0.638447462	0.087519918	0.130601692	0.682773959	0.541244437	0.416117494
7	10	0.54858904	0.043143622	0.075890525	0.667744979	0.44618251	0.356310135
7	11	0.638270892	0.194356754	0.128982555	0.703160803	0.538000643	0.44055433
7	12	0.668673152	0.30337332	0.256998851	0.745450869	0.595892982	0.514077835
7	13	0.683810074	0.319803975	0.375509245	0.647122254	0.619578039	0.529164717
7	14	0.732928826	0.376131205	0.354852188	0.651772476	0.509208622	0.524978663
7	15	0.777312273	0.494738583	0.327640238	0.619591589	0.432939253	0.530444387

7	16	0.823461427	0.729833739	0.321085344	0.563081278	0.517934695	0.591079297
7	17	0.85917686	0.757689186	0.588112399	0.576560183	0.53684789	0.663677304
7	18	0.887797361	0.672514356	0.761986838	0.546771802	0.662658839	0.706345839
7	19	0.837683393	0.719671688	0.887443853	0.634991239	0.815613104	0.779080655
7	20	0.932036341	0.816977842	0.917685156	0.8509907	0.940552785	0.891648565
7	21	0.884105429	0.897853342	0.910842996	0.867333872	0.956892392	0.903405606
7	22	0.913095123	0.905204293	0.876997806	0.834310554	0.927993137	0.891520183
7	23	0.88266076	0.92319834	0.792698214	0.789156221	0.883075974	0.854157902
7	0	0.75610774	0.920778088	0.752402591	0.750101092	0.802343038	0.79634651
7	1	0.727535394	0.934157121	0.766504753	0.726614099	0.808642968	0.792690867
7	2	0.744373816	0.908481405	0.825211532	0.714516781	0.786043644	0.795725436
7	3	0.673922116	0.798262229	0.799409798	0.62548861	0.786258109	0.736668173
7	4	0.713185014	0.719070383	0.750522302	0.615615312	0.723097957	0.704298194
7	5	0.719702077	0.633519738	0.511490651	0.61194231	0.698085894	0.634948134
7	6	0.692943594	0.45858513	0.425101849	0.498989082	0.671934481	0.549510827
7	7	0.528973643	0.288987102	0.297869007	0.42044076	0.453286687	0.39791144
7	8	0.38018877	0.301930189	0.231092656	0.338623804	0.406278484	0.331622781
7	9	0.400317827	0.246459818	0.128590828	0.291818304	0.410889497	0.295615255
7	10	0.407059617	0.253044106	0.104512692	0.356045289	0.362152163	0.296562773
7	11	0.485810138	0.508974475	0.166509976	0.40578245	0.452884564	0.403992321
7	12	0.591592025	0.561844202	0.353233051	0.376331042	0.558763605	0.488352785
7	13	0.543035089	0.503938547	0.411339183	0.376465831	0.500737226	0.467103175
7	14	0.45678834	0.402859204	0.300245482	0.329761423	0.445847408	0.387100371
7	15	0.399707856	0.456270106	0.311422751	0.359280226	0.469116937	0.399159575
7	16	0.287890462	0.357024744	0.314687141	0.263512603	0.316444158	0.307911822
7	17	0.222463	0.256757163	0.321659877	0.123298288	0.178475685	0.220530803
7	18	0.577546631	0.352920838	0.615716076	0.149851732	0.224103265	0.384027709
7	19	0.712013227	0.481554974	0.850334273	0.351091791	0.453822851	0.569763423
7	20	0.835339818	0.730931121	0.926956022	0.515231163	0.814259289	0.764543483
7	21	0.848694982	0.815955624	0.900109683	0.655108505	0.851871213	0.814348002
7	22	0.711724293	0.800862872	0.887469968	0.589499933	0.853962254	0.768703864
7	23	0.509277986	0.658909834	0.715736969	0.557453835	0.748391507	0.637954026
7	0	0.384298051	0.540753435	0.655332707	0.517657366	0.743619645	0.568332241
7	1	0.414010081	0.34472806	0.756946621	0.407703195	0.579794649	0.500636521
7	2	0.603053068	0.311490935	0.744124099	0.364469605	0.610423034	0.526712148
7	3	0.579986516	0.561498452	0.620260107	0.360897695	0.709533001	0.566435154
7	4	0.61024431	0.562204985	0.459704377	0.394898234	0.76733151	0.558876683
7	5	0.534736268	0.518039145	0.395304502	0.263681089	0.72666345	0.487684891
7	6	0.410237889	0.419229729	0.142562415	0.312104057	0.678355048	0.392497828
7	7	0.275691033	0.223865789	0.043246631	0.232308937	0.409951209	0.23701272
7	8	0.136569392	0.127145907	0.010654967	0.08916296	0.229170018	0.118540649
7	9	0.087659315	0.048390006	0.002036979	0.073999191	0.201986489	0.082814396
7	10	0.073501557	0.055545534	0	0.098901469	0.167497721	0.079089256
7	11	0.104240907	0.15647455	0.000156691	0.186076291	0.157752935	0.120940275
7	12	0.208128672	0.275397613	0.066410739	0.196219167	0.236863975	0.196604033
7	13	0.257135061	0.24647485	0.136085866	0.130239925	0.281218165	0.210230773
7	14	0.308533179	0.239108866	0.185443435	0.089297749	0.226864511	0.209849548
7	15	0.380236926	0.256817294	0.08377729	0.085894325	0.16256501	0.193858169

7	16	0.362547754	0.282132227	0.04972318	0.040537808	0.126521366	0.172292467
7	17	0.419708498	0.41103695	0.056095268	0.027126297	0.273202509	0.237433905
7	18	0.655719285	0.589263702	0.324088582	0.069382666	0.621615463	0.45201394
7	19	0.744261453	0.795706684	0.211924162	0.270757514	0.714412096	0.547412382
7	20	0.770233394	0.869231232	0.5440562	0.371579728	0.80434025	0.671888161
7	21	0.753828373	0.876176303	0.830277865	0.436244777	0.897391561	0.758783776
7	22	0.685463418	0.862361324	0.879609318	0.484566653	0.78061498	0.738523139
7	23	0.638030113	0.891975587	0.870051186	0.453026014	0.6478473	0.70018604
7	0	0.632010658	0.783199543	0.85067377	0.40197466	0.546860758	0.642943878
7	1	0.591351247	0.685968552	0.835814269	0.389169699	0.537196397	0.607900033
7	2	0.531991396	0.574712125	0.723545388	0.45147594	0.66684092	0.589713154
7	3	0.573373142	0.535582213	0.678209548	0.552702521	0.532290494	0.574431583
7	4	0.712526887	0.523766573	0.642013998	0.572011053	0.569929226	0.604049547
7	5	0.604786671	0.541054087	0.696777395	0.538313789	0.644187979	0.605023984
7	6	0.562987576	0.51250714	0.638201191	0.471525812	0.574352582	0.55191486
7	7	0.404619731	0.371937104	0.498903165	0.389843645	0.330317409	0.399124211
7	8	0.332643103	0.346050931	0.408388175	0.285483219	0.320358158	0.338584717
7	9	0.537160101	0.590812062	0.409223859	0.26920744	0.569527103	0.475186113
7	10	0.780394234	0.858347614	0.537919148	0.357494271	0.765441531	0.65991936
7	11	0.790715593	0.913953279	0.788049723	0.462157973	0.809849338	0.752945181
7	12	0.786445793	0.934112023	0.888540687	0.496765063	0.723419656	0.765856644
7	13	0.866335998	0.943898259	0.9037658	0.563081278	0.740590317	0.80353433
7	14	0.845709333	0.91384805	0.894703855	0.580806039	0.804072168	0.807827889
7	15	0.863173778	0.853477045	0.883787736	0.524228333	0.758525012	0.776638381
7	16	0.826238403	0.861489432	0.850908806	0.431055398	0.76351134	0.746640676
7	17	0.85832611	0.820645801	0.886477593	0.448072517	0.810144228	0.76473325
7	18	0.927252881	0.821532726	0.911104147	0.55529721	0.829901882	0.809017769
7	19	0.842900254	0.798502751	0.931761203	0.519611808	0.837314353	0.786018074
7	20	0.880895053	0.807838008	0.910320694	0.662286022	0.893370329	0.830942021
7	21	0.845548814	0.936968221	0.892249034	0.793132498	0.910031634	0.87558604
7	22	0.893110533	0.945326358	0.916483861	0.823695916	0.942925312	0.904308396
7	23	0.937397669	0.949340068	0.916640552	0.792087882	0.949037585	0.908900751
7	0	0.943930784	0.944213944	0.922568683	0.747337916	0.918891748	0.895388615
7	1	0.93006196	0.946919816	0.948944949	0.753807791	0.873518846	0.890650673
7	2	0.887636842	0.941673431	0.909276089	0.692141798	0.824071095	0.850959851
7	3	0.766557514	0.919635609	0.947430273	0.506503572	0.831644416	0.794354277
7	4	0.651545796	0.879663871	0.876109892	0.370804691	0.720591389	0.699743128
7	5	0.648752769	0.789618472	0.73187611	0.390686076	0.688756635	0.649938012
7	6	0.681803589	0.693740417	0.6097096	0.419800512	0.69836738	0.6206843
7	7	0.653744904	0.491521602	0.551107281	0.367064294	0.61370704	0.535429024
7	8	0.600548974	0.373380235	0.238352659	0.247978164	0.59396279	0.410844564
7	9	0.597643584	0.348606476	0.09500679	0.267589972	0.56468822	0.374707008
7	10	0.450463899	0.299434773	0.095764128	0.415082895	0.488780762	0.349905292
7	11	0.53313108	0.385466462	0.179880915	0.633845532	0.463701678	0.439205133
7	12	0.787264439	0.493551006	0.22861172	0.766680146	0.581698032	0.571561069
7	13	0.816462808	0.686780313	0.335056931	0.790841084	0.698702482	0.665568724
7	14	0.814488427	0.686028682	0.439674083	0.681965224	0.711262131	0.666683709
7	15	0.743330444	0.72966838	0.539590515	0.59273487	0.707884296	0.662641701

7	16	0.713714726	0.776194342	0.502637627	0.511187492	0.668422605	0.634431358
7	17	0.669668368	0.801328884	0.61986838	0.529485106	0.731488928	0.670367933
7	18	0.754004944	0.73551607	0.900057453	0.55812778	0.861120047	0.761765259
7	19	0.827570709	0.316075885	0.77710749	0.741036528	0.857206048	0.703799332
7	20	0.846672445	0.868389405	0.583855636	0.774093544	0.915647955	0.797731797
7	21	0.915021349	0.871937104	0.608168808	0.883710743	0.948863332	0.845540267
7	22	0.920430832	0.802997505	0.567220307	0.839264052	0.928086966	0.811599932
7	23	0.877572314	0.399702354	0.84281312	0.781506942	0.880153879	0.756349722
7	0	0.846431667	0.258591143	0.859291758	0.739621243	0.867500402	0.714287243
7	1	0.83116633	0.445987794	0.815470594	0.6958148	0.883022358	0.734292375
7	2	0.793187582	0.338549653	0.424945158	0.665824235	0.822744089	0.609050143
7	3	0.731516261	0.35786657	0.789303249	0.609751988	0.762894751	0.650266564
7	4	0.848727086	0.504434623	0.638854069	0.621444939	0.708581309	0.664408405
7	5	0.844810427	0.513980337	0.553979944	0.597284001	0.794662485	0.660943439
7	6	0.913400109	0.576155257	0.193591351	0.719537674	0.740523296	0.628641537
7	7	0.837121577	0.511620216	0.13911522	0.657871681	0.717977588	0.572741256
7	8	0.656297152	0.482366736	0.114619242	0.564968325	0.699520133	0.503554317
7	9	0.603679091	0.353431947	0.216442077	0.570831648	0.659642915	0.480805536
7	10	0.636954637	0.56905986	0.163820119	0.594756706	0.869832717	0.566884808
7	11	0.775851552	0.85281561	0.094641178	0.855236555	0.898222615	0.695353502
7	12	0.904025811	0.710261267	0.109683485	0.904097587	0.902096402	0.706032911
7	13	0.939099169	0.508959442	0.129034785	0.918014557	0.864176184	0.671856827
7	14	0.922244695	0.365352816	0.132612556	0.884249899	0.851321645	0.631156322
7	15	0.907348551	0.366931241	0.35634075	0.879768163	0.862540883	0.674585917
7	16	0.910735497	0.34002285	0.443721926	0.866828414	0.895260308	0.691313799
7	17	0.897508748	0.444334205	0.651310979	0.92081143	0.916184119	0.766029896
7	18	0.901553822	0.481780464	0.849916432	0.920642944	0.770588708	0.784896474
7	19	0.759302064	0.282117194	0.622819388	0.920002696	0.535614712	0.623971211
7	20	0.870332916	0.389630498	0.590436645	0.932032619	0.33286419	0.623059373
7	21	0.725914155	0.328147079	0.360101327	0.724356382	0.367822101	0.501268209
7	22	0.204516999	0.579357205	0.36660399	0.036426742	0.032437939	0.243868575
7	23	0.423721468	0.260019242	0.642249034	0.234634048	0.003257198	0.312776198
7	0	0.097788051	0.147274586	0.672333647	0.327941771	0.243552625	0.297778136
7	1	0.099136409	0.317549082	0.649091194	0.542458552	0.229786607	0.367604369
7	2	0.039583935	0.368314242	0.569205056	0.525812104	0.067516487	0.314086365
7	3	0.010192944	0.246324524	0.737464745	0.306139641	0.036861294	0.26739663
7	4	0.081190407	0.132392291	0.703201713	0.200161747	0.013229854	0.226035202
7	5	0.089489229	0.097546676	0.720333229	0.147492924	0.019020428	0.214776497
7	6	0.034142348	0.547773669	0.828319231	0.142910096	0.256929923	0.362015053
7	7	0.526228771	0.885481495	0.639689752	0.156052029	0.806404482	0.602771306
7	8	0.776108382	0.880295241	0.483782513	0.112751045	0.910152271	0.63261789
7	9	0.673055315	0.618532215	0.275070511	0.125758188	0.868425286	0.512168303
7	10	0.710022794	0.488845795	0.396166301	0.623433077	0.85365396	0.614424385
7	11	0.571382709	0.412284658	0.512561371	0.403828009	0.773148893	0.534641128
7	12	0.581511445	0.322224227	0.589600961	0.544143416	0.503337623	0.508163534
7	13	0.57335709	0.274630949	0.552178001	0.638327268	0.552168785	0.518132418
7	14	0.436129571	0.346847659	0.344876214	0.81021701	0.521580612	0.491930213
7	15	0.170101769	0.387435736	0.350020892	0.753336029	0.575800225	0.44733893

7	16	0.20700504	0.397161841	0.267679933	0.872826526	0.454908584	0.439916385
7	17	0.431891875	0.354243709	0.260446046	0.690187357	0.356026487	0.418559095
7	18	0.486404058	0.424521211	0.345868589	0.572617603	0.480577449	0.461997782
7	19	0.593694822	0.467048495	0.360545284	0.42623669	0.463661466	0.462237351
7	20	0.665543035	0.282026999	0.238535464	0.190187357	0.448112702	0.364881111
7	21	0.646890751	0.191846306	0.155411052	0.252426203	0.550895394	0.359493941
7	22	0.545844168	0.117885812	0.158649326	0.345026284	0.65430808	0.364342734
7	23	0.441731677	0.185743062	0.143110833	0.784270117	0.706262399	0.452223618
7	0	0.36208225	0.277877995	0.116212264	0.636676102	0.545573964	0.387684515
7	1	0.262993997	0.226721987	0.041888645	0.502695781	0.362353225	0.279330727
7	2	0.195993451	0.086768287	0.023242453	0.374410298	0.250013404	0.186085579
7	3	0.111351889	0.026277021	0.009714823	0.267926944	0.155246367	0.114103409
7	4	0.082602973	0.000586272	0.00010446	0.299231702	0.113532786	0.099211639
7	5	0.09342194	0	0	0.236891764	0.101214412	0.086305623
7	6	0.121079328	0.047412886	0	0.229512064	0.181344164	0.115869688
7	7	0.04244117	0.01841496	0	0.122556948	0.081966114	0.053075839
7	8	0.013339112	0.004269264	0	0.021364065	0.049260093	0.017646507
7	9	0.000626023	1.50326E-05	0	0.000134789	0.005375047	0.001230178
7	10	0	0.000420913	0	0.010311363	0.005428663	0.003232188
7	11	0	0.013138511	0.003055469	0.037639844	0.001380623	0.011042889
7	12	0	0.086948679	0.021962812	0.012670171	9.38287E-05	0.024335098
7	13	0	0.013950272	0.030006268	0.002291414	5.36164E-05	0.009260314
7	14	0	0.011018911	0.005510289	3.36973E-05	5.36164E-05	0.003323303
7	15	0	0.001909143	0.005170793	0.000202184	0.002385931	0.00193361
7	16	0	0.00625357	0.000313381	0	0.003096349	0.00193266
7	17	0	0.008598659	0.000156691	0	0.000134041	0.00177878
7	18	0.000240778	0.092781335	0.009819283	0.000168486	2.68082E-05	0.020607338
7	19	0.062104722	0.342428069	0.13472788	0.004212158	0.158744839	0.140443534
7	20	0.364843173	0.60731788	0.258774679	0.020454239	0.436290279	0.33753605
7	21	0.389643327	0.578259824	0.34725269	0.045221728	0.467066109	0.365488736
7	22	0.453272978	0.575704278	0.531259793	0.037538752	0.473245402	0.414204241
7	23	0.394073646	0.620411293	0.527525332	0.007312306	0.48573803	0.407012121
7	0	0.26447077	0.670950964	0.526715763	0	0.527813522	0.397990204
7	1	0.236781277	0.613255765	0.390394861	0	0.452884564	0.338663293
7	2	0.371408392	0.659676498	0.477567116	0	0.569192	0.415568801
7	3	0.38744422	0.714094585	0.498850935	0.000572853	0.657203367	0.451633192
7	4	0.385373527	0.798457653	0.417006163	0.014523521	0.645809876	0.452234148
7	5	0.513242801	0.77228586	0.405358822	0.065507481	0.569969439	0.46527288
7	6	0.457013066	0.61230871	0.546693826	0.179303141	0.502922095	0.459648168
7	7	0.209894379	0.243768979	0.376031547	0.124747271	0.220577985	0.235004032
7	8	0.152685479	0.107393043	0.164577457	0.066787977	0.173475953	0.132983982
7	9	0.201691868	0.067210848	0.11078032	0.058195175	0.178274623	0.123230567
7	10	0.16883367	0.039671086	0.110179672	0.015433347	0.138598467	0.094543248
7	11	0.10085396	0.103409398	0.179280267	0.002156625	0.147619431	0.106663936
7	12	0.07335709	0.212922041	0.313903687	0.001651166	0.187670902	0.157900977
7	13	0.119538348	0.274615917	0.266739789	0.001448982	0.202576269	0.172983861
7	14	0.141962824	0.341601275	0.208163585	0.001381588	0.169856844	0.172593223
7	15	0.128431089	0.48284778	0.252480936	0.004650222	0.109632191	0.195608444

7	16	0.12912132	0.543143622	0.360910895	0.001246799	0.109913678	0.228867263
7	17	0.217021413	0.601981299	0.462472579	0.003403424	0.150675567	0.287110856
7	18	0.30256188	0.68664502	0.689230126	0.004481736	0.319553911	0.400494535
7	19	0.424941411	0.836490184	0.791496918	0.030159051	0.498458528	0.516309218
7	20	0.660759575	0.885210908	0.858482189	0.083535517	0.671612782	0.631920194
7	21	0.771629908	0.889450107	0.930220412	0.097351395	0.784341322	0.694598629
7	22	0.826768115	0.903851357	0.932492427	0.149346273	0.737493968	0.709990428
7	23	0.722575364	0.893418719	0.899274	0.331345195	0.689520669	0.707226789
7	0	0.621737455	0.868720123	0.876266583	0.382800917	0.695753579	0.689055731
7	1	0.756091688	0.89113376	0.880784498	0.605506133	0.76524047	0.77975131
7	2	0.860043661	0.939704158	0.892457955	0.513445208	0.807986167	0.80272743
7	3	0.825323445	0.933285229	0.832915491	0.533360291	0.815264597	0.788029811
7	4	0.721210954	0.911653288	0.873472266	0.557487532	0.862245992	0.785214006
7	5	0.734421651	0.888548149	0.906351196	0.553915622	0.765454935	0.769738311
7	6	0.705143022	0.82665885	0.844197221	0.289627982	0.650018766	0.663129168
7	7	0.524061768	0.713162563	0.787762457	0.120130745	0.437134738	0.516450454
7	8	0.348133166	0.519662668	0.789930011	0.091892438	0.441933408	0.438310339
7	9	0.393319208	0.469604041	0.758591873	0.087410702	0.543067396	0.450398644
7	10	0.419740602	0.402573585	0.878146871	0.098699286	0.446450592	0.449122187
7	11	0.511798132	0.505667298	0.913402277	0.143786225	0.493726878	0.513676162
7	12	0.552104401	0.637307958	0.924945158	0.318371748	0.587971154	0.604140084
7	13	0.674451828	0.673987553	0.89922177	0.37660062	0.60845263	0.64654288
7	14	0.679427911	0.68016596	0.852684634	0.316248821	0.607206048	0.627146675
7	15	0.701178208	0.625883166	0.826360598	0.254448039	0.544608868	0.590495776
7	16	0.617178722	0.554688674	0.764937846	0.272240194	0.551887298	0.552186547
7	17	0.672605862	0.596223806	0.820510812	0.257548187	0.581416546	0.585661043
7	18	0.744903528	0.698325366	0.888880184	0.342633778	0.684587958	0.671866163
7	19	0.774519246	0.859775713	0.907813643	0.476411915	0.832488875	0.770201878
7	20	0.859128704	0.903370314	0.953619555	0.626533226	0.915540722	0.851638504
7	21	0.916080773	0.902468356	0.953306174	0.743698612	0.925446357	0.888200054
7	22	0.9487624	0.924912059	0.952287684	0.735274296	0.887754008	0.889798089
7	23	0.948826608	0.911457864	0.950250705	0.763310419	0.880917913	0.890952702
7	0	0.894153905	0.906767686	0.892719106	0.731971964	0.879416653	0.861005863
7	1	0.886770041	0.884489342	0.841481249	0.650222402	0.83397673	0.819387953
7	2	0.87352724	0.881167133	0.781155333	0.478433751	0.759181813	0.754693054
7	3	0.796815307	0.886383452	0.875221978	0.49568675	0.790225725	0.768866643
7	4	0.802288998	0.855746971	0.891204429	0.528642674	0.795225457	0.774621706
7	5	0.715063084	0.763777397	0.782905045	0.670946219	0.746863439	0.735911037
7	6	0.675880446	0.653543189	0.784158571	0.562508424	0.715806123	0.678379351
7	7	0.496131497	0.389254683	0.683510916	0.311430112	0.385609351	0.453187312
7	8	0.339288581	0.321607889	0.588948083	0.171957137	0.253431451	0.335046628
7	9	0.380574015	0.349989477	0.432126815	0.170710338	0.260642861	0.318808701
7	10	0.399386818	0.455518475	0.402172778	0.226681493	0.337461798	0.364244273
7	11	0.527930271	0.663058838	0.536482816	0.324572045	0.488887995	0.508186393
7	12	0.696972615	0.794053095	0.596025279	0.414173069	0.627767948	0.625798401
7	13	0.734277184	0.790099516	0.733913089	0.388091387	0.584700552	0.646216346
7	14	0.760923304	0.769655152	0.762091298	0.410196792	0.546860758	0.649945461
7	15	0.789174612	0.732885361	0.771309934	0.451138968	0.620650367	0.673031849

7	16	0.800908536	0.711644268	0.76817612	0.484094891	0.71112809	0.695190381
7	17	0.794230954	0.75289378	0.766400292	0.508997169	0.760173717	0.716539183
7	18	0.753106039	0.815143862	0.918259689	0.471121445	0.808361482	0.753198503
7	19	0.752656586	0.904798413	0.944975452	0.492418116	0.783188569	0.775607427
7	20	0.867925134	0.948242687	0.949284446	0.645605877	0.914334352	0.865078499
7	21	0.892372147	0.940771474	0.949388906	0.786595228	0.936410916	0.901107734
7	22	0.90905005	0.940756441	0.932544657	0.81699016	0.900930245	0.900054311
7	23	0.907589329	0.907835002	0.900893137	0.796569619	0.893651815	0.88130778
7	0	0.852531381	0.881347524	0.924161705	0.815979242	0.873666291	0.869537229
7	1	0.742126553	0.867487448	0.879530973	0.715460305	0.847018927	0.810324841
7	2	0.757600565	0.774766243	0.712968766	0.566484701	0.784676425	0.71929934
7	3	0.664788597	0.786341361	0.604904419	0.441905917	0.71622165	0.642832389
7	4	0.779495329	0.796999489	0.563015774	0.454205419	0.670098118	0.652762826
7	5	0.752367652	0.733847449	0.437741565	0.590948915	0.630368345	0.629054785
7	6	0.754020996	0.513183608	0.351692259	0.522813048	0.638652083	0.556072399
7	7	0.719204469	0.478353026	0.338921968	0.526755627	0.533201973	0.519287413
7	8	0.641914668	0.364961967	0.309855845	0.449588893	0.424414241	0.438147123
7	9	0.547593823	0.231622621	0.297921237	0.313721526	0.432242239	0.364620289
7	10	0.368503002	0.237500376	0.381933563	0.273857663	0.41902579	0.336164079
7	11	0.302963177	0.296307988	0.302987569	0.19261356	0.324486623	0.283871783
7	12	0.289880895	0.381993927	0.363496292	0.153996495	0.303616428	0.298596807
7	13	0.251035346	0.435615285	0.523451374	0.134014018	0.281432631	0.325109731
7	14	0.267055122	0.472114488	0.509192521	0.106213775	0.310023591	0.3329199
7	15	0.327169412	0.628047864	0.491643163	0.174821405	0.327569567	0.389850282
7	16	0.437590292	0.625311927	0.376475504	0.212393854	0.272344646	0.384823245
7	17	0.521557674	0.59297676	0.267810509	0.238745114	0.332877594	0.39079353
7	18	0.588734791	0.613466222	0.482424527	0.262198409	0.429467589	0.475258308
7	19	0.68599313	0.709960615	0.670166092	0.405883542	0.594378318	0.613276339
7	20	0.765867283	0.826252969	0.838138515	0.624713573	0.787317034	0.768457875
7	21	0.765305467	0.909338264	0.821006999	0.730287101	0.898021554	0.824791877
7	22	0.864762914	0.919049337	0.794265121	0.699285618	0.883987454	0.832270089
7	23	0.809801278	0.887661225	0.702052648	0.617097992	0.711892124	0.745701053

**Appendix B – The PSS/E Load Flow Data Format and Sample
Power System Load Flow Data for the Western Kansas Power
System**

Case Identification Data

IC, SBASE

where

IC = change code; 0 for base case, 1 to add data to working case

SBASE = system base MVA

Bus Data

I, 'NAME', BASKV, IDE, GL, BL, AREA, ZONE, VM, VA

where

I = bus number

NAME = bus name

BASKV = bus base voltage in KV

IDE = bus type code; 1 for load bus, 2 for generator bus 3 for swing bus, 4 for disconnected bus

GL = real component of shunt admittance to ground

BL = reactive component of shunt admittance to ground

AREA = area number

ZONE = zone number

VM = bus voltage magnitude

VA = bus voltage phase angle

Load Data

I, ID, STATUS, AREA, ZONE, PL, QL, IP, IQ, YP, YQ

where

I = bus number

ID = load identifier which is used to distinguish among multiple loads at bus I

STATUS = initial load status ; 1 for in-service, 0 for out-of-service

AREA = area to which the load is assigned

ZONE = zone to which the load is assigned

PL = real power component of constant MVA load in MW

QL = reactive power component of constant MVA load in MVAR

IP = real power component of constant current load in MW

IQ = reactive power component of constant current load in MVAR

YP = real power component of constant admittance load in MW

YQ = reactive power component of constant admittance load in MVAR

Generator Data

I, ID, PG, QG, QT, QB, VS, IREG, MBASE, ZR, ZX, RT, XT, GTAP, STAP,
RMPCT, PT, PB

where

I = bus number

ID = machine identifier which is used to distinguish among multiple machines at bus I

PG = generator real power output in MW

QG = generator reactive power output in MVAR

QT = maximum generator reactive power output in MVAR

QB = minimum generator reactive power output in MVAR

VS = regulated voltage set point in p.u.

IREG = bus number of a remote type one bus whose voltage is to be regulated by this plant to the value specified by VS

MBASE = total MVA base of the units represented by this machine

ZR, ZX = machine impedance, ZSOURCE in p.u.

RT, RX = step-up transformer impedance, XTRAN in p.u.

GTAP = step-up transformer off-nominal turns ratio in p.u.

STAT = initial machine status; 1 for in-service, 0 for out-of-service

RMPCT = percent of the total MVARs required to hold the voltage at bus

IREG

PT = maximum generator real power output in MW

PB = minimum generator real power output in MW

Branch Data

I, J, CKT, R, X, B, RATEA, RATEB, RATEC, RATIO, ANGLE, GI, BI, GJ, BJ,

ST, LEN

where

I = branch "from bus" number

J = branch "to bus" number

CKT = branch circuit identifier

R = branch resistance in p.u.

X = branch reactance in p.u.

B = total branch charging susceptance in p.u.

RATEA = first current rating in MVA

RATEB = second current rating in MVA

RATEC = third current rating in MVA

RATIO = transformer off-nominal turns ratio in p.u.

ANGLE = transformer phase shift angle in degrees.

GI, BI = complex admittance of the line shunt at the bus "I" end of the branch in p.u.

GJ, BJ = complex admittance of the line shunt at the bus "J" end of the branch in p.u.

ST = initial branch status; 1 for in-service, 0 for out-of-service

LEN = line length

Transformer Adjustment Data

I, J, CRT, ICONT, RMA, RMI, VMA, VMI, STEP, TABLE, CNTRL, CR, CX

where

I = "from bus" number

J = "to bus" number

CRT = circuit identifier

ICONT = bus number of the bus whose voltage is to be controlled by the transformer turns ratio adjustment option

RMA = upper limit of either off-nominal ratio for voltage in p.u. or phase shift angle in degrees

RMI = lower limit of either off-nominal ratio for voltage in p.u. or phase shift angle in degrees

VMA = upper limit of either controlled bus voltage in p.u. or real power flow through the phase shifter in MW or reactive power flow through the transformer in MVAR

VMI = lower limit of either controlled bus voltage in p.u. or real power flow through the phase shifter in MW or reactive power flow through the transformer in MVAR

STEP = transformer turns ratio step increment

TABLE = zero, or the number of a transformer impedance correction table

CNTRL = adjustment enable flag; 1 for the automatic adjustment, 0 for prohibiting the automatic adjustment

CR, CX = load drop compensation impedance for voltage controlling transformers in p.u.

Figure B.1 The Western Kansas Power System Sample One-Line Diagram

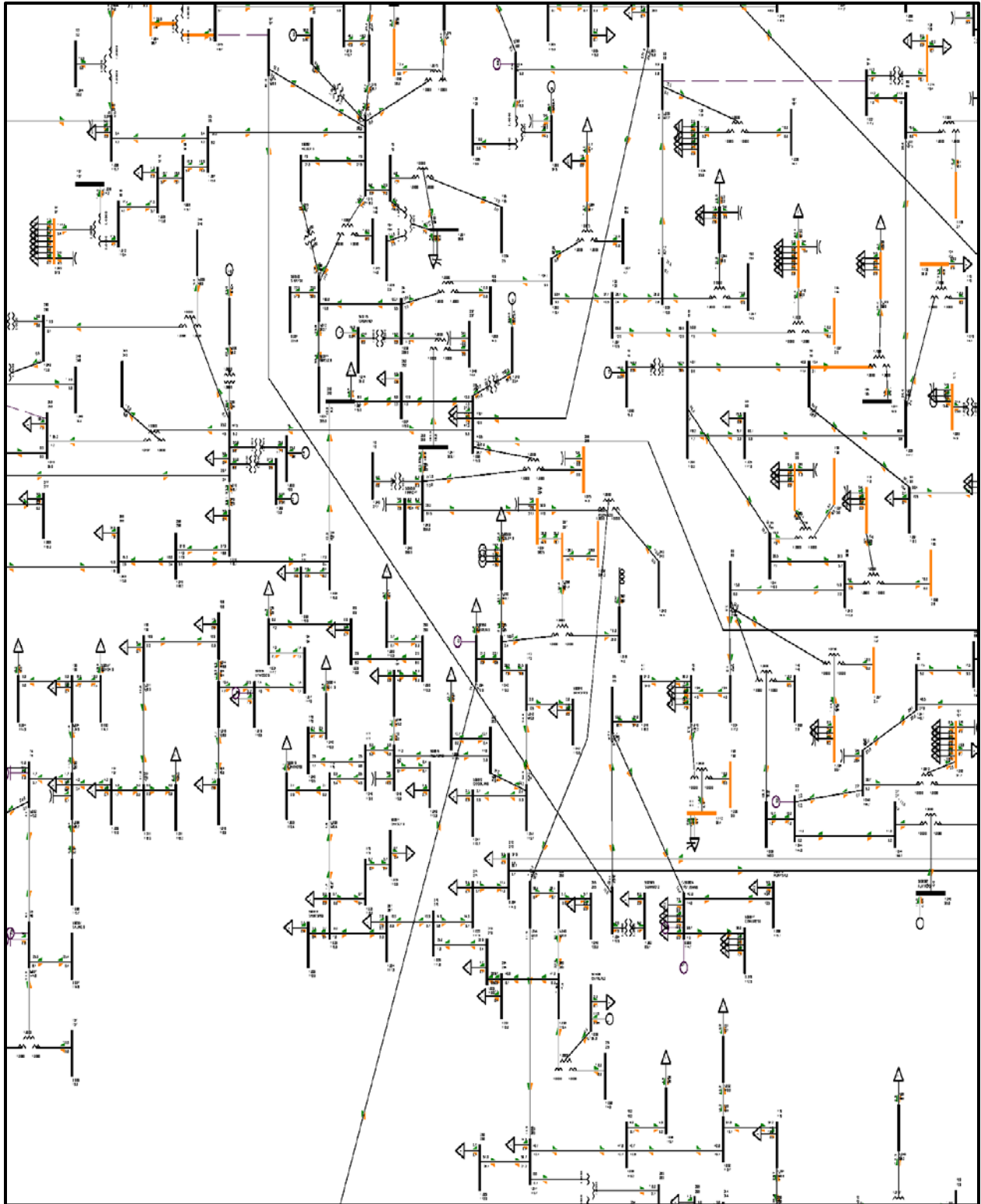


Table B.1 The Western Kansas Power System Load Flow Sample Data in PSS/E

0, 100.00 MVA, 60.00 Hz / PSS@E-32.0 SAT, JUN 04 2011 23:58
 2010 SUMMER PEAK

BUS DATA

1,'1	;', 115.0000,1, 534,1541, 534,1.00937, -32.9454
2,'2	;', 115.0000,1, 534,1549, 534,0.99254, -40.1006
3,'3	;', 69.0000,1, 534,1545, 534,0.98589, -40.1631
4,'4	;', 115.0000,1, 534,1544, 534,0.98553, -38.8736
5,'5	;', 115.0000,1, 534,1549, 534,0.99008, -29.2993
6,'6	;', 34.5000,1, 534,1549, 534,0.97946, -27.4440
7,'7	;', 115.0000,1, 534,1549, 534,1.01525, -33.7416
8,'8	;', 115.0000,1, 534,1549, 534,1.02499, -32.9775
9,'9	;', 22.0000,2, 534,1549, 534,1.03732, -18.5266
10,'10	;', 115.0000,1, 534,1549, 534,0.99136, -39.5873
11,'11	;', 13.8000,2, 534,1549, 534,1.00800, -15.9511
12,'12	;', 13.8000,1, 534,1549, 534,1.03576, -22.3997
13,'13	;', 13.2000,2, 534,1549, 534,1.00000, -16.7807
14,'14	;', 13.2000,2, 534,1549, 534,1.00800, -16.3213
15,'15	;', 69.0000,1, 534,1545, 534,1.09036, -44.9185
16,'16	;', 26.0000,1, 534,1549, 534,1.03928, -26.5549
17,'17	;', 13.8000,2, 534,1630, 539,1.02000, -41.5851
18,'18	;', 13.8000,2, 534,1630, 539,1.02000, -25.3074
19,'19	;', 15.0000,2, 534,1630, 539,1.00000, -31.5006
20,'20	;', 13.8000,2, 534,1630, 539,1.02000, -31.2631
21,'21	;', 34.5000,1, 534,1630, 539,0.99513, -42.5522
22,'22	;', 34.5000,1, 534,1630, 539,1.09405, -41.1547
23,'23	;', 34.5000,1, 534,1630, 539,1.01236, -55.0587
24,'24	;', 34.5000,1, 534,1630, 539,1.00067, -45.0254
25,'25	;', 34.5000,2, 534,1630, 539,1.00000, -33.4851
26,'26	;', 13.8000,1, 534,1630, 539,1.03356, -42.0167
27,'27	;', 138.0000,1, 534,1630, 539,1.03340, -42.4441
28,'28	;', 13.8000,1, 534,1630, 539,1.02516, -28.4234
29,'29	;', 230.0000,1, 534,1630, 539,1.02504, -28.3725
30,'30	;', 13.8000,1, 534,1630, 539,1.02373, -28.8929
31,'31	;', 230.0000,1, 534,1630, 539,1.02368, -28.8696
32,'32	;', 138.0000,2, 534,1630, 539,1.03285, -42.6301
33,'33	;', 230.0000,2, 534,1630, 539,1.02320, -29.0455
34,'34	;', 115.0000,1, 534,1630, 539,0.99277, -37.8624
35,'35	;', 115.0000,1, 534,1630, 539,0.99849, -39.4336
36,'36	;', 115.0000,1, 534,1630, 539,0.99628, -39.7262
37,'37	;', 115.0000,1, 534,1630, 539,1.00415, -39.3087
38,'38	;', 115.0000,1, 534,1630, 539,0.99984, -37.1723
39,'39	;', 115.0000,1, 534,1630, 539,0.98207, -44.5973
40,'40	;', 115.0000,1, 534,1630, 539,1.01724, -35.9654

41,'41 ', 115.0000,1, 534,1630, 539,0.99771, -45.1774
42,'42 ', 115.0000,1, 534,1630, 539,1.00564, -45.2076
43,'43 ', 115.0000,1, 534,1630, 539,1.02263, -35.2157

0 / END OF BUS DATA, BEGIN LOAD DATA

1,'1 ',1, 534, 341, 0.871, 0.030, 0.747, 0.026, 1.283, 0.044, 534,1
3,'1 ',1, 534, 345, 6.128, 1.502, 5.252, 1.287, 9.027, 2.212, 534,1
4,'1 ',1, 534, 344, 0.991, 0.000, 0.850, 0.000, 1.460, 0.000, 534,1
7,'1 ',1, 534, 349, 1.081, 0.240, 0.927, 0.206, 1.593, 0.354, 534,1
8,'1 ',1, 534, 349, 3.635, 0.511, 3.115, 0.438, 5.354, 0.752, 534,1
10,'1 ',1, 534, 349, 1.772, 0.871, 1.519, 0.747, 2.611, 1.283, 534,1
15,'1 ',1, 534, 345, 2.794, 0.180, 2.394, 0.154, 4.115, 0.265, 534,1
17,'1 ',1, 534,1635, 10.003, 3.575, 8.574, 3.064, 14.735, 5.266, 539,1
21,'1 ',1, 534,1630, 6.098, 1.502, 5.227, 1.287, 8.983, 2.212, 539,1
21,'K1',1, 534,1630, 1.382, 0.451, 1.184, 0.386, 2.035, 0.664, 550,1
21,'K2',1, 534,1630, 0.391, 0.060, 0.335, 0.051, 0.575, 0.088, 550,1
22,'1 ',1, 534,1630, 10.304, 3.785, 8.831, 3.244, 15.177, 5.575, 539,1
22,'K1',1, 534,1630, 0.571, 0.090, 0.489, 0.077, 0.841, 0.133, 550,1
22,'K2',1, 534,1630, 0.240, 0.120, 0.206, 0.103, 0.354, 0.177, 550,1
22,'K4',1, 534,1630, 0.481, 0.150, 0.412, 0.129, 0.708, 0.221, 550,1
22,'K5',1, 534,1630, 0.631, 0.060, 0.541, 0.051, 0.929, 0.088, 550,1
22,'KN',1, 534,1630, 1.382, 0.511, 1.184, 0.438, 2.035, 0.752, 550,1
23,'1 ',1, 534,1630, 5.047, -0.421, 4.325, -0.360, 7.434, -0.619, 539,1
23,'K1',1, 534,1630, 0.270, 0.090, 0.232, 0.077, 0.398, 0.133, 550,1
23,'K2',1, 534,1630, 1.142, 0.270, 0.978, 0.232, 1.681, 0.398, 550,1
23,'K3',1, 534,1630, 1.262, 0.360, 1.081, 0.309, 1.858, 0.531, 550,1
24,'1 ',1, 534,1630, 5.437, -0.150, 4.660, -0.129, 8.009, -0.221, 539,1
24,'K1',1, 536,1583, 1.200, 0.200, 0.000, 0.000, 0.000, 0.000, 550,1
24,'K2',1, 536,1630, 0.200, 0.200, 0.000, 0.000, 0.000, 0.000, 550,1
24,'K3',1, 536,1630, 1.100, 0.700, 0.000, 0.000, 0.000, 0.000, 550,1
24,'K4',1, 536,1630, 0.400, 0.400, 0.000, 0.000, 0.000, 0.000, 550,1
38,'1 ',1, 534,1630, 4.566, 1.772, 3.914, 1.519, 6.726, 2.611, 539,1
39,'1 ',1, 534,1630, 0.781, 0.210, 0.669, 0.180, 1.150, 0.310, 539,1
45,'1 ',1, 534,1630, 0.270, 0.090, 0.232, 0.077, 0.398, 0.133, 539,1
45,'K1',1, 534,1630, 0.481, 0.150, 0.412, 0.129, 0.708, 0.221, 550,1
48,'1 ',1, 534,1630, 3.064, -0.030, 2.626, -0.026, 4.513, -0.044, 539,1
48,'K1',1, 536,1583, 4.900, 1.500, 0.000, 0.000, 0.000, 0.000, 550,1
51,'1 ',1, 534,1630, 0.360, 0.120, 0.309, 0.103, 0.531, 0.177, 539,1
54,'K1',1, 536,1630, 0.400, 0.600, 0.000, 0.000, 0.000, 0.000, 550,1
60,'1 ',1, 534,1630, 0.000, 0.000, 0.000, 0.000, 0.000, 0.000, 539,1
62,'K1',1, 534,1630, 5.407, 1.772, 4.634, 1.519, 7.965, 2.611, 550,1
62,'KN',1, 534,1630, 4.806, 3.425, 4.120, 2.935, 7.080, 5.044, 550,1
76,'1 ',1, 534,1630, 6.969, 3.815, 5.973, 3.270, 10.266, 5.620, 539,1
76,'K1',1, 536,1583, 11.400, 1.700, 0.000, 0.000, 0.000, 0.000, 550,1
76,'K2',1, 536,1630, 2.400, 0.300, 0.000, 0.000, 0.000, 0.000, 550,1
80,'1 ',1, 534, 345, 2.854, 0.421, 2.446, 0.360, 4.204, 0.619, 534,1

87,'1 ',1, 534,1630, 0.391, -0.090, 0.335, -0.077, 0.575, -0.133, 539,1
87,'K1',1, 536,1583, 0.500, 0.100, 0.000, 0.000, 0.000, 0.000, 550,1
90,'1 ',1, 534,1630, 1.292, 0.090, 1.107, 0.077, 1.903, 0.133, 539,1
91,'1 ',1, 534,1630, 0.691, 0.180, 0.592, 0.154, 1.018, 0.265, 539,1

0 / END OF LOAD DATA, BEGIN FIXED SHUNT DATA

0 / END OF FIXED SHUNT DATA, BEGIN GENERATOR DATA

9,'9 ', 446.596, 33.091, 253.000, -175.000,1.00800, 284, 384.000, 0.00000E+0,
2.45000E-1, 0.00000E+0, 0.00000E+0,1.00000,1, 100.0, 500.000, 90.000, 534,1.0000
11,'11', 97.000, 9.411, 25.000, -15.000,1.00800, 0, 97.000, 0.00000E+0,
1.98000E-1, 0.00000E+0, 0.00000E+0,1.00000,1, 100.0, 97.000, 25.000, 534,1.0000
13,'13', 57.000, 0.503, 25.000, -15.000,1.00000, 0, 57.000, 0.00000E+0,
1.77000E-1, 0.00000E+0, 0.00000E+0,1.00000,1, 100.0, 57.000, 5.000, 534,1.0000
14,'14', 55.000, 5.317, 25.000, -15.000,1.00800, 0, 55.000, 0.00000E+0,
1.77000E-1, 0.00000E+0, 0.00000E+0,1.00000,1, 100.0, 55.000, 5.000, 534,1.0000
17,'17', 58.000, -6.602, 5.000, -15.000,1.02000, 0, 58.800, 0.00000E+0, 1.45000E-
1, 0.00000E+0, 0.00000E+0,1.00000,1, 100.0, 58.000, 25.000, 539,1.0000
18,'18', 70.000, -8.812, 25.000, -15.000,1.02000, 0, 74.000, 0.00000E+0,
1.80000E-1, 0.00000E+0, 0.00000E+0,1.00000,1, 100.0, 70.000, 5.000, 539,1.0000
19,'19', 143.000, 26.066, 50.000, -15.000,1.00000, 0, 175.000, 0.00000E+0,
1.64000E-1, 0.00000E+0, 0.00000E+0,1.00000,1, 100.0, 143.000, 40.000, 539,1.0000
20,'20', 93.000, 9.878, 25.000, -15.000,1.02000, 0, 96.000, 0.00000E+0,
1.30000E-1, 0.00000E+0, 0.00000E+0,1.00000,1, 100.0, 93.000, 30.000, 539,1.0000
25,'25', 36.000, -15.157, 0.000, -30.000,1.00000, 0, 110.000, 0.00000E+0,
1.30000E-1, 0.00000E+0, 0.00000E+0,1.00000,1, 100.0, 110.000, 0.000, 540,0.6667,
539,0.3333
32,'32', 100.000, 0.000, 0.000, 0.000,1.00000, 0, 100.000, 0.00000E+0, 1.50000E-
1, 0.00000E+0, 0.00000E+0,1.00000,0, 100.0, 100.000, 0.000, 539,1.0000
58,'58', 100.000, 0.000, 0.000, 0.000,1.00000, 0, 100.000, 0.00000E+0, 1.50000E-
1, 0.00000E+0, 0.00000E+0,1.00000,0, 100.0, 100.000, 0.000, 539,1.0000
62,'62', 100.000, 0.000, 0.000, 0.000,1.00000, 0, 100.000, 0.00000E+0, 1.50000E-
1, 0.00000E+0, 0.00000E+0,1.00000,0, 100.0, 100.000, 0.000, 539,1.0000
75,'75', 100.000, 0.000, 0.000, 0.000,1.00000, 0, 100.000, 0.00000E+0, 1.50000E-
1, 0.00000E+0, 0.00000E+0,1.00000,0, 100.0, 100.000, 0.000, 539,1.0000

0 / END OF GENERATOR DATA, BEGIN BRANCH DATA

1, 173,'1 ', 4.30000E-3, 1.00000E-2, 0.00120, 83.00, 98.00, 98.00, 0.00000, 0.00000,
0.00000, 0.00000,1,1, 1.70, 534,1.0000
1, 175,'1 ', 8.03000E-2, 1.86600E-1, 0.02190, 83.00, 98.00, 98.00, 0.00000, 0.00000,
0.00000, 0.00000,1,2, 30.90, 534,1.0000
1, 267,'1 ', 5.13000E-2, 1.19000E-1, 0.01400, 83.00, 98.00, 98.00, 0.00000, 0.00000,
0.00000, 0.00000,1,1, 19.70, 534,1.0000
1,530616,'1 ', 0.00000E+0, 2.00000E-4, 0.00000, 0.00, 0.00, 0.00, 0.00000, 0.00000,
0.00000, 0.00000,1,1, 0.00, 534,1.0000

2, 192,'1 ', 2.00000E-4, 2.00000E-4, 0.00020, 16.00, 16.00, 16.00, 0.00000, 0.00000,
 0.00000, 0.00000,1,2, 0.01, 534,1.0000
 3, 207,'1 ', 2.17000E-2, 4.58000E-2, 0.00080, 50.00, 59.00, 59.00, 0.00000, 0.00000,
 0.00000, 0.00000,1,2, 3.00, 534,1.0000
 4, 193,'1 ', 0.00000E+0, 1.00000E-4, 0.00000, 120.00, 143.00, 143.00, 0.00000,
 0.00000, 0.00000, 0.00000,1,1, 0.01, 534,1.0000
 5, 257,'1 ', 0.00000E+0, 1.00000E-4, 0.00000, 12.00, 12.00, 12.00, 0.00000, 0.00000,
 0.00000, 0.00000,1,2, 0.01, 534,1.0000
 6, 258,'1 ', 0.00000E+0, 1.00000E-4, 0.00000, 20.00, 20.00, 20.00, 0.00000, 0.00000,
 0.00000, 0.00000,1,2, 0.00, 534,1.0000
 7, 299,'1 ', 2.10000E-3, 8.10000E-3, 0.00110, 120.00, 143.00, 143.00, 0.00000, 0.00000,
 0.00000, 0.00000,1,2, 1.50, 534,1.0000
 8, 282,'1 ', 1.94000E-2, 4.35000E-2, 0.00550, 83.00, 98.00, 98.00, 0.00000, 0.00000,
 0.00000, 0.00000,1,2, 1.00, 534,1.0000
 10, 291,'1 ', 2.70000E-3, 1.05000E-2, 0.00140, 120.00, 143.00, 143.00, 0.00000,
 0.00000, 0.00000, 0.00000,1,2, 1.90, 534,1.0000
 15, 205,'1 ', 8.13000E-3, 3.23300E-2, 0.00053, 106.00, 106.00, 106.00, 0.00000,
 0.00000, 0.00000, 0.00000,1,1, 2.00, 534,1.0000
 27, 32,'1 ', 5.69000E-3, 3.14200E-2, 0.00000, 110.00, 110.00, 0.00, 0.00000, 0.00000,
 0.00000, 0.00000,1,1, 4.10, 539,1.0000
 29, 31,'1 ', 1.42000E-2, 8.25900E-2, 0.00000, 319.00, 319.00, 0.00, 0.00000, 0.00000,
 0.00000, 0.00000,1,1, 10.50, 539,1.0000
 31, 33,'1 ', 3.45000E-3, 2.00600E-2, 0.00000, 319.00, 319.00, 0.00, 0.00000, 0.00000,
 0.00000, 0.00000,1,2, 5.10, 539,1.0000
 32, 59,'1 ', 8.71400E-2, 1.87630E-1, 0.00000, 110.00, 110.00, 0.00, 0.00000, 0.00000,
 0.00000, 0.00000,1,1, 23.20, 539,1.0000
 32, 64,'1 ', 3.41200E-2, 7.34400E-2, 0.00000, 110.00, 110.00, 0.00, 0.00000, 0.00000,
 0.00000, 0.00000,1,2, 9.00, 539,1.0000
 33, 49,'1 ', 2.63000E-3, 1.77700E-2, 0.03462, 319.00, 319.00, 0.00, 0.00000, 0.00000,
 0.00000, 0.00000,1,2, 11.80, 539,1.0000
 33,532861,'1 ', 1.39200E-2, 9.37200E-2, 0.18313, 319.00, 319.00, 0.00, 0.00000,
 0.00000, 0.00000, 0.00000,1,2, 62.44, 539,0.8120, 536,0.1880
 34, 69,'1 ', 7.90000E-3, 3.07000E-2, 0.00000, 120.70, 129.50, 0.00, 0.00000, 0.00000,
 0.00000, 0.00000,1,1, 5.33, 539,1.0000
 35, 36,'1 ', 1.23600E-2, 2.90500E-2, 0.00000, 88.00, 99.00, 99.00, 0.00000, 0.00000,
 0.00000, 0.00000,1,2, 4.75, 539,1.0000
 35, 67,'1 ', 8.76900E-2, 1.87900E-1, 0.02120, 83.90, 89.60, 0.00, 0.00000, 0.00000,
 0.00000, 0.00000,1,1, 30.72, 539,1.0000
 35, 90,'1 ', 1.42700E-2, 3.05000E-2, 0.00350, 83.90, 89.60, 0.00, 0.00000, 0.00000,
 0.00000, 0.00000,1,1, 5.00, 539,1.0000
 36, 51,'1 ', 4.45100E-2, 1.46500E-1, 0.00000, 88.00, 99.00, 99.00, 0.00000, 0.00000,
 0.00000, 0.00000,1,2, 17.11, 539,1.0000
 37, 82,'1 ', 1.05730E-1, 2.26080E-1, 0.02574, 59.80, 59.80, 0.00, 0.00000, 0.00000,
 0.00000, 0.00000,1,2, 37.04, 539,1.0000
 37, 87,'1 ', 2.28300E-2, 4.88200E-2, 0.00556, 59.80, 59.80, 0.00, 0.00000, 0.00000,
 0.00000, 0.00000,1,2, 8.00, 539,1.0000

38, 61,'1 ', 8.30000E-3, 1.94300E-2, 0.00000, 83.90, 89.60, 0.00, 0.00000, 0.00000,
0.00000, 0.00000,1,2, 3.25, 539,1.0000
38, 125,'1 ', 2.37000E-3, 6.71000E-3, 0.00000, 83.90, 89.60, 0.00, 0.00000, 0.00000,
0.00000, 0.00000,1,1, 1.17, 539,1.0000
39, 45,'1 ', 5.52000E-3, 1.97500E-2, 0.00243, 120.70, 129.50, 0.00, 0.00000, 0.00000,
0.00000, 0.00000,1,2, 3.37, 539,1.0000

0 / END OF BRANCH DATA, BEGIN TRANSFORMER DATA

9, 284, 0,'1 ',1,1,1, 0.00000E+0, 0.00000E+0,2,'HOLGENXF ',1, 534,1.0000
0.00000E+0, 1.91200E-2, 100.00
1.02632, 0.000, 0.000, 600.00, 600.00, 600.00, 0, 0, 1.50000, 0.51000, 1.50000,
0.51000, 159, 0, 0.00000, 0.00000, 0.000
1.00000, 0.000
11, 283, 0,'1 ',1,1,1, 0.00000E+0, 0.00000E+0,2,'S2 GENXF ',1, 534,1.0000
0.00000E+0, 1.09500E-1, 100.00
1.00000, 0.000, 0.000, 123.00, 123.00, 123.00, 0, 0, 1.50000, 0.51000, 1.50000,
0.51000, 159, 0, 0.00000, 0.00000, 0.000
1.00000, 0.000
12, 260, 0,'1 ',1,1,1, 0.00000E+0, 0.00000E+0,2,'S3 GENXF ',1, 534,1.0000
0.00000E+0, 5.88300E-1, 100.00
1.00000, 0.000, 0.000, 20.00, 20.00, 20.00, 0, 0, 1.50000, 0.51000, 1.50000, 0.51000,
159, 0, 0.00000, 0.00000, 0.000
1.00000, 0.000
13, 283, 0,'1 ',1,1,1, 0.00000E+0, 0.00000E+0,2,'S4 GENXF ',1, 534,1.0000
0.00000E+0, 1.59500E-1, 100.00
1.00000, 0.000, 0.000, 78.00, 78.00, 78.00, 0, 0, 1.50000, 0.51000, 1.50000, 0.51000,
159, 0, 0.00000, 0.00000, 0.000
1.00000, 0.000
14, 283, 0,'1 ',1,1,1, 0.00000E+0, 0.00000E+0,2,'S5 GENXF ',1, 534,1.0000
0.00000E+0, 1.81300E-1, 100.00
1.00000, 0.000, 0.000, 78.00, 78.00, 78.00, 0, 0, 1.50000, 0.51000, 1.50000, 0.51000,
159, 0, 0.00000, 0.00000, 0.000
1.00000, 0.000
16, 285, 0,'1 ',1,1,1, 0.00000E+0, 0.00000E+0,1,' ',1, 534,1.0000
3.30000E-4, 1.46400E-2, 100.00
1.00000, 0.000, 0.000, 600.00, 600.00, 600.00, 0, 0, 1.50000, 0.51000, 1.50000,
0.51000, 159, 0, 0.00000, 0.00000, 0.000
1.00000, 0.000
17, 46, 0,'1 ',2,2,1, 0.00000E+0, 0.00000E+0,2,'CIM-PLT3 ',1, 539,1.0000
1.16500E-2, 2.21550E-1, 100.00
13.8000, 13.800, 0.000, 50.00, 50.00, 50.00, 0, 0, 0.00000, 0.00000, 0.00000, 0.00000,
33, 0, 0.00000, 0.00000, 0.000
115.000, 115.000
18, 47, 0,'1 ',2,2,1, 0.00000E+0, 0.00000E+0,2,'CLIFTON3 ',1, 539,1.0000
5.44000E-3, 1.48140E-1, 100.00

13.8000, 13.800, 0.000, 95.00, 95.00, 95.00, 0, 0, 0.00000, 0.00000, 0.00000, 0.00000,
33, 0, 0.00000, 0.00000, 0.000
115.000, 115.000
19, 61, 0, '1', 2, 2, 1, 0.00000E+0, 0.00000E+0, 2, 'FORTDGE3', 1, 539, 1.0000
2.39000E-3, 6.06600E-2, 100.00
15.0000, 15.000, 0.000, 187.00, 187.00, 0.00, 0, 0, 0.00000, 0.00000, 0.00000,
0.00000, 33, 0, 0.00000, 0.00000, 0.000
117.875, 115.000

0 / END OF TRANSFORMER DATA, BEGIN AREA DATA

534, 9, -120.000, 1.000, 'SUNC'

536, 532663, -279.000, 1.000, 'WERE'

0 / END OF AREA DATA, BEGIN TWO-TERMINAL DC DATA

0 / END OF TWO-TERMINAL DC DATA, BEGIN VSC DC LINE DATA

0 / END OF VSC DC LINE DATA, BEGIN IMPEDANCE CORRECTION DATA

0 / END OF IMPEDANCE CORRECTION DATA, BEGIN MULTI-TERMINAL DC DATA

0 / END OF MULTI-TERMINAL DC DATA, BEGIN MULTI-SECTION LINE DATA

0 / END OF MULTI-SECTION LINE DATA, BEGIN ZONE DATA

1541, 'GREAT PL'

1542, 'LANE-SCO'

1544, 'NORTON-D'

1545, 'PIONEER'

1546, 'VICTORY'

1547, 'WESTERN'

1548, 'WHEATLAN'

1549, 'SEPC'

1583, 'WEST'

0 / END OF ZONE DATA, BEGIN INTER-AREA TRANSFER DATA

0 / END OF INTER-AREA TRANSFER DATA, BEGIN OWNER DATA

1, '1'

534, 'SEPC 534'

536, 'WERE_536'

539, 'MKEC 539'

550, 'KEPC'

0 / END OF OWNER DATA, BEGIN FACTS DEVICE DATA

0 / END OF FACTS DEVICE DATA, BEGIN SWITCHED SHUNT DATA

17, 0, 0, 1, 1.04000, 0.98500, 0, 100.0, ' ', 33.00, 5, 3.00, 6, 3.00

21, 0, 0, 1, 1.04500, 1.00000, 58, 100.0, ' ', 9.60, 2, 4.80

22, 0, 0, 1, 1.04500, 1.00000, 61, 100.0, ' ', 9.60, 2, 4.80

23, 0, 0, 1, 1.04500, 0.97000, 62, 100.0, ' ', 0.00, 1, 4.80

24, 0, 0, 1, 1.04500, 0.97000, 75, 100.0, ' ', 4.80, 1, 4.80

25, 0, 0, 1, 1.04500, 1.00000, 58, 100.0, ' ', 12.00, 6, 2.40

29, 0, 0, 0, 1.05000, 0.95000, 0, 100.0, ' ', 27.00, 1, 27.00

59, 0, 0, 1, 1.05000, 0.95000, 0, 100.0, ' ', 24.00, 2, 12.00

62, 0, 0, 1, 1.05000, 1.00000, 0, 100.0, ' ', 24.00, 1, 24.00

74, 0, 0, 0, 1.05000, 0.95000, 0, 100.0, ' ', 44.00, 1, 44.00

75,0,0,0,1.05000,0.95000,	0, 100.0,'	,	29.00, 1,	29.00
76,0,0,1,1.05000,0.98000,	0, 100.0,'	,	24.00, 2,	12.00
90,0,0,1,1.05000,0.95000,	0, 100.0,'	,	0.00, 1,	9.60
93,0,0,1,1.04000,0.98500,	47, 100.0,'	,	0.00, 1,	4.80
94,0,0,1,1.04000,0.98500,	48, 100.0,'	,	0.00, 2,	4.80
96,0,0,1,1.04000,0.98500,	52, 100.0,'	,	7.80, 1,	4.80, 1, 3.00
97,0,0,1,1.04000,0.98500,	53, 100.0,'	,	5.40, 1,	3.00, 1, 2.40
98,0,0,1,1.04000,0.98500,	54, 100.0,'	,	0.00, 2,	4.80
99,0,0,1,1.04000,0.98500,	55, 100.0,'	,	7.20, 1,	4.80, 1, 2.40
100,0,0,1,1.04000,0.98500,	56, 100.0,'	,	4.80, 1,	4.80
101,0,0,1,1.04000,0.98500,	59, 100.0,'	,	0.00, 1,	4.80
102,0,0,1,1.04000,0.98500,	60, 100.0,'	,	0.00, 1,	3.60
103,0,0,1,1.04000,0.98500,	63, 100.0,'	,	4.80, 1,	4.80
104,0,0,1,1.04000,0.98500,	66, 100.0,'	,	4.80, 1,	4.80, 1, 2.40
106,0,0,1,1.04000,0.98500,	69, 100.0,'	,	6.00, 1,	6.00
107,0,0,1,1.04000,0.98500,	70, 100.0,'	,	7.20, 1,	4.80, 1, 2.40
109,0,0,1,1.04000,0.98500,	73, 100.0,'	,	2.40, 1,	2.40
110,0,0,1,1.04000,0.98500,	74, 100.0,'	,	4.80, 1,	4.80
111,0,0,1,1.04000,0.98500,	76, 100.0,'	,	4.80, 1,	4.80
112,0,0,1,1.04000,0.98500,	77, 100.0,'	,	7.80, 1,	4.80, 1, 3.00
113,0,0,1,1.04000,0.98500,	78, 100.0,'	,	7.80, 1,	4.80, 1, 3.00
114,0,0,1,1.04000,0.98500,	79, 100.0,'	,	4.80, 1,	4.80
115,0,0,1,1.04000,0.98500,	219, 100.0,'	,	3.60, 1,	3.60
116,0,0,1,1.04000,0.98500,	82, 100.0,'	,	4.80, 1,	4.80
118,0,0,1,1.04000,0.98500,	86, 100.0,'	,	3.00, 1,	3.00
120,0,0,1,1.04000,0.98500,	88, 100.0,'	,	0.00, 1,	4.80
121,0,0,1,1.04000,0.98500,	89, 100.0,'	,	9.60, 2,	4.80
178,1,0,1,1.03500,0.97500,	0, 100.0,'	,	12.00, 1,	12.00
192,1,0,1,1.03500,0.99560,	0, 100.0,'	,	8.00, 1,	8.00
204,1,0,1,1.04000,1.00000,	0, 100.0,'	,	24.00, 2,	12.00
213,1,0,1,1.04000,0.99130,	0, 100.0,'	,	24.00, 2,	12.00
225,1,0,1,1.04493,0.99493,	0, 100.0,'	,	0.00, 1,	7.50
286,1,0,1,1.01700,0.90400,	284, 100.0,'	,	0.00, 1,	-50.00
288,1,0,1,1.05500,0.94500,	265, 100.0,'	,	-25.00, 2,	-25.00
294,1,0,1,1.05000,0.97000,	0, 100.0,'	,	0.00, 1,	-60.00
297,1,0,1,1.05500,0.94500,	0, 100.0,'	,	0.00, 2,	-25.00

0 / END OF SWITCHED SHUNT DATA, BEGIN GNE DATA
0 / END OF GNE DATA

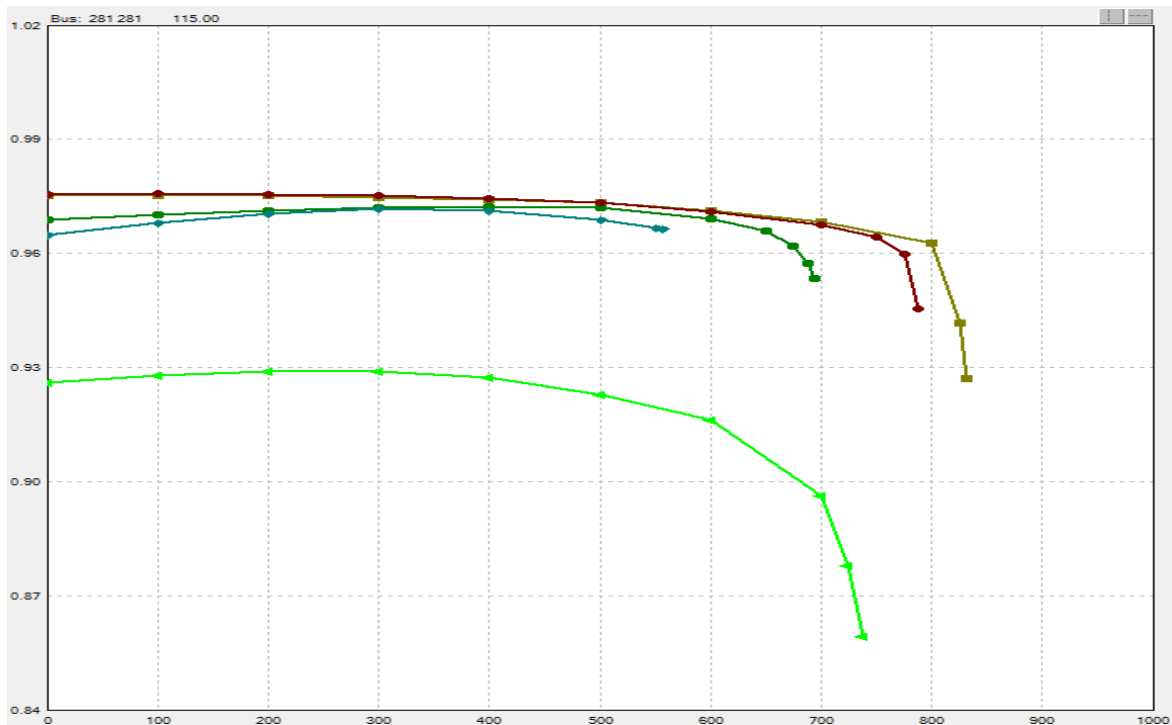
Appendix C - Additional Results of Simulations “Load Modeling Impact on Voltage Stability”

C.1 Constant Current (I) Load Modeling Impact on Voltage Stability Using the P-V Curve Method (Area I to Area II Transfer)

Table C.1 P-V Curve Analysis Results for Constant Current (I)

PV Contingencies (Constant Current (I) Load Type)		
CON#	Max MW	DESCRIPTION
BASE CASE	831.25	BASE CASE
1	693.75	OPEN BRANCH FROM BUS 61 [61 115.00] TO BUS 128 [128 115.00]
2	787.5	OPEN BRANCH FROM BUS 63 [63 115.00] TO BUS 86 [86 115.00]
3	556.25	OPEN BRANCH FROM BUS 83 [83 115.00] TO BUS 128 [128 115.00]
4	737.5	OPEN BRANCH FROM BUS 215 [215 115.00] TO BUS 284 [284 115.00]

Figure C.1 P-V Curve Analysis Results for Constant Current (I)



MARK	DESCRIPTION
—■—	BASE CASE
—■—	OPEN BRANCH FROM BUS 61 [61 115.00] TO BUS 128 [128 115.00]
—■—	OPEN BRANCH FROM BUS 63 [63 115.00] TO BUS 86 [86 115.00]
—■—	OPEN BRANCH FROM BUS 83 [83 115.00] TO BUS 128 [128 115.00]
—■—	OPEN BRANCH FROM BUS 215 [215 115.00] TO BUS 284 [284 115.00]

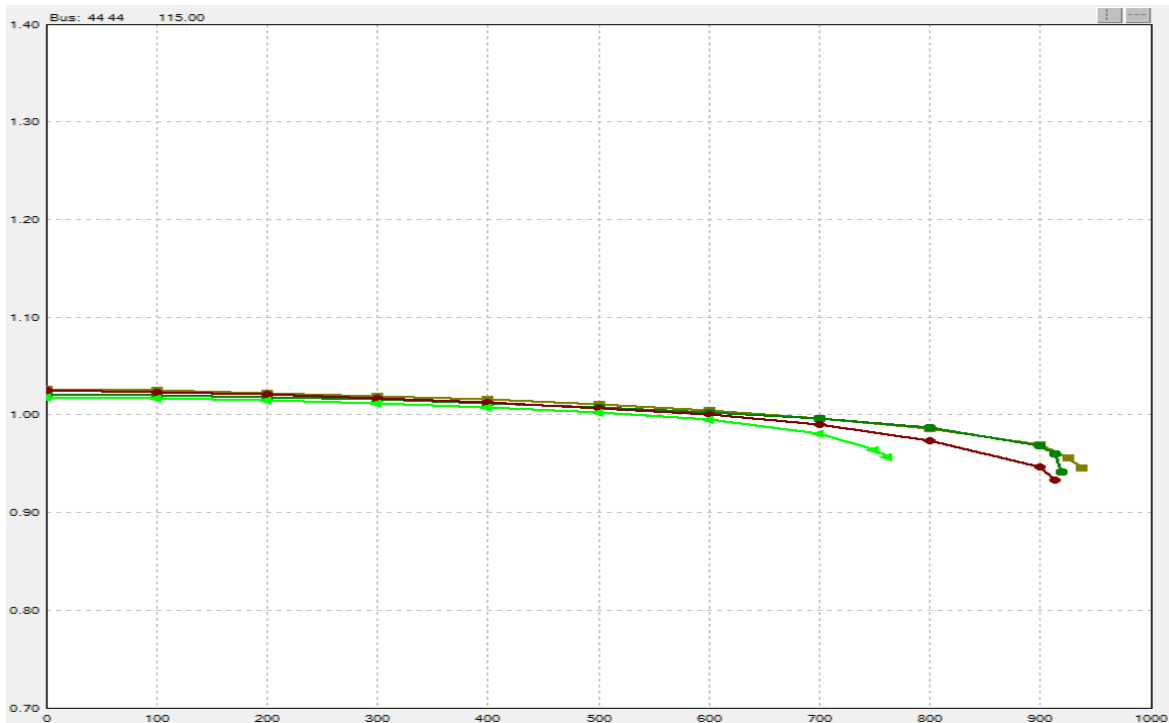
C.2 Constant Impedance (Z) Load Modeling Impact on Voltage Stability

Using the P-V Curve Method (Area I to Area II Transfer)

Table C.2 P-V Curve Analysis Results for Constant Impedance (Z)

PV Contingencies (Constant Impedance (Z) Load Type)		
CON#	Max MW	DESCRIPTION
BASE CASE	937.5	BASE CASE
1	918.75	OPEN BRANCH FROM BUS 61 [61 115.00] TO BUS 128 [128 115.00]
2	912.5	OPEN BRANCH FROM BUS 63 [63 115.00] TO BUS 86 [86 115.00]
3	912.5	OPEN BRANCH FROM BUS 83 [83 115.00] TO BUS 128 [128 115.00]
4	762.5	OPEN BRANCH FROM BUS 215 [215 115.00] TO BUS 284 [284 115.00]

Figure C.2 P-V Curve Analysis Results for Constant Impedance (Z)



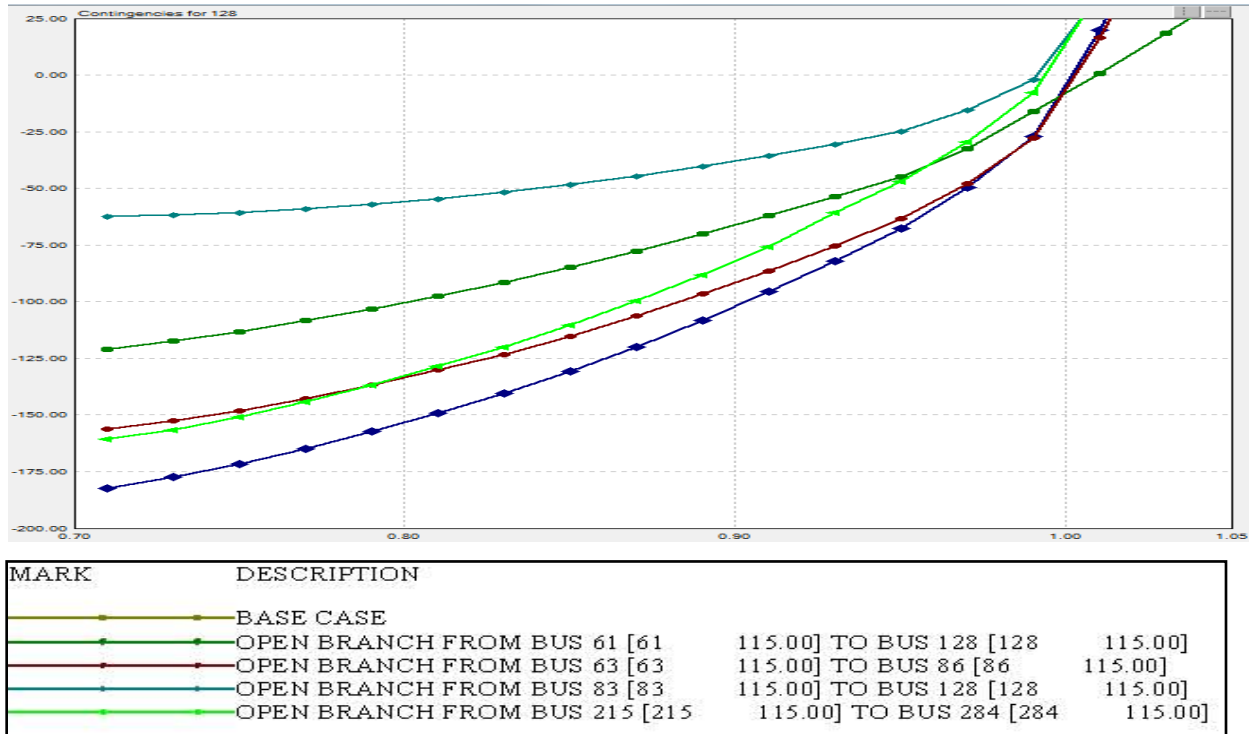
MARK	DESCRIPTION
—●—	BASE CASE
—●—	OPEN BRANCH FROM BUS 61 [61 115.00] TO BUS 128 [128 115.00]
—●—	OPEN BRANCH FROM BUS 63 [63 115.00] TO BUS 86 [86 115.00]
—●—	OPEN BRANCH FROM BUS 83 [83 115.00] TO BUS 128 [128 115.00]
—●—	OPEN BRANCH FROM BUS 215 [215 115.00] TO BUS 284 [284 115.00]

C.3 Constant Current (I) Load Modeling Impact on Voltage Stability Using the Q-V Curve Method

Table C.3 Q-V Curve Analysis Results for Constant Current (I)

Q-V Contingencies (Constant Current (I) Load Type)				
CON#	Min MVAR	Max MVAR	Max Mismatch	DESCRIPTION
BASE CASE	-182.377	111.059	0.881	BASE CASE
1	-121.069	36.972	0.603	OPEN BRANCH FROM BUS 61 [61 115.00] TO BUS 128 [128 115.00]
2	-156.363	101.687	0.882	OPEN BRANCH FROM BUS 63 [63 115.00] TO BUS 86 [86 115.00]
3	-62.238	105.825	0.846	OPEN BRANCH FROM BUS 83 [83 115.00] TO BUS 128 [128 115.00]
4	-160.738	128.494	0.932	OPEN BRANCH FROM BUS 215 [215 115.00] TO BUS 284 [284 115.00]

Figure C.3 Q-V Curve Analysis Results for Constant Current (I)

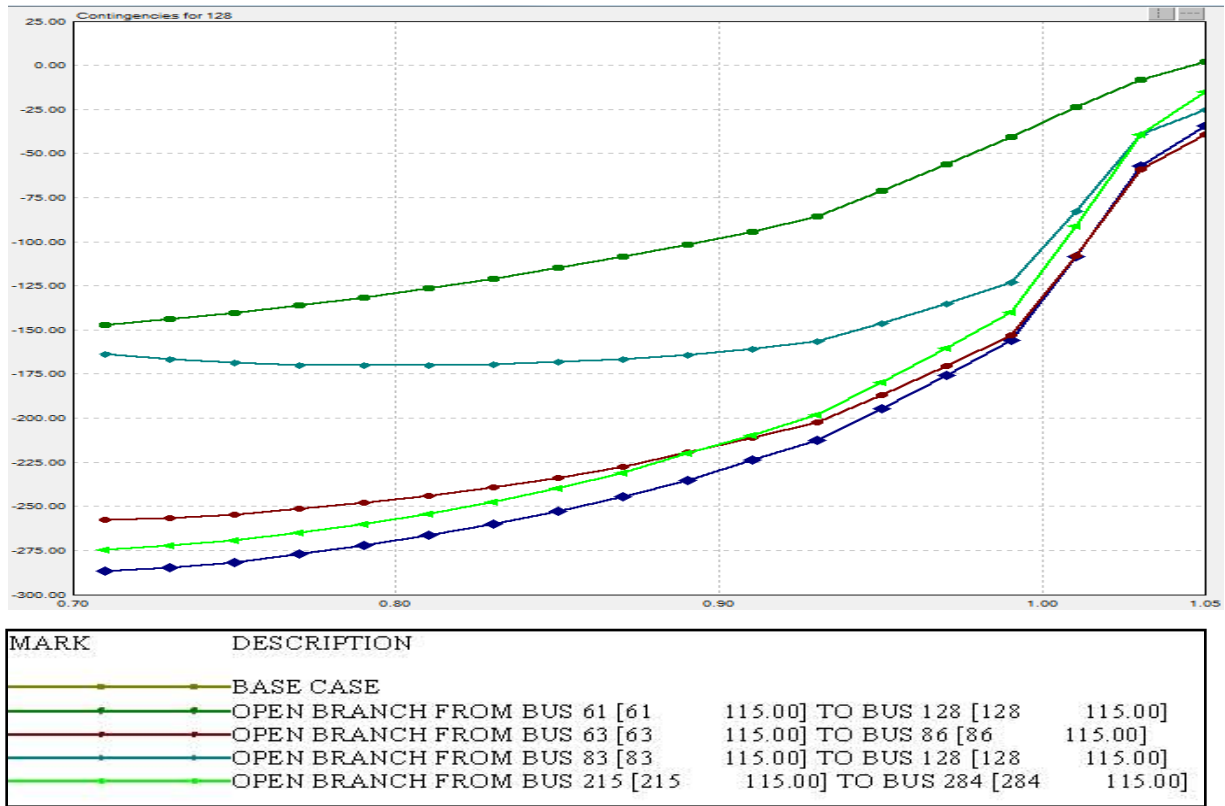


C.4 Constant Impedance (Z) Load Modeling Impact on Voltage Stability Using the Q-V Curve Method

Table C.4 Q-V Curve Analysis Results for Constant Impedance (Z)

Q-V Contingencies (Constant Impedance (Z) Load Type)				
CO N#	LABEL	Min MVAR	Max MVAR	DESCRIPTION
	BASE CASE	-286.761	34.358	BASE CASE
1	1	-147.138	2.166	OPEN BRANCH FROM BUS 61 [61 115.00] TO BUS 128 [128 115.00]
2	2	-257.517	39.365	OPEN BRANCH FROM BUS 63 [63 115.00] TO BUS 86 [86 115.00]
3	3	-170.044	25.067	OPEN BRANCH FROM BUS 83 [83 115.00] TO BUS 128 [128 115.00]
4	4	-274.360	14.891	OPEN BRANCH FROM BUS 215 [215 115.00] TO BUS 284 [284 115.00]

Figure C.4 Q-V Curve Analysis Results for Constant Impedance (Z)



**Appendix D – Additional Modal Analysis Results of Simulation for
Wind Integration in the Western Kansas Power System**

**D.1 Additional Results of Simulation for Western Kansas Power System
Critical Eigenvalues and the “Normalized” Participation Factors for
Individual Buses for Wind Injections Using DFIG Wind Turbine Type**

Bus 95 Wind Injection

Figure D.1 Bus 95 “Zero” MW of Wind Injection at Bus # 95

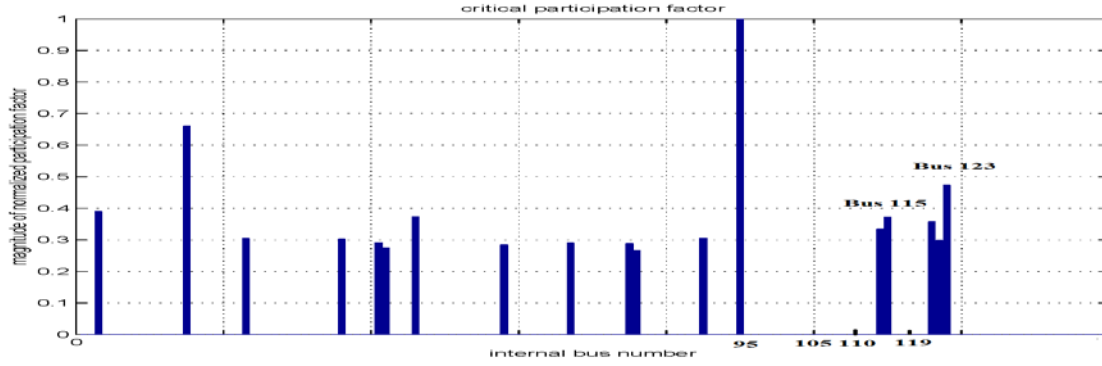


Figure D.2 Bus 95 “10” MW of Wind Injection at Bus # 95

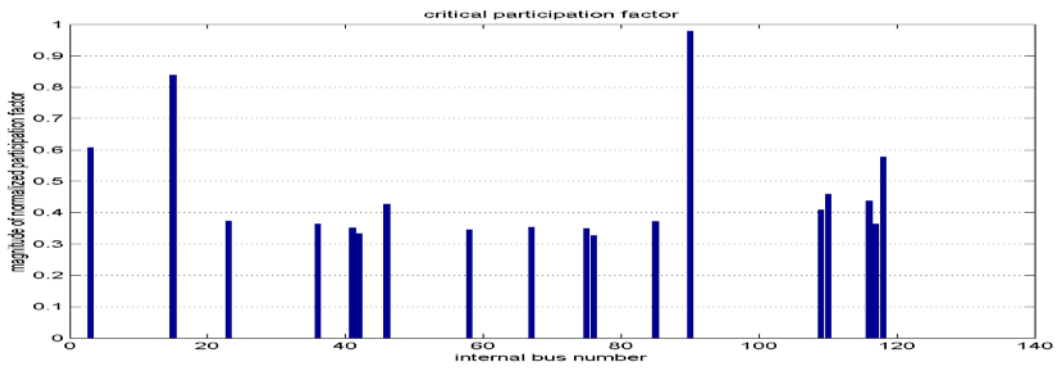


Figure D.3 Bus 95 “20” MW of Wind Injection at Bus # 95

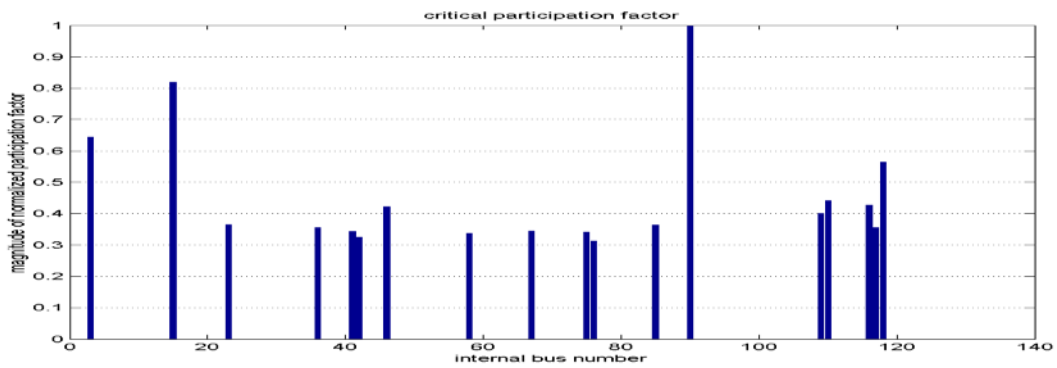


Figure D.4 Bus 95 “30” MW of Wind Injection at Bus # 95

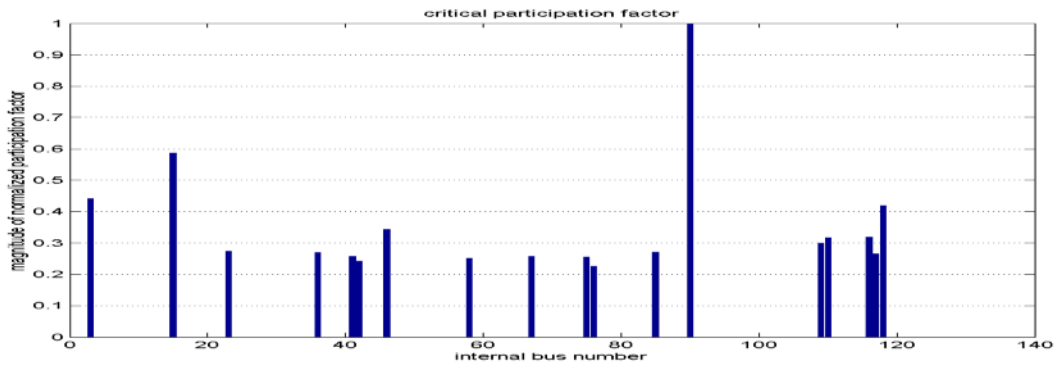


Figure D.5 Bus 95 “40” MW of Wind Injection at Bus # 95

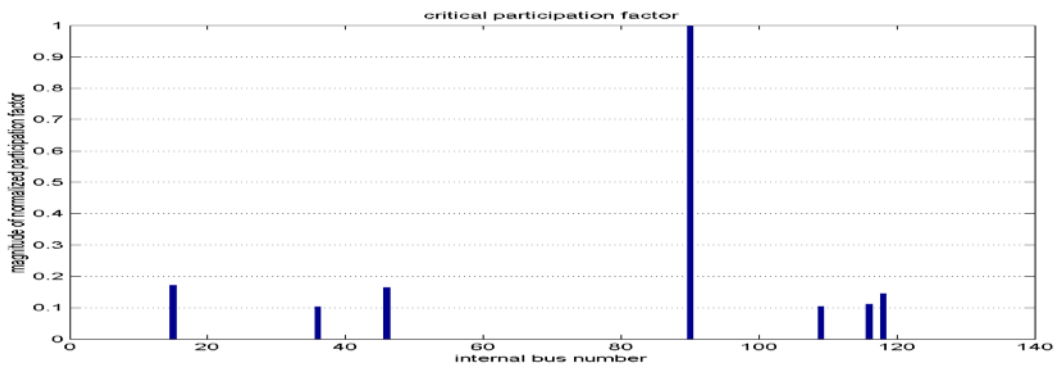
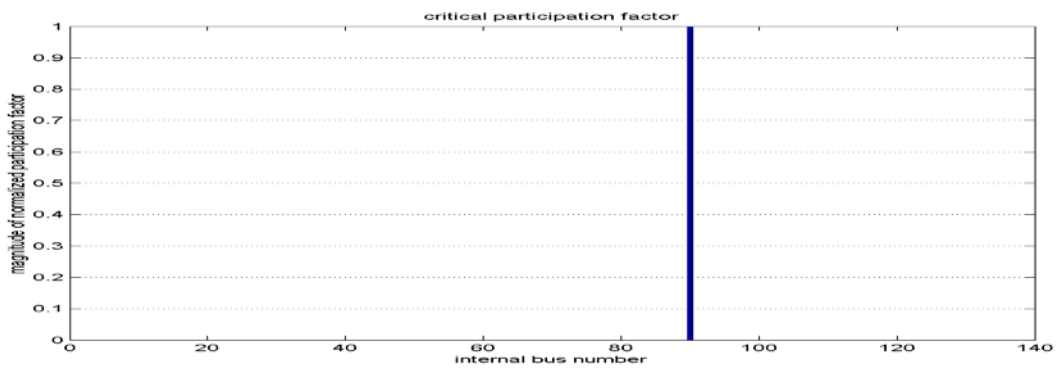


Figure D.6 Bus 95 “45” MW of Wind Injection at Bus # 95



Bus 115 Wind Injection

Figure D.7 Bus 115 “Zero” MW of Wind Injection at Bus # 115

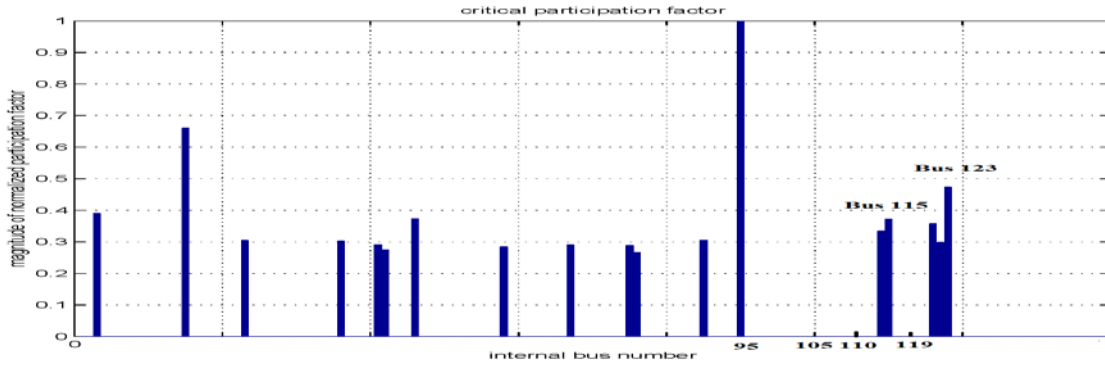


Figure D.8 Bus 115 “10” MW of Wind Injection at Bus # 115

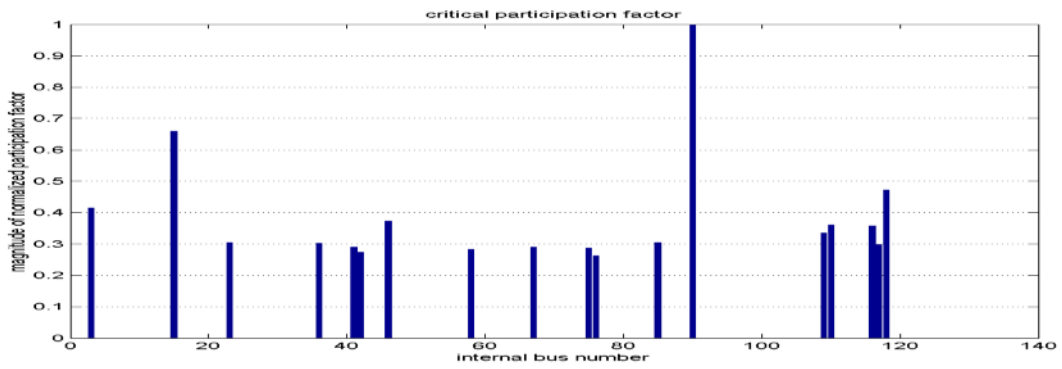


Figure D.9 Bus 115 “20” MW of Wind Injection at Bus # 115

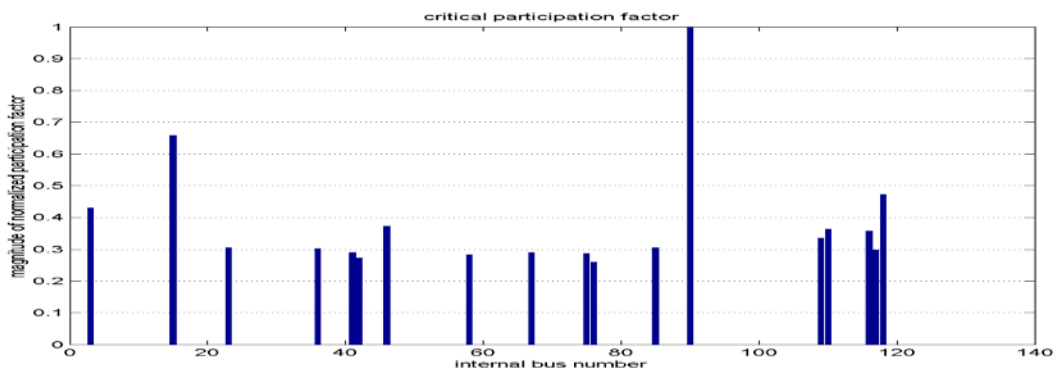


Figure D.10 Bus 115 “30” MW of Wind Injection at Bus # 115

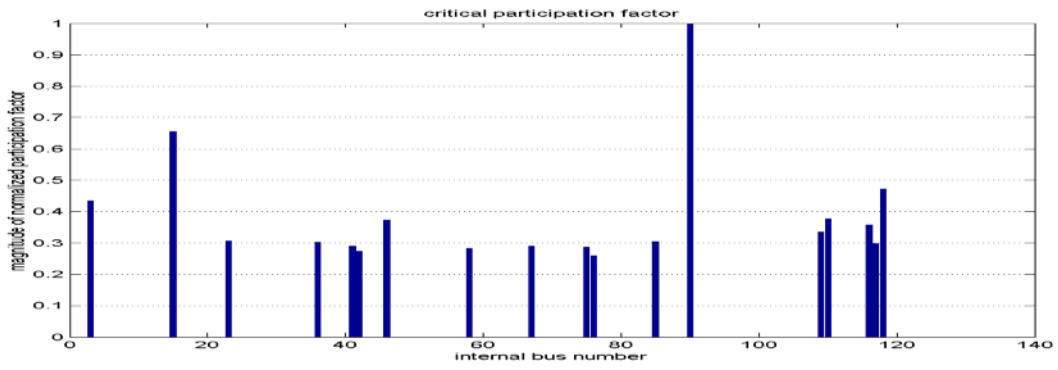


Figure D.11 Bus 115 “40” MW of Wind Injection at Bus # 115

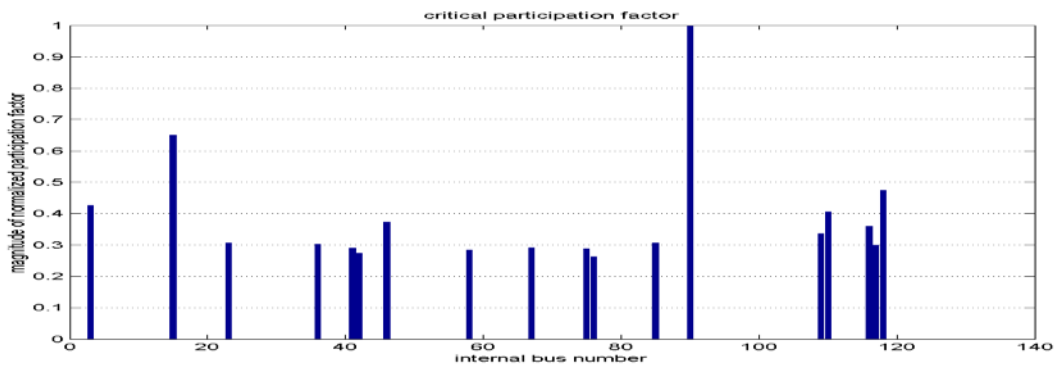


Figure D.12 Bus 115 “50” MW of Wind Injection at Bus # 115

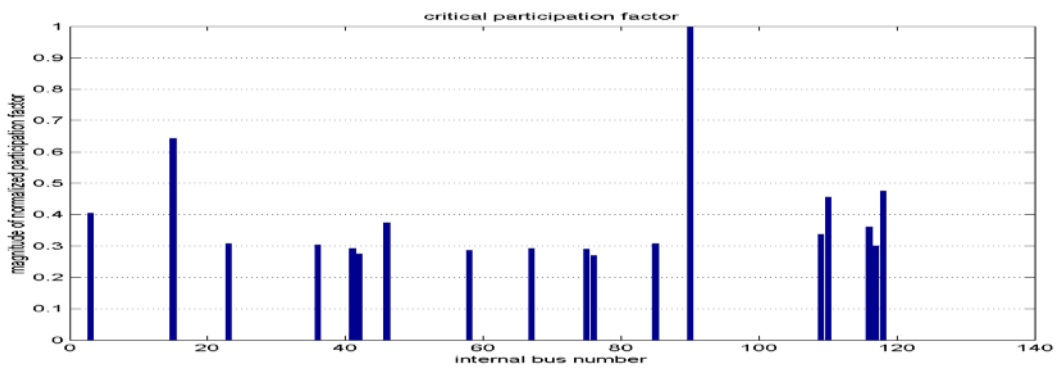


Figure D.13 Bus 115 “60” MW of Wind Injection at Bus # 115

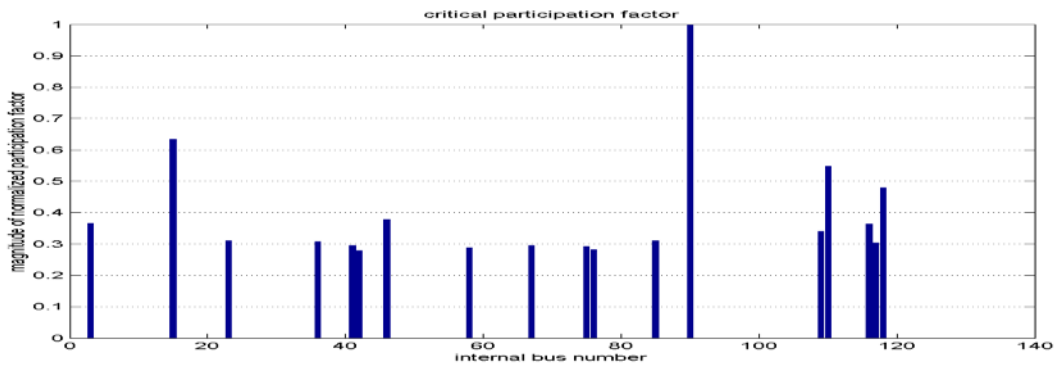


Figure D.14 Bus 115 “70” MW of Wind Injection at Bus # 115

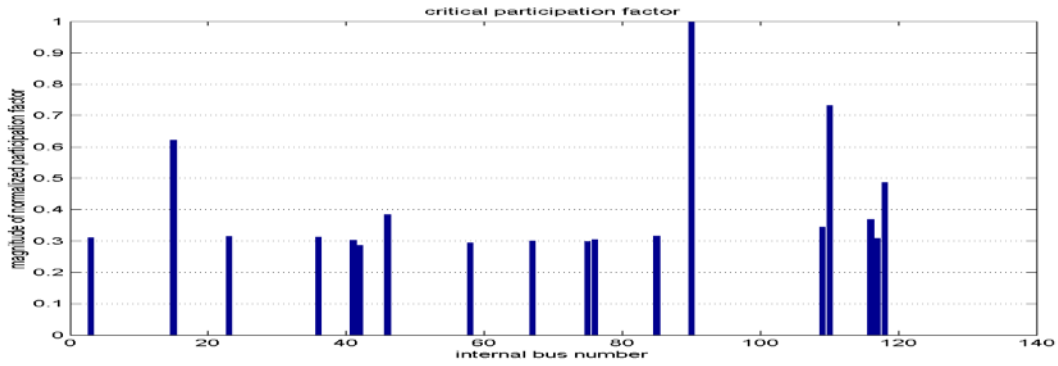


Figure D.15 Bus 115 “80” MW of Wind Injection at Bus # 115

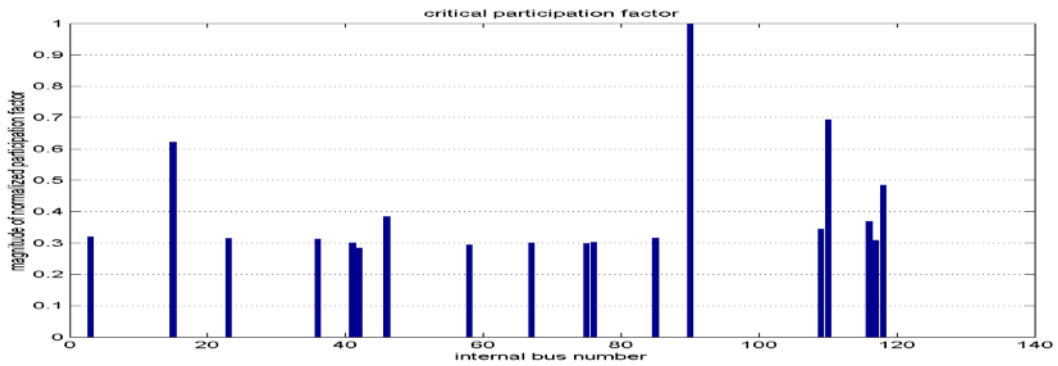
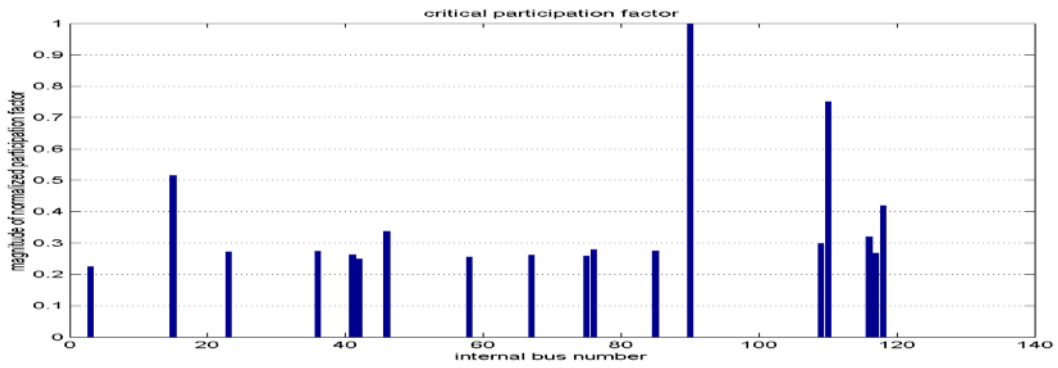


Figure D.16 Bus 115 “88” MW of Wind Injection at Bus # 115



Bus 123 Wind Injection

Figure D.17 Bus 123 “Zero” MW of Wind Injection at Bus # 123

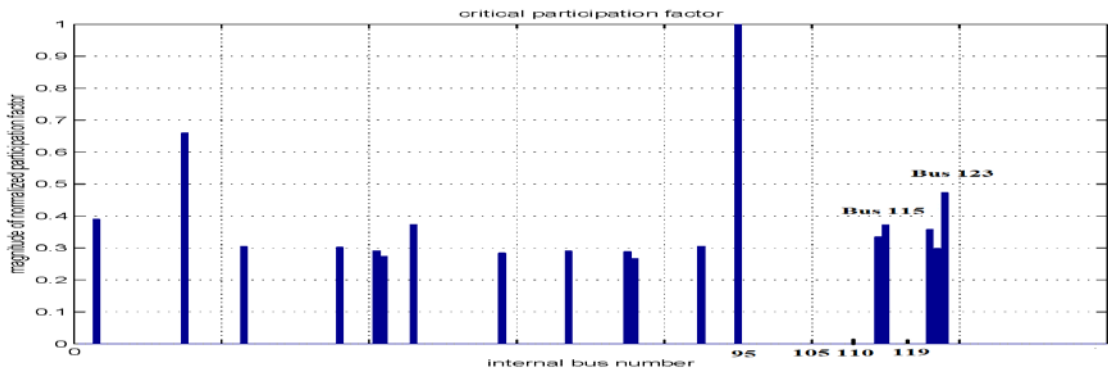


Figure D.18 Bus 123 “10” MW of Wind Injection at Bus # 123

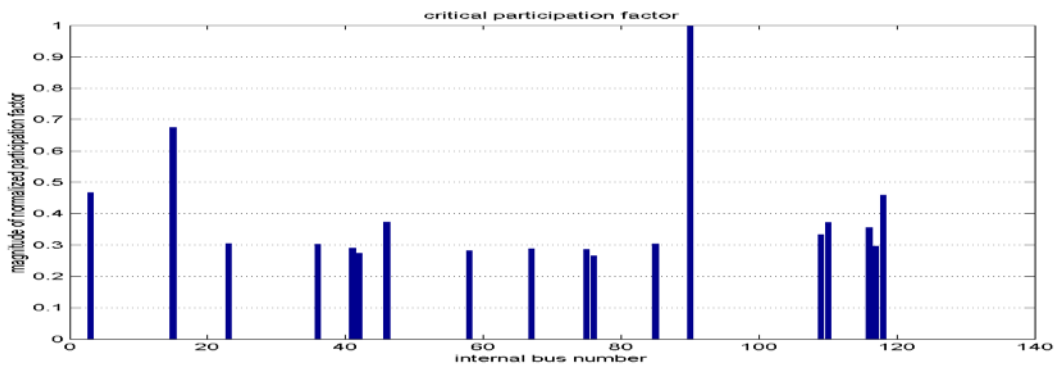


Figure D.19 Bus 123 “20” MW of Wind Injection at Bus # 123

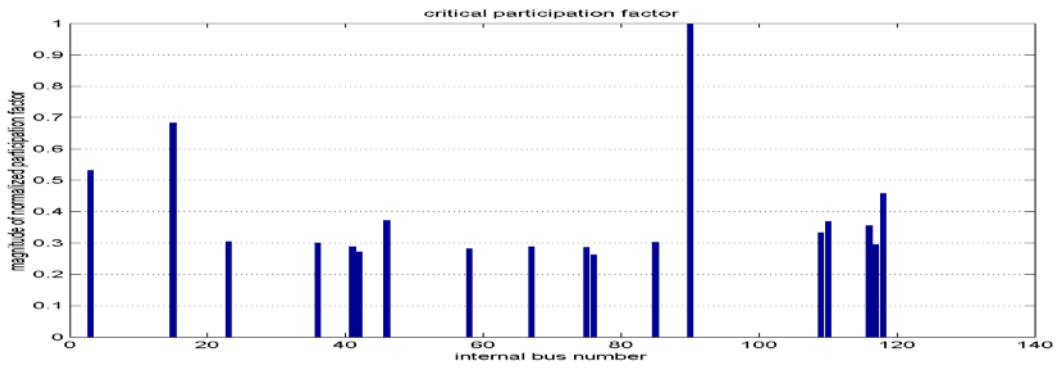


Figure D.20 Bus 123 “30” MW of Wind Injection at Bus # 123

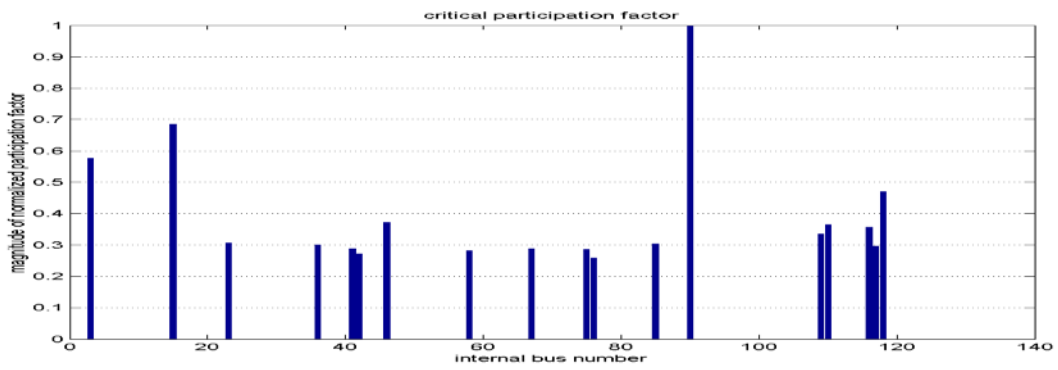


Figure D.21 Bus 123 “40” MW of Wind Injection at Bus # 123

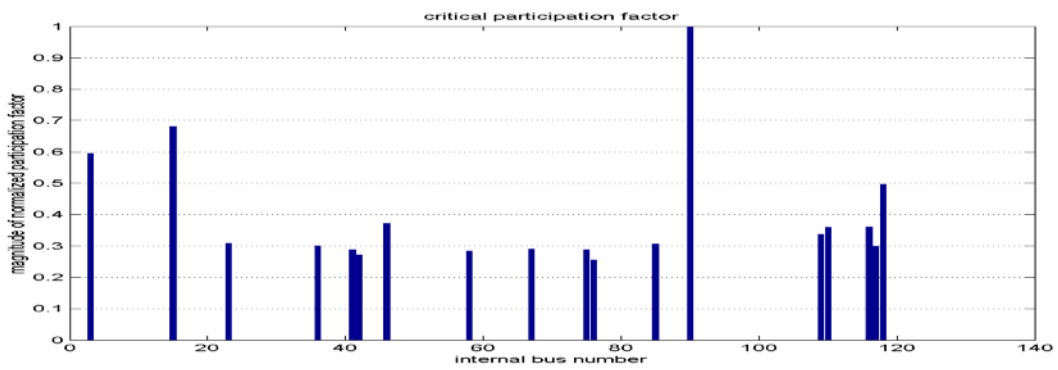


Figure D.22 Bus 123 “50” MW of Wind Injection at Bus # 123

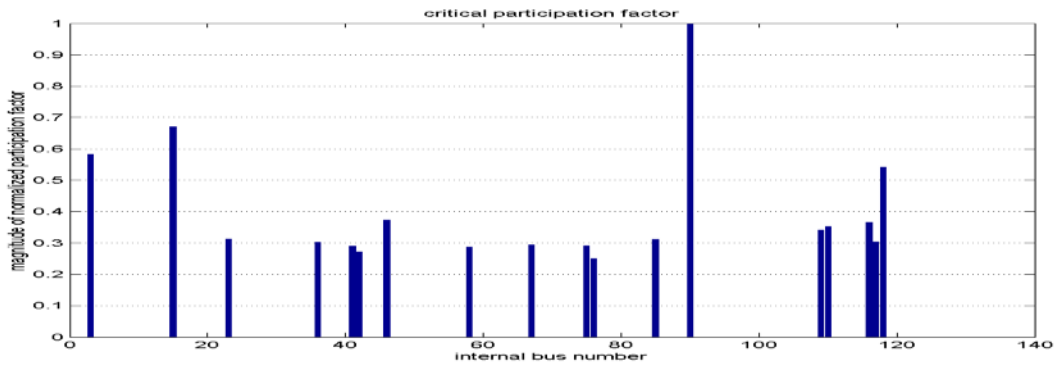


Figure D.23 Bus 123 “60” MW of Wind Injection at Bus # 123

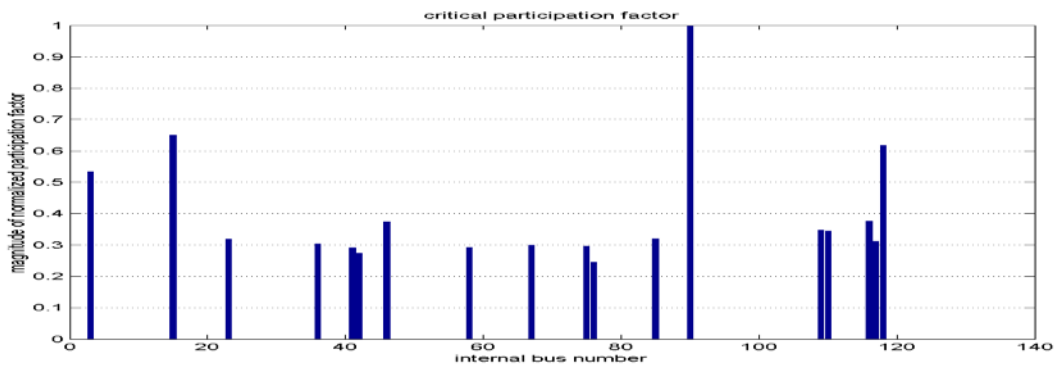


Figure D.24 Bus 123 “70” MW of Wind Injection at Bus # 123

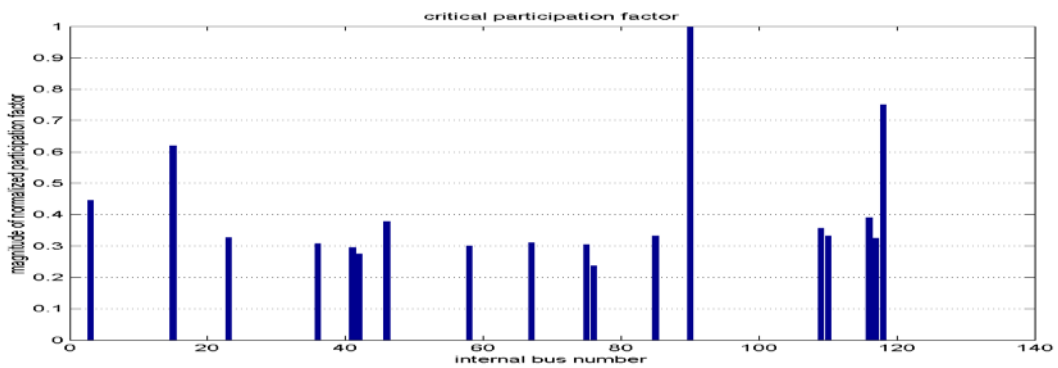


Figure D.25 Bus 123 “80” MW of Wind Injection at Bus # 123

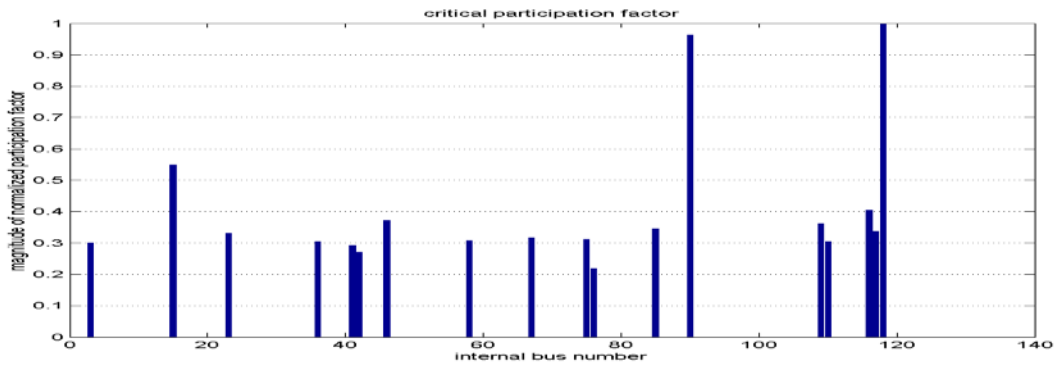
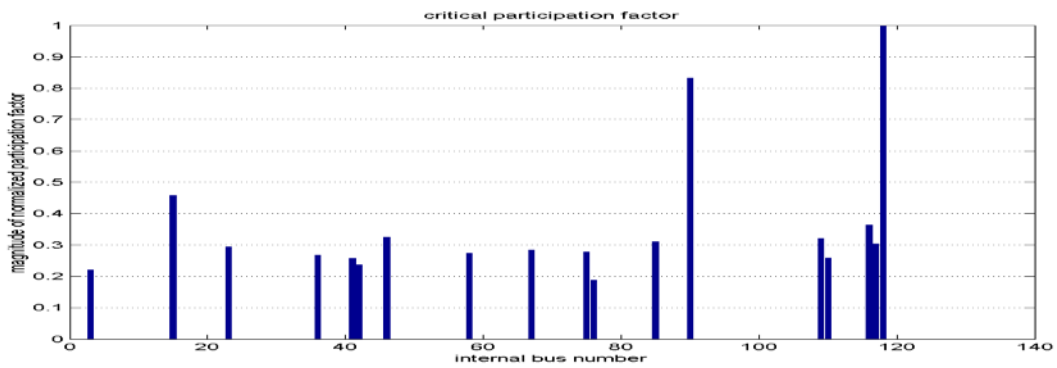


Figure D.26 Bus 123 “83” MW of Wind Injection at Bus # 123



Bus 110 Wind Injection

Figure D.27 Bus 110 “Zero” MW of Wind Injection at Bus # 110

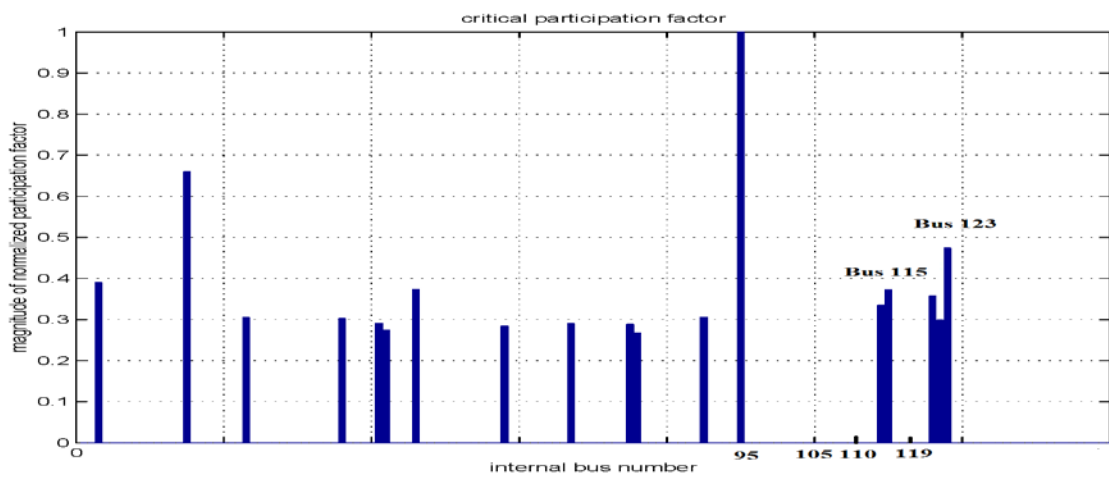


Figure D.28 Bus 110 “10” MW of Wind Injection at Bus # 110

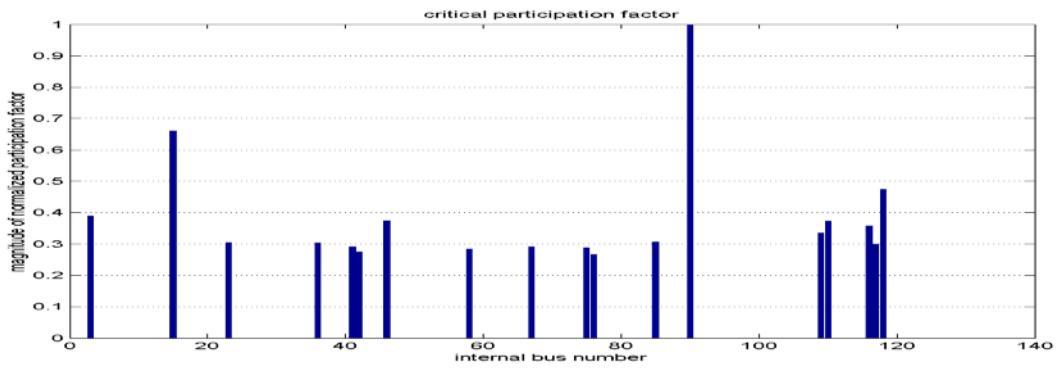


Figure D.29 Bus 110 “20” MW of Wind Injection at Bus # 110

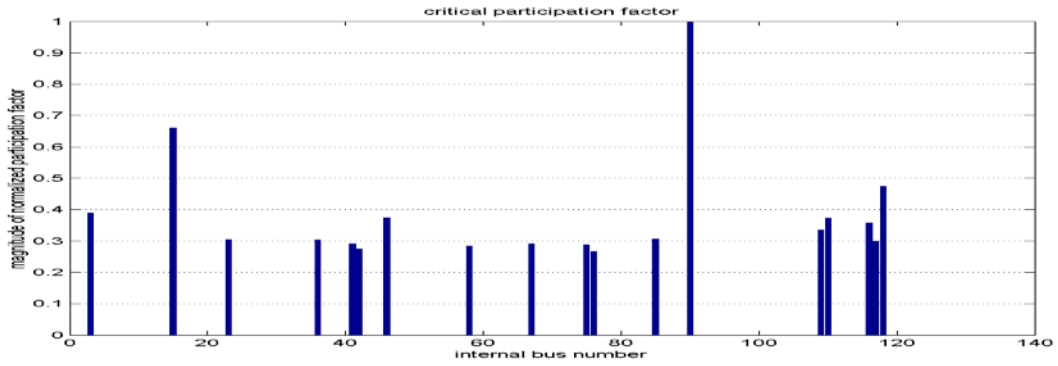


Figure D.30 Bus 110 “30” MW of Wind Injection at Bus # 110

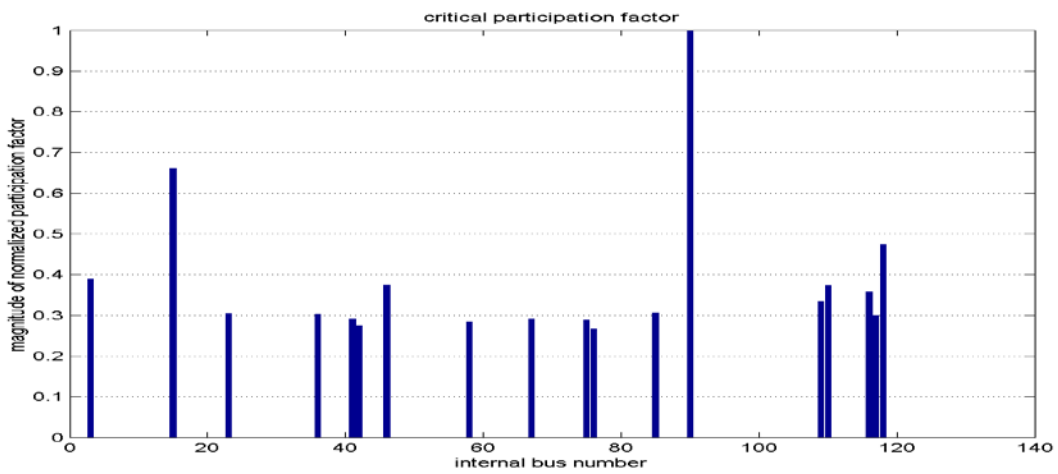


Figure D.31 Bus 110 “40” MW of Wind Injection at Bus # 110

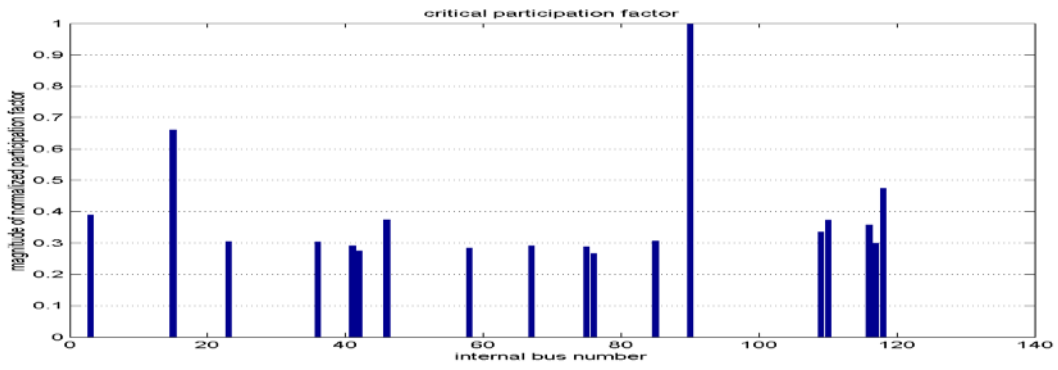


Figure D.32 Bus 110 “50” MW of Wind Injection at Bus # 110

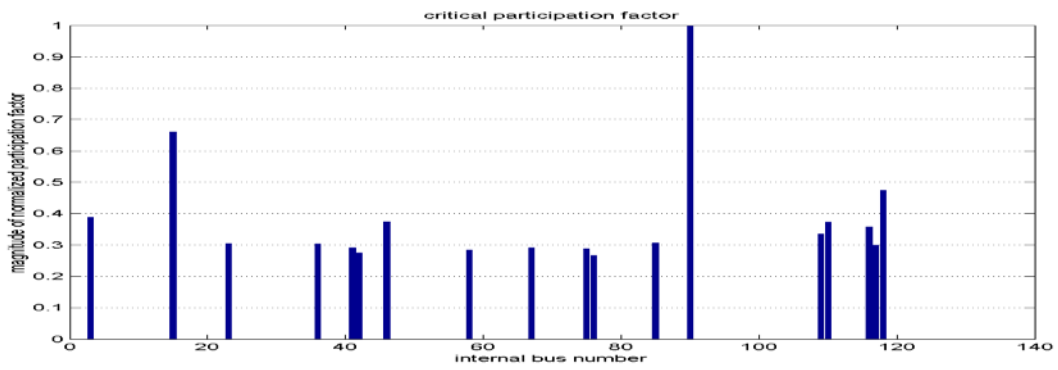


Figure D.33 Bus 110 “60” MW of Wind Injection at Bus # 110

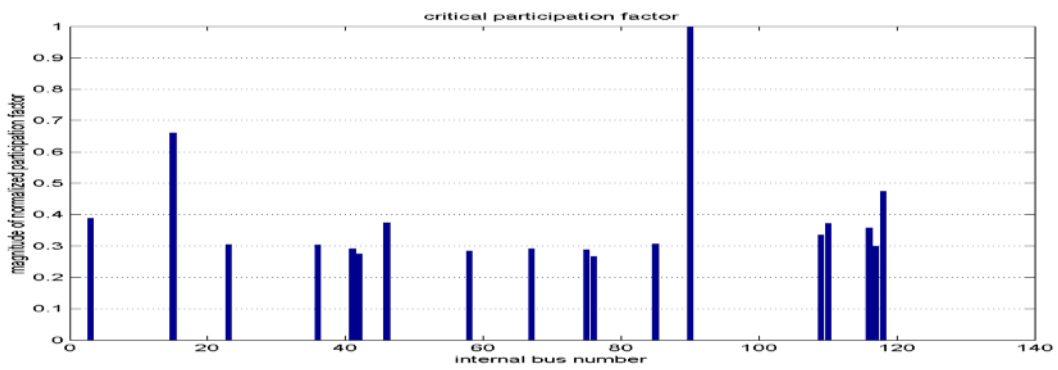


Figure D.34 Bus 110 “70” MW of Wind Injection at Bus # 110

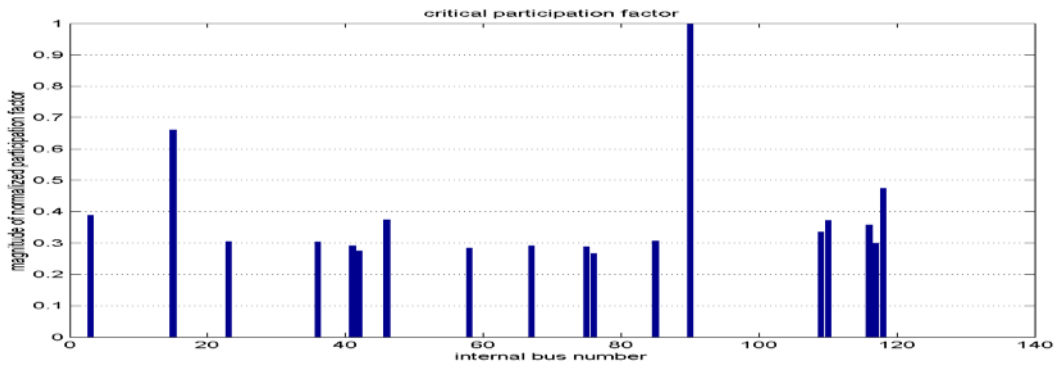


Figure D.35 Bus 110 “80” MW of Wind Injection at Bus # 110

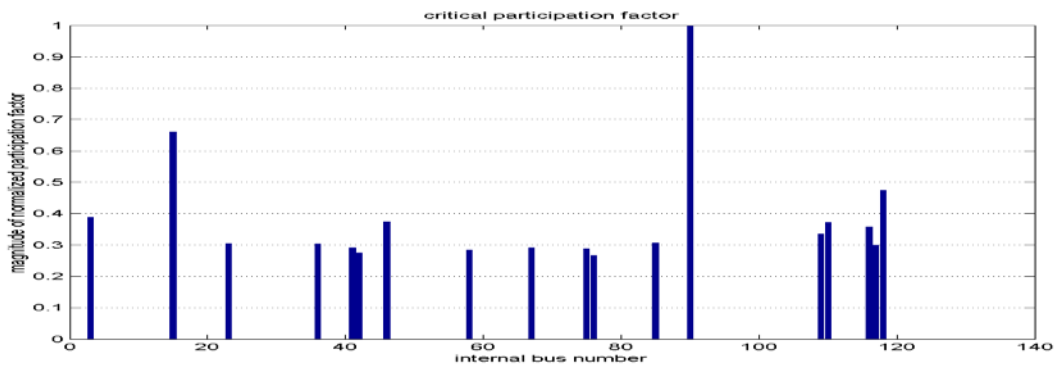


Figure D.36 Bus 110 “90” MW of Wind Injection at Bus # 110

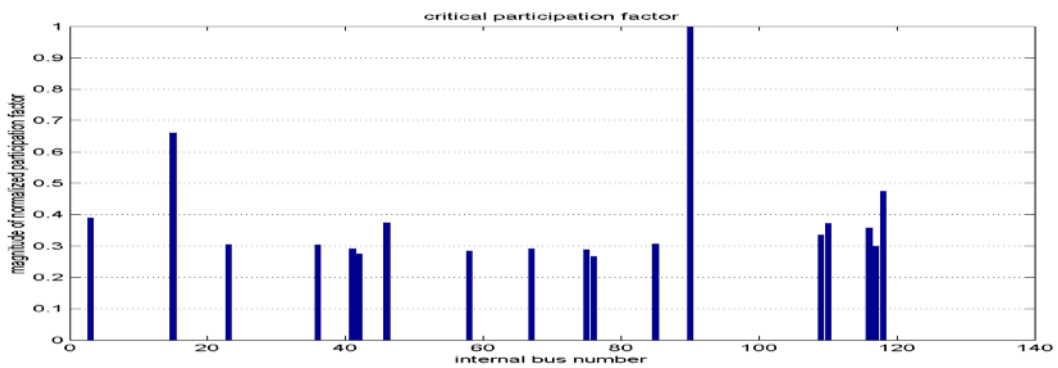


Figure D.37 Bus 110 “100” MW of Wind Injection at Bus # 110

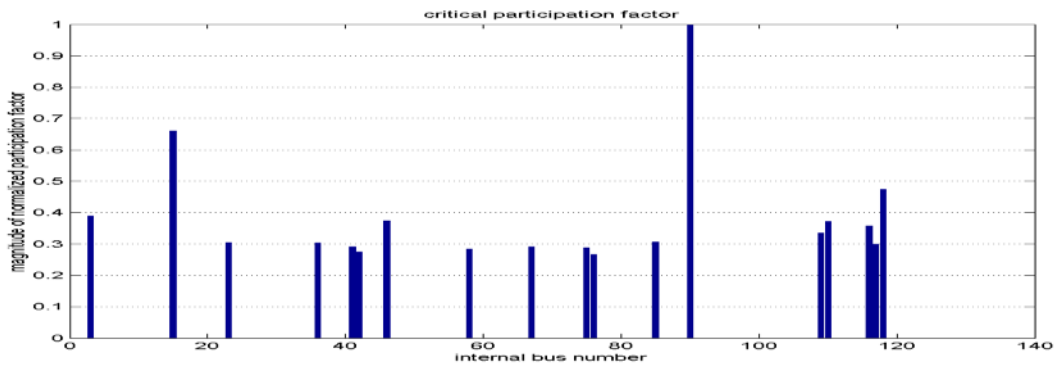
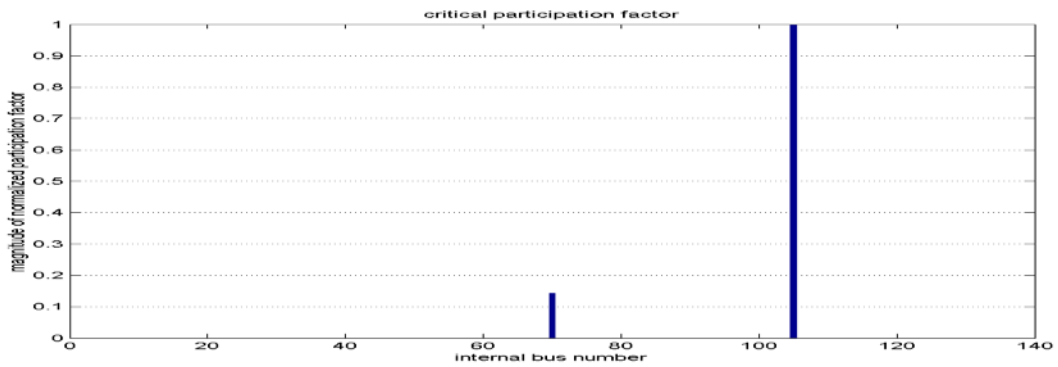


Figure D.38 Bus 110 “109” MW of Wind Injection at Bus # 110



Bus 119 Wind Injection

Figure D.39 Bus 119 “zero” MW of Wind Injection at Bus # 119

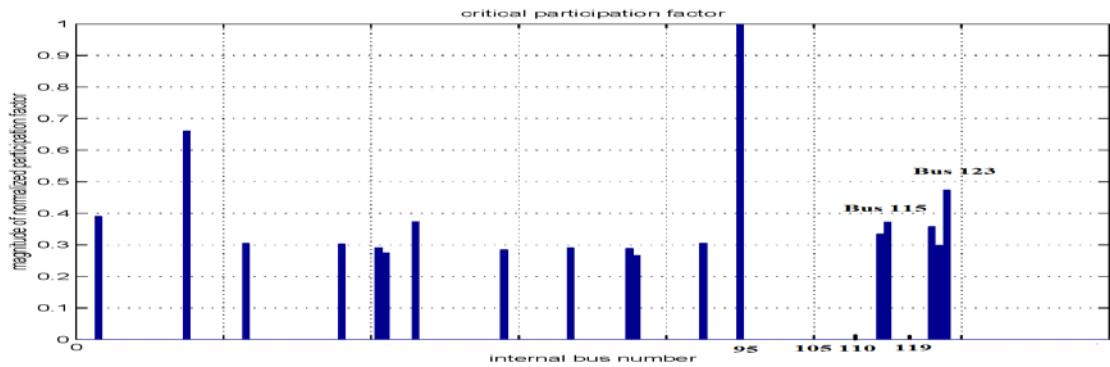


Figure D.40 Bus 119 “10” MW of Wind Injection at Bus # 119

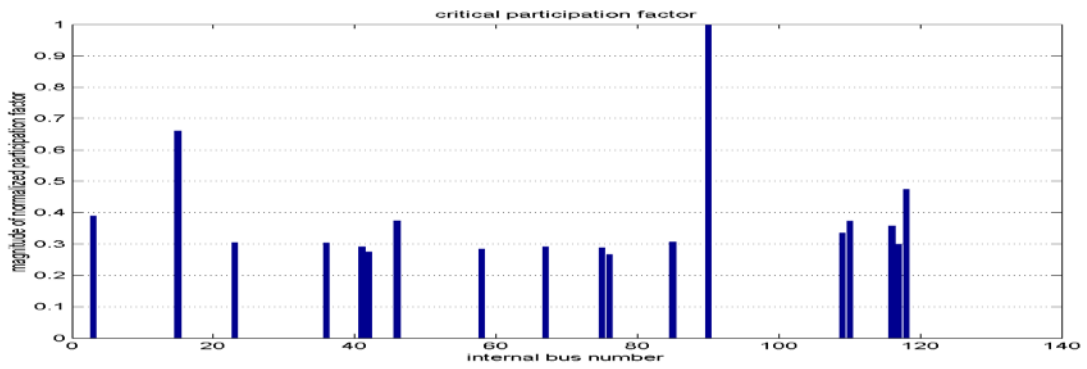


Figure D.41 Bus 119 “20” MW of Wind Injection at Bus # 119

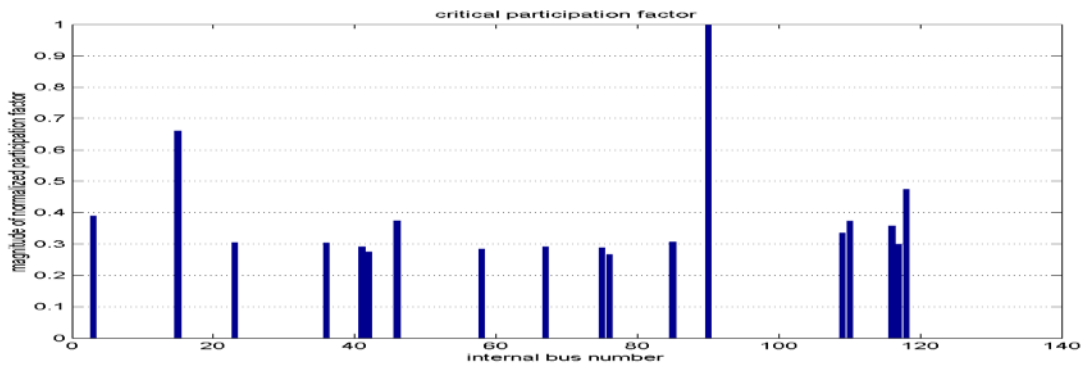


Figure D.42 Bus 119 “30” MW of Wind Injection at Bus # 119

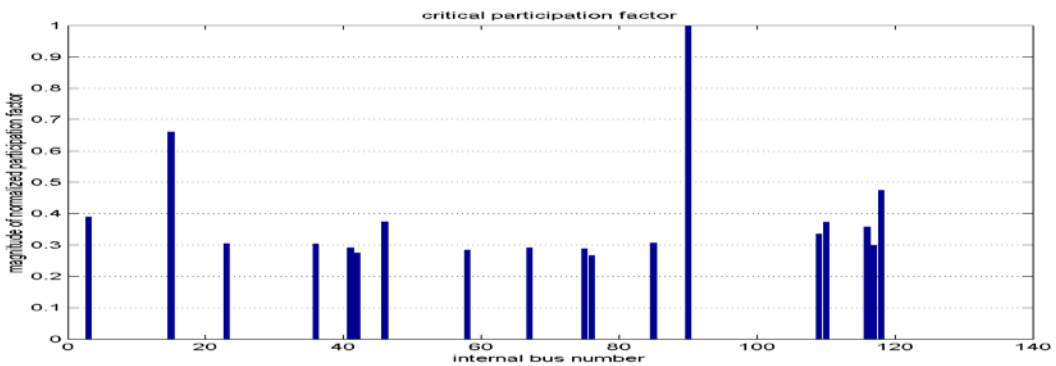


Figure D.43 Bus 119 “40” MW of Wind Injection at Bus # 119

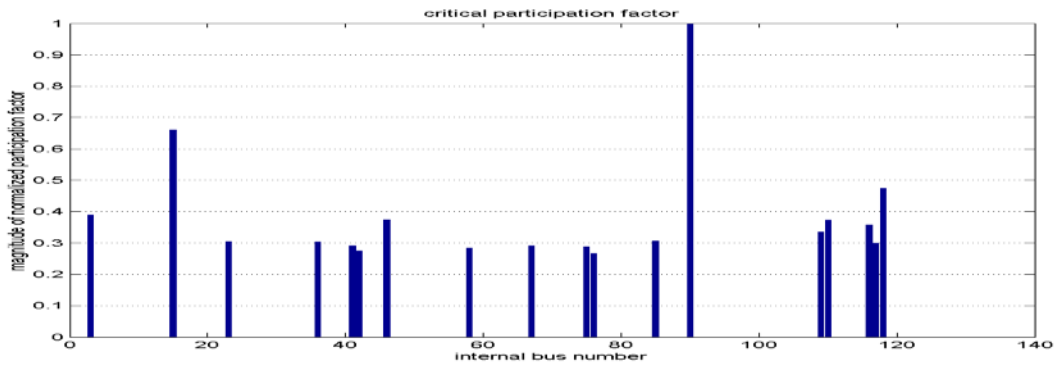


Figure D.44 Bus 119 “50” MW of Wind Injection at Bus # 119

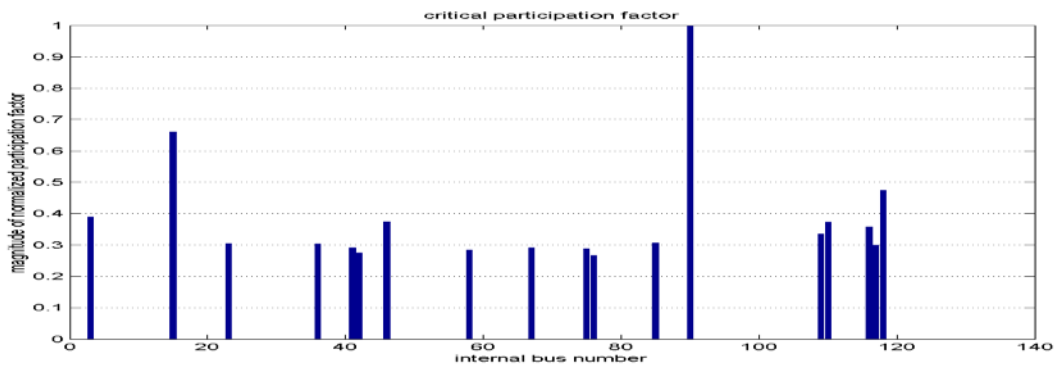


Figure D.45 Bus 119 “60” MW of Wind Injection at Bus # 119

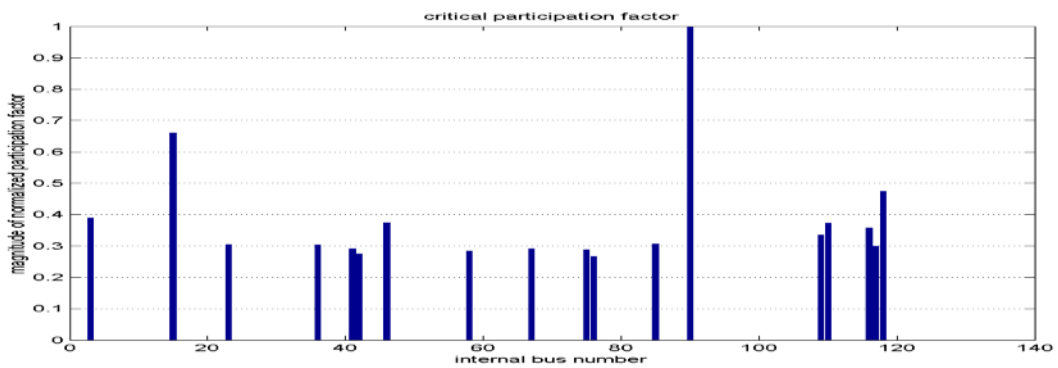


Figure D.46 Bus 119 “70” MW of Wind Injection at Bus # 119

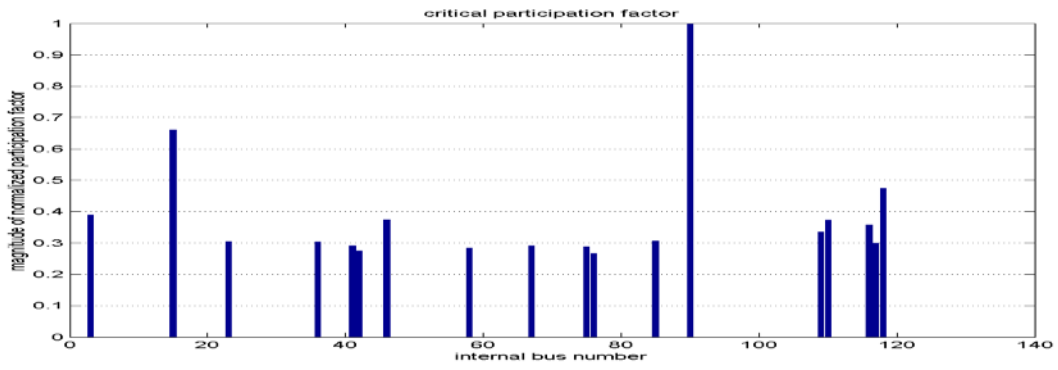


Figure D.47 Bus 119 “80” MW of Wind Injection at Bus # 119

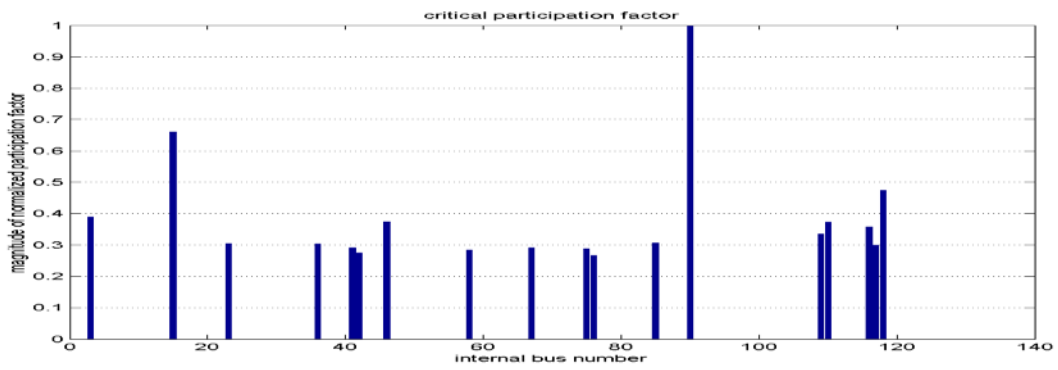


Figure D.48 Bus 119 “90” MW of Wind Injection at Bus # 119

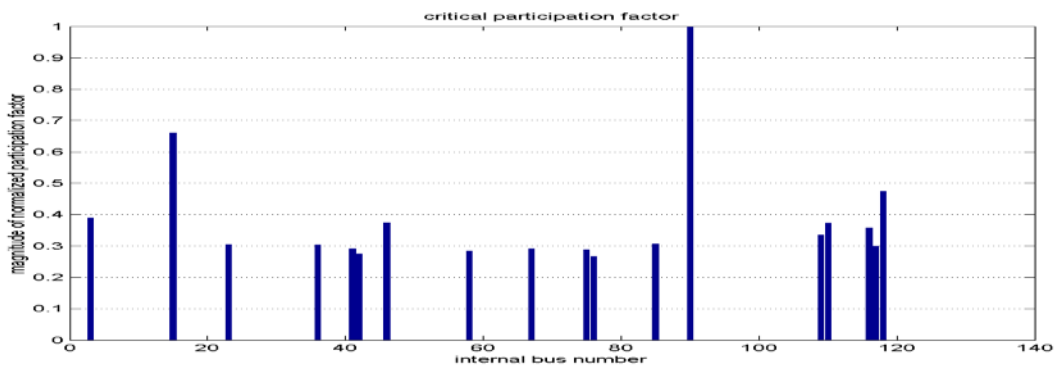


Figure D.49 Bus 119 “100” MW of Wind Injection at Bus # 119

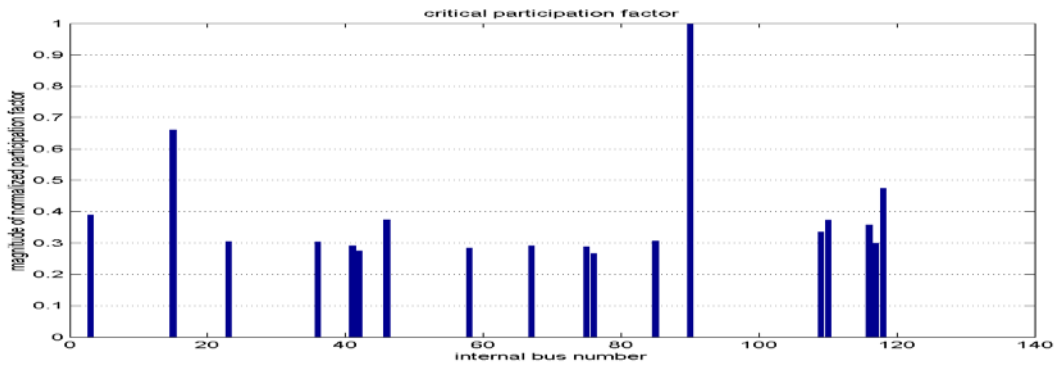


Figure D.50 Bus 119 “110” MW of Wind Injection at Bus # 119

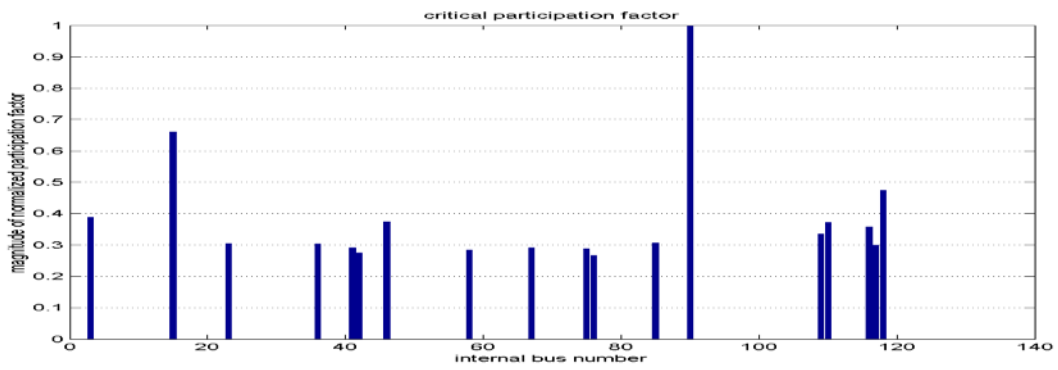


Figure D.51 Bus 119 “120” MW of Wind Injection at Bus # 119

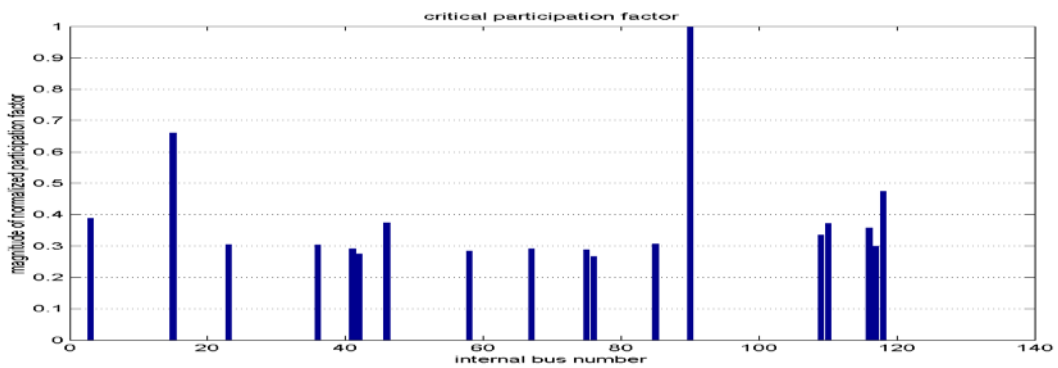


Figure D.52 Bus 119 “130” MW of Wind Injection at Bus # 119

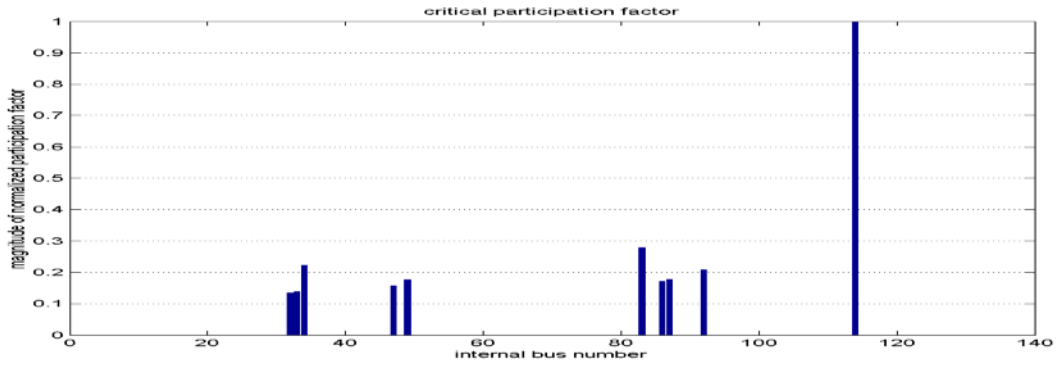
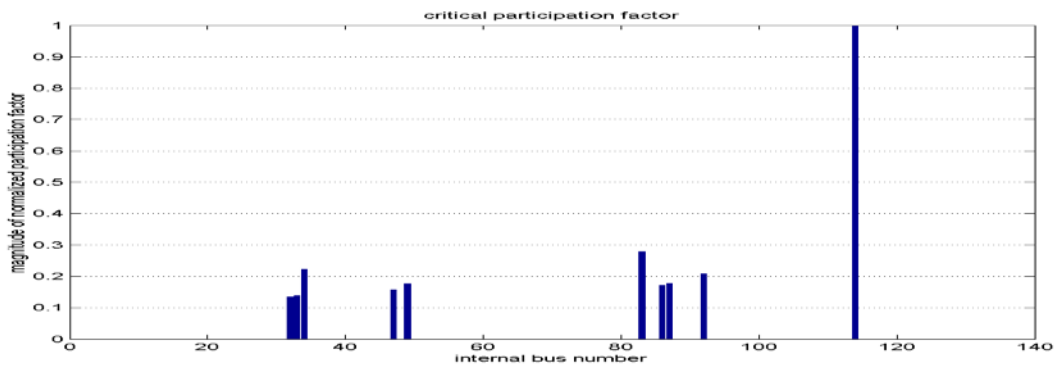


Figure D.53 Bus 119 “131” MW of Wind Injection at Bus # 119



Bus 105 Wind Injection

Figure D.54 Bus 105 “Zero” MW of Wind Injection at Bus # 105

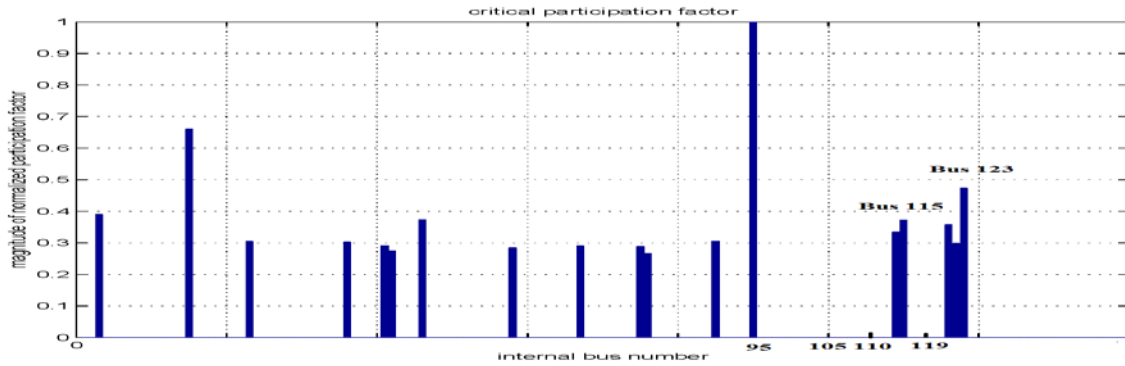


Figure D.55 Bus 105 “10” MW of Wind Injection at Bus # 105

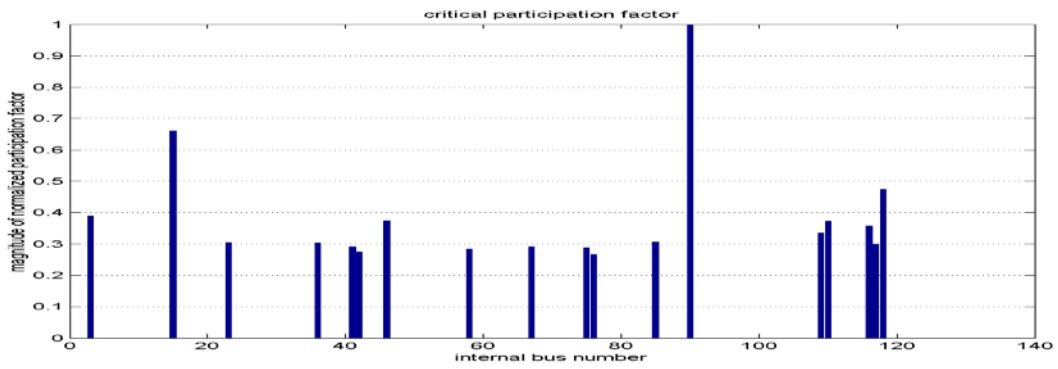


Figure D.56 Bus 105 “20” MW of Wind Injection at Bus # 105

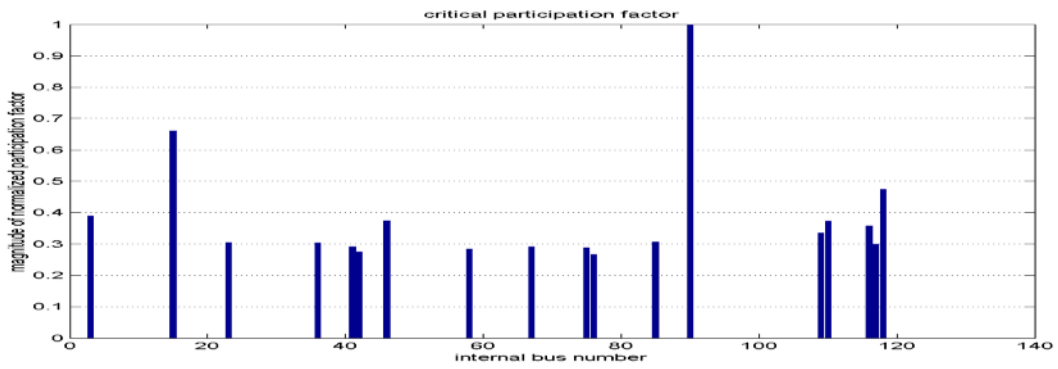


Figure D.57 Bus 105 “30” MW of Wind Injection at Bus # 105

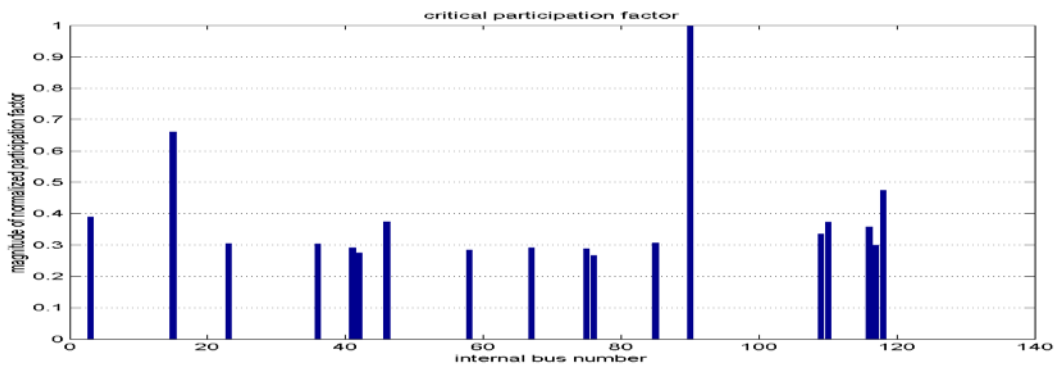


Figure D.58 Bus 105 “40” MW of Wind Injection at Bus # 105

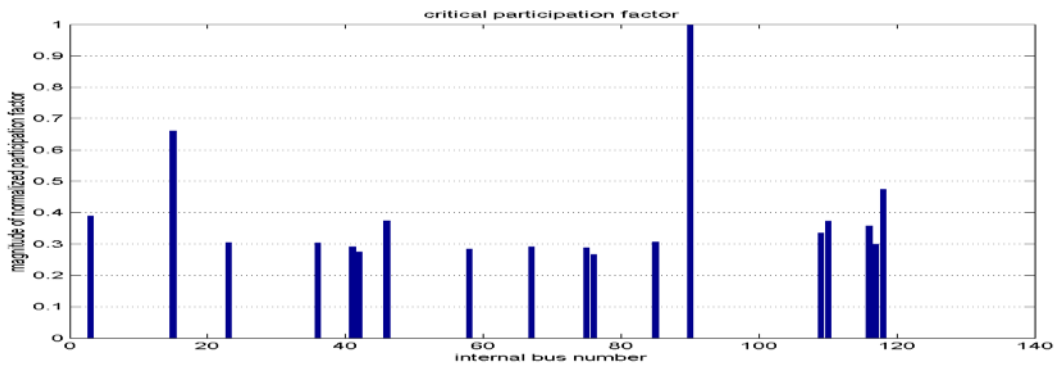


Figure D.59 Bus 105 “50” MW of Wind Injection at Bus # 105

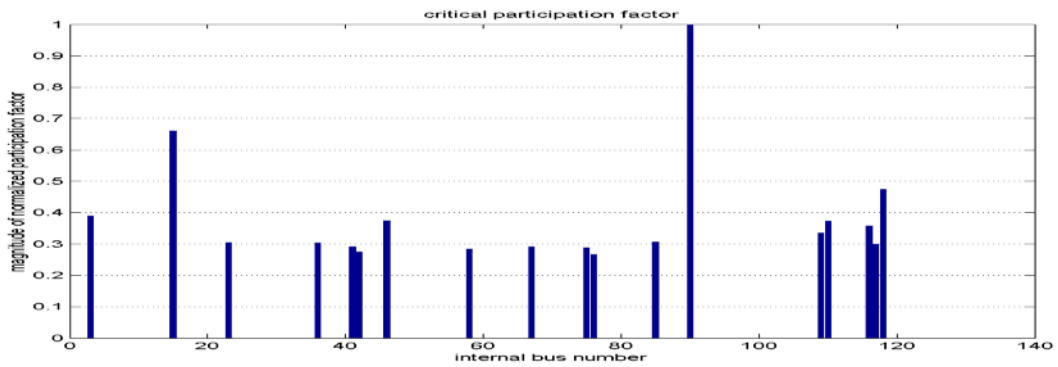


Figure D.60 Bus 105 “60” MW of Wind Injection at Bus # 105

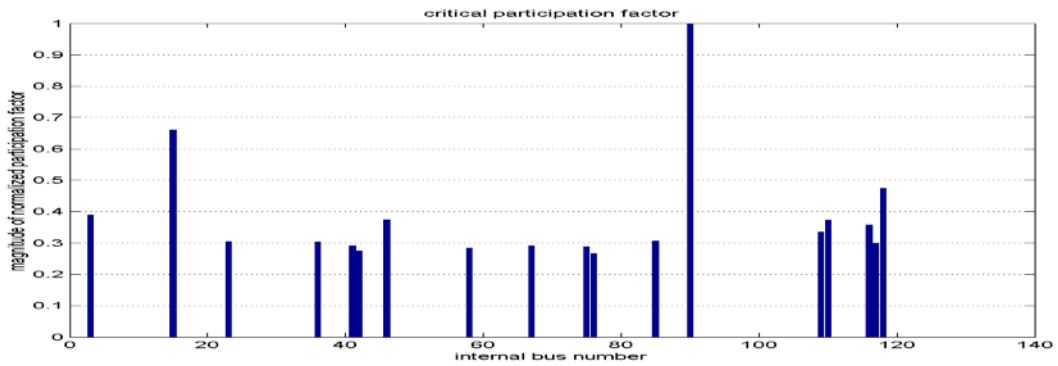


Figure D.61 Bus 105 “70” MW of Wind Injection at Bus # 105

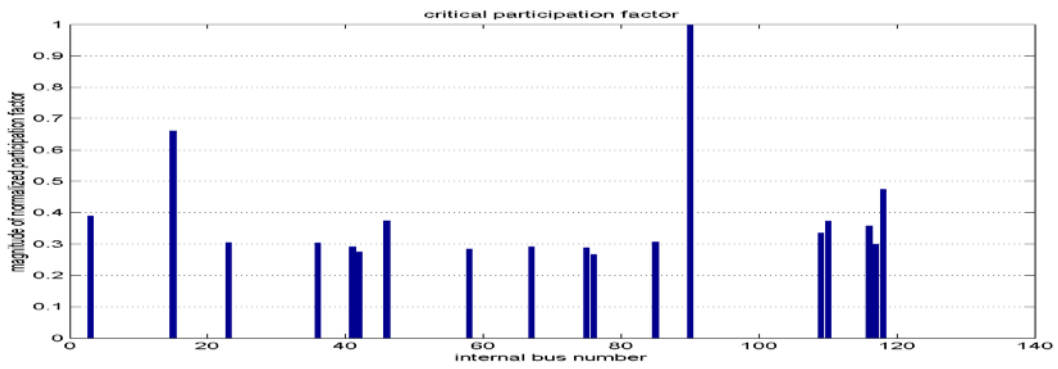


Figure D.62 Bus 105 “80” MW of Wind Injection at Bus # 105

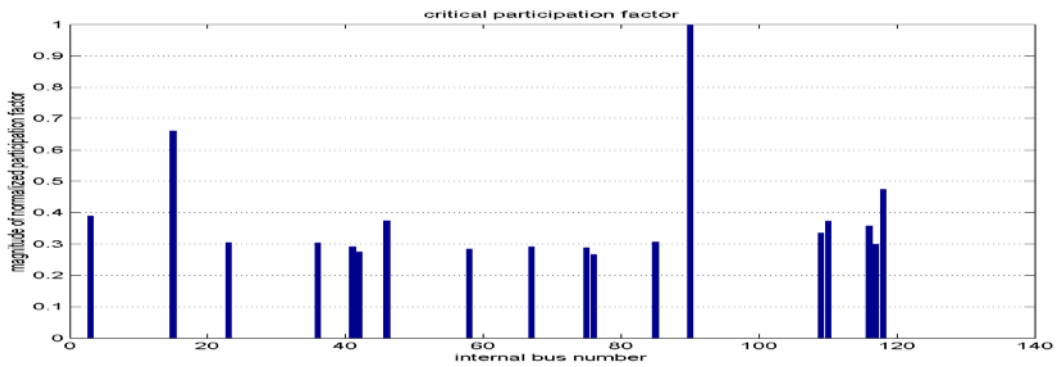


Figure D.63 Bus 105 “90” MW of Wind Injection at Bus # 105

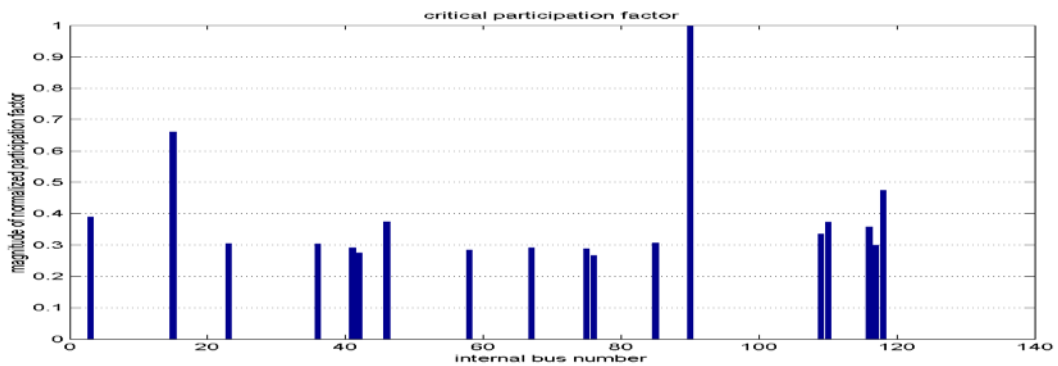


Figure D.64 Bus 105 “100” MW of Wind Injection at Bus # 105

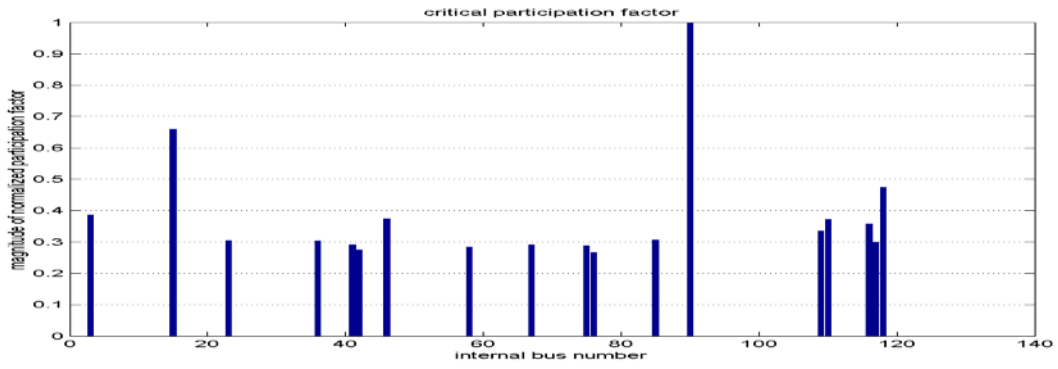


Figure D.65 Bus 105 “110” MW of Wind Injection at Bus # 105

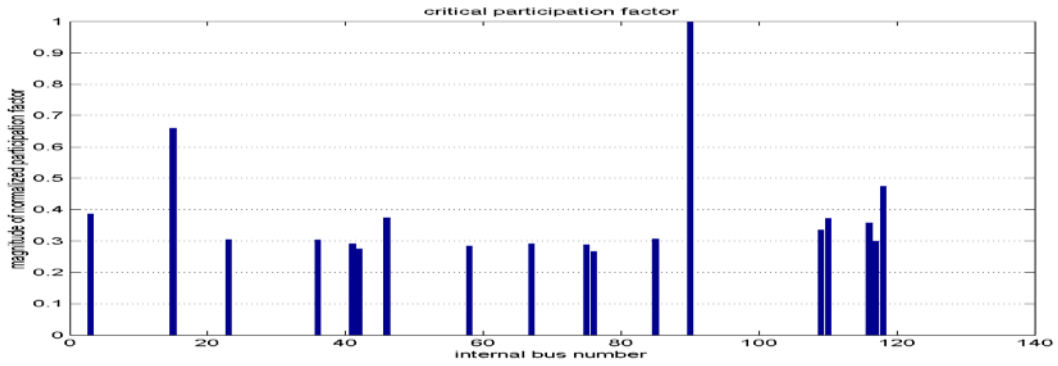


Figure D.66 Bus 105 “120” MW of Wind Injection at Bus # 105

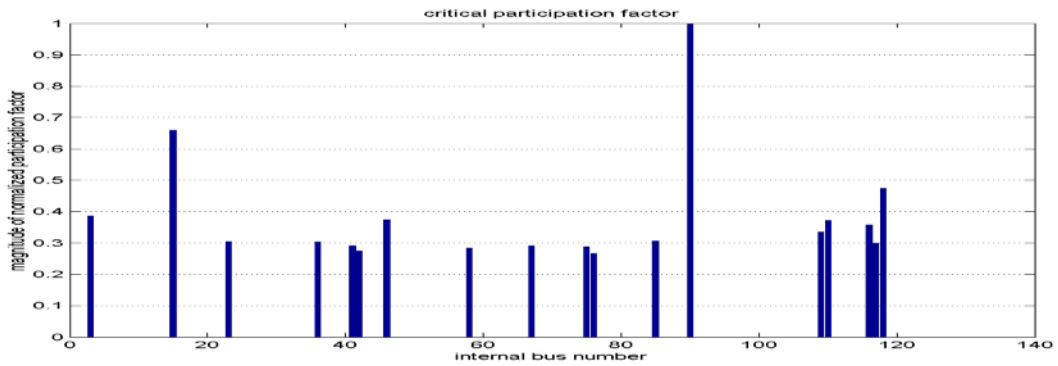


Figure D.67 Bus 105 “130” MW of Wind Injection at Bus # 105

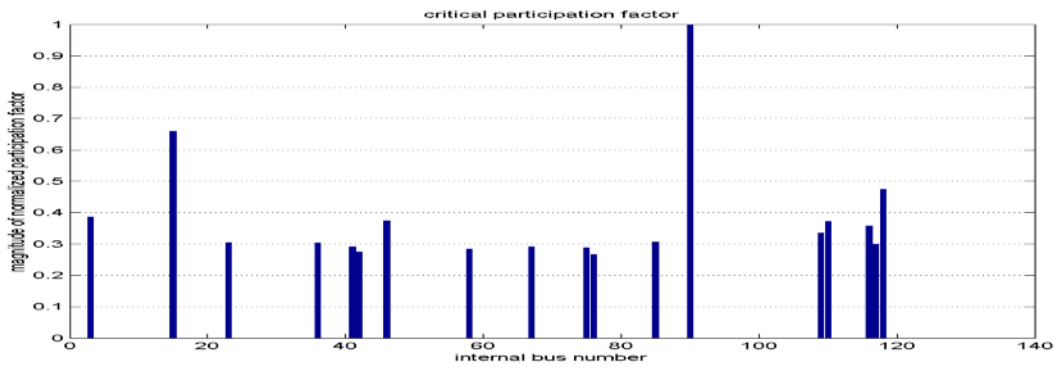


Figure D.68 Bus 105 “140” MW of Wind Injection at Bus # 105

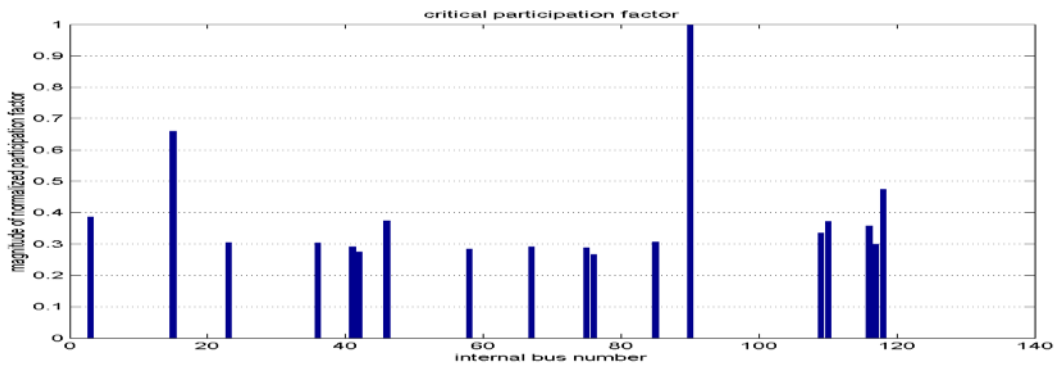


Figure D.69 Bus 105 “150” MW of Wind Injection at Bus # 105

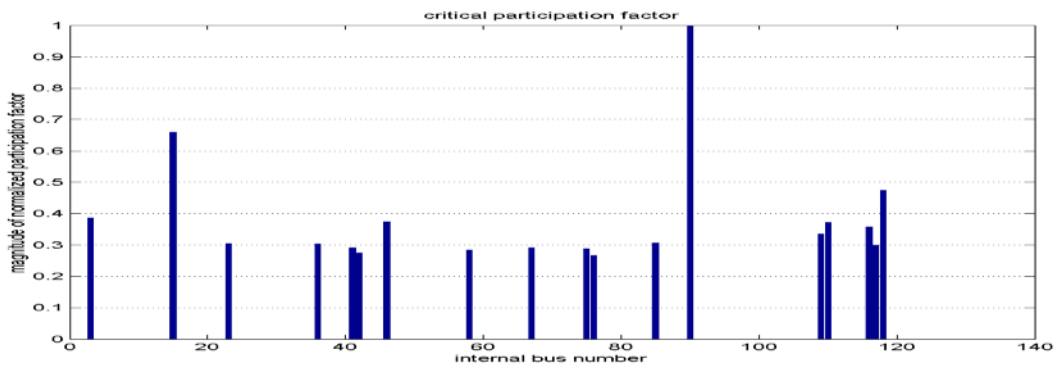
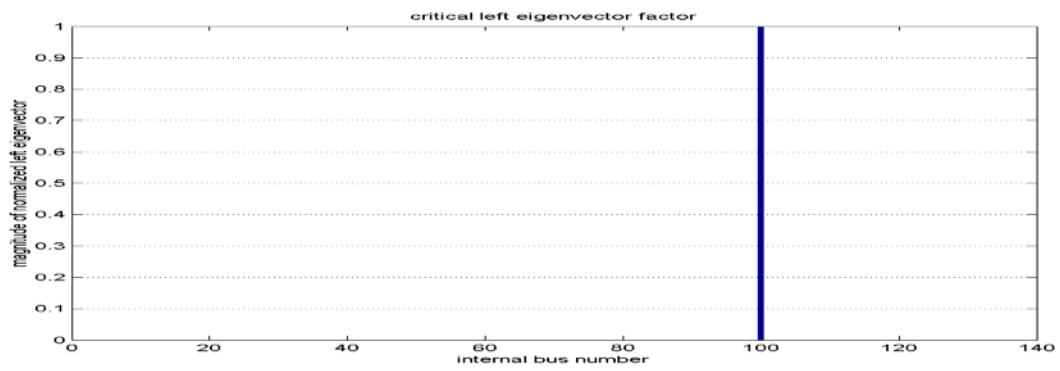


Figure D.70 Bus 105 “156” MW of Wind Injection at Bus # 105



**D.2 Additional Results of Simulation of System Critical Eigenvalue and
“Normalized” Participation Factors for the 3-Weak Bus Combination Wind
Injections Using DFIG Wind Turbine Type**

Figure D.71 Combined Wind Injection from Buses 95-115-123 “Zero” MW of Wind Injection

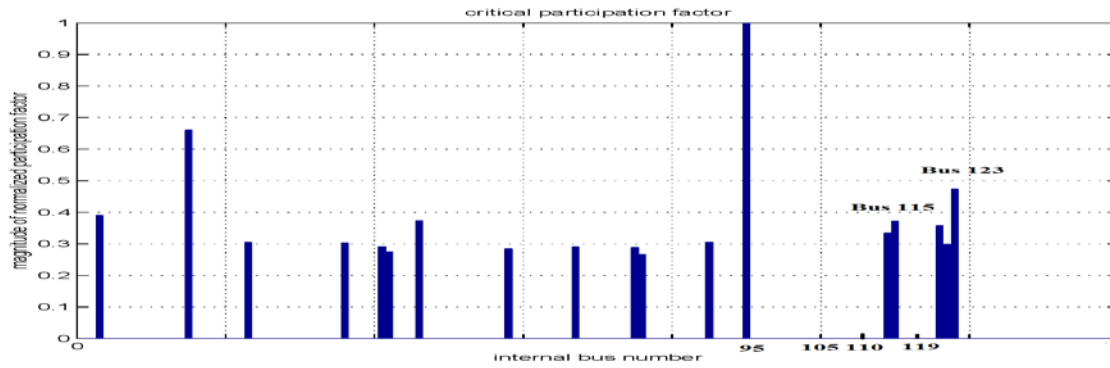


Figure D.72 Combined Wind Injection from Buses 95-115-123 “30” MW of Wind Injection

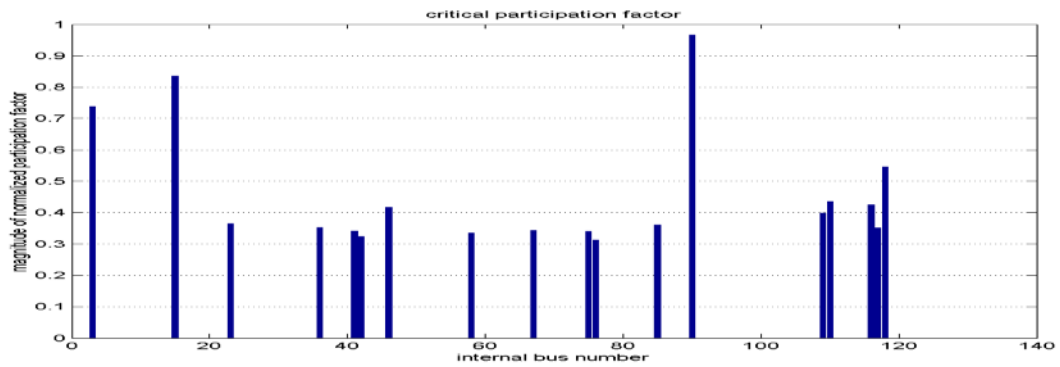


Figure D.73 Combined Wind Injection from Buses 95-115-123 “60” MW of Wind Injection

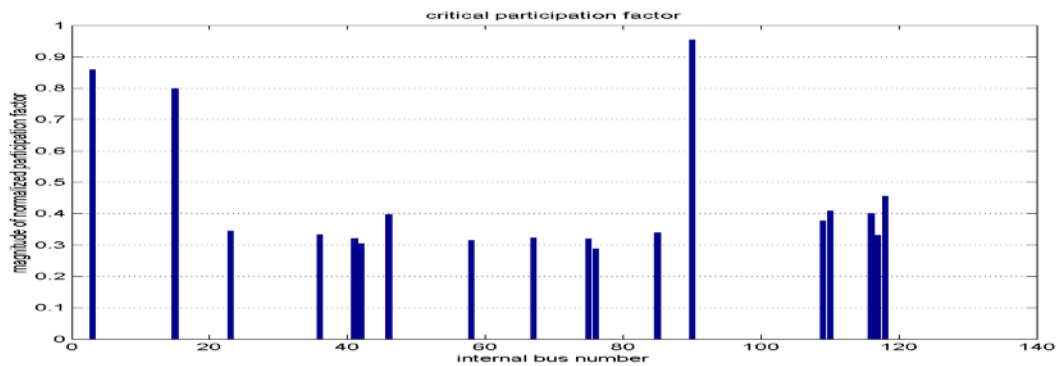


Figure D.74 Combined Wind Injection from Buses 95-115-123 “90” MW of Wind Injection

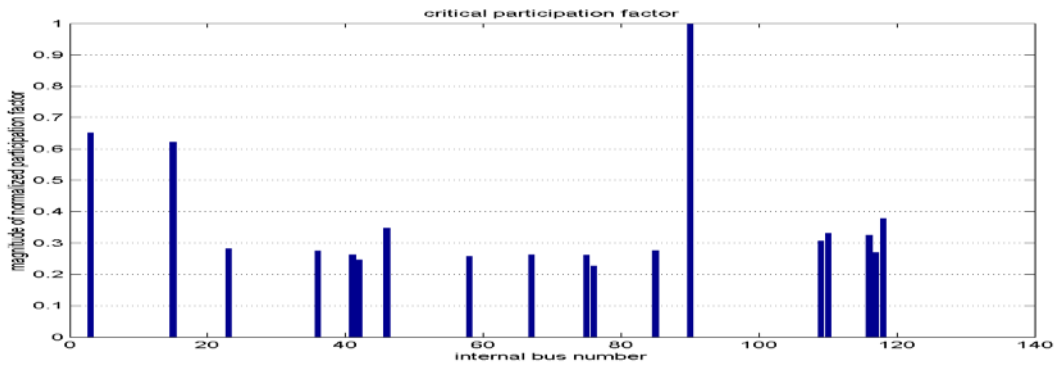


Figure D.75 Combined Wind Injection from Buses 95-115-123 “120” MW of Wind Injection

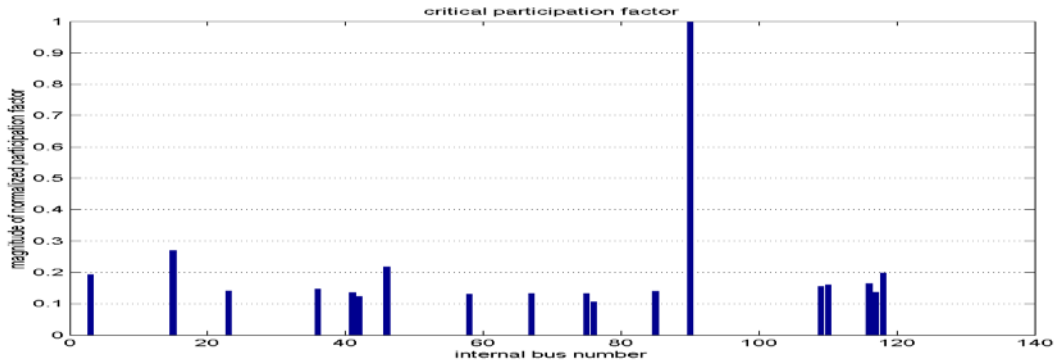


Figure D.76 Combined Wind Injection from Buses 95-115-123 “123” MW of Wind Injection

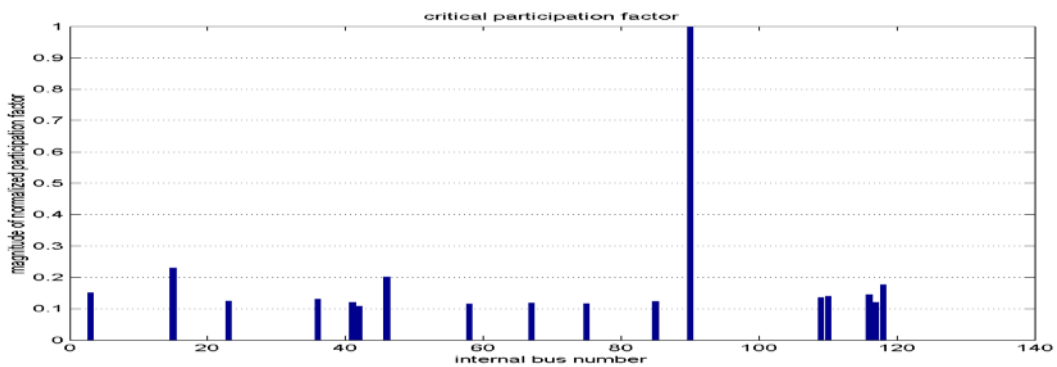


Figure D.77 Combined Wind Injection from Buses 95-115-123 “126” MW of Wind Injection

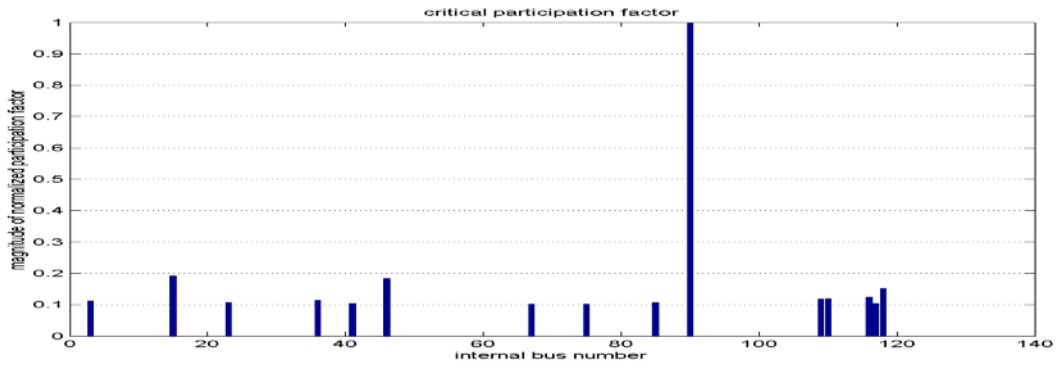
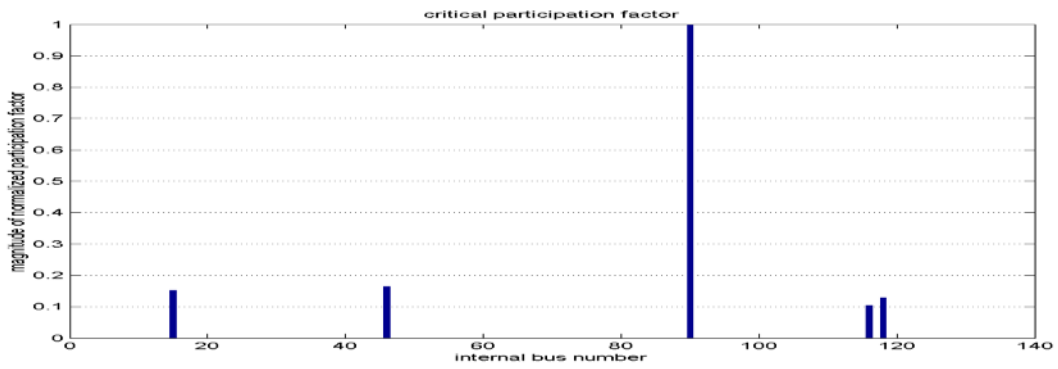


Figure D.78 Combined Wind Injection from Buses 95-115-123 “129” MW of Wind Injection



**D.3 Additional Results of Simulation of System Critical Eigenvalue and
“Normalized” Participation Factors for the 3-Strong Bus Combination Wind
Injections Using DFIG Wind Turbine Type**

Figure D.79 Combined Wind Injection from Buses 105-110-119 “Zero” MW of Wind Injection

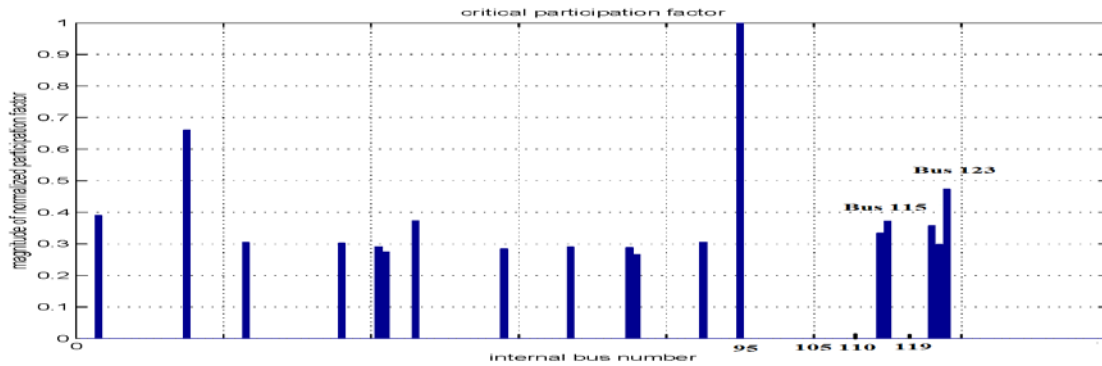


Figure D.80 Combined Wind Injection from Buses 105-110-119 “30” MW of Wind Injection

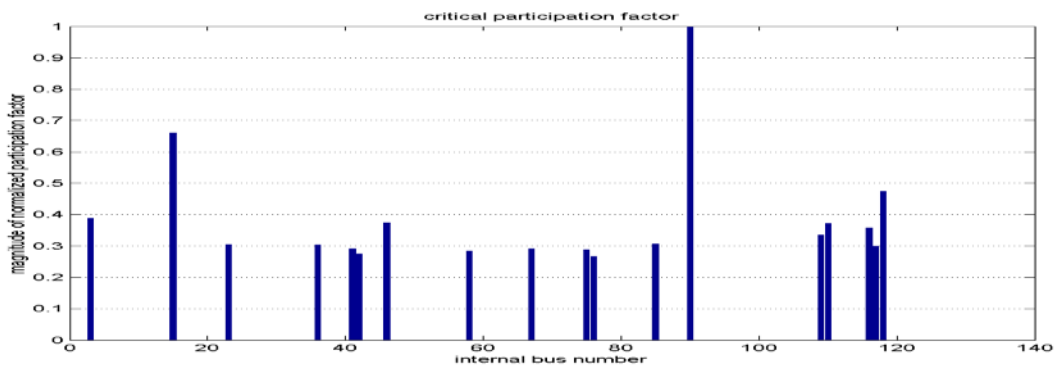


Figure D.81 Combined Wind Injection from Buses 105-110-119 “60” MW of Wind Injection

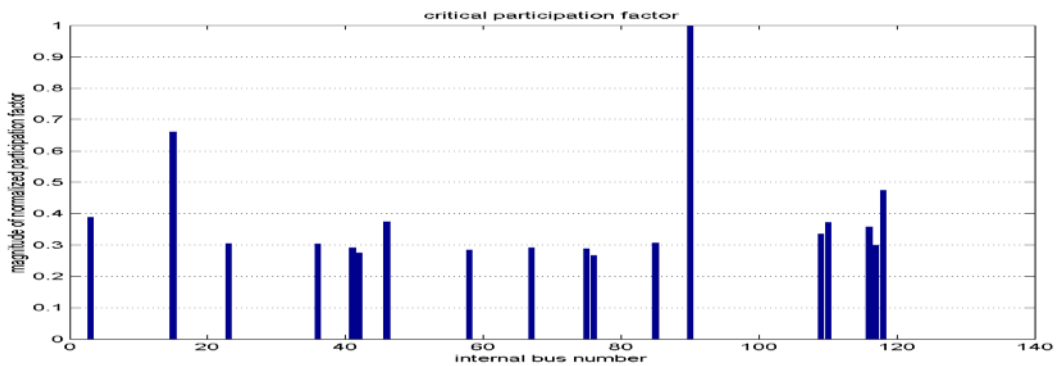


Figure D.82 Combined Wind Injection from Buses 105-110-119 “90” MW of Wind Injection

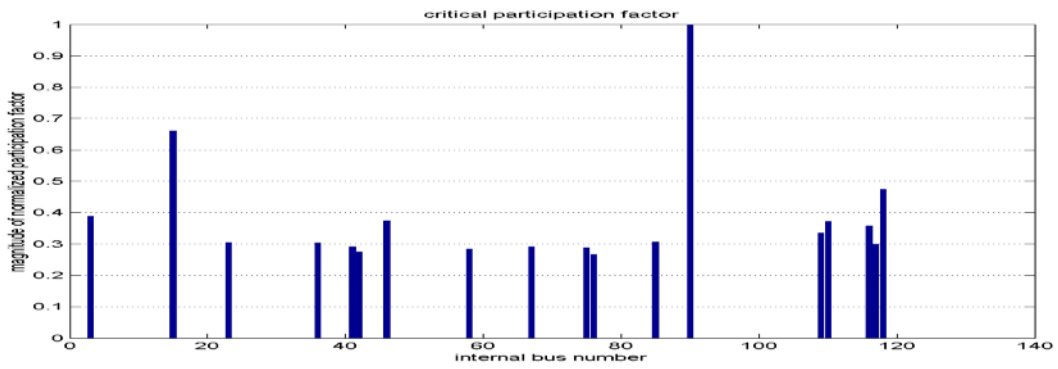


Figure D.83 Combined Wind Injection from Buses 105-110-119 “120” MW of Wind Injection

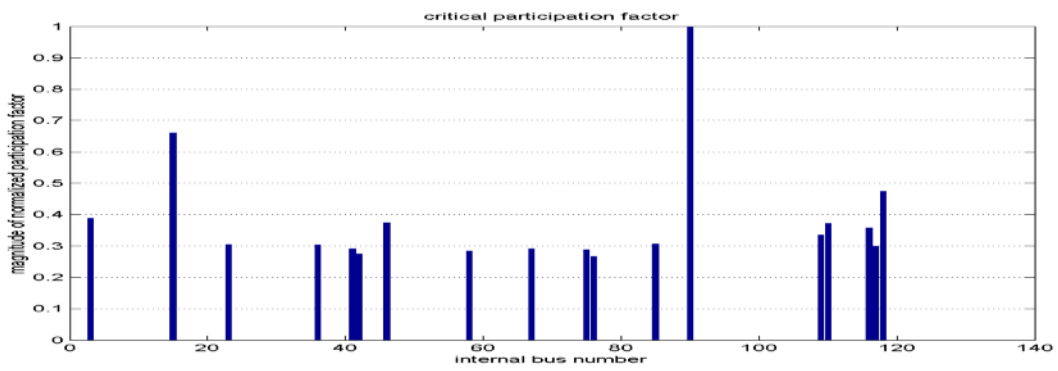


Figure D.84 Combined Wind Injection from Buses 105-110-119 “150” MW of Wind Injection

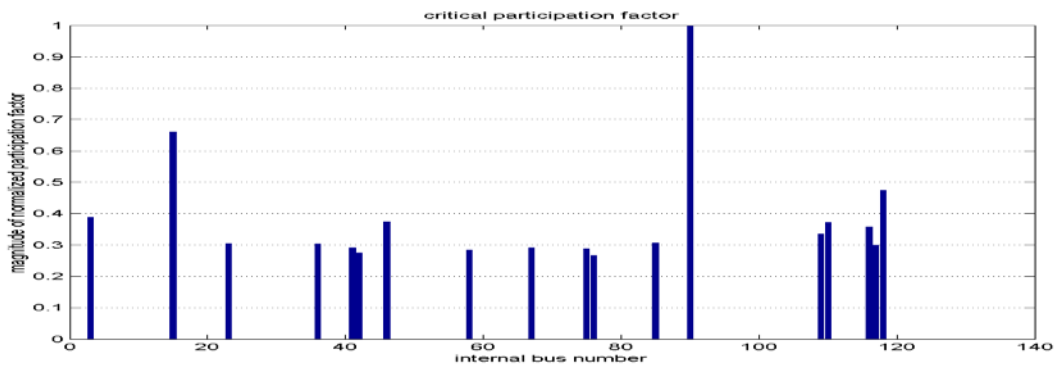


Figure D.85 Combined Wind Injection from Buses 105-110-119 “180” MW of Wind Injection

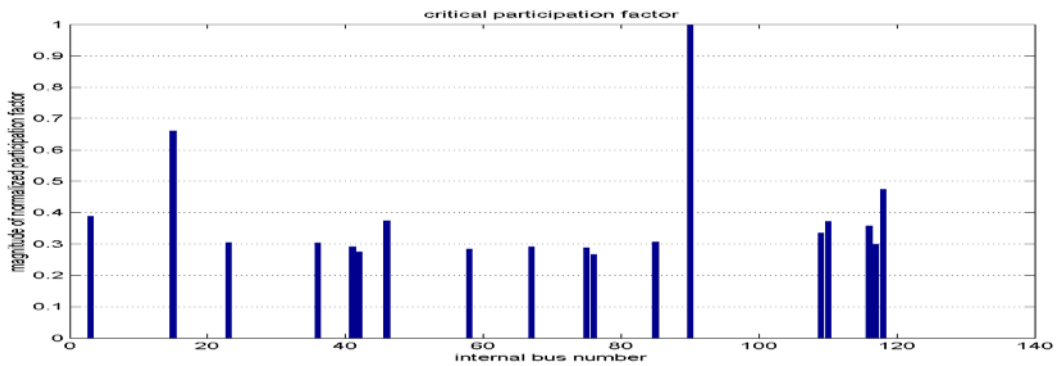


Figure D.86 Combined Wind Injection from Buses 105-110-119 “210” MW of Wind Injection

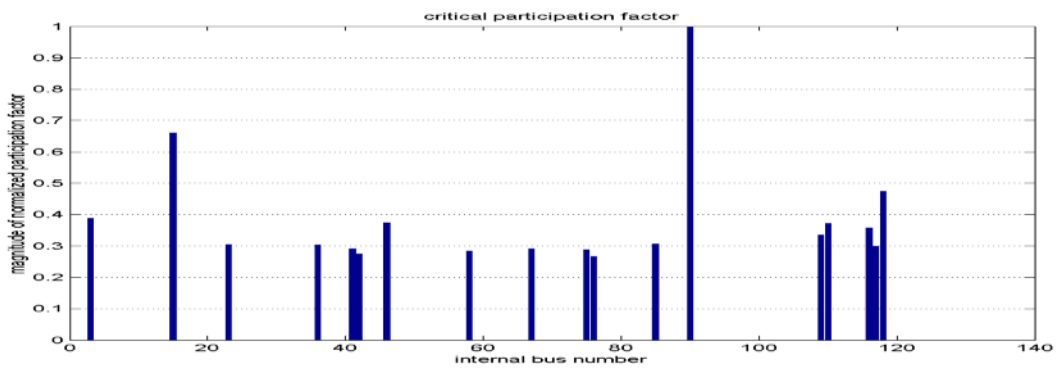


Figure D.87 Combined Wind Injection from Buses 105-110-119 “240” MW of Wind Injection

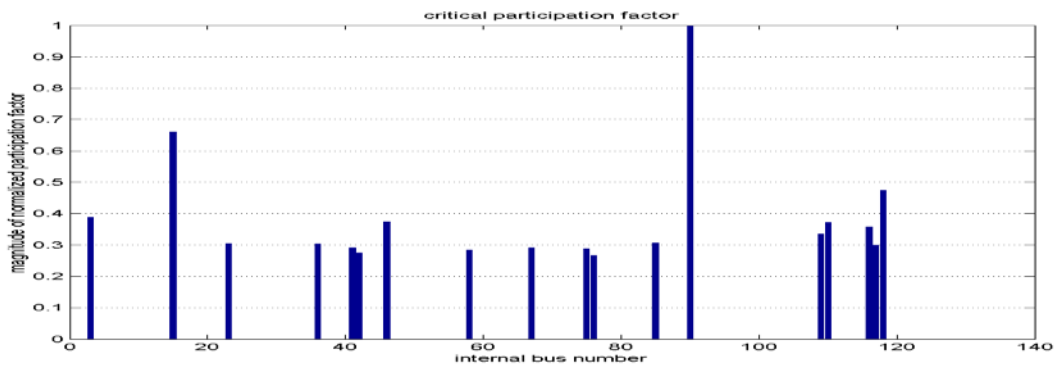


Figure D.88 Combined Wind Injection from Buses 105-110-119 “270” MW of Wind Injection

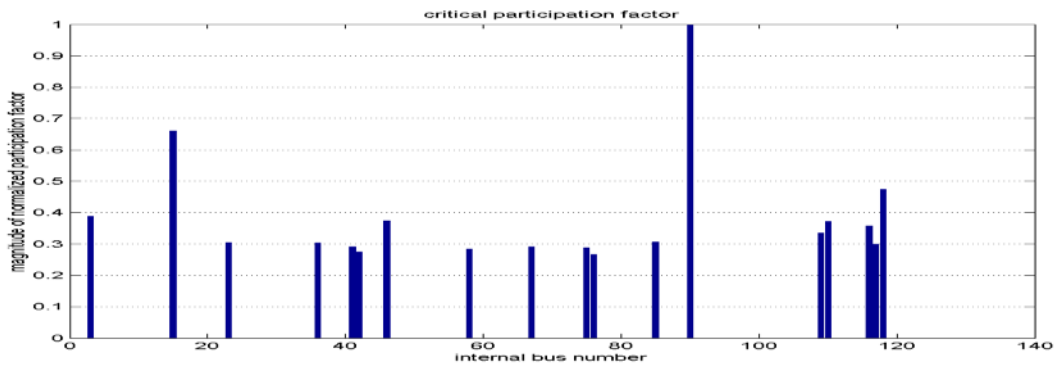


Figure D.89 Combined Wind Injection from Buses 105-110-119 “300” MW of Wind Injection

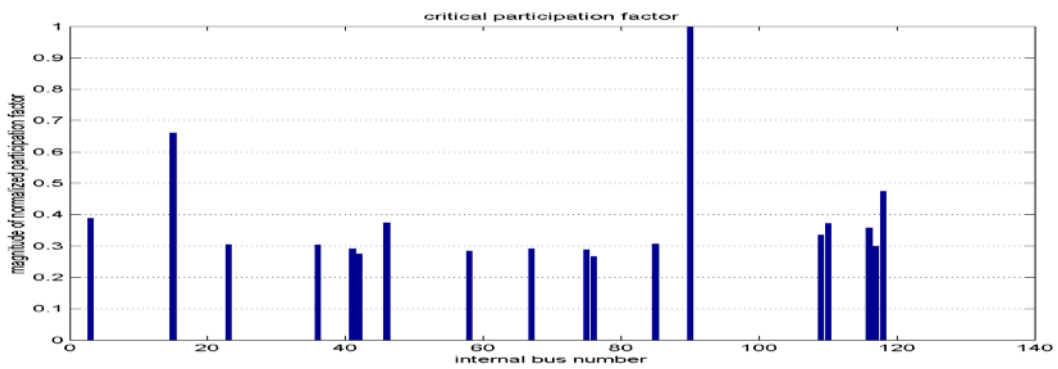
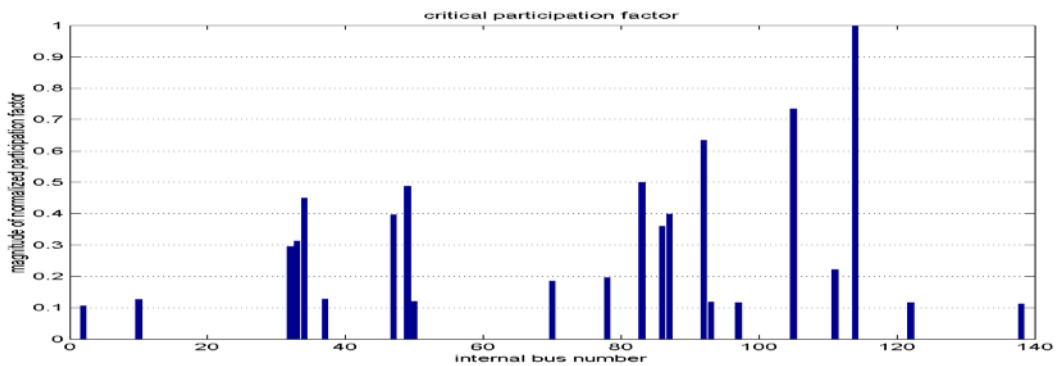


Figure D.90 Combined Wind Injection from Buses 105-110-119 “321” MW of Wind Injection



**D.4 Additional Results of Simulation of System Critical Eigenvalue and
“Normalized” Participation Factors for the 3-Strong Bus Combination Wind
Injections Using DFIG Wind Turbine Type and Using SVCs to Increase Wind
Penetration**

Figure D.91 Combined Wind Injection from Buses 105-110-119 “321” MW of Wind Injection “Bus with Highest Participation Factor is Bus Number 119”

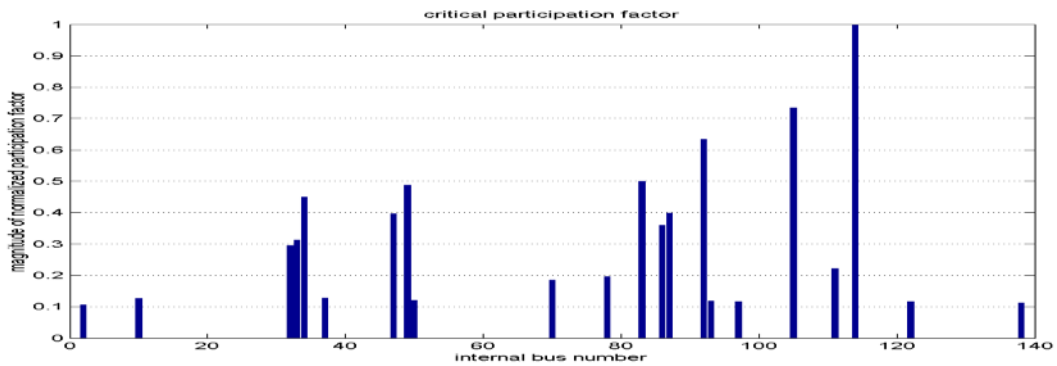


Figure D.92 Combined Wind Injection from Buses 105-110-119 “330” MW of Wind Injection “Bus with Highest Participation Factor is Bus Number 110”

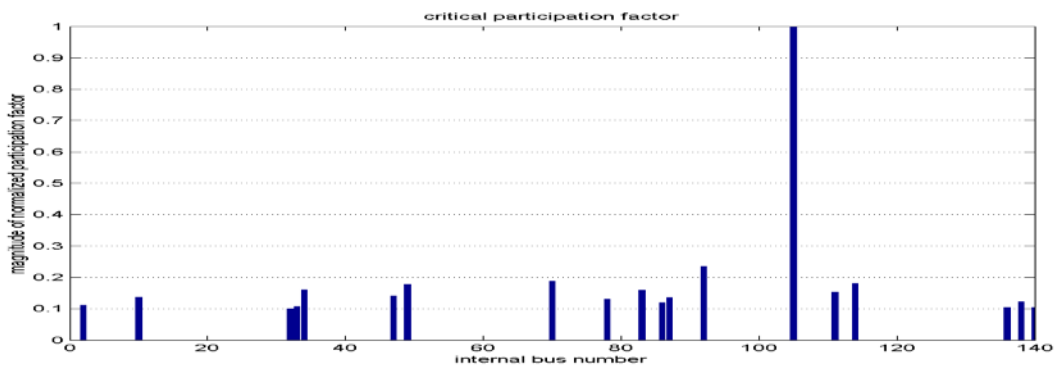


Figure D.93 Combined Wind Injection from Buses 105-110-119 “360” MW of Wind Injection “Bus with Highest Participation Factor is Bus Number 95”

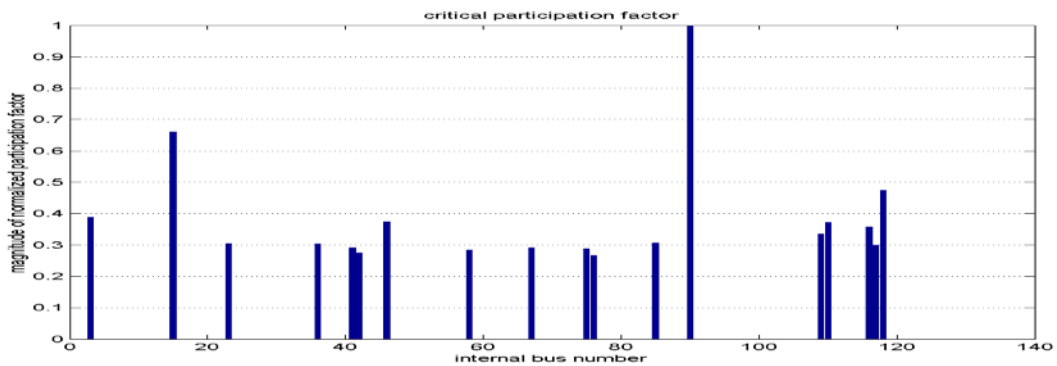


Figure D.94 Combined Wind Injection from Buses 105-110-119 “390” MW of Wind Injection “Bus with Highest Participation Factor is Bus Number 97”

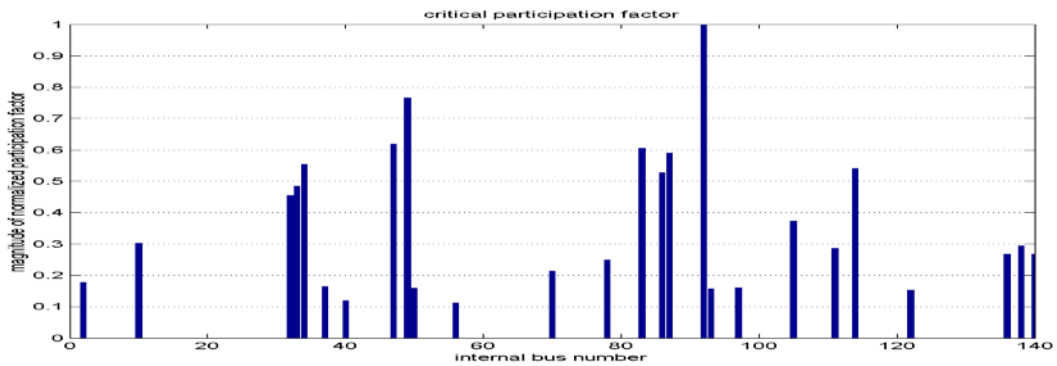
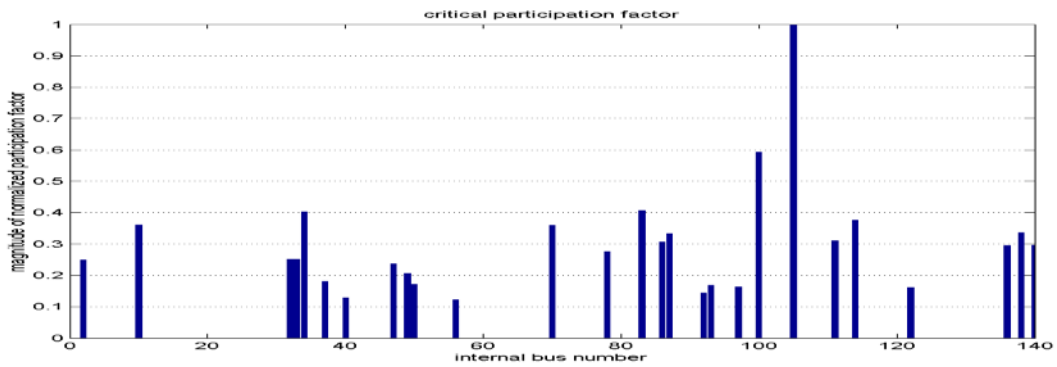


Figure D.95 Combined Wind Injection from Buses 105-110-119 “410” MW of Wind Injection “Bus with Highest Participation Factor is Bus Number 110”



**D.5 Sample of Additional Results of Simulation of System Critical Eigenvalue
and “Normalized” Participation Factors for Individual Bus Wind Injections
Using SCIG Wind Turbine Type**

Bus 95 Wind Injection

Figure D.96 Bus 95 “Zero” MW of Wind Injection at Bus # 95

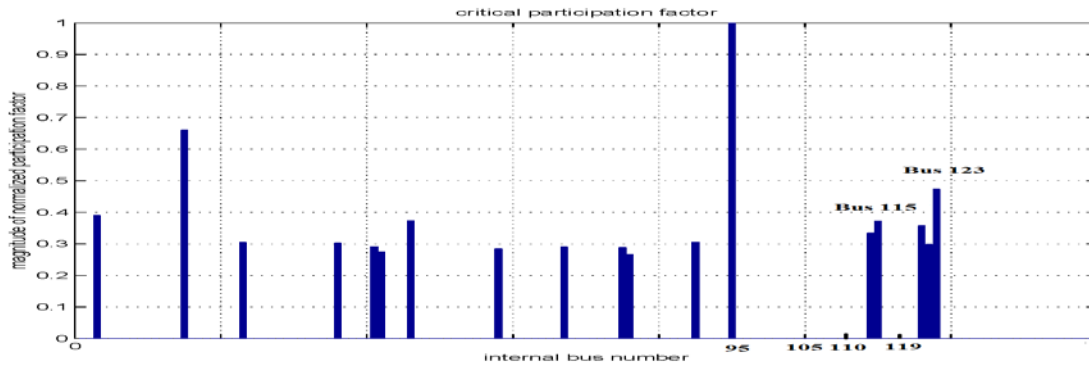


Figure D.97 Bus 95 “20” MW of Wind Injection at Bus # 95

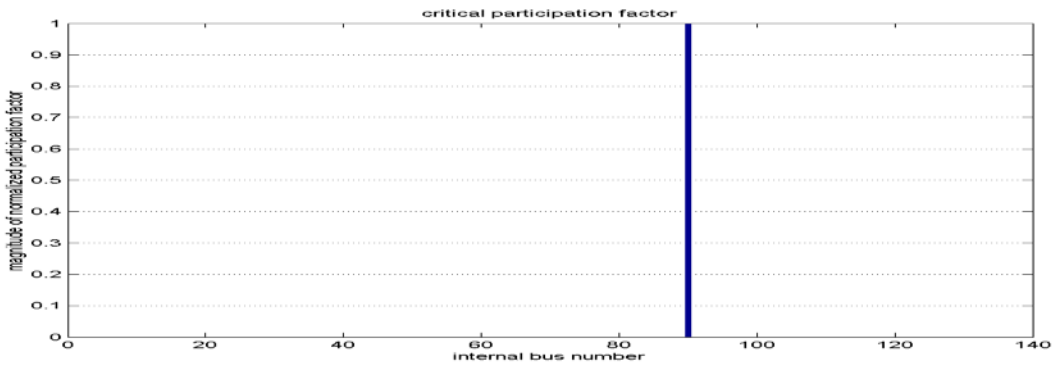
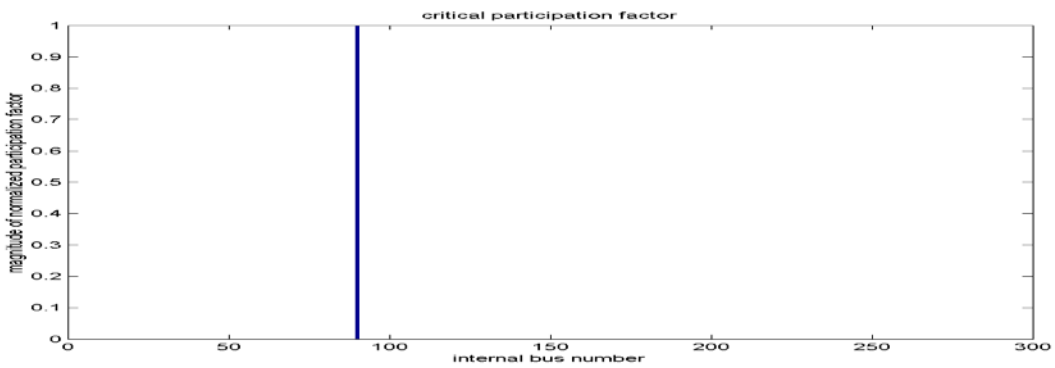


Figure D.98 Bus 95 “25” MW of Wind Injection at Bus # 95



Bus 115 Wind Injection

Figure D.99 Bus 115 “20” MW of Wind Injection at Bus # 115

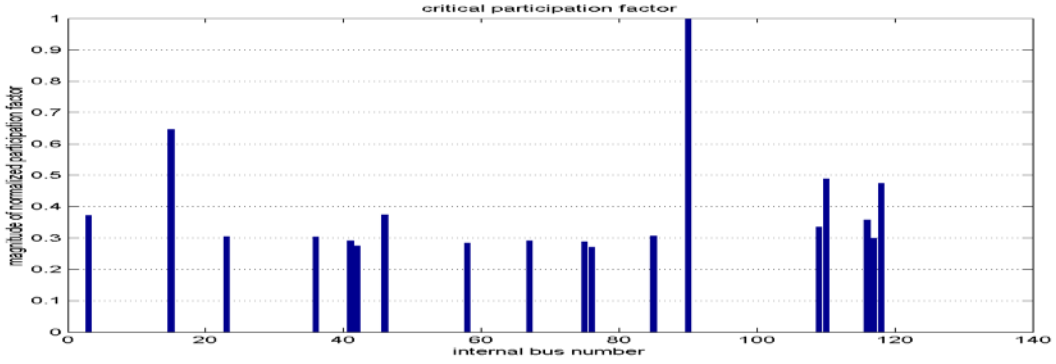


Figure D.100 Bus 115 “40” MW of Wind Injection at Bus # 115

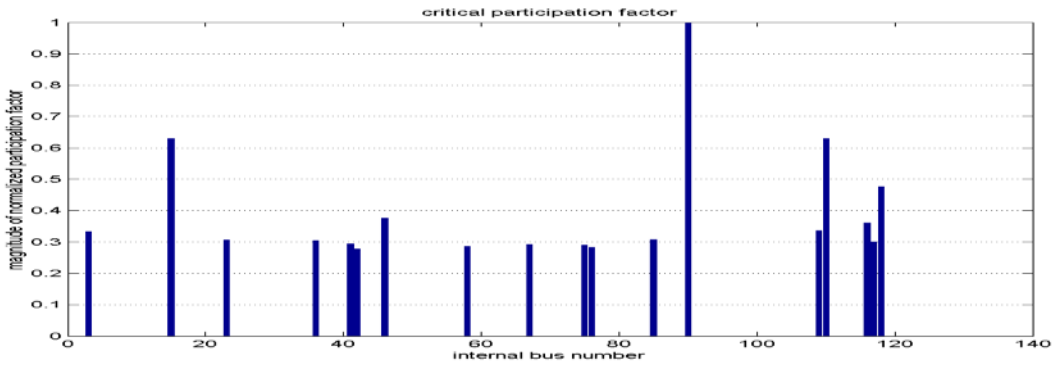


Figure D.101 Bus 115 “50” MW of Wind Injection at Bus # 115

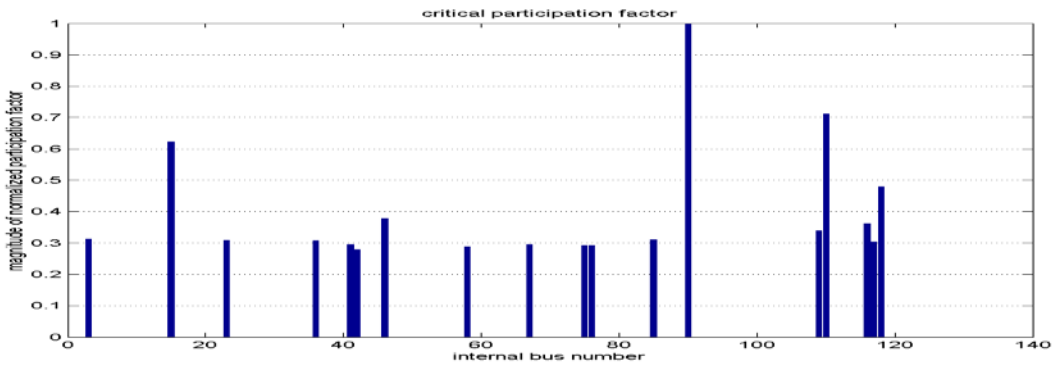


Figure D.102 Bus 115 “60” MW of Wind Injection at Bus # 115

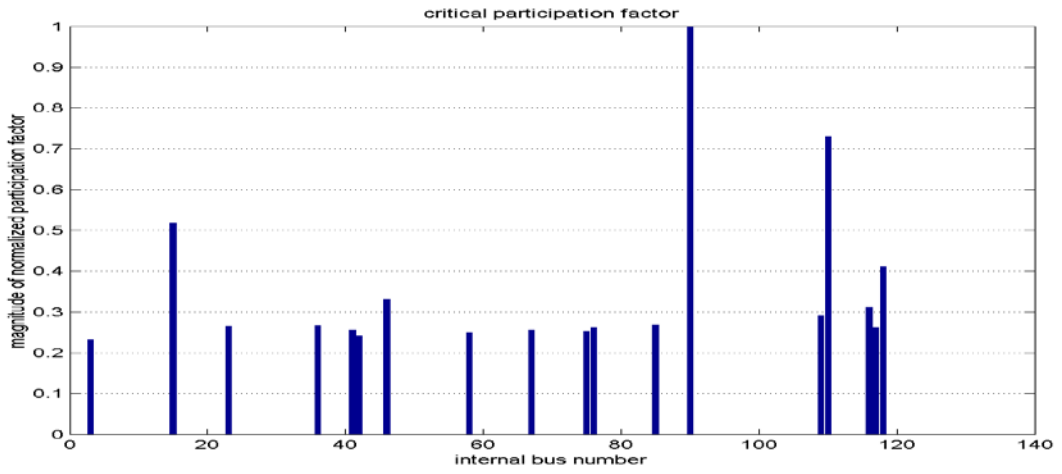
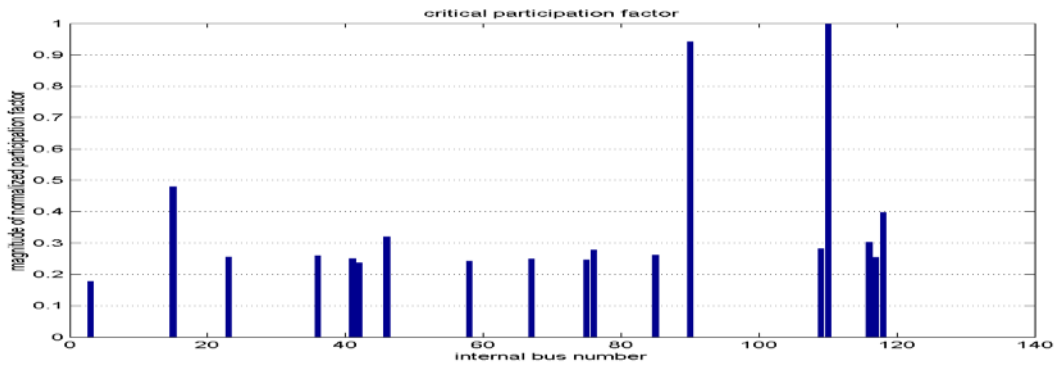


Figure D.103 Bus 115 “65” MW of Wind Injection at Bus # 115



Bus 123 Wind Injection

Figure D.104 Bus 123 “20” MW of Wind Injection at Bus # 123

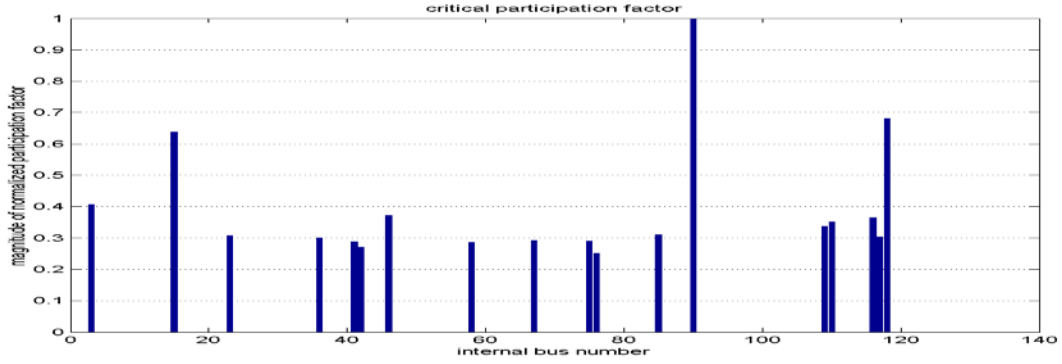


Figure D.105 Bus 123 “40” MW of Wind Injection at Bus # 123

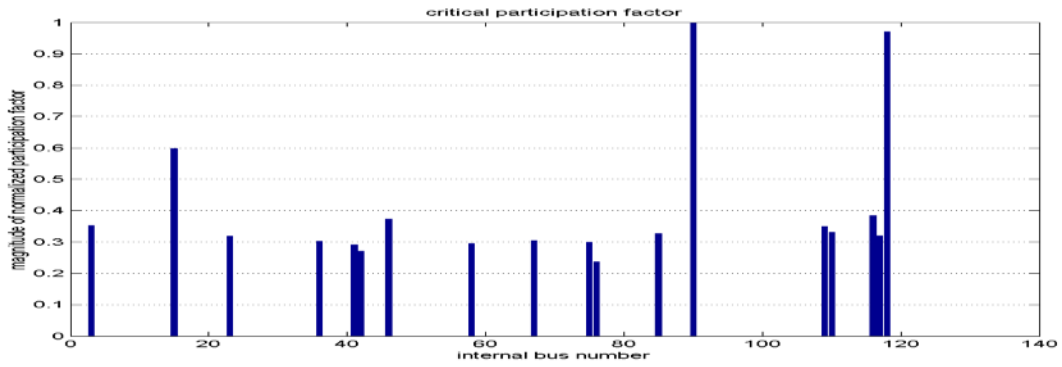
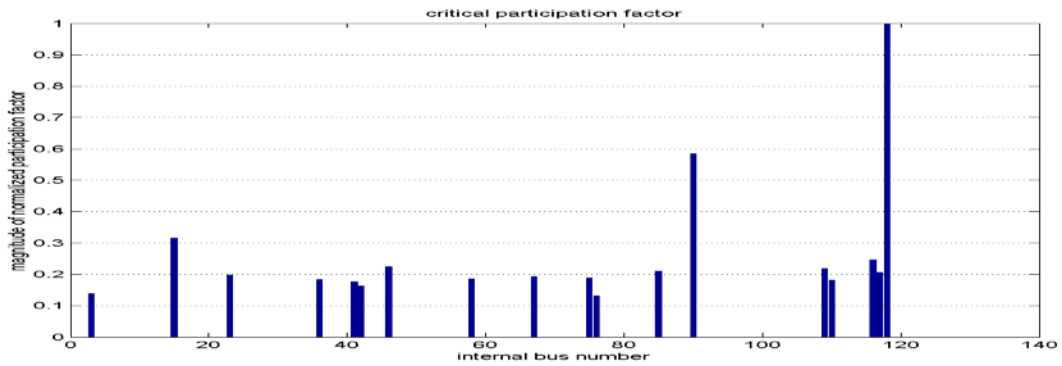


Figure D.106 Bus 123 “52” MW of Wind Injection at Bus # 123



Bus 110 Wind Injection

Figure D.107 Bus 110 “20” MW of Wind Injection at Bus # 110

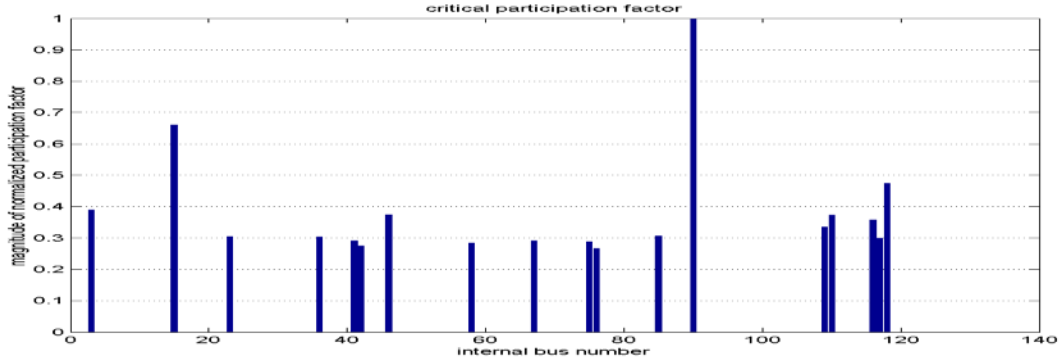


Figure D.108 Bus 110 “40” MW of Wind Injection at Bus # 110

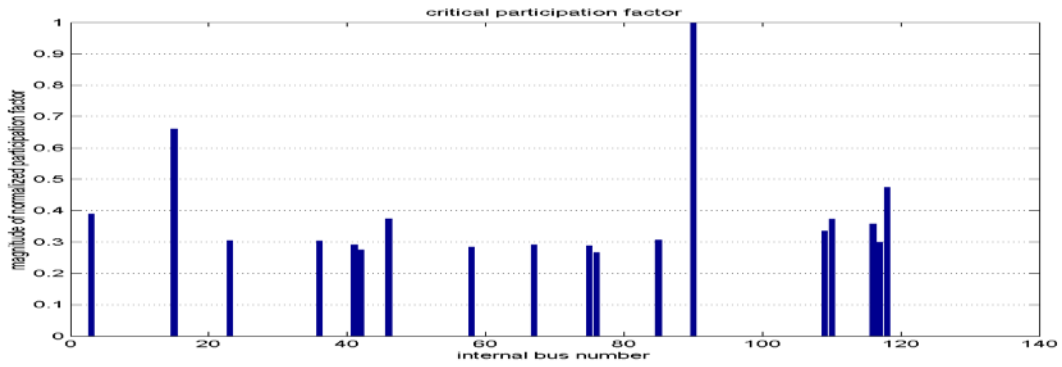


Figure D.109 Bus 110 “60” MW of Wind Injection at Bus # 110

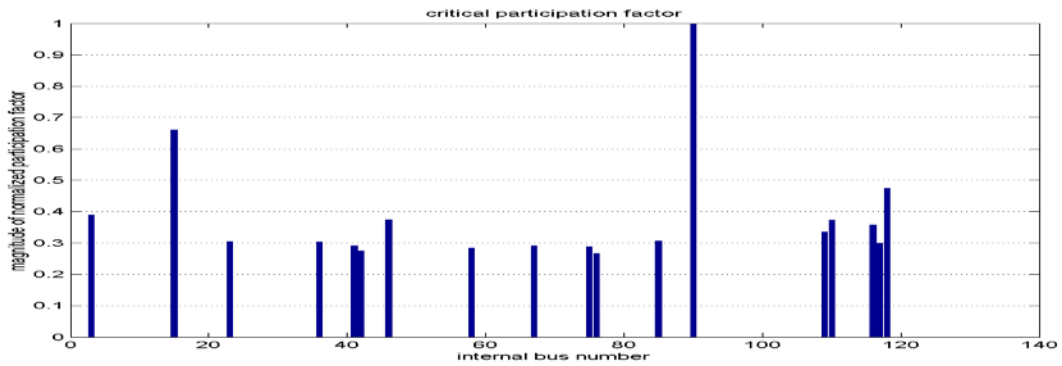
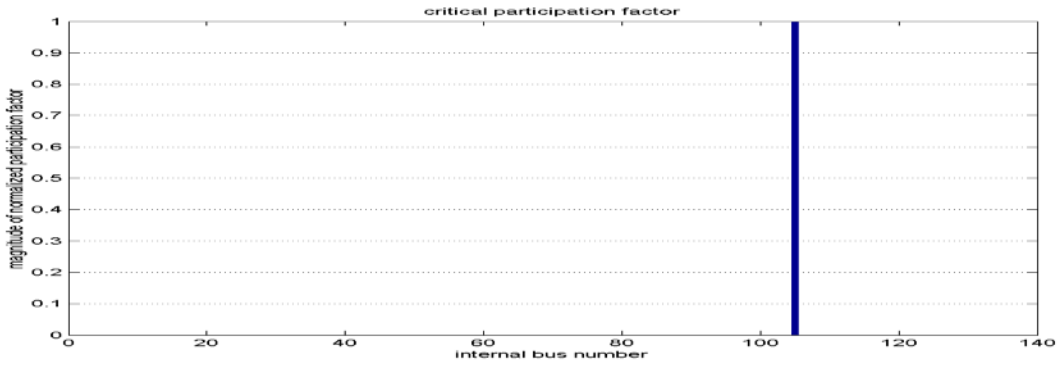


Figure D.110 Bus 110 “66” MW of Wind Injection at Bus # 110



Bus 119 Wind Injection

Figure D.111 Bus 119 “20” MW of Wind Injection at Bus # 119

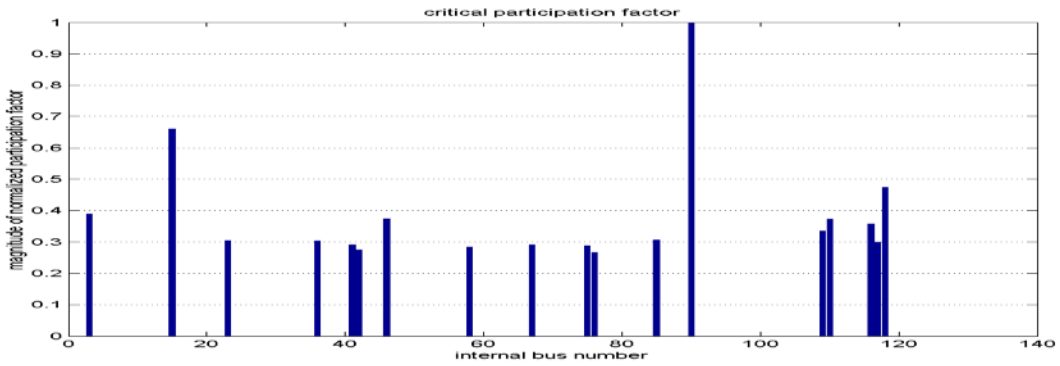


Figure D.112 Bus 119 “40” MW of Wind Injection at Bus # 119

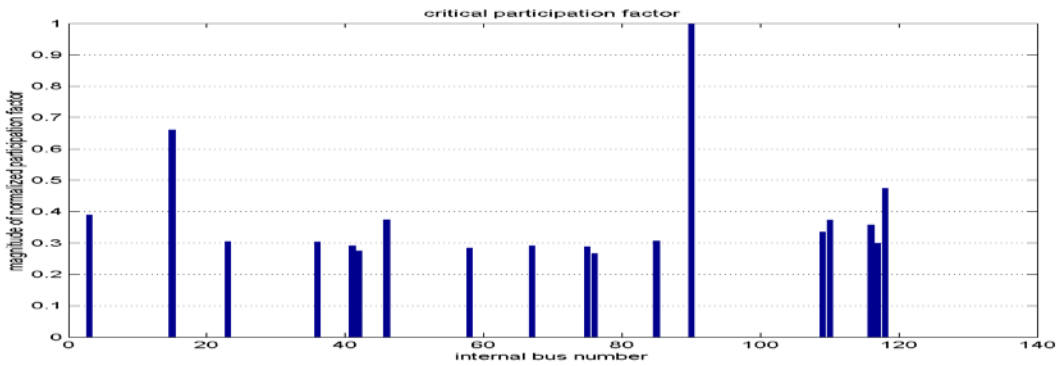


Figure D.113 Bus 119 “60” MW of Wind Injection at Bus # 119

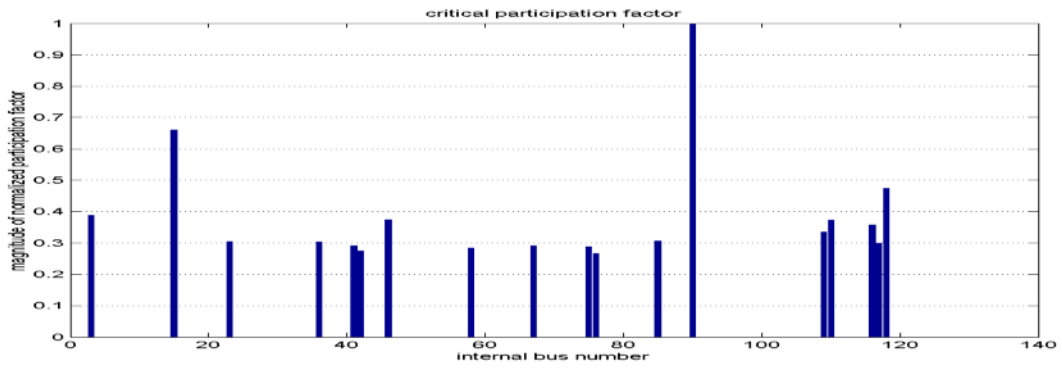
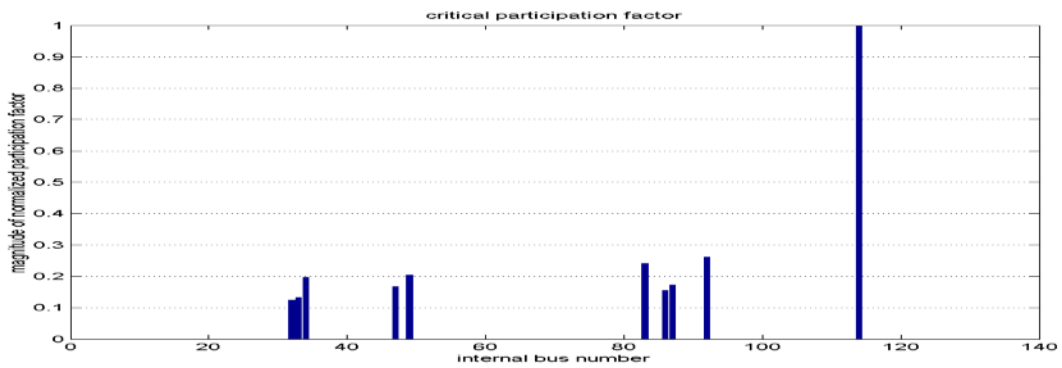


Figure D.114 Bus 119 “80” MW of Wind Injection at Bus # 119



Bus 105 Wind Injection

Figure D.115 Bus 105 “20” MW of Wind Injection at Bus # 105

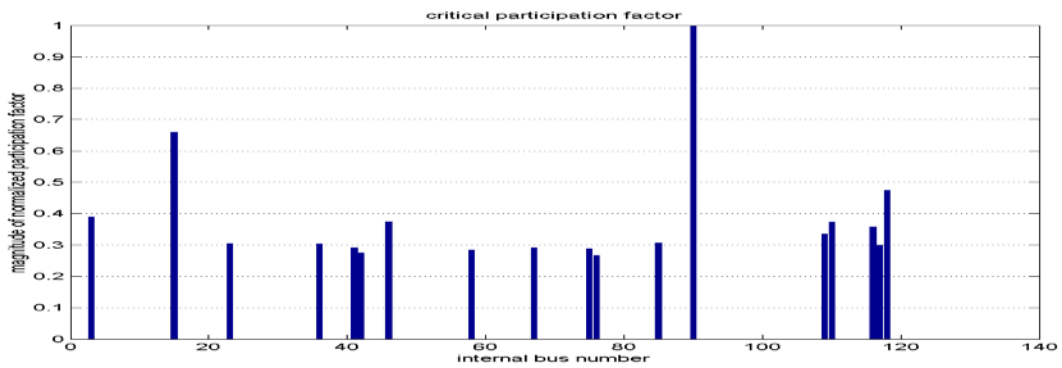


Figure D.116 Bus 105 “40” MW of Wind Injection at Bus # 105

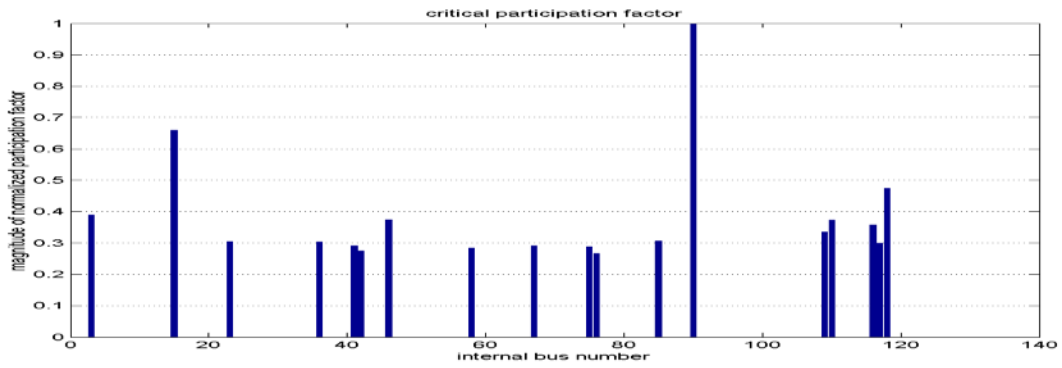


Figure D.117 Bus 105 “60” MW of Wind Injection at Bus # 105

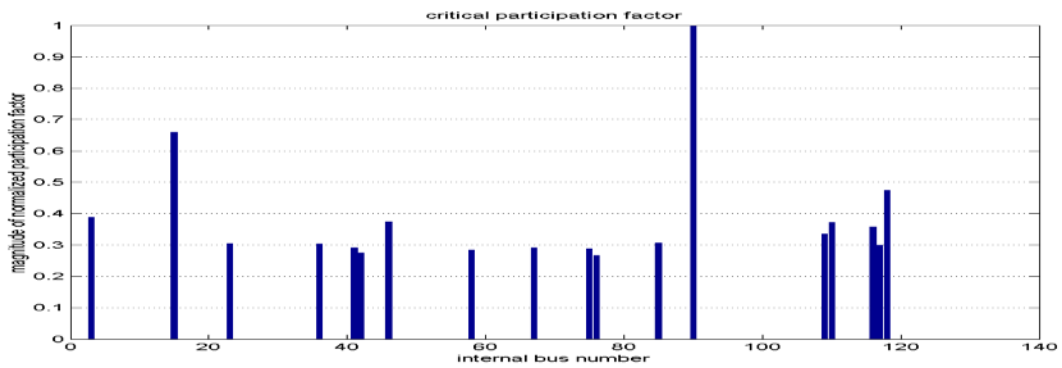


Figure D.118 Bus 105 “80” MW of Wind Injection at Bus # 105

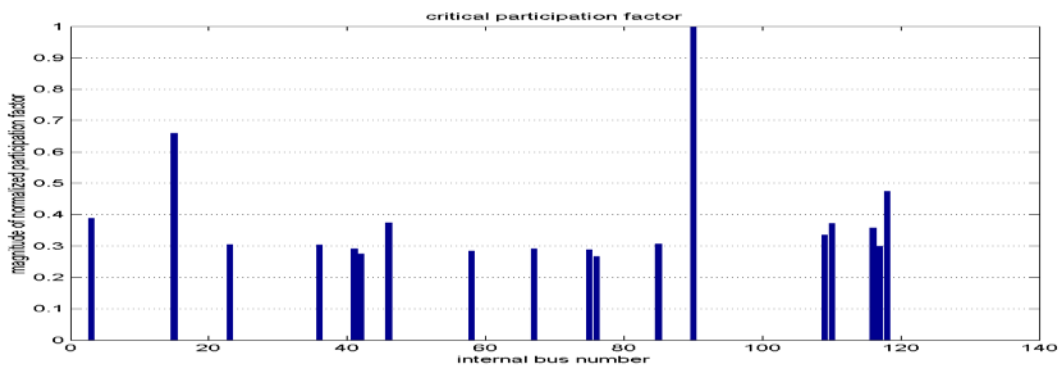


Figure D.119 Bus 105 “100” MW of Wind Injection at Bus # 105

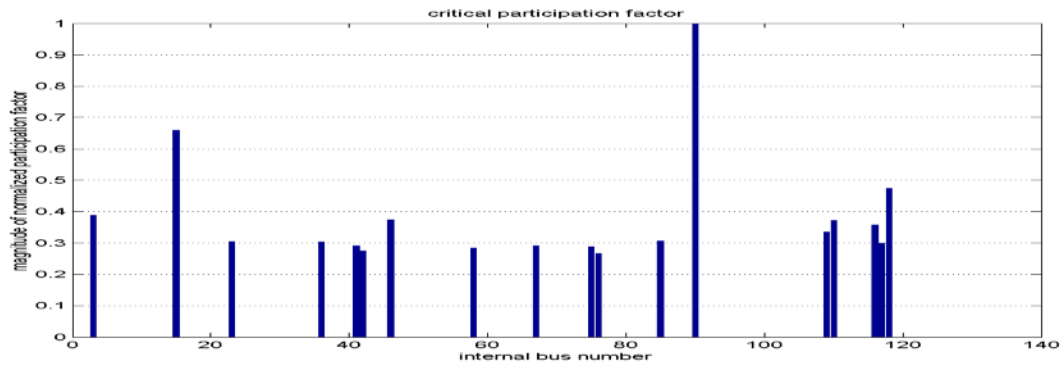
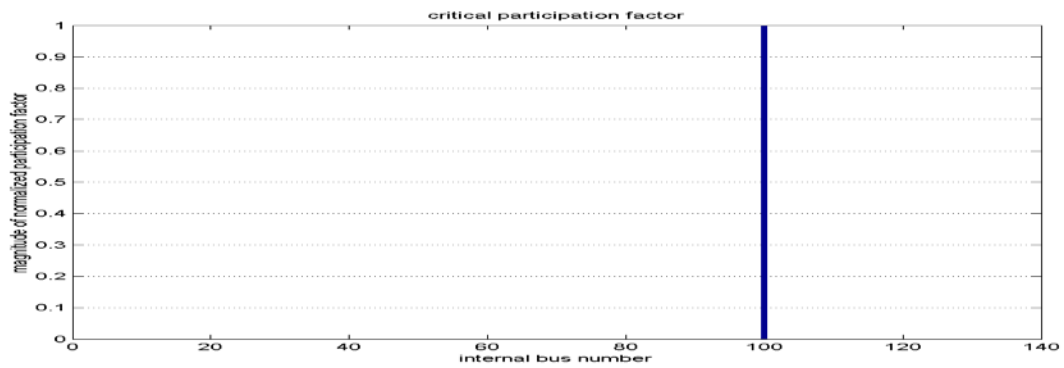


Figure D.120 Bus 105 “106” MW of Wind Injection at Bus # 105



**D.6 Additional Results of Simulation of System Critical Eigenvalue and
“Normalized” Participation Factors for the 3-Weak Bus Combination Wind
Injections Using SCIG Wind Turbine Type**

Figure D.121 Combined Weak Buses 95_115_123 of Total “30” MW of Wind Injection

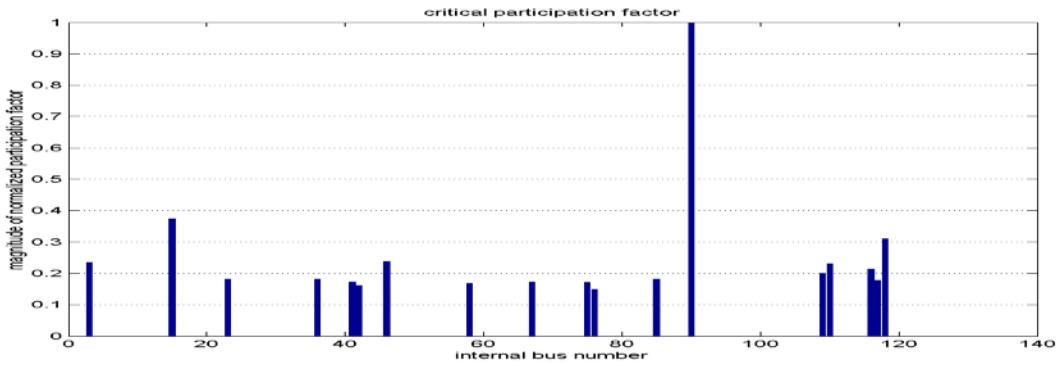


Figure D.122 Combined Weak Buses 95_115_123 of Total “60” MW of Wind Injection

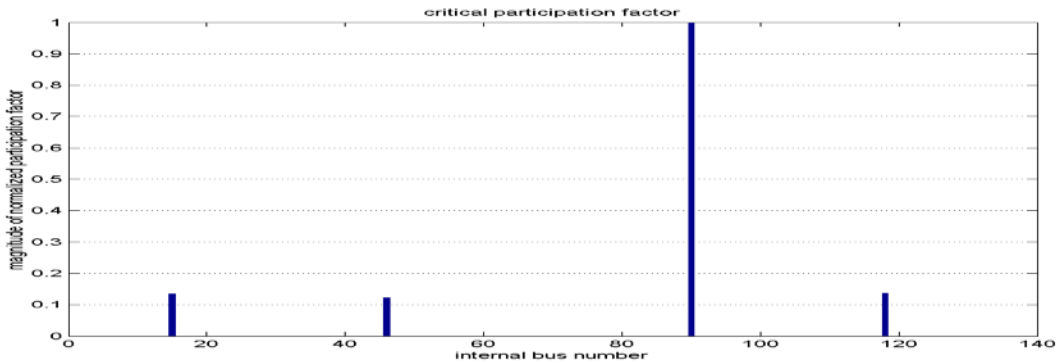
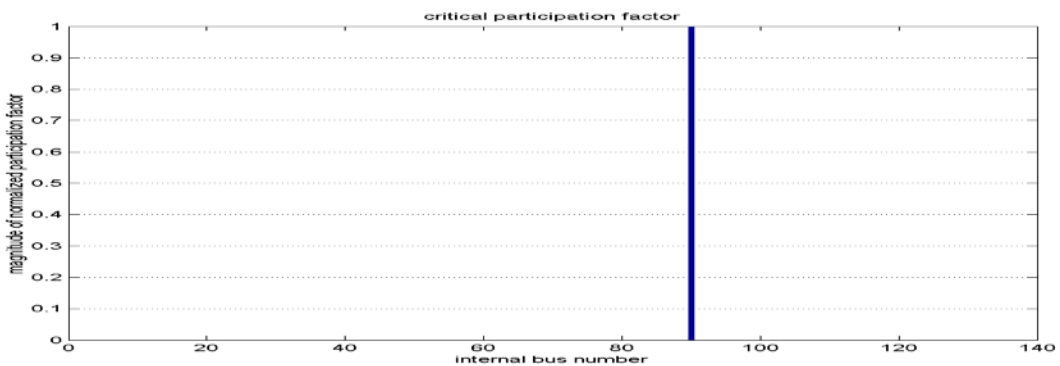


Figure D.123 Combined Weak Buses 95_115_123 of Total “90” MW of Wind Injection



**D.7 Additional Results of Simulation of System Critical Eigenvalue and
“Normalized” Participation Factors for the 3-Strong Bus Combination Wind
Injections Using SCIG Wind Turbine Type**

Figure D.124 Combined Strong Buses 105_110_119 of Total “30” MW of Wind Injection

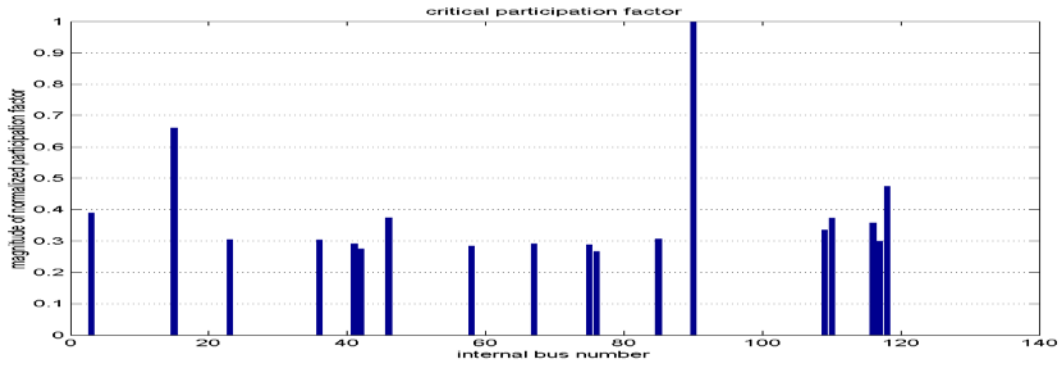


Figure D.125 Combined Strong Buses 105_110_119 of Total “60” MW of Wind Injection

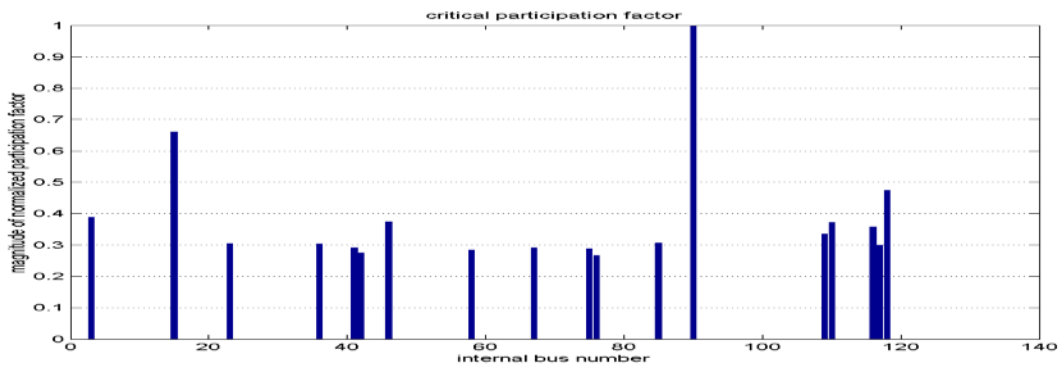


Figure D.126 Combined Strong Buses 105_110_119 of Total “90” MW of Wind Injection

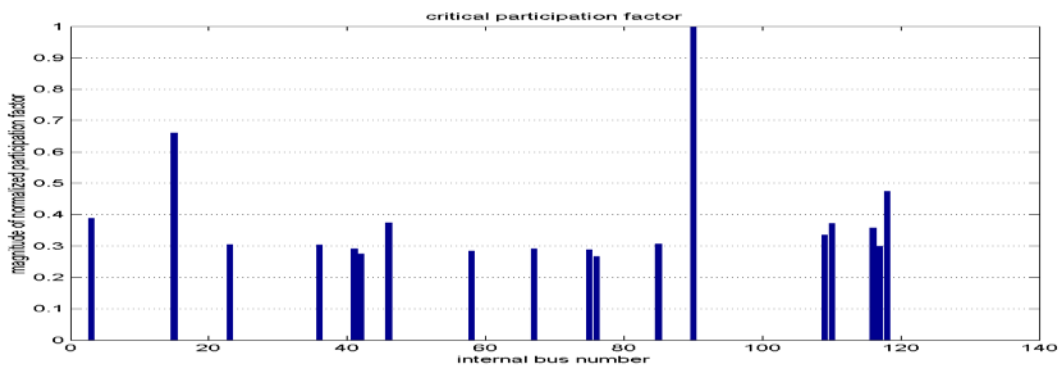


Figure D.127 Combined Strong Buses 105_110_119 of Total “120” MW of Wind Injection

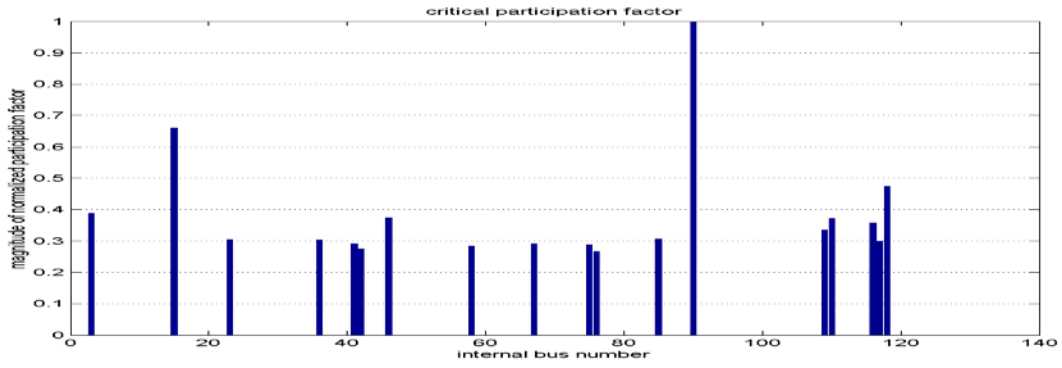


Figure D.128 Combined Strong Buses 105_110_119 of Total “150” MW of Wind Injection

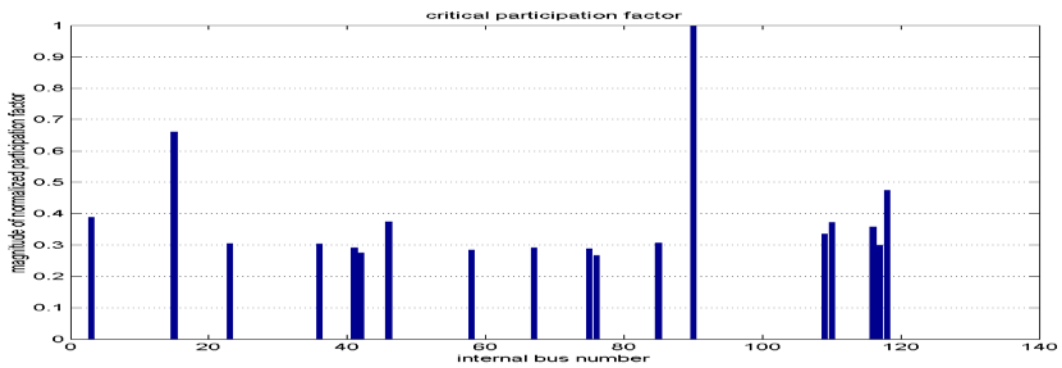
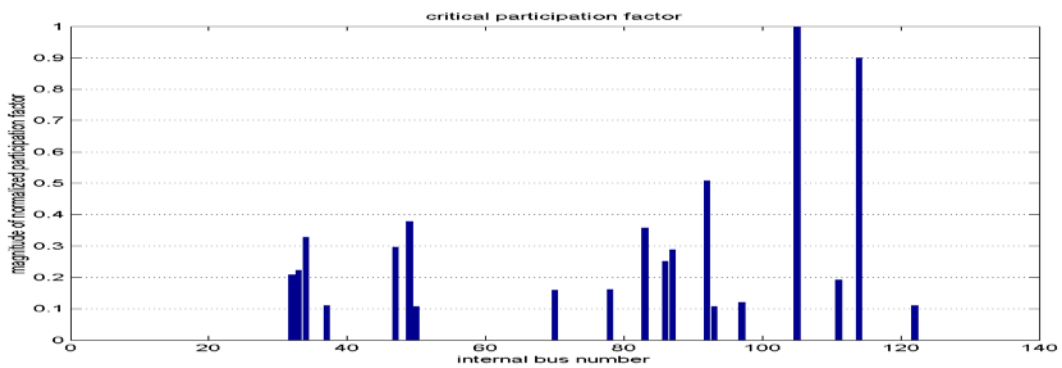


Figure D.129 Combined Strong Buses 105_110_119 of Total “180” MW of Wind Injection



**D.8 Additional Results of Simulation of System Critical Eigenvalue and
“Normalized” Participation Factors for Individual Bus Wind Injections Using
DDSG Wind Turbine Type**

Bus 95 Wind Injection

Figure D.130 Bus 95 “20” MW of Wind Injection at Bus # 95

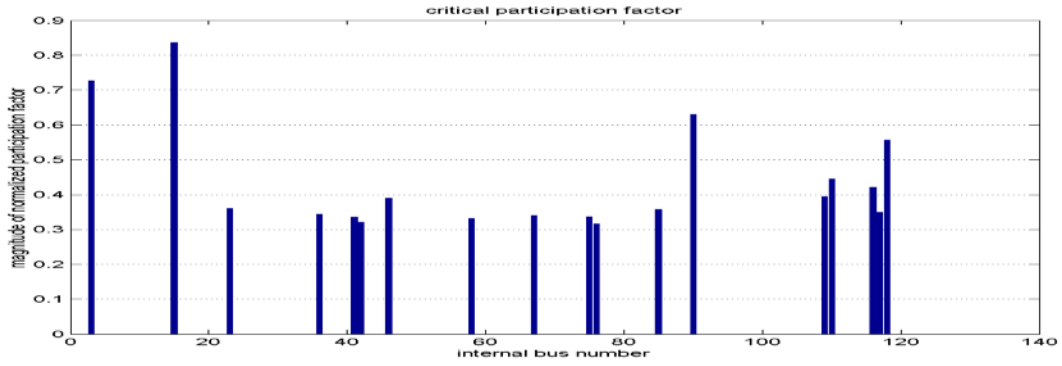


Figure D.131 Bus 95 “40” MW of Wind Injection at Bus # 95

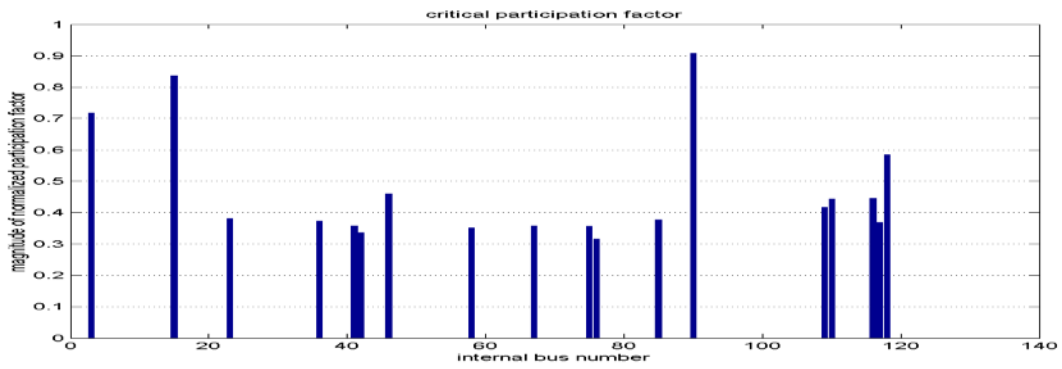


Figure D.132 Bus 95 “50” MW of Wind Injection at Bus # 95

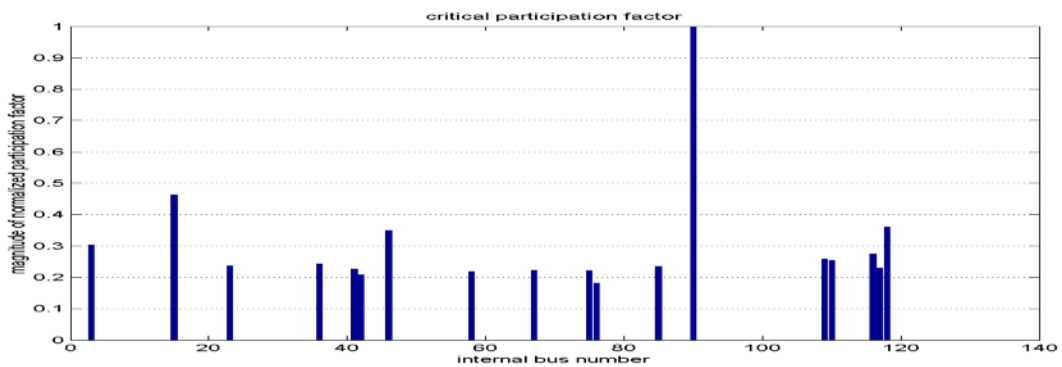
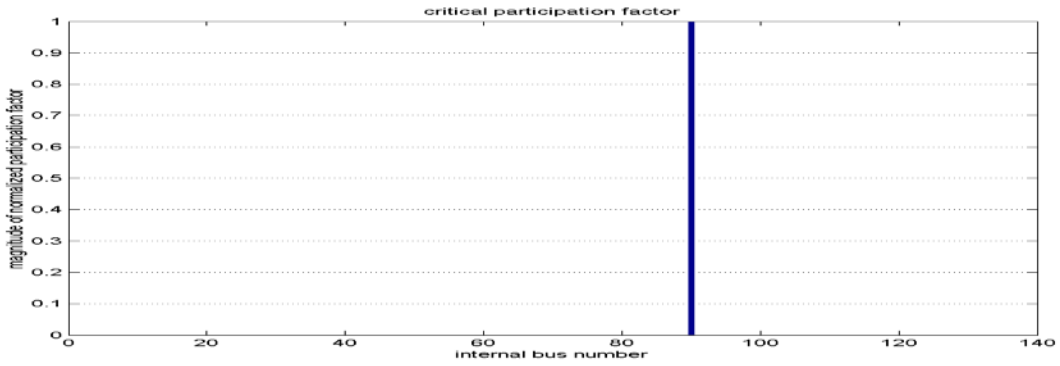


Figure D.133 Bus 95 “57” MW of Wind Injection at Bus # 95



Bus 123 Wind Injection

Figure D.134 Bus 123 “20” MW of Wind Injection at Bus # 123

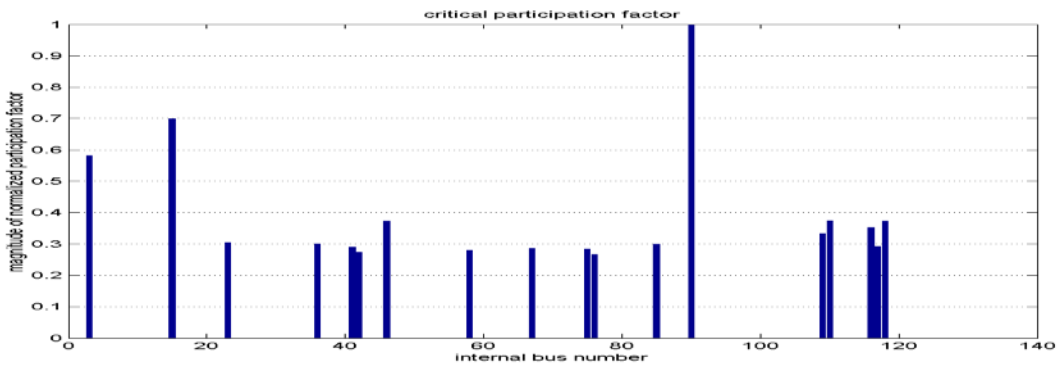


Figure D.135 Bus 123 “40” MW of Wind Injection at Bus # 123

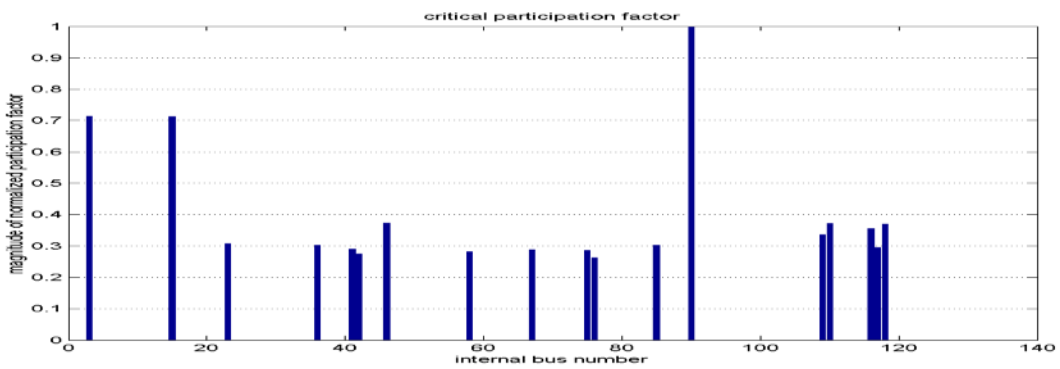


Figure D.136 Bus 123 “60” MW of Wind Injection at Bus # 123

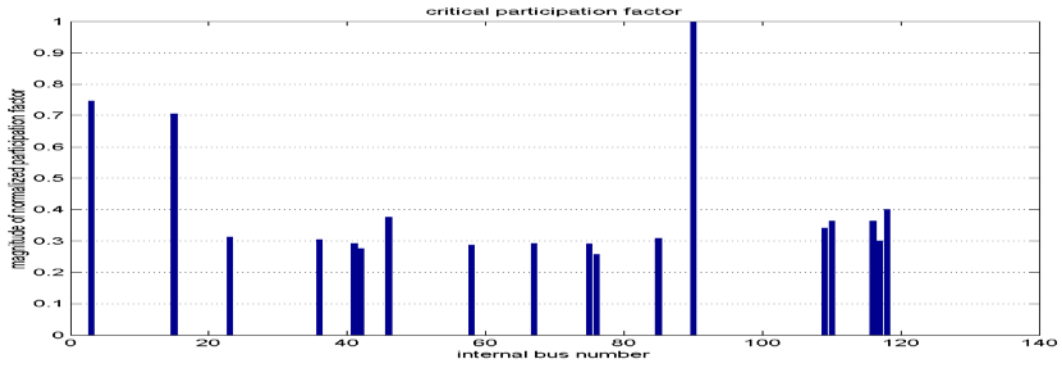


Figure D.137 Bus 123 “80” MW of Wind Injection at Bus # 123

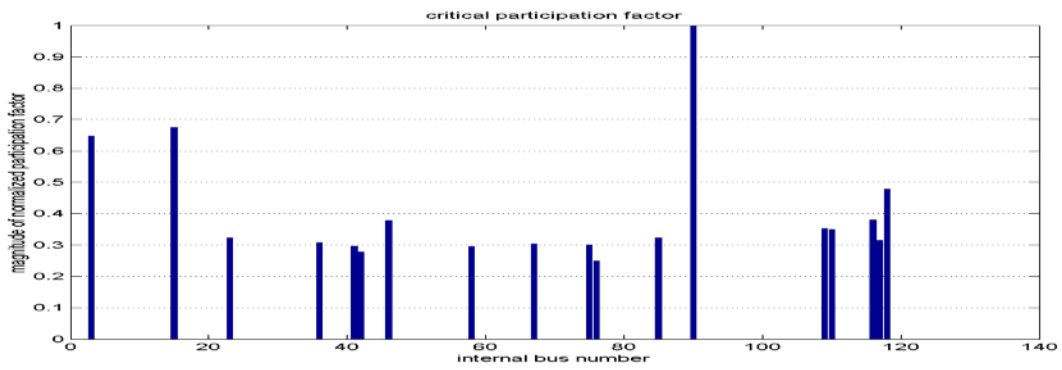
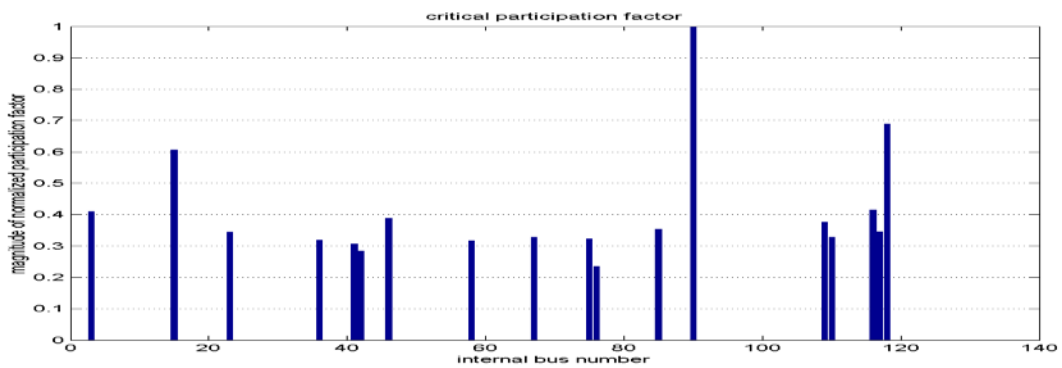


Figure D.138 Bus 123 “100” MW of Wind Injection at Bus # 123



Bus 115 Wind Injection

Figure D.139 Bus 115 “20” MW of Wind Injection at Bus # 115

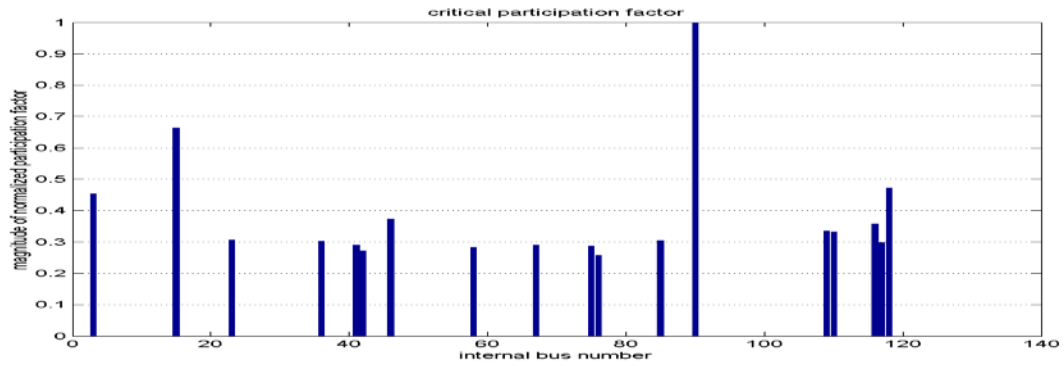


Figure D.140 Bus 115 “40” MW of Wind Injection at Bus # 115

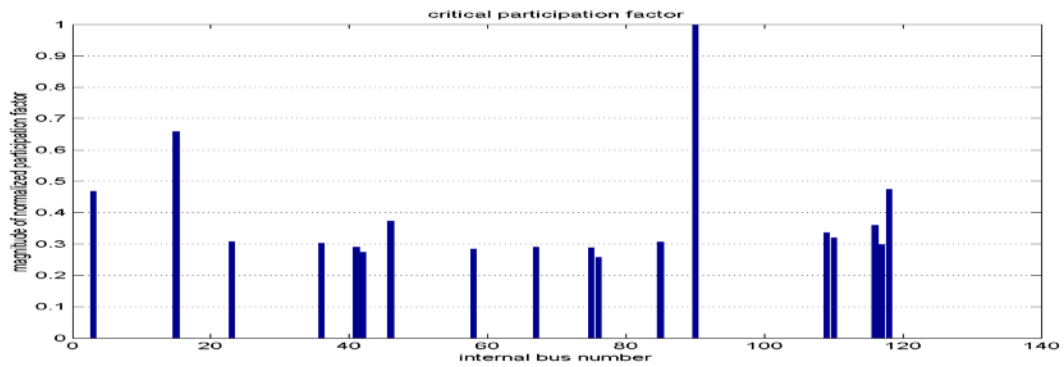


Figure D.141 Bus 115 “60” MW of Wind Injection at Bus # 115

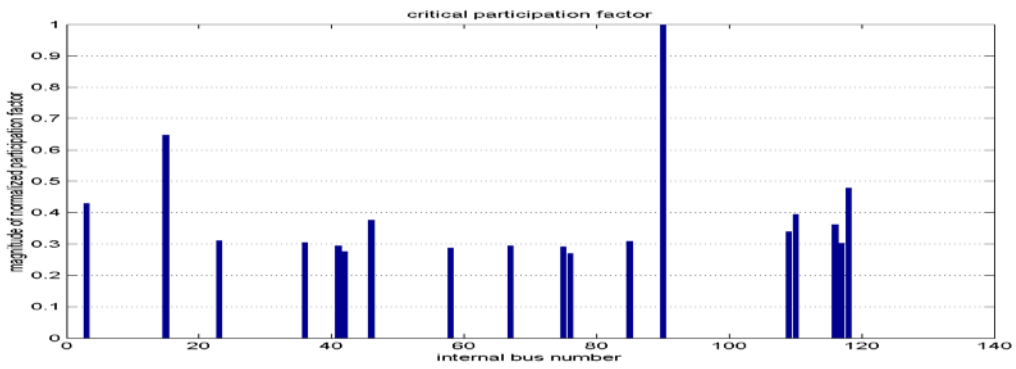


Figure D.142 Bus 115 “60” MW of Wind Injection at Bus # 115

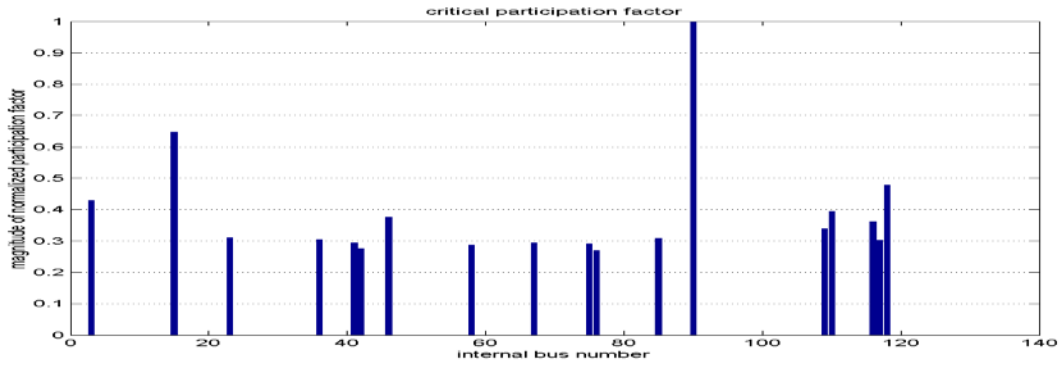


Figure D.143 Bus 115 “80” MW of Wind Injection at Bus # 115

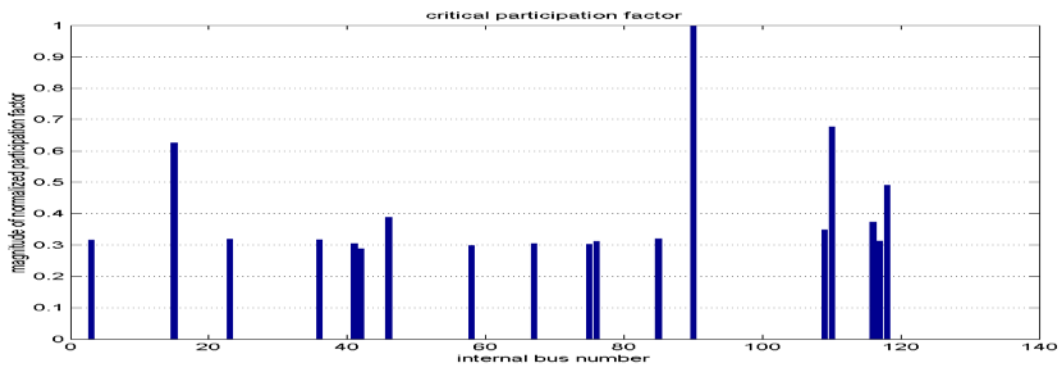
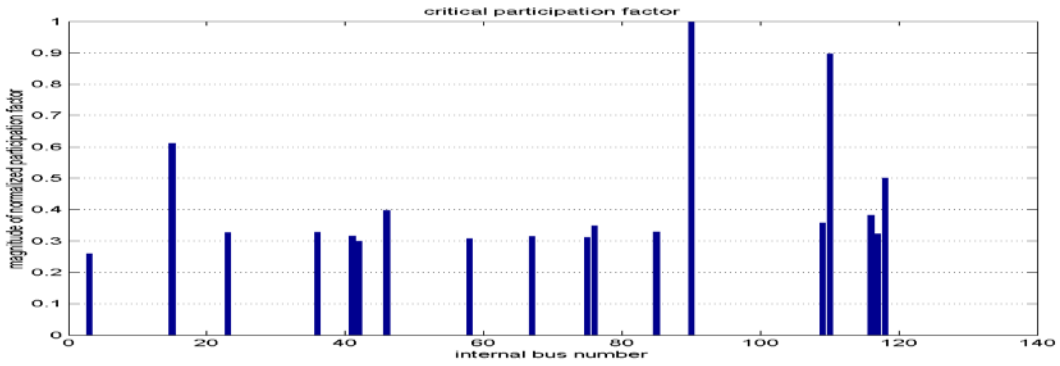


Figure D.144 Bus 115 “100” MW of Wind Injection at Bus # 115



Bus 110 Wind Injection

Figure D.145 Bus 110 “20” MW of Wind Injection at Bus # 110

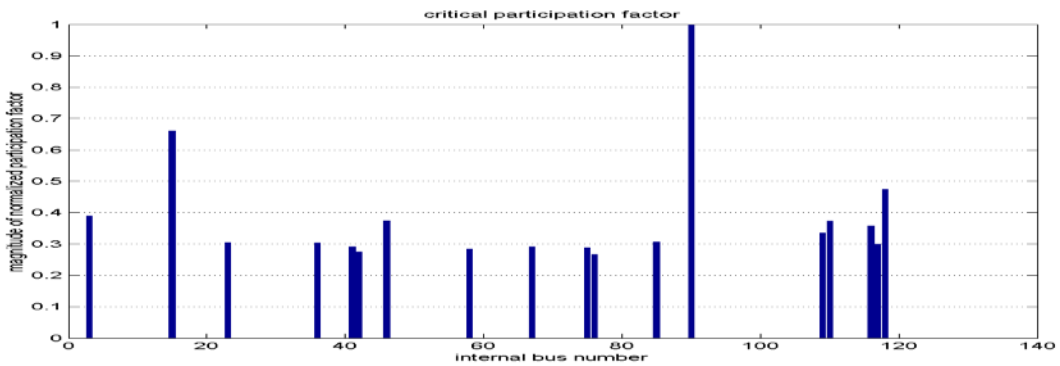


Figure D.146 Bus 110 “40” MW of Wind Injection at Bus # 110

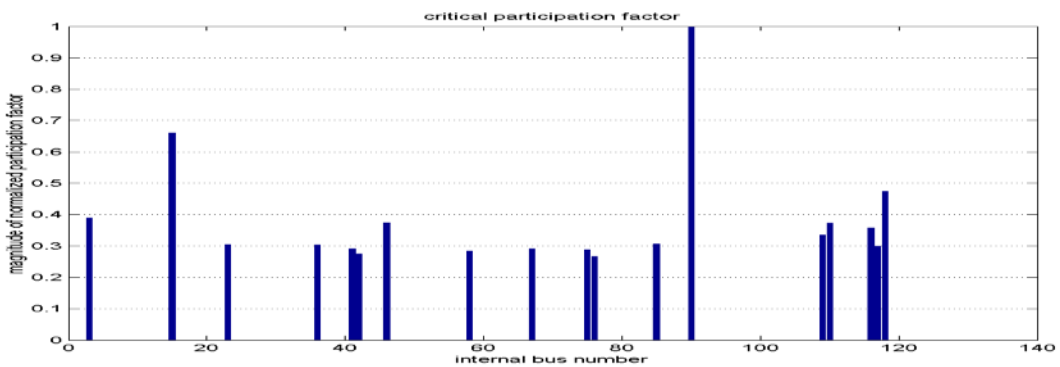


Figure D.147 Bus 110 “60” MW of Wind Injection at Bus # 110

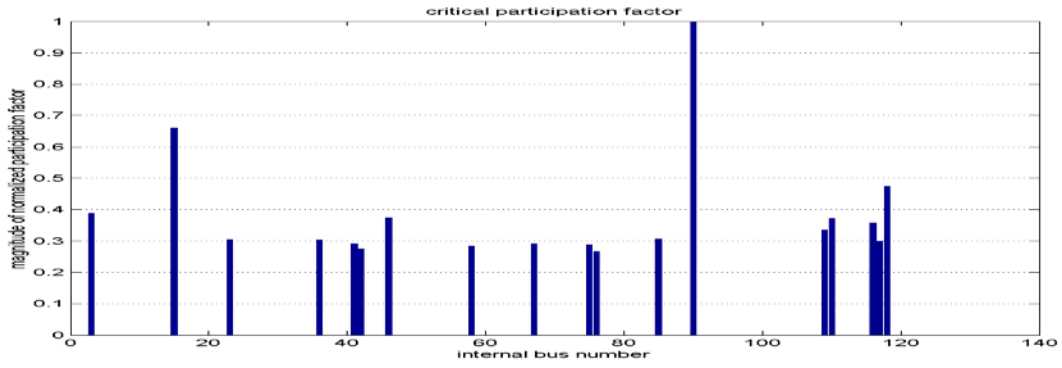


Figure D.148 Bus 110 “80” MW of Wind Injection at Bus # 110

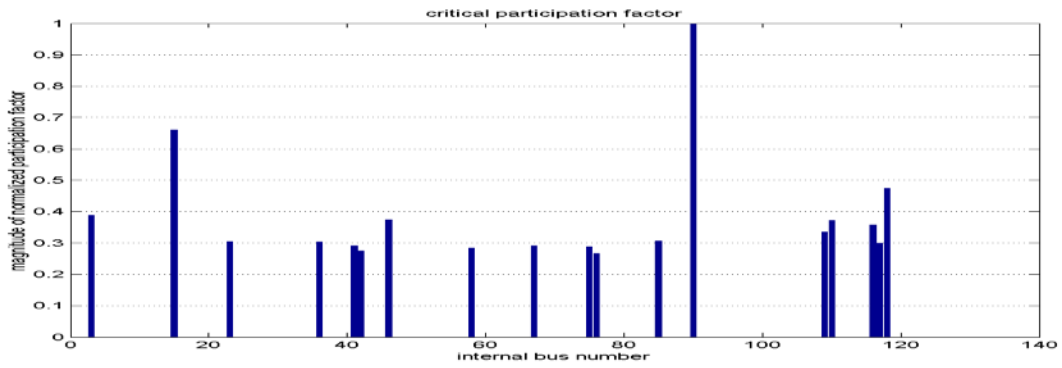


Figure D.149 Bus 110 “100” MW of Wind Injection at Bus # 110

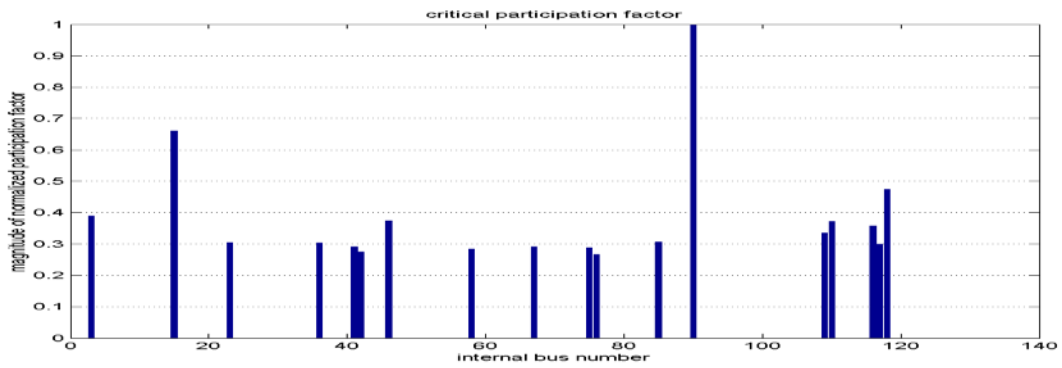
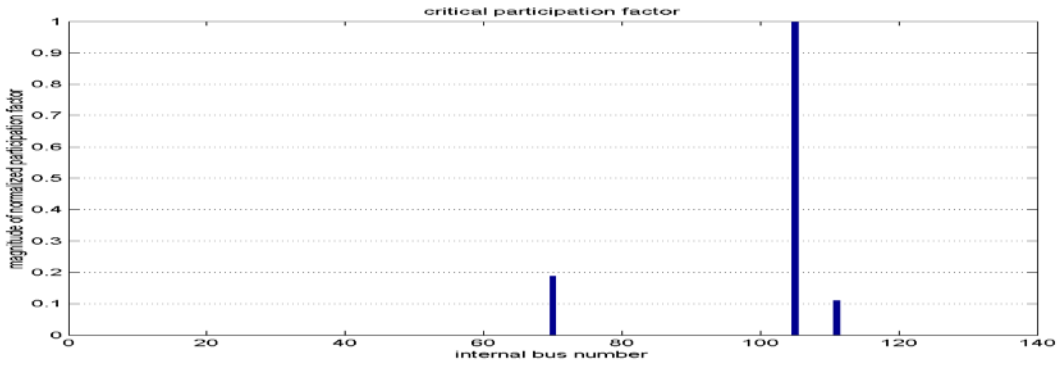


Figure D.150 Bus 110 “115” MW of Wind Injection at Bus # 110



Bus 119 Wind Injection

Figure D.151 Bus 119 “20” MW of Wind Injection at Bus # 119

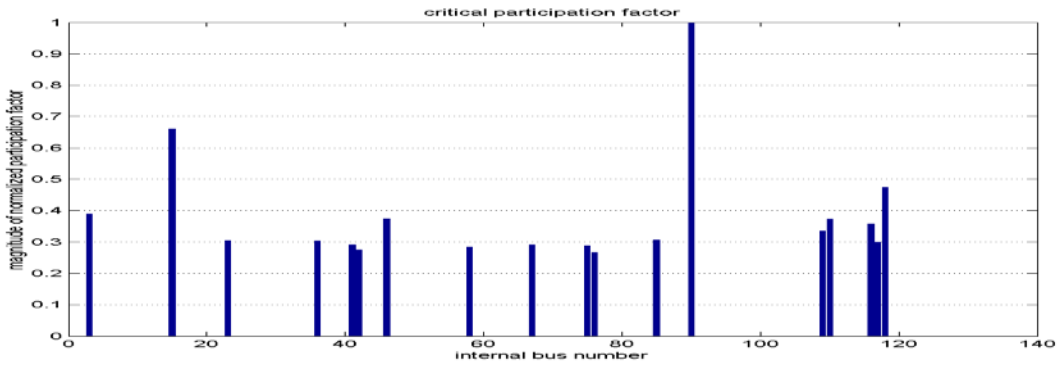


Figure D.152 Bus 119 “40” MW of Wind Injection at Bus # 119

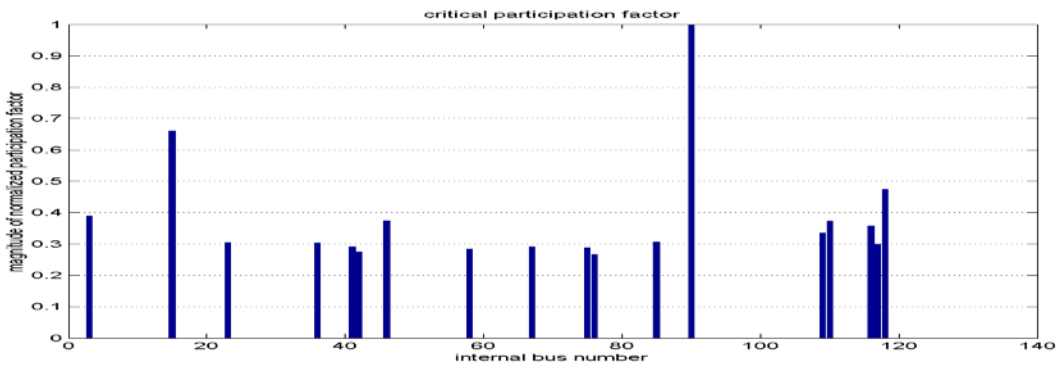


Figure D.153 Bus 119 “60” MW of Wind Injection at Bus # 119

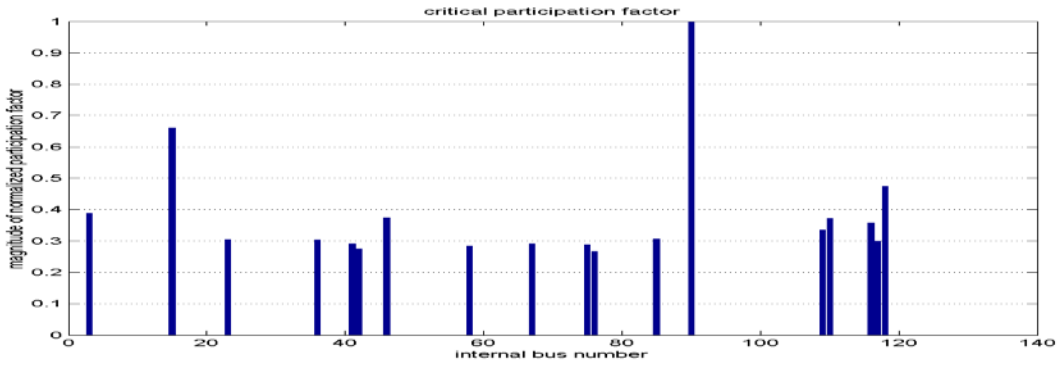


Figure D.154 Bus 119 “80” MW of Wind Injection at Bus # 119

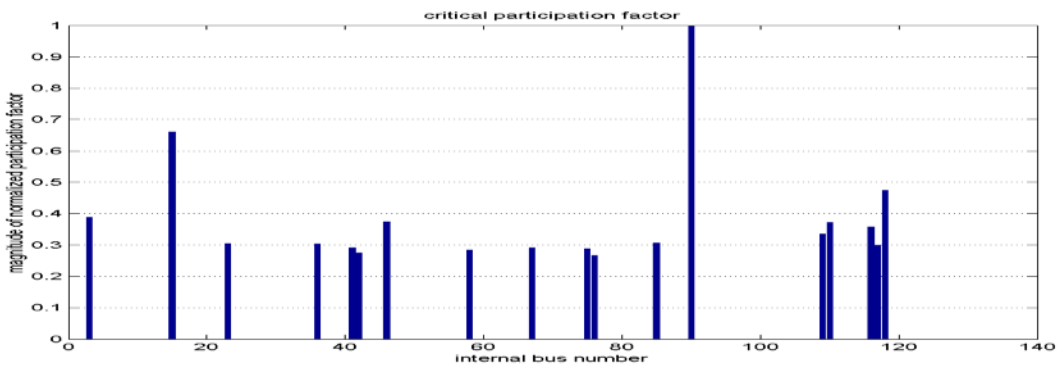


Figure D.155 Bus 119 “100” MW of Wind Injection at Bus # 119

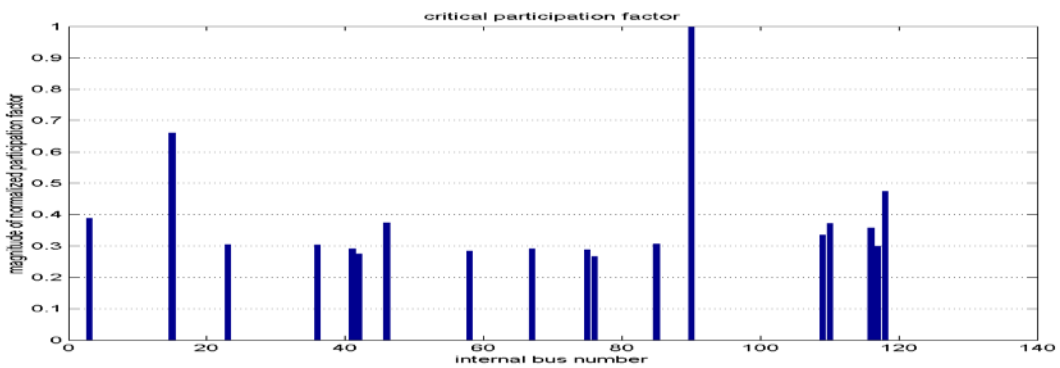


Figure D.156 Bus 119 “120” MW of Wind Injection at Bus # 119

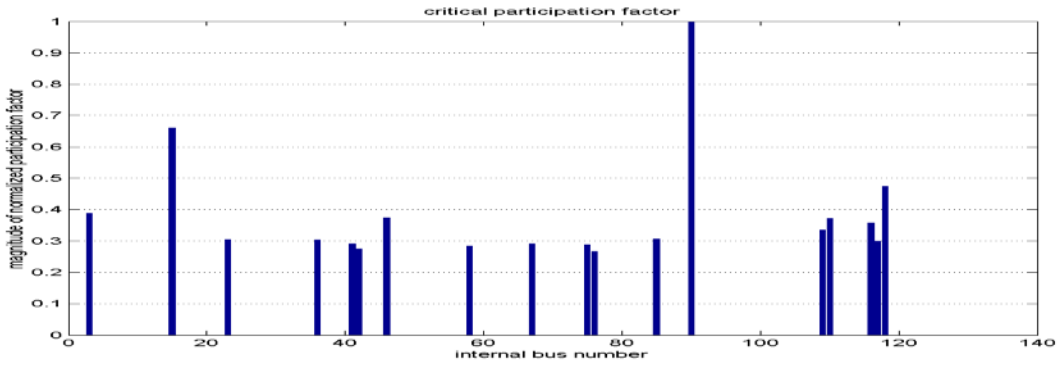
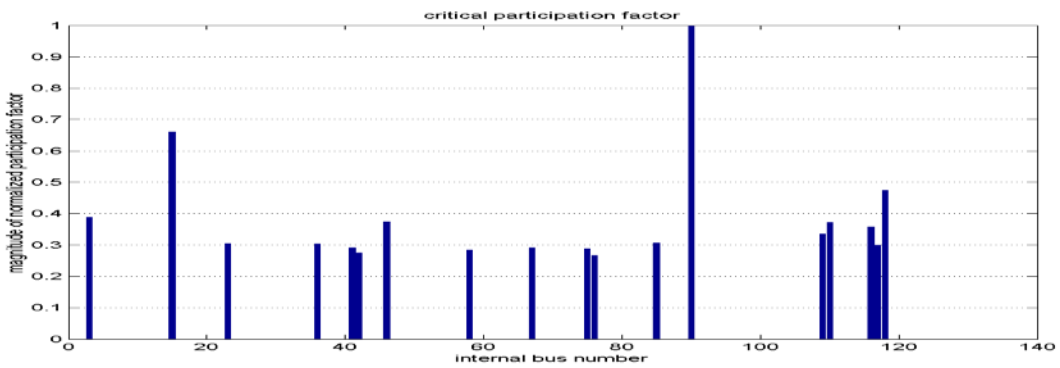


Figure D.157 Bus 119 “135” MW of Wind Injection at Bus # 119



Bus 105 Wind Injection

Figure D.158 Bus 105 “20” MW of Wind Injection at Bus # 105

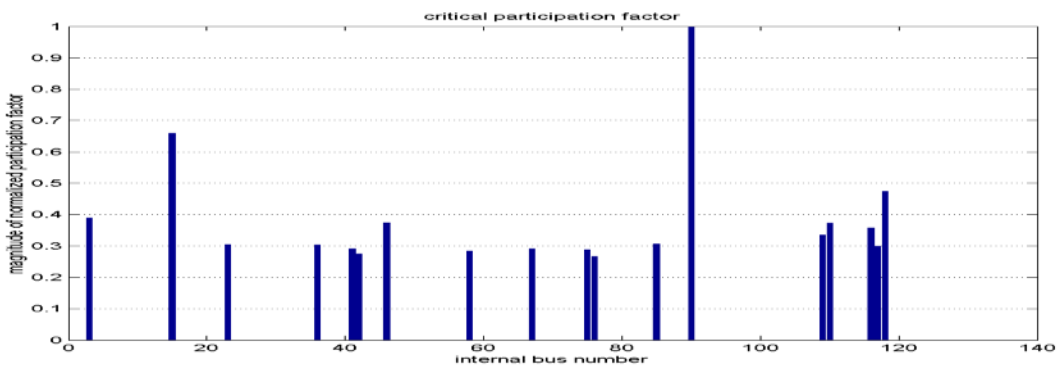


Figure D.159 Bus 105 “40” MW of Wind Injection at Bus # 105

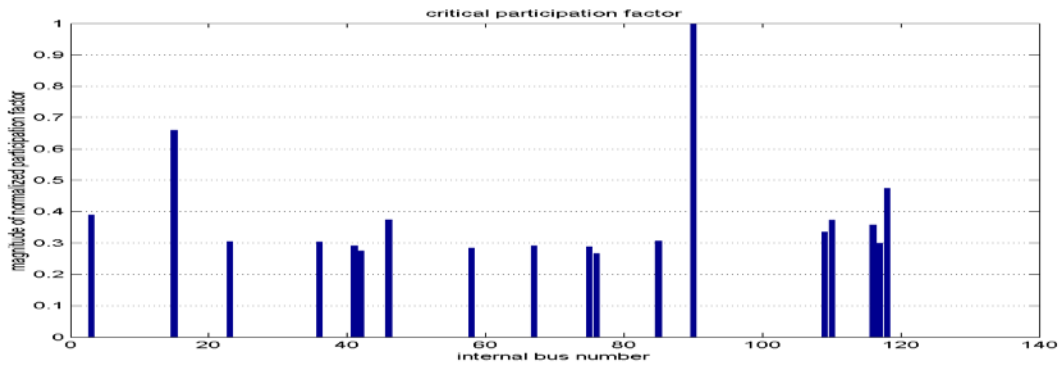


Figure D.160 Bus 105 “60” MW of Wind Injection at Bus # 105

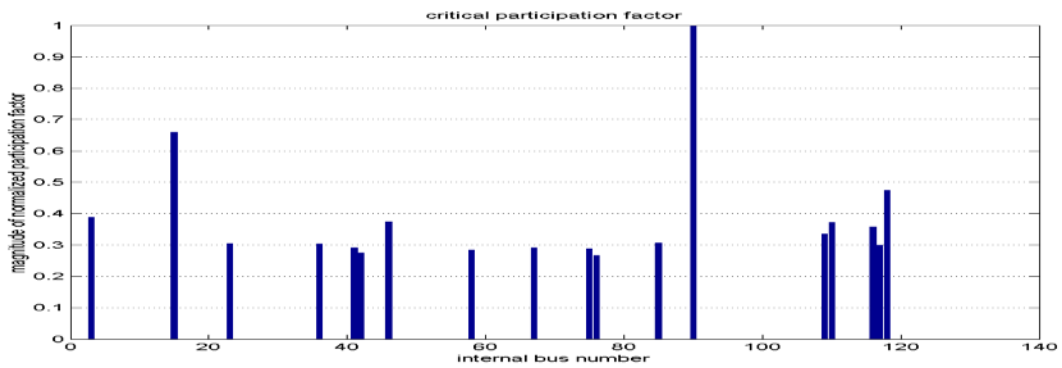


Figure D.161 Bus 105 “80” MW of Wind Injection at Bus # 105

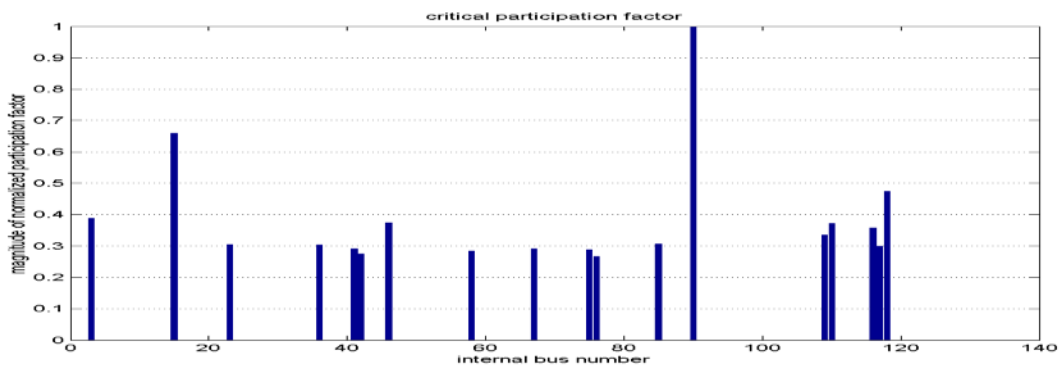


Figure D.162 Bus 105 “100” MW of Wind Injection at Bus # 105

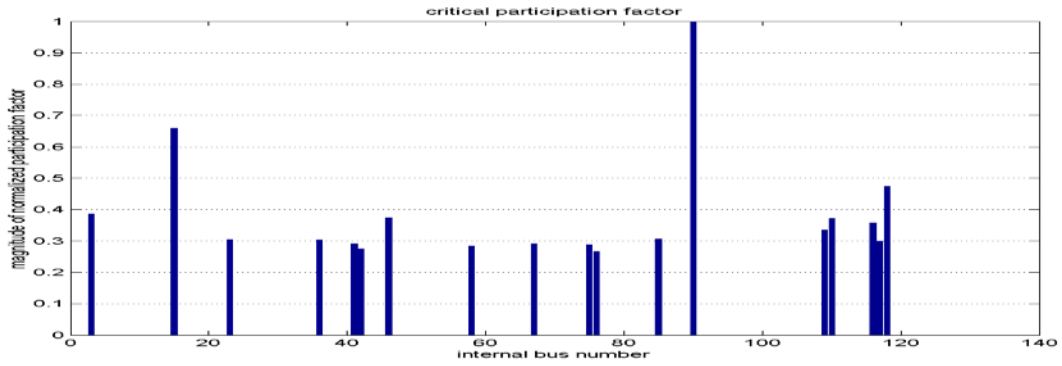


Figure D.163 Bus 105 “120” MW of Wind Injection at Bus # 105

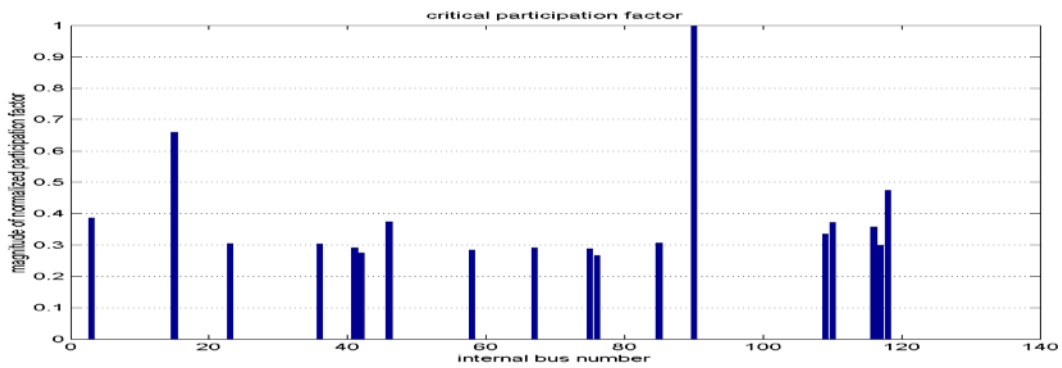


Figure D.164 Bus 105 “140” MW of Wind Injection at Bus # 105

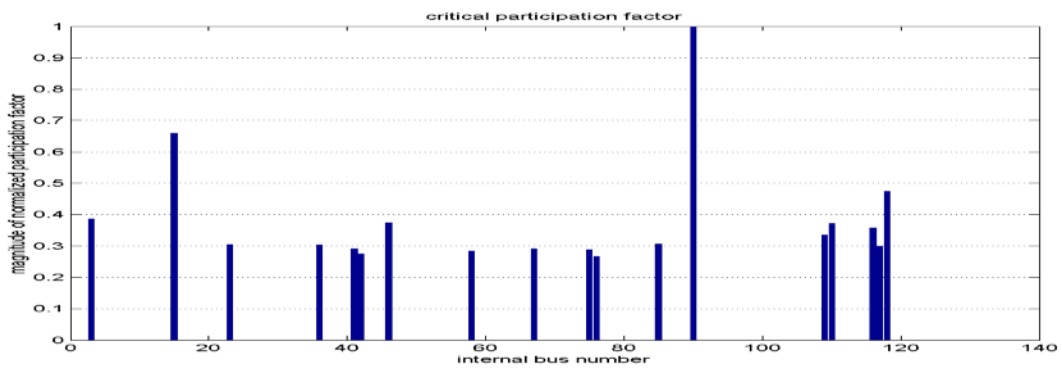


Figure D.165 Bus 105 “160” MW of Wind Injection at Bus # 105

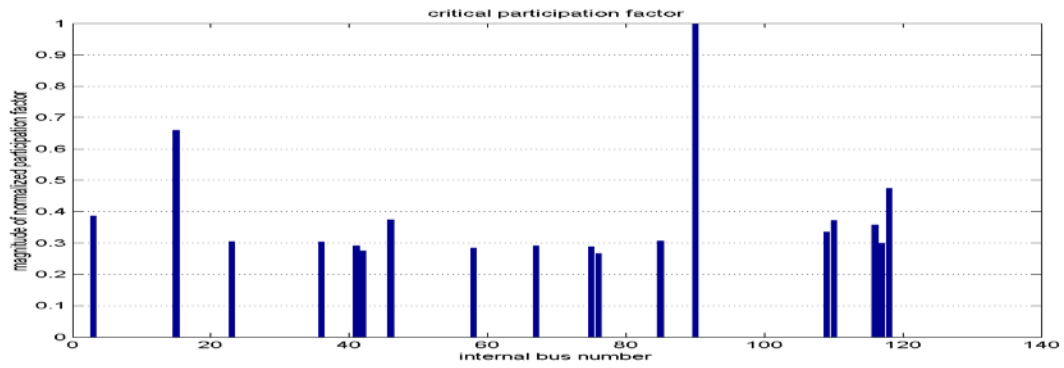
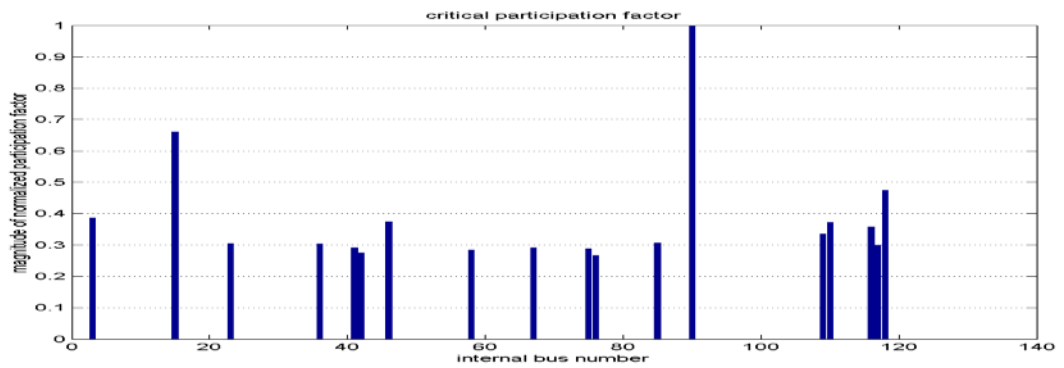


Figure D.166 Bus 105 “165” MW of Wind Injection at Bus # 105



**D.9 Additional Results of Simulation of System Critical Eigenvalue and
“Normalized” Participation Factors for the 3-Weak Bus Combination Wind
Injections Using DDSG Wind Turbine Type**

Figure D.167 Combined Weak Buses 95_115_123 of Total “30” MW of Wind Injection

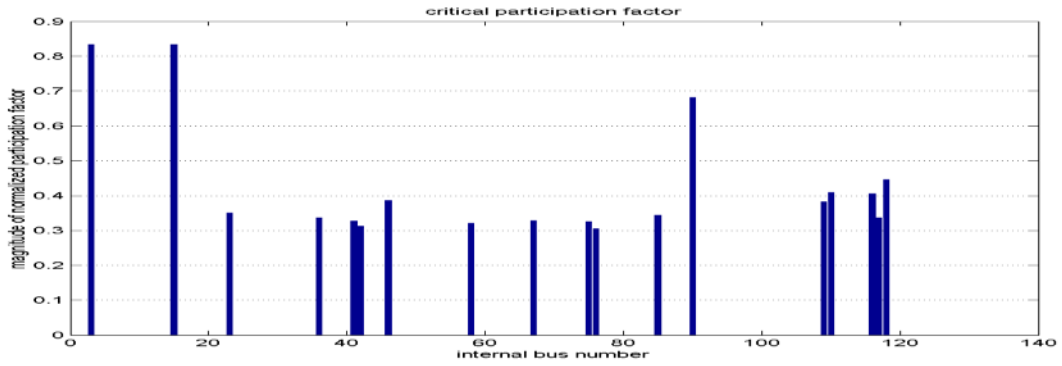


Figure D.168 Combined Weak Buses 95_115_123 of Total “60” MW of Wind Injection

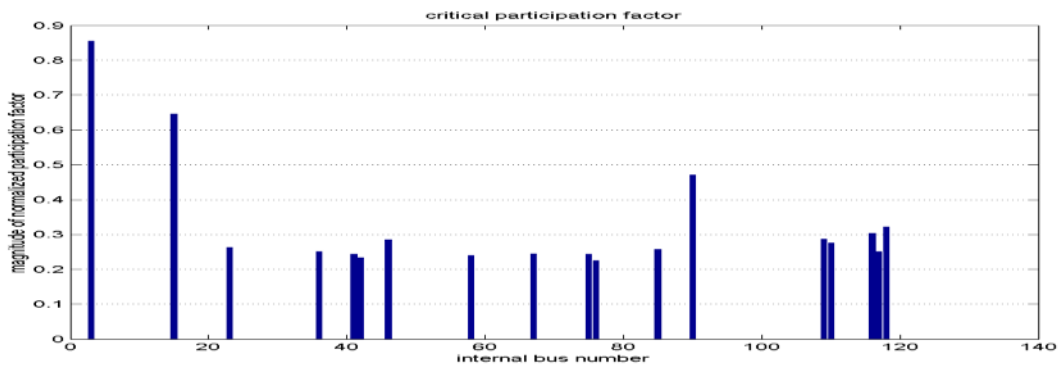


Figure D.169 Combined Weak Buses 95_115_123 of Total “90” MW of Wind Injection

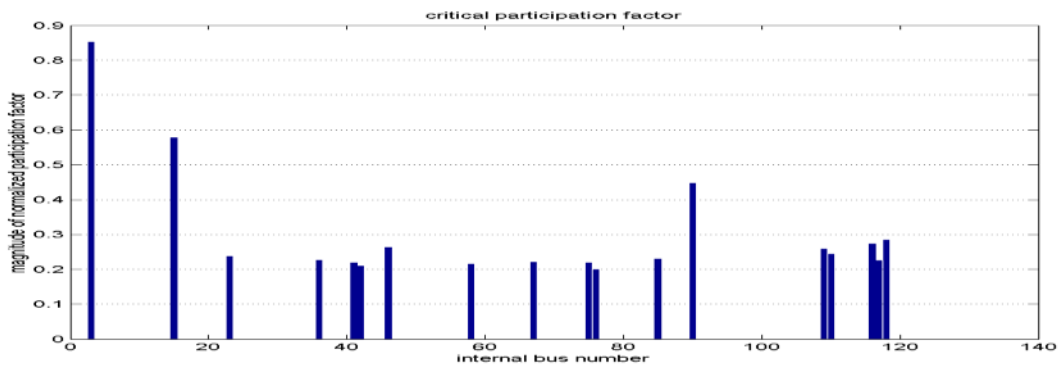


Figure D.170 Combined Weak Buses 95_115_123 of Total “120” MW of Wind Injection

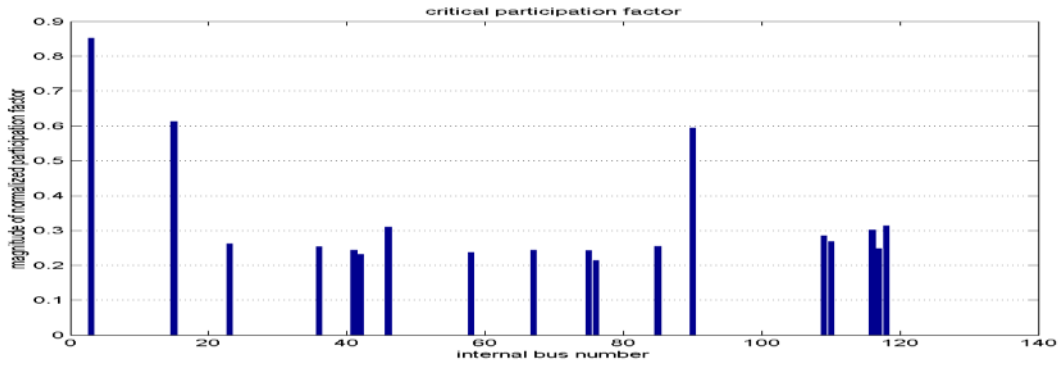
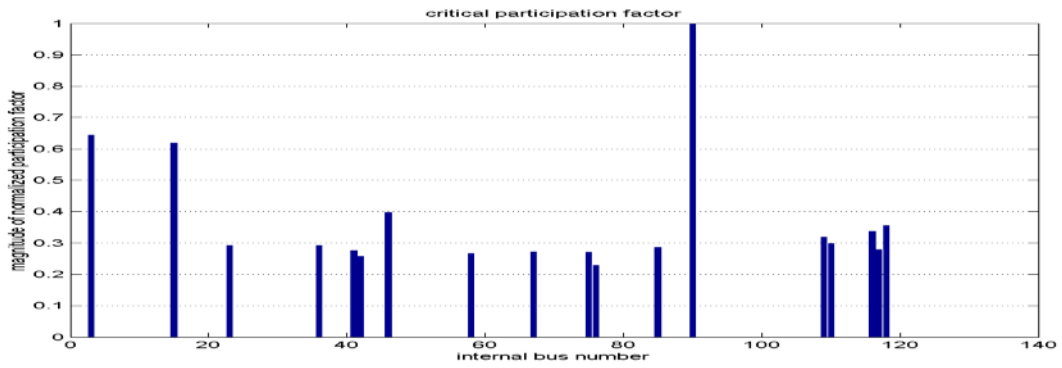


Figure D.171 Combined Weak Buses 95_115_123 of Total “150” MW of Wind Injection



**D.10 Additional Results of Simulation of System Critical Eigenvalue and
“Normalized” Participation Factors for the 3-Strong Bus Combination Wind
Injections Using DDSG Wind Turbine Type**

Figure D.172 Combined Strong Buses 105_110_119 of Total “30” MW of Wind Injection

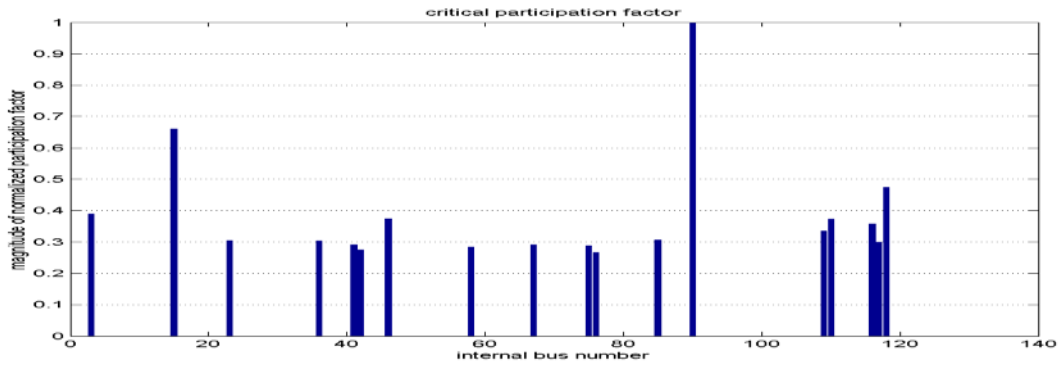


Figure D.173 Combined Strong Buses 105_110_119 of Total “60” MW of Wind Injection

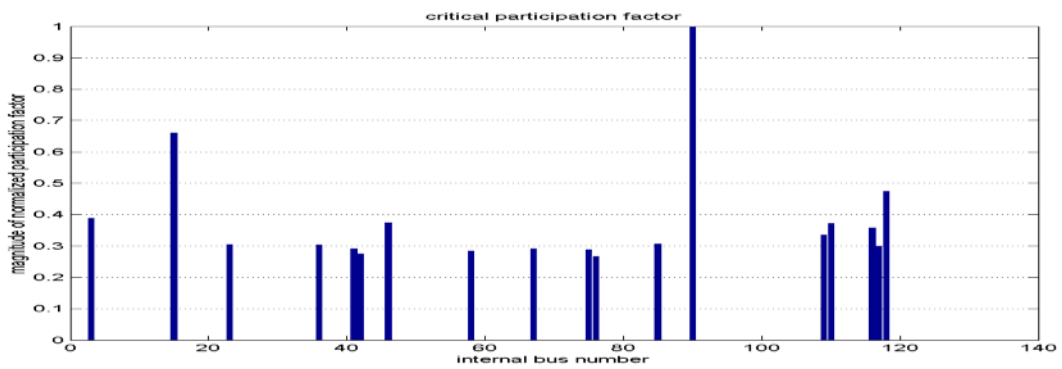


Figure D.174 Combined Strong Buses 105_110_119 of Total “90” MW of Wind Injection

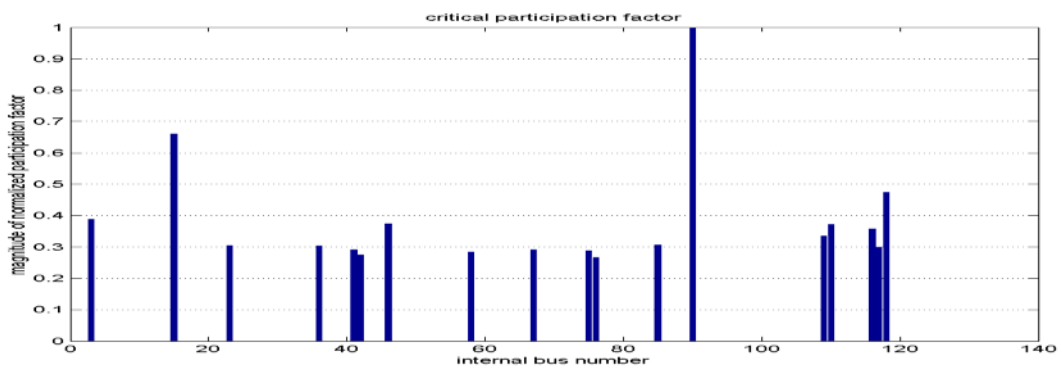


Figure D.175 Combined Strong Buses 105_110_119 of Total “120” MW of Wind Injection

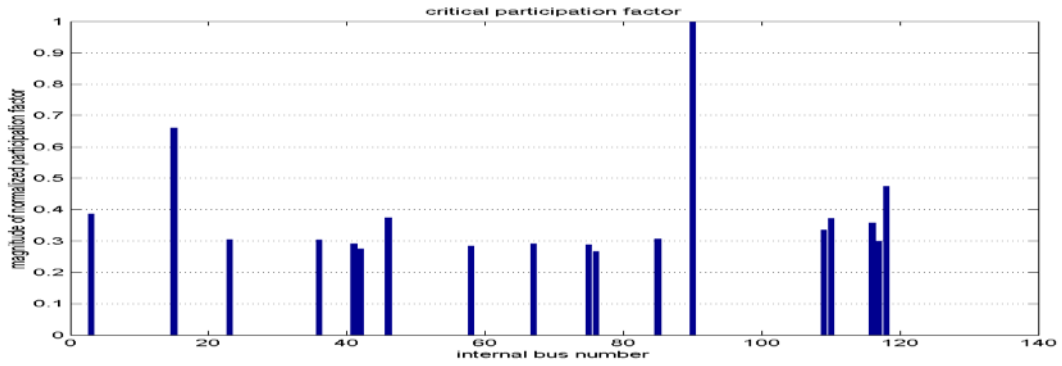


Figure D.176 Combined Strong Buses 105_110_119 of Total “150” MW of Wind Injection

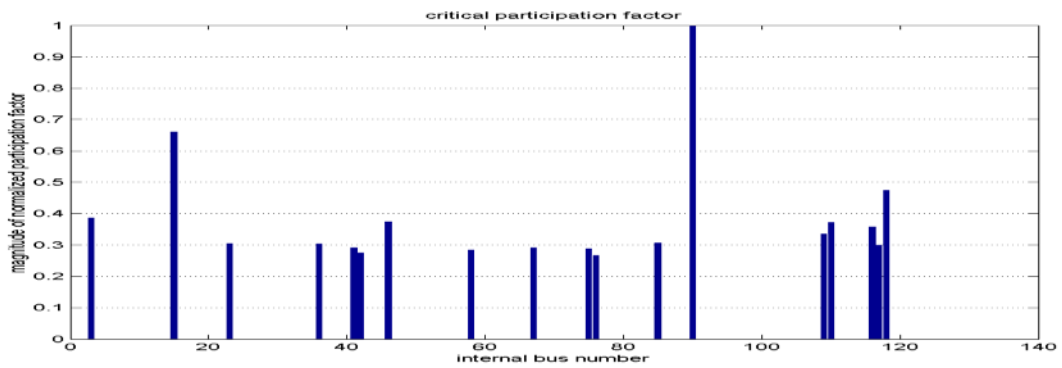


Figure D.177 Combined Strong Buses 105_110_119 of Total “180” MW of Wind Injection

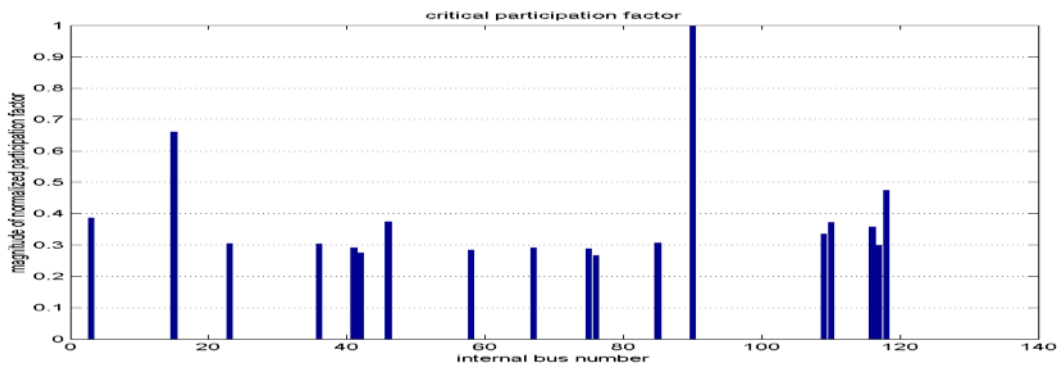


Figure D.178 Combined Strong Buses 105_110_119 of Total “210” MW of Wind Injection

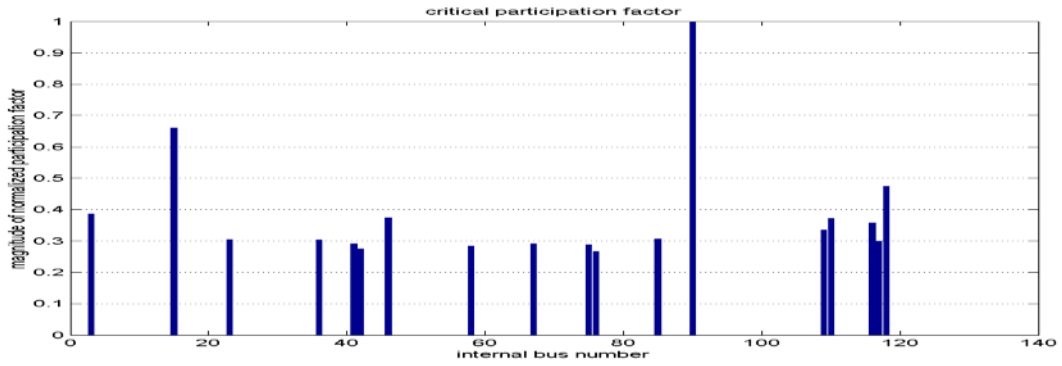


Figure D.179 Combined Strong Buses 105_110_119 of Total “240” MW of Wind Injection

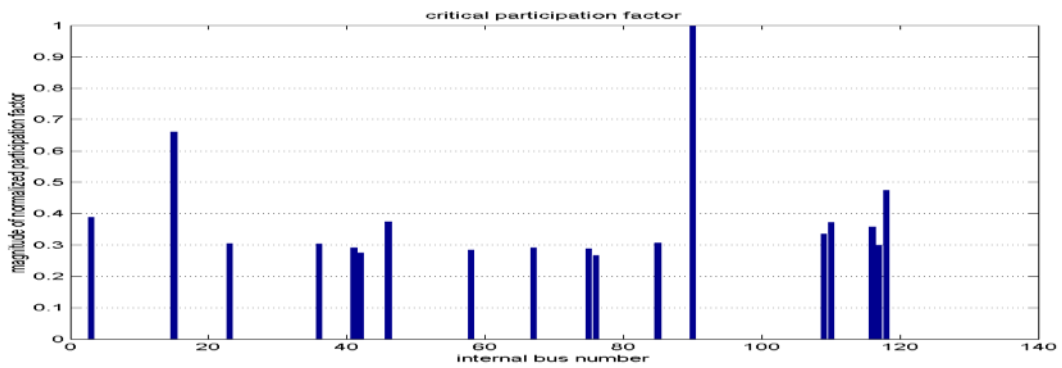


Figure D.180 Combined Strong Buses 105_110_119 of Total “270” MW of Wind Injection

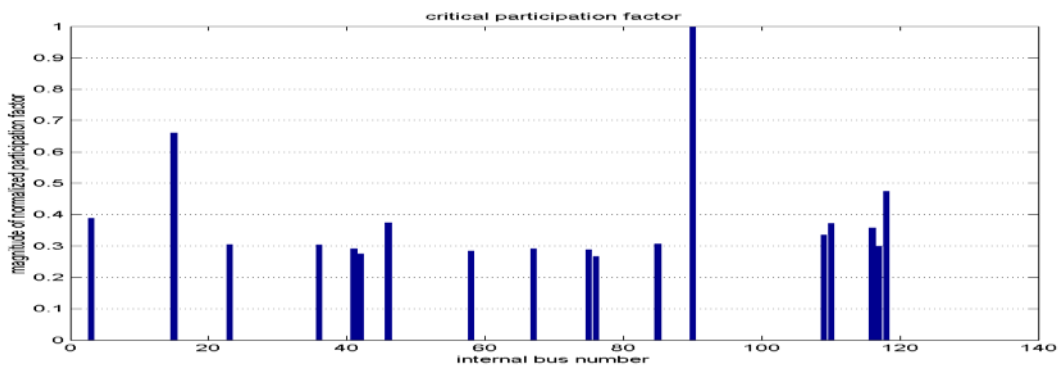


Figure D.181 Combined Strong Buses 105_110_119 of Total “300” MW of Wind Injection

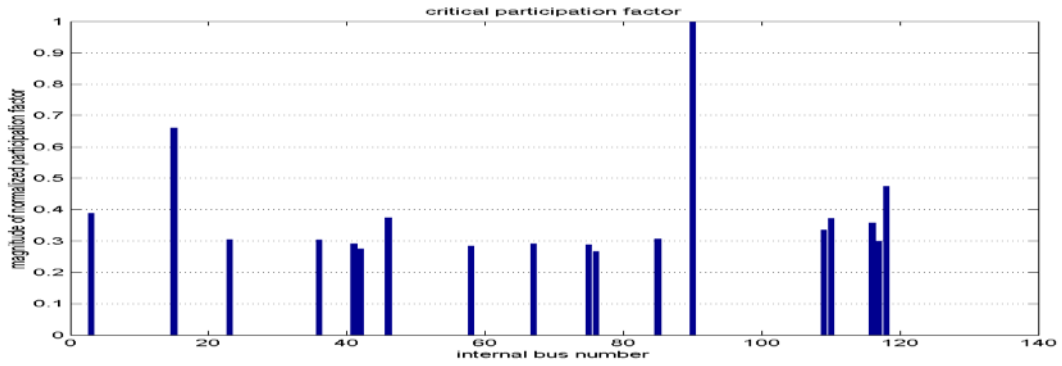


Figure D.182 Combined Strong Buses 105_110_119 of Total “330” MW of Wind Injection

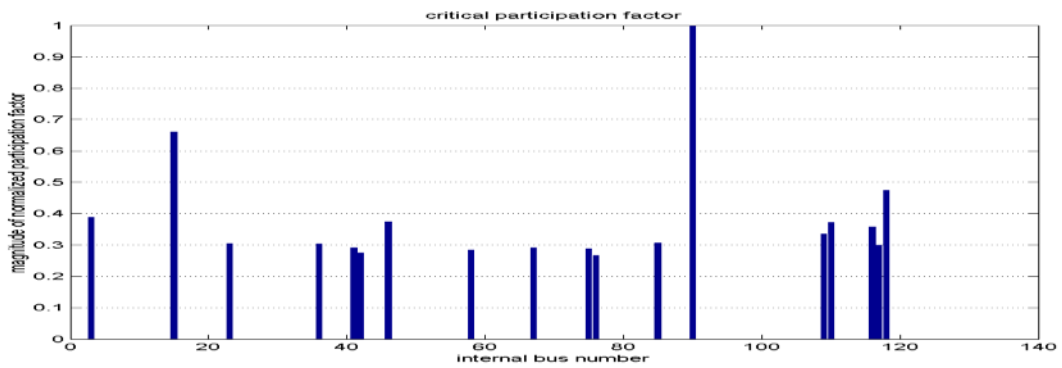


Figure D.183 Combined Strong Buses 105_110_119 of Total “350” MW of Wind Injection

